Synthesis, Modification And Click Of Arylopeptoids Using Carbene-Based Catalysts

Ayman Akhdar

UNIVERSITÉ
Clermont Auvergne
& associés

UNIVERSITE CLERMONT AUVERGNE

ECOLE DOCTORALE DES SCIENCES FONDAMENTALES

THESE

Présentée pour obtenir le grade de

DOCTEUR D'UNIVERSITE

Spécialité : Chimie organique, minérale et industrielle

Par **Ayman AKHDAR**

SYNTHESIS, MODIFICATION AND CLICK OF ARYLOPEPTOIDS USING CARBENE-BASED CATALYSTS

Date de soutenance prévue le 09 décembre 2022 devant la Commission d'Examen :

Membres du jury :

M. Xavier BANTREIL, Maître de conférences HDR, IBMM, Université de Montpellier (rapporteur)
M. Victor MAURIZOT, Chargé de Recherche CNRS HDR, IECB, Université de Bordeaux (rapporteur)
Mme Sylvie DUCKI, Professeur, ICCF, Université Clermont Auvergne (UCA) (examinatrice)
M. Thomas HJELMGAARD, Docteur, ROCKWOOL International (examinateur)
Mme Sophie FAURE, Directrice de Recherche CNRS, ICCF, UCA (co-directrice de thèse)
M. Arnaud GAUTIER, Directeur de Recherche CNRS, ICCF, UCA (directeur de thèse)

Institut de Chimie de Clermont-Ferrand

It is with a deep feeling of gratitude that I thank the Universite Clermont Auvergne and CNRS-France for the financial support throughout my thesis. I take advantage of these few lines to thank all those who have accompanied me over the last three years and these whom without this work would never have been possible. My gratitude goes to my thesis supervisors, Arnaud GAUTIER and Sophie FAURE who have supervised me over the past three years, for their support especially in difficult and important times, also for having learned to be organized, harmonious and rigorous in the work. They gave me the confidence and encouragement to face all the vagaries of science. They were always available to me and thanks to their scientific minds, their knowledge and especially their remarks, many aspects of this report work have been improved.

I would like to thank M. Xavier BANTREIL Maître de conferences, HDR, at Université de Montpellier and M. Victor MAURIZOT Chargé de Recherche CNRS HDR, at Université de Bordeaux who agreed to be the rapporteurs of this work. I would also like to thank M. Thomas HJELMGAARD, Doctor at ROCKWOOL international and Pr. Sylvie DUCKI at Université Clermont Auvergne to accept to examine this thesis.

I sincerely thank Olivier ROY and Lionel NAUTON for their technical assistance, their availability and for the richness of our exchanges and for their constant support. I would like to also thank Aurélie JOB for helping with the HPLC, Martin LEREMBOURE and Frederic EMENEGER for carrying out LCMS experiments and Jean-michel ANDANSON for the IR studies. I would like also to show my gratitude to Mounir TRAIKA for his support as a godfather during my thesis. Your contributions were essential.

Furthermore, I would also like to show my gratitude to the permanent members of the team (Claude TAILLEFUMIER and Florence POUGET) and to all my friends in COM and ICCF: Maha, Maxime, Nassirine, Laura, Cassandra, Zein, Amelie, Cedric, Ali, Zacharie, Xavier and Yael. Also, I would like to show my appreciation to the tarot team (Yael, Arnaud, Olivier, and Lionel) for all the good times during the last years. I thank the stagiares whom I had the opportunity to meet during my thesis and with whom I had a very good time work: Cristina, Teodor, Romane and Adriana. I would also like to show my gratitude to my friends in Clermont-Ferrand: Mohammad, Houssein and Carine who supported me during the last years.

To my wife Dana, it is beyond words to show my gratitude for the invaluable presence you have been in my life. Throughout my journey over the past years, your support has been my rock during the challenging times. I am forever grateful for your unwavering commitment, patience, and love. Your presence has made all the difference, and I am truly blessed to have you as my partner in life.

No words can express my feelings and gratitude to my family including my mother and father, who have stood by my side over the past five years through my ups and downs and their unconditional support that allowed me to continue my studies. To my sisters Reem, Yomna and Ghida, and my brothers in law Ali, Ahmad and Mohammad., I am truly blessed to have you in my life.

Finally, I had the chance to be hosted in France in the recent years by nice and adorable people in Clermont-Ferrand. I would like to show my love to France which has given me the opportunity to improve my skills, my lifestyle, and my scientific knowledge.

Table of Contents

List of Abbreviations

AAC : Azide-Alkyne [3 + 2] Cycloaddition

Boc : tertbutyloxycarbony

Cl_2Phen : 4,7-dichloro-1,10-phenanthroline

CuAAC : Copper catalaysed Azide-Alkyne [3 + 2] Cycloaddition

DFT : Density Functional Theory

DIC : *N,N*'-diisopropylcarbodiimide

DIPEA (Hunig base): *N,N*-Diisopropylethylamine

Dipp : 2,6-diisopropylphenyl

DMAP : 4-Dimethylaminopyridine

DMF : Dimethylformamide

DMSO : Dimethyl sulfoxide

HATU : Hexafluorophosphate Azabenzotriazole Tetramethyl Uronium

HFIP : 1,1,1,3,3,3-Hexafluoro-2-propanol

HPLC : High-performance liquid chromatography

HRMS : High Resolution Mass Spectrometry

IAd : 1,3-bis(admantyl)imidazol-2-ylidene

IC_{50} : 50% inhibitory concentration

ICy : 1,3-bis(cyclohexyl)imidazol-2-ylidene

IMe : 1,3-bis(methyl)imidazol-2-ylidene

IPr : 1,3-bis(2,6-diisopropylphenyl)imidazol-2-ylidene

M : mol.liter^{-1}

min : minute

mmol : millimole

Mol : mole

Nem : *N*-ethynylmethylglycine

NHC : *N*-heterocyclic carbene

Nme : *N*-methoxyethylglycine

NMP : 1-methyl-2-pyrrolidone

NMR : Nuclear magnetic resonance

Npm : *N*-phenylmethylglycine

Ns1tbe : *N*-(S)-1-tertbutylethylglycine

NtBu : *N-tert*butylglycine

OTf : Trifluoromethanesulfonate

PyBOP : Benzotriazol-1-yloxytripyrrolidinophosphonium Hexafluorophosphate

qNMR : Quantitative Nuclear magnetic resonance

SICy : 1,3-bis(cyclohexyl)imidazolin-2-ylidene

SIMes : 1,3-Bis(2,4,6-trimethylphenyl)imidazolin-2-ylidene

SIPr : 1,3-bis(2,6-diisopropylphenyl)imidazolin-2-ylidene

tBuOK : Potassium tert-butylate

TFA : Trifluoroacetic acid

THF : Tetrahydrofuran

TIS : Triisopropylsilane

General introduction

Click chemistry was very recently awarded by the Nobel price of chemistry to Sharpless, Meldal and Bertozzi. “This year’s Prize in Chemistry deals with not overcomplicating matters, instead working with what is easy and simple. Functional molecules can be built even by taking a straightforward route”; says Johan Åqvist, Chair of the Nobel Committee for Chemistry. Click chemistry has been developed over the years and served in chemical diversity and ligation. Also, click chemistry proved its application in diverse areas such as material science, radio chemistry and drug discovery. As we have been driven by the desire to build increasingly elaborated non-natural oligoamides, we take advantage of CuAAC reaction to straightforward introduce chemical diversity and access complex architectures.

N-alktylated oligoamides constitute important class of peptide mimics. Indeed, they are more resistant to hydrolysis in biological conditions. Recent findings demonstrate their importance in many fields, especially in polymer and co-polymers synthesis as well as antibacterials developpment.

Chapter I will introduce the copper-carbenes used as catalyst in CuAAC Click chemistry. Also, the literature about peptoid-type oligoamides, particularly arylopetoids, is introduced, in addition to early CuAAC reactions on peptoid-type oligomers.

To assess the purity of the catalysts we report in chapter II an extension of the quantitative NMR technic to the organometallic field. This chapter not only deals with a method for copper catalyst but also extended the interest to other metals such as silver, palladium and gold as well as the ligands or pre-ligands used. The quantitative NMR reported in this manuscript is based on proton and ^{19}F fluorine nucleus. The scope and limitation of the method are discussed.

In chapter III, the Click CuAAC reaction on supported *N*-alkylated aromatic oligoamides bearing several alkyne groups will be discussed. Methodological study is conducted and moreover, we will debate about the possibility of combinatorial library generation through Click chemistry in order to increase the diversity.

In chapter IV, methylation of triazoles-containing arylopeptoids to form triazolium-based oligomers is studied. The synthesized triazolium-based arylopeptoids represent new type of amphiphilic structures and are tested for their antibacterial activities.

More complex 3-dimentional structures are described in chapter V. The advantage of the use of carbene-copper catalyst is explored to access to 3-D dimensional crown- and tube-like structures from constrained arylopeptoid macrocycles.

Finally, Chapter VI will introduce a preliminary work corresponding to the synthesis of cyclic and cyclodimeric aromatic oligoamides on support.

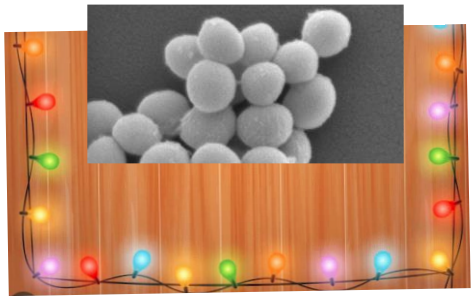

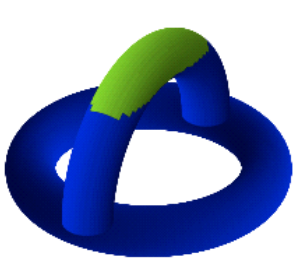

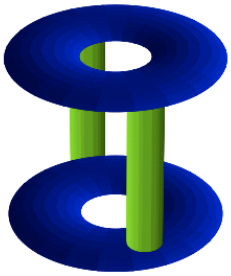

Chapter III + IV

Chapter V

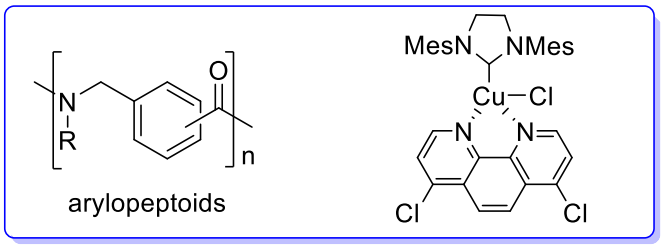

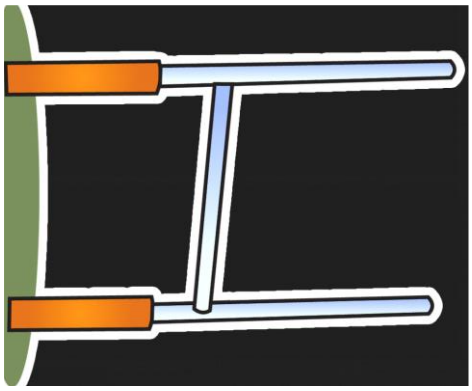

Chapter VI

Chapter I. Bibliography.

I.A. Carbene and metal carbenes.

The interest in carbenes species predates even before the proof of their real existence. It is almost 180 years since the existence of these molecules, containing a divalent carbon atom linked to two covalently adjacent groups, was first mentioned. This introduction will describe the history of these species from the suspicion of their existence to their isolation and characterization through their indirect studies (in the form of organometallic complexes). We will see in the following sections that these species alone and especially as a ligand of organometallic complexes have many applications.

I.A.1. Exploring unstable species.

In 1835, before the establishment of tetravalence of carbon, Dumas become the first chemist who evokes the existence of a new carbonaceous species, the methylene ("the simplest carbon species"), which would consist of 86% carbon and 14% hydrogen as mass percentage, corresponding to a CH_2.[1] He started dehydrating methanol using concentrated sulfuric acid or phosphorous pentoxide to prove his hypothesis, but finished without any evidence. Later, Bulterov also suggested the formation of a divalent carbon as an intermediate for the synthesis of ethylene from methyl iodide and copper (0).[2] Geuther also proposed a dichlorocarbene in the alkaline hydrolysis of chloroform to explain the formation of monoxide and formate anion (this hypothesis was demonstrated in 1954 by Doering).[2] In 1897, the divalent carbon intermediate was also proposed by J. Nef for the ortho-formylation of phenols (the Reimer-Tiemann reaction), and the transformation of pyrrole to *meta*-chloropyridine in chloroform (Scheme I.1).[3]

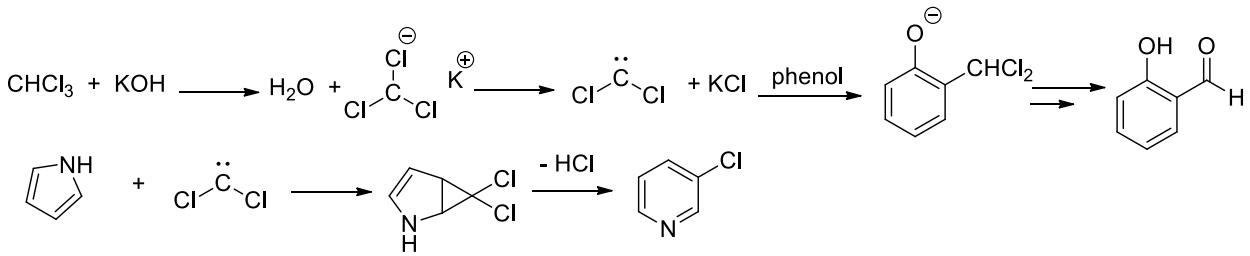

Scheme I.1. Nef's proposal.

In 1912, Staudinger contributed in the recognition of the formation of carbene intermediates while studying the reactivity of diazomethane.[4] He succeeded in converting alkenes **I.1** into cyclopropanes **I.3** using diazomethane under light irradiation and proposed the methylene **I.2** as an intermediate (Scheme I.2).

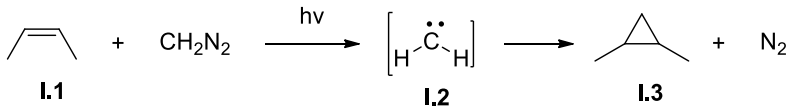

Scheme I.2. Cyclopropanation of alkene using diazomethane.

[1] Dumas, J.; Péligot, E. *Annal. chim. phys.* **1835**.
[2] Kirmse, W.; *Carbene Chemistry*. academic press, london, New York: **1971**.
[3] Nef, J. U. *Eur. J. Org. Chem.* **1897**, *298*, 202-374.
[4] Staudinger, H.; Kupfer, O. *Chem. Ber.* **1912,** *45*, 501-509.

In 1950's, Doering proposed the existence of dihalomethylene intermediate by the first addition of bromoform or chloroform to an alkene producing a cyclopropanation (Scheme I.3).[5]

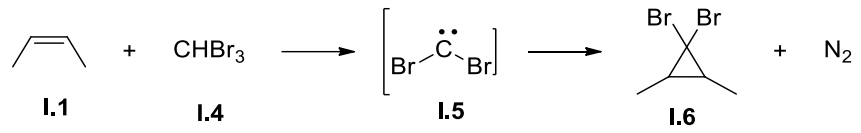

Scheme I.3. Cyclopropanation using bromoform.

Impressively, he also reported a very efficient synthesis of tropolones, a natural compound possessing important pharmaceutic properties, *via* the addition of methylene to benzene derivatives (Scheme I.4).

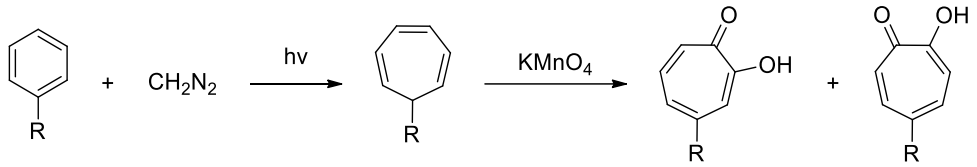

Scheme I.4. Doering's tropolone synthesis.

Later, Conia provided a new synthetic route for natural compounds taking advantage of the decomposition of trimethylsilylcyclopropanols.[6] He added chloromethylcarbene to silyl enol ethers followed by thermal rearrangement in order to form trisubstituted enones (Scheme I.5).

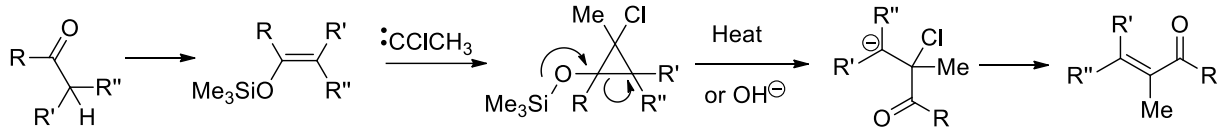

Scheme I.5. Synthesis of trisubstituted enones.

Due to this long history, the carbene intermediates were widely used in the synthesis of natural products affording shorter synthetic paths and better yields. Some selected examples among the plethora of total synthesis are presented below.

Kats-Hegan and Herzon used the carbene generated from bromoform and sodium hexamethyldisilazide in the synthesis of the highly substituted troplone (−) gukulenins A (Scheme I.6).[7]

[5] Von E. Doering, W.; Hoffmann, A. K. *J. Am. Chem. Soc.* **1954,** *76*, 6162-6165.
[6] Conia, j.M.; Salaun, J.R. *Acc. Chem. Res.* **1972**, *5*, 33-40.
[7] Kats-Kagan, R.; and Herzon, S.B. *Org. Lett.* **2015**, *17*, 2030-2033.

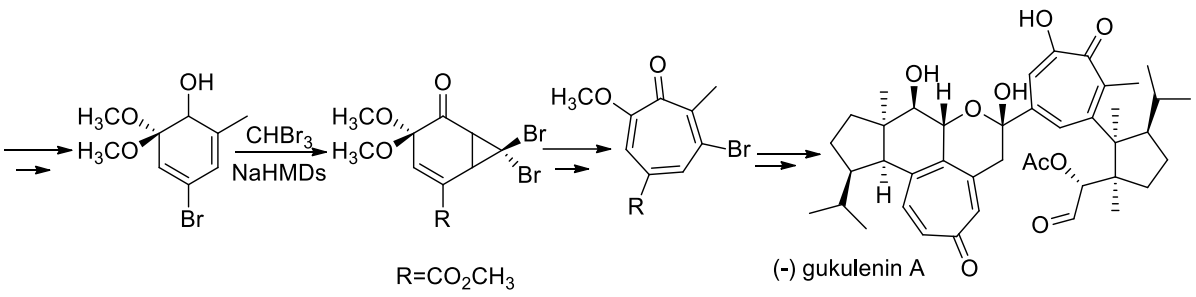

Scheme I.6. Synthesis of (-)-gukulenin.

Dibromocyclopropanation are accessible via metal-halogen exchange between methyl lithium and carbon tetrabromide. Indeed, Cory and M[c] Laren applied this method at an early stage of the total synthesis of ishwarane (extracted from the roots of Aiistolochia iridica Linn).[8]

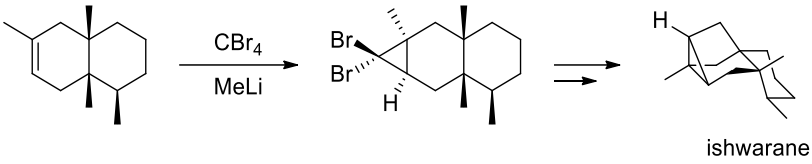

Scheme I.7. Synthesis of Ishwarane.

Conia also used cyclopropanation to obtain natural products containing the α-methyl α-ethylenic motif such as Eucarvone **I.7**, (±) Nuciferal **I.8** (an extract from the wood oil Japanese Kaya) and (±) Manicone **I.9** (an ants's alarm pheromone), (Scheme I.8).[9]

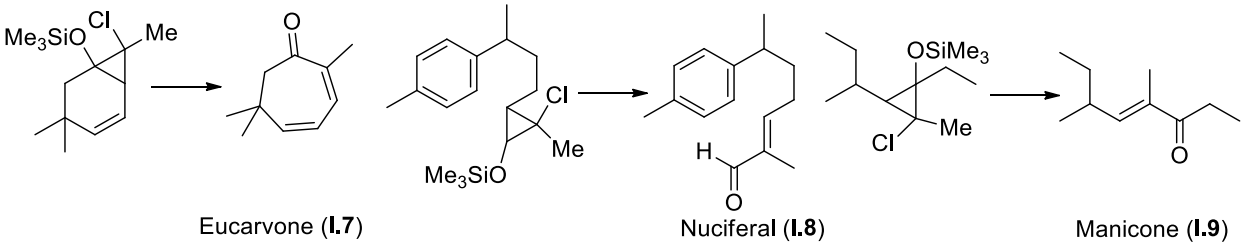

Scheme I.8. Synthesis of natural products.

Later, cyclopropanation was used to synthesize a wide range of natural products such as (−) Bolivianine,[10] (diazo photo decomposition, scheme I.2) or Steenkrotin A[11] (free carbenes, Scheme I.9).

[8] Cory, M.R.; McLaren, F.R *Chem. Commun* **1977**, 587-588.
[9] Blanco, L.; Slougui, N.; Rousseau, G.; Conia, J.M. *Tetrahedron Lett.* **1981**, *22*, 645-648.
[10] Yuan, C.; Du, B.; Li, Y.; Liu, B. *J. Am. Chem. Soc*. **2013**, *135*, 9291-9294.
[11] Pan, S.; Jun, X.; Gao, B.; An, Z.; Ding, H. *Angew. Chem. Int. Ed.* **2015**, *54*, 6905-6908.

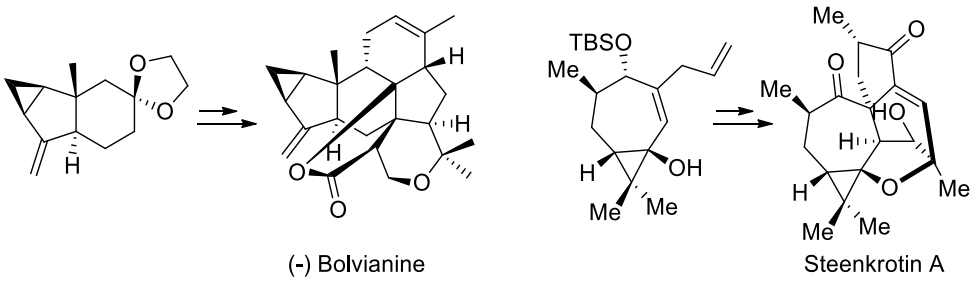

Scheme I.9. Synthesis of natural products by diazo photo decomposition.

As we could see, there has been a long interest in the isolation of carbenes. These carbenes also proved their importance in the synthetic routes of different natural products which make it more attractive. After the high interest that carbenes gained, these molecules were classified according to the electronic configuration and geometry as singlet and triplet carbenes.

I.A.1.1. Singlet and triplet Carbenes.

Carbenes adopt sp2 hybrid structure. They are classified as singlet or triplet depending of their spin pairing. Triplet carbenes have two unpaired electrons with a total spin of one and are consequently paramagnetic, thus they can be characterized by Electron Spin Resonance spectroscopy (ESR). Oppositely, singlet carbenes are spin-paired, possessing a full and an empty orbital (Scheme I.10).

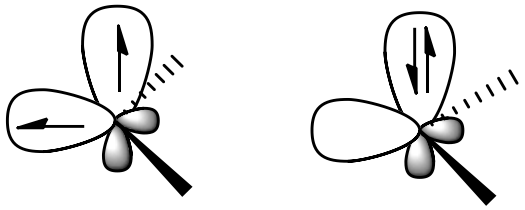

Scheme I.10. Singlet and triplet carbenes.

Triplet carbenes possess a diradical-like behavior that makes them very reactive and difficult to isolate. However, they can be stabilized by an extended aromatic network as shown by Tomioka *et al.* who obtained a triplet carbene stable up to one week at room temperature in solution (Scheme I.11).[12]

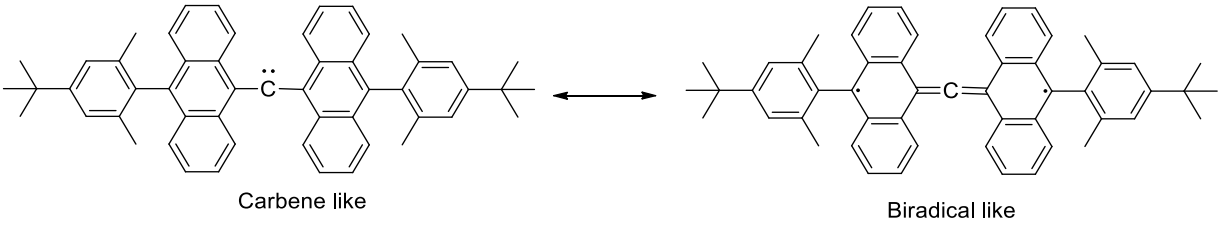

Scheme I.11. Stable triplet carbene.

Singlet carbene stability is favored by adding σ-electron withdrawing substituents. Another possibility for the stabilization consists in pushing electrons in the empty orbital, for example by placing a heteroatom (possessing nonbonding electrons) adjacent to the carbene center.

[12] Iwamoto, E.; Hirai, K.; Tomioka, H. *J. Am. Chem. Soc*. **2003**, *125*, 14664-14665.

I.A.1.2. Fischer carbenes.

In the early 1960s, the name of Fischer starts to strike in the scientific community due to his work on alkene-metal-carbonyl complexes. In 1964, methoxyphenylmethylene tungsten (0) pentacarbonyl **I.13** (Scheme I.12) was fully characterized and became the first metal-carbene complex reported.[13] After this achievement, Fischer and his collaborators extended the synthesis to other transition metals such as chromium (0),[14] iron (0) and manganese (0) complexes with different alkoxy and alkyl groups.[15]

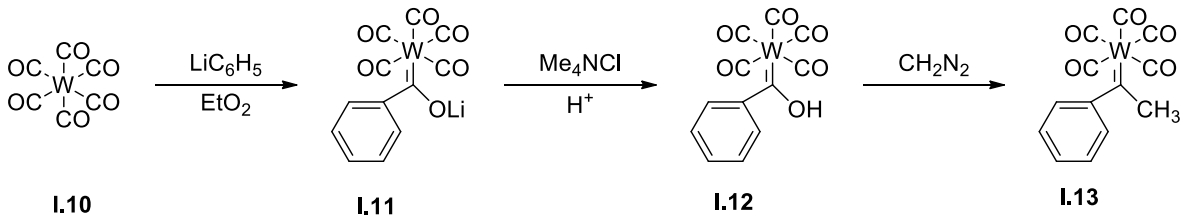

I.10 **I.11** **I.12** **I.13**

Scheme I.12. Synthesis of 1st Fischer metal carbene.

Fischer carbenes are defined as well stabilized singlet carbenes, such as alkoxycarbenes and aminocarbenes, having a significant gap between singlet and triplet ground states. They form a main σ-type carbene-metal donation with a weak π-back metal-carbene donation, this is the reason of the partial-double bond character of the metal-carbon bond. These carbenes are electrophilic at their carbene-metal-center making them susceptible to a nucleophilic attack. The main characteristics of these carbenes are:

– Low oxidation state metal center

– π-acceptor metal ligands (carbonyls)

– π-donor substituent groups R (like alkoxy, or amines) linked to the carbene

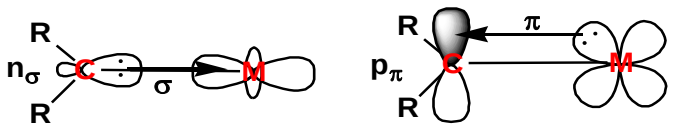

Scheme I.13. Metal-carbon bonding in Fischer-carbene complexes.

I.A.1.3. Schrock carbenes.

In 1974, Schrock synthesized the first metal-carbene complex with high oxidation state (d^0) by intermolecular α-hydrogen elimination on the tri-(2,2-dimethylpropyl)methyl tantalum (V) dichloride precursor **I.14** (Scheme I.14).[16]

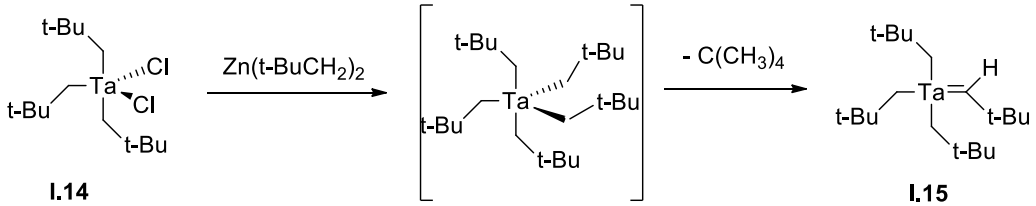

I.14 **I.15**

[13] Fischer, E. O.; Maasböl, A. *Angew. Chem., Int. Ed. Engl*. **1964**, *3*, 580-581.

[14] Fischer, E. O.; Maasböl, A. *Chem. Ber*. **1967**, *100*, 2445-2456.

[15] Cardin, D. J.; Cetinkaya, B.; Doyle, M. J.; Lappert, M. F. *Chem. Soc Rev*. **1973**, *2*, 99-144

[16] Schrock, R. R. *J. Am. Chem. Soc.* **1975**, *97*, 6577-6578.

Scheme I.14. Synthesis of 1st Schrock complex.

Schrock carbenes are defined as weakly stabilized triplet carbenes such as dialkylcarbenes and alkylidenes, with a small gap between singlet and triplet ground states. These carbenes form a covalent metal-carbene bond. The π-electrons are distributed equally between the carbene and metal center, leading to consider the metal-carbon as a true double bond. Schrock carbene complexes are nucleophilic at the metal-carbene center. The main characteristics of these complexes are:

–High oxidation state metal center (d^0)
–π-donor metal ligands or ligands σ-donors
–Early transition metals

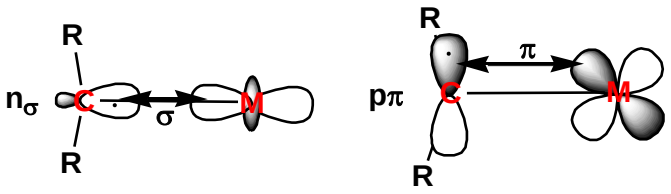

Scheme I.15. Metal-carbon bonding in Schrock-carbene complexes.

I.A.2. Bertrand and Arduengo's stable Carbenes.

I.A.2.1. Historical breakthrough

Due to the importance of carbenes in organic synthesis and biological processes, chemists had tried to isolate these unstable species. Indeed, Breslow hypothesized that carbenes are not restricted to a laboratory curiosity but are also species used by enzymes.[17] Thiamines (vitamin B1) is a precursor of the thiamine pyrophosphate, a co-enzyme presented in living organisms. It is involved in many enzymatic reactions such as pyruvate dehydrogenase and decarboxylase, alpha-ketoglutarate dehydrogenase or transketolase. Breslow was the first to postulate the existence of a free stable carbene: the thiazol-2-ylidene, stabilized by the presence of the two adjacent heteroatoms. Indeed, Breslow reported the H-D exchange at the C2 carbon in D_2O (Scheme I.16); therefore, this rises the question of the existence of the free carbene or the ylide forms.

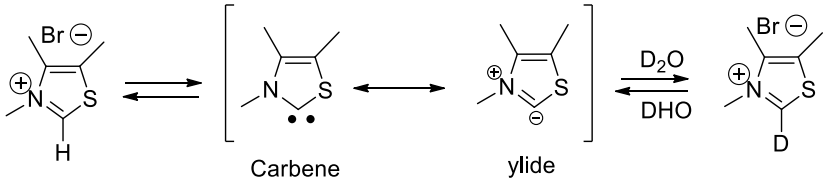

Scheme I.16. Breslow's hypothesis.

The question stays open for many years. In 1960s, Wanzlick and Öfele, both interested in carbenes isolation to test the Breslow's hypothesis, propose that the presence of heteroatoms around the carbene center (such as diaminocarbenes) can increase the stability.[18] However, all attempts to isolate a free carbene were unsuccessful. Indeed, Wanzlick team tries to isolate a so-called *N*-heterocyclic Carbene (NHC) from imidazolium derivatives but didn't succeed.

[17] Breslow, R. *J. Am. Chem. Soc.* **1958,** *80,* 3719-3726.
[18] Wanzlick, H. W. *Angew. Chem. Int. Ed* **1962,** *1*, 75-80; (b) Öfele, K. *J. Organomet. Chem* **1968,** *12*, 42-43; (c) Wanzlick, H. W.; Schönherr, H. J. *Angew. Chem. Int. Ed* **1968,** *7*, 141-142.

They end up with a dimer, the tetraamino olefin **I.16** (Scheme I.17), proposing an equilibrium between the free carbene and its dimer, a tetraaminoethylene derivative. They argue that the carbene couldn't be isolable due to its high instability.

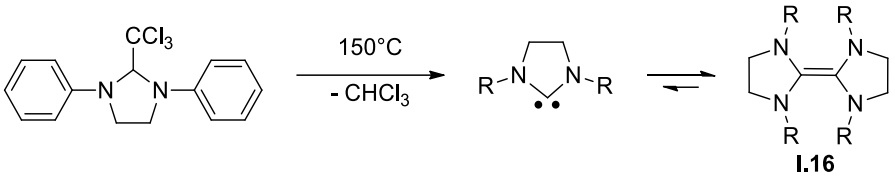

Scheme I.17. Wanzlick equilibrium.

The reality of this equilibrium was proved by Herrmann and Ma who performed NMR studies and obtained metathesis product of mixed olefin originated from symmetrical olefins.[19]

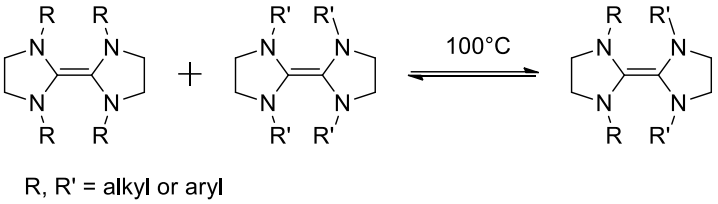

Scheme I.18. Catalyst free metathesis.

In 1988, Bertrand reports a breakthrough by isolating the first persistent and distillable carbene, a phosphinocarbene (Scheme I.19), which proved to have enough stability for NMR analysis and to be used in reaction with different substrates.[20]

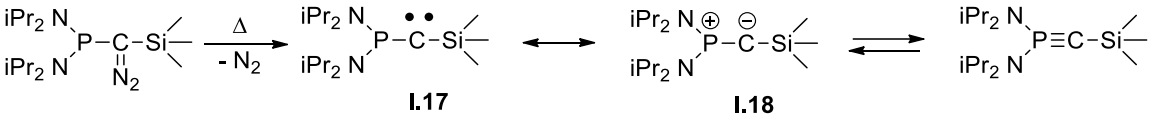

Scheme I.19. First isolated carbene by Bertrand.

Later, in 1991, Arduengo reports the successful isolation of a stable singlet carbene, structurally close to Wanzlick's, the 1,3-bis(adamantyl)imidazol-2-ylidene[21]. Arduengo concentrates on the steric hindrance of one substituent on nitrogen atoms surrounding the carbene center. As the easily accessible azolium salts have a pka ranging between 20 to 24, strong bases should be used for the deprotonation. He used sodium hydride in presence of catalytic amount of dmso (to form dimsyl anion), to deprotonate an imidazolium chloride and form the diaminocarbenes (Scheme I.20). The steric hindrance was a main hypothesis for the isolation of this diaminocarbene, displacing the Winzlack's equilibrium to the carbene side. However, the isolation of tetramethylimidazolydene proved that the steric aspect was not the exclusive reason of the stability.

[19] (a) Böhm, V. P. W.; Herrmann, W. A. *Angew. Chem. Int. Ed.* **2000,** *39*, 4036-4038; (b) Denk, M. K.; Hatano, K.; Ma, M. *Tetrahedron Lett.* **1999,** *40*, 2057-2060.
[20] Igau, A.; Grutzmacher, H.; Baceiredo, A.; Bertrand, G. *J. Am. Chem. Soc.* **1988**, *110*, 6463-6466.
[21] Arduengo, A. J.; Harlow, R. L.; Kline, M. *J. Am. Chem. Soc.* **1991**, *113*, 361-363.

Scheme I.20. The first stable *N*-heterocyclic carbene (NHC).

I.A.2.2. Synthesis of imidazolium and imidazolidinium

The most widely used imidazoliums as NHC precursors are represented in Scheme (I.21).

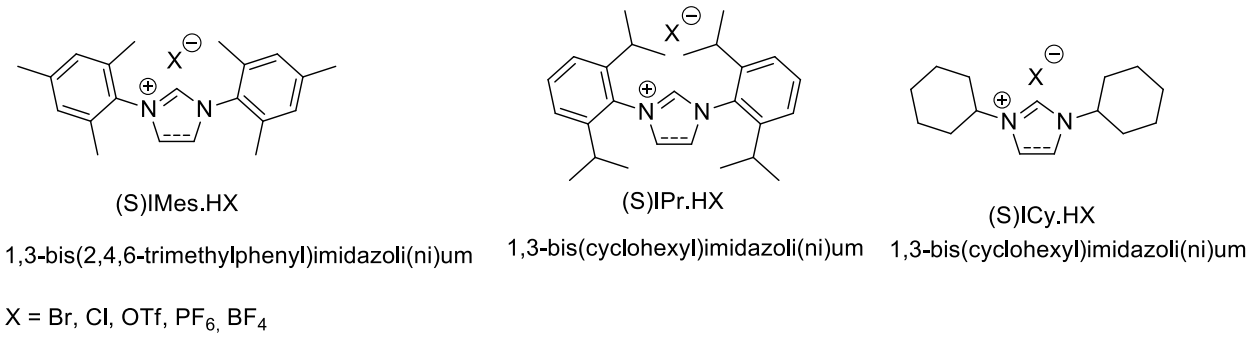

Scheme I.21. Examples of NHCs precursors.

However, this series represents only a very small part of the structures reported in the literature, which has found plethora of applications as phosphine substitute in catalysis. If most of the applications in transition metal catalysis are based on symmetrical ligand, a large number of publications reported the utilization of unsymmetrical ligands.

I.A.2.2.1. Synthesis of symmetrical imidazolium

One of the most straightforward synthetic paths is a one pot synthesis using glyoxal, primary amine and formaldehyde under aqueous acidic conditions (Scheme I.22), patented in 1991 by Arduengo.[22]

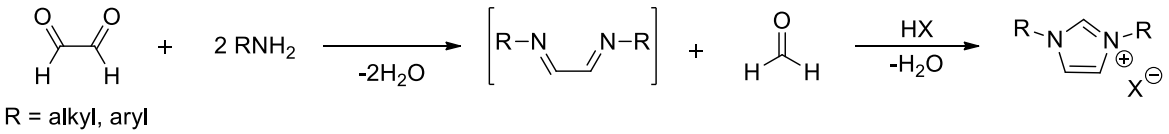

Scheme I.22 One pot synthesis of imidazolium salts.

Due to low yields obtained generally with the one pot sequence, probably due to the problematic removal of water, and the poor scope of the procedure, the reaction was splitted into two steps.[23] At first, the diimine was isolated then cyclization was performed separately. This procedure allows the synthesis of symmetrically *N,N'*-substituted imidazolium salts with various alkyl and aryl groups such as 1,3-bis(isobutyl)imidazolium (I^{t}Bu.HX), 1,3-bis(dodecyl)imidazolium (IDD.HX), 1,3-bis(2,6-diisopropylphenyl)imidazolium (IPr.HX), 1,3-

[22] Arduengo III, A. J. Patent: WO 9114678, **1992**

[23] (a) Arduengo III, A. J.; Krafczyk, R.; Schmutzler, R. *Tetrahedron* **1999**, *55*, 14523-14534. (b) Jafarpour, L.; Stevens, E. D.; Nolan, S. P. *J. Organomet. Chem.* **2000**, *606*, 49-54.

bis(cyclohexyl)imidazolium (ICy.HX), and 1,3-bis(2,4,6-trimethylphenyl)imidazolium (IMes.HX) (Scheme I.23).[24]

Arduengo used this two steps procedure using MOMCl (chloromethylethylether) as formaldehyde equivalent and obtained straightforwardly IMes.HCl and IPr.HCl, in moderate 40% yields.[23a] Nolan modified Arduengo's procedure by replacing the toxic MOMCl by paraformaldehyde in presence of a protic acid (such as HCl, HBF_4, or HPF_6, and preferably HCl) in a dry solvent at room temperature, (Scheme I.23).[25] In 2007, Hintermann proposes a variation of the cyclization protocol by replacing HCl catalyst by trimethylsilyl chloride in ethyl acetate.[26] This produces IPr.HCl, IMes.HCl and IXy.HCl, in better yields than one-pot synthesis, reaching up to 80% (Scheme I.23).

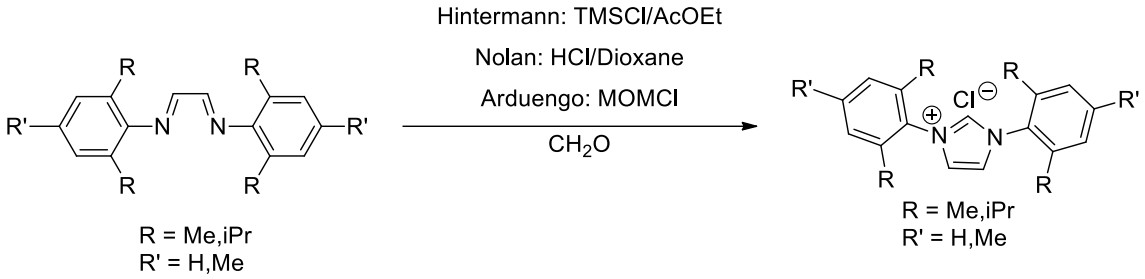

Scheme I.23. Arduengo, Nolan and Hintermann protocols.

The general mechanism for the cyclization was proposed by Hintermann.[27] It involves an *N*-alkylation of the azadiene by activated formaldehyde. The elimination of acid chloride furnishes the dipole imino-azomethin-ylide which will undergo a 6π electrocyclization (1,5-dipolar cyclization).

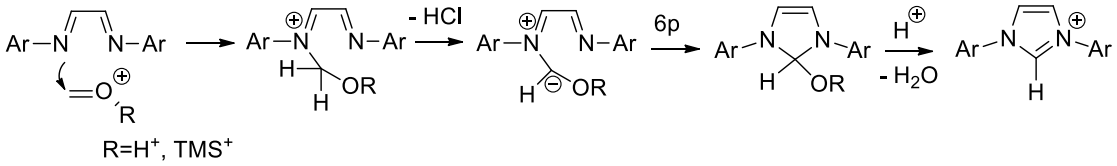

Scheme I.24. General mechanism of cyclization proposed by Hintermann.

Nevertheless, this route becomes problematic when C_4 and C_5 positions are substituted, making the cyclization step disfavored. Glorius proposed a useful alternative[27]. The reaction of silver triflate with chloromethyl pivalate generates, *in situ*, an alkylating reagent (trifluoromethylsulfonyloxymethyl pivalate) which efficiently cyclizes hindered and non-hindered diimines (Scheme I.25).

[24] (a) de Frémont, P.; Scott, N. M.; Stevens, E. D.; Nolan, S. P. *Organometallics* **2005**, *24*, 2411- 2418. (b) de Frémont, P.; Scott, N. M.; Stevens, E. D.; Ramnial, T.; Lightbody, O. C.; MacDonald, C. L. B.; Clyburne, J. A. C.; Nolan, S. P. *Organometallics* **2005**, *24*, 6301-6309. (c) de Frémont, P.; Singh, R.; Stevens, S. P.; Petersen, J.; Nolan, S. P. *Organometallics* **2007**, *26*, 1376-1385.
[25] Jafarpour, L.; Stevens, E. D.; Nolan, S. P. J. *Organomet. Chem.* **2000**, *606*, 49–54.
[26] Hinterman, L. *Beilstein J. Org. Chem.* **2007**, *3*, 22.
[27] (a) Glorius, F.; Altenhoff, G.; Goddard, R.; Lehmann, C. W. *Chem. Commun.* **2002**, 2704- 2705. (b) Altenhoff, G.; Goddard, R.; Lehmann, C. W.; Glorius, F. *J. Am. Chem. Soc.* **2004**, *126*, 15195-15201.

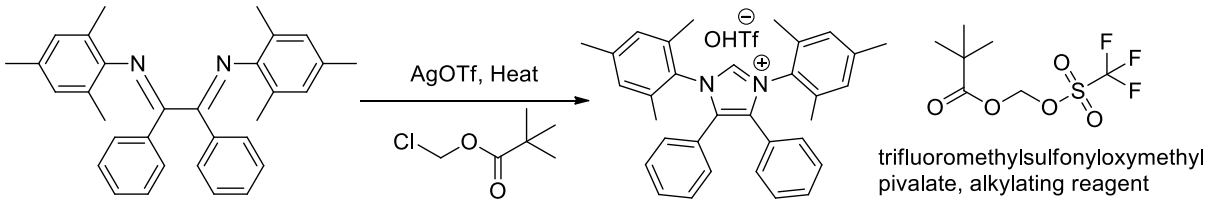

Scheme I.25. Glorius synthesis of imidazolium salts.

Markó described an efficient three step-synthesis of the hindered NHC, IPr*.[28] The synthesis of IPr* starts with the dialkylation of *p*-toluidine followed by the treatment with aqueous glyoxal to afford the diimine. The IPr*.HCl salt was produced by the cyclization of the formed diimine (Scheme I.26).

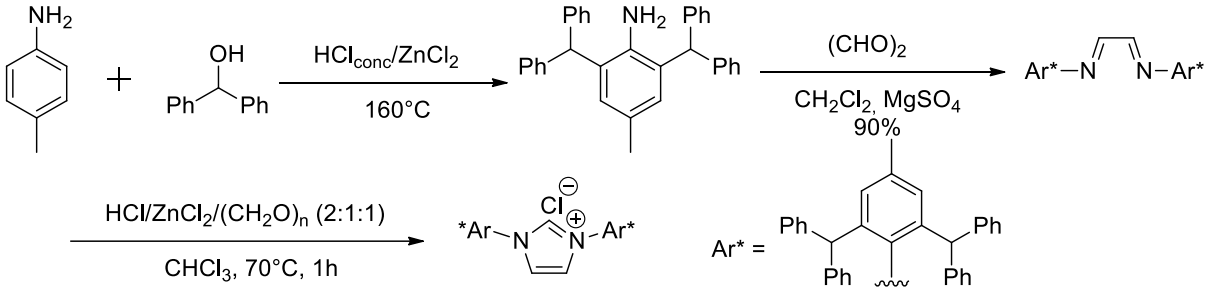

Scheme I.26. Synthesis of IPr*.HCl by Markó.

Recently, Lamaty described a mechanochemical one pot, two-step synthesis.[29] The first step is the formation of 1,4-diazadiene in quantitative yield *via* milling 2,6-diisopropylphenylamine and 2,3-butanedione (1.0 equiv.) for 2h in a zirconium oxide 20 mL jar. The ring closure is performed by addition of paraformaldehyde and 4M HCl in dioxane with 3h of milling (imine formation and 3h cyclization, Scheme I.27). Finally, the imidazolium salt is recovered upon precipitation in EtOAc.

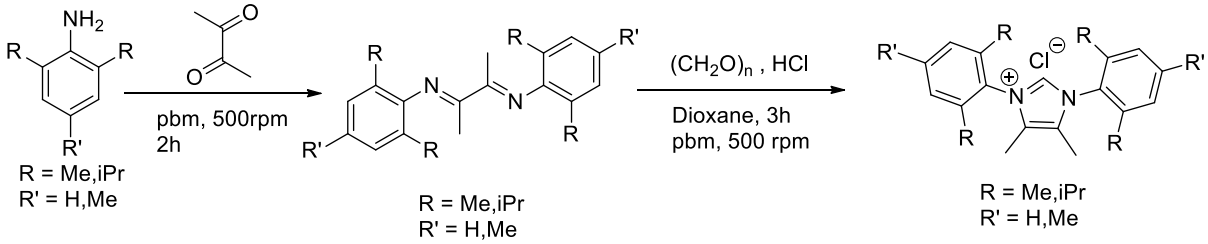

Scheme I.27. Synthesis of imidazolium salts using mechanochemistry.

I.A.2.2.2. Synthesis of unsymmetrical Imidazolium

The route for the synthesis of non-symmetrical dialkylated imidazolium salts is a step-by-step reaction of the imidazolide anion followed by alkylation with an alkyl halide (Scheme I.28).[30] This is the standard procedure for the synthesis of ionic liquids.

[28] Berthon-Gelloz, G.; Siegler, M. A.; Spek, A. L.; Tinant, B.; Reek, J. N. H.; Marko, I. E. *Dalton Trans.* **2010**, *39*, 1444–1446.
[29] Beillard, A.; Bantreil, X.; Métro, T.-X.; Martinez, J.; Lamaty, F. *Green Chem.* **2018**, *20*, 964–968.
[30] Herrmann, W.A. *Angew. Chem. Int. Ed.* **2002**, *41*, 1290-1309.

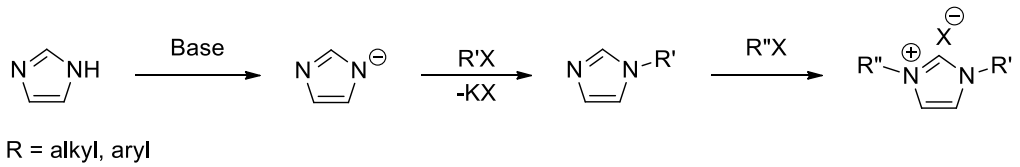

Scheme I.28. Synthesis of dialkylated non-symmetrical imidazoliums.

Using one equivalent of the alkyl or aromatic primary amines mono *N*-substituted, imidazoles are produced. Further *N*-alkylation can be performed by the reaction with alkyl or benzyl halide forming an unsymmetrical *N,N'*-substituted imidazolium salt (Scheme I.29).[31]

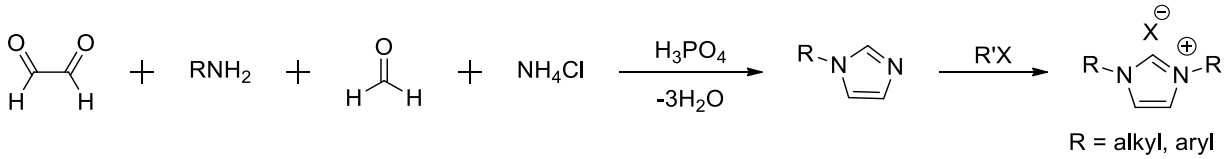

Scheme I.29. Synthesis of non-symmetrical imidazolium salts.

The synthesis of unsymmetrical diaryl imidazolium usually requires more steps. Fürstner reported a route *via* oxazolinium salts[31]. The key intermediate could be synthesized by two ways. First route affords α-aminoketones which is *N*-formylated using formic acetic anhydride. Cylclization to oxazolium occurs in acetic anhydride catalyzed by strong mineral acids. A variant route starts from bromoacetaldehyde diethylacetal (Scheme I.30). In both cases, addition of the second aniline followed by dehydration affords the desired imidazolium.

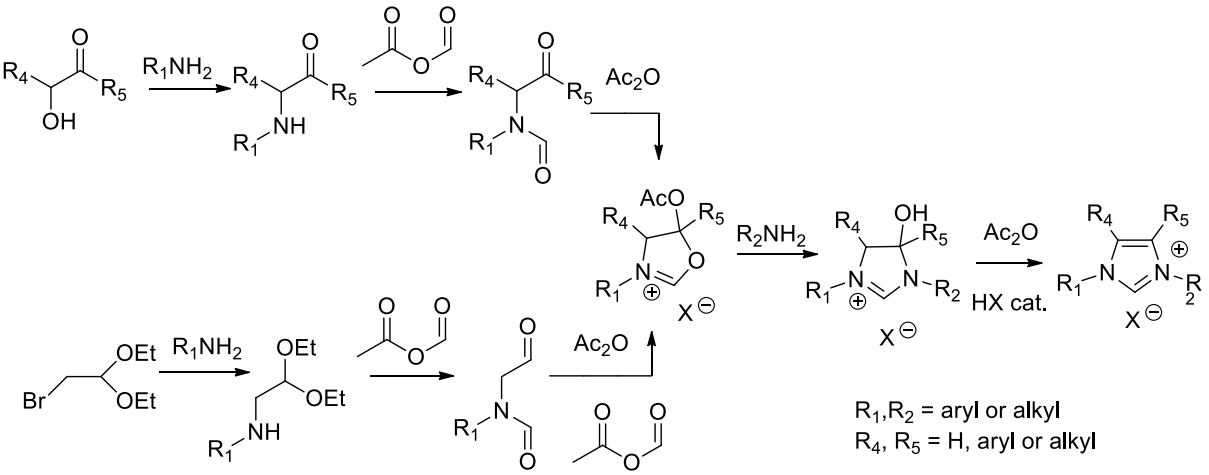

Scheme I.30. Furstner's synthesis of non-symmetrical imidazolium salts.

Glorius developed an efficient method for the one-pot synthesis of various highly substituted imidazolium salts.[32] The coupling of formamidines with readily available α-halo ketones produce a hydroxyimidazolinium halide in presence of Hünig base, followed by a dehydration similar to Fürstner's one (Scheme I.31).

[31] Furstner, A.; Alcazaro, M.; Céesar, V.; Lehmann, C.W. *Chem. Commun.* **2006**, 2176–2178.

[32] Hirano, k.; Urban, S.; Wang, C.; Glorius, F. *Org. Lett.* **2009**, *11*, 1019–1022

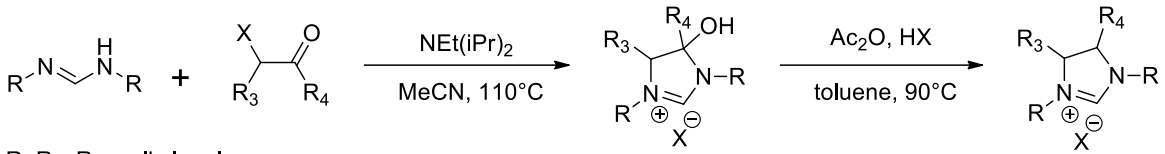

R, R_3, R_4 = alkyl,aryl
X = Cl, Br

Scheme I.31. Glorius's synthesis of imidazolium salts.

An even shorter method for the synthesis of non-symmetrical imidazolium salts is the quaternization of well-known *N*-substitued imidazoles with diversely substituted phenyl boronic acids in DMF, catalyzed by $Cu(OAc)_2$ and $FeCl_3$ (Scheme I.32).[33]

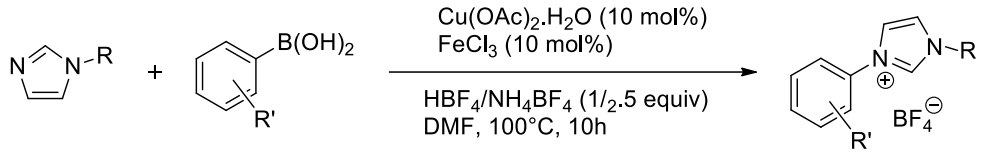

R, R' = aryl, alkyl

Scheme I.32. Imidazolium salts via boronic acids.

I.A.2.2.3. Symmetrical Imidazolinium

Arduengo used the reduction of azadiene by sodium borohydride to obtain 1,2-diaminomethane. Then, imidazolinium salts are formed by the reaction of the reduced amines with triethyl orthoformate under acidic conditions (Scheme I.33).[23a] Recently, it was proved that time could be reduced from hours to few minutes using microwave heating.[34] This method is usually used for the synthesis of symmetrical imidazolinium salts with various aryl groups.

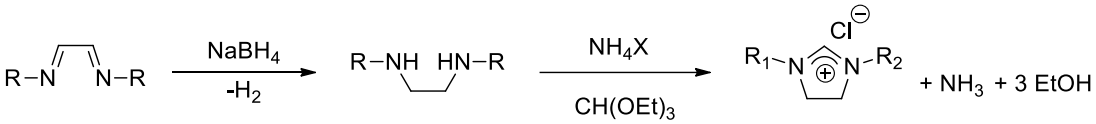

Scheme I.33. Synthesis of symmetrical imidazolinium salts.

This 3 steps synthesis requires the adjustment of the oxidation level by $NaBH_4$, which on large scale is exothermic and thus could be troublesome. Direct formation of the diamine is possible by the alkylation of 3-4 equivalents of anilines with dibromoethane[35]. Refluxing the reagent in methanol at high concentrations affords the desired dihydrobromid salts that crystalize from the reaction mixture. Further anion exchange and orthoformate cyclization affords the desired imidazolidinium salt.

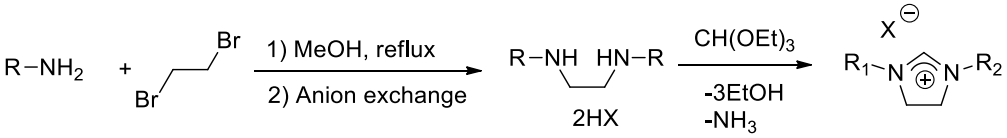

Scheme I.34. Synthesis of symmetrical imidazolinium salts.

[33] Li, S.; Yang, F.; Lv, T.; Lan, J.; Gao, G.; You, J. *Chem. Commun.* **2014**, *50*, 3941-3943.
[34] Aidouni, A.; Demonceau, A.; Delaude, L. *Synlett* **2006**, 493-495.
[35] Roche, S. P.; Teyssot, M-L.; Gautier, A. *Tetrahedron Lett.* **2010**, *51*, 1265–1268.

I.A.2.2.4. unsymmetrical Imidazolidinium

Ethyl chloroglyoxylate could react in stepwise manner with two different amines to produce unsymmetrical oxalamide. Borane or lithium aluminum hydride are good reagents to reduce the oxalamide into 1,2-diaminoethanes. Further cyclization into unsymmetrically *N,N'*-substituted imidazolinium salts using triethyl orthoformate under acidic conditions is applied according to well established procedures (Scheme I.35).[36]

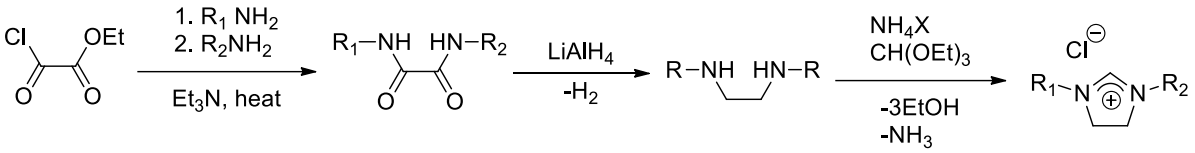

Scheme I.35. Synthesis of unsymmetrical imidazolinium salts.

Imidazolinium salts are deprotonated using the same route as imidazolium salts, using strong bases. However, it is important to mention that nucleophilic bases such as alkoxides and ammonia should be avoided due to the fact that adducts with the imidazolidin-2-ylidene could be formed.

I.A.3. Synthesis of NHCs

I.A.3.1. Deprotonation of azoliums.

After the first NHC isolation by Arudengo using dimsyl anion (Scheme I.20), other bases were tested by Arduengo such as *t*BuOK or KH in THF. In 1996, Herrmann described a new route for the deprotonation of azolium salts in liquid ammonia.[37] The azolium salts are deprotonated by sodium anhydride (NaH) in a solution of liquid ammonia with THF at around -50°C (Scheme I.36). Generally, potassium or sodium hydride with a catalytic amount of *t*BuOK are employed, but not *t*BuOK itself, lithium aluminium hydride, butyllithium, potassium hexamethyldisilazide (KHMDS) and DBU are also efficient alternatives bases.

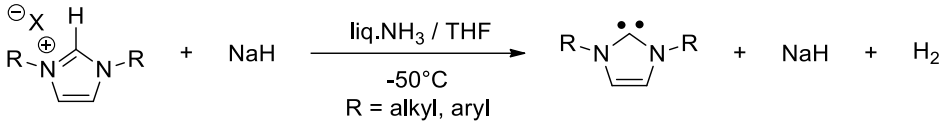

Scheme I.36. Ammonium route for the deprotonation of imidazolium salts.

I.A.3.2. Reduction of azoliums.

Imidazol-2-ylidenes can be synthesized by a single electron reduction of imidazolium salts using excess of potassium in boiling THF (Scheme I.37).[38]

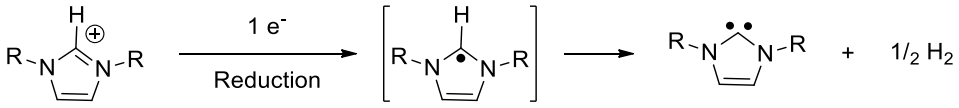

Scheme I.37. Synthesis of imidazolylidenes by chemical reduction

[36] (a) Clavier, H.; Coutable,L.; Guillemin, J.-C.; Mauduit, M. *Tetrahedron* **2005**, *17*, 921. (b) Paczal, A.;Bényei, A.C.; Kotschy, A. *J. Org. Chem.* **2006**, *71*, 5969.

[37] Herrman, W.; Elison, M.; Fisher, J.; Kocher, C.; Artus, G. R. *J. Eur. J. Chem.* **1996**, *2*, 772-780.

[38] Arduengo III, A. J.; Krafczyk, R.; Schmutzler, R. *Tetrahedron* **1999**, *55*, 14523-14534. (b) Gorodetsky, B.; Ramnial, T.; Branda, N. R.; Clyburne J. A. C. *Chem. Commun.* **2004**, 1972-1973.

Astruc reports a reduction with a 19-electron sandwich complex of Fe(I) to produce a radical anion peroxide in presence of air, which in its turn deprotonate the imidazolium salt (Scheme I.38).[39]

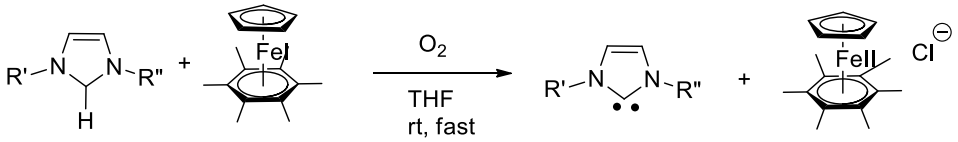

Scheme I.38. Astruc synthesis.

I.A.3.3: Reduction of imidazol-2-thione.

Both symmetrical and non-symmetrical imidazol-2-thiones are simply transformed to imidazol-2-ylidenes by desulfurization. The corresponding NHC is formed after addition of excess potassium to the thione in boiling THF (Scheme I.39).[40] Although the conditions seem to be drastic, the yields are almost quantitative.

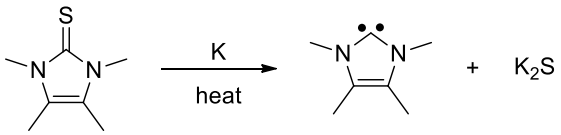

Scheme I.39. Desulfurization of imidazole-2-thiones.

I.A.3.4. Imidazolidin-2-ylidenes via imidazolidine adducts

Imidazolidine adducts, represents a masked form of NHC. They could be produced by the reaction of alcohols or chloroform in presence of a base with imidazolinium halides[41]. As masked form of NHCs they are chemically stable and could be manipulated in air. They can generate imidazolidinylidenes directly by thermolysis in a similar manner to first Wanzlick tries (Scheme I.40).

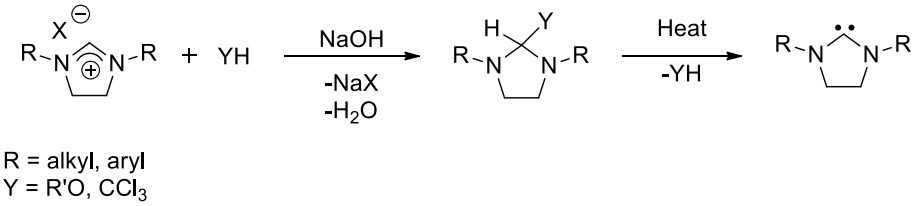

Scheme I.40. Synthesis of masked NHCs and thermal generation of NHC.

Another stable, masked form is the carbon dioxide adduct. As reported by Louie, these species produce a stable NHC-carbene upon the loss of CO_2, able to combine with metal salts without the use of base (Scheme I.41).[42]

---

[39] Méry, D.; Ruiz Aranzaes, J.; Astruc, D. *J. Am. Chem. Soc.* **2006**, *128*, 5602-5603.

[40] (a) Hahn, F.E.; Paas, M.; Le Van, D.; Lügger, T. *Angew. Chem., Int. Ed.* **2003**, *42*, 5243-5246; (b) Hahn, F.E.; Paas, M.; Le Van, D.; Fröhlich, R. *Dalton Trans.* **2006**, 860-864.

[41] (a) Scholl, M.; Ding, S.; Lee, C. W.; Grubbs, R. H. *Org. Lett.* **1999**, 1, 953-956. (b) Trnka, T. M.; Morgan, J. P.; Sanford, M. S.; Wilhelm, T. E.; Scholl, M.; Choi, T.-L.; Ding, S.; Day, M. W.; Grubbs, R. H. *J. Am. Chem. Soc.* **2003**, 125, 2546-2558. (c) Cetinkaya B.; Cetinkaya, E.; Chamizo, J. A.; Hitchcock, P. B.; Jasim, H. A.; Kücükbay, H.; Lappert, M. F. J. *Chem. Soc., Faraday Trans.* **1998**, 2047-2054. (d) Blum, A. P.; Ritter, T.; Grubbs, R. H. *Organometallics* **2007**, 26, 2122-2124.

[42] (a) Duong, H. A.; Tekavec, T. N.; Arif, A. M.; Louie, *J. Chem. Commun.* **2004**, 112-113. (b) Voutchkova, A. M.; Appelhans, L. N.; Chianese, A. R.; Crabtree, R. H. *J. Am. Chem. Soc.* **2005**, 127, 17624-17625.

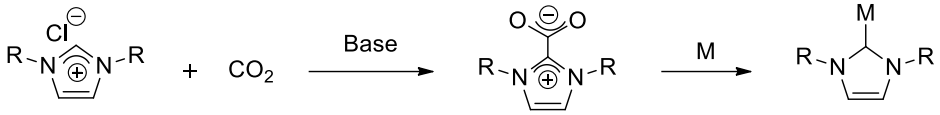

Scheme I.41. Synthesis of imidazole-2-ylidenes via carboxylate adducts.

Similarly, Taton obtained the hydrogen carbonate salt of imidazolium by simple anion metathesis with $KHCO_3$ (Scheme I.42).[43]

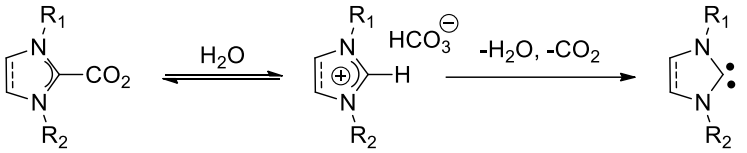

Scheme I.42. Synthesis of imidazolium hydrogen carbonate salts by anion metathesis.

I.A.4. *N*-heterocyclic metal carbenes (NHC).

To the best of our knowledge, the first metal carbene was reported in 1925 by Chugaev, however he was not able to report the exact nature of this platinum complex.[44] Wanzlick succeeded in synthetizing the first NHC-metal complex in 1968 by the reaction of imidazolidinium with mercury acetate (Scheme I.43)[45].

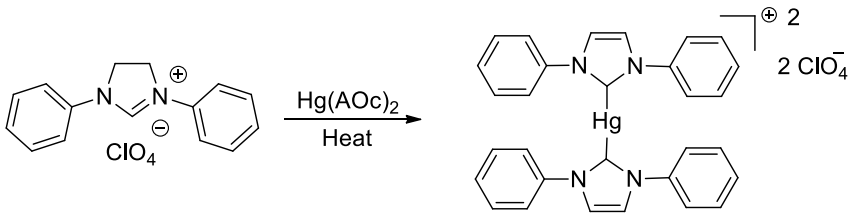

Scheme I.43. First isolated NHC-metal complex.

In 1970, Lappert's takes advantage of the Wanzlick equilibrium to synthesize a series of metal-NHCs (platinum, palladium and ruthenium), proving that the tetraaminoethylenes serves a 'carbene reservoir' as previously proposed (Scheme I.44).[46]

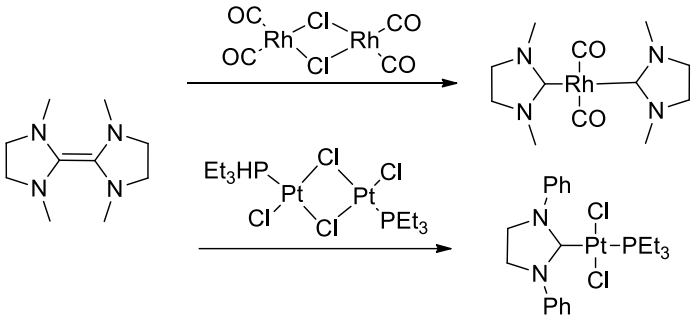

Scheme I.44. Metal-carbene of Lappert.

[43] Fevre, M.; Coupillaud, P.; Mique, k.; Sotiropoulos, J-M., Vignolle, J.; Taton, D. *J. Org. Chem.* **2012**, 77, 10135−10144.

[44] Chugaev, L.; Skanavy Grigorieva, M.; Posniak, A. *Z. Anorg. Allg. Chem.* **1925**, *148*, 37–42.

[45] Wanzlick, H. W.; Schoenherr, H. J. *Angew. Chem., Int. Ed. Engl.* **1968**, *7*, 141-142.

[46] Cardin, D. J.; Cetinkaya, B.; Lappert, M. F. *Chem. Rev.* **1972**, *72*, 545-574.

I.A.4.1. Metal-NHC of Group 11

Group 11 includes copper, silver, gold and roentgenium (synthetic element of short half-life) according to IUPAC. Copper, silver and gold are among the most used metals by humans and among the first used (about 5000 years BC).[47] These metals are widely used for their appearance (jewelry, decorations, status…), their low resistivity (electronics, wires), their resistance to corrosion (water proofing, coins), their pharmacological properties (antifungals, antimicrobial) and for their importance in catalysis. The first work on metal-NHC on this group is very recent, belonging to 1990s. These transition metals–NHC complexes have applications in many fields, being most studied in the fields of catalysis, biological applications and in nano-sciences.

Three synthetic routes are commonly used to access metal-NHCs. They comprise:

- The synthesis through the free carbene (generated separately or from a masked form),
- The trans-metalation of a metal-NHC possessing $C_{carbene}$-Metal bond of a low energy (silver, copper, manganese),
- The direct reaction with a metal oxide which serves as base and metal source.

I.A.4.1.1. Copper-NHCs.

I.A.4.1.1.a. Addition of free carbene on the metal.

In 1993, Arduengo's team described the first Cu-NHC access simply by the addition of SIMes on copper triflate (I) to form the cationic homoleptic complex [Cu(SIMes)$_2$], OTf (Scheme I.45-a).[48] One year later, Raubenheimer reported a synthesis route of neutral copper complexes using the CuCl or CuI (Scheme I.45-b).[49]

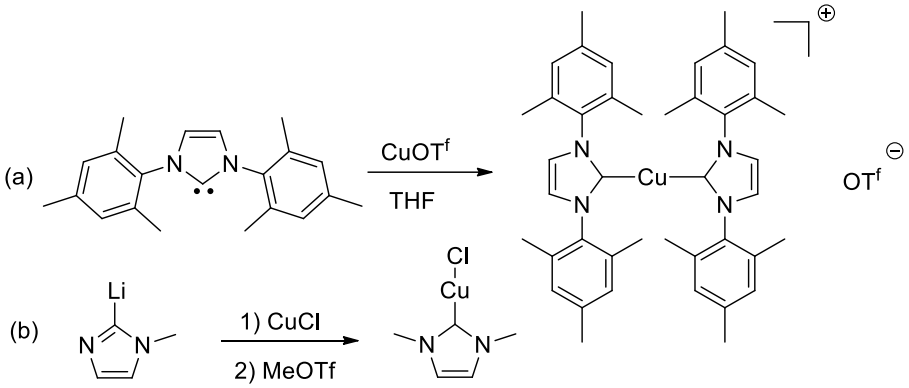

Scheme I.45. Synthesis of Cu-NHC complexes (a) by Arduengo's team, (b) by Raubenheimer.

In 2010, Nolan's team synthesized Cu-NHC complexes bearing ICy and ItBu using isolated carbenes. This method assures the synthesis of [Cu(ICy)X] and [Cu(ItBu)X] in good yields ranging between 71-85% (Scheme I.46).[50]

[47] Dainian, Fan. Chinese Studies in the History and Philosophy of Science and Technology. p. 228

[48] Arduengo III, A. J.; Dias, H. V. R.; Calabrese, J. C.; Davidson, F. *Organometallics* **1993**, *12*, 3405-3409.

[49] Raubenheimer, H. G.; Cronje, S.; Olivier, P. J. *J. Chem. Soc., Dalton Trans.* **1995**, 313-316.

[50] Dıez-Gonzalez, S.; Escudero-Adan, E. C.; Benet-Buchholz, J.; Stevens, E. D.; Slawin, A. M. Z.; Nolan, S. P. *Dalton Trans.* **2010**, *39*, 7595–7606.

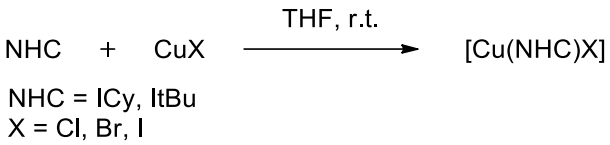

Scheme I.46. Preparation of complexes bearing ICy and ItBu ligands.

I.A.4.1.1.b. One pot procedure using a strong base.

Several methods to prepare Cu-NHCs complexes by the reaction of imidazoli(ni)um salt with a strong base in the presence of copper (I) salt were reported in the literature (Scheme I.47).[51]

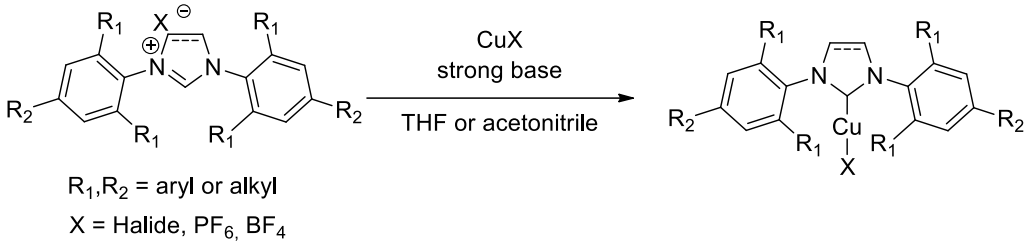

Scheme I.47. Synthesis of Cu^{I}-NHC through direct metalation.

In 2001, Fraser and Woodward reported the first application of Cu-NHC complex as a catalyst.[52] They synthesized their complex after deprotonation of the imidazolium with tBuOK in THF followed by the addition of $Cu(OTf)_2$ to produce SIMes.Cu.OTf *in situ*, which served as an effective catalyst in copper catalyzed conjugate addition of $ZnEt_2$ to enones.

In 2003, Buchwald's team prepared [Cu(IPr)Cl] from an imidazolium salt in the presence of NaOtBu as strong base and CuCl (Figure I.48).[53]

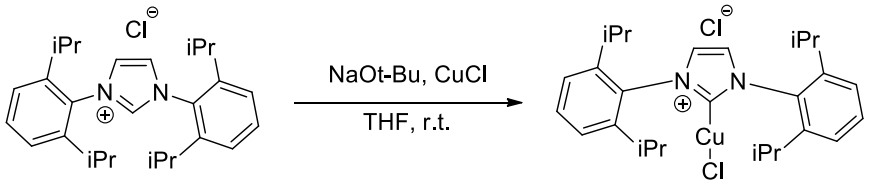

Scheme I.48. Synthesis of Cu^{I}-NHC using strong bases.

Nolan extends the method to [Cu(IMes)X], [Cu(SIMes)X], [Cu(SIPr)X], [Cu(SIPr)X] by optimization of the base, the metal source and the solvent.[54]

I.A.4.1.1.c. One pot procedure using the 'soft bases route'.

Cazin's team used potassium carbonate to synthesize Cu-NHCs in moderate to excellent yields. This synthesis takes place under mild condition, 60°C temperature with 2 equivalents of K_2CO_3 during 24h (Scheme I.49)[55].

[51] (a) Jurkauskas, V.; Sadighi, J. P.; Buchwald, S. L. *Org. Lett.* **2003**, *5*, 2417-2420. (b) Lake, B. R. M.; Bullough, E. K.; Williams, T. J.; Whitwood, A. C.; Little, M. A.; Willans, C. E. *Chem. Commun*. **2012**, *48*, 4887-4889.
[52] raser, P. K.; Woodward, S. *Tetrahedron Lett.* **2001,** *42* , 2747-2749.
[53] Jurkauskas, V.; Sadighi, J. P.; Buchwald, S. L. *Org. Lett.* **2003,** *5*, 2417-2420.
[54] Nolan, S. P. *Eur. J. Inorg. Chem.* **2015**, 2012–2027.
[55]Santoro, O.; Collado, A.; M. Z. Slawin, A.; Nolan, S. P.; S. J. Cazin, C. *Chem. Commun.* **2013**, *49*, 10483—10485.

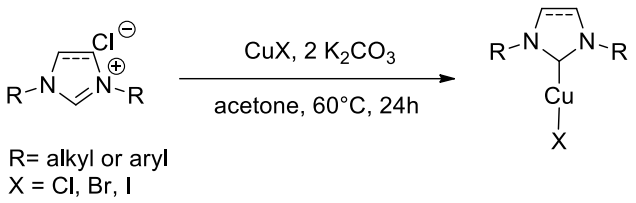

Scheme I.49. Cazin's methodology to synthesize Cu-NHCs.

In 2013, another metalation method was introduced by Cisnetti using aqueous ammonia as a weaker base.[56] This method allows the access to homoleptic complexes $[Cu(NHC)_2]^+$ for soft counter ions in ethanol and heteroleptic complexes [Cu(NHC)-X] in the presence of halides in water (Scheme I.50). Variation of the metal source and counterion allows the access to a μ-OH cationic complex.

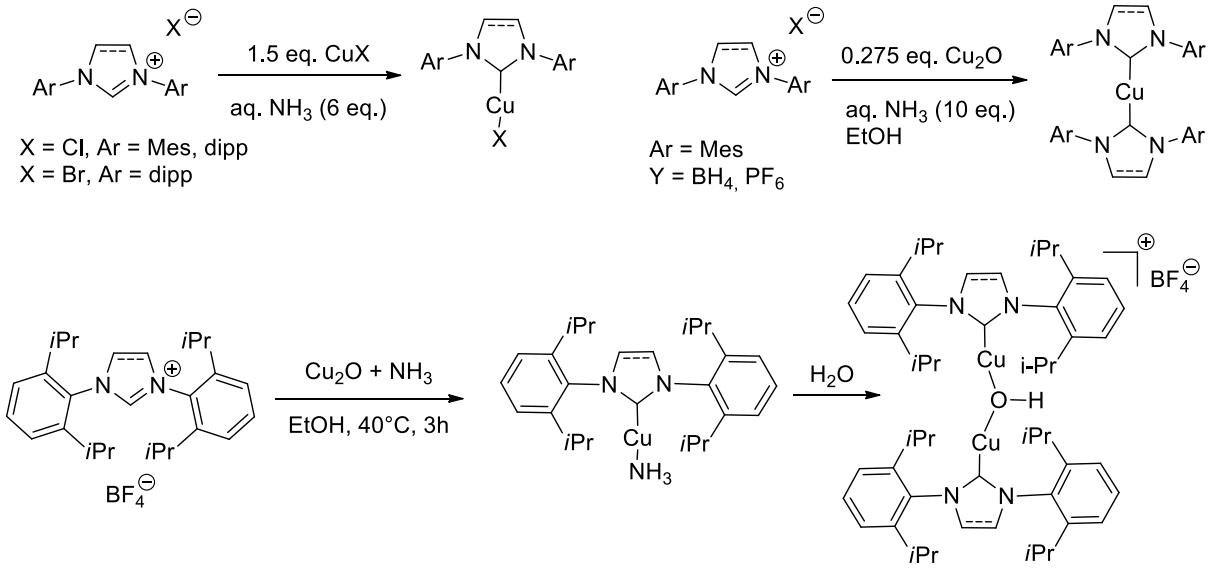

Scheme I.50. Synthesis of Cu-NHC using ammonia.

The versatility of the soft base route has been reviewed by Nolan for various metals.

I.A.4.1.1.d. Using metal oxide as base.

Donopoulos reported the synthesis of Cu-NHCs using copper oxide for the metalation of imidazolium salts functionalized with pyridine dissolved in chlorinated solvents (Scheme I.51).[57] Later in 2010, Cazin's team reports the synthesis of monodentate NHCs (such as SIMes, IMes, SIPr, IPr,etc.) in toluene or water (Scheme I.51)[58]. In both cases, the reaction is carried out at reflux for 24hrs.

[56] Gibard, C.; Ibrahim, H.; Gautier, A.; Cisnetti, F. *Organometallic* **2013,** *32*, 4279-4283.

[57] Tulloch, A. A. D.; Danopoulos, A. A.; Kleinhenz, S.; Light, M. E.; Hursthouse, M. B.; Eastham, G.,*Organometallic* **2001,** *20*, 2027-2031.

[58](a) Okamoto, S.; Tominaga, S.; Saino, N.; Kase, K.; Shimoda, K. *J. Organomet. Chem.* **2005,** *690*, 6001-6007; (b) Goj, L. A.; Blue, E. D.; Munro-Leighton, C.; Gunnoe, T. B.; Petersen, J. L. *Inorg. Chem.* **2005,** *44*, 8647-8649.

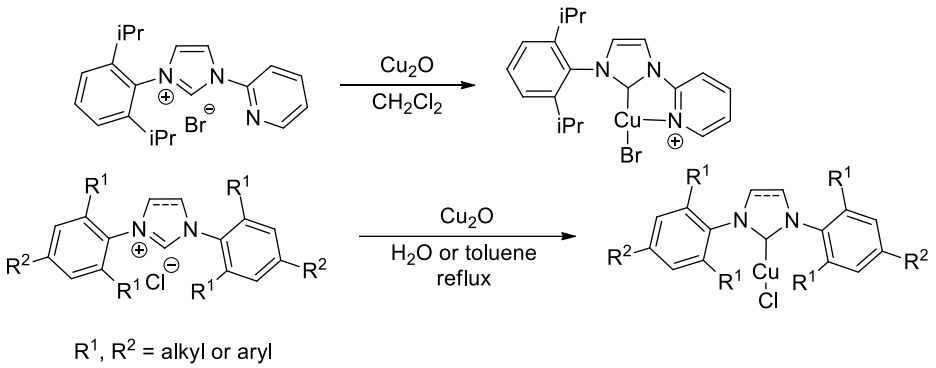

Scheme I.51. Synthesis of Cu-NHC using imidazolium salts and copper (I) oxide.

I.A.4.1.1.e. Transmetallation

Lin used Ag-NHC complexes for transmetalation to other metals complexes.[59] This discovery strikes fast in the field of NHC complexes, and a huge number of complexes were synthetized using this 'silver route'. Several reviews were published on this important topic.[60] Regarding the synthesis of Cu-NHC, Ag-NHC complexes are reacted with copper (I) halides to form the expected Cu-NHC complexes (Scheme I.52).

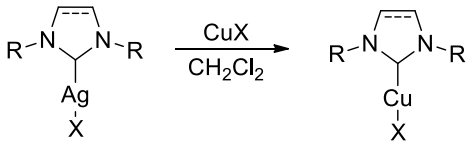

Scheme I.52. Synthesis of Cu-NHC by transmetallation.

However, there are several limitations of this method such as halogen exchange in the case of dichloromethane solvent,[61] an additional step for the preparation of silver-NHC complexes in addition to the inorganic byproducts (AgX) with their difficult recoverability.

I.A.4.2.2.f. Other methods

- **Via masked or free carbenes**

In 2012, Olszewski described a new method through CO_2-NHC adduct as a masked carbene to synthesize Cu-NHC (Scheme I.53).[62] This method allows a controlled release of free carbene under neutral conditions with CO_2 as the only byproduct, thus making it possible to dispense with the use of strong bases, avoiding possible parasitic reactions.

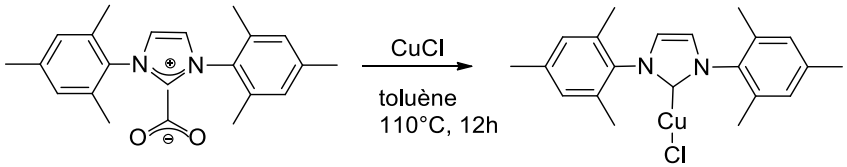

Scheme I.53. Synthesis of Cu-NHC via CO_2 carbene adducts.

[59] Wang, H. M. J.; Lin, I. J. B. *Organometallic* **1998,** *17*, 972-975.
[60] Lin, I. J. B.; Vasam, C. S. *Coord. Chem. Rev.* **2007,** *251*, 642-670
[61] Lee, K. M.; Wang, H. M. J.; Lin, I. J. B. *Dalton Trans*. **2002**, 2852-2856.
[62] Olszewsk, T. K.; Jaskolska, D. E. *Heteroat. Chem.* **2012**, *23*, 605−609.

- **Electrosynthesis**

In 2012, Willans described a new method for the synthesis of Cu-NHCs by electrochemistry using copper sacrificial anode (Scheme I.54).[63] This method allows for the synthesis of wide range of Cu-NHCs in high yields and releases dihydrogen as the only byproduct. The methodology was extended to electrochemical-flow cell technique.[64]

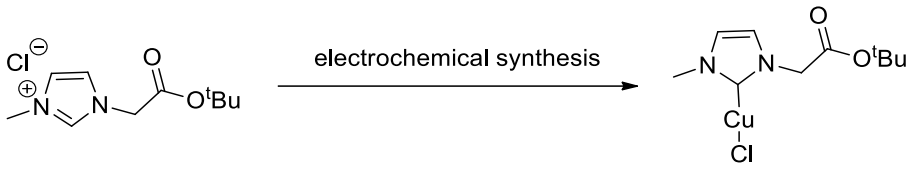

Scheme I.54. Electrochemical synthesis of Cu-NHC complexes.

I.A.4.2.3. Silver-NHCs.

Due to its high importance in the transmetallation route, the synthesis of silver complexes was well studied. The synthesis of hetero and homoleptic complexes are well reported by Nolan using silver oxide or silver chloride.[65]

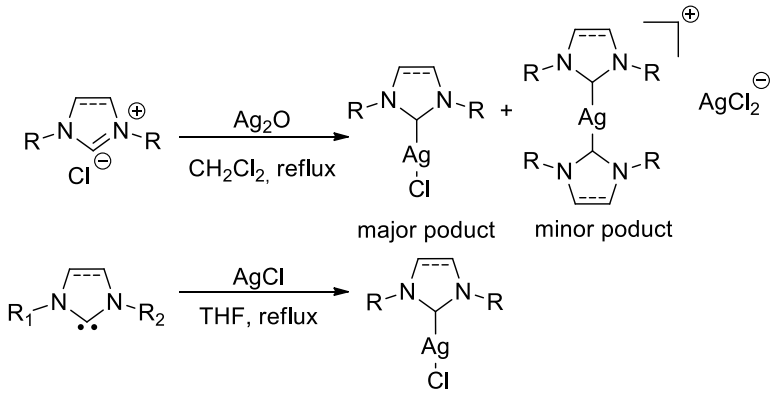

Scheme I.55. Synthesis of silver complexes by Nolan.

The aqueous ammonia route is also useable among many other reported procedures.[66] When the azolium contains chloride ion as counter ion, a mixture of homo and heteroleptic complexes is obtain. Using the non-coordinating ion PF_6, reaction forms the homoleptic complex if mesityl is used or an ammonia intermediate for IPr.

[63] Lake, B. R. M.; Bullough, E. K.; Williams, T. J.; Whitwood, A. C.; Little, M. A.; Willans C. E. *Chem. Commun.* **2012**, *48*, 4887-4889.

[64] Chapman, M. R.; Shafi, Y. M.; Kapur, N.; Nguyen, B. N.; Willans C. E. *Chem. Commun.* **2015**, *51*, 1282-1284.

[65] Scattolin, T.; Nolan, S. P. *Trends Chem.* **2020**, *2*, 721-736.

[66] Gibard, C. ; Fauche, K. ; Guillot, R. ; Jouffret, L. ; Gautier, A. ; Cisnetti, F. *J. Organomet. Chem.* **2017**, *840*, 70-74

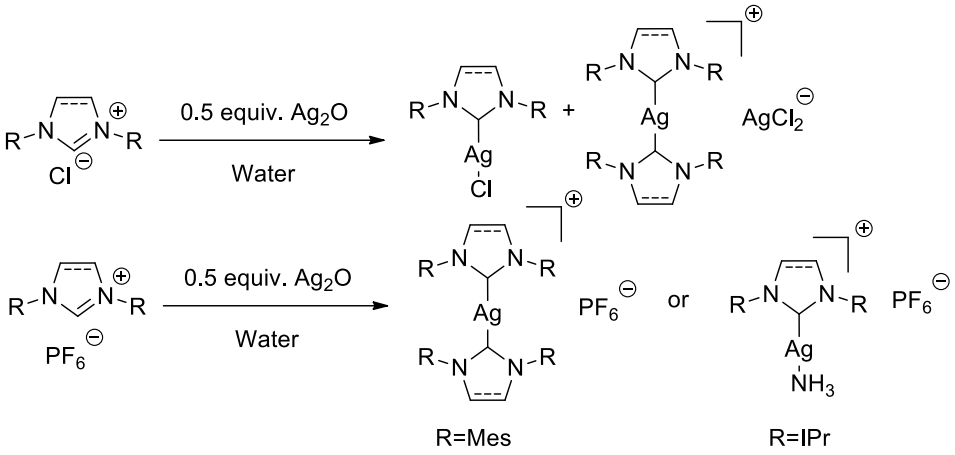

Scheme I.56. Synthesis of silver complexes using soft ammonia route.

I.A.4.2.4. Gold-NHCs.

The Lin's method is so far is the mostly used to obtain heteroleptic complexes from silver-NHC. Recently, copper has been reported as a transfer agent for the transmetallation by Cazin's team (Scheme I.57).[67]

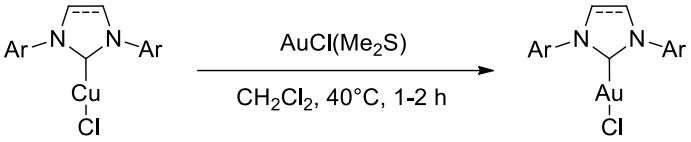

Scheme I.57.Carbene transfer from Cu to Au.

Many other routes could be found in the literature.[68]

I.A.5. Click Chemistry.

Described by Kolb, Finn and Sharpless in 2001, click chemistry comprise a collection of organic reactions inspired by the natural ligation.[69] Click reactions are one-pot, irreversible reactions (high thermodynamically driving force). It forms the desired product quickly, in high yields and without generating byproducts. This concept is commonly used in material science, drug discovery, polymers and bio-conjugation.[70]

---

[67] Furst, M. R. L.; Cazin, C. S. J. *Chem. Commun.* **2010,** *46*, 6924-6925

[68] Collado, A.; Gomez-Suarez, A.; Martin, A. R.; Slawin, A. M. Z.; Nolan, S. P. *Chem. Commun.* **2013**, *49*, 5541−5543.(b) Visbal, R.; Laguna, A.; Gimeno, M. C. *Chem. Commun.* **2013**, *49*, 5642−5644. (c) Nahra, F.; Tzouras, N. V.; Collado, A.; Nolan, S. P. *Nat. Protoc.* **2021**, *16*, 1476. (d) Voloshkin, V. A.; Tzouras, N. V.; Nolan, S. P. *Dalton Trans.* **2021**, *50*, 12058-12068. (d) Nahra, F.; Gomez-Herrera, A.; Cazin, C. S. J. *Dalton Trans.* **2017**, *46*, 628-631.

[69] Kolb, H. C.; Finn, M. G. *Angew. Chem. Int. Ed.* **2001,** *40*, 2004.

[70] (a) Martin, D.; Kehrli, S.; d'Augustin, M.; Clavier, H.; Mauduit, M.; Alexakis, A., *J. Am. Chem. Soc.* **2006,** *128* (26), 8416-8417; (b) Lazreg, F.; Slawin, A. M. Z.; Cazin, C. S. J. *Organometallic* **2012,** *31*, 7969-7975.(c) Selim, K. B. a. M. Y. a. Y. K.-i. a. T. K. *Angew. Chem. Int. Ed.* **2009,** *48* (46), 8733--8735; (d) Fujihara, T. *Angew. Chem. Int. Ed.* **2011,** *50* (2), 523-527; (e) Lee, Y.; Hoveyda, A. H. *J. Am. Chem. Soc.* **2009,** *131* (9), 3160-3161; (f) Munro-Leighton, C.; Delp, S. A.; Alsop, N. M.; Blue, E. D.; Gunnoe, T. B. *Chem. Commun.* **2008**, 111-113. (g) Deutsch, C. *Angew. Chem. Int. Ed.* **2007,** *46* (10), 1650--1653; (h) Lebel, H.; Davi, M.; Díez-González, S.; Nolan, S. P. *J. Org. Chem.* **2006,** *72* (1), 144-149; (i) Fructos, M. R.; Belderrain, T. R.; Nicasio, M. C.; Nolan, S. P.; Kaur, H.; Díaz-Requejo, M. M.; Pérez, P. J. *J. Am. Chem. Soc.* **2004,** *126* (35), 10846-10847; (j) Biffis, A.; Tubaro, C.; Scattolin, E.; Basato, M.; Papini, G.; Santini, C.; Alvarez, E.; Conejero, S. *Dalton Trans.* **2009,** (35), 7223-7229; (k) Sai, M. *Angew. Chem. Int. Ed.* **2011,** *50* (14), 3294-3298; (l) Dubinina, G. G.; Furutachi, H.; Vicic, D. A. *J.*

I.A.5.1: General criteria.

The reactions must meet strict criteria to be considered as "click". As Sharpless described, the reactions should:

- allow high yield of the desired product with inoffensive byproducts that can be removed easily (without chromatography).
- be valid on a wide scope of substrates
- be regio and stereospecific
- be performed in a simple way, requiring benign solvents.

This implies that, the reaction should have a high thermodynamically driven force with ΔG greater than 20 kCal.mol^{-1}. In addition, the starting materials and reagents should be readily available. Some well-known reactions meet the criteria of click chemistry such as nucleophilic opening of small ring (azidirines, epoxides, aziridinium ions, etc.), formation of non-soluble oximes, urea and hydrazones, cycloaddition reactions (Diels-Alder) and 1-4 additions (Michael).[70]

I.A.5.2. CuAAC.

One of the first click reaction described by Sharpless was the Huisgen 1,3-dipolar cycloaddition of alkynes (terminal or internal) and azides to produce 1,2,3-triazoles. Huisgen cycloaddition requires high temperature and produces mixture of 1,4 and 1,5 regioisomers,[71]therefore it didn't meet all the click criteria. However, strong acceleration occurs in the presence of Cu(I) with terminal alkyne, leading to the sole 1,4 regioisomer at room temperature.[72] This variant of click is named Copper (I)-catalyzed Azide-Alkyne Cycloaddition (CuAAC). With an appropriate choice of solvent and reagents, the product precipitates from the reaction media and a simple filtration is used for purification. This reaction was named the "cream of the crop" of click chemistry.

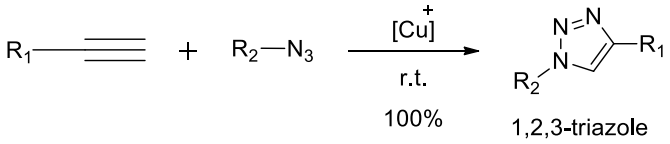

Scheme I.58. First CuAAC reaction.

As copper (I) is sensible to oxidation, it is essential to keep the Cu catalyst at its +1 oxidation state. A large variety of Cu sources could be used as precatalyst. For example, a Cu (II) salt can be used combined with a reducing agent (usually sodium ascorbate).[73] Another protocol uses Cu (I) (CuBr or CuOAc) combined with a base or amine ligand (such as DIPEA) and a reducing agent (sodium ascorbate). Also, Cu (0) compounds (wires, powder, or nanoparticles) could be used to generate Cu(I) at their surface. In addition, cupric salts such as $Cu(OAc)_2$ could work as pre-catalyst due to their tendency for reduction in presence of alkynes (Scheme I.59). The solvent could range from organic to aqueous, which is a great advantage.

Am. Chem. Soc. **2008,** *130* (27), 8600-8601; (m) Díez-González, S.; Kaur, H.; Zinn, F. K.; Stevens, E. D.; Nolan, S. P. *J. Org. Chem.* **2005,** *70* (12), 4784-4796.

[71] Huisgen, R. *Proc. Chem. Soc.* **1961**, 357-396.

[72] (a) Tornøe, C. W.; Christensen, C.; Meldal, M. *J. Org. Chem.* **2002**, *67*, 3057-3064. (b) Rostovtsev, V. V.; Green, L. G.; Fokin, V. V.; Sharpless, K. B. *Angew. Chem. Int. Ed.* **2002**, *41*, 2596-2599.

[73] Meldal, M.; Tornoe, C. W. *Chem. Rev.* **2008,** *108*, 2952-3015.

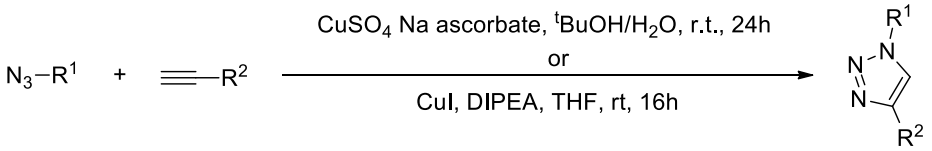

Scheme I.59 Most common catalytic systems for CuAAC

Some ligands possess a strong acceleration effect leading to reduced levels of copper and reducing agents. This acceleration effect is due to the additional electronic density around the metal center. Sharpless and his group reported a series of tris(triazolyl)methyl amine ligands that proved their usefulness for bio-conjugation. The tris(benzyltriazolylmethyl)amine (TBTA) was introduced first; it is composed of a tertiary amine holding three triazoles (Figure I.1).[74] In 2005, Finn described a new ligand derived from bathophenanthroline having the same rate characteristics than TBTA.[75] This new ligand allows better solubility in aqueous media. Later he also described, [tris(3-hydroxypropyltriazolylmethyl)amine ,THPTA , an aqueous soluble version of TBTA.[76] Wu also reported several new ligands that proves their efficiency to accelerate CuAAC such as 2-[4-{(bis(1-tert-butyltriazolyl)methyl]amino)methyl}-triazolyl]ethyl hydrogen sulfate (BTTES) and 2-[4-{(bis(1-tert-butyltriazolyl)methyl]amino)methyl}-triazolyl]acetic acid (BTTAA) (Figure I.1).[77] Moreover, Sieber's team reported the cationic {3-[4-({bis[(1-tertbutyltriazolyl)methyl] amino}methyl)-triazolyl]propyl}trimethylammonium (TABTA) as an accelerating ligand to CuAAC (Figure I.1).[78]

[74] Chan, T. R.; Hilgraf, R.; Sharpless, K. B.; Fokin, V. V. *Org. Lett.* **2004,** *6*, 2853-2855.
[75] Lewis, W. G.; Magallon, F. G.; Fokin, V. V.; Finn, M. G. *J. Am. Chem. Soc.* **2004**, *126*, 9152-9153.
[76] Hong, V.; Presolski, S. I.; Ma, C.; Finn, M. G. *Angew. Chem. Int. Ed.* **2009,** *48* (52), 9879-9883.
[77] Wang, W.; Hong, S.; Tran, A.; Jiang, H.; Triano, R.; Liu, Y.; Chen, X.; Wu, X. *Chem. Asian J.* **2011**,6, 2796-2802.
[78] Rudolf, G. C.; Sieber, S. A. *ChemBioChem*. **2013**, *14*, 2447-2455.

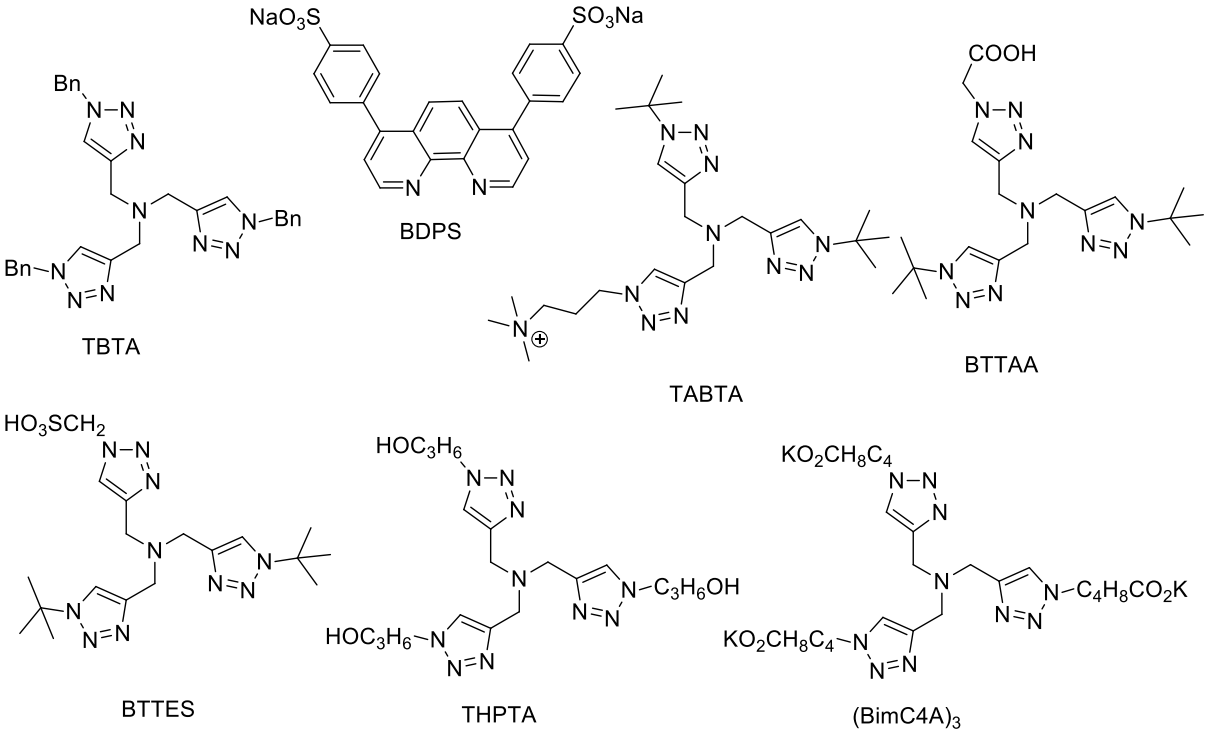

Figure I.1. Most efficient polydentate nitrogen donors for the CuAAC reaction.

Although the CuAAC reactions are effective in several fields, there are some limitations considering the use of copper, base, or ligands:

The sensitivity of Cu(I) to oxygen presents a main limitation of CuAAC for modification of sensitive biological substrates.[79] The oxidation of the metal produces hydroxyl radicals that can also react with substrates and/or products, leading to unexpected species (Scheme I.60).[80]

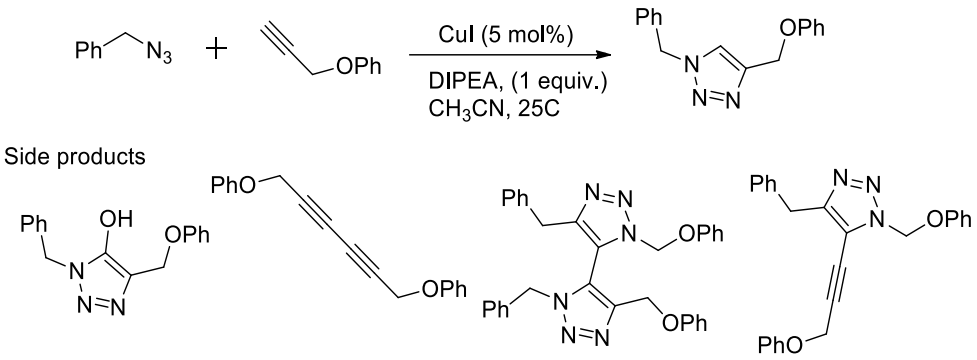

Scheme I.60. Undesired side products of CuAAC.

If excess of ascorbic acid could overcome the problem of the metal deactivation, it produces dehydro-ascorbate and decomposition products such as glyoxal that could react with the side chains of peptide and proteins.[81]

[79] Gupta, S. S.; Kuzelka, J.; Singh, P.; Lewis, W. G.; Manchester, M.; Finn, M. G. *Bioconjugate Chem.* **2005,** *16* (6), 1572-1579.
[80] Ornoe, C. W.; Christensen, C.; Meldal, M. *J. Org. Chem.* **2002,** *67*, 3057-3064.
[81] Hong, V.; Presolski, S. I., Ma, C.; Finn, M. G. *Angew. Chem., Int. Ed*. **2009**, 48, 9879

Moreover, as ascorbate participates to the recycling of copper, it amplifies the oxidation processes.

- The high quantity of copper and base could lead to the formations of secondary products such as bis-triazoles, 5-hydroxytriazoles or diynes by Glaser couplings (Scheme I.61).[82]
- The case of internal alkynes is considered also as a restriction, where the catalytic conditions derived by Sharpless and Meldal are only applicable to true alkynes since it is necessary to form an acetylide-Cu^{I} σ-complex in the first catalytic step of the accepted mechanism.[83]

Therefore, it is necessary to afford new systems in order to overcome these limitations. For example, more ligands and complexes should be afforded to obtain CuAAC reactions while using lower amounts of copper, without the formation of Cu(II) and being deactivated in the presence of oxygen.

I.A.5.3. CuAAC mechanism with 'classical ligands'.

The CuAAC mechanism has been studied by many teams due to its importance and effectivity. A first mechanism was proposed soon after the discovery of CuAAC reactions (Scheme I.61).[84] It proposed a first formation of a σ-complex between the metal and the alkyne followed by a chelation of the N1 atom of the azide on the copper(I). A cyclometallation takes place leading to a 6-membered ring containing a copper (III) intermediate that further undergoes reductive elimination to furnish a triazolide copper(I) complex. Protonation could occur with the aid of a protic solvent or through the intervention of the alkyne.

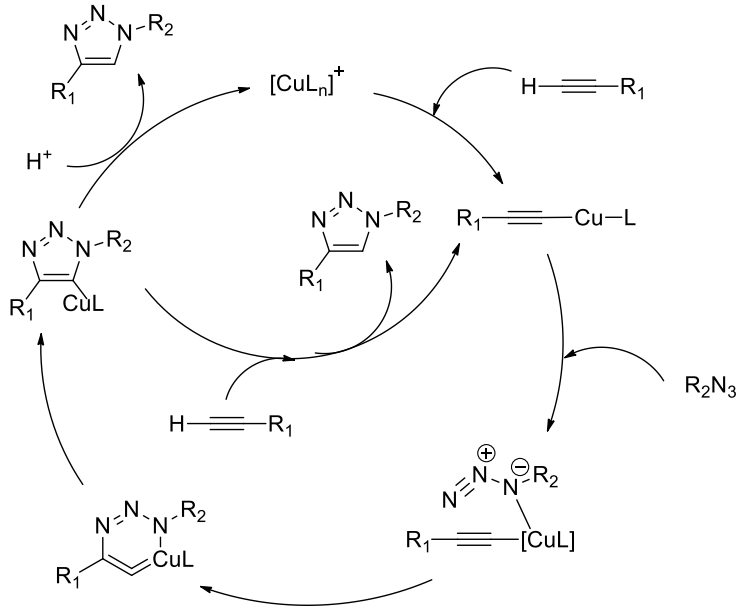

[82] Luczkowski, M.; Kozlowski, H.; Stawikowski, M.; Rolka, K.; Gaggelli, E.; Valensin, D.; Valensin, G. *J. Chem. Soc., Dalton. Trans.* **2002**, 2269-2274.

[83] (a) Candelon, N.; Lastecoueres, D.; Diallo, A. K.; Ruiz Aranzaes, J.; Astruc, D.; Vincent, J.-M. *Chem. Commun.* **2008**, 741-743; (b) Hein, J. E.; Tripp, J. C.; Krasnova, L. B.; Sharpless, K. B.; Fokin, V. V. *Angew. Chemi. Int. Ed.* **2009,** *48*, 8018-8021.

[84] Himo, F.; Lovell, T.; Hilgraf, R.; Rostovtsev, V. V.; Noodleman, L.; Sharpless, K. B.; Fokin, V. V. *J. am. Chem. soc.* **2005**, *127*, 210-216.

Scheme I.61. First proposed mechanism

However, several observations contracted this hypothesis.[85] Indeed, it has been observed that reaction rate is first order in alkyne and azide and second order in copper, as depicted in the following formula:

$$v = k.[Cu]^2[Alkyne].[Azide]$$

Therefore, a stepwise mechanism involving a copper(I)-acetylide, a copper(I) species and a binuclear copper(I) complex was proposed and supported by DFT calculations. Indeed, the complexations of the alkyne with a second metal center decreases the activation energy barrier by 4-6 Kcal/mol.

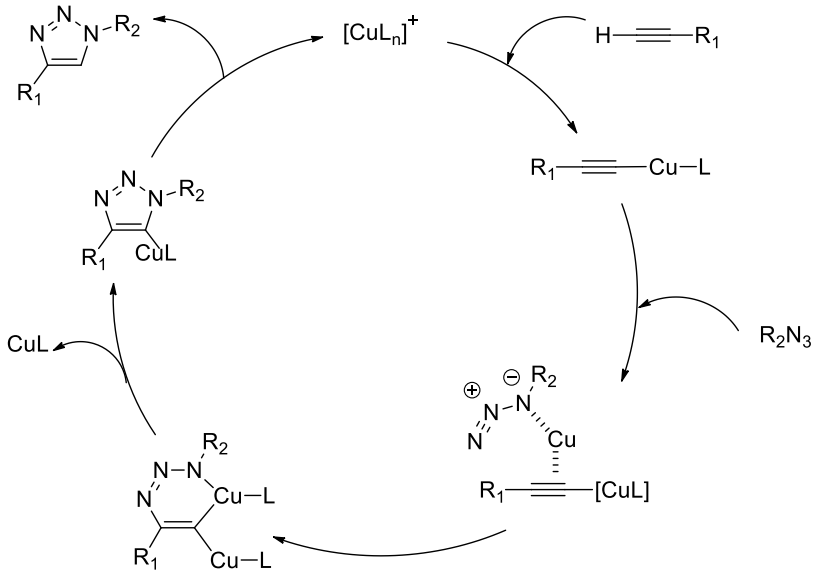

Scheme I.62. Currently accepted mechanism.

This mechanism is commonly accepted but many factors such as pH, presence of salts and the nature of reagents or the ligand perturbate the rate equation by slowing down one of the steps compared to the others. Therefore, a real and clear picture of what predominates in a studied reaction is case depend.

I.A.5.4. CuAAC mechanism with Cu(I)-NHCs.

In 2006, Straub proved the enrollment of copper (I) acetylide species for Cu-NHCs catalysts.[86] Complex **I.19** was synthesized starting from the reaction of copper (I) acetate complex with lithium phenyl acetylide. After the addition of azidodi-4-tolylmethane, the copper (I) triazolide complex **I.20** precipitates from the solvent (toluene) at room temperature (Scheme I.63).

[85](a) Rodionov,V. O.; Fokin, V. V.; Finn, M. G. *Angew. Chem. Int. Ed.* **2005**, *44*, 2210-2215. (b) Worell, B. T.; Malik, J. A.; Fokin, V. V. *Science* **2013**, *340*, 457-460. (c) Iacobucci, C. ; Reale, S. ; Gal, J-F. ; De Angelis F. *Angew. Chem. Int. Ed.* **2015**, *54*, 3065–3068 (c) Ozkilic, Y.; Tuzun, N. S. *Organometallics* **2016**, *35* (16): 2589–2599.

[86] Nolte, C.; Mayer, P.; Straub, B. F. *Ange. Chem. Int. Ed.* **2007,** *46*, 2101--2103.

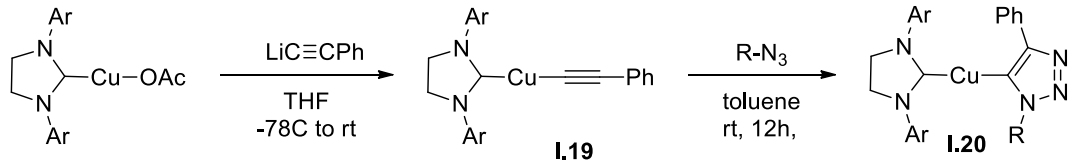

Scheme I.63. Synthesis of copper (I) triazolide complex.

Moreover, the copper (I) triazolide complex **I.20** is an efficient catalyst for click reactions. Therefore, it was proposed by Straub that binuclear complexes are not mandatory for CuAAC reactions catalyzed by Cu-NHCs. However, Fokin reported the involvement of a binuclear complex based on experimental arguments. He observed statistical enrichment of the triazolide between ^{63}Cu and ^{65}Cu while combining isotopically enriched copper complex to the reaction of Cu-acetylide with the organic azide (Scheme I.64).

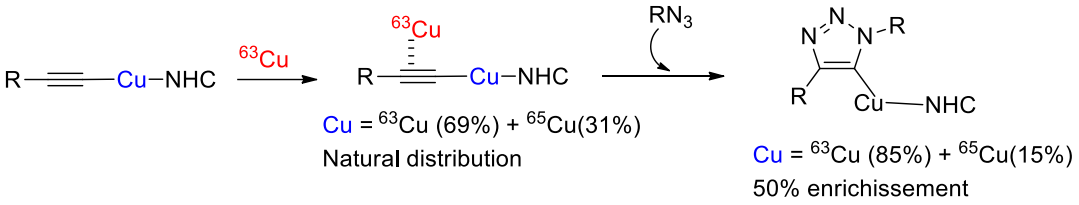

Scheme I.64 Isotopic crossover studies.

Thus, he proposes that the reaction starts with the formation of σ-bound Cu-acetylide followed by the formation of the catalytically active complex via recruitment of a second π-bound copper atom. The arrival of an organic azide makes a reversible coordination on the π-bounded copper followed by a stepwise cycloaddition. Based on the enrichment of copper isotopes, it was proposed that ligand exchange occurs between the two metal centers in a binuclear intermediate. Also, it was suggested that σ-bond copper acetylide coordinates reversibly with the organic azide, followed by forming the first covalent bond via the nucleophilic attack of N_3 of the azide to the β-carbon of the acetylide. Finally, the ligand exchange occurs during the formation of the second covalent bond.

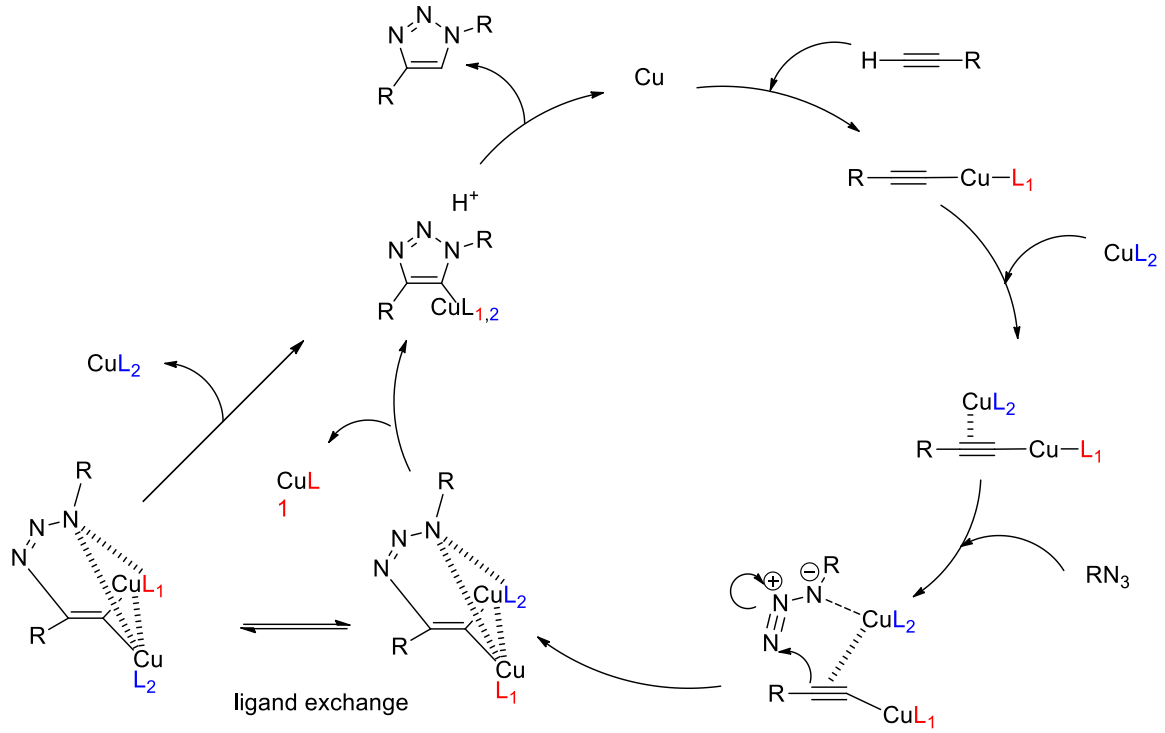

Scheme I.65. Mechanism of CuAAC with CuI-NHC.

Moreover, a calorimetric tracking shows that exogenous copper such as $[Cu(PPh_3)_2NO_3]$ strongly accelerates the reaction of the NHC-Cu^I-acetylide (completion within 20min) while in its absence the reaction shows slow conversion to the triazolide (Scheme I.66).[85b]

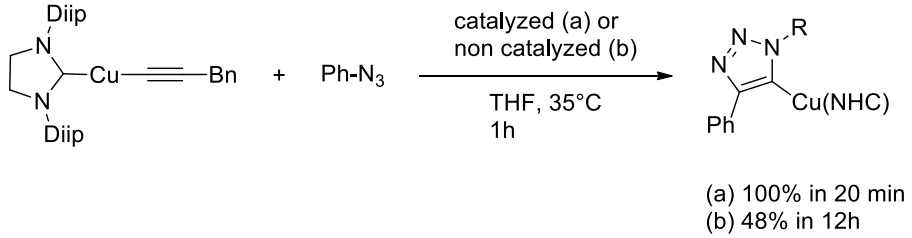

Scheme I.66. Calorimetric studies by Fokin.

I.A.5.4.1. Heteroleptic Cu(I)-NHCs in CuAAC reaction

Nolan's group was the first to report Cu-NHCs complexes for azide-alkyne cycloaddition.[87] These complexes proved to be efficient, leading to high yields, but in solventless or 'on water' conditions. Therefore, care should be taken when performing a catalyzed exothermic reaction in neat conditions. Interestingly, internal alkynes are reactive substrates using higher temperature and extended reaction time.

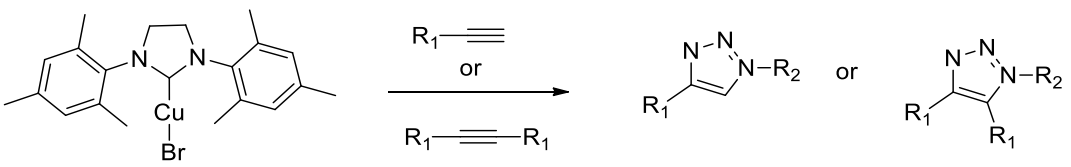

Scheme I.67. Heteroleptic Cu(I)-NHC example in CuAAC reaction.

[87] Díez-González, S.; Kaur, H.; Zinn, F. K.; Stevens, E. D.; Nolan, S. P. *J. Org. Chem.* **2005**, *70*, 4784–4796.

Nolan extended his studies to a larger collection of copper catalysts such as [Cu (NHC) X] (NHC = (S) IPr, ItBu, (S) IMes, IAd or ICy and X = Cl, Br, I); in neat conditions. The following three systems [Cu(ICy)Cl], [Cu(IAd)Br] and [Cu(IAd)I] were considered as the best requiring less than 10 minutes to convert the entire substrate.[88] The [Cu(IAd)I] is the best system yielding quantitative triazoles within 1h with only 0.25% loading. A trend concerning the efficiency of catalysts with respect to the halides could be, in general, described as iodine > bromine > chlorine. Also, Nolan describes [Cu(SIPr)Cl] as a latent catalyst for CuAAC. The catalyst is considered latent because its activation needs an external stimulation such as thermal activation. The addition of [Cu(SIPr)Cl] to the benzyl azide and phenylacetylene in dry DMSO at room temperature, do not finished any product even after one week. But, after the addition of water to the reaction medium and raising the temperature to 60°C, the clicked product was yielded quantitatively.

I.A.5.4.2. Homoleptic Cu(I)-NHCs in CuAAC reaction

Homoleptic complexes of formula $[Cu(NHC)_2]Y$ (Y = PF_6 or BF_4) were also tested for CuAAC by Nolan[89]. After screening some homoleptic catalysts (2 mol% loading, room temperature, "on water" conditions), $[Cu(ICy)_2],PF_6$ proved to be the best (total conversion after 90 min). Moreover, neat reactions proceeds smoothly with a significant decrease in the catalytic loading while slightly increasing temperatures around 40-50°C. Impressively, the authors reported 81% conversion after 4hr while conducting the experiment with 40 ppm catalyst loading at 40°C. Mechanistic studies using ^{1}H-NMR show that if no visible interaction occurs between benzyl azide and the catalyst, the copper complex reacts with phenylacetylene to release one imidazolium and forms a NHC-Cu-acetylide (Scheme I.67). Therefore, it was proposed that one of the carbene ligands acts as a base to deprotonate the alkyne, forming a copper σ-complex containing the second ligand.

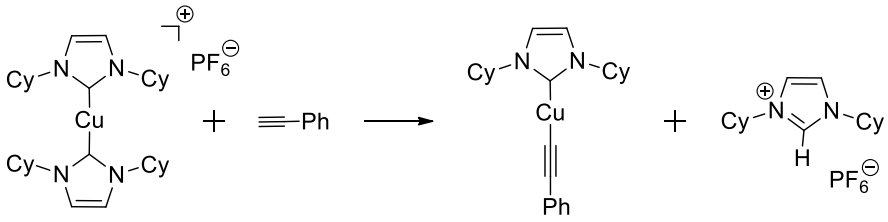

Scheme I.68. Stoichiometric reaction of phenyl acetylene with the homoleptic catalyst.

Later in 2012, Cazin published the first examples of heteroleptic bis-NHC copper (I) complexes containing a phosphine.[70b] Screening of the newly synthesized complexes was done at a loading of 0.5 mol%. Quantitative yields of the triazoles were obtained for $[Cu(IPr)(ICy)]BF_4$ and $[Cu(IPr)(ItBu)]BF_4$, the most actives. Thanks to the presence of two different NHC ligands, it become possible to know which ligand plays the role of base and which one stays complexed to the metal center while forming the σ-complex (Scheme I.69). It turns out that ICy plays the role of the base while IPr stays chelated on the reactive copper center. Also, the NHC/phosphine $[Cu(IPr)(PtBu_3)]BF_4$ complex showed a good catalytic activity that is compared to the best NHC complexes $[Cu(IPr)(ICy)]BF_4$.

[88] Díez-González, S.; Correa, A.; Cavallo, L.; Nolan, S. P. *Chem. Eur. J.* **2006**, *12*, 7558-7564.
[89] Díez-González, S.; Nolan, S. P. *Angew. Chem. Int. Ed.* **2008**, *47*, 8881—8884.

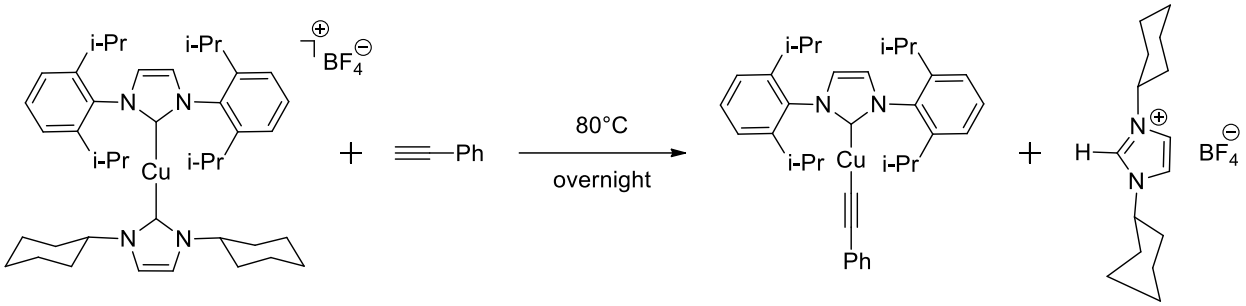

Scheme I.69. Reactions of mechanistic studies by Cazin.

I.A.5.4.3. The phenanthroline effect

In 2009, Gautier studied the effect of external *N*-donor ligands such as phenanthroline or 4-dimethylaminopyridine (4-DMAP) on [Cu(NHC)Cl].[90] The addition of phenanthroline on Cu-NHC results in the apparition of a red color, typical of the electronic metal-to-ligand transfer (MLT) effect. In addition, the complex presents remarkable solubility in hydro-alcoholic solvents that do not occurs with [Cu(NHC)Cl]. The signals of phenanthroline shows extreme broadening on ^{1}H NMR spectra. This reveals a reversible chelation of the *N*-donor on the copper center. UV-Vis spectroscopy was used to determine the equilibrium constant *via* studying of the charge transfer band from copper (I) to ligand (d to π) at 450 nm in dichloromethane. The comparison of the equilibrium constant with other complexes (such as $[Cu(Phen)]^{+}$ and $[Cu(Phen)_2]^{+}$) shows that the complexes formation are weaker. The X-ray diffraction was done on the red crystals of the complex obtained by the saturation of a solution of the complex in dichloromethane with diethyl ether. The X-ray showed that the copper atom lays in a distorted tetrahedral environment, contrary to [CuSIMesCl] which presents a linear geometry (Figure I.2). Interestingly, a 30% elongation of the Cu-Cl bond was noted. The complex is stable in solutions for few days and several weeks or months in solid state (non-crystallized). In the case of crystallized complex, samples are stable for several years. The addition of equimolar amount of phenanthroline to [Cu(SIMes)Cl] shows a great increase in its activity, reaching a similar activity compared to that of TBTA/$CuSO_4$/ascorbic acid system. Subsequently, the 4 ligands SIMes, IMes, SIPr, and IPr were studied in presence of phenanthroline to end up with [CuCl(SIMes)(Phen)] as the best complex. Also, 19 aromatic *N*-donors (derivatives of different pyridines and phenanthrolines) were screened to finish with 1,10–phenanthroline and 4,7-dichloro-1,10–phenanthroline as best additives.[91] For long time stability and storage purpose, the latter was selected. Gratifyingly, the complex could be stored for several years under air and light as uncrystallized purple powder. The structure of two complexes has been resolved using X-ray diffraction showing almost total similarity (Figure I.3.).

[90] Teyssot, M.-L.; Chevry, A.; Traïkia, M.; El-Ghozzi, M.; Avignant, D.; Gautier, A., *Chem. Eur. J.* **2009**, 15, 6322—6326.
[91] Teyssot, M.-L.; Nauton, L.; Canet, J.-L.; Cisnetti, F.; Chevry, A.; Gautier, A. *Eur. J. Org. Chem.* **2010**, 3507-3515.

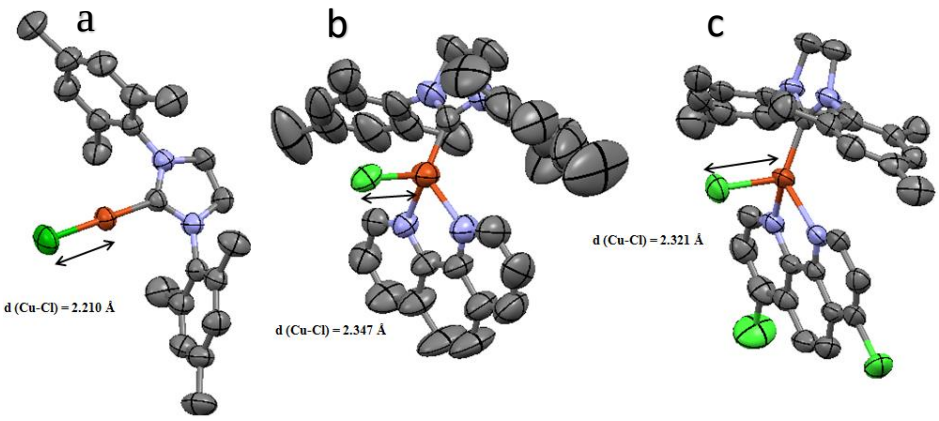

Figure I.2. X-ray structures of (a) [Cu(SIMes)Cl]; (b) [CuCl(SIMes)(Phen)] (1,10–phenanthroline) and (c) [CuCl(SIMes)(Phen)] (4,7-dichloro-1,10–phenanthroline).

I.A.5.4.4. Functionalized Cu-NHCs

The introduction of ammonium groups to the ligands is a classic modification for organometallic catalysis in aqueous medium.[92] In 2011, Wang's team described new modified complexes with ammonium groups.[93] Catalytic studies of the water-soluble catalysts were done using 0.5 mol-% and 5 mol-% for the cycloaddition of the three-component system, benzyl bromide and sodium azide with phenylacetylene. These studies show a trend activity of the modified catalysts with respect to the counter ions was Cl > I >> Br, different from the trend of the neutral complex described before by Nolan. The complex [Cu(SIPr)Cl-N^+Et_3] shows the best efficiency allowing the access to 98% yield.

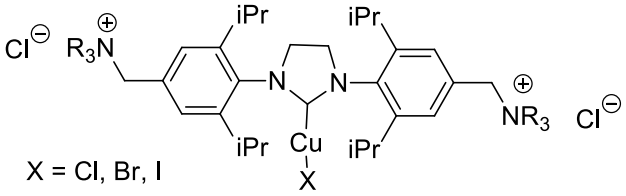

Figure I.3. Modified complexes formed by Wang's team.

In the same year, Gautier also introduced a water-soluble complex by modifying the core of SIMes by two triazolyl-choline arms as cationic and hydrophilic[94]. Thanks to the introduction of azide at position 4 of the aromatics, this compound could be obtained by a CuAAC reaction. The authors were able to achieve the synthesis of this compound on gram scale using only simple filtrations without any chromatography.

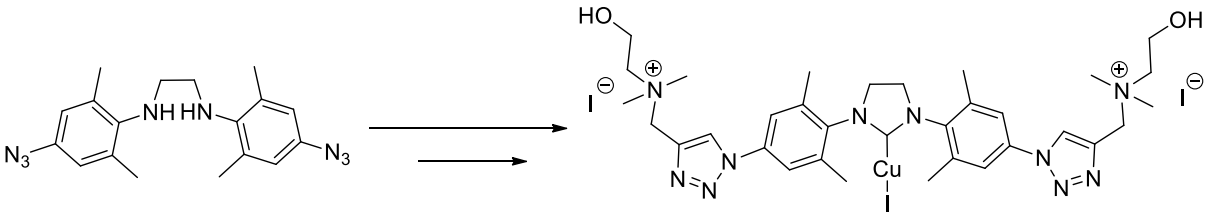

Scheme I.70. Water-soluble catalyst synthesized by Gautier.

[92] Shaughnessy, K. H. *Chem. Rev.* **2009**, 109, 643-710.
[93] Wang, W.; Wu, J.; Xia, C.; Li, F. *Green. Chem.* **2011**, 13, 3440-3445.
[94] Gaulier, C.; Hospital, A.; Legeret, B.; Delmas, A. F.; Aucagne, V.; Cisnetti, F.; Gautier, *A.Chem. Commun.* **2012**, 48, 4005-4007.

In collaboration with Delmas's team, this complex was tested for the conjugation of amino acids and peptides[94]. It shows high efficiency in pure water and in the two weakly coordinating buffers (Good's buffers) HEPES and MES at pH = 7.6 and 6.2. Completion versus time curves determined from ^{1}H NMR show that the reaction is faster at pH 7.2. In all cases the reaction reach completion which proves its stability in oxygenated medium. Therefore, the catalyst was applied to the repetitive N-terminal octapeptide of the human prion protein, which is known to strongly bond Cu^{II}. Quantitative conversion to a copper free peptide was obtained which demonstrates the stability of the catalyst. Moreover, no degradation products were obtained even in presence of sensitive histidine, methionine, tryptophane or cysteine.

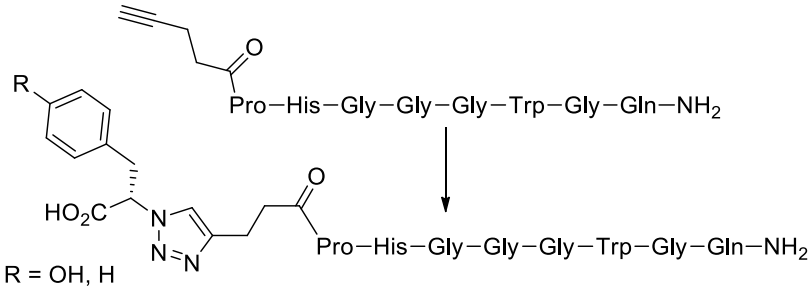

Scheme I.71. Catalyzed reactions of peptides.

I.A.5.4.5. Abnormal Cu(I)-NHCs

In 2011, Fukuzawa was the first to describe a copper complex bearing 1,2,3-triazole carbene.[95] These carbenes are called abnormal or mesoionic carbenes due to the inability to write their mesomeric forms without formal charges. Since the carbene center is surrounded with only one nitrogen atom, the inductive effect of the substituents is less and the carbene is richer in electrons. The complexes were synthesized by the treatment of triazolium with silver oxide/ammonium chloride followed by transmetallation by CuCl to produce air-stable 1,2,3-triazol-5-ylidene-copper (I) complexes (Scheme I.72).

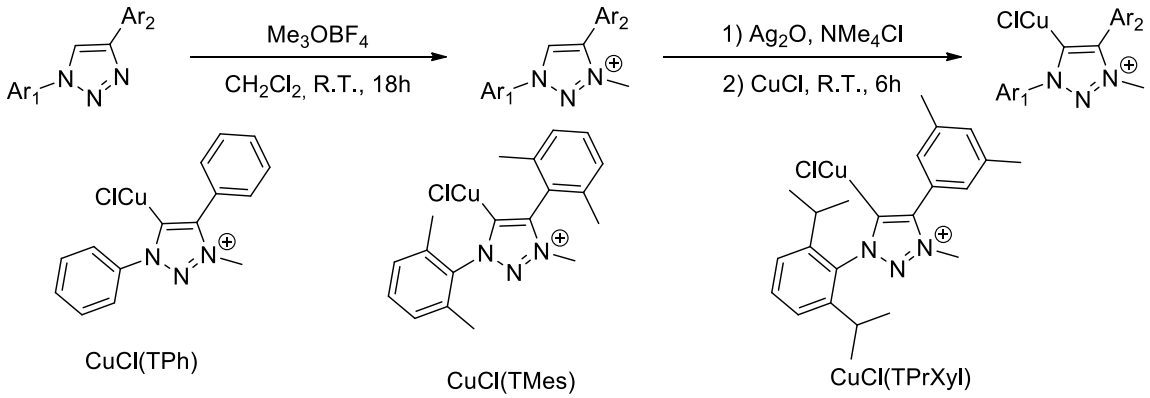

Scheme I.72. Synthesis of copper (I) complexes bearing 1,2,3-triazole carbene.

Fukuzawa tested the catalytic activity of the complexes and compared them with [CuCl(IMes)]. A very good activity, surpassing [(IMes)CuCl]'s, is found for all the complexes in neat conditions, especially [CuCl(TPh)] that yields 95% product in 30 min at 1 mol% catalyst loading (Scheme I.73).

[95] Nakamura, T.; Terashima, T.; Ogata, K.; Fukuzawa, S. *Org. Lett.* **2011**, *13*, 620-623.

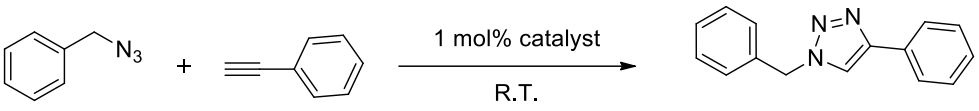

CuCl(TPh): 30min. 97%
CuCl(TMes): 60min. 35%; 90min. 100%

CuCl(TPrXyl): 60min. 95%
CuCl(IMes): 60min. 25%

Scheme I.73. Catalytic tests in CuAAC.

It was found that [CuCl(TPh)] was the most efficient catalyst. The catalyst proved its superiority on hindered azides and alkynes (mesitylacetylene with mesitylazide) yielding 71% of the product after 100 min at 30°C.

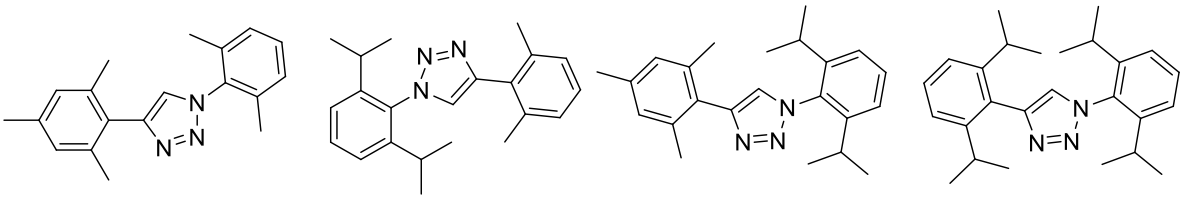

30min, 71% yield | 45min, 69% yield | 5.5h, 71% yield | 18h, 63% yield

Figure I.4. Sterically hindered azides and alkynes CuAAC reactions.

Sarkar also described the synthesis of abnormal copper (I) complexes with σ-NHC (1,2,3-triazol-3-ium-5-ylidene) as a ligand (Figure I.5).[96]

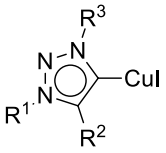

R^1 = Ph, R^2 = Bn, R^3 = Me
R^1 = Ph, R^2 = Thioanisole, R^3 = Me

Figure I.5. Complexes synthesized by Sarkar.

The high catalytic activity of these complexes proved that the copper (I) complex with mesoionic carbene (σNHC = 3-methyl-1-[2-(methylthio)phenyl]-4-phenyl-1H-1,2,3-triazol-3-ium-5-ylidene) shows the best activity (up to 0.05% catalyst loading), producing the product in quantitative yields after 2h (Scheme I.75). Gratifyingly, these complexes are able to catalyze the reactions between bulky azides and alkynes which are incapable to perform under Sharpless conditions (Cu^{II}/ascorbate/TBTA mixture).

In 2013, Sarkar and Gautier studied the influence of phenanthroline additive to mesoionic systems in aqueous/alcoholic solutions and report a strong acceleration.[97] The optimization of the system showed quantitative yield after 5 min at room temperature with 0.5 mol% catalytic charge in solution. To the best of our knowledge, it is the most active catalyst *in solution* reported so far. However, the mesoionic carbenes containing phenanthrolines are easily oxidizable by air and therefore should be used with care.

[96] Hohloch, S.; Su, C.-Y.; Sarkar, B. *Eur. J. Inorg. Chem.* **2011**, 3067--3075.
[97] Hohloch, S.; Sarkar, B.; Nauton, L.; Cisnetti, F.; Gautier, A. *Tetrahedron Lett.* **2013**, 54, 1808-1812.

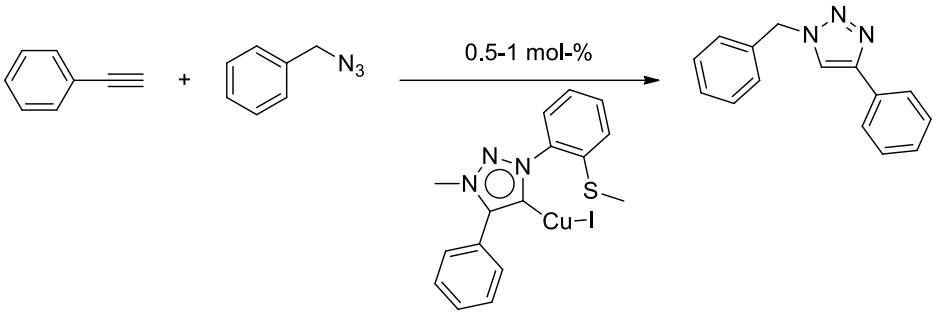

Scheme I.74. Precatalyst example in CuAAC.

Sarkar's team continued pioneering the mesoionic by reporting the synthesis of several neutral and cationic mesoionic copper (I) complexes (Figure I.6).[98] A screening shows that the cationic, halide-free complexes show better catalytic activity (0.005 mol% in neat conditions).

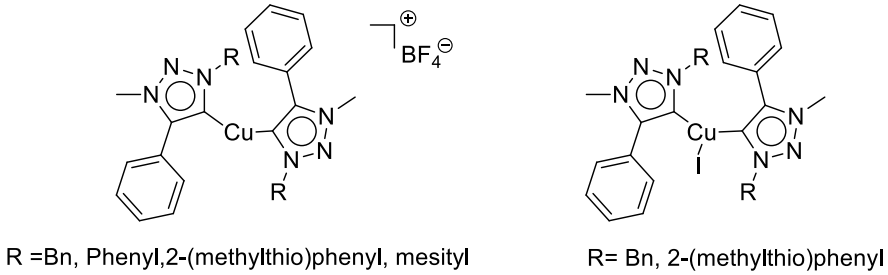

Figure I.6. Mesoionic catalysts Sarkar's team.

I.A.5.4.6. Binuclear Cu(I)-NHCs

As CuAAC reactions is believed to involve two copper atoms in the rate determining step, the proximity of two copper (I) atoms carried by ditopic ligand should provide a favorable gain. Therefore, Straub reported two μ-acetato binuclear copper carbene complexes (Figure I.7).[99]

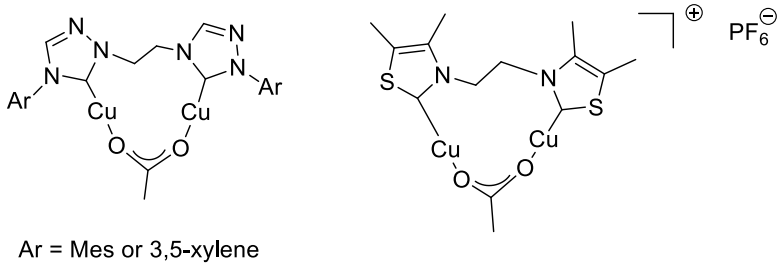

Figure I.7. Binuclear complexes by Straub.

Both complexes afford strong acceleration effects. The first binuclear catalyst shows a very strong rate enhancement compared to $[ICy]^{2+}$ and CuOAc (Figure I.7).

The thiazolylidine complex shows stability for at least several days in air. In order to test the activity of the new complex, series of reactions were performed under argon atmosphere. The click reaction was followed by NMR spectroscopy. Figure I.8 shows the better activity of the binuclear catalyst compared to CuOAc, in the reaction of both phenylacetylene and ethyl

[98] Hohloch, S.; Scheiffele, D.; Sarkar, B. *Eur. J. Inorg. Chem.* **2013**, 3956--3965.

[99] (a) Berg, R.; Straub, J.; Schreiner, E.; Mader, S.; Rominger, F.; Straub, B. F. *Adv. Synth. Catal.* **2012**, *354*, 3445-3450. (b) Schoffler, A. L.; Makarem, A., Rominger, F.; Straub, B. F. *Beilstein J. Org. Chem.* **2016**, *12*, 1566–1572.

propiolate with benzyl azide. Importantly, acetic acid (9 mol% added) strongly accelerates the reaction suggestion that protonation of the triazolyl copper species is now part of reaction rate.

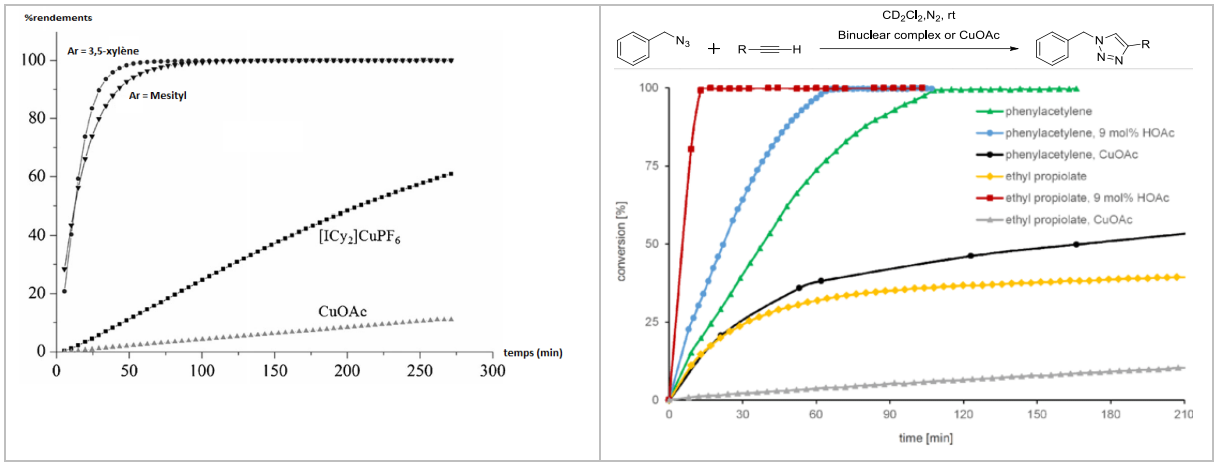

Figure I.8. Reactions of benzyl azide with phenylacetylene in CD_2Cl_2 at 23°C. The time diagram of the CuAAC reaction of benzyl azide with either ethyl propiolate in the presence of 0.9 mol% of binuclear complex or phenylacetylene in the presence of 1.8 mol% of the binuclear complex with saturated homogenous solution of CuOAc in both experiments.

Gautier and Sarkar extend this important finding to mesoionic copper(I) carbenes (Figue I.9).[100] The catalytic activity of this complex was studied between phenylacetylene and benzyl azide in $CDCl_3$, to result in a rapid reaction and more than 95% yield of triazole as a product with only 1 mol% catalyst loading.

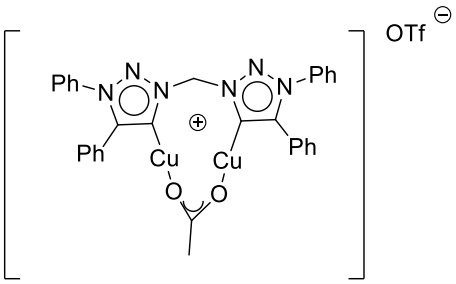

Figure I.9. Mesoionic copper(I) carbene catalyst.

The laboratory further studied the kinetic and reported that only azide and copper appears in the rate law. Also, the order in copper catalyst is estimated to be 0.8. This non-integer value is attributed to a fast and reversible formation of an inactive complex out of the catalytic cycle (Scheme I.75).

$$v = k.[Azide].[Cu]^{0.8}$$

[100] Beerhues, J.; Fauche, K.; Cisnetti, F.; Sarkar, S.; Gautier, A. *Dalton Trans.* **2019**, *48*, 8931-8936.

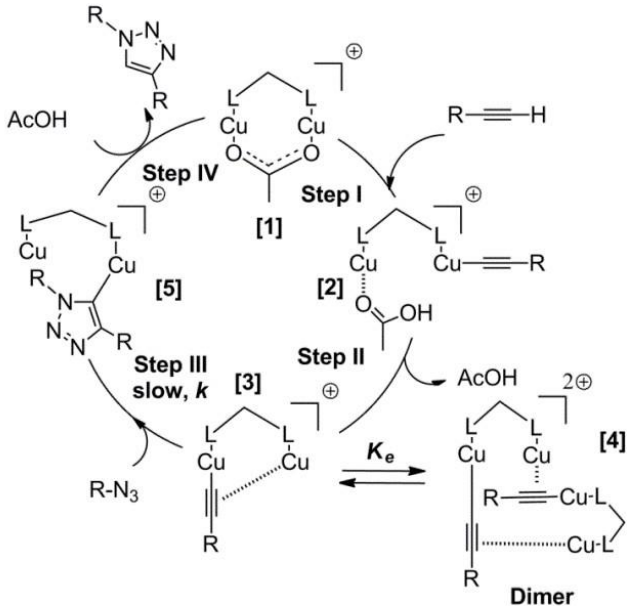

Scheme I.75. Catalytic cycle proposed for binuclear catalysts.

Overall, the fast alkyne deprotonation can be explained by the presence of an intramolecular base (step I). In step II, the key σ–π complex **[3]** is formed with expulsion of acetic acid. The rate determining step III, consists in the formation of the triazole. The last step (IV) is the protonation of the copper-triazolide helped by the acid formed previously.

I.B. Peptoids and related family members.

I.B.1. Generalities

α-peptoids are *N*-substituted glycine oligomers that mimic natural peptides with side chains on the nitrogen atoms rather than the α-carbons as in peptides. They were synthesized for the first time in 1992 at Chiron by Bartlett and Zuckermann.[101] At first, α-peptoids were introduced as peptidomimetics resistant to hydrolysis by protease enzymes. Therefore, it could be expected that, with proper choice of the *N*-substituents, peptoids may keep peptides activity but with better therapeutic profile. In addition, α-peptoids are not isolated structures but are part of the more general family of peptoids, *i.e.* oligoamides featuring *N*,*N*-disubstituted amides (Figure I.10). β-peptoids introduced by Hamper in 1998,[102] are constituted by lengthening the backbone chain with one additional methylene (*i.e.* *N*-substituted β-alanine oligomers), mimicking β-peptides.[103] Alternating oligomers such α,β-peptoids have been introduced by Taillefumier.[104] We should also mention *N*-substituted aromatic oligoamides which are constituted of the α-peptoid backbone extended with an aromatic ring.[105] These oligomers could be considered as proteomimetics rather than peptidomimetics. We can cite three main types: arylopeptoids,[106]

[101] Simon, R. J.; Kania, R. S.; Zuckermann, R. N.; Huebner, V. D.; Jewell, D. A.; Banville, S.; Ng, S.; Wang, L.; Rosenberg, S.; Marlowe, C. K *PNAS* **1992**, *89*, 9367-9371.
[102] Hamper, B. C.; Kolodziej, S. A., Scates, A. M.; Smith, R. G.; Cortez, E. *J. Org. Chem. Res.* **1998**, *63*, 708-718.
[103] Olsen, C. A. *Peptide Sci.* **2011**, *96*, 561-566.
[104] Hjelmgaard, T.; Faure, S.; Caumes, C.; De Santis, E.; Edwards, A. A.; Taillefumier, C. *Org. Lett.* **2009**, *11*, 4100-4103.
[105] Akhdar, A.; Gautier, A.;Hjelmgaard, T.; Faure, S.*; ChemPlusChem* **2021**, *86*, 298-312.
[106] Hjelmgaard, T.; Faure, S.; Staerk, D.; Taillefumier, C.; Nielsen, J. *Eur. J. Org. Chem.* **2011**, 4121–4132.

benzylopeptoids[107] and azole peptoids[108] as a family in which aromatic ring is added in the peptoid backbone. These last peptoid family members belong to the class of *N*-substituted aromatic oligoamides which were the subject of a review written during my PhD and published in a special issue on foldamers in *ChemPlusChem* (see section I-B-6).

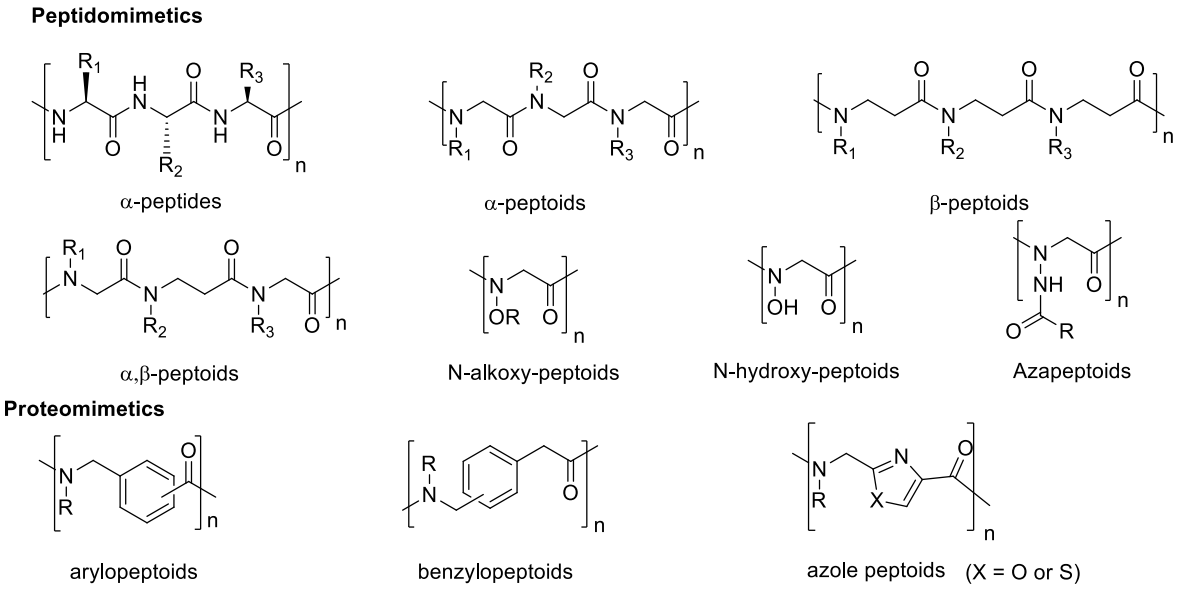

Figure I.10 Generic structures of peptide and peptoid-type oligomers.

In addition to the lack of intramolecular hydrogen bonds, the tertiary character of *N*,*N*-disubstituted amides promotes the establishment of a cis-trans isomerism and induce an inherent flexibility to the peptoid-type skeleton.[109] Therefore, peptoid oligomers exhibit more conformational flexibility than peptides as well as altered and/or different physiochemical properties. Rabenstein showed that the rate of cis/trans isomerization is slow and can be controlled by steric and electronic effects on the side chain, which allows them to be involved in different fields.[110] Peptoids are studied as peptidomimetics (inhibitors of protein/protein and RNA/protein interactions, amphiphilic antibacterials, surfactants …)[111]and as biomaterials.[112] Peptoids hold immense potential as therapeutic agents due to the fact that they are more proteolytically stable and cell-permeable than peptides.[111] Moreover, some groups are interested in studying peptoids as presenting platforms of pharmacophores (porphyrins, sugars, phthalocyanines, etc..) or effector molecules.[113]

[107] Meli, A.; Gambaro,S.; Costabile, C.; Talotta, C.; Della Sala, G.; Tecilla, G.; Milano, D.; Tosolini, M.; Izzoa, I.; De Riccardis, F. *Org. Biomol. Chem.* **2016**, *14*, 9055-9062.

[108] Mohan, A.; Koh, A. H. M.; Gate, G.; Calkins, A. L.; McComans, K. N.; Fuller, A. A. *Molecules* **2018**, *23*, 1035-1047.

[109] Yoo, B.; Kirshenbaum, K. *Curr. Opin. Chem. Biol.* **2008**, *12*, 714-721.

[110] Sui, Q.; D. Borchardt, D.; Rabenstein, D.L. *J. Am. Chem. Soc.* **2007**, *129*, 12042–12048.

[111] a) Zuckermann, R. N.; Kodadek, T. *Curr. opin. mol. ther.***2009**, *11*, 299-307. (b) T Dohm, M.; Kapoor, R.; E Barron, A. *Curr. Pharm. Des.* **2011**, *17*, 2732-2747. (c) Horne, W. S. *Expert Opin. Drug Discov*. **2011**, *6*, 1247-1262.

[112] (a) Ganesh, S. D.; Saha, N.; Zandraa, O.; Zuckermann, R. N.; Saha, P. *Polymer Bulletin* 2017, *74*, 3455–3466. (b) Gangloff, N.; Ulbricht, J.; Lorson, T.; Schlaad, H.; Luxenhofer, R. *Chem. Rev.* **2015**, *116*, 1753-1802.

[113] (a) Szekely, T.; Roy, O.; Dériaud, E.; Job, A.; Lo-Man, R.; Leclerc, C.; Taillefumier, C. *J. Med. Chem*. **2018**, *61*, 9568-9582. (b) Caumes, C.; Gillon, E.; Legeret, B.; Taillefumier, C.; Imberty, A.; Faure, S. Chem. Commun. **2015**, *51*, 12301-12304. (c) Yang, W.; Jo, J.; Oh, H.; Lee, H.; Chung, W-J.; Seo, J. *J. Org. Chem.* **2020**, *85*, 1392−1400.

The amide bonds of peptides are secondary in nature, and they prefer the trans geometry. However, the tertiary character of *N,N*-disubstituted amides in the peptoids are prone to cis/trans isomerism as we mentioned earlier.[109] Cis and trans amide forms could be in equilibrium in many cases since the cis and trans confirmations are energetically close (Scheme I.76). Therefore, for a peptoid made up of n monomers, a mixture of 2^{n-1} isomers in equilibrium or of 2^n if it is acylated in the *N*-terminal position may be found in solution.

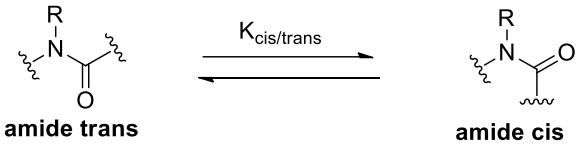

Scheme I.76. *Cis* and *trans* confirmations of the *N,N*-disubstituted amide.

The NMR spectra of peptoids is usually difficult to study due to the combination of many rotamers which makes it complex especially in the case of long oligomers that present high degenerated spectra. Therefore, many researchers have studied the development of strategies to control the *N,N*-disubstituted conformation and induce privileged secondary structures, particularly for α-peptoids. The strategies of conformational control were mainly based on the establishment of weak non-covalent interactions and/or steric interactions between the side chain and the peptoid backbone.[114] For example, the studies revealed the effect of n→π* interaction between the backbone amide carbonyl oxygen and an aromatic residue on the side chain or even the re-establishment of hydrogen bonds between skeletal carbonyl and a specially designed side chain.[115] Nevertheless, the macrocyclization has also proved to restrict the conformational freedom and aim for the structuration.

I.B.2. Peptidomimetic peptoids

I.B.2.1. α-peptoids

I.B.2.1.1. Synthesis methods

First, the synthesis of α-peptoids was done using a monomer-based method similar to Fmoc solid-phase peptide synthesis (SPPS) (Scheme I.12).[101] This method requires the synthesis of the Fmoc-protected peptoid monomers in big quantities which is expensive and time-consuming (Zuckerman: '1 year to prepare monomers consumed in days'!). Besides, the coupling of peptoid monomers is more difficult than amino acids coupling due to the secondary amine. To overcome these limitations, Zuckermann developed a more efficient synthesis, the solid-phase submonomer method.[116] The submonomer synthesis is a cycle of two chemical steps, the first step involves the acylation of a resin bounded secondary amine with bromoacetic acid in the presence of DIC (*N,N'*-diisopropylcarbodiimide) as a coupling reagent. The introduction of the nitrogen and the side chain is performed using an SN_2 reaction with a primary amine. Both reactions are fast and the cycle is repeated until getting the targeted peptoid sequence. However, the use of bromoacetic acid could result in undesired side reactions in the presence of side-chain functionalities that contain unprotected heteroatoms, especially these

[114] (a) Roy, O.; Caumes, C.; Esvan, Y.; Didierjean, C.; Faure, S.; Taillefumier, C. *Org. Lett*. **2013**, *15*, 2246-2249. (b) Stringer, J. R.; Crapster, J. A.; Guzei, I. A.; Blackwell, H. E. *J. Am. Chem. Soc.* **2011**, *133*, 15559-15567.
[115] (a) Caumes, C.; Roy, O.; Faure, S.; Taillefumier, C. *J. Am. Chem. Soc*. **2012**, *134*, 9553-9556. (b) Gorske, B. C.; Stringer, J. R.; Bastian, B. L.; Fowler, S. A.; Blackwell, H. E. *J. Am. Chem. Soc*. **2009**, *131*, 16555-16567.
[116] Zuckermann, R. N.; Kerr, J. M.; Kent, S. B.; Moos, W. H. *J. Am. Chem. Soc*. **1992**, *114*, 10646-10647.

occurring in many heterocycles (ex: pyridines, imidazoles, indoles and pyrazines).[117] This limitation of the bromoacetic acid is overcomed by using chloroacetic acid which is less prompt to react.[118]

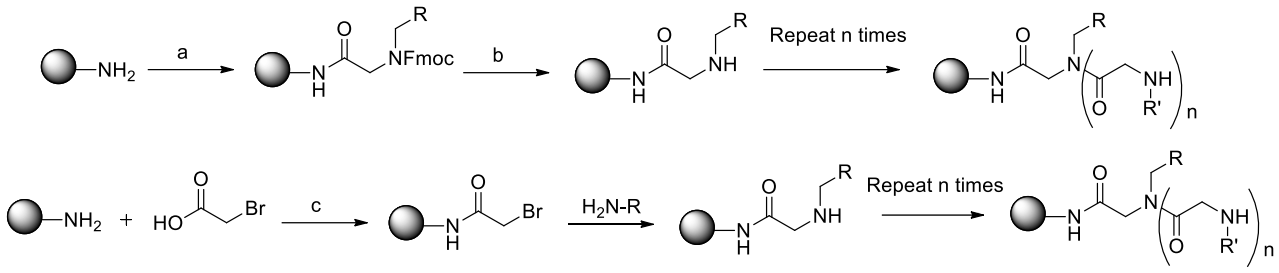

Scheme I.77. Monomer and submonomer methods: Conditions (a) Fmoc-protected glycine monomers and coupling reagent, (b) 20% piperidine and (c) coupling reagent.

This method is considered as one of the most efficient techniques known in terms of yields and monomers diversity/availability.[119] The reactions are neither air nor moisture sensitive and both acylation and substitution steps can be accelerated using conventional heating or microwave irradiation.[120] Thanks to these facts, the whole process could be automated and adapted to nearly all the commercial peptide synthesizers.[121] Peptoids with high number of monomers can be synthesized; the longest peptoids reported with reasonable yield are about 50 monomers, suggesting +99% yield for one coupling cycle.[122]

The side chains of interest could be easily introduced in peptoids, using submonomer method, as only a reactive primary amine is required in the substitution step. Unlike peptides whose side chain diversity is limited due to the presence of only 20 natural amino acids, peptoid libraries containing high side chain diversity can be prepared using hundreds of commercially available amines[119,121] If the acylation step is fast, the substitution is slower (up to 2h at room temperature) and requires high concentrations of amine (0.5-2M) to avoid double alkylation. Moreover, amines with poor nucleophiles or hindered amines are incorporated slower leading to low yields.

Nevertheless, the scaling up of this synthesis was rare in academia for cost reasons. The submonomer method also could be applied in solution to overcome the cost limitation. However, it will require additional steps of purifications and intermediate treatments that obviously lengthen the time of the synthesis but allows scale up using cheap materials. The first step is the acylation of the secondary amine by the chloro or the bromoacetyl bromide to elongate the skeleton followed by the substitution of bromine by a primary amine (Scheme I.78)[104]. Note that no coupling reagent is need in this solution-phase submonomer method.

[117] Uno, T.; Beausoleil, E.; Glodsmith, R.; Levine, B.; Zuckermann, R. *Tet Lett* **1999**, *40*(8), 1475-1478.
[118] Burkoth, T.; Fafarman, A.; Charych, D.; Connolly, M.; Zuckermann, R. *J Am Chem Soc* **2003**,*125*(29), 8841-8845.
[119] (a) Culf, A. S.; Ouellette, R. J. *Molecules* **2010**, *15*, 5282-5335. (b) Connolly, M. D.; Xaun, S.; Malchanova, N.; Zuckermann, R. N. *Meth. Enzymol.* **2021**, *656*, 241-270.
[120] Olivos, H.; Alluri, P.; Reddy, M.; Salony, D.; Kodadek, T. *Org Lett* **2002**, *4*(23):4057-4059.
[121] Igliozzi, G.; Goldsmith, R.; Ng, S.; Banville, S.; Zuckermann, R. *Methods Enzymol* **1996**, *267*, 437-447.
[122] Burkoth, T.; Beausoleil, E.; Kaur, S.; Tang, D.; Cohen, F.; Zuckermann, R. *Chem Biol* **2002**, *9*(5), 647-654.

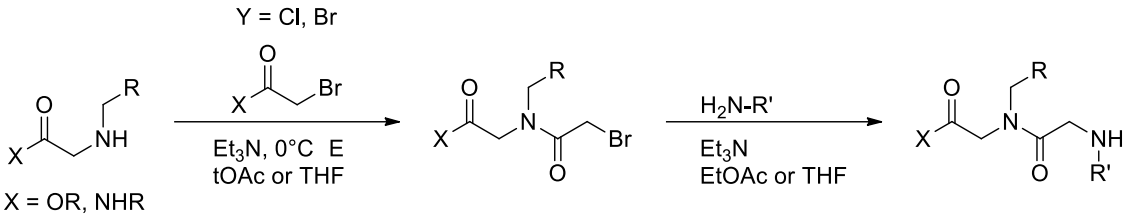

Scheme I.78. Synthesis of α-peptoids in solution using submonomer method.

I.B.2.1.2: Structuration

Peptoids has similar amide bonds to that in polyprolines, in which it undergoes the polyproline I (PPI) or polyproline II (PPII) helical structures. In α-peptoids, the helical structure could be controlled by the nature of the side chains, as PPII-type helix is formed in the case of backbone *trans* amides while the PPI-type helix is formed in case of *cis* amides. PPI-type secondary structures were much more studied in peptoids than PPII-type. Studies have proved that PPI peptoid helices have good thermal and chemical (denaturation by chemical agents) resistance compared to peptides.[123]

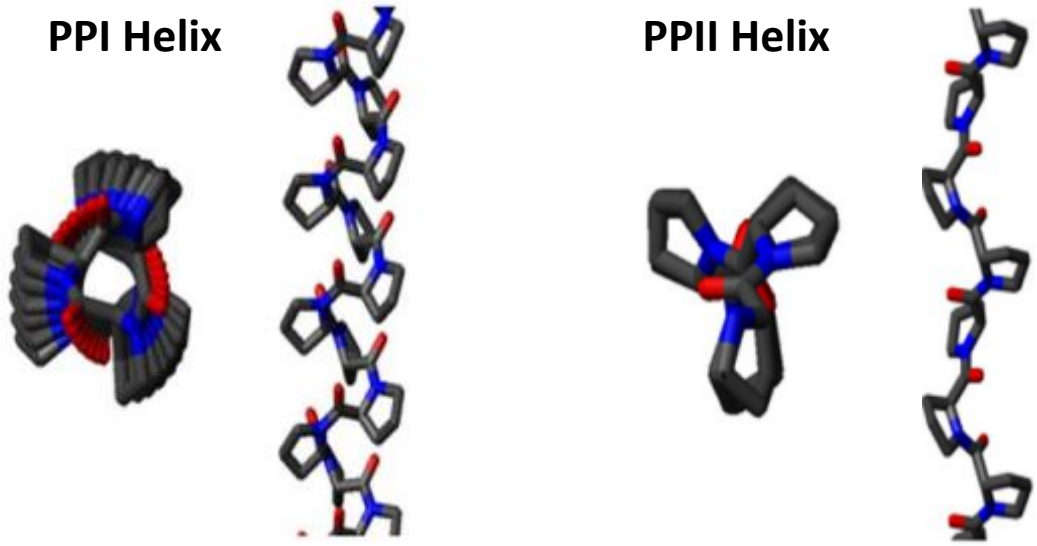

Figure I.11. Representation of the two types of polyproline helices.

Over the years, many strategies were extensively investigated for the incorporation of specific side chains stabilizing *cis* conformation of peptoid amide bonds. The *cis* confirmation is favored by the incorporation of *N*α-chiral aromatic side chains by steric and electronic interactions.[124] The 1-phenylethyl side chain is the most used and studied side chain in building PPI helices. It was even studied in both asymmetric configurations S and R (Figure I.12). As the peptoid is an achiral molecule, a stereogenic center placed on the Nα side chain could control the sense of helicity, to be right or left. Also, *N*α-achiral electron deficient aromatic side chain, *N*α-chiral aliphatic side chains and achiral α-branched aliphatic side chains have been less studied but proved to be more efficient for the stabilization of *cis*-amide (Figure I.12).

[123] Miller, S. M.; Simon, R. J.; Ng, S.; Zuckermann, R. N.; Kerr, J. M.; Moos, W. H. *Drug Dev. Res.* **1995**, *35*, 20-32.
[124] Armand, P.; Kirshenbaum, K.; Falicov, A.; Dunbrack Jr, R. J.; Dil, K. A.; Zuckermann, R. N.; Cohen, F. E. *Folding Des.* **1997**, *2*, 369–375.

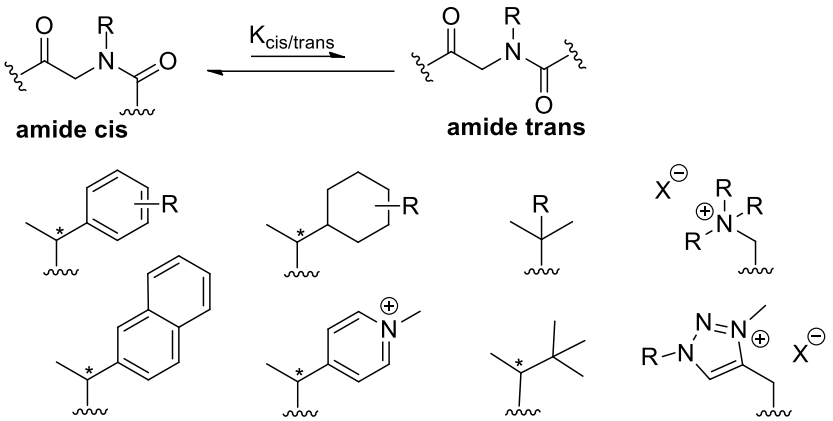

Figure I.12. Some examples of side chains used for the *cis* amide control.

Barron observed that at least 50% Nα-chiral, aromatic side chain is required for peptoids to form stable secondary structures in hexameric sequences.[125] Also, the presence of aromatic side chain serves in the stabilization of the propeller since it allows aromatic π-π interactions along the axis of the helix. Moreover, they prove the importance of a bulky chiral side chain in the *C*-terminus, especially in short sequences to form a PPI helix. The effect of these three factors was limited to short oligomers (up to 12 monomers) to form the secondary helix structures; but this influence is vanished on oligomers longer than 15 monomers.

Nevertheless, Blackwell reported that Nα-chiral aromatic 1-phenylethyl side chain doesn't lead to full geometry control skeletal amides caused by conformational heterogeneity by the *cis* and *trans* conformations[115b]. For this reason, $K_{cis/trans}$ was calculated in two different pentameric homooligomers, the first one with (S)-N-(1-phenylethyl) glycine (named Ac-$(Nspe)_5$-OtBu) and second with (S)-N-(1-naphthylethyl) glycine (named as Ac-$(Ns1pe)_5$-OtBu) as side chain (Figure I.13). The calculated equilibrium constant of Ac-$(Nspe)_5$-OtBu was 3.3 which only corresponds to around 75% confirmation while the equilibrium constant of Ac-$(Ns1npe)_5$-OtBu was $K_{cis/trans}$> 19 which shows much better confirmation control. The threshold value of 19 means that no more *trans* amide is identified by NMR. Oligomers of Ns1npe form the most stable helices described to date for peptoid bearing aromatic side chains. The CD studies shows that the structuration increases with the elongation of the oligomers, thus showing cooperative effect. Our team also reported the chiral 1-triazolium-ethyl side chain which strongly induces the *cis* conformation (Figure I.13).[115a] It was demonstrated that n → π* interactions between C=O and the aromatic is stabilizing the cis conformation either by molecular modeling studies or NMR studies on monomers or dimers.

On the other hand, Barron investigated the conformational properties of a set of peptoid homooligomers with *N*α-chiral aliphatic side chains and proved helical structuring.[126] For example, homooligomers (R)-*N*-(1-cyclohexylethyl) glycine (*N*rch) form PPI-type helical structure in acetonitrile. The first crystal structure of a peptoid oligomer reported in the literature is that of the pentamer $(Nrch)_5$, it adopts a left-handed helical conformation with

[125] Wu, C. W.; Sanborn, T. J.; Huang, K.; Zuckermann, R. N.; Barron, A. E. *J. Am. Chem. Soc.* **2001**, *123*, 6778–6784.

[126] Wu, C. W.; Kirshenbaum, K.; Sanborn, T. J.; Patch, J. A.; Huang, K.; Dil, K. A.; Zuckermann, R. N.; Barron, A. E. *J. Am. Chem. Soc.* **2003**, *125*, 13525– 13530.

repeating *cis*-amide bonds (Figure I.12). However, according to NMR study, the hexamer Ac-(*N*sch)$_6$-OtBu $K_{cis/trans}$ is around 1 which is a sign of heterogeneity in solution.

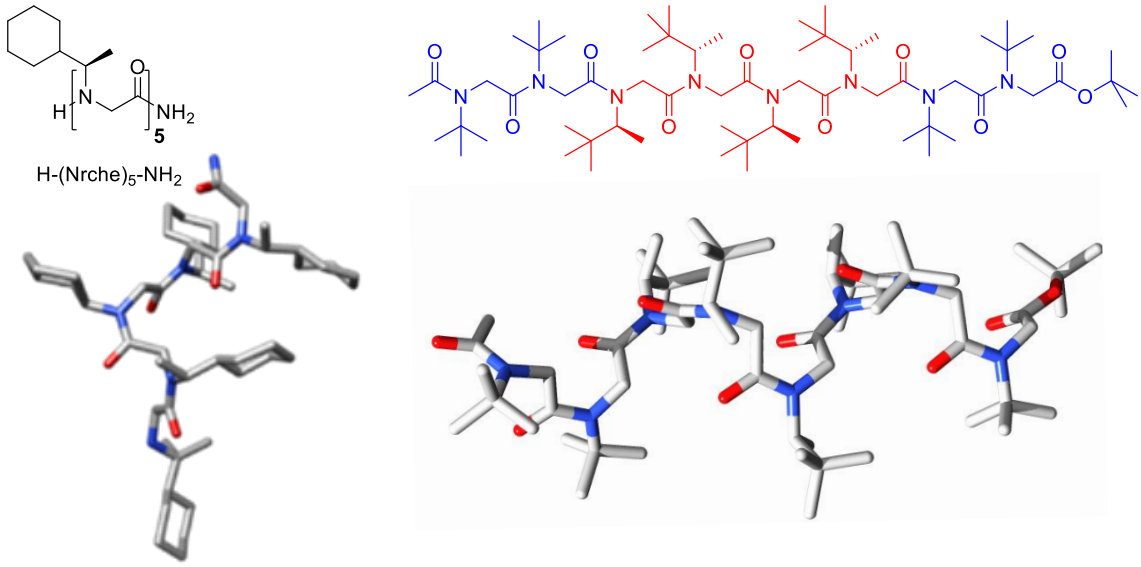

Figure I.13. Crystal structures of the pentamer H-(*N*rch)$_5$-NH_2 and the octamer Ac-(*N*tBu)$_2$-(*N*stbe)$_4$-*N*tBu)^2-OtBu.

Recently, our team reported two sterically hindered aliphatic side chains: the achiral tert-butyl chain (Figure I.12) and the chiral 1-*tert*-butylethyl, whose monomers have been named N*t*Bu and Ns1tbe, respectively.[127] The *cis* amide bond preference and PPI type helical confirmations were observed in Ns1tbe. The *t*Bu, also known as NCα-gem-dimethyl amines, are the first side chain capable of completely displace balance toward *cis*-amide conformation (Kcis/trans>19), regardless the length of the oligomer.[128] This complete displacement toward *cis*-amide was also recently achieved by Zuckermann using cationic alkyl ammonium ethyl side chains.[129] The molecular modeling studies proved that N*t*Bu oligomers adopt PPI-type helix despite the absence of chiral side chains. The study shows that the helix would be the most stable conformation because it allows the establishment of a greater number of weak non-covalent interactions such as London interactions between *t*Bu groups positioned on the same face of the helix (between residues i and i+3). Connections by weak hydrogen CH--O=C along the peptoid skeleton would also contribute to the helical structure.[130]

The *trans* isomerization is less explored in peptoids. Shah observed that PPII-type structure, in which all amides are *trans*, are observed when *N*-aryl side chains are incorporated in peptoids.[131] The computational studies showed that *trans* isomers are more stable than *cis* isomers (Figure I.14.a). Also, Stringer showed by NMR studies that peptoids having N-aryl side chains with hydrogen bond donor groups at *ortho* position stabilizes *trans*-amide (Figure

[127] Roy, O.; Dumonteil, G.; Faure, S.; Jouffret, L.; Kriznik, A.; Taillefumier, C. *J. Am. Chem. Soc.* **2017**, *139*, 13533-13540.
[128] Shyam, R.; Nauton, L.; Angelici, G.; Roy, O.; Taillefumier, C.; Faure, S. *Biopolymers* **2019**, *110*, e23273.
[129] Wijaya, A. W.; Nguyen, A. I.; Roe, L. T.; Butterfoss, G. L.; Spencer, R. K.; Li, N. K.; Zuckermann, R. L. *J. Am. Chem. Soc.* **2019**, *141*, 19436−19447.
[130] Angelici, G.; Bhattacharee, N.; Roy, O.; Faure, S.; Didierjean, C.; Jouffret, L.; Taillefumier, C. *Chem. Comm.* **2016**, *52*, 4573-4576.
[131] Shah, N. H.; Butterfoss, G. L.; Nguyen, K.; Yoo, B.; Bonneau, R.; Rabenstein, D. L.; Kirshenbaum, K. *J. Am. Chem. Soc.* **2008**, *130*, 16622-16632

I.14.b).[132] Proulx reported the synthesis of peptoids containing *N*-imino and *N*-alkylimino glycines.[133] These residues was proved to induce a *trans*-amide preference. Recently, our group reported the synthesis of *N*-alkylamino peptoid homooligomers.[134] The *trans*-amide configuration was obtained after conformational analysis of these homooligomers.

Other structures have been also detected such as threaded loop,[135] sheet structure[136] and the ribbon structure.[137]

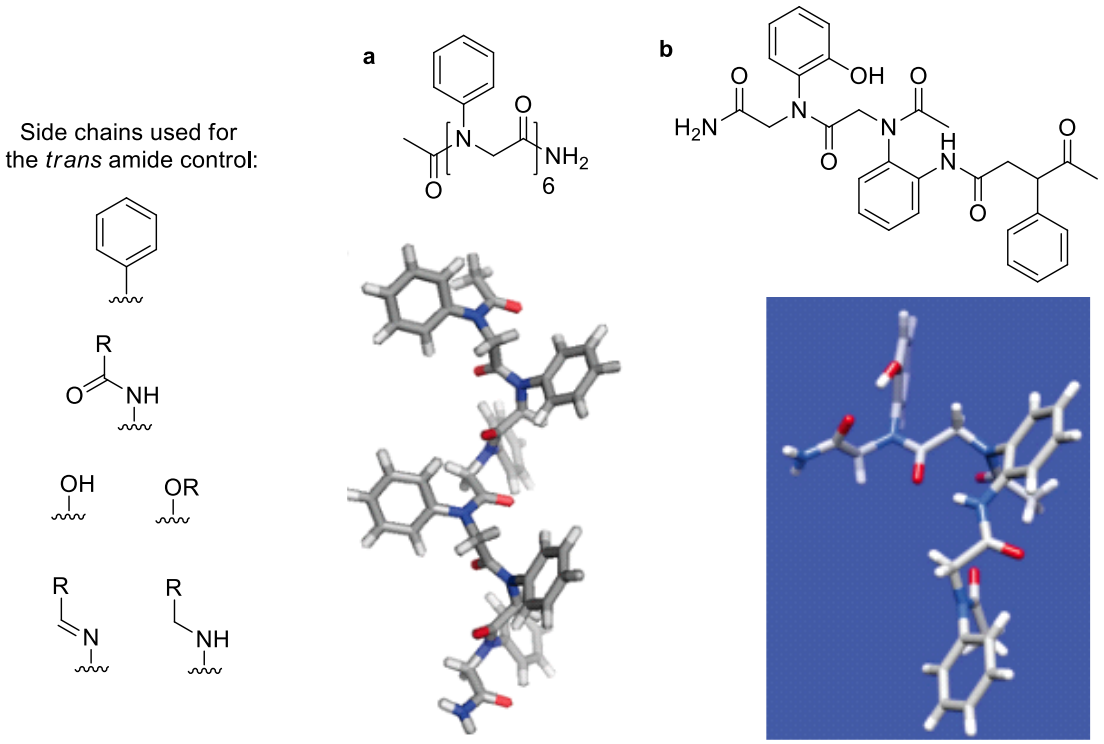

Figure I.14. Side chains inducing trans amide conformations and PPII-type structure of *trans* amide peptoids calculated by molecular modeling

I.B.2.1.3. Applications

The peptoids are active in a wide range of applications. For example, peptoids are used as platforms for phase-transfer and metallo-peptoid oxidation catalytic ensembles;[138] fluorescent sensors of pH, cyanide and mercury ions; platforms for multicomponent photocatalytic centers and designable chelators for specific metals.[139] Also, peptoids shows an important role as sensors of biomacromolecules (proteins, nucleics acids and polysaccharides), medical

[132] Stringer, J. R.; Crapster, J. A.; Guzei, I. A.; Blackwell, H. E. *J. Org. Chem.* **2010**, *75*, 6068–6078.
[133] Davern, C. M.; Lowe, B. D.; Rosfi, A.; Ison, E. A.; Proulx, C. *Chem. Sci.* **2021**, *12*, 8401–8410.
[134] Pypec, M.; Jouffret, L.; Taillefumier, C.; Roy, O. *Beilstein J Org Chem.* **2022**, *18*, 845-854.
[135] (a) Huang, K.; Wu, C. W.; Sanborn, T. J.; Patch, J. A.; Kirshenbaum, K.; Zuckermann, R. N. *J. Am. Chem. Soc.* **2006**, 128, 1733-1738. (b) Fowler, S. A.; Blackwell, H. E. *Org. Biomol. Chem.* **2009**, *7*, 1508-1524.
[136] Crapster, J. A.; Stringer, J. R.; Guzei, I. A.; Blackwell, H. E. *Peptide Sci.* **2011**, *96*, 604-616.
[137] Crapster, J. A.; Guzei, I. A.; Blackwell, H. E. Angew. *Chem., Int. Ed.* **2013**, *52*, 5079-5084.
[138] (a) Schettini, R.; Nardone, B.; De Riccardis, F.; Sala, G. D.; Izzo, I. *Eur. J. Org. Chem.* **2014**, *2014*, 7793-7797. (b) Schettini, R.; De Riccardis, F. ; Sala, G. D. ; Izzo *J. Org. Chem.* **2016**, *81*, 2494-2505. (c) Della Sala, G.; Nardone, B. ; De Riccardis, F.; Izzo I. *Org. Biomol. Chem.* **2013**, *11*, 726731. (d) Schettini, R.; D'Amato, A.; De Riccardis, F.; Sala, G. D.; Izzo I. *Synthesis* **2017**, *49*, 1319-1326.
[139] Culf, A.S. *Biopolymers* **2019**, *110*, e23285.

imaging,[140] and as cellular transporters.[141] Similarly, their resistance to enzymes, especially proteolysis makes peptoids prime candidates for therapeutic development.[142]

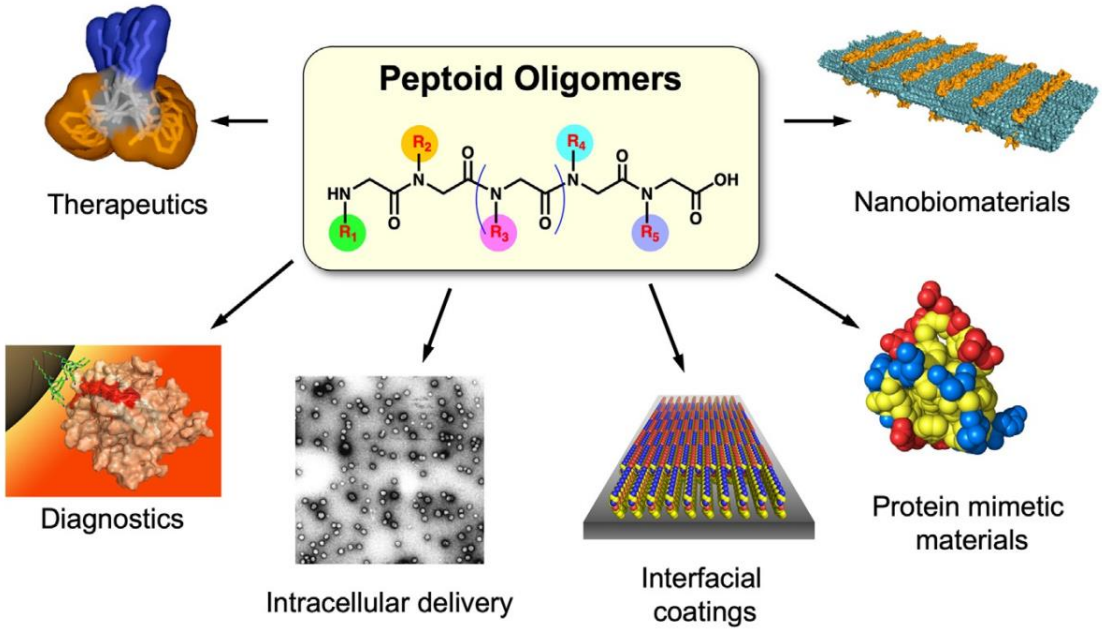

Figure I.15. Examples of peptoid applications (adapted from reference 119b)

I.B.2.2. β-peptoids

I.B.2.2.1. Synthesis

In 1998, Hamper *et al*. developed a solid-phase synthesis for the preparation of β-peptoids, defined as oligomers of *N*-substituted β-alanine.[102] The backbone of β-peptoid oligomers was synthesized by the treatment of Wang's resin with acryloyl chloride followed by Michael addition of primary amine (Scheme I.79). These two steps are repeated to form a library of dimers and trimers.

[140] (a) Cai, W; Hong, H. *Am. J. Nucl. Med. Mol. Imaging* **2011**, *1*, 76-79. (b) Hao, G.; Hajibeigi, A.; De León-Rodríguez, L. M.; Öz, O. K.; Sun, X. *Am. J. Nucl. Med. Mol. Imaging* **2011**, *1*, 65-75. (c) Seo, J.; Ren, G.; Liu, H.; Miao, Z.; Park, M.; Wang, Y.; Miller, T. M.: Barron, A. E.; Cheng, Z. *Bioconjugate Chem.* **2012**, *23*, 1069-1079.
[141] (a) Kölmel, D. K.; Hörner, A.; Rönicke, F.; Nieger, M.; Schepers, U.; Bräse, S. *Eur. J. Med. Chem.* **2014**, *79*, 2314 (b) Jong, T.; Pérez-López, A. M.; Johansson, E. M. V.; Lilienkampf, A.; Bradley, M. *Bioconjugate Chem*. **2015**, *26*, 1759-1765.
[142] https://maxwellbiosciences.com/development-programs

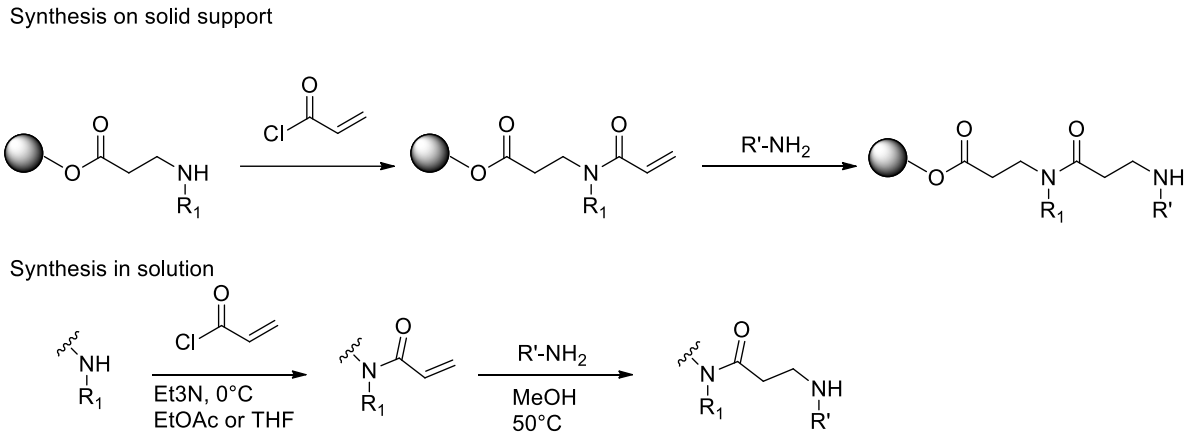

Scheme I.79. Synthesis of β-peptoids on support and in solution.

Unlike in α-peptoids, the supported submonomer method was less studied and optimized for β-peptoids. The purities and yields are insufficient, and it doesn't allow the synthesis of long oligomers. However, Shuey *et al.* have developed an approach supported by block couplings which made it possible to obtain oligomers up to 18 units.[143] In 2011, Caumes *et al.* developed a new method of synthesis in solution that allows the preparation of tetramers on gram scale.[144] The method involves the introduction of volatile primary amines on the chain which make it efficient and quick by excluding any intermediate purification (Scheme I.80).

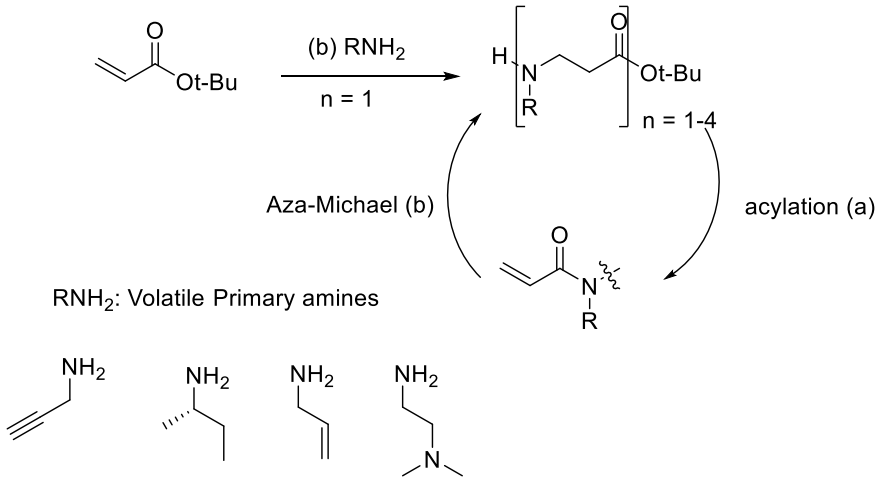

Scheme I.80. β-Tetrapeptoids synthesis in solution.

I.B.2.2.2. Structuration

The effect of the side chain on the conformational behavior was also studied for β-peptoid oligomers. A wide range of β-peptoids monomers containing various side chains as well as thioamidation and trifluoroacetylation were synthesized.[145] The NMR spectroscopy revealed that the model compounds with different side chains exhibit *cis-trans* isomerization similar to that of α-peptoids. For example, (S)-1-(1-naphthyl)ethyl side chain induces strongly the *cis*-amide conformation, while *N*-aryl gives rise to *trans.* Also, this study revealed that an α-

[143] Shuey, S. W.; Delaney, W. J.; Shah, M. C.; Scialdone, M. A. *Bioorg. Med. Chem. Lett.* **2006**, *16*, 1245-1248.
[144] Caumes, C.; Hjelmgaard, T.; Remuson, R.; Faure, S.; Taillefumier, C. *Synthesis* **2011**, *2011*, 257-264.
[145] (a) Laursen, J. S.; Engel-Andreasen, J.; Fristrup, P.; Harris, P.; Olsen, C. A. *J. Am. Chem. Soc.* **2013**, *135*, 2835−2844. (b) Laursen, J. S.; Engel-Andreasen, J.; Olsen, C. A. *Acc. Chem. Res.* **2015**, *48*, 2696-2704.

branching of the bulky substituent is mandatory for the *cis*-amide preference, as the diphenyl-substituted benzyhydryl side chain was not efficiently sterically demanding. The electronic effects of the carbonyl donor-acceptor capabilities were studied in the model systems containing trifluoroacetyl groups and thioamides. The NMR studies showed an interaction of the *N*-terminal carbonyl/thiocarbonyl lone pair with the aromatic side chain without evidence for conformational stabilization through non-covalent carbonyl-carbonyl interactions.

Olsen synthesized two series of homooligomeric β-peptoids and studied their folding propensity.[146] During the synthesis, the precipitation of two hexamers with *N*-1-(1-naphthyl)ethyl side chain was observed. The crystals were studied by X-ray diffraction which revealed helical structures with all *cis*-amide and a highly ordered arrangement of the naphthyl groups along three faces of the helix to give an equilateral triangle when viewed down the helical axis. Thus, a triangular prism shape was adopted by the main helix not taking into consideration *N*-terminal side chain.[146] However, the *N*-terminal acetylation introduced fully helical arrangement through the hexamer by forcing the final side chain into cisoid conformation. This work reports the first example of ordered secondary structures in linear oligomeric β-peptoids with a high-resolution evidence. In addition to that, a trend was obtained by increasing of the folding activity by increasing the oligomer length, caused by the increase of $K_{cis/trans}$ values.

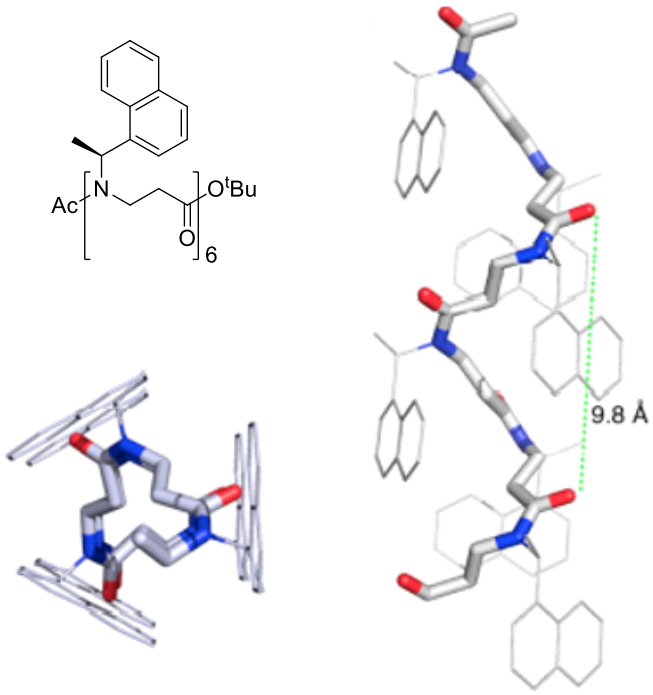

Figure I.14. X ray structures (side and top views) of homooligomeric β-peptoid (β–*N*s1npe).

Later, Olsen synthesized a hexamer series of bis-functionalized β-peptoids (Scheme I.81).[147] These functionalized β-peptoids show better solubility compared to the previous ones, thus allowing for more investigation of helical folding propensity in different solvents and pH

[146] Laursen, J. S.; Harris, P.; Fristrup, P.; Olsen, C. A. *Nat. Commun.* **2015**, *6*, 7013.
[147] (a) Wellhöfer, I.; Frydenvang, K.; Kotesova, S.; Christiansen, A. M.; Laursen, J. S.; Olsen, C. A. *J. Org. Chem.* **2019**, *84*, 3762-3779. (b) Wellhöfer, I.; Beck, J.; Frydenvang, K.; Bräse, S.; Olsen, C. A. *J. Org. Chem.* **2020**, *85*, 10466-10478. (c) Laursen, J. S.; Engel-Andreasen, J.; Fristrup, P.; Harris, P.; Olsen, C. A. *J. Am. Chem. Soc.* **2013**, *135*, 2835–2844.

effects. The β-peptoids with the functionalized triazole side chains showed denaturation and refolding upon heating and cooling the compounds, respectively. Helical folding was indicated by the high degree of *cis*-amide bond formation showed by NMR. Also, the high solubility introduced has revealed the ability of the amino- and carboxy-functionalized oligomers to reversibly respond to the addition of acid and base.

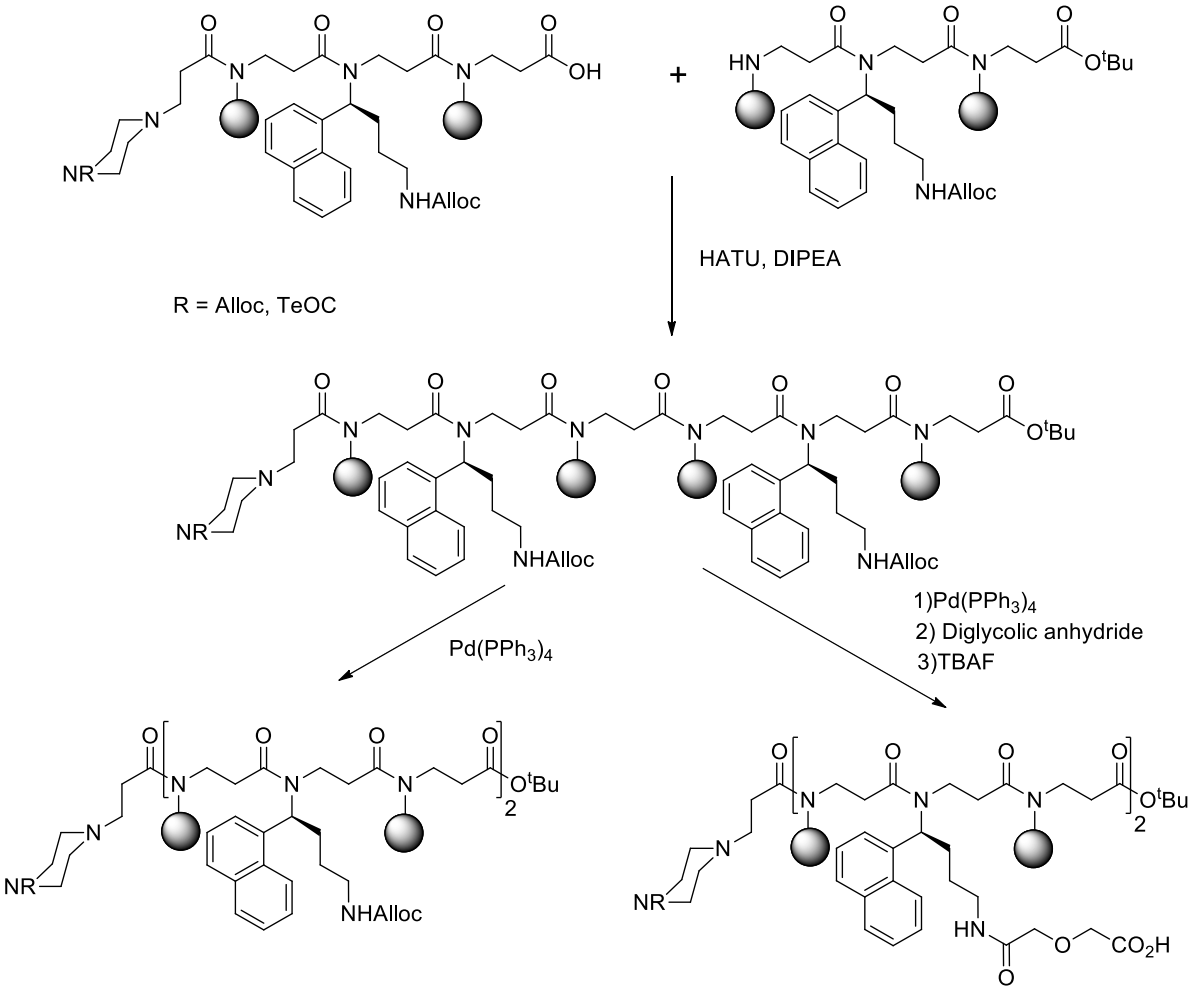

Scheme I.81. Synthesis of amino- and carboxy-functionalized β-peptoid hexamers.

I.B.2.2.3. Applications

The applications of β-peptoids were less studied and observed compared to the α-peptoids. Faure shows an application of β-peptoids as a multivalent platform for sugar display. It was shown that an efficient binding potency for bacterial lectins LecA and Bc2L-A was obtained with the cyclic β-peptoid scaffold displaying 1-thio-b-D-galactose or 1-thio-a-Dmannose.[148] Also, Faure deployed the β-peptoids in the synthesis of SRIF mimics and studied their efficiency.[149]

[148] Caumers, C.; Gillon, E.; Legeret, L.; Taillefumier, C.; Imberty, A.; Faure, S. *Chem. Commun.* **2015**, *51*, 12301-12304.
[149] Caumes, C.; Hejlmgaard, T.; Roy, O.; Reynaud, M.; Servent, D.; Taillefumier, C.; Faure, S. *Med. Chem. Commun.* **2012**, *3*, 1531-1535

In addition to α-and β-peptoids, there are other kinds of peptidomimetic peptoids such as *N*-hydroxypeptoids,[150] *N*-alkoxypeptoids[151] and azapeptoids[152] which are also obtained using the submonomer method. These types will not be described in detail in this bibliographic part.

I.B.3. Proteomimetic peptoids

I.B.3.1. Arylopeptoids

I.B.3.1.1. Synthesis methods

Arylopeptoids or oligomeric *N*-substituted aminomethyl benzamides, were first patented in 1996 by Zuckermann at Chiron[153]. Later, in 2007, Combs and Lokey described the synthetic access on solid phase using the submonomer method. In their procedure, they amidate *meta* or *para*-bromomethyl benzoic acids using DIC followed by the addition of different primary amines to elongate the skeleton on Wang resin (Scheme I.82).[154] This method was limited in terms of the amines diversity and the isolated yield of pentamers was only 37% on *meta*-aryl substituents.

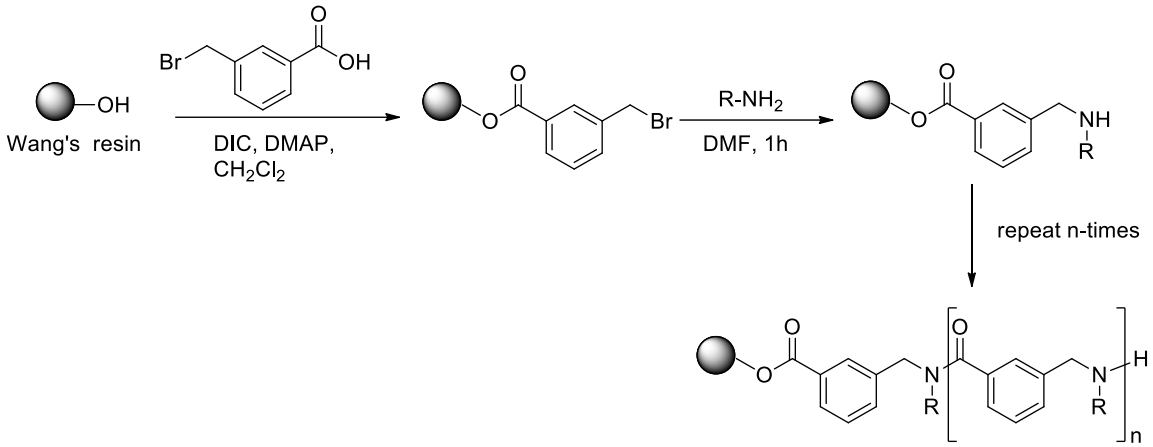

Scheme I.82. Synthesis of arylopeptoids by Lokey.

Meta- and *para*-regioisomers display room temperature ^{1}H NMR spectra highly complex because of the amide bond rotamers. However, in dmso-d_6 at 100°C the coalescent of the signals is overpass giving rise to greatly simplified spectra. Importantly, compound incorporating morpholine are highly soluble in water (80 mg/mL) indicating that backbone's hydrophobicity can be overcomed with an appropriate choice of hydrophilic side chains.

In 2011, Faure and Nielsen reported the first solution-phase synthesis of *meta*- and *para*-arylopeptoids using bromomethyl benzoyl bromides as the aromatic building blocks (Scheme I.83).[106] This method could be adaptable to gram scale and the usage of COMU (1-Cyano-2-ethoxy-2-oxoethylidenaminooxy)dimethyl amino-morpholino-carbenium) as a coupling reagent gives access to hexamers and nonamers by coupling of trimeric blocks. This method

[150] Crapster, J. A.; Stringer, J. R.; Guzei, I. A.; Blackwell, H. E. *Peptide Sci.* **2011**, *96*, 604-616.
[151] Jordan, P. A.; Paul, B.; Butterfoss, G. L.; Renfrew, P. D.; Bonneau, R.; Kirshenbaum, K. *Peptide Sci.* **2011**, *96*, 617-626.
[152] Aubin, S.; Martin, B.; Delcros, J. G.; Arlot-Bonnemains, Y.; Baudy-Floc'h, M. *J. Med. Chem.* **2005**, 48, 330-334.
[153] Zuckermann, R. N.; Goff, D. A.; Ng, S.; Spear, K.; Scott, B. O.; Sigmund, A. C.; Goldsmith, R. A.; Marlowe, C. K.; Pei, Y.; Richter, L.; Simon, R. WO9640202A1, **1996**.
[154] Combs, D. J.; Lokey, R. S. *Tetrahedron Lett.* **2007**, *48*, 2679–2682.

was further modified to use the chloromethyl benzoyl chloride in the acylation step which gives access to more side chains and increased the isolated yields.

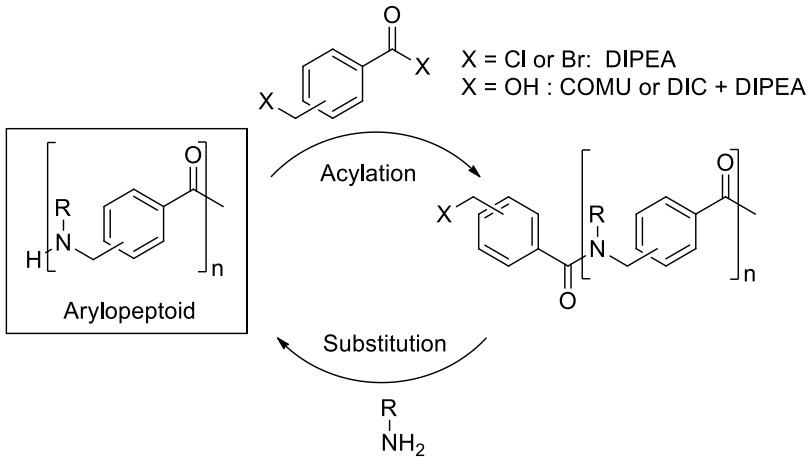

Scheme I.83. Synthesis of *para*- and *meta*-arylopeptoids in solution.

In 2012, an improved method for the synthesis of arylopeptoids on solid support was reported.[155] The chloromethyl benzoyl chloride was used in the acylation step instead of DIC activation of benzoic acid (Scheme I.84). Thus, this procedure is cheaper, faster (10 minutes versus 1h) and more atom economic. Therefore, it enables the access to oligomers carrying a wide range of side chains that were previously inaccessible and results in higher isolated yields than the former procedure (on 2-chlorotrityl resin or rink amide resin).

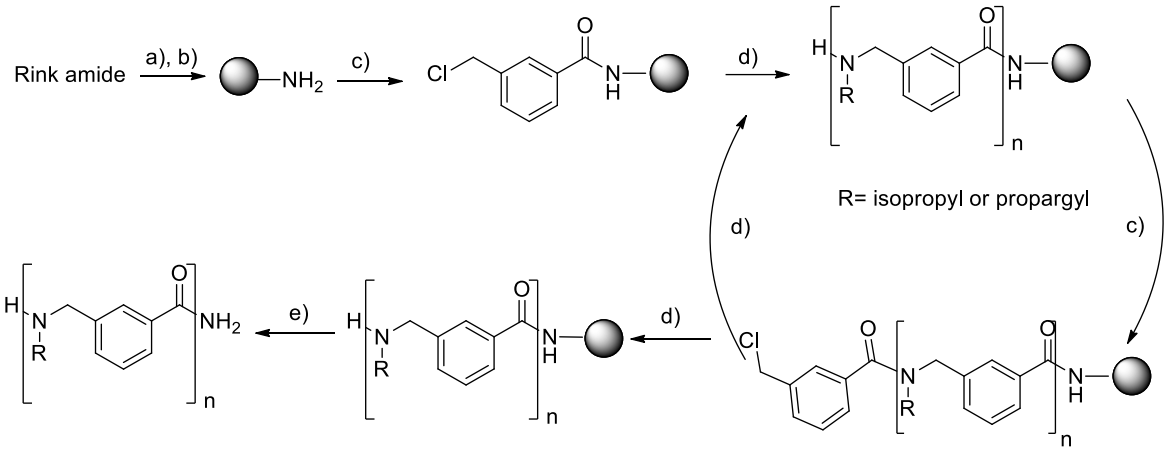

Scheme I.84. Solid-phase submonomer synthesis on Rink amide resin.

Later in 2013, Hjelmgaard and Nielsen reported the synthesis of *ortho*-arylopeptoids for the first time, as a new type of aromatic oligoamides with an *ortho*-connection pattern in the backbone.[156] The submonomer method was used to efficiently synthesize these arylopeptoids both in solution and on solid phase. The solution-phase synthesis comprises two consecutive steps, the acylation using *ortho* (bromomethyl)benzoyl bromide followed by the substitution

[155] Hjelmgaard, T.; Faure, S.; De Santis, E.; Staerk, D.; Alexander, B. D.; Edwards, A. A.; Taillefumier, C.; Nielsen, J. *Tetrahedron* **2012**, 68, 4444-4454.
[156] Hjelmgaard, T.; Nielsen, J. *Eur. J. Org. Chem.* **2013**, 3574–3589.

step using the primary amine (Scheme I.85). The solution-phase synthesis could be applied for gram scale synthesis of short oligomers (dimers and trimers).

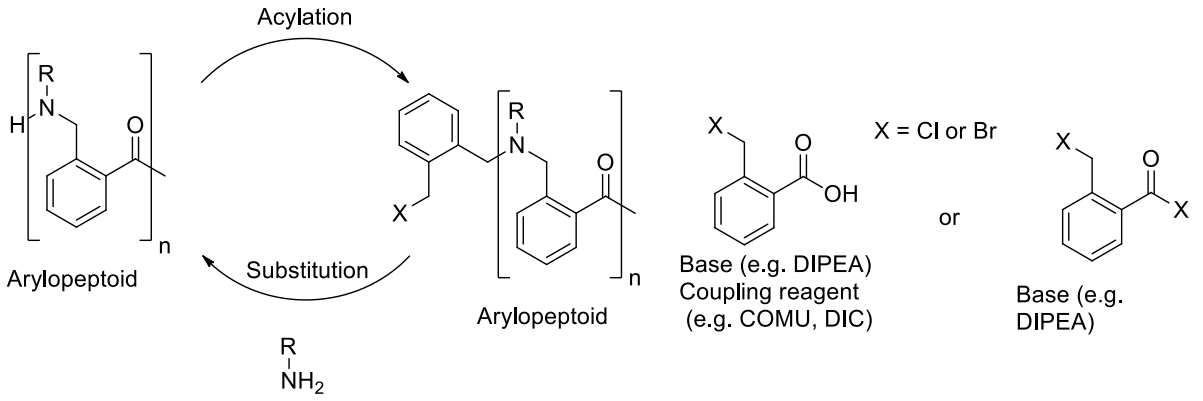

Scheme I.85. Synthesis of *ortho*-arylopeptoids in solution.

The synthesis on solid-phase also results in higher yield using the same procedure of that used for *meta*- and *para*- but was more efficient on rink acid in the case of *ortho*-arylopeptoids (Scheme I.86). The same conditions also could be applied to synthesize the *ortho*-arylopeptoids on rink amide and it was observed in high crude yields.

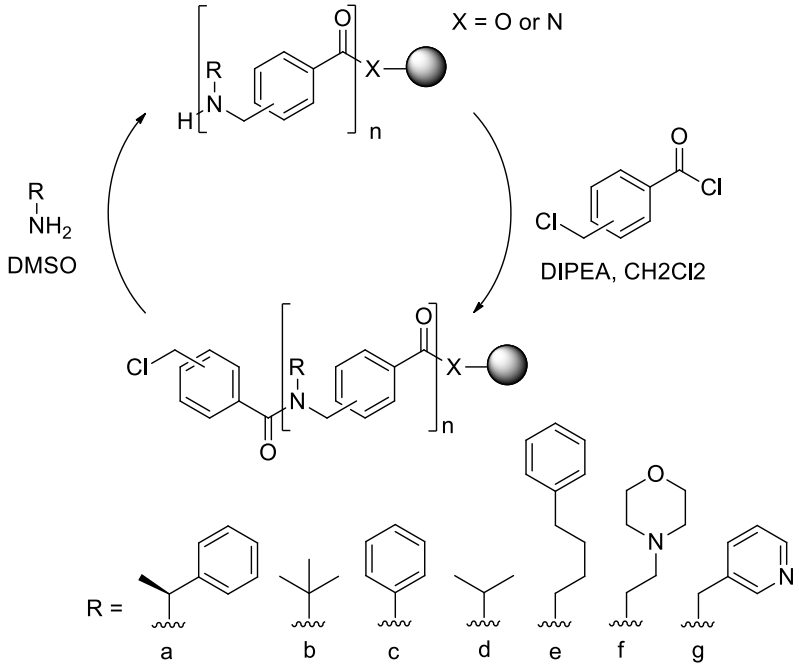

Scheme I.86. Improved solid-phase synthesis of arylopeptoids and some of the side chain diversity available.

I.B.3.1.2. Structuration

The conformational studies using NMR was done on *ortho*-, *meta*- and *para*-arylopeptoid models to evaluate the *cis*-*trans* preferences of the backbone *N*,*N*-disubstituted amide depending on the side chain.[106,156,157] 100% cis confirmation was obtained with *tert*-butyl side chain and 100% trans confirmation in the presence of phenyl as a side chain whatever the

[157] (a) Gillis, E. P.; Eastman, K. J.; Hill, M. D.; Donnelly, D. J.; Meanwell, N. A. *J. Med. Chem.* **2015**, *58*, 8315–8359. (b) Hunter, L.; *Beilstein J. Org. Chem.* **2010**, *6*, 38.

backbone substitution in *ortho*, *meta* and *para* (Figure I.17). However, NMR showed that there is more restricted rotation around the amide bonds for *ortho*-oligomers than for their *para*- and *meta*- counterparts.

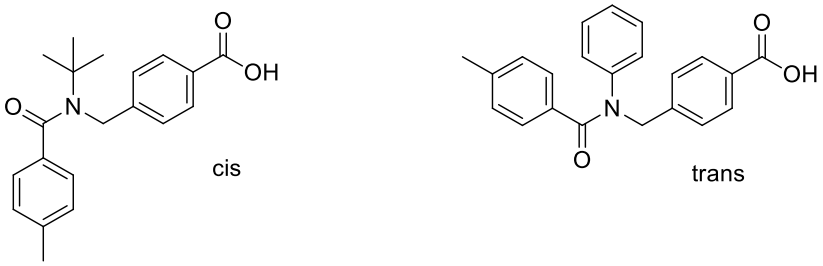

Figure I.17. Side chains exerting a complete control over of the conformation of the amide in cis or trans in a *para*-arylopeptoid model.

Actually, no particular secondary structure was identified for linear arylopeptoids. Conformational restriction by macrocyclisation was therefore studied and has led to conformationally well-defined macrocycles. Reported studies about cycloarylopeptoids will be presented in Chapter V.

I.B.3.1.3. Applications

All the applications of arylopeptoids were mentioned in the review below.

I.B.3.2. Benzylopeptoids

I.B.3.2.1. Synthesis methods

De Riccardis introduced benzylopeptoids as a new family of extended macrocyclic peptoids. *N*-alkylaminomethyl phenylacetate monomer replaced the *N*-alkylamino acetyl unit of the peptoid backbone, thus forming the benzylopeptoid.[158] The monomer approach was used to synthesize the benzylopeptoids on solid-phase. The three different substituted monomers were synthesized using two routes. After the protection of the carboxyl group in the *para*- and *meta*- isomers using the methyl group, the amination reaction in the presence of excess of methoxymethylamine was applied to form the free amines. The deprotection of the carboxyl group by the hydrolysis with lithium hydroxide followed by the protection of the amino groups yields the para- and *meta*- monomer in 46% and 44% yields, respectively (Scheme I.87).

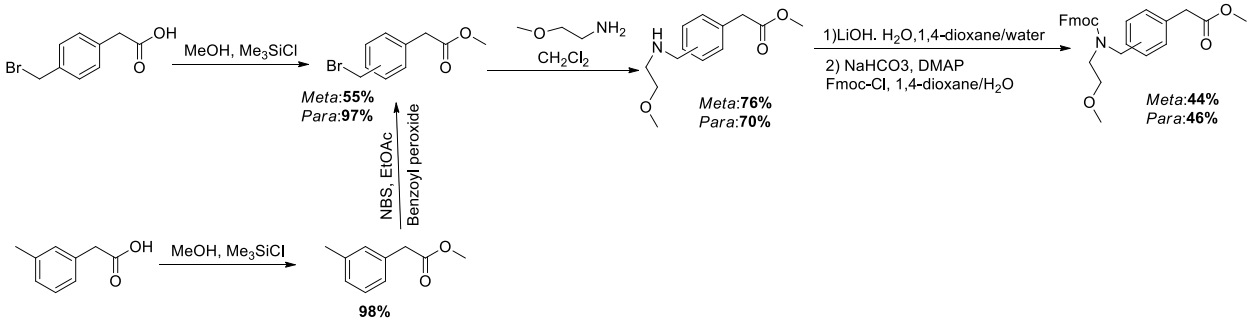

Scheme I.87. Synthesis of *meta*- and *para*- benzylopeptoid monomers.

The second route used for the synthesis of ortho-monomers implies the protection of the carboxyl group with t-butyl ester to prevent possible base-induced intramolecular macrolactamization. Then, the radical bromination and subsequent SN_2 halogen displacement,

[158] Meli, A. ; Gambaro, S.; Costabile, C.; Talotta, C.; Della Sala, G.; Tecilla, P.; Milano, D.; Tosolini, M.; Izzo, I.; De Riccardis, F. *Org. Biomol. Chem.* **2016**, *14*, 9055–9062.

in the presence of methoxyethylamine, followed by the Fmoc protection and deproptection of the carboxyl group afforded the *ortho*-monomer with 25% yield (Scheme I.88).

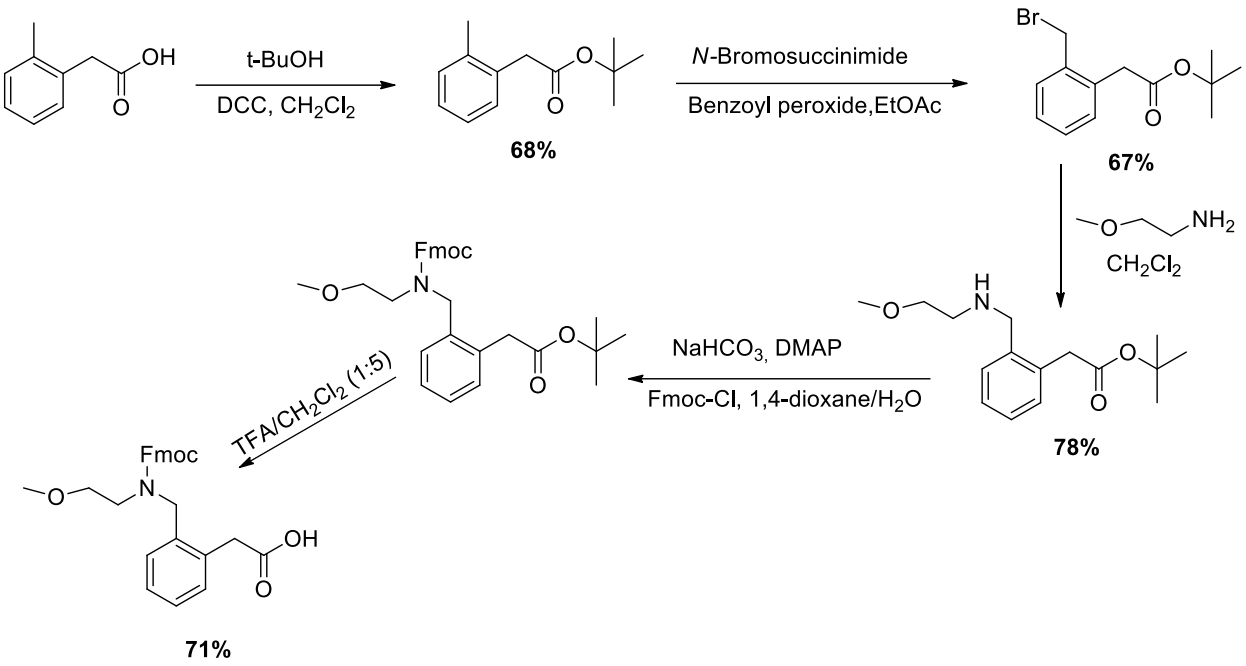

Scheme I.88. Synthesis of *ortho*-benzylopeptoid monomer.

After the synthesis of the Fmoc protected monomers, the oligomers were synthesized on the 2-chlorotrityl resin with excellent yield of coupling (>98%). The trimers and tetramers of the different isomers were synthesized in good overall yield (60-84%). Then, the crude oligomers were cyclized in DMF in the presence of HATU and DIPEA in high dilution ($3*10^{-3}$M) to furnish the cyclized trimers and tetramers in good yields ranging between 32% to 72% (Scheme I.89).

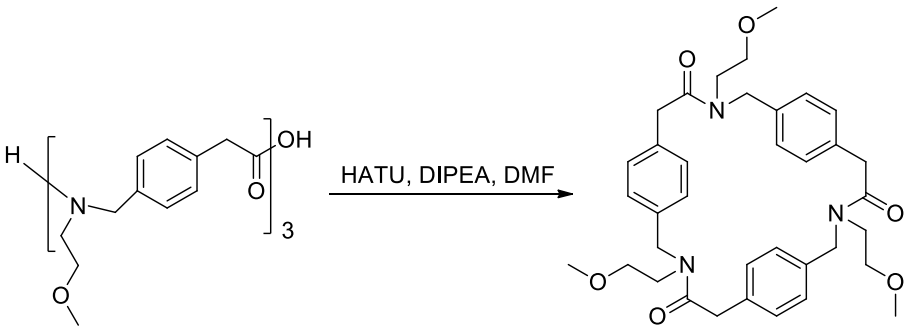

Scheme I.89. Macrocyclization of the linear trimer.

I.B.3.2.2. Applications

The complexing studies of the macrocyclic benzylopeptoids shows its efficiency as host due to its cation complexation properties.[158] Also, the ionophoric activity of these molecules was studied and shows their inactivity as a transporter.

I.B.3.3. Azole-peptoids

I.B.3.3.1. Synthesis methods

In 2012, Kodadek introduced heteraromatics such as oxazoles, thiazoles, furanes and pyrazines into the peptoid backbone.[159] Thus, the submonomer method using free acid activated with COMU in the acylation steps was used to synthesize trimer azole peptoids with isolated yields ranging from 13 to 63%. Then, Fuller introduced the synthesis of azole peptoids as *N*-substituted azole homooligomers.[108] The solid phase submonomer method was used in the synthesis of azole peptoids, by replacing the bromoacetic acid with the functionalized azole in the acylation step. The synthesis starts with the addition of azole (thiazole or oxazole) to the 2-chlorotrityl resin in the presence of DIPEA in dichloromethane, followed by the substitution with the addition of amine at 50°C. After the synthesis of the first monomer, the acylation was modified by the addition of COMU as a coupling reagent, and the same cycle of acylation and substitution was continued to produce trimers with good isolated yields up to 61% (Scheme I.90).

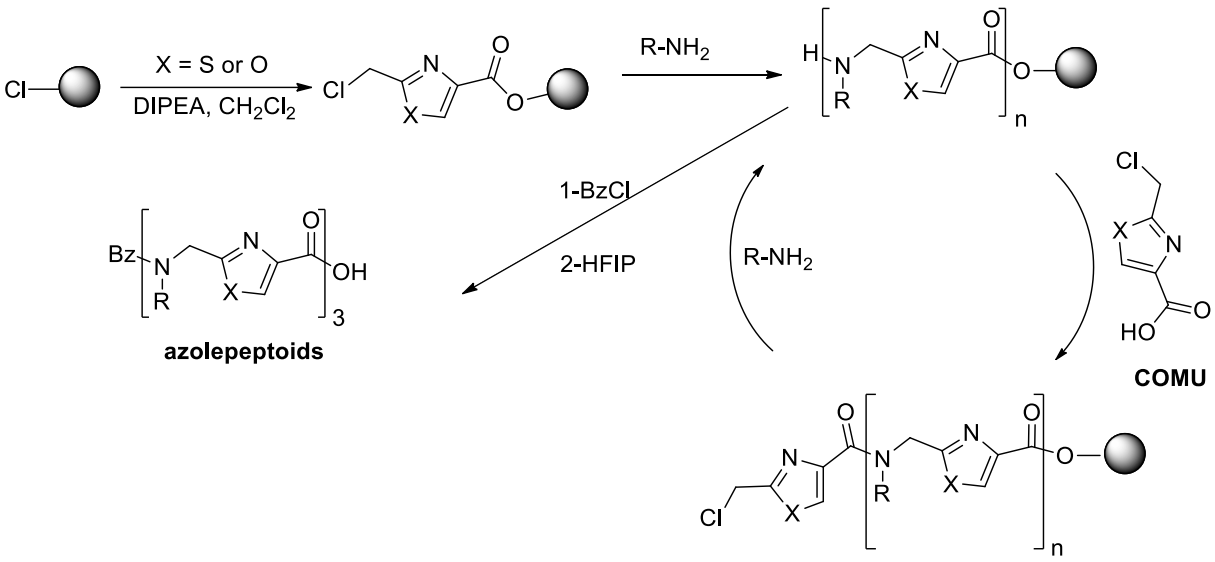

Scheme I.90. Synthesis of azole peptoid homooligomers.

I.B.3.3.2. Applications

The azolepeptoid is an attractive scaffold for a range of uses due to its similarities with the azole-rich natural products. Fuller proves its application for coordinating to transition metals in water.

Convenient synthesis methods are now in place to access this different type of *N*-alkylated aromatic oligoamides, particularly by the submonomer strategy but the potential applications of this class of aromatic oligoamides in drug discovery or material science are still understudied

I.B.4. CuAAC in α-peptoids and related family members.

Click chemistry based on the CuAAC reaction has been widely used in peptide-based drug research in the last two decades.[160] The selectivity, efficiency and mild conditions of CuAAC

[159] Aditya, A.; Kodadek, A. *ACS Comb. Sci.* **2012**, *14*, 164–169

[160] (a) Li, H.; Aneja, R.; Chaiken, I. *Molecules* **2013**, *18*(8), 9797-9817. (b) Castro, V. ; Rodriguez, H.; Albericio, F. *ACS Comb. Sci.* **2016**, *18*, 1, 1–14. (c) Agrahari, A. K.; Bose, P.; Jaiswal, M. K.; Rajkhowa, S.; Singh, A.S.; Hotha, S.; Mishra, N.; Tiwari, V. K. *Chem. Rev.* **2021**, *121*, 7638–7956.

make it a convenient way to link functional groups to the peptides and to achieve peptide cyclization.[161] Also, its structural similarity makes it efficient to introduce a surrogate of amide and disulfide bonds, in addition to mimic or promote the secondary structure of peptides that could be caused by the triazoles.[162] The various functional groups introduced by the triazoles such as carbohydrates, polyethylene glycol, and radiolabeling/photolabeling reagents, can efficiently increase the functionality of peptides.[163]

I.B.4.1. CuAAc on solid support.

CuAAC click reaction on solid support was first introduced by Meldal in 2002 for the synthesis of peptides (Scheme I.91).[164] The original procedure uses Copper Iodide (2 equivalents) as a catalyst in presence of Hünig base (50 equivalents).

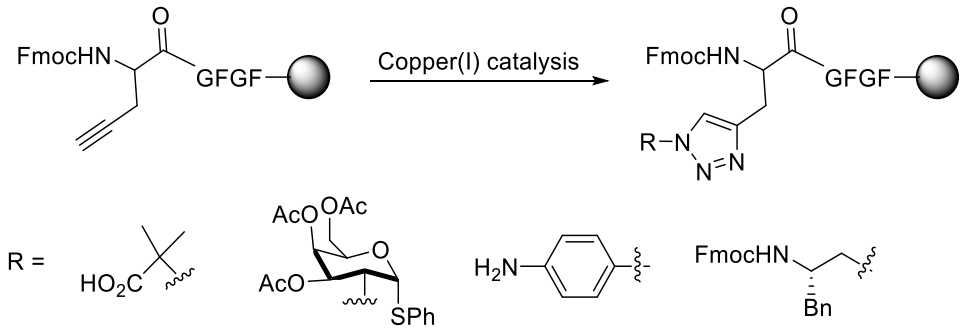

Scheme I.91. CuAAC on solid support by Meldal.

By analogy with peptides, similar and modified procedures were applied for the click chemistry of peptoids on solid support, with most of these conditions applying high quantity of Copper and other additives.[160b] For example, in 2006, Kirshenbaum applied click chemistry on peptoids on rink amide resin, by adding 40 equiv. of CuI, 20 equiv. of ascorbic acid, 50 equiv. of DIPEA and 21 equiv. of the alkyne in DMF-pyridine (7:3; v/v).[165] The reaction proceeded with 95% conversion and sequential cycles of click chemistry could be done to result in 75% crude yield purity by HPLC. Bräse applied multivalent click chemistry on solid support using 5 equivalences of CuI, 50 equivalences of DIPEA, 12 equivalences of azide in THF for 18h at room temperature. These conditions yield 1% of the desired product on both Rink amide and 2-chlorotrityl resin after HPLC purification (Scheme I.92).[166]

[161] (a) Turner, R. A.; Oliver, A. G.; Lokey, R. S. *Org. Lett.* **2007**, *9*, 5011−5014. (b) Li, H.; Aneja, R.; Chaiken, I. *Molecules* **2013**, 18, 9797−9817. (c) Vlieghe, P.; Lisowski, V.; Martinez, J.; Khrestchatisky, M. *Drug Discovery Today* **2010**, *15*, 40−56.

[162] (a) Franke, R.; Doll, C.; Eichler, J. *Tetrahedron Lett.* **2005**, *46*, 4479−4482. (b) Proteau-Gagne, A.; Rochon, K.; Roy, M.; Albert, P.-J.; Gue´rin, B.; Gendron, L.; Dory, Y. L. *Bioorg. Med. Chem. Lett.* **2013**, *23*, 5267−5269.

[163] Holub, J. M.; Kirshenbum, K. *Chem. Soc. Rev.* **2010**, *39*, 1325-1337.

[164] Tornøe, C. W.; Christensen, C.; Meldal, M. *J. Org. Chem.* **2002**, *67*, 3057−3064.

[165] Holub, J. M.; Jang, H.; Kirshenbum, K. *Org. Biomol. Chem.* **2006**, *4*, 1497–1502.

[166] Vollrath, S. B. L.; Fürniss, D.; Schepers, U.; Bräse, S. *Org. Biomol. Chem.* **2013**, *11*, 8197−8201.

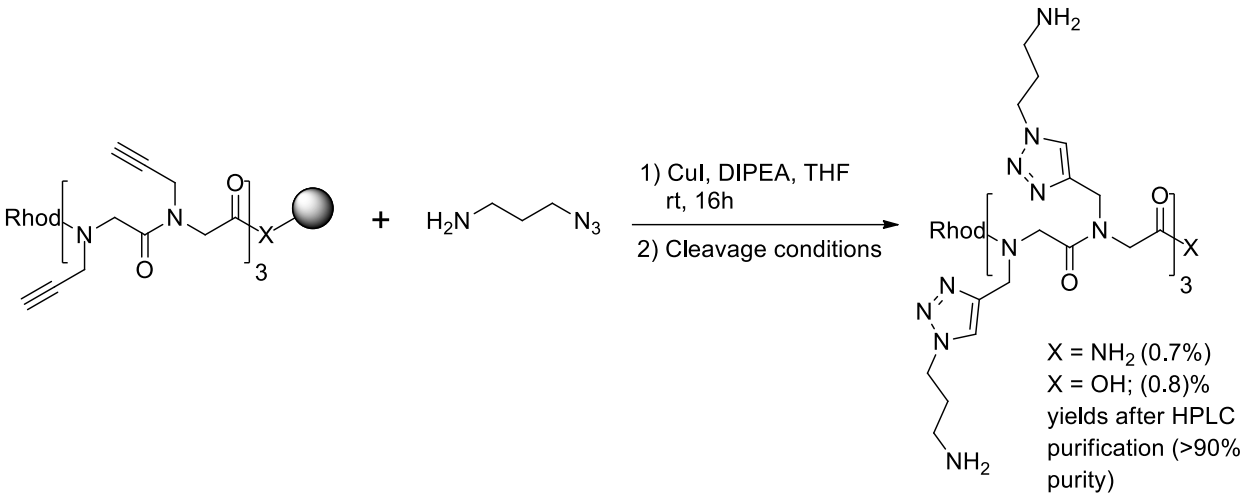

Scheme I.92. Synthesis of linear hydrophilic peptoids.

In 2013, Förniss synthesized the glycosylated peptoids using multivalent click chemistry.[167] After synthesis of the peptoid backbone on 2-chlorotrityl chloride resin, multivalent CuAAC was carried out by using 1.85 equivalence of $Cu(CH_3CN)_4PF_6$ in THF with 8.4 equivalence of 2,6-lutidine as base in the presence of 7 equivalence of the azido sugar (Scheme I.93). The full conversion was observed after 18 h at room temperature and 19% of the desired poly-triazole was isolated after the cleavage using 33% HFIP in CH_2Cl_2.

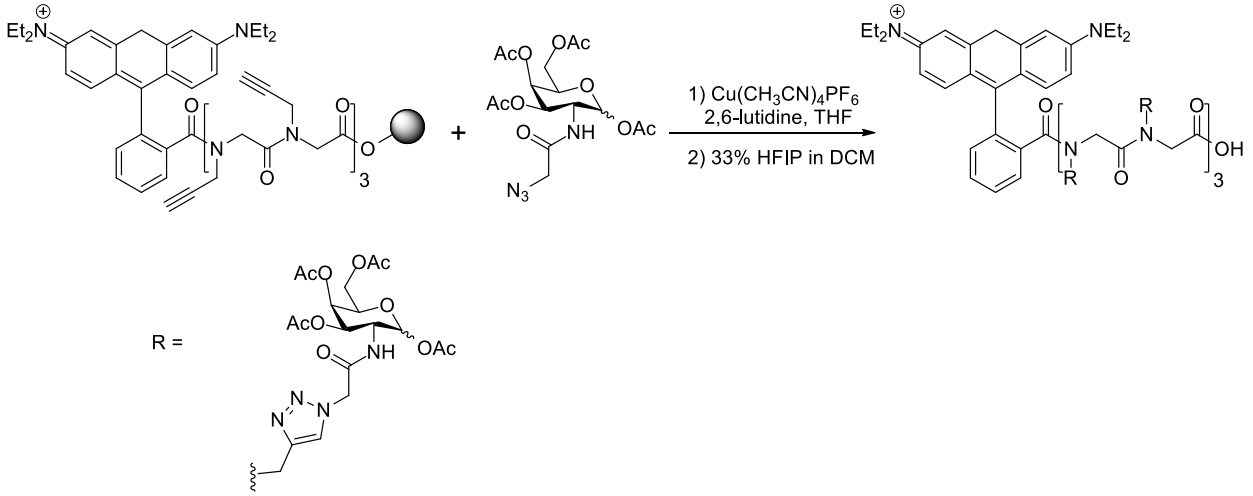

Scheme I.93. Synthesis of hexaglycosylated peptoid by CuAAC.

Bräse describes an improved procedure of the multivalent click chemistry of peptoids on solid support. In this procedure 0.2 equivalence of $Cu(CH_3CN)_4PF_6$, 0.2 equivalence of 2,6-lutidine in dry THF under argon atmosphere were used. After 2 days at 40°C, the conversion of 92 % was obtained.

All these studies are pointing the necessity to use a very large excess of catalyst which is opposite to what is used for standard solution protocols.

[167] Förniss, D.; Mack, T.; Hahn, F.; Vollrath, S. B. L.; Koroniak, K.; Schepers, U.; Bräse, S. *Beilstein J. Org. Chem.* **2013**, *9*, 56−63.

I.B.4.2. CuAAc in solution.

The CuAAC reaction was also applied on peptoids in solution. The conditions were less harsh than that on solid support, but it still uses a large amount of copper and several other additives. The CuAAC has been studied for the macrocyclization of linear peptoids in solution, through installing alkyne and azide as side chains. In 2008, our group introduced the CuAAC of peptoids in solution for the first time. The cyclic peptoid was dissolved in *t*-BuOH/H_2O and 5 equivalents of Benzyl azide was added in the presence of 4 mol% $CuSO_4$,12% ascorbic acid and 4% TBTA under argon atmosphere (Scheme I.94).[168] Then, another example was shown in 2012 by the addition of 0.08 equivalence of CuSO4 in the presence of 0.24 equivalence of ascorbic acid and 2 equivalences of azide, all mixed in tert-BuOH (0.1 M) at rt under Ar atmosphere.[115a] This reaction yields up to 88% of the triazole after flash chromatography on silica gel.

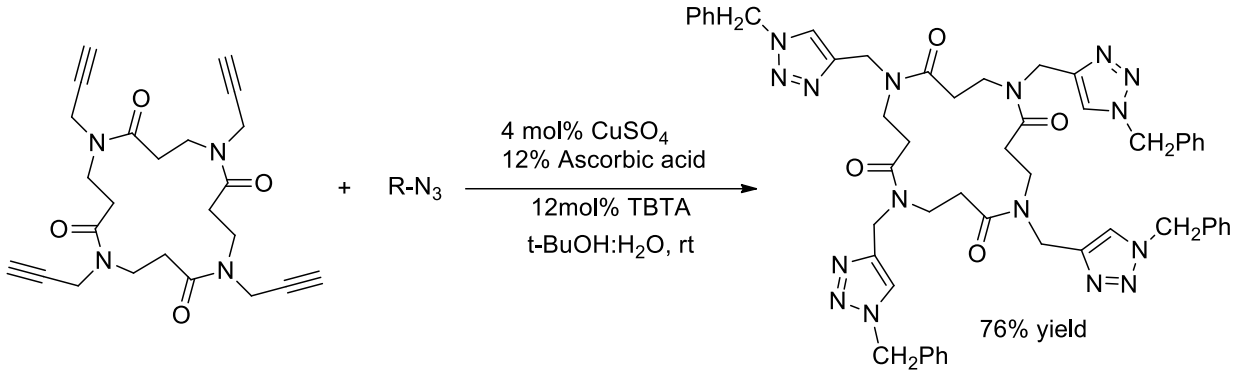

Scheme I.94. First poly-CuAAC of peptoids in solution.

Kirshenbaum also applied CuAAC in solution by the addition of 2 equivalents of 2,6-Lutidine, 0.5 equivalence of $Cu(CH_3CN)_4PF_6$ into MeOH/CH_2Cl_2 (1:1, v/v) solution with 0.5 mM of the peptoid macrocycle.[169] The complete conversion was observed after 2 days at room temperature. Recently, the same conditions were applied by Bräse to synthesize tube-like structure from peptoid macrocycles in dry CH_2Cl_2 for 3 days.[170] The isolated yield was only 7% of the tube-like molecules (Scheme I.95).

[168] Roy, O.; Faure, S.; Thery, V.; Didierjean, C.; Taillefumier, C. *Org. Lett.* **2008**, *10*, 5, 921–924.

[169] Vollrath, S. B. L.; Bräse, S.; Kirshenbaum, K. *Chem. Sci.* **2012**, *3*, 2726-2731. B) C. N. Herlan, K. Sommer, P. Weis, M. Nieger and S. Bräse, *Molecules* 2021, **26**, 150.

[170] Herlan, C. N.; Sommer, K.; Weis, P; Nieger, M.; Bräse, S. *Molecules* **2021**, *26*, 150.

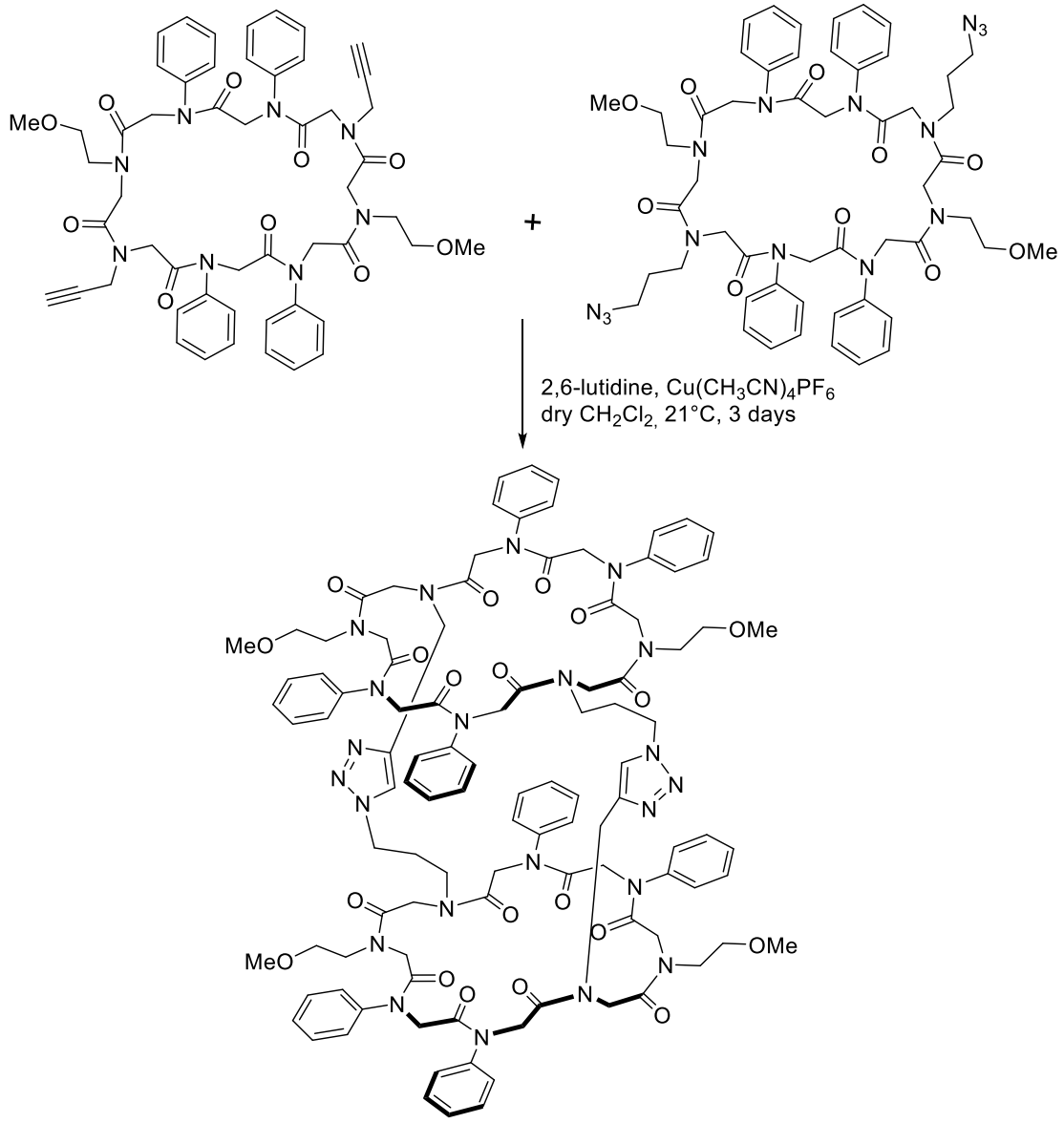

Scheme I.95. Tube-like structure synthesized by Bräse.

Recently, our group also applied CuAAC in solution for linear peptoids.[171] The reaction was done using the traditional conditions of click[172] and a high yield of triazoles was isolated after column chromatography purifications.

[171] Aliouat, H.; Caumes, C.; Roy, O.; Zouikri, M.; Taillefumier, C. ; Faure, S. *J. Org. Chem.* **2017**, *82*, 2386−2398.
[172] Rostovtsev, V. V.; Green, L. G.; Fokin, V. V.; Sharpless, K. B. *Angew. Chem., Int. Ed.* **2002**, *41*, 2596-2599.

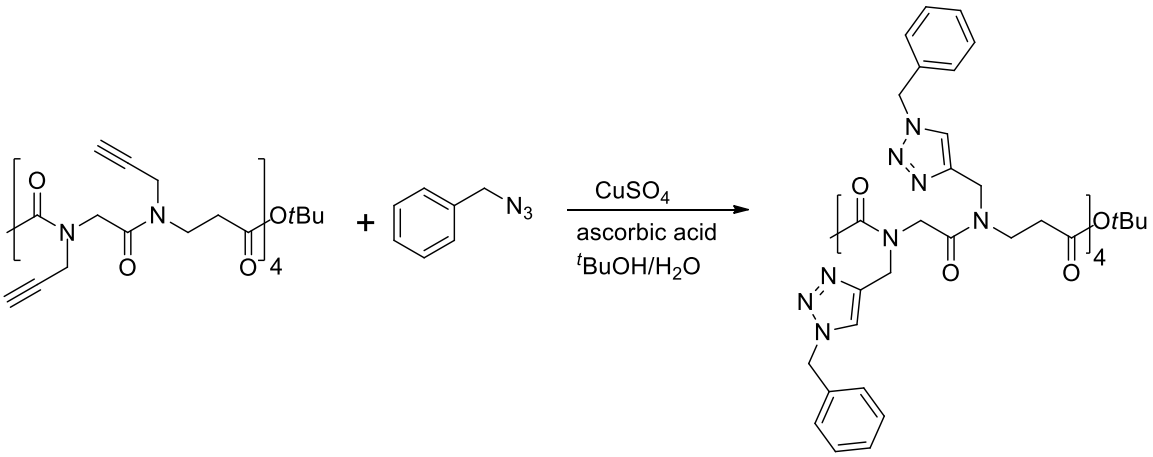

Scheme I.96. CuAAC of linear peptoids in solution.

I.B.5. Associated publication.

My PhD principal topic concerned *N*-substituted aminomethyl benzamides also named arylopeptoids. They can be regarded as extended peptoid oligomers incorporating aryl groups into the backbone but they primarily belong to the class of *N*-substituted aromatic oligoamides. We thought therefore to review the field of this particular type of aromatic oligoamides. In this review, we discuss about their different classes, their synthesis, their foldameric properties and their applications. This mini-review was submitted soon after the first covid-19 lock-down.

Reference: Akhdar, A., Gautier, A., Hjelmgaard, T. and Faure, S. *N*-Alkylated Aromatic Poly- and Oligoamides, *ChemPlusChem* **2021**, *86*, 298-312. DOI: 10.1002/cplu.202000825

Authors file is provided here after

* *N*-Alkylated Aromatic Poly- and Oligoamides

Ayman Akhdar,[a] Dr. Arnaud Gautier,[a] Dr. Thomas Hjelmgaard,*[b] and Dr. Sophie Faure*[a]

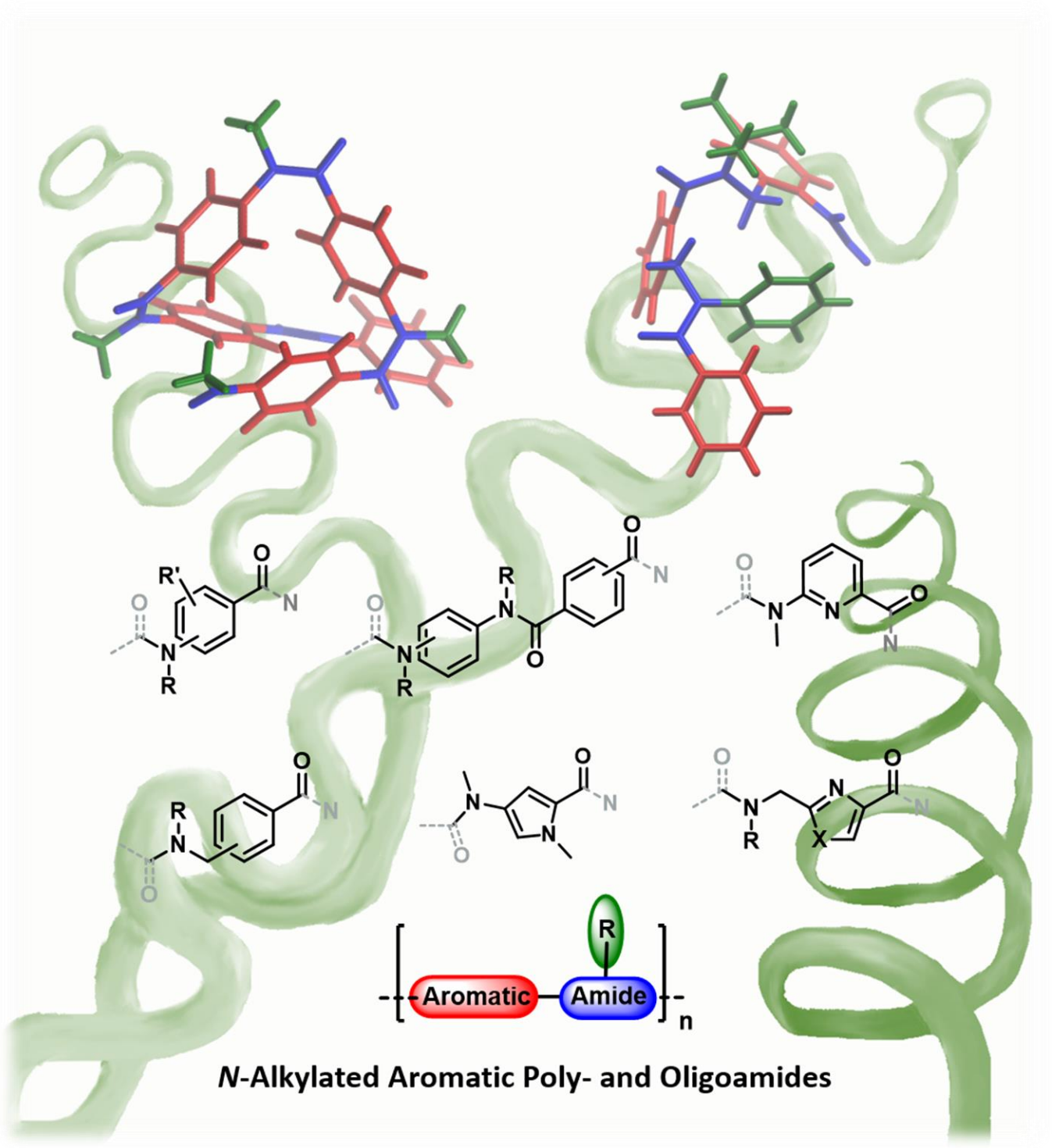

N-Alkylated Aromatic Poly- and Oligoamides

Ayman Akhdar,[a] Dr. Arnaud Gautier,[a] Dr. Thomas Hjelmgaard,*[b] and Dr. Sophie Faure*[a]

[a] Ayman Akhdar, Dr. Arnaud Gautier, Dr. Sophie Faure
Université Clermont Auvergne, CNRS, SIGMA Clermont, ICCF, F-63000 Clermont−Ferrand, France
E-mail: sophie.faure@uca.fr
[b] Dr. Thomas Hjelmgaard
Rockwool International A/S, Hovedgaden 584, 2640 Hedehusene, Denmark
E-mail: thomas.hjelmgaard@rockwool.com

Abstract: *N*-alkylated aromatic poly- and oligoamides are a particular class of abiotic foldamers that is deprived of the capability of forming intramolecular hydrogen-bonding networks to stabilize their tri-dimensional structure. The alkylation of the backbone amide nitrogen atoms greatly increases the chemical diversity accessible for aromatic poly- and oligoamides. However, the nature and the conformational preferences of the *N*,*N*-disubstituted amides profoundly modify the folding properties of these aromatic poly- and oligoamides. In this review, representative members of this class of aromatic poly- and oligoamides will be highlighted, among them *N*-alkylated phenylene terephthalamides, benzanilides, pyridylamides and aminomethyl benzamide oligomers. The principal synthetic pathways to the main classes of *N*-alkylated aromatic polyamides with narrow to broad molecular-weight distribution, or oligoamides with specific sequences, will be detailed and their foldameric properties will be discussed. The review will end with describing the few applications reported to date and the future prospects.

1. Introduction

Aromatic oligoamides constitute a particularly important class of abiotic foldamers with a high propensity to adopt well-defined conformations.[1] Many types have been designed that fold into secondary as well as tertiary structures owing to their highly constrained backbones. The most studied are oligoamides comprising benzene, pyridine and/or quinoline scaffolds with the amide connections arranged in either a “one-way sequence” manner using amino acid building blocks or in a symmetric manner using a combination of diamine and diacid building blocks (Figure 1). These oligoamides quickly proved to be highly conformationally stable, predictable and modular foldamers.[2] Their well-defined conformations arise from intramolecular hydrogen-bonding networks, restricted rotation about the aryl-amide bonds and the intrinsic rigidity and planarity of the aromatic units.[1a] The high predictability and the robustness of their tridimensional structuration have made aromatic oligoamides promising unnatural oligomers for applications in biological and material sciences. For example, α-helix or β-sheet-like foldamers exhibiting tailored functions have been designed to mimic or bind to protein surfaces.[3] Although the aromatic oligoamide backbones are inherently only distantly related to the parent peptides and proteins, the aim is still to mimic the side chain presentation of these biopolymers. To address this challenge, it is therefore necessary to increase the tunability of aromatic oligoamides. To introduce further chemical diversity, substitution of the aromatic entities was studied extensively but the synthetic access to the required diversely functionalized building blocks is time-consuming and can sometimes be particularly challenging.[1] Given that most of the aromatic oligoamides such as benzamide and pyridylamide oligomers are deprived of aliphatic carbons in their backbone, the remaining way to further enhance chemical diversity is alkylation of the backbone amide nitrogen (Figure 1).

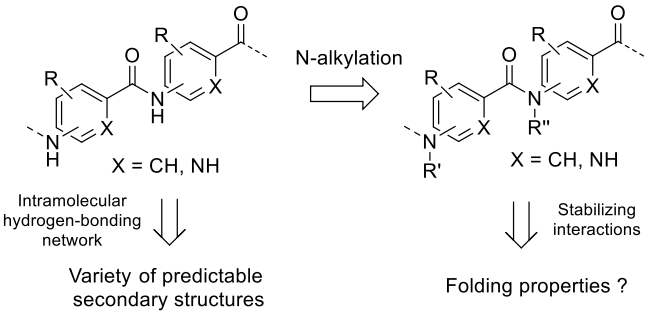

Figure 1. Schematic representation of aromatic oligoamides and their *N*-alkylated counterparts.

This strategy appears particularly appealing considering the large variety of side chains potentially accessible. However, the stabilizing interactions involving the amide protons that serve to restrict the rotation about the NHCO-aryl bond will unfortunately no longer be available. Indeed, local hydrogen bonding represents the most versatile means to block rotation about the CONH-aryl and NHCO-aryl bonds and lead to robust, well-defined secondary structures such as crescents and helices (Figure 2). For example, in *ortho*-connected benzamide oligomers, intramolecular hydrogen bonds between adjacent amide-NH and-CO groups lead to a planar arrangement of the substituents and formation of a linear strand structure of oligoanthranilamides as demonstrated by Hamilton and coll.[4] An exocyclic hydrogen-bond acceptor (such as an alkoxy group) at the ortho position on the aryl group was found to stabilize the anti-conformation through a six- or five-membered hydrogen-bonded ring.[5] This strategy was particularly efficient for the design of α-helix proteomimetics.[6] Based on the same principle, Gong and co-workers showed that a three-center hydrogen bonding system can exist and totally block rotation around the amide linkage.[7] Repetition of this motif into *meta*- and/or *para*-benzamide oligomers gave rise to rigid crescent and pseudo-cyclic structures with various curvatures. In aza-aromatic oligoamides such as pyridine and quinolone amide

oligomers, three-center hydrogen bonding systems are also the key of their robust and predictable secondary structures. [1]

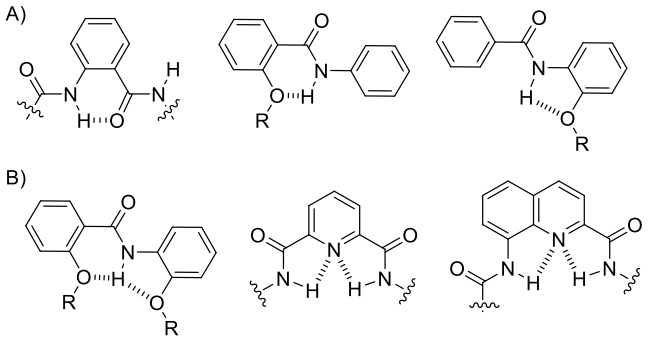

Figure 2. Examples of hydrogen bonding systems: A) two-center hydrogen bonding systems; B) three-center hydrogen bonding systems found in aromatic and aza-aromatic amide oligomers.

These examples show that the absence of the amide-NH group will considerably alter the foldameric properties of aromatic oligoamides. Besides this, *N*-alkylated aromatic oligoamides also have to deal with another major feature of the *N*,*N*-disubstituted amides; the low-energy rotameric *cis*/*trans* barrier.[8] Thus, while most secondary aromatic amides exhibit a *trans* conformation, *N,N*-disubstituted amides are prone to *cis*/*trans* isomerism (Figure 3). The preferred conformation depends on various steric and/or electronic interactions that take place between the backbone and the side chain on the nitrogen.

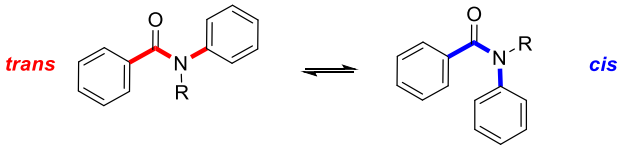

Figure 3. *Cis*/*trans* isomerism of *N*-alkylated aryl amides.

Thomas Hjelmgaard, obtained his PhD in total synthesis from the Technical University of Denmark (Prof. D.Tanner, 2005). He then continued as postdoctoral fellow within total synthesis (Prof. J. Nielsen, 2005), linear and macrocyclic peptides (Prof. D. J. Aitken, 2006), linear and macrocyclic peptoids (Prof. C. Taillefumier, 2008), and arylopeptoids (Prof. J. Nielsen). In 2012, he became assistant professor at the University of Copenhagen, working on arylopeptoid conctructs. In 2013, Thomas moved to an R&D position at Rockwool International, focusing on research within green chemistry.

Sophie Faure, studied chemistry at the University of Reims-Champagne-Ardennes where she received her PhD in organic photochemistry in 1999. As postdoctoral fellow, she worked with Prof. D. Enders in Aachen and at the faculty of pharmacy Paris-Descartes. She joined the CNRS in 2002 as Chargé de Recherche to work on natural macrocyclic peptides with Prof. D.J. Aitken. In 2007, she turned her interest towards the synthesis and study of the foldameric properties of α-peptoid oligomers and related family members such as β-peptoids and arylopeptoids.

This review will focus on *N*-alkylated poly- and oligoamides. The main type of *N*-alkylated aromatic poly- and oligoamides developed to date will be reviewed. The various synthetic strategies used to access either polymers or oligomers will then be detailed, followed by the foldameric properties. At the end of the review, the applications reported in the literature and the future prospects will be discussed.

2. Classes of *N*-alkylated aromatic oligoamides

The *N*-alkylated aromatic poly- or oligoamides developed to date can be divided into different classes depending on the backbone aromatic or heteroaromatic ring nature, the mono- or bi-directional amide arrangement and the presence or absence of aliphatic carbons in the backbone (Figure 4).

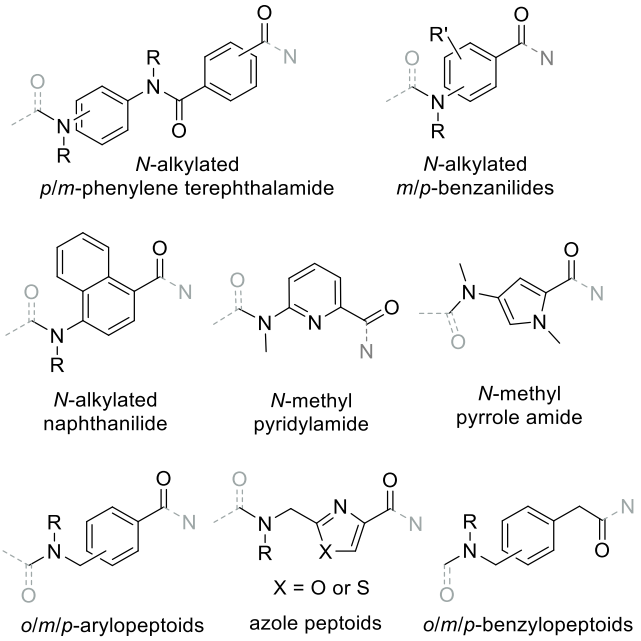

Figure 4. Some classes of *N*-alkylated oligoamides developed in the literature.

The first example of *N*-substituted aromatic amide repeating sequences appeared back in the 1980s in the polymer field with the study of poly(*m*- or *p*-phenylene terephthalamide) derivatives to modulate the physical properties of Kevlar® (poly(*p*-phenylene terephthalamide, PPTA) and Nomex® (poly(*m*-phenylene terephthalamide, MPDI), and in particular in an attempt to increase the solubility of these types of polymers.[9] *N*-substituted PPTA and MPDI are composed of alternating symmetric aryl diacid and aryl diamine residues with *para* and *meta* substitution patterns, respectively (Figure 4). and can be obtained by direct polymerization of secondary aromatic diamines and terephthaloyl chloride or by alkylation of the formed PPTA (section 3.1).
Introduced ten years later by Shudo and co-workers,[10] *N*-alkylated benzamides represent one of the most studied type of *N*-substituted aromatic oligoamides (Figure 4). Various *meta*-[11] and *para*-oligobenzamides[10] were studied, including mixed

backbones.[12] Although more difficult to obtain, the conformational preference of *ortho*-connected benzanilides have been studied by the Clayden group.[13] However, the synthetic methods developed to access these oligobenzamides in general do not allow for the preparation of chemically defined oligomers.
In spite of the wide structural diversity that is potentially available by the introduction of various side chains on the nitrogen of the backbone amides, this approach is thus far less exploited than for other classes of *N*-alkylated oligoamides such as peptoids (*i.e.* oligomeric of *N*-substituted glycines).[14] Indeed, mainly homooligomers have been studied and only scarce examples of heterooligomers have been reported.[15] The secondary structures adopted by these oligomers have been studied in detail and some of them were shown to exhibit helical conformations (section 4.2).[16] Among anilide-type oligomers, the more hindered *N*-alkylated oligo-1,4-naphthanilide have also briefly been addressed but a preferred structuration could not be evidenced (Figure 4).[16b] Pyridine-containing *N*-methyl heteroaromatic amides were studied by Okamoto and co-workers. The hydrogen bond acceptor ability of the pyridine ring was exploited to design aromatic oligoamides that were conformationally switchable under exposure to external stimuli (section 5).[17] Inspired by the structure of natural oligoamides, netropsin and distamycin A that bind in the minor groove of DNA,[18] polyamides containing *N*-methylpyrrole amino acids were also studied.[19] Tanatani and co-workers have recently explored the conformational preferences of the *N*-alkylated amide bonds on the pyrrole group in heterooligomers containing both pyrrole and arene rings.[20] More related to *N*-alkylated benzamides, oligomeric *N*-substituted aminomethyl benzamides, or arylopeptoids, possess a backbone-methylene group adjacent to the phenyl ring. In connection with their pioneering work on peptoids,[14] Zuckermann and co-workers briefly mentioned the synthesis of such oligomers in few patents back in the 1990's,[21] but arylopeptoids were further developed by other groups taking advantages of the great chemical diversity available by variation of the substituents on the nitrogen.[22] The replacement of the phenyl group by heteroaromatic rings such as thiazole and oxazole led to azole peptoid-type oligomers.[23] The addition of a second backbone-methylene between the aromatic and the acid function resulted in benzylopeptoids which were briefly studied by De Riccardis and co-workers to access macrocycles with complexing properties.[24]

3. Synthesis of *N*-alkylated aromatic poly- and oligoamides

This section describes the principal synthetic pathways to the main classes of *N*-alkylated aromatic poly- or oligoamides.
The synthetic approaches leading to polymers with broad to narrow molecular-weight distribution are detailed in section 3.1 (Alkylation of polyamides and direct polymerization) and those leading to oligoamides with precise and defined sequences are detailed in sections 3.2 (Monomer synthesis) and 3.3 (Submonomer synthesis).

3.1. Alkylation of polyamides and direct polymerization

N-substituted poly(m-phenylene terephthalamide) were originally prepared by polycondensation of symmetrical *N*,*N'*-disubstituted diamines and arylene diacid chlorides but suffer from the poor solubility of the formed polymers and the lability of the secondary diamines at high temperature leading to polyamides with broad molecular-weight distribution.[9b] This method was rapidly replaced by alkylation of poly(*p*-phenylene terephthalamide) (PPTA) or poly(*m*-phenylene terephthalamide) (MDPI) with a selected alkyl or aryl halide *via* a metalation reaction.[9a] However, the major issue is achieving full completion of the reaction in order to obtain homogeneous *N*-substituted polymers.[25] A high degree of alkylation and aralkylation could be obtained by using sodium methylsulfinylmethylide in dimethyl sulfoxide as solvent, improving the solubility of the *N*-metalated PPTA compared to sodium in liquid ammonia (Scheme 1).[9a] Applying these conditions, a panel of alkyl or aryl halides, bromo acetic acid, propylene oxide and acrylonitrile were used as reagents for the *N*-alkylation reaction.[9a, 26] A high degree of substitution (86 to 100%) was observed for PPTA polymers with both low and high average molecular weights (4100 and 24 000 g.mol^{-1}), except for 9-anthrylmethyl and carboxymethyl substituents. However, this method of access could not provide polyamides with narrow polydispersity.

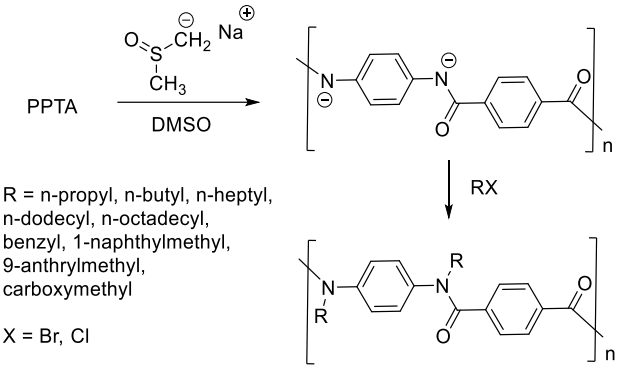

Scheme 1. Alkylation of poly(p-phenylene terephthalamide).

To access polymers of *N*-alkylated benzamides with a polydispersity (M_w/M_n) close to 1, Yokozawa and co-workers have developed a chain-growth polycondensation process[27] using phenyl aminobenzoate derivatives.[28] To provide aromatic polybenzamides having precisely controlled molecular weights and quite narrow molecular weight distributions (MWD), the process relies on the use of a small amount of reactive initiator and the formation of a polymer with more reactive end groups than the monomer to avoid step-growth polycondensation. Thus, an *N*-alkylated *p*-benzamide polymer with high molecular weight (M_n = 10 000 g.mol^{-1}) and narrow distribution (M_w/M_n = 1.12) was synthesized using *N*-triethylsilyl-*N*-octyl aniline in presence of cesium fluoride as base to deprotonate the phenyl 4-(alkylamino)benzoate building blocks. A highly reactive anilide anion is then formed while the ester group in the *para* position undergoes a strong deactivating effect (Scheme 2).[29] Phenyl 4-nitrobenzoate as initiator is therefore required to enable the formation of the first amide bond. The propagation is then ensured by reaction of the reactive monomer with the ester of the growing chain. Shortly thereafter, Ueda and co-workers reported a similar polycondensation process with the metal amide anion of 4-(*N*-octylamino)benzoylbenzoxazolin-2-thione generated using EtMgBr in the presence of LiCl and *p*-nitrobenzoyl chloride as initiator.[30] *N*-octyl *p*-benzamide polymers with M_n ranging from 4 700 to 20 100 g.mol^{-1} were prepared using this new protocol with narrow distributions (M_w/M_n = 1.13-1.17).

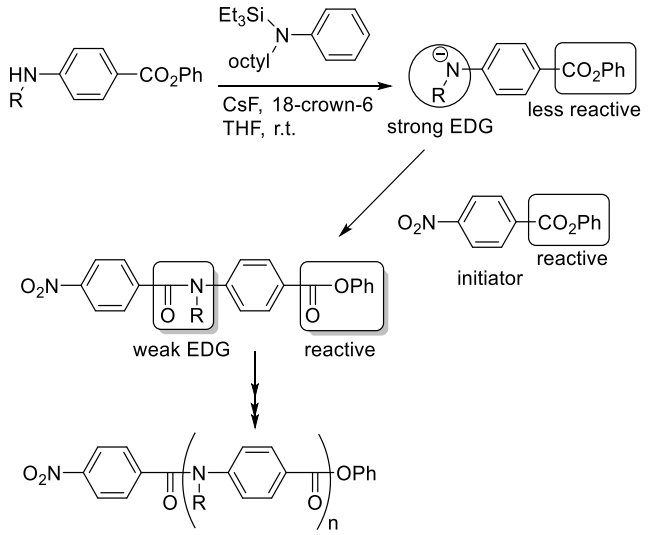

R = octyl, 4-octyloxybenzyl, (S)-2-(methoxyethoxyethoxy)propyl
EDG = electron donating group

Scheme 2. Chain-growth polycondensation to access *N*-alkylated poly(*p*-benzamides).

The same methodology is applicable to access poly(benzamides) of the *meta*-series since the inductive effect of the nucleophilic site is enough strong to deactivate the electrophilic site at the *meta* position of the monomer.[31] Nevertheless the use of a lithium amide base having bulky alkyl substituents (LiHMDS) was necessary in order to obtain polymers with narrow molecular weight distribution (M_n = 4 380 g.mol^{-1}; M_w/M_n = 1.27). The inclusion of a coordinating additive such as *N*,*N*,*N*′,*N*′-tetramethylethylenediamine (TMEDA) could furthermore be beneficial.[31b],[32] This type of polycondensation enables the synthesis of well-defined block copolyamides having different aminoalkyl side chains or different aryl substitution patterns (*meta* /*para*)[31a], [33] as well as telechelic poly(*p*-benzamide)s (*i.e.* reactive polymers possessing reactive functional groups at the chain ends)[34] and cross-linked star polymers with aromatic polyamide arms.[35] It is worth noting that this type of polycondensation in the absence of an initiator was efficiently applied to access aromatic oligoamide macrocycles such as calix[3]amides.[36] One drawback of the chain-growth polymerization is the difficulty of accessing high molecular weight polymers since only polyaramides up to 24 000 g.mol^{-1} could be formed. To this end, Kilbinger and coworkers have studied a modified procedure using highly reactive pentafluorophenol esters in a step-growth manner, enabling the preparation of polyaramides of up to M_n 50 000 g.mol^{-1} but with higher polydispersity (M_w/M_n = 2-3).[37]

A particularly appealing asymmetric polymerization catalyzed by planar−chiral cyclopentadienyl ruthenium complexes (I) followed by thiol-ene post-modification or ring-closing metathesis was developed by Onitsuka and co-workers to access optically active poly-*N*-alkoxyamides.[38] These are closely related to *N*-substituted poly(aminomethyl benzamide)s with one asymmetric center on the backbone (Scheme 3). However, conformational properties of these poly-*N*-alkoxyamides were not studied and the *N*-alkoxyamide groups were readily transformed to secondary amide groups by the reductive cleavage of N−O bonds.[39]

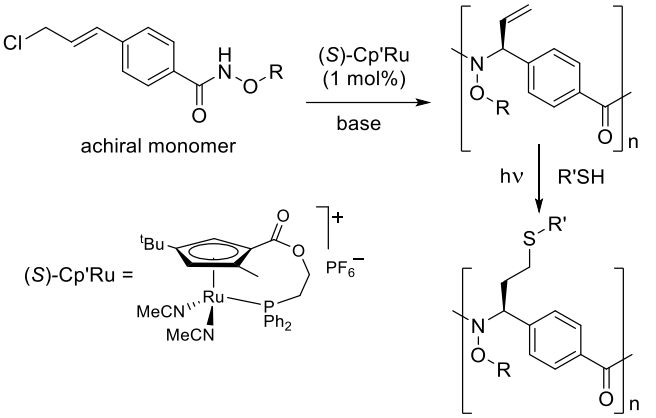

Scheme 3. Asymmetric polymerisation to access optically active poly-*N*-alkoxyamides.

Even though the chain-growth polymerization process has proven to be efficient to access *N*-alkylated polyamides with narrow polydispersity, only polyamides carrying one type of side chain or at the best two types of side chains in the case of block copolymers, can be obtained. The development of other synthetic pathways was necessary to prepare oligoamides with specific sequences and lengths.

3.2. Monomer synthesis

Short *N*-alkylated aromatic oligoamides with specific sequences were synthesized in solution by the successive introduction of selected monomers in a mono-directional manner. This was mostly achieved using *N*-protected *N*-alkylated monomeric aromatic derivatives, activating the carboxylic acid as the corresponding acid chloride prior to the coupling step. Various *N*-protecting groups were employed, comprising for example trifluoroacetate[40] and *o*- or *p*-nitrobenzenesulfonyl (nosyl) to access oligo(*p*-benzamide)s[41] and oligo(pyridyl amide)s (Scheme 4).[42]

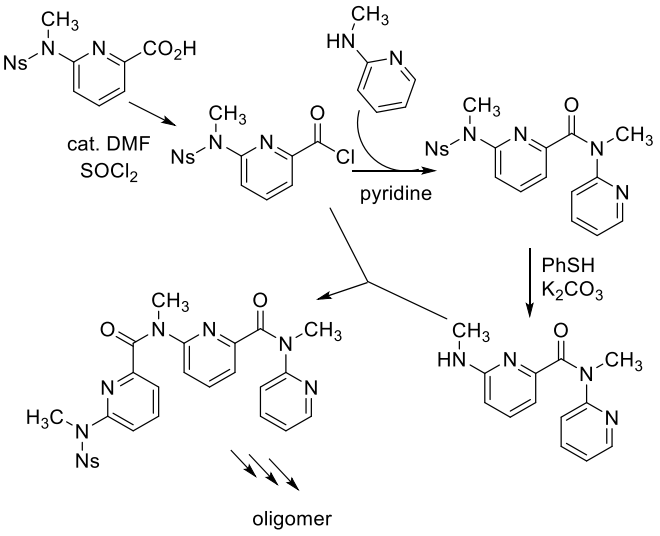

Scheme 4. Solution phase synthesis of a *N*-methyl oligoamide bearing pyridine 2-carboxamide.

The latter could also serve for the synthesis of secondary amines by means of Fukuyama's nosyl methodology.[41],[43] Even though this synthetic pathway is theoretically applicable to a wide variety of monomers, only a few side-chains have been studied and essentially only homooligomers have been prepared. A few groups have opted for the coupling of a primary amine usually obtained by reduction of nitroarene derivative, followed by alkylation using a selected alkyl halide. Using this approach, Clayden and co-workers have synthesized short oligomers of *o*-, *m*- and *p*-linked benzamides as well as of 1,4-naphthanilides with good to excellent yield for each step.[16b] This methodology was also employed by Tanatani to prepare *N*-methyl oligoamides with alternating arene and pyrrole rings but was less efficient.[20] Again, only one type of side chain was used to prepare the oligomer. To access longer oligomers, an efficient block-coupling approach was preferred as illustrated by Ueda and co-workers in the preparation of *N*-alkylated oligo(*p*-benzamide)s comprising up to sixteen residues.[40]

The monomer synthesis using acid chloride derivatives was also performed in a bi-directional manner to access symmetrical pyridine-containing *N*-methyl aromatic oligoamides[17c] and unsymmetrical *N*-methyl aromatic amide oligomers. [12a]

Kilbinger and coworkers were the first to describe the solid-phase synthesis of *N*-substituted oligo(*p*-benzamide)s up to decamer length using a Wang resin support and a Fmoc-based strategy. This strategy involves the acylation of a secondary aromatic amine by *N*-Fmoc- and *N*-PMB-protected *p*-amino benzoyl chloride or *N*-Fmoc-protected *N*-alkyl *p*-amino benzoyl chloride (Scheme 5).[15a] This methodology was used to access homooligomers and heterooligomers with, at best, two types of side chains.

Except for the first residue attachment, peptide-type coupling reagents proved to be inefficient even when using coupling reagents employed for the synthesis of aromatic amides (DBOP, TPP). Instead, activation of the acid as the corresponding acid chloride was achieved using thionyl chloride in NMP (Scheme 5).[15a] At the end of the iterative process, the oligomer was obtained by nucleophilic cleavage from the resin using hexylamine in toluene without loss of p-methoxy benzyl groups. The yield of the solid-phase synthesis was, however, not reported. A slightly modified methodology in which the acid chloride derivative was generated using bis(trichloromethyl)carbonate (triphosgene) instead of thionyl chloride was automatized using a commercial peptide synthesizer to access up to a 15-mer heterooligoamide in 54% overall yield (30 synthetic steps).[44]

A solid-phase strategy was also used to access series of *p*-benzamide trimers carrying various substituents on the nitrogen and also on the aryl ring.[15b,c] For the first time, the accessibility to diverse side chains was exploited. In these publications, the acid chloride was generated using 1-chloro-*N,N*,2-trimethyl-1-propenylamine (Ghosez's reagent)[45] in chloroform followed by addition of *N*-methylimidazole as base prior to the ensuing reaction. This solid-phase methodology was adapted to the use of a microwave assisted peptide synthesizer, allowing facile library generation of functionalized oligomers in excellent yield and good purity for a panel of hydrophobic side chains but an incompatibility of some side chains was observed.[46]

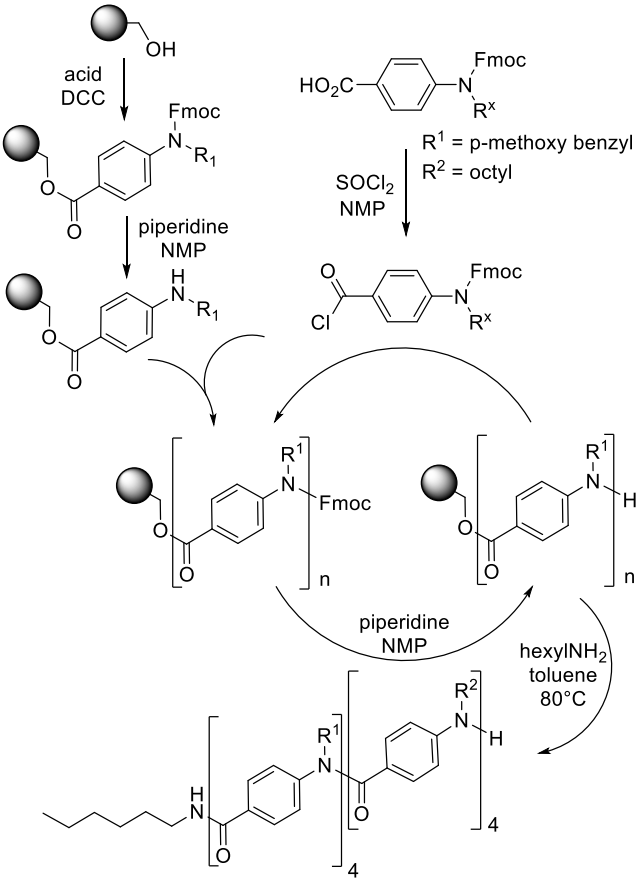

Scheme 5. Solid-phase synthesis of heterooligomers of *N*-substituted *p*-benzamides carrying two types of *N*-substituents.

To the best of our knowledge, synthesis on solid-support of *N*-alkylated *o*- or *m*-benzamide, naphtanilide, pyridylamide, pyrrole amide oligomers have not been reported in the literature. By contrast with other classes of *N*-alkyl aromatic oligoamides, classical Fmoc-based solid-phase peptide synthesis (SPPS) using HATU as coupling reagent could efficiently be performed to access benzylopeptoid trimers and tetramers on a 2-chlorotrityl chloride resin with yields ranging from 60 to 84%, prior to macrocyclisation to access cyclic compounds.[24] Monomer synthesis has not been applied to the preparation of arylopeptoids since the submonomer approach appears much more convenient as will be discussed in the following section.

3.3. Submonomer synthesis

The backbone structure of oligomeric *N*-substituted aminomethyl benzamides, or arylopeptids, allow for their synthesis *via* a unique "submonomer" method wherein each of the aromatic amide residues can be created in two steps directly on the growing chain (Scheme 6). This convenient iterative cycle comprises an acylation reaction with an activated chloro- or bromomethyl benzoic acid followed by a substitution reaction with a primary amine. The submonomer method thus enables complete control over the backbone sequence, and potentially provides access to highly diverse structures.

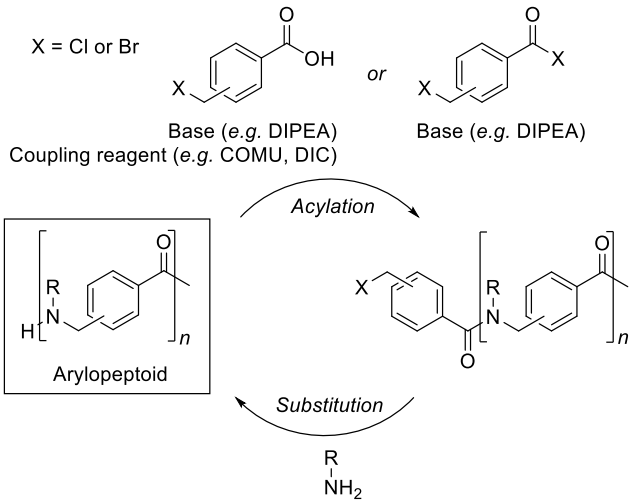

Scheme 6. Acylation and substitution steps in "submonomer" synthesis of arylopeptoids.

As previously mentioned, the first disclosure of arylopeptoids appeared in a series of patents in the mid to late 1990's.[21] A few pentameric *para*-arylopeptoids were synthesized on solid phase using the above submonomer method wherein 0.5 equiv. of *N,N'*-diisopropylcarbodiimide (DIC) was employed to activate the benzoic acid building blocks as their corresponding anhydrides. In 2007, Lokey and Combs disclosed the solid phase synthesis of a limited number of short oligomers (tetra- and pentamers) of *para*- and *meta*-arylopeptoids, activating the bromomethyl benzoic acid building blocks with 1.0 equiv. DIC.[22a] In 2011, the first solution phase synthesis of trimeric *para*- and *meta*-arylopeptoids was reported, using bromomethyl benzoyl bromides as the aromatic building blocks.[22b] Each acylation-substitution cycle was carried out in a one-pot procedure and the method is adaptable to gram-scale synthesis. Furthermore, head-to-tail coupling of suitably deprotected trimers in the presence of 1-Cyano-2-ethoxy-2-oxoethylidenaminooxy)dimethyl amino-morpholino-carbenium (COMU) as coupling agent gave access to arylopeptoid hexamers and nonamers.

After studying a range of conventional peptide coupling reagents, COMU was also found to be the most efficient reagent for submonomer synthesis of arylopeptoids on solid phase.[47] Both *para*- and *meta*-arylopeptoids with acid or amide groups at the *C*-terminus were synthesized, and the efficiency of the method was demonstrated by the synthesis of two model hetereo-dodecamer arylopeptoids in 25-27% yield and >99% purity (58-62% crude purity). Although generally broadly applicable, this method proved inadequate for the incorporation of very bulky side chains such as *tert*-butyl and for the use of the less reactive anilines. This was later solved in 2012 by using chloromethyl benzoyl chlorides in the acylation step (Scheme 7).[48] This modification not only allowed for installation of previously inaccessible side chains but generally provided higher crude purities (59-99% for hexamer synthesis) and purified yields (23-69% of hexamers with HPLC purity >99%) than the previous methods.

The following year, the synthesis of the first arylopeptoids with *ortho*-backbones was then reported.[49] Examples of such *ortho*-linked "one-way sequence" aromatic oligoamides remain very rare. Nonetheless, the efficient synthesis of a wide variety of *ortho*-arylopeptoids both in solution and on solid phase was demonstrated. On solid phase, activation of the aromatic building block as the corresponding acid chloride was in this case found to be considerably more efficient than using the free acid in combination with a peptide coupling reagent. This is presumably due to the increased steric hindrance.

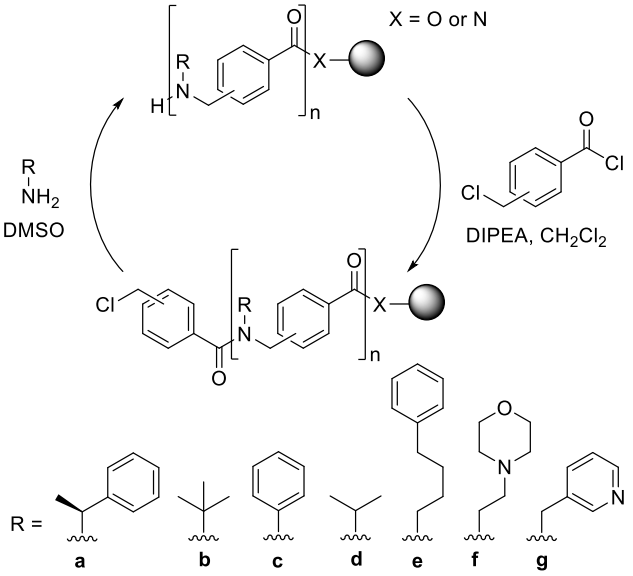

Scheme 7. Improved solid-phase synthesis of arylopeptoids and some of the side chain diversity available.

The solid phase methodology based on the use of chloromethyl benzoyl chlorides in the acylation step has furthermore been adapted to semi-automated microwave synthesis.[50] Strongly reduced reaction times were achieved in this way and the synthesis of a model arylopeptoid nonamer with alternating *ortho*-, *meta*-, and *para*-substituted backbone pattern carrying very challenging side chains was demonstrated.

Intriguingly, the submonomer method may also be adapted for installation of heteroaromatics such as furanes, pyrazines, oxazoles and thiazoles in the aromatic oligoamide backbone.[23] Thus, various trimeric azole peptoids (or heteroarylopeptoids) with oxazoles or thiazoles in the backbone were efficiently synthesized with isolated yields ranging from 13 to 63% *via* the submonomer method using free acids activated with COMU in the acylation steps (Scheme 8).[23b]

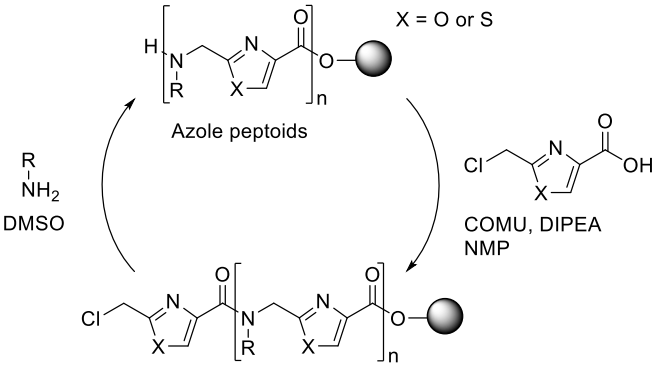

Scheme 8. Submonomer synthesis of azole peptoids.

The synthetic methodology of the submonomer method for the solid-phase synthesis of arylopeptoid architectures was furthermore recently broadened by the development of an iterative cycle based on acylation – reductive amination rather than the above acylation – substitution cycle (Scheme 9).[22c],[51] In this technique, formylbenzoyl chloride was used in the acylation step and the installation of the side chain was then achieved by reaction with an amine in the presence of picoline-borane. Only introduction of phenyl and 4-methoxyphenyl side chains have been studied. This alternative method allows for using a smaller excess of reagent when using aromatic amines in the second step of the iterative cycle.

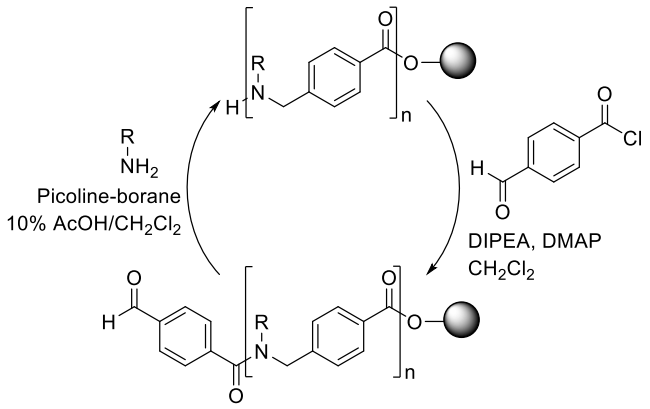

Scheme 9. Submonomer synthesis of arylopeptoids using an alternative acylation – reductive amination cycle.

4. Foldameric properties

The folding properties of *N*-alkylated aromatic poly- and oligoamides have been studied in solution by NMR and circular dichroism analysis, as well as by X-ray crystallography in the solid-state. The conformational behavior of the oligomers primarily depends on the *cis*/*trans* conformational preference of the *N,N*-disubstituted amides and the syn/anti arrangement of the arene rings. These local preferences may then act cooperatively along the backbone to induce well-defined secondary structures.

4.1. Local conformational preferences of *N,N*-disubstituted amides

For aromatic amides, the local possible conformations result from rotation about the Ar-N, Ar-CO and N-CO bonds. Depending on the *N*-substituents and aryl substitution, one conformation may be privileged (Figure 5). The preference for *cis* amide conformation (formally *E*) of *N*-methylbenzanilide monomer in solution in aprotic and protic organic solvents and in the solid-state was early shown by Shudo and co-workers.[52] They thoroughly investigated the *cis*-amide preference of *N*-methylanilides by means of crystallography and NMR[8a] as well as by theoretical studies.[53] Recently, the conformational preferences of *N*-alkyl anilides were thoroughly reinvestigated by Bloomfield using density functional theory (DFT) and NBO deletion strategies to discriminate energy differences due to orbital mixing from those due to steric strain.[8c] The *N*-alkyl *N*-aryl amide conformation appears to be governed by an interplay of steric and orbital delocalization effects.

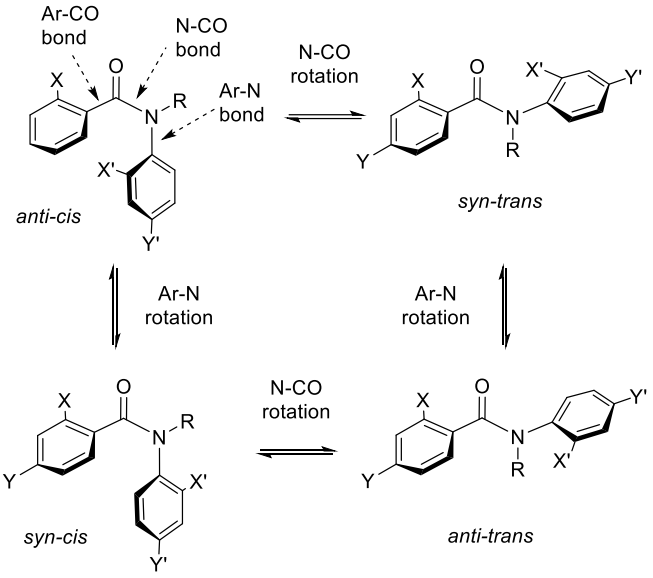

Figure 5. Different conformations accessible by rotation about the Ar-N, Ar-CO and N-CO bonds

In the *cis* conformation, allylic strain ($A^{1,3}$) between the aryl and the *N*-alkyl groups causes the aryl substituent to rotate out of the amide plane and the *trans* conformation is destabilized by a repulsive effect between the π system of the aromatic moiety and the lone pairs on the oxygen atom of the carbonyl. The *cis* conformation is even more stable for electron-rich arenes (for example Y'=OCH_3), leading to an increase in the interaction with the carbonyl oxygen, and a higher repulsive effect due to the increased electron density in the π system. The conformation ratio may be modified by the presence of *ortho*-substituent(s) on the arene (X and/or X' = I, CH_3) or a bulky substituent R on the nitrogen.[13] The proportion of *cis* and *trans* conformers may often be determined by NMR since the rotation about the C-N amide-bond of *N*,*N*-disubstituted amides is hindered and at the NMR time scale, two resonance peaks will often be observed for the protons adjacent to the amide, even at low to ambient temperature.[54] Similarly to *N*-methyl benzanilide, *N*-methyl-*N*-phenyl pyrrole 2-carboxamide exhibits predominantly the *cis* conformation but the proportion of *cis* conformer decreases in *N*-methyl-*N*-(4-pyrrole) benzamide as demonstrated by ^{1}H NMR at low temperature in CD_2Cl_2.[20] A *cis* to *trans* switching effect induced by an environmental change (solvent or pH) was demonstrated by Okamoto and co-workers for *N*-methyl aromatic amides containing 2,6-disubstituted pyridine (Figure 6).[17]

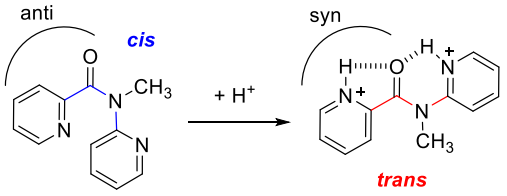

Figure 6. Acid-induced *cis*-*trans* switching of *N*-methyl-*N*-(2-pyridyl)-pyridine-2-carboxamide.

The protonation of the pyridyl ring under acidic conditions leads to a pyridinium core which is able to stabilize the *trans*

conformation through the establishment of hydrogen-bonding with the oxygen of the adjacent carbonyl group. This conformational switch was evidenced by ^{1}H NMR in CD_3CN upon addition of TFA-d or $DClO_4$.

Cis-*trans* amide isomerism in arylo- and benzylopeptoids was found to be more side chain specific due to the presence of the backbone-methylene. Indeed, the study of the *cis*/*trans* ratio in *meta*-, *para*- and *ortho*-arylopeptoid monomeric models carrying various side-chains showed conformational preferences similar to those of peptoid-type amides (Figure 7).[22b],[48],[49] As expected with *N*-phenyl substitution, exclusively the *trans* amide is observed. With aliphatic side chains, an equilibrium between *cis* and *trans* takes place, with the *cis* conformation being increasingly favored with increasing bulk of the side chain. The *tert*-butyl group thus results in a 100% *cis* conformation.

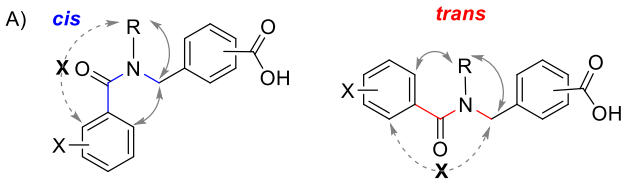

B)

R	*para*	*meta*	*ortho**
Et	64:36	65:35	50:50
*i*Pr	82:18	84:16	80:20
(S)-phenylethyl	83:17	81:19	80:20
*t*Bu	100:0	100:0	100:0
Ph	0:100	0:100	0:100

Figure 7. A) Representation of *cis* and *trans* amides in arylopeptoids and main NOESY correlations observed for amide conformation attribution; B) *cis*/*trans* proportion determined by NMR at 278K or 293K* in $CDCl_3$.

X-ray crystallographic studies of two arylopeptoid dimers recrystallized from chloroform containing a few drops of methanol, confirmed the *trans* and *cis*-directing effects of the phenyl and *tert*-butyl groups, respectively.[55] The phenyl side chain resulted in a more open, extended backbone structure, where the phenyl side chain points inwards into the twist created by the backbone. Conversely, the *tert*-butyl side chain resulted in a more packed structure where the *tert*-butyl group points outwards from the twist created by the backbone aromatic rings.

These studies of *N*-alkylated aromatic amide models show that good to high degrees of conformational control may be obtained around the aromatic amide. However, in order to construct oligomers with well-defined secondary structures, these conformational restrictions observed locally should act cooperatively to stabilize one preferred overall conformation.

4.2. Secondary structures

N-unsubstituted aromatic polyamides such as poly(*p*-phenylene terephthalamide) and poly(*p*-benzamide) display extended rodlike structures due to their *trans*-amide conformation and intermolecular hydrogen bonding between polymer chains.[56] Despite their higher flexibility compared to aromatic oligoamides with free amide protons on the backbone, *N*-alkylated poly(para-benzamide)s with narrow polydispersity (M_w/M_n<1) were shown to form helical conformations in solution and solid-state.[16a] Well-defined poly(para-benzamide)s with hydrophilic chiral oligo(ethylene glycol) *N*-side chains exhibited chain length dependent circular dichroism (CD) spectra in acetonitrile or chloroform, indicative of a chiral conformation. However, the high temperature dependency indicated thermodynamic control of the conformation. X-ray crystallographic analysis of *N*-methyl *para*-benzamide tetramers and pentamers, whose single crystals were obtained by recrystallization from CCl_4 and ethyl acetate, respectively, revealed a helical conformation in solid-state with three monomer units per turn, *cis* conformation of the amide bonds and a *syn* arrangement of the benzene rings (Figure 8). Supported by these results, a helical conformation in solution was assigned and the helicity was deduced from inspection of the CD spectra and exciton model analysis of the absorption.

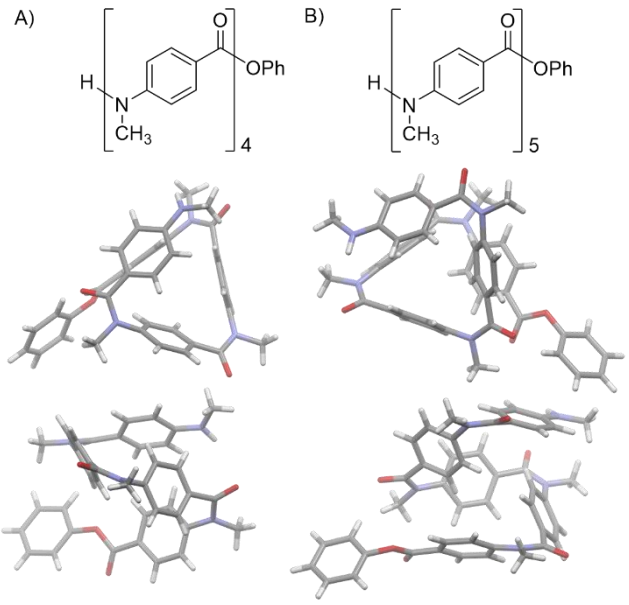

Figure 8. The crystal structures of 4-(methylamino)benzoic acid oligomers: A) a tetramer (top and side views) and B) a pentamer (top and side views). (adapted from reference [16a] with permission from American Chemical Society)

Induction of a one-handed helical chirality on the otherwise achiral *N*-methyl oligo(*para*-benzamide)s was performed *via* a domino effect based on the planar-axial-helical chirality relay caused by an (*S*)-*N*,*N*-methylphenyl-2-iodoferroceneamide transition-metal complex introduced at the *N*-terminal position of the oligobenzamide.[57] According to CD analysis performed in chloroform, the chiral induction led to a one-handed helix for a trimer but the screw-sense preference appeared less marked for longer oligomers. However, in absence of a marker that acts as a diastereotopic probe at the other terminal,[58] it was difficult to evaluate the chiral transmission in solution of these systems.

Conformational analysis of *N*-alkylated poly(meta-benzamide)s was also performed by Yokozawa and co-workers.[31b] As for the *para* series, CD studies in protic or aprotic solvents of *N*-substituted poly(*meta*-benzamide)s carrying chiral aliphatic side chains showed a Cotton effect not due to the intrinsic chirality of the monomer units. The highly temperature dependent CD spectra were indicative of a chiral conformation of the polymer gradually becoming disordered with increasing temperature. The preferred conformation could not be determined since even if only *cis* conformation of amide bonds was observed, different conformations could arise from the variation of the dihedral angles

between the amide linkages and benzene units (*syn* and *anti* arrangements) as previously observed for short *N*-methyl aromatic amide oligomers by Yashima and co-workers.[59] Clayden and co-workers have studied the conformational behaviour in different solvents of series of *ortho*-, *meta*- and *para*-linked oligobenzanilides as well as hybrid *ortho*/*meta* or *para*/*meta* oligomers and oligo-1,4-naphthanilides by NMR.[13],[60] The evidence of a single conformation or dynamic mixtures of conformers was difficult to establish. In these studies, substituents were introduced on aromatic ring to slow down rotation about the Ar-CO and Ar-N axis. However, despite conformational restriction observed on dimers and trimers, the degree of control degraded significantly in longer oligomers.

Tanatani and co-workers have taken advantage of the *cis*- or *trans*-conformation preference of tertiary and secondary amides to build a helical structure with a large cavity that could host guest molecules having a suitable molecular shape and size.[41] This helical construct was made from alternately *N*-alkylated and non-alkylated *para*-benzamides. NMR, UV, CD studies in polar aprotic solvents and theoretical analysis showed a helical conformation in solution with a cavity size of approximately 9Å and stabilization through intramolecular hydrogen bond interactions of secondary amides (Figure 9).

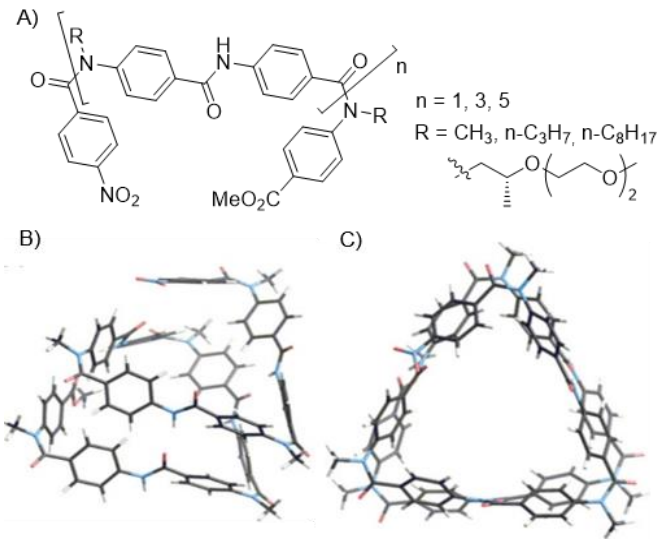

Figure 9. A) Structure of alternating *N*-alkylated and non-alkylated *para*-benzamides and B) side-view and C) top-view conformation of a *N*-methylated pentamer obtained by DFT geometry optimization at the RI-B3LYP/def-SV(P) level based on the crystal structure of (*cis*, *trans*, *cis*) form monomer (adapted from reference [41] with permission from American Chemical Society).

This type of helical structure with a large cavity was also accessible from polyamides with a diphenylacetylene backbone bearing (*S*)-α- and (*S*)-β methyl-substituted triethyleneglycol (TEG) side chains on the amide nitrogens (Scheme 10).[61] The large triangular cavity was first evidenced by X-ray analysis of a single crystal of a cyclic triamide, obtained by recrystallization from CH_3CN/CH_2Cl_2.[62] A polyamide (M_n = 14200, M_w/M_n=1.31) and oligoamides (5- to 7-mers) carrying the (*S*)-β methyl-substituted triethyleneglycol side chain were found to exhibit similar CD curves in chloroform with a negative Cotton effect at 305-310 nm and a positive one at 350 nm. Polyamides *N*-substituted with α- or β-chiral side chains were found to adopt a left- or right-handed helical structure, respectively, according to CD analysis in various solvents at 0°C and theoretical study. [61]

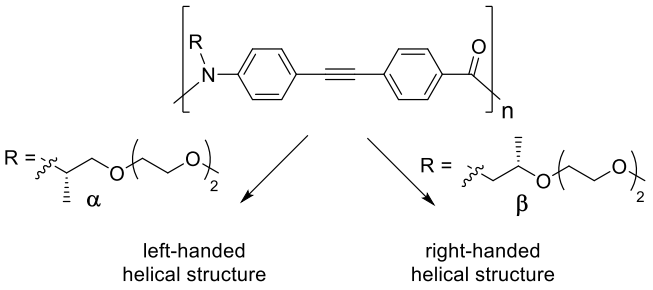

Scheme 10. Structure of diphenylacetylene-based oligoamide and chain-dependent helical folding.

Some reports from Wilson and Barnard suggested that short *N*-alkylated *para*-oligobenzamides, especially those bearing an *ortho*-substituent on the aromatic rings, might also, under certain conditions, be able to adopt extended conformations with *trans* amide bonds in solution.[15b,c] Up to now, this type of conformation has not been evidenced though. However, it should be noted that a crystallographic structure exhibiting *N*-alkylated benzamides in the *trans* form and a fully extended conformation, was obtained from DMSO-d_6 for a hybrid *N*-alkylated and non-alkylated *para*-benzamide trimer.[41]

Interesting features were also obtained when combining pyrrole and phenyl rings in *N*-methyl aromatic oligoamides.[20] NMR studies in CD_2Cl_2 showed that the *N*-methylated amide attached at the 2-position of the pyrrole ring predominantly adopted the *cis* conformation, while the *cis*/*trans* ratio decreased when the *N*-methylated amide bond was at the 4-position of the pyrrole ring (Scheme 11). Chain-length and solvent dependent CD spectra reflected different folding properties than *N*-alkylated *para*-oligobenzamides, suggesting the presence of a combination of *cis*-amide bonds with an anti/syn conformational preference but this unique conformation has not yet been confirmed.

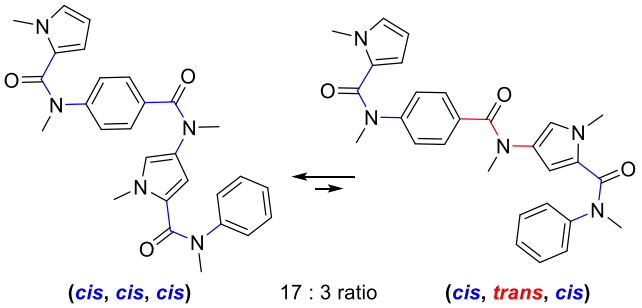

Scheme 11. Proportion of conformers observed by NMR in CD_2Cl_2 at 233K.

The identification of the folding behaviour of oligomeric *N*-substituted aminomethyl benzamides (arylopeptoids) proved to be difficult since the amide conformation preference was markedly less pronounced in these oligoamides due to the additional backbone-methylene group. Some particular side chains, *i.e. tert*-butyl and aryl groups, inducing complete control of the *cis* or *trans* conformation, respectively, were identified

(section 4.1) but their achiral nature made studies by circular dichroism impossible. Attempts to evidence a privileged conformation by CD was then performed using the (*S*)-*N*-(1-phenylethyl) (*spe*) side chain which has been used extensively in the conformational studies of peptoids.[14b] However, the control of this side chain on the *cis*-amide conformation is not total, inducing additional flexibility to the system. This made NMR and circular dichroism analysis difficult. [48] Efforts thus still need to be made to better understand conformational preferences of arylopeptoids.

Another area of interest in the field of foldamers is the development of oligomers exhibiting external stimuli responsive structures.[63] Many examples of anion- or ligand-responsive folding/unfolding systems have been described but far less foldamers whose conformational preference depends on acid-base stimuli. To this end, Okamoto and co-workers have developed pH-responsive conformation-switching foldamers based on the particular properties of the pyridine ring under acidic conditions (section 4.1).[17c],[42] Symmetrical *N*-methyl oligoamides, made from 2,6-disubstituted pyridines, were able to switch from a layered to a spiral form upon addition of TFA or a small amount of perchloric acid which protonate only the terminal mono-substituted pyridines. This was observed by NMR in CD_3CN upon addition of TFA-d or $DClO_4$ and confirmed by the crystal structure of a perchlorate salt obtained from the studied oligomer and two equivalents of perchloric acid. Protonation of inner pyridine rings occurs upon further addition of perchloric acid which leads to a flat form with all *N*-methyl amides in a *trans* configuration according to the correlations observed between the N-methyl and pyridine protons in NOESY experiments (Scheme 12).

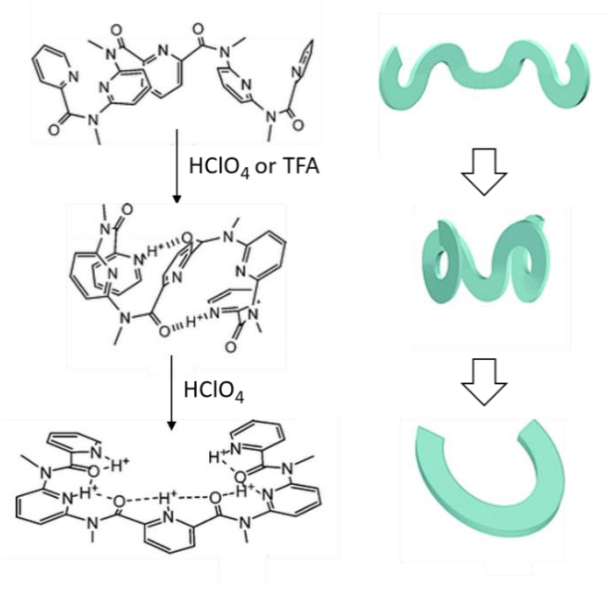

Scheme 12. Acid-responsive conformations of an *N*-methyl aromatic oligoamide made from 2,6-disubstituted pyridines (adapted from reference [17c] with permission from American Chemical Society).

The nature of the interactions involved in the folding of *N*-alkylated oligoamides combined with the low energy barrier of the *cis*/*trans* isomerism of *N*,*N*-disubstituted amides are responsible for the dynamic character of their secondary structures. In many cases, circular dichroism studies highlighted temperature-dependent folding but the privileged conformation in solution was difficult to assign by classical techniques such as NMR due to the absence of stabilizing hydrogen bonding and dynamic exchange of conformers. Fortunately, solid-state structures could be resolved in some cases which has assisted in the identification of the conformation in solution. The different conformational behaviours of *N*-substituted aromatic oligoamides compared to the parent non-substituted oligomers confers them unique properties that may be exploited for various applications.

5. Applications

In material sciences, the unique properties of *N*-substituted poly(benzamide)s have allowed for the preparation of a number of polymers and co-polymers intended for use in the fabrication of self-assembled architectures. Indeed, one of their important properties is a good solubility in organic solvents which has greatly facilitated the preparation of well-defined polymers and co-polymers. To this end, the 4-(octyloxy)benzyl (OOB) or *N*-p-methoxybenzyl (PMB) groups were efficiently used as *N*-substituents to prevent aggregation during oligomer synthesis and to facilitate purification. [35],[44] The protecting groups could then be removed to obtain highly interesting shape-persistent materials. This strategy has for example led to the development of strongly aggregating poly(benzamide)s with a rod-like conformation or rod-coil conformation when associated with PEG coil block polymers.[44a] In addition, the well-controlled chain-growth polycondensation developed by Yokosawa and co-workers for the synthesis of poly(benzamide)s with narrow polydispersity,[27] has allowed for the access to a wide range of polymer and copolymer architectures: star-shaped polymers with a porphyrin core[64] or a microgel core made from diacrylamides,[35] tadpole-shaped dendrimers[40] and hyperbranched polymers. [65]

The optical properties of oligothiophenes attached to cyclic *meta*- or *para*-benzamides trimers and polymers were studied by Takagi and co-workers.[32],[36a] The alignment of the π-conjugated oligothiophene chromophores in a controlled fashion is particularly important in the context of development of active materials for optoelectronic devices.

Ikeda and co-workers have shown that an N-(4-methoxy)phenyl-substituted arylopeptoid pentamer featuring *all*-trans amide bonds, linked to a polyethylene glycol monomethyl ether (MPEG) polymer can self-assemble to form spherical-shaped nanostructures in aqueous media (10 mM HEPES at pH 7.4) (Figure 10).[51] This first report on the self-assembling ability of hydrophobic arylopeptoids bearing hydrophilic polymers lends promise of access to nanostructures with various shapes and functions which may for example be used in the development of drug carriers.

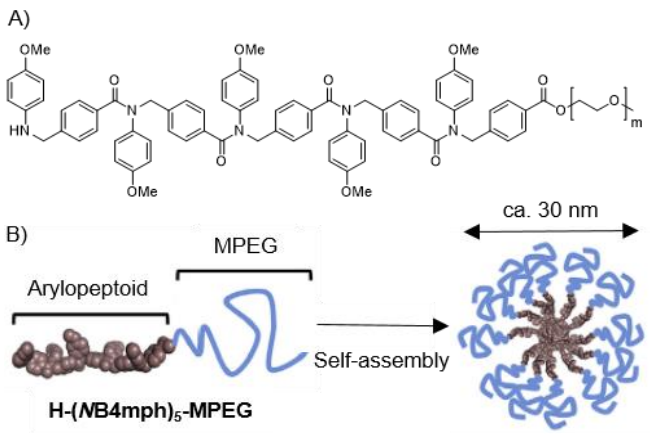

Figure 10. A) Structure of the arylopeptoid pentamer H-(*N*B4mph)$_5$-MPEG; B) Schematic illustration of the formation of self-assembled nanostructures from H-(*N*B4mph)$_5$-MPEG (adapted from reference [51] with permission from American Chemical Society).

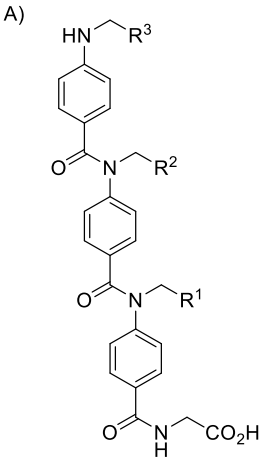

B)

Cpds	IC50 (μM)
p53(15-31)	1.2 (± 0.4)
1	3.8 (± 0.8)
2	4.1 (± 0.9)
3	3.3 (± 0.9)
4	2.8 (± 0.8)

1 R^1 = *i*Pr, R^2 = Ph, R^3 = Ph
2 R^1 = Ph, R^2 = Ph, R^3 = *i*Pr
3 R^1 = Ph, R^2 = *i*Pr, R^3 = Ph
4 R^1 = *i*Pr, R^2 = naphtyl, R^3 = Ph

Figure 11. A) Proteomimetics of *h*DM2 binding domain; B) IC50 values determined by fluorescence anisotropy competition assay for inhibition of the p53–hDM2 interaction.

The robustness of the methodologies developed for the submonomer synthesis of arylopeptoids make these types of *N*-alkylated aromatic oligomers highly suitable for educational purposes.[66] In the context of the Distributed Drug Discovery (D3) program,[67] a library of arylopeptoid dimers was screened to evaluate their activity on bacteria and yeasts.[66c] One dimer was found "partially active" on *Cryptococcus neoformans*. Nielsen and co-workers have also developed short arylopeptoids as agonists of the peroxisome proliferator-activated receptor γ (PPARγ) involved in metabolic disorders.[68] However, these agonists were designed as small molecule ligands by analogy with existing PPARγ agonists rather than as proteomimetics.

By contrast, *N*-alkylated oligobenzanilides were used as proteomimetics to target protein-protein interactions. By analogy with the parent oligobenzanilides,[1c],[3a],[69] they have been developed as α-helix mimics by Wilson and Barnard with interesting features such as amenability to library construction with high diversity and also to multifacial mimicry by the introduction of *O*-substituents on the backbone aromatic rings.[15c] Even though the *cis*-amide conformation of *N*-alkyl benzanilide is not favorable for the formation of extended conformations able to mimic one face of an α-helix, trimeric *N*-alkylated benzanilides carrying hydrophobic side chains, developed by Wilson and co-workers were found to be potent inhibitors of the p53–hDM2 interaction (Figure 11).[15b] According to the ^{1}H–^{15}N HSQC chemical shift perturbations observed, and a mapping onto the crystal structure of p53–hDM2, an extended conformation of the aromatic benzanilides appears to interact with the hydrophobic groove of p53 protein, even though this is not the preferred arrangement in solution. In addition, the all-*trans* conformation enables a side chain arrangement that match the spatial presentation of side chains located at the *i*, *i* + 4 and *i* + 7 positions of an α-helix. Further studies are necessary to better understand the conformational behavior and interactions involved in this context. Compared to non-alkylated benzamides, these oligomers thus possess a certain degree of plasticity that may be beneficial for protein-surface recognition. Resolution of the structure of proteomimitic-protein complexes would be of high interest to further understand these interactions.

In the pursuit of new oligoamide biomimetic scaffolds capable of transition metal binding, Fuller and co-workers have studied the ability of a thiazole-based aromatic oligoamide bearing a terpyridine group to bind Zn^{2+} by UV analysis of a trimeric arylopeptoid in aqueous buffer upon addition of $ZnCl_2$.[23b] The authors speculated that a distorted octahedral complex with two oligomers bound to one metal cation was formed. However, the conformational change upon metal coordination was difficult to evaluate due to the conformational heterogeneity of the thiazole-based oligomers. Changes in folding behavior upon binding were easier to evaluate on more highly-structured aromatic oligoamides such as arylopeptoid and benzylopeptoid macrocycles.[70],[24] These few studies have shown the promising binding potential of these types of macrocyclic oligoamides.

6. Summary and Outlook

N-alkylated aromatic poly- and oligoamides have so far been by less studied than aromatic foldamers built from secondary amides. Nevertheless, very efficient pathways for their synthesis have been developed both in solution-phase and on solid support. Notable highlights comprise the chain-growth polycondensation to access aromatic poly(para- and meta-benzamide)s with narrow polydispersity and the solid-phase submonomer synthesis to prepare arylopeptoids and azole peptoids with a large diversity of side chains. Although, convenient processes are thus in place, the level of accessible chemical diversity has not yet been fully exploited to design specific sequences directed to a particular application. Due to the inherent properties of the *N,N*-substituted amides, the studied *N*-alkylated aromatic oligoamides have revealed dynamic conformational preferences. The *para*-benzamide polymers bearing *N*-chiral aliphatic side-chains were found to adopt helical structure and pyridyl oligoamides have pH-responsive conformation. Nevertheless, further studies need to be carried out in order to increase the understanding of the interactions involved in the folding processes and to identify the preferred conformation of most oligoamides discussed herein. A number of polymer and co-polymer architectures with various shapes have been efficiently prepared owing to the good organosolubility of these polymers. However, the self-assembling properties of this class of aromatic foldamers remains under

explored despite a promising potential. More attention should be paid towards their ability to form supramolecular edifices. The application of *N*-alkylated aromatic oligoamides as proteomimetic foldamers is still at an early development stage. Although their conformational behaviors can be difficult to establish, the modularity and adaptability of this type of oligomers represent tremendous opportunities for application within a plethora of areas as outlined above. There is no doubt that further studies in this area of research will emerge in the coming years.

Acknowledgements

Financial support (AA grant) from Université Clermont Auvergne (UCA) is gratefully acknowledged.

Keywords: aromatic oligoamides • conformational preferences • foldamers • helical structures • proteomimetics

[1] a) I. Huc, *Eur. J. Org. Chem.* **2004**, 17-29; b) D.-W. Zhang, X. Zhao, J.-Li Hou, Z.-T. Li, *Chem. Rev.* **2012**, *112*, 5271-5316; c) I. Saraogi, A. D. Hamilton, *Chem. Soc. Rev.* **2009**, *38*, 1726-1743.

[2] a) Z.-T. Li, J.-L. Hou, C. Li, *Acc. Chem. Res.* **2008**, *41*, 1343-1353; b) I. Huc, L. Cuccia in *Foldamers : structures, properties and applications*, (Eds.: S. Hecht, I. Huc), Wiley-VCH, Weinheim, **2007**, pp. 3-34.

[3] a) W.S. Horne, T.N. Grossmann, *Nat. Chem.* **2020**, *12***,** 331–337; b) R. Gopalakrishnan, A. I. Frolov, L. Knerr, W. J. Drury, E. Valeur, *J. Med. Chem.* **2016,** *59*, 9599-9621; c) L. Sebaoun, V. Maurizot, T. Granier, B. Kauffmann, I. Huc, *J. Am. Chem. Soc.* **2014**, *136*, 2168-2174.

[4] Y. Hamuro, S. J. Geib, A. D. Hamilton, *J. Am. Chem. Soc.* **1996**, *118*, 7529-7541.

[5] a) I. Saraogi, C. D. Incarvito, A. D. Hamilton, *Angew. Chem. Int. Ed.* **2008**, *47*, 9691-9694; b) P. Prabhakaran, V. Azzarito, T. Jacobs, M. J. Hardie, C. A. Kilner, T. A. Edwards, S. L. Warriner, A. J. Wilson, *Tetrahedron* **2012**, *68*, 4485-4491.

[6] a) S. Thompson, R. Vallinayagam, M. J. Adler, R. T. W. Scott, A. D. Hamilton, *Tetrahedron* **2012**, *68*, 4501-4505; b) G. M. Burslem, A. J. Wilson, *Synlett* **2014**, *25*, 324-335.

[7] J. Zhu, R. D. Parra, H. Zeng, E. Skrzypczak-Jankun, X. C. Zeng, B. Gong, *J. Am. Chem. Soc.* **2000**, *122*, 4219-4220.

[8] a) A. Itai, Y. Toriumi, S. Saito, H. Kagechika, K. Shudo, *J. Am. Chem. Soc.* **1992**, *114*, 10649-10650; b) Q. Sui, D. Borchardt, D. L. Rabenstein, *J. Am. Chem. Soc.* **2007**, *129*, 12042-12048; c) G. J. Pros, A. J. Bloomfield, *J. Phys. Chem. A* **2019**, *123*, 7609-7618.

[9] a) M. Takayanagi, T. Katayose, *J. Polym. Sci. Pol. Chem.* **1981**, *19*, 1133-1145; b) J. Preston, *J. Polym. Sci.* **1966**, *4*, 529-539.

[10] I. Azumaya, H. Kagechika, K. Yamaguchi, K. Shudo, *Tetrahedron* **1995**, *51*, 5277-5290.

[11] K. Yamazaki, A. Yokoyama, T. Yokozawa, *Macromolecules* **2006**, *39*, 2432-2434.

[12] a) T. Nishimura, K. Maeda, E. Yashima, Chirality **2004**, *16*, S12-S22; b) A. Yokoyama, S. Saito, Y. Shimizu, T. Yokozawa, *Macromol. Rapid Commun.* **2005**, *26*, 1931-1935.

[13] J. Clayden, L. Vallverdù, M. Helliwell, *Org. Biomol. Chem.* **2006**, *4*, 2106-2118.

[14] a) R. Zuckermann, T. Kodadek, *Curr. Opin. Mol. Ther.* **2009**, *11*, 299-307; b) M. A. Kline, L. Guo, R. N. Zuckermann in *Sequence-Controlled Polymers,* (Ed.: J.-F. Lutz), Wiley-VCH, Weinheim, **2018**, 183-227.

[15] a) H. M. König, R. Abbel, D. Schollmeyer, A. F. M. Kilbinger, *Org. Lett.* **2006**, *8*, 1819-1822; b) F. Campbell, J. P. Plante, T. A. Edwards, S. L. Warriner, A. J. Wilson, *Org. Biomol. Chem.* **2010**, *8*, 2344-2351; c) T. Flack, C. Romain, A. J. P. White, P. R. Haycock, A. Barnard, *Org. Lett.* **2019**, *21*, 4433-4438.

[16] a) A. Tanatani, A. Yokoyama, I. Azumaya, Y. Takakura, C. Mitsui, M. Shiro, M. Uchiyama, A. Muranaka, N. Kobayashi, T. Yokozawa, *J. Am. Chem. Soc*. **2005**, *127*, 8553-8561; b) L. Chabaud, J. Clayden, M. Helliwell, A. Page, J. Raftery, L. Vallverdù, *Tetrahedron*, **2010**, *66*, 6936-6957.

[17] a) I. Okamoto, M. Nabeta, M. Yamamoto, M. Mikami, T. Takeya, O. Tamura, *Tetrahedron Lett.* **2006**, *47*, 7143-7146; b) I. Okamoto, M. Nabeta, T. Minami, A. Nakashima, N. Morita, T. Takeya, H. Masu, I. Azumaya, O. Tamura, *Tetrahedron Lett.* **2007**, *48*, 573-577; c) I. Okamoto, M. Nabeta, Y. Hayakawa, N. Morita, T. Takeya, H. Masu, I. Azumaya, O. Tamura, *J. Am. Chem. Soc*. **2007**, *129*, 1892-1893.

[18] M. L. Kopka, C. Yoon, D. Goodsell, P. Pjura, R. E. Dickerson, *Proc. Natl. Acad. Sci. U.S.A.* **1985**, *82*, 1376-1380.

[19] E. E. Baird, P. B. Dervan, *J. Am. Chem. Soc.* **1996**, *118*, 6141-6146.

[20] Y. Tojo, K. Urushibara, S. Yamamoto, H. Mori, H. Masu, M. Kudo, T. Hirano, I. Azumaya, H. Kagechika, A. Tanatani, *J. Org. Chem.* **2018**, *83*, 4606-4617.

[21] a) R. N. Zuckermann, D. A. Goff, S. Ng, K. Spear, B. O. Scott, A. C. Sigmund, R. A. Goldsmith, C. K. Marlowe, Y. Pei, L. Richter, R. Simon, *US005877278A*, 1999; b) R. N. Zuckermann, D. A. Goff, S. Ng, K. Spear, B. O. Scott, A. C. Sigmund, R. A. Goldsmith, C. K. Marlowe, Y. Pei, L. Richter, R. Simon, *WO9640202A1*, 1996; c) R. N. Zuckermann, J. M. Kerr, S. Kent, W. H. Moos, R. J. Simon, D. A. Goff, *WO9406451A1*, 1994.

[22] a) D. J. Combs, R. S. Lokey, *Tetrahedron Lett.* **2007**, *48*, 2679-2682; b) T. Hjelmgaard, S. Faure, D. Staerk, C. Taillefumier, J. Nielsen, *Eur. J. Org. Chem.* **2011**, 4121-4132; c) M. Ikeda, K. Horio, T. Tsuzuki, R. Torii, A. Shibata, Y. Kitamura, H. Katagiri, Y. Kitade, *Tetrahedron Lett.* **2015**, *56*, 6726-6729.

[23] a) A. Aditya, T. Kodadek, *ACS Comb. Sci.* **2012**, *14*, 164-169; b) A. Mohan, A. H. M. Koh, G. Gate, A. L. Calkins, K. N. McComas, A. A. Fuller, *Molecules* **2018**, *23*, 1035.

[24] A. Meli, S. Gambaro, C. Costabile, C. Talotta, G. Della Sala, P. Tecilla, D. Milano, M. Tosolini, I. Izzo, F. De Riccardis, *Org. Biomol. Chem.* **2016***, 14*, 9055–9062.

[25] H. A. Kashani, J. A. Barrie, M. H. George, *J. Polym. Sci. Pol. Chem. Ed.* **1978**, *16*, 533-537.

[26] a) M. Takayanagi, T. Katayose, *J. Polym. Sci. Pol. Chem.* **1983**, *21*, 31-39; b) H. G. Rogers, R. A. Gaudiana, R. A. Minns, D. M. Spero, *J. Macromol. Sci. A* **1986**, *23*, 905-914.

[27] T. Yokozawa, A. Yokoyama, *Chem. Rev.* **2009,** *109*, 5595-5619.

[28] A. Yokoyama, T. Yokozawa, *Macromolecules* **2007**, *40*, 4093-4101.

[29] a) T. Yokozawa, T. Asai, R. Sugi, S. Ishigooka, S. Hiraoka, *J. Am. Chem. Soc.* **2000**, *122*, 8313-8314; b) A. Tanatani, A. Yokoyama, I. Azumaya, Y. Takakura, C. Mitsui, M. Shiro, M. Uchiyama, A. Muranaka, N. Kobayashi, T. Yokozawa, *J. Am. Chem. Soc.* **2005**, *127*, 8553-8561.

[30] Y. Shibasaki, T. Araki, M. Okazaki, M. Ueda, *Polymer J.* **2002**, *34*, 261-266.

[31] a) R. Sugi, A. Yokoyama, T. Furuyama, M. Uchiyama, T. Yokozawa, *J. Am. Chem. Soc.* **2005**, *127,* 10172-10173; b) K. Yamazaki, A. Yokoyama, T. Yokozawa, *Macromolecules* **2006**, *39*, 2432-2434.

[32] K. Takagi, K. Nobuke, Y. Nishikawa, R. Yamakado, *Polym. J.* **2013**, *45*, 1171–1176.

[33] a) A. Yokoyama, S. Saito, Y. Shimizu, T. Yokozawa, *Macromol. Rapid Commun.* **2005**, *26*, 1931-1935; b) A. Yokoyama, T. Masukawa, Y. Yamazaki, T. Yokozawa, *Macromol. Rapid Commun.* **2009**, *30*, 24-28.

[34] M. Alizadeh, A. F. M. Kilbinger, *Macromolecules* **2018**, *51*, 4363-4369.

[35] T. Ohishi, T. Masukawa, S. Fujii, A. Yokoyama, T. Yokozawa, *Macromolecules* **2010**, *43*, 3206–3214.

[36] a) K. Takagi, S. Sugimoto, R. Yamakado, K. Nobuke, *J. Org. Chem.* **2011**, *76*, 2471–2478; b) T. Ohishi, T. Suzuki, T. Niiyama, K. Mikami, A. Yokoyama, K. Katagiri, I. Azumaya, T. Yokozawa, *Tetrahedron Lett.* **2011**, *52*, 7067-7070; c) C.Storz, M. Badoux, C. M. Hauke, T. Šolomek, A. Kühnle, T. Bally, A. F. M. Kilbinger, *J. Am. Chem. Soc.* **2014**, *136*, 12832−12835.

[37] M. Badoux, A. F. M. Kilbinger, Macromolecules **2017**, *50*, 4188−4197.

[38] a) N. Kanbayashi, T. Okamura, K. Onitsuka, *Macromolecules* **2014**, *47*, 4178-4185; b) N. Kanbayashi, T. Okamura, K. Onitsuka, *Macromolecules* **2015**, *48*, 8437-8444.

[39] Y. Ishido, N. Kanbayashi, T. Okamura, K. Onitsuka, *Macromolecules* **2017**, *50*, 5301-5307.

[40] Y. Ito, I. Washio, M. Ueda, *Macromolecules* **2008**, *41*, 2778-2784.

[41] K. Urushibara, H. Masu, H. Mori, I. Azumaya, T. Hirano, H. Kagechika, A. Tanatani, *J. Org. Chem.* **2018**, *83*, 14338-14349.

[42] R. Yamasaki, S. Fujikake, A. Ito, K. Migita, N. Morita, O. Tamura, I. Okamoto, *Tetrahedron Lett.* **2016**, *57*, 56–59.

[43] T. Fukuyama, C. K. Jow, M. Cheung, *Tetrahedron Lett.* **1995**, *36*, 6373-6374.
[44] a) H. M. König, T. Gorelik, U. Kolb, A. F. M. Kilbinger, *J. Am. Chem. Soc*. **2007**, *129*, 704-708; b) H. M. König, A. F. M. Kilbinger, Chimia **2013**, *67*, 788–790.
[45] A. Devos, J. Remion, A. M. Frisque-Hesbain, A. Colens, L. Ghosez, *J. Chem. Soc., Chem. Commun.,* **1979**, 1180–1181.
[46] K. Long, T. A. Edwards, A. J. Wilson, *Bioorg. Med. Chem.* **2013**, *21*, 4034-4040.
[47] T. Hjelmgaard, S. Faure, D. Staerk, C. Taillefumier, J. Nielsen, *Org. Biomol. Chem.* **2011**, *9*, 6832-6843.
[48] T. Hjelmgaard, S. Faure, E. De Santis, D. Staerk, B. D. Alexander, A. A. Edwards, C. Taillefumier, J. Nielsen, *Tetrahedron* **2012**, *68*, 4444-4454.
[49] T. Hjelmgaard, J. Nielsen, *Eur. J. Org. Chem.* **2013**, 3574-3589.
[50] J. E. Rasmussen, M. M. Boccia, J. Nielsen, C. Taillefumier, S. Faure, T. Hjelmgaard, *Tetrahedron Lett.* **2014**, *55*, 5940-5943.
[51] T. Tsuzuki, H. Katagiri, Y. Kitamura, Y. Kitade, M. Ikeda, *Tetrahedron* **2016**, *72*, 6886-6891.
[52] A. Itai, Y. Toriumi, N. Tomioka, H. Kagechika, I. Azumaya, K. Shudo, *Tetrahedron Lett.* **1989**, *30*, 6177-6180.
[53] S. Saito, Y. Toriumi, N. Tomioka, A. Itai, *J. Org. Chem.* **1995**, *60*, 4715-4720.
[54] L. A. LaPlanche, M. T. Rogers, *J. Am. Chem. Soc*. **1963**, *85*, 3728-3730.
[55] T. Hjelmgaard, M. Plesner, M. M. Dissing, J. M. Andersen, K. Frydenvang, J. Nielsen, *Eur. J. Org. Chem.* **2014**, 3971-3975
[56] K. Tashiro, M. Kobayashi, H. Tadokoro, *Macromolecules* **1977**, *10*, 413-420.
[57] K. Kamikawa, K. Fukumoto, K. Yoshihara, M. Furusyo, M. Uemura, S. Takemotoa, H. Matsuzaka, *Chem. Commun.* **2009**, 1201-1203.
[58] a) J. Clayden, L. Lemiègre, G. A. Morris, M. Pickworth, T. J. Snape, L. H. Jones, *J. Am. Chem. Soc.* **2008,** *130*, 15193-15202; b) J. Clayden, A. Castellanos, J. Solà, G. A. Morris, *Angew. Chem. Int. Ed.* **2009**, *48*, 5962-5965.
[59] T. Nishimura, K. Maeda, E. Yashima, *Chirality* **2004**, 16:S12–S22.
[60] L. Chabaud, J. Clayden, M. Helliwell, A. Page, J. Raftery, L. Vallverdú, *Tetrahedron* **2010**, *66*, 6936-6957.
[61] K. Urushibara, T. Yamada, A. Yokoyama, H. Mori, H. Masu, I. Azumaya, H. Kagechika, T. Yokozawa, A. Tanatani *J. Org. Chem.* **2020**, *85*, 2019-2039.
[62] A. Yokoyama, T. Maruyama, K. Tagami, H. Masu, K. Katagiri, I. Azumaya, T. Yokozawa, *Org. Lett.* **2008**, *10*, 3207-3210.
[63] a) D.-W. Zhang, X. Zhao, Z.-T. Li *Acc. Chem. Res.* **2014**, *47*, 1961-1970; b) E. A. John, C. J. Massena, O. B. Berryman, *Chem. Rev.* **2020,** *120*, 2759-2782.
[64] K. Yoshino, A. Yokoyama, T. Yokozawa, *J. Polym. Sci., Part A: Polym. Chem.* **2011**, *49*, 986−994.
[65] Y. Ohta, S. Fujii, A. Yokoyama, T. Furuyama, M. Uchiyama, T. Yokozawa, *Angew. Chem., Int. Ed.* **2009**, *48*, 5942−5945.
[66] a) A. Fuller, *J. Chem. Educ.* **2016**, *93*, 953-957; b) A. R. Van Dyke, D. H. Gatazka, M. M. Hanania, *ACS Chem. Biol.* **2018**, *13*, 26-35; c) A. A. Fuller, A. B. Dounay, D. Schirch, D. G. Rivera, K. A. Hansford, A. G. Elliott, J. Zuegg, M. A. Cooper, M. A. T. Blaskovich, J. R. Hitchens, S. Burris-Hiday, K. Tenorio, Y. Mendez, J. G. Samaritoni, M. J. O'Donnell, W. L. Scott, *ACS Chem. Biol.*, **2020**, *15*, 3187-3196.
[67] W. L. Scott, R. E. Denton, K. A. Marrs, J. D. Durrant, J. G. Samaritoni, M. M. Abraham, S. P. Brown, J. M. Carnahan, L. G. Fischer, C. E. Glos, P. J. Sempsrott, M. J. O'Donnell, *J. Chem. Educ.* **2015**, *92*, 819-826.
[68] K. Worm-Leonhard, T. Hjelmgaard, R. K. Petersen, K. Kristiansen, J. Nielsen, *Bioorg. Med. Chem. Lett.* **2013**, *23*, 4162-4165.
[69] V. Azzarito, K. Long, N. S. Murphy, A. J. Wilson, *Nature Chem.* **2013**, *5*, 161-173.
[70] T. Hjelmgaard, L. Nauton, F. De Riccardis, L. Jouffret, S. Faure *Org. Lett.* **2018**, *20*, 268-271.

Chapter II. Purity evaluation of organometallic compounds and NHC-catalyst synthesis.

II.A. Introduction.

The full description of a chemical compound not only requires the determination of its structure but also its purity which is particularly important in the context of medical drugs. Classically, purity is determined using chromatography techniques (HPLC, GC), however this requires a calibration from a sample of the pure compound as detection cannot take into account contaminants such as non-absorbing residual solvents, inorganic impurities, sorbent (silica, celite) or even water. Moreover, accurate determination using these techniques requires many adjustments to find a proper separation of the compounds and therefore cannot be used as a real routine procedure.

To overcomes these limitations, ^{1}H NMR offer a good alternative. Indeed, the integrations of the proton signals of the compound and its contaminants should be proportional to their concentrations. To realize this task, relaxation time (T1) should be determined and relatively long delay (usually 30-60 seconds), 5 time the T1, should be used. The absolute purity can be determined using an internal standard of known purity and this technique is denoted quantitative NMR (qNMR). Indeed, 'gold standard' are provided by suppliers such as Aldrich. Once this realized, the purity is given by the following formula:

$$P(\%) = \frac{n_{st}.Int_s.MW_s.m_{st}}{n_s.Int_{st}.MW_t.m_s}.P_{st}$$

where *Int* denotes the integral, *MW* the molecular weight, *m* the mass, *n* the number of protons, *P* the purity (in %); *St* stands for the internal standard and *s* the sample. Thus, compared with chromatography qNMR uses nearly universal detection and provides a versatile routine method of purity evaluation.

qNMR was explored by Hanna during the years between 1984 and 2006 at the US Food and Drug Administration and further developed by Pauli at the university of Chicago.[173] Early work milestones consist in the qNMR of dicyclomine in 1984;[174] the combination of identification and quantitation by (q)NMR and the concept of quantitating two compounds simultaneously in 1988.[175] Finally, the use of qNMR for the analysis of optical purity of an active pharmaceutical ingredient (API) using a lanthanide shift reagent. qNMR present a great unexploited potential for identification, impurity analysis, degradation, and stability studies of API. This pioneer work is described in a review publication.[159a] Now it has received a large attention, for example by becoming a standard technique replacing HPLC as described in the J. Med. Chem.'s guidelines for Authors. Importantly, qNMR is also referred by the Bureau International des Poids et Mesures (BIPM's).[176] The focus of the BIPM's qNMR programme concerns the best-practice for performing

[173] (a) Jaki, B. U.; Bzhelyansky, A.; Pauli, G. F. *Magn Reson Chem.***2021**, *59*, 7–15. (b)Bishizaki, Y.; Lankin, D. C.; Chen, S-N.; Pauli, G. F. *Anal. Chem.* **2021**, *93*, 2733−2741

[174] Hanna, G. M. *J. Assoc. Off. Anal. Chem.* **1984**, *67*, 222

[175] Hanna, G. M.; Lau-Cam, C. A. *Drug Dev. Ind. Pharm.* **1988**, *14*, 43.

[176] https://www.bipm.org/en/organic-analysis/qnmr

qNMR measurements and the identification of a small suite of compounds that constitute a set of primary internal standards.

The literature reveals many examples of purity determination for natural product (Figure II.1).

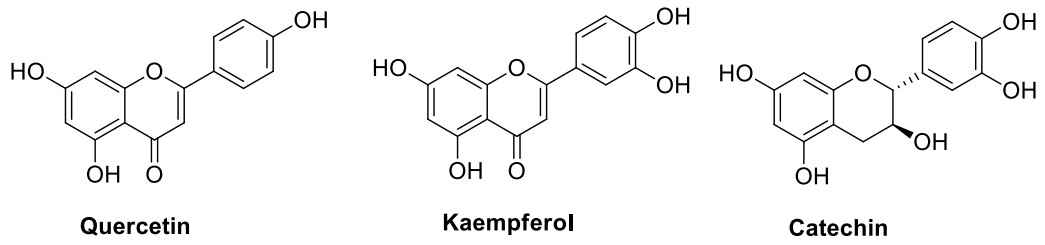

Figure II.1. Some example of natural products studied by ^{1}H-qNMR.

Thanks to its short T1, the classical nucleus used in qNMR is the proton. However, ^{19}F possesses also a short T1 and compared to proton, fluorine appears in a larger window which avoid the overlap of signals. The presence of ^{19}F in many pharmaceutical compounds make this nucleus also attractive. Some studies have been reported regarding this matter and suppliers provide fluorine 'gold standards', however these publications remain rare.

Attracted by this technique, we were interested in its application for organometallics and catalysis, especially in metal-NHCs. Strangely, examination of the literature reveals that qNMR for such compounds have not been applied. Indeed, the synthesis of organometallics requires a good purity of the ligand or the pre-ligand or at least its determination of adapt the exact stoichiometry of the reagents (ie: presence of water, sorbents…). This will avoid contamination by counter ions or traces of metal that are not easily quantifiable. Regarding the field of catalysis, a known purity is essential to obtain reproductible results. As example, it is well-known that silver contamination during the synthesis of gold-NHCs strongly perturbates the processes in gold catalysis.[177] In addition, the determination of accurate rate constant, turn over or frequency is dependant of the catalyst purity. Some ligands or metal-NHCs counter ions are introduced by metathesis and incomplete process will afford a mixture of compounds. Finally, it is important to note that many ligands or complexes contains PF_6 or BF_4 counter anions offering the possibility of determining purity by two independent measurements (^{19}F and ^{1}H NMR). As final argument, most of the organometallics gives simple spectra, well adapted for qNMR.

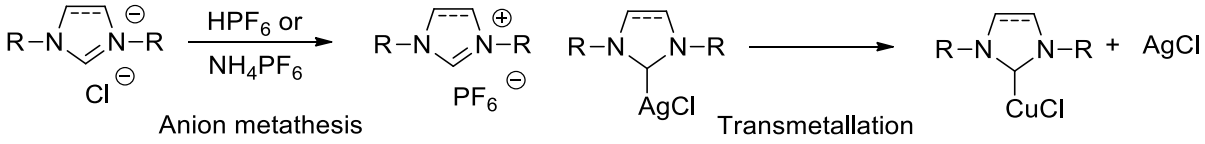

Scheme II.I. Some reactions considered in the context of qNMR.

[177] Garrison, J. C.; Youngs, W. J. *Chem. Rev.* **2005,** *105*, 3978–4008.

For the concern of this thesis, we decided to use qNMR to assess the quality of the numerous batches of the catalyst SIMesCuCl that we will routinely use. Therefore, qNMR will allow us to secure the reproducibility of our reactions. The following publication describe our findings in this field.

Reference : Akhdar, A.; Andanson, J-M.; Faure, S.; Traika, M.; Gautier, A. *J. Organomet. Chem.* **2021**, *950*, 12199. DOI : 10.1016/j.jorganchem.2021.121991

Authors file is provided here after

II.B. Associated publication.

Application of Quantitative ^{1}H and ^{19}F NMR to Organometallics

Ayman Akhdar,[a] Jean-Michel Andanson,[a] Sophie Faure,[a] Mounir Traïkia,[a] and Arnaud Gautier[a*]
CNRS-UMR 6296, Université Clermont Auvergne, ICCF, F-63000 Clermont-Ferrand, France.

Abstract

Purity assessment of organometallics is particularly important for catalytic applications. While quantitative NMR is a well-known method in pharmaceutic chemistry, the present work illustrates its usefulness for the determination of the ligands and organometallics purities using proton and fluorine NMR. This method is fast, straightforward and provides accuracy results.

Keywords.

Purity, NMR, Analytic Chemistry, Imidazolium, Organometallics.

1. Introduction.

The structure determination of ligands and organometallic complexes is usually performed by NMR, infrared (IR), Ultraviolet-Visible (UV-vis) and X-ray spectroscopies. The purity is determined accurately by HPLC for ligands if analytical pure samples of the constituent(s) of a mixture are available. However, this technique cannot be applied routinely to organometallic complexes. Elemental analysis is useful to establish elemental composition and molecular formula. However, it does not provide a direct measurement of the molar purity. Quantitative NMR (qNMR) presents a valuable alternative because the measured signals represent a direct measurement of the composition. [1] Therefore, in presence of an internal reference of known purity, the composition of a synthetic sample can be determined accurately using a single spectrum/ integration sequence (so-called absolute quantification). Equation 1 affords the purity value after accurate weight and NMR measurements.

$$P_s = \frac{I_s}{I_{std}} \cdot \frac{N_{std}}{N_s} \cdot \frac{M_s}{M_{std}} \cdot \frac{m_{std}}{m_s} \cdot P_{std} \qquad \text{Eq. 1}$$

(where s and std stand for the sample and the standard respectively; I being the sum of integrals, N the total number of nucleus (^{1}H, ^{19}F for example), M the molecular mass, m the measured masses, and P the purities of the standard). This method gives a direct access to the sample purity regardless the content of water or residual solvents, inorganic or organic chemicals, and sorbents, such as silica gel or celite. qNMR, especially using proton measurement is now a technique of choice routinely used in natural product and pharmaceutical chemistry with a reported accuracy of 1-2%. [1a] Several reviews are available, [1b] reporting the acquisition parameters and this protocol is recently entered into the guideline for authors of the Journal of Medicinal Chemistry.[2] Chemical suppliers are commercializing 'gold standard' which are used as internal or external standards. Expensive 'gold standards' can also be used to determine the

purity of a cheaper or more adequate secondary standard, especially if the commercial standard is not compatible with the chemical stability of the organometallic complexes. The purity is of importance for the synthesis of the desired complexes. For example, the starting material could contain residual water, a metathesis could afford a mixture of counter ions or a transmetallation leading to a contamination. In addition, in the case of kinetic studies the determination of the concentrations in stock solutions (reactants and catalyst) should be taken into consideration to perform accurate measurements. In this communication, the application of ^{1}H and ^{19}F qNMR for ligands and organometallics is reported (ESI for NMR parameters and protocols). In brief, after proper weight measurements, choice of the adequate solvent, recording of ^{1}H and ^{19}F spectrum takes 30 to 60 minutes making this technic attractive for routine determination.

2. Results and discussion.

2.1. Choice of the standard.

To make this method straightforward and broadly applicable to a wide variety of ligands and organometallics, the standard should be cheap and inert in presence of the organometallics. This prohibits standards containing some functional groups that could chelate or react such as carbonyls, reducing agents (formic salts), double bonds, acidic or redox compounds (phenol, quinones). We find that 1,4-dimethoxy benzene (1,4-DMB) is a good secondary standard for ^{1}H qNMR as it is cheap, easily purified by recrystallization from hexane or sublimation [3] and presents a good solubility in all common NMR solvents. Using maleic acid as primary gold standard (99.995% traceable certified reference materials, TraceCERT®) we find a purity of 99.5 % for our recrystallized sample of 1,4-DMB (Karl Fisher analysis demonstrates the absence of residual water). ^{1}H NMR of 1,4-DMB shows two well defined, sharp singlets at 6.7 and 3.7 ppm. Regarding ^{19}F qNMR, we used the commercially available 'gold standard' 2-chloro-4-fluoro toluene that is found inert in presence of the compounds described below. It is also interesting to note that the chemical shift of this standard is well positioned between the signals displayed by BF_4 and PF_6 anions. PF_6 appears as a doublet due to the coupling with phosphorus whereas BF_4 appears as two close signals, a singlet (^{10}B) and a quadruplet (^{11}B, S=3/2, J=1.1Hz) in a ratio 2:8. Chemical shifts (δ) and relaxation times (T1) are collected in Table 1. The relaxation times show that 30 seconds of inter-pulse delay (>5 T1) could be used for ^{19}F qNMR.

Table 1: Chemical shifts (δ) and relaxation times (T1)**.**

compound	Solvent	δ (ppm)	T1 (s)
2-chloro-4-fluoro Toluene	dmso-d_6	-115.3	3.3[a]
	Acetone-d_6	-117.0	6.5[b]
	MeOH-d_4	-117.7	4.8[a]
	MeCN-d_3	-117.3	4.7[a]
	$CDCl_3$	-115.8	4.4[a]
BF_4^-	dmso-d_6	-148.3	^{10}B: 6.8 ^{11}B: 5.9[c]

	Acetone-d_6	-151.8	^{10}B: 5.5 ^{11}B: 5.2[c]
	MeOH-d_4	-154.8	^{10}B: 5.4 ^{11}B: 4.9[c]
	MeCN-d_3	-151.8	^{10}B: 6.2 ^{11}B: 5.5[c]
	$CDCl_3$	-151.9	^{10}B: 2.9 ^{11}B: 2.8[d]
PF_6^-	dmso-d_6	-70.0	3.8[e]
	Acetone-d_6	-72.6	3.4[e]
	MeOH-d_4	-74.7	3.1[e]
	MeCN-d_3	-72.8	3.5[e]
	$CDCl_3$	-72.3	2.0[f]

[a]: taken from Aldrich, TraceCERT® CRMs for quantitative NMR. [b]: this work. [c]: using SIPr.HBF_4. [d]: using $N(Pr)_4$, BF_4. [e]: using SIPr.HPF_6. [f]: using $N(Bu)_4$, PF_6.

2.2.Ligands.

As illustration of this methodology due to their actual increasing interest in catalysis, we decided to focus on imidazolium and imidazolinium that are used for *N*-heterocyclic carbenes (NHCs) and metal-NHCs synthesis.[4] In his seminal communications, Arduengo reports a convenient synthesis of these azoliums that consists of refluxing diamines in triethyl orthoformate (Scheme 1).[4b] After filtration, salt/triethyl orthoformate adduct are obtained and simple purification can be achieved by repeated recrystallizations from acetonitrile/ether.

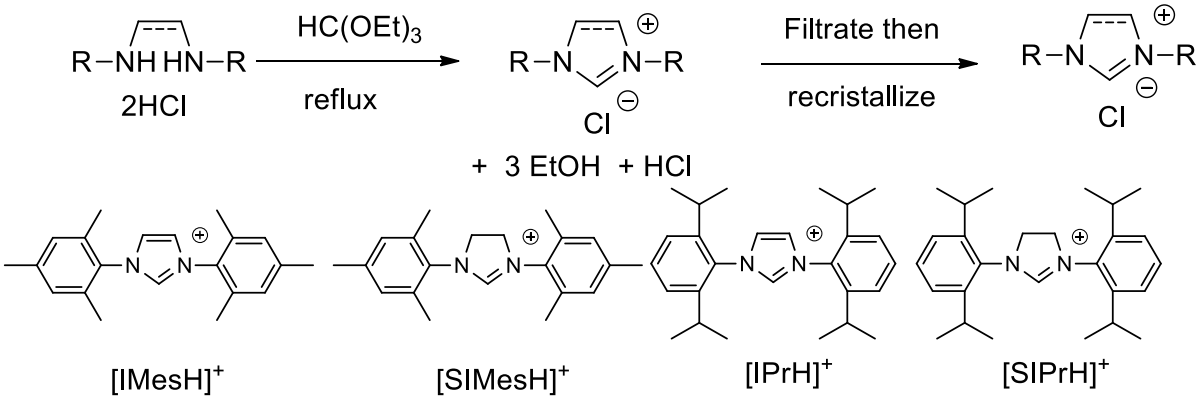

Scheme 1: Imidazolium and imidazolinium synthesis.

At first, we followed the Arduengo's procedure for SIMes.HCl and find, using 1,4-DMB, a purity of 72% for the crude product after filtration (Table 2, entry 1). Simple recrystallization [4b] and determination of the water content by Karl-Fisher analysis (0.5 molecule of water, Table 2, entry 2) affords a purity of 91%. For the azolium series, the amount of water varies from 0 to 1 molecule. This first screening of classical imidazolium and imidazolinium highlights the importance of the purity determination that should be corroborated with Karl-Fisher analysis results.

Table 2: purity of azolium chlorides.

Entries[(a)]	Azolium	Purity[(b)]
1	SIMes.HCl[(c)]	72%
2	SIMes.HCl, $0.5H_2O$[(d)]	91% (±2%)
3	IMes.HCl, $1H_2O$	98% (± 1%)
4	SIPr.HCl, $0H_2O$	91% (± 2%)
5	IPr.HCl, $0.5H_2O$	96% (± 2%)

(a): in dmso-d6. (b): uncertainty from 3 experiments. (c): before recrystallization. (d): after recrystallization.

The same procedure was followed for the non-coordinating anions PF_6 and BF_4, commonly used for metal carbene complexes. Importantly, both ^1H qNMR and ^{19}F qNMR should give comparable results. We simply synthesize the PF_6 and BF_4 salts by anion metathesis from the corresponding azolium chloride as previously described (Table 3). [5] We obtained high yields and in contrast to the chloride series, Karl-Fisher analysis demonstrates the absence of residual water (less than 0.1%). The results show a good correspondence between both technics with a maximum deviation of 3% (entries 6) and an averaged deviation of 1.8%. In all cases, good purity was observed.

Table3: Purity of azolium with non-coordinating salts.

Entry[(a)]	Azolium	Yield	Purity by ^1H qNMR[(b)]	Purity by ^{19}F qNMR[(b)]
1	SIMes.HPF_6	90%	98% (± 2%)	97% (± 1%)
2	IMes.HPF_6	91%	99% (± 3%)	99% (± 1%)
3	SIPr.HPF_6	76%	96% (± 2%)	97% (± 2%)
4	IPr.HPF_6	86%	95% (± 2%)	96% (± 1%)
5	SIMes.HBF_4	89%	98% (± 2%)	99% (± 1%)
6	IMes. HBF_4	90%	94% (± 2%)	97% (± 1%)
7	SIPr. HBF_4	78%	95% (± 2%)	97% (± 1%)
8	IPr. HBF_4	91%	93% (± 2%)	95% (± 1%)

(a): in dmso-d_6. (b) Uncertainty from 2 experiments.

2.3.Metal-NHCs.

The purity of a selection of useful metal-NHCs was determined. We used well-established literature procedures to synthetize silver, copper, gold and palladium complexes. Indeed, Ag(I)-NHCs and Cu(I)-NHCs are important synthons for transmetallation. [6] Silver(I)-NHCs is used in A3 coupling reactions and oxazole synthesis, copper(I)-NHCs are used in CuAAC, reduction, conjugated additions, allylic substitutions, alkene and alkyne transformations, nitrene transfert, allene synthesis, hydrocarboxylation, A3 coupling, oxidative coupling of phenol. [7] Regarding gold(I)-NHCs, they are used

in a wide range of catalysis including enyne cycloisomerization, alkyne hydration, C-C coupling reactions; [8] and palladium(II)-NHCs has gained high importance in homogeneous cross-coupling. [9]

IMesAgCl, SIMesAgCl, IPrAgCl and SIPrAgCl were synthesized by the classical silver oxide route [4a], [10] and recrystallized from dichloromethane/pentane affording good purities (Table 4, entries 1-4) in $CDCl_3$. At this stage, we noticed that a decomposition of the complex in presence of the maleic acid standard takes place after few hours; therefore 1,4-DMB as secondary standard was selected. The copper complexes SIMesCuCl and IPrCuCl (entry 5-6) were obtained by a soft, direct metalation of the azolium using the ammonia protocol. [11] Both complexes are obtained with good purity, 93 and 98% respectively. IPrAuCl was synthetized by transmetallation from IPrAgCl affording 93% purity (entry 7). The cationic complex [IPrAu(MeCN)], BF_4 was obtained from Strem chemical (95%) and analyzed by ^1H and ^{19}F qNMR to give an average purity of 95% in perfect agreement with the supplier's specifications (entry 8). Pd(PEPPSI)IPr was synthetized from the well-established procedure from the Organ's group.[12a] We find small amounts of indefinite materials in the crude mixture that were removed by washing with dichloromethane/pentane (1:5). The NMR spectrum shows the presence of 0.8 molecules of CH_2Cl_2 that cannot be removed under reduced pressure (2mbar) for several hours. [12b] The Pd(PEPPSI)IPr's purity in this mixture is found to be 87% and, taking the dichloromethane amount into account, a 96% purity is obtained (entry 9).

Table 4: Purity of metal-NHCs.

Entries	M-NHC	Solvent	Purity
1	IMesAgCl	$CDCl_3$	97% (± 1%)
2	SIMesAgCl	$CDCl_3$	95% (± 2%)
3	IPrAgCl	$CDCl_3$	97% (± 1%)
4	SIPrAgCl	$CDCl_3$	98% (± 1%)
5	SIMesCuCl	$CDCl_3$	93% (± 2%)
6	IPrCuCl	$CDCl_3$	98% (± 1%)
7	IPrAuCl	dmso-d_6	93% (± 1%)
8	[IPrAu,MeCN], BF_4	dmso-d_6	94% (± 1%) [(b)] 96% (± 1%) [(c)]
9	Pd(PEPPSI)IPr,[(d)] $0.8CH_2Cl_2$	$CDCl_3$	96% (± 2%)

(a): average of two measurements. (b): by ^1H qNMR. (c): by ^{19}F qNMR. (d): Pd(PEPPSI)IPr: Dichloro[1,3-bis(2,6-diisopropylphenyl)imidazol-2-ylidene)](3-chloropyridyl)palladium(II).

3. Conclusion

In conclusion, we have applied ^1H and ^{19}F quantitative NMR to organometallics complexes and their corresponding ligands. According to previous reports, this technique is easy to conduct, affording purity

of compounds in approximately 30 minutes to 1h experiment. Care should be taken regarding the choice of the solvent and if possible, Karl Fisher analysis should be considered, especially regarding the ligands.

4. Acknowledgment

Financial support from the Centre National de la Recherche Scientifique (CNRS) and the Université Clermont-Auvergne are acknowledged.

Appendix.

Supplementary material: procedure, NMR sequence and spectra can be found, in the online version.

References.

[1] (a) G.F. Pauli, S. N. Chen, C. Simmler, D. C. Lankin, T. Gödecke, B.U. Jaki, J. B. Friesen, J. B. McAlpine, J. G. Napolitano, Importance of purity evaluation and the potential of quantitative ^{1}H NMR as a purity assay. J. Med. Chem. 57 (2014) 9220-31. https://doi.org/10.1021/jm500734a. (b) S.K. Bharti, R. Roy, Quantitative ^{1}H NMR spectroscopy Trends in analytical Chemistry 35 (2012) 5-26. https://doi.org/10.1016/j.trac.2012.02.007.

[2] M. Cushman, G. I. Georg, U. Holzgrabe, S. Wange, Absolute Quantitative ^{1}H NMR Spectroscopy for Compound Purity Determination. J. Med. Chem. 57 (2014) 9219. https://doi.org/10.1021/jm501683w.

[3] Purification of laboratory chemicals 6thEds, p279.

[4] (a) M. N. Hopkinson, C. Richter, M. Schedler, F. Glorius, An overview of N-heterocyclic carbenes. Nature 510, (2014), 485-496. https://doi.org/10.1038/nature13384. (b) A. J. Arduengo, R. Krafczyk, R. Schmutzler, H. A. Craig, J. R. Goerlich, W. J. Marshall, M. Unverzagt, Imidazolylidenes, imidazolinylidenes and imidazolidines, Tetrahedron 55 (1999) 14523-34. https://doi.org/10.1016/S0040-4020(99)00927-8.

[5] X. Bantreil, S. P. Nolan, Synthesis of N-heterocyclic carbene ligands and derived ruthenium olefin metathesis catalysts. Nat. Protocols 6 (2011) 69–77. https://doi.org/10.1038/nprot.2010.177.

[6] (a) I. J. B Lin, C. S. Vasam, Preparation and application of N-Heterocyclic carbene complexes of Ag(I) Coord. Chem. Rev. 251 (2007) 642-670. https://doi.org/10.1016/j.ccr.2006.09.004. (b) F. Nahra, A. Gómez-Herrera, C. S. J. Cazin, Copper(I)–NHC complexes as NHC transfer agents. *Dalton Trans. 46 (2017)* 628-631. https://doi.org/10.1039/C6DT03687B.

[7] (a) V. A. Peshkov, O. P. Pereshivko, E. V. Van der Eycken, A walk around the A3-coupling. Chem. Soc. Rev. 41 (2012) 3790-3807. https://doi.org/10.1039/C2CS15356D. (b) R. Heath, H. Müller-Bunz, M. Albrecht, Silver(I) NHC mediated C–C bond activation of alkyl nitriles and catalytic efficiency in oxazoline synthesis. Chem. Commun. 51 (2015) 8699-8701. https://doi.org/10.1039/C5CC02558C.

[8] S. P. Nolan, The Development and Catalytic Uses of N-Heterocyclic Carbene Gold Complexes. Acc. Chem. Res. 44 (2011) 91-100. https://doi.org/10.1021/ar1000764.

[9] G. C. Fortman, S. P. Nolan *N*-Heterocyclic carbene (NHC) ligands and palladium in homogeneous cross-coupling catalysis: a perfect union. Chem. Soc. Rev. 40 (2011) 5151-5169. https://doi.org/10.1039/C1CS15088J.

[10] P. de Frémont, N. M. Scott, E. D. Stevens, T. Ramnial, O. C. Lightbody, C. L. B. Mac Donald, J. A. C. Clyburne, C. D. Abernethy, S. P. Nolan *Synthesis of Well-Defined N-Heterocyclic Carbene Silver(I) Complexes*. Organometallics 22 (2005) 6301-6309. https://doi.org/10.1021/om050735i.

[11] C. Gibard, H. Ibrahim, A. Gautier, F. Cisnetti, Simplified Preparation of Copper(I) NHCs Using Aqueous Ammonia. Organometallics 15 (2013) 4279-4283. https://doi.org/10.1021/om400440b.

[12] (a) J. Nasielski, N. Hadei, G. Achonduh, E. Ass en, B. Kantchev, C. J. O'Brien, A. Lough, M. G. Organ. Structure-Activity Relationship Analysis of Pd-PEPPSI Complexes in Cross-Couplings: A Close Inspection of the Catalytic Cycle and the Precatalyst Activation Mode. Chem. Eur. J. 16 (2010) 10844–53. https://doi.org/10.1002/chem.201000138.

II.C. Discussion

In this publication, we have used the qNMR technique to determine the purity of ligands and organometallics, a field left unexploited. We have found out that if many of the 'gold standards' are well-adapted for the ligands, they are not all well-adapted for organometallics because of their acidic, redox properties or bonding abilities. We then introduce 1,4-dimethoxybenzene (1,4-DMB) as secondary standard but we still believe that this choice depends on the species studied. We obtained a very good correlation between the mass weighted of the sample and its mass recalculated from the qNMR spectrum containing the standard (Graph II.1).

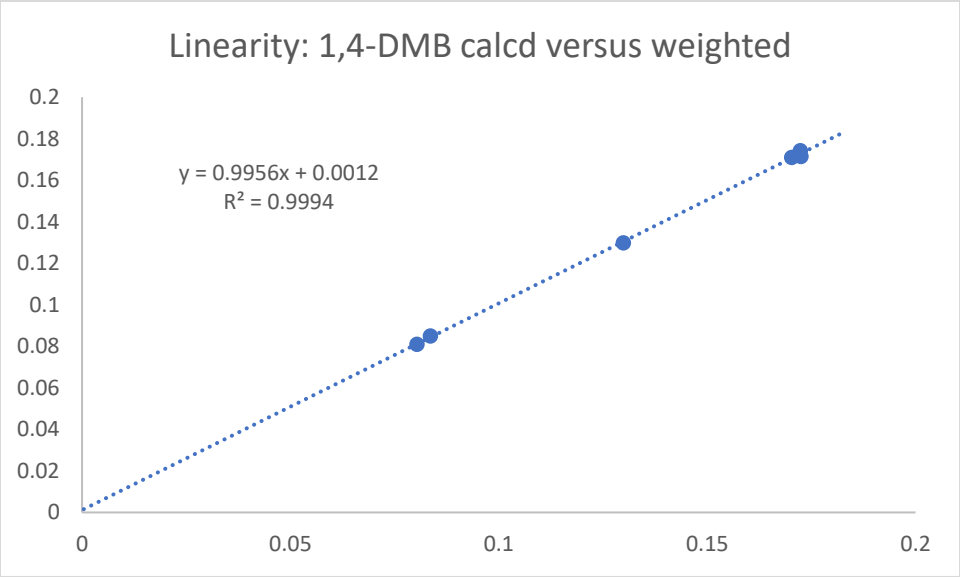

Graph II.1. Correlation between measured and recalculated mass of 1-4 DMB.

We have also used ^{19}F qNMR for the first time in the organometallic field. Thanks to the determination of the T1 for PF_6 and BF_4 anions, we have reported that the two orthogonal techniques of ^{19}F and ^{1}H qnmr furnish similar results. Representative spectrum of PF_6 and BF_4 anions are presented in (Figure II.2).

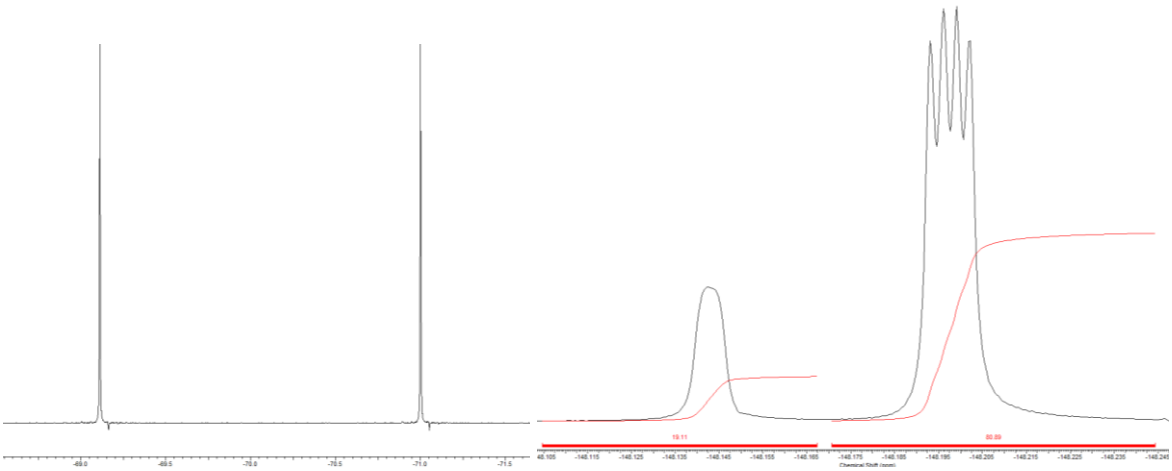

Figure II.2. ^{19}F spectra of (a) PF_6 and (b) BF_4 anions.

PF_6 anion appears at -72 ppm as a double (J^1=710 Hz) due to the coupling of the phosphorus nucleus with the fluorines. Bore appears as two signals at -148ppm. As it appears in the form of two stable isotopes, ^{10}B and ^{11}B in 19 and 81% respectively, two signals are visible. ^{10}B possesses a spin of 3 and gives a broad signal. The ^{11}B isotope possesses a spin of 3/2 giving rise to four signals of equal intensity. The ^{19}F qNMR method could be also applied to the field of ionic liquids where BF_4 and PF_6 anions are commonly found. qNMR technique could also be extended to phosphorus nucleus of PF_6, as certified standards are provided by Aldrich (phosphonoacetic acid, potassium phosphate, triphenyl phosphate) but we do not study.

Regarding our particular interest for SIMesCuCl, we have shown that the synthesis of SIMes.HCl requires a recrystallization step, as mentioned by Arduengo, which allows a great improvement in the ligand purity. Moreover, Karl-Fisher revealed the presence of crystallisation water (0.5 or 1 molecule) in most of the ligands studied. This should be taken into consideration for the synthesis of sensitive NHCs using strong bases. Regarding this residual solvent matter, we discovered in our synthesis of Pd(PEPPSI)IPr that it contains 0.8 molecules of dichloromethane which cannot be remove even after an extended time under reduced pressure. The qNMR technique allows then for a better determination of the amount of active catalyst in a reaction.

It would be interesting in the future to estimate the efficiency of the different routes employed to obtain a metal-NHC. Indeed, many complexes are obtain using two mature routes: the transmetallation (from silver) and the direct route using a soft base. Therefore, residual contamination with salts such as AgCl (transmetallation) or ammonium (soft base route) could be estimated. It is important to note here that transmetallation from copper-NHCs is becoming a popular route that should also be evaluated.

However, we find some limitations of the technique. For silver salts, in agreement with Rolland reports,[178] we saw an equilibrium between homoleptic and heteroleptic species in dmso. This equilibrium should also occur with copper and therefore, we used $CDCl_3$ as NMR solvent in which this equilibrium occurs slowly. An equilibrium also occurs in the case of our complex [(SIMesCu)(Cl_2-Phen)]Cl that equilibrates with free SIMesCuCl and Cl_2-Phen at a rate comparable with the NMR precession. As could be seen in table II.1, the signals of the phenanthroline become broad in $CDCl_3$ and dmso-d_6, whereas the NHC's signals stay well defined.

[178] Caytan, E.; Roland, S. *Organometallics* **2014**, *33*, 2115−2118.

dmso-d_6 ^{1}H spectra

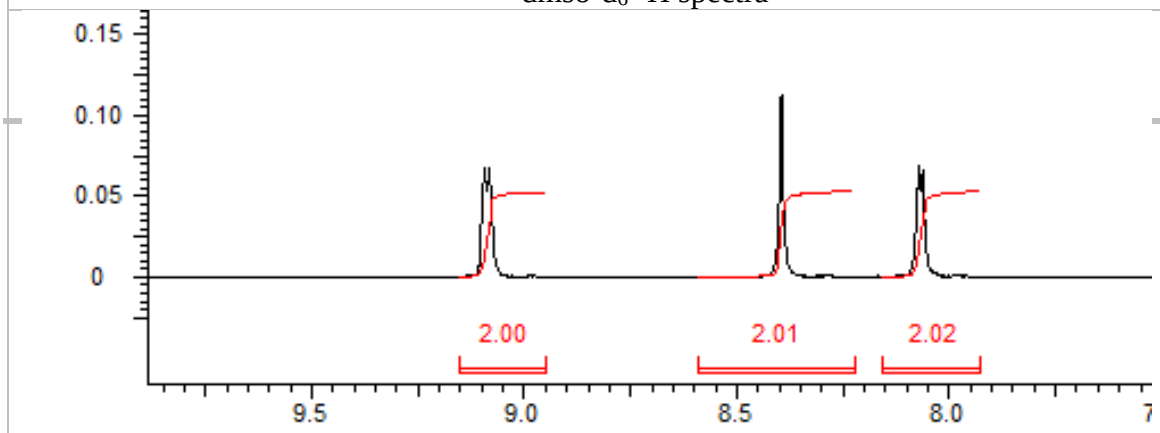

Figure II.2. 4,7-Cl_2-Phen

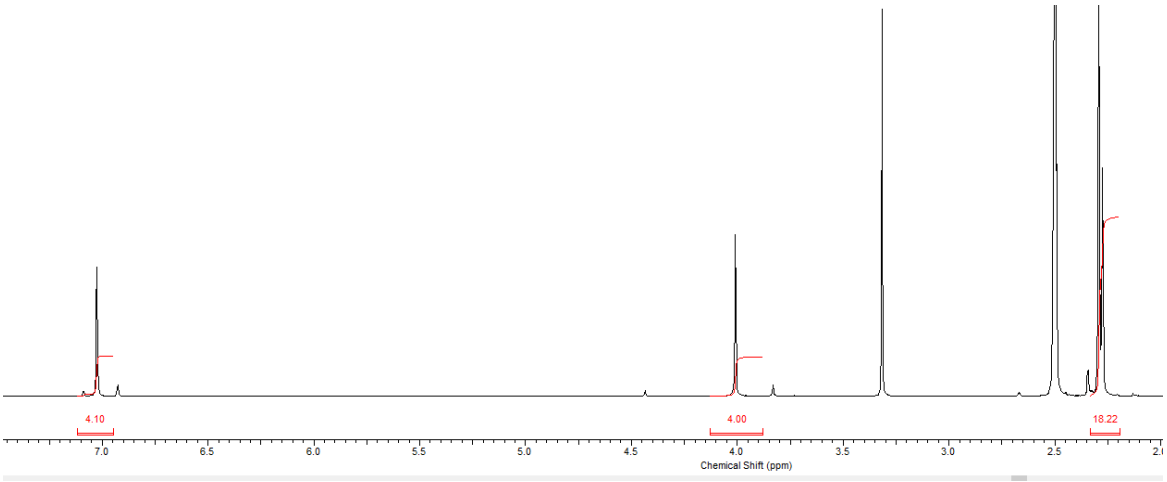

Figure II.3 of SIMesCuCl.

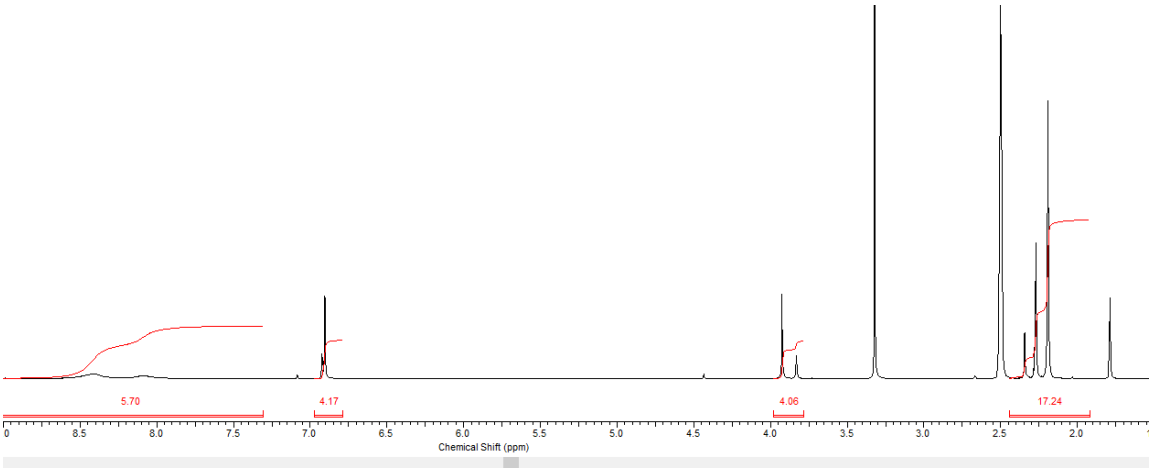

Figure II.4. [(SIMes)(4,7-Phen)CuCl].

$CDCl_3$ ^{1}H spectra

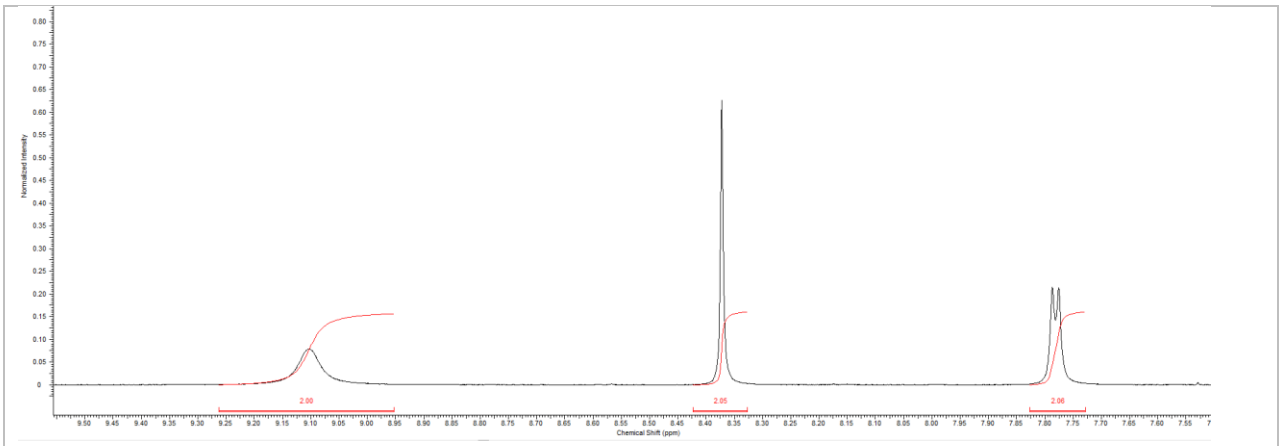

Figure II.5. 4,7-Cl_2-Phen

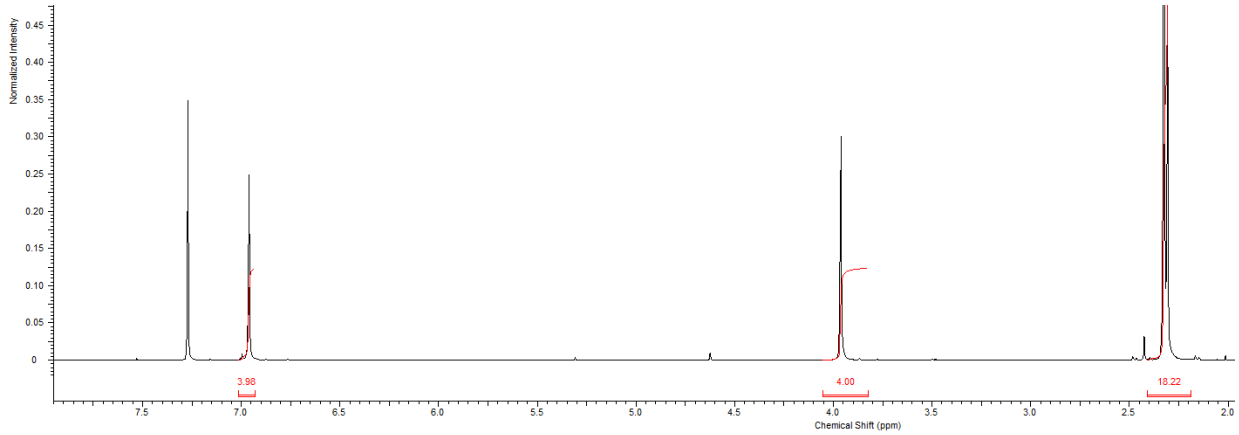

Figure II.6. SIMesCuCl.

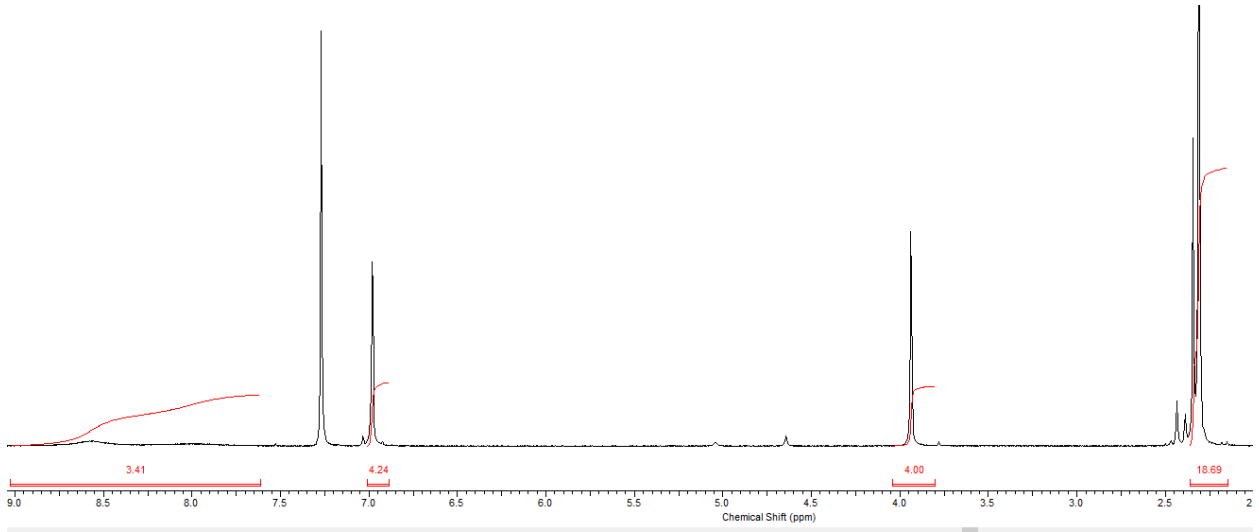

Figure II.7. [(SIMes)(4,7-Phen)CuCl].

Table II.1. Comparison of the different ^{1}H-NMR Spectra

We therefore take advantage of the well-defined signals of the copper(I)-NHC moity to conduct a ^{1}H qNMR purity determination using the 1,4-dimethoxy benzene as secondary standard (Figure II.8)

The calculation revealed that our catalyst, routinely used in the research work, was 96% pure.

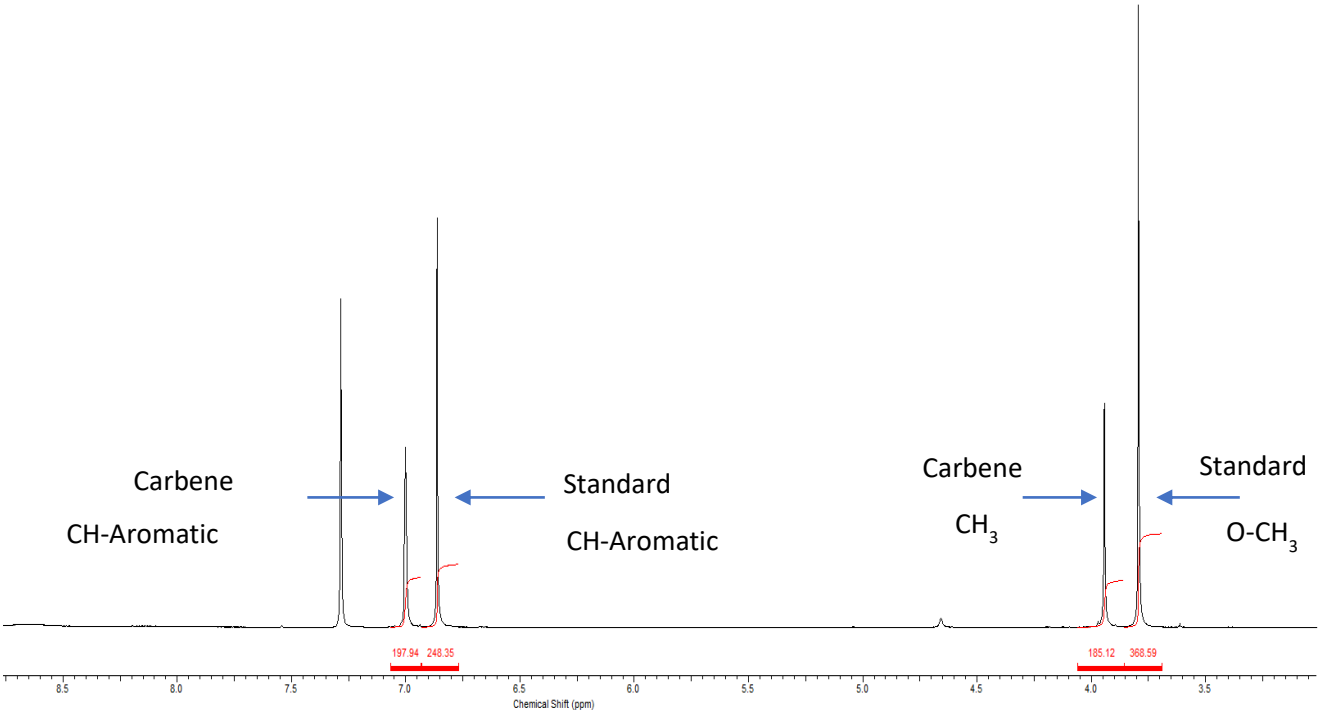

Figure II.8. qNMR of the catalyst to calculate its purity.

II.D. Synthesis of the [SIMesCu(4,7 Cl-Phen)Cl] catalyst.

The synthesis of [SIMesCu(4,7Cl-Phen)Cl] was performed in 5 step as depicted in scheme II.1.

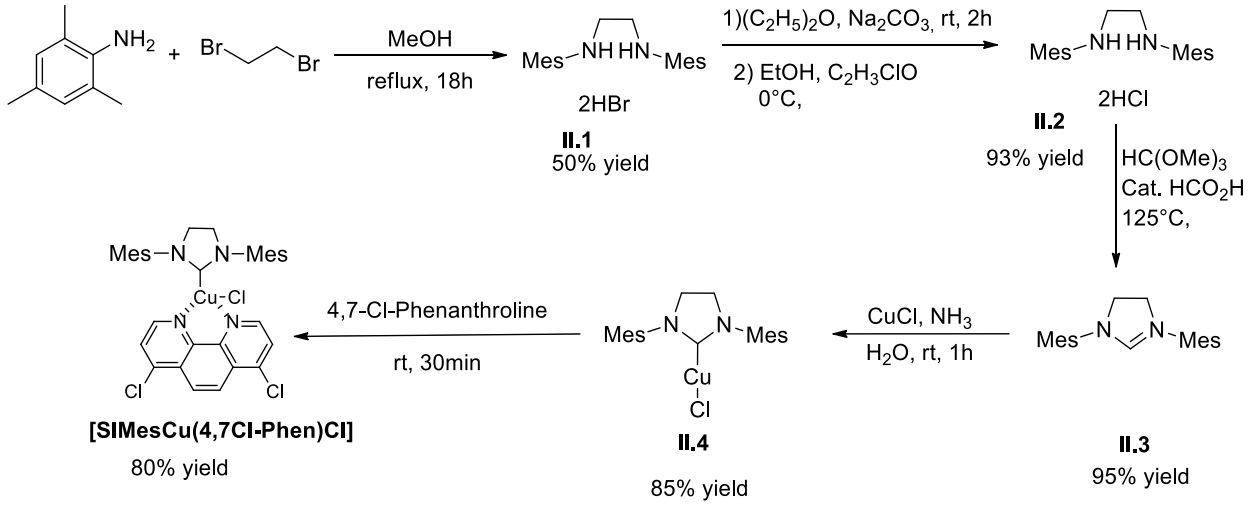

Scheme II.1. Synthesis of [(SIMes)(4,7-Phen)CuCl].

First, SIMes was prepared according to a known and well described procedure.[35,179] First, we start with the synthesis of *N,N'*–bis–(2,4,6–trimethylphenylamino)ethane dihydrobromide **(II.I)** by the reflux of 2,4,6–trimethylaniline and 1,2–dibromoethane in methanol for 18h, to end up with 50% isolated yield. Quantitative ^{1}H NMR of this product show 89% purity.

The diamine was freed from the bromide by a basic aqueous solution and extracted in diether ether. Addition ethanoic HCl to the ether forms the diamine hydrochloride salt as a white precipitate, **II.2** in 93% isolated yield. Karl Fischer indicates the presence of 0.5 equiv. of water in the product, which makes the purity 96% (q^{1}HNMR)

1,3–bis–(2,4,6–trimethylphenyl)imidazolinium chloride, **II.3** was obtained after reflux in triethyl formate as a white precipitate in 72% purity as described in the publication. [23a] Recrystallization in acetonitrile/ether affords **II.3** as 0.5 hydrate (determined by karl-fisher) in 95% isolated yield and 91% purity.

The overall yield of this 2 step synthesis is 44% and compare well with arduengo's report which is 54%

SIMesCuCl (**II.4)** was synthetized using the aqueous ammonia protocole and was obtained in 85% yield and 93% purity after recrystallization.

Addition of 4,7-dichloro-1,10-phenanthroline to a SIMesCuCl (0.1 M) dissolved in anhydrous CH_2Cl_2, followed by slow addition of pentane over 20 minutes affords the final complex [SIMesCu(4,7Cl-Phen)Cl], **II.5** in 80% yield as a dark purple powder.

II.E. Application of qNMR to measure alcohol concentration in handgels.

In 2020, we all lived in the episode of COVID-19 pandemic. The virus was accelerating and spreading more every day. The first means of protection were the precautions such as wearing a mask and washing hands with hydro-alcoholic gels. In the laboratory, we applied the World Health Organization (WHO) protocol to fabricate several dozens of litres of hydro alcoholic mixture at our institute. As we were already developing our publication concerning the qNMR (See chapter II), we used the same method to determine the quantity of alcohol (ethanol or isopropanol) in the mixture. This method was also applied to several hand gels that I brought from my origin country. However, all the hand gels coming from my country were insufficient according to the WHO procedures and to the French legislation, as less than 60% of alcohol were found inside, the minimal quantity needed to eliminate COVID-19 virus. In fact, this matter was also occurring in France. The 'direction générale de la Concurrence, de la Consommation et de la Répression des frauds', DGCCRF, asked to bring back several solutions to the furnishers.

[179] https://protocols.scienceexchange.com/protocols/synthesis-of-1-3-bis-2-4-6-trimethylphenyl-imidazolinium-salts-simes-hcl-simes-hbr-simes-hbf4-and-simes-hpf6

DGCCRF

Avis de rappel

solution hydroalcoolique "Gel Mains"

Nom du produit :
GEL MAINS GEL HYDROALCOOLIQUE
Risque : L'utilisateur pense légitimement utiliser un produit le protégeant des bactéries et virus existants. Or au regard de la teneur en éthanol retrouvée, ce produit ne peut apporter la protection nécessaire. De plus, l'étiquetage n'apporte pas les informations nécessaires eu égard au risque inhérent à l'utilisation du produit.

Figure II.9. Example of a call-back from the DGCCRF.

These facts encourage us to prepare two different communications and rapidly submit them in open access journals to raise awareness about this matter and try to afford a solution to this important societal problem. Importantly, the use of a simple alcohol-meter (as asked for the WHO's recipe) was not accurate for liquids containing gelling agents; therefore, our papers take all their importance. These communications are attached below.

II.E.1. Ethanol dosage in hydro-alcoholic gels.

Reference: Akhdar, A., Hersant, Y. and Gautier, A., Ethanol Dosage in Hydro-Alcoholic Gels, **2020**, DOI: 10.26434/chemrxiv.13060220

Authors file is provided here after

Ethanol dosage in hydro-alcoholic gels.

Ayman Akhdar, Yael Hersant and Arnaud Gautier*

CNRS-UMR 62394, Université Clermont Auvergne, SIGMA,

ICCF, F-63000 Clermont-Ferrand, France.

Abstract

A method of determination of the ethanol content in hydro-alcoholics is reported. Based on quantitative ^{1}HNMR (q^{1}HNMR), the results are obtained rapidly and accurately. The method is available for viscous solutions to which other simpler technics do not apply.

Introduction

As the spread of the COVID-19 pandemic accelerates around the world, many low- and middle-income countries are still struggling to access the diagnostic tests they desperately need to control the disease. Moreover, passive protection methods such as masks and hydro-alcoholic gels are the first means of defence to avoid chaotic spread of the virus among the population. The World Health Organization (WHO) provides a protocol that was taken into consideration in many national legislations.[1] In France, at the beginning of the pandemic, we applied this protocol to fabricate several dozens of litters of hydro-alcoholic mixture at our institute and the content of ethanol in grams per grams of solution was determined by ^{1}H quantitative NMR (qNMR). If the content of ethanol in liquids gels can be approximatively measured using a simple alcohol-meter, this technic is less appropriate for viscous liquids containing gelling agents. We report here a method of ethanol content measurement using ^{1}H quantitative NMR (^{1}H qNMR). Our intention is to remind the scientific community of this well-known

technic, and of the fact that several samples obtained from abroad do not contain the adequate amount of ethanol.

Quantitative NMR is a valuable method because the measured signals represent a direct measurement of the composition if correct inter-pulse delay are adequately chosen.[2] Therefore, in presence of an internal reference of known purity, the composition of a sample can be determined accurately using a single spectrum/ integration sequence (so-called absolute quantification). For this purpose, we used 3-(trimethylsilyl)-1-propanesulfonic acid di sodium salt (TSPA, CAS: 2039-96-5, 97% purity) as standard (also used as chemical shift reference) and D_2O for NMR solvent. After proper weighting of the standard and the gel, the mass of ethanol contained in the sample is calculated by equation 1:

$$masse(Ethanol) = \frac{46.1*15*0.97}{5*218.3} * \frac{\sum I^{Ethanol} * m^{std}}{\sum I^{Std}} \qquad \text{Eq.1}$$

Where ΣInt stands for the sum of the integral of ethanol and standard, m is the weighted mass of the standard, 46.1 and 218.3 are the molar masses, 5 and 15 represent the total number of protons of ethanol and standard respectively; 0.97 is the purity of the standard.

Results

The following spectrum depicts a typical qNMR of a home-made hydro-alcoholic solution using the WHO protocol. The amount of gel and TSPA is 34.69 and 18.14 mg respectively.

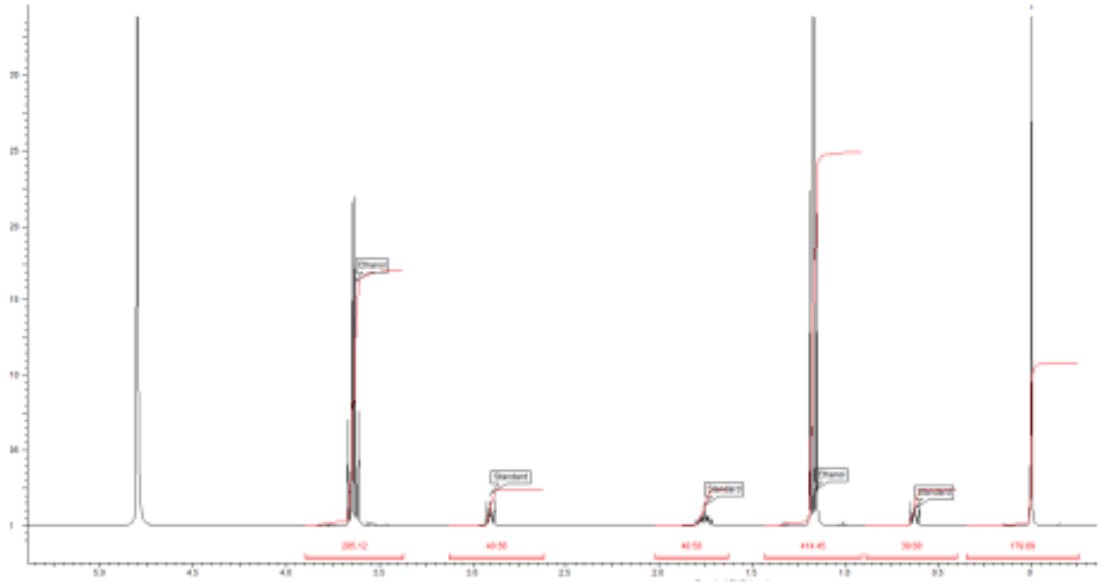

As it can be seen, ethanol and standard signals are well separated, allowing a clean integration. As the amount of gelling agent is usually lesser than a few percents, its signals are not visible. Only signals coming from the traces of glycerol are visible below the CH_2OH signal at 3.6 ppm, which makes its integration slightly overestimated. The accuracy of the measurement can be determined by the calculation of the deviation of each integration: the measured number of protons versus the theoretical number at each peak calculated by:

$$Dev = 100 * \left(\frac{Int * \sum Proton}{\sum Int} - NbProton\right) / NbProton \qquad \text{Eq.2}$$

Table 1.

Standard	TSPA:	18.14mg			Sum	Int/^{1}H	Mmol
δ(ppm)	2.8	1.65	0.52	0			
Number of ^{1}H	2	2	2	9	15		
Integration	40.56	40.58	39.6	179.7	300.4	20.0	0.0831
Deviation(%)[(a)]	-1.2	-1.3	-1.1	0.3			
Ethanol		34.69mg					

δ(ppm)	3.60	1.18					
Number of ^{1}H	2	3			5		
Integration	285.1	414.5			699.6	139.9	0.563
Deviation(%)[a]	1.9	-1.3					

A: Deviation more than 5% should be discarded.

Indeed, the number of mmol of ethanol contained in the mass of the sample is simply obtained from the cross product between the blue numbers. In our typical case, 34.69 mg of gel contains 0.58 mmol of ethanol which makes 26.8 mg. Therefore, the masse percentage is 75%.

Discussion

We followed the WHO protocol and recorded the masses of the constituents added: 833 mL ethanol (96%): 666 g; H2O2 (3%): 42mL of H_2O_2(3%): 42 g; 14.7mL of glycerol: 18 g; water to complete the 1000mL: 133 g. The total mass is therefore 859g. The mass percentage of ethanol in the gel is therefore 77.5%, in agreement with our findings (see WHO's quality control, Ref. 1, p3). During the last months, we have noticed that some gels do not fulfil WHO's requirements, some of them being so viscous that the use of an alcoholmeter becomes useless. Therefore, NMR determination of the mass percentage becomes an interesting alternative.[3]

Method

Sample Preparation. *Use of screw necked vials with PTFE closure is strongly recommended in order to minimize the ethanol evaporation.* Masses are weighed using a Mettler Toledo balance (0.01 mg accuracy) into a 4 mL flat bottom screw neck vial equipped with a centred hole, screw closure closed by a silicone PTFE (Macherey-Nagel, Germany). The standard is weighted first (Table 1) then 2 mL of D_2O is introduced. The vial is closed and gently shaken until all the solid dissolves. The gel is added (Table 1) into the vial with a syringe (Inject®-F 1 ml) equipped with a needle (Henke Sass Wolf, Germany, 0.6X25mm) through the silicone join in order to minimize the evaporation of ethanol. The

solution was shaken, then 600 µL were transferred into a 3 mm standard NMR tubes (Norell) for analysis.

Pulse Program. Sample Temperature: 19 °C (regulated ± 0.1 K). Single pulse, without carbon decoupling ('zg' with 90° pulse). Data Points (acquired): 64 K. NS=64. Relaxation delay: D1=60s. Acquisition Time: 4s. Spectral window for proton: SW=30ppm and O1: 7.5 ppm

Post-Acquisition Processing. Performed with ACDLABS software (1.2, academic version). Zero Filling: to 256K. Line Broadening: LB = 0.1 Hz. Phasing: manually. Baseline Correction: 6th order polynomial. For each signal measured a ratio signal/noise>100 is verified.

References

1. Guide to Local Production: WHO-recommended Handrub Formulations. https://www.who.int/gpsc/5may/Guide_to_Local_Production.pdf?ua=1

2. Pauli, G.F.; Chen, S.N.; Simmler, C.; Lankin, D.C.; Gödecke, T.; Jaki, B.U.; Friesen, J.B.; McAlpine, J.B.; Napolitano, J.G. Importance of purity evaluation and the potential of quantitative ^{1}H NMR as a purity assay. *J Med Chem*., **2014** *57*, 9220-31.

3. For some of these gels gathered from colleagues travelling from abroad, the mass percentage were found far away the WHO requirement, one of them reaching only 5-7%. We therefore recommend this procedure for the analysts having the possibility to access to the equipment described inhere.

II.E.2. A protocol for alcohol dosage in handrub gels.

Reference: Akhdar, A., Hersant, Y. and Gautier, A., A protocol for ethanol or isopropanol dosage in hand rub gels, *Protoc. Exch.* **2020**, DOI: 10.21203/rs.3.pex-1205/v1.

A protocol for alcohol dosage in handrub gels

Abstract

A method of determination of the ethanol content in hydro-alcoholics handrub solutions is reported. Based on quantitative ^{1}HNMR (q^{1}HNMR), the results are obtained rapidly and accurately. The method is available for viscous solutions to which other simpler technics do not apply.

Introduction

As the spread of the COVID-19 pandemic accelerates around the world, many low- and middle-income countries are still struggling to access the diagnostic tests they desperately need to control the disease. Moreover, passive protection methods such as masks and hydro-alcoholic gels are the first means of defence to avoid chaotic spread of the virus among the population. The World Health Organization (WHO) provides a protocol that was taken into consideration in many national legislations.[1] In France, at the beginning of the pandemic, we applied this protocol to fabricate several dozens of litres of hydro-alcoholic mixture at our institute and the contents of ethanol and isopropanol in grams per grams of solution was determined by ^{1}H quantitative NMR (qNMR). If the contents of alcohols in liquids gels can be approximatively measured using a simple alcohol-meter, this technic is less appropriate for viscous liquids containing gelling agents. We report here a method of ethanol content measurement using ^{1}H quantitative NMR (^{1}H qNMR). Our intention is to remind the scientific community of this well-known technic.

Reagents

NMR Brucker 400MHz.

3mm NMR tubes (Norell).

Balance (0.01 mg accuracy).

4 mL flat bottom screw neck vial equipped with a centred hole, screw closure closed by a silicone PTFE

syringe (Inject®-F 1 ml)

needle (Henke Sass Wolf, Germany, 0.6X25mm)

D_2O

3-(trimethylsilyl)-1-propanesulfonic acid di sodium salt (TSPA), CAS: 2039-96-5 (97% purity).

Procedure

Sample preparation:

- Masses are weighed using a Mettler Toledo balance (0.01 mg accuracy) into a 4 mL flat bottom screw neck vial equipped with a centred hole closed by a silicone PTFE (Macherey-Nagel, Germany).

- The standard is weighted first, then 2 mL of D_2O are introduced.

- The vial is then closed and gently shaken until all the solid dissolves.

- The gel is added into the vial with a syringe (Inject® -F 1 ml) equipped with a needle (Henke Sass Wolf, Germany, 0.6X25mm) through the silicone join in order to minimize the evaporation of ethanol. - The solution was shaken, then 600 mL were transferred into 3 mm standard NMR tubes (Norell) for analysis.

Pulse Program.

Single pulse, without carbon decoupling ('zg' with 90° pulse). Data Points (acquired): 64 K. NS=64. Relaxation delay: D1=60s. Acquisition Time: 4s. Spectral window for proton: SW=30ppm and O1: 7.5 ppm (the sample Temperature is fixed at 19 °C ± 0.1 K).

Post-Acquisition Processing.

Performed with ACDLABS software (1.2, academic version). Zero Filling: to 256K. Line Broadening: LB = 0.1 Hz. Phasing: manually. Baseline Correction: 6th order polynomial. For each signal measured a ratio signal/noise>100 is verified.

Troubleshooting

It is important to use a screw neck vial closed by a silicone PTFE and an appropriate syringe and needle to minimize ethanol evaporation during the sample preparation.

Time Taken

Sample preparation: 10 minutes

NMR acquisition: 1h

NMR processing: 10 minutes

Anticipated Results

Quantitative NMR is a valuable method because the measured signals represent a direct measurement of the composition if correct inter-pulse delay are adequately chosen.[2] Therefore, in presence of an internal reference of known purity, the composition of a sample can be determined accurately using a single spectrum/ integration sequence (so-called absolute quantification). For this purpose, we used 3-(trimethylsilyl)-1-propanesulfonic acid di sodium salt (TSPA, CAS: 2039-96-5, 97% purity) as standard (also used as chemical shift reference) and D_2O for NMR solvent.

After proper weighting of the standard and the gel, the masses of ethanol or isopropanol contained in the samples are calculated by equations 1:

$$Masse = [\ 15 \times 0.97 \times M^{(Alc)} \times SInt^{Alc} \times m^{(Std)}\ ]/[\ 218.3 \times n^1H^{(Alc)} \times SInt^{(Std)}\ ]$$

$$= [\ 0.06665 \times M^{(Alc)} \times SInt^{Alc} \times m^{(Std)}\ ]/[\ n^1H^{(Alc)} \times SInt^{(Std)}\ ] \quad \text{Eq.1}$$

Where $M^{(Alc)}$, $n^1H^{(Alc)}$ and $m^{(Std)}$ are respectively the molecular mass, the number of integrated proton and the weighted masse of the chosen alcohol; $SInt^{(Alc)}$ and $SInt^{(Std)}$ being the sum of the integrals for the chosen alcohol and the standard; 15 and 218 and 0.97 being the total number of proton, the molecular mass and the purity of the standard.

For ethanol and isopropanol respectively, the equation resumes to:

$$Mass^{(ethanol)} = [\ 0.615 \times SInt^{(Alc)} \times m^{(Std)}\ ]/\ SInt^{(Std)} \quad \text{Eq. 2}$$

$$Mass^{(isopropanol)} = [\ 0.572 \times SInt^{(Alc)} \times m^{(Std)}\ ]/\ SInt^{(Std)} \quad \text{Eq. 3}$$

We found 75% and 68% for handrub solutions produced according to the WHO protocols. The weighted masses were TSPA, 18.14mg, ethanolic gel: 34.69mg (Figure 1) and TSPA: 41.85mg, isopropanol gel: 25.95mg (Figure 2).

References

1. https://www.who.int/gpsc/5may/Guide_to_Local_Production.pdf?ua=1

2. Pauli, G.F.; Chen, S.N.; Simmler, C.; Lankin, D.C.; Gödecke, T.; Jaki, B.U.; Friesen, J.B.; McAlpine, J.B.; Napolitano, J.G. Importance of purity evaluation and the potential of quantitative ^1H NMR as a purity assay. *J Med Chem*., 57, 9220-31 (2014).

Chapter III. Access to clicked arylopeptoids on resin.

III.A. Introduction.

The click chemistry, especially the CuAAC reaction, has a great importance for post-functionalization and ligation of oligoamides such as peptides or peptidomimetics, as it yields the 1,2,3-triazoles with high yields and in addition is suitable for generation of combinatorial libraries. As we mentioned before, the CuAAC reaction was applied in solution and on solid support to access peptoids functionalized with triazole-type side chains but, to our knowledge, not on arylopeptoids or other *N*-alkylated aromatic oligoamides.[180] The application of click chemistry on solid support usually requires high quantity of copper catalyst, in addition to other additives such as DIPEA, pyridine, and ascorbic acid.[160b] These additives could result in side reactions decreasing the global yield. Also, the quantities of copper are usually high which make it hard to remove from the expected oligomers. Also, combinatorial chemistry is highly interesting as it allows the synthesis of large combinatorial libraries easily, especially on the solid support. The combinatorial libraries could be used for the screening of wide range of peptoids for potential application in medicine and material sciences[181]. This could make the screening more efficient and effective by screening several compounds with different side chains with less time and materials used.[182] In this chapter, we will discuss the CuAAC on *meta*- and *ortho*-arylopeptoids using copper(I)-*N*-heterocyclic carbene catalyst. The main objectives are: 1) Optimization of the on-support CuAAC process; 2) Exploration of the accessible chemical diversity by combinatorial chemistry and stepwise synthesis and 3) Preliminary study of the kinetics of this reaction.

Based on literature precedents that we have presented before, we selected naturally the solid support synthesis of oligomers of medium length (6-12 mers). For the methodological study we selected four different resins: 2-chlorotrityl resin, rink acid, Chemmatrix resin, which provides an acid at the *C*-terminal position, and Rink amide which provides a primary amide in *C*-terminal position. Indeed, these resins are well known to be efficient for the synthesis of many peptides and peptoids, including modification by CuAAC reactions. Chemmatrix resin was recently shown to be efficient with the copper catalyst of interest, [Cu(SIMes)(Cl_2-Phen)]Cl.[183]

Regarding the triazole side chain, two possibilities are offered. Either we could introduce them during the substitution step (route A), or introduce propargyl amine and/or an azide, then click on the solid support (routes B and C).

[180] Angell, Y. L.; burgess, K.; *Chem. Soc. Rev.* **2007**, *36*, 1674–1689.

[181] Molchanova, N.; Hansen, P. R.; Franzyk, H. *Molecules* **2017**, 22, 1430-1490.

[182] Ng, S.; Goodson, B.; Ehrhardt, A.; Moss, W. H.; Siani, M.; Winter, J. *Bioorg. Med. Chem.* **1999**, *7*, 1781-1785.

[183] Bruyat, P.; Gautier, A.; Jean, L.; Renard, P-Y. *J. Org. Chem.* **2018**, *83*, 13515−13522.

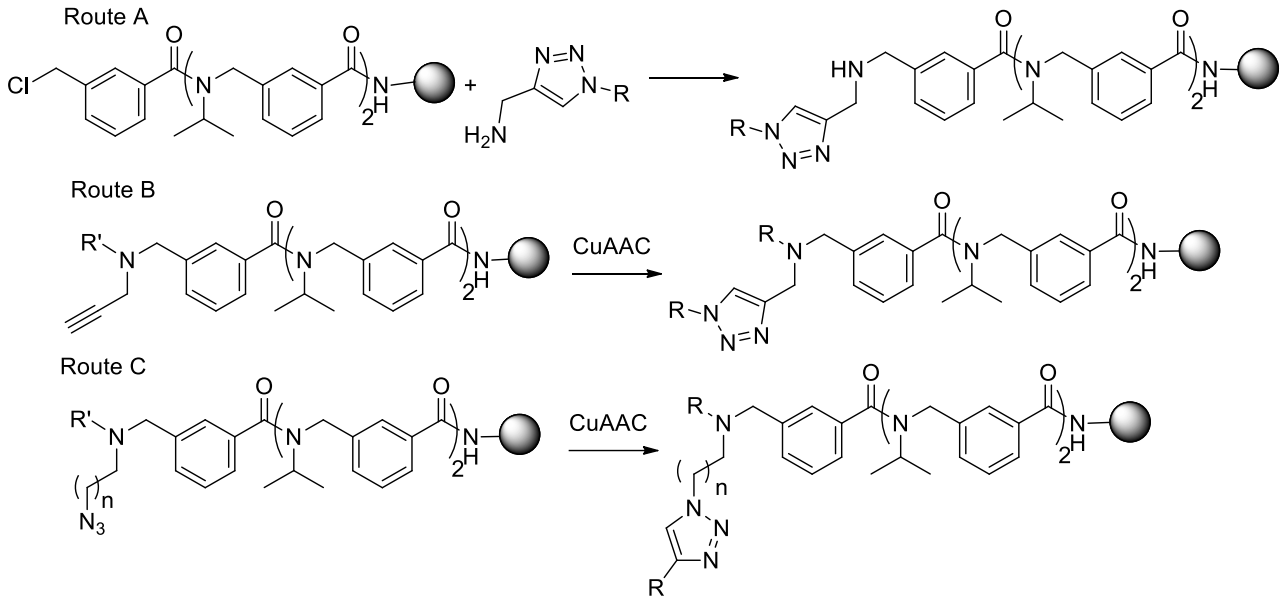

Scheme III.1. Different routes to introduce the triazole side chain.

The route A supposes a pre-synthesis of the triazoles of interest. Obviously, as the side chain substituents (amine, alcohols…) could react during the elongation of the oligomer, they require a protection. Moreover, from an atom economy point of view, this route doesn't seem to be efficient, and it was ruled out. We then embark on the more challenging route B which includes at first the synthesis of the supported oligomer containing alkynes that will be 'clicked' afterwards. It is important to note that, we do not select azide side chain (route C) because this will imply the synthesis of small azides (*i.e.* azido ethyl amine, azido propyl amine) that are potentially explosive. Indeed, this is explained in the rule of 6 : a minimum of six carbons (or other atoms of about the same size) per energetic functional group (azide, diazo, nitro, etc.) and by the the equation:$(N_{Carbon} + N_{Oxygen}) / N_{Nitrogen} \geq 3$.[184]

For the other substituents, we selected isopropyl amines as it is high yielding and hydrophobic. Therefore, we could alternate hydrophobic and cationic hydrophilic side chains (after conversion of triazoles into triazoliums) to generate amphipathic character of interest for antimicrobial activity (see Chapter IV).

Regarding the diversity, we used five azide partners, either hydrophilic containing amine, alcohol, acid groups, either hydrophobic containing benzyl or cyclohexyl groups. With these groups in hands, we through also to explore the possibility of building combinatorial library. Indeed, the maximum number of products arising from the CuAAC reaction of an oligomer containing n alkynes in its backbone and m external azides is m^n. As could be seen in the following table, the number of products accessible in only one step grows explosively.

[184] Bräse, S.; Gil, C.; Knepper, K.; Zimmermann, V. *Angew. Chem. Int. Ed.* **2005**, *44*, 5188-5240.

n(Alkyne)/m(Azide)	1	2	3	4	5
1	1	2	3	4	5
2	2	4	9	16	25
3	3	8	27	64	125
4	4	16	81	256	625

Table III.1. Number of products possible with the different numbers of alkyne and azide.

If a biological activity is found in a mixture arising from combinatorial library, owing to the difference affinity in chromatography (hydrophilic, hydrophobic, polar properties) an active fraction could be found. However, it could still contain several compounds. Therefore, it is important to be able to re-synthetize a specific compound for identification purposes.

In the following article published in Organic & Biomolecular Chemistry in January 2022, we tried to response to the preceding questions. This publication deals with the CuAAC post-modification of *meta*-arylopeptoid oligomers on support using copper (I) *N*-heterocyclic carbene as catalyst. The methodology, the optimization and the application in combinatorial chemistry and step-wise synthesis to access oligomers containing various triazole side-chains were exposed.

Reference: Akhdar, A.; Faure, S.; Gautier, A. *Org. Biomol. Chem.* **2022**, *20*, 2402-2406. DOI : 10.1039/D2OB00163B

Authors file is provided here after

III.B. Associated publication.

Access to functionalised arylopeptoid oligomers by combinatorial or sequential on-resin click chemistry using Copper(I)-*N*-heterocyclic carbene catalyst

Ayman Akhdar,[a] Sophie Faure*[b] and Arnaud Gautier*[b]

Efficient on-resin click chemistry protocol using Copper (I)-*N*-heterocyclic carbene catalyst is developed for post-functionalization of *N*-alkylated aminomethylbenzamide oligomers. The accessibility to polyfunctionalized oligomers is demonstrated using combinatorial and sequential approaches.

N-alkylated aromatic oligoamides is a class of oligomers still underexplored.[1] Contrary to other aromatic oligoamides relying on hydrogen-bonding networks for their structuration,[2] the conformational modularity and adaptability of *N*-substituted aromatic oligoamides make them particularly interesting abiotic oligomers for applications in the medical and/or materials field.[1] One major issue for their development is the ability to provide well-defined sequences with high chemical diversity. To this aim, *N*-substituted aminomethylbenzamide oligomers are particularly well adapted and represent particularly promising aromatic oligoamides.[3] They were named arylopeptoids[4] since their backbone can be considered as the peptoid (*N*-substituted glycine oligomer)[5] backbone in which a phenyl group is inserted (Figure 1). Sequence-defined arylopeptoids are accessible *via* solid-phase submonomer method wherein each residue is created in two steps: acylation/substitution[6] or acylation/reductive amination.[7] The submonomer method potentially provides access to highly diverse structures.[8] Another way to introduce chemical diversity is the post-functionalization of formed oligomers. This strategy is particularly attractive in the context of multivalent display[9] and has never been studied to access functionalised arylopeptoid oligomers. Therefore, click chemistry and especially the CuAAC reaction which was introduced two decades ago by Kolb, Finn and Sharpless, could be of particular importance as it is modular and high yielding.

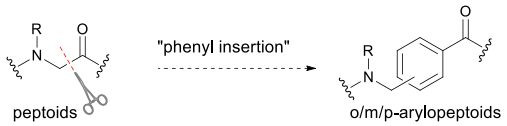

Figure 1 Analogy between peptoid and arylopeptoid oligomeric structures.

From the point of view of the synthetic chemist, combinatorial synthesis on solid support allows the rapid preparation of large and organized collections of compounds (molecular libraries) which constitute an essential source in drug discovery.[10] Nevertheless, CuAAC on solid support requires sometimes large amount of copper catalyst that is difficult to remove and therefore could contaminate the samples.[11] Also, several drawbacks from ascorbic acid has been reported.[12] Moreover, some sensible functional groups are damaged by the hydroxy radicals that are produced by the reaction of Cu(I) and oxygen.[13] Therefore, copper(I)-*N*-heterocyclic carbenes (Cu-NHCs) that are recognized as stable source of Cu(I) offer great opportunities in this field. Indeed, several publications from our group report applications in the peptide field.[14] Here, we report the application of [SIMesCu(4,7 Cl-Phen)Cl] as CuAAC catalyst to the on-resin construction of an arylopeptoid library.

To examine the possibility of post-functionalisation of *meta*-arylopeptoid oligomers by 'on support' click chemistry process, we started our investigation by reacting benzyl azide (**Ia**) with synthesized resin-bound hexamer **II-6(Alk$_{3,6}$)** containing four isopropylamine and two propargylamine side chains (Scheme 1; see ‡ for the nomenclature). This model reaction was studied on four different resins; three polystyrene-based resins: 2-chlorotrityl chloride, Rink Acid and Rink Amide, and one (polyethylene glycol)-based resin: trityl-OH ChemMatrix®. The Rink amide resin providing oligomers with a primary amide in C-terminal (X = NH) and the others leading to oligomers with an acid function (X = O).

First, the hexamer **II-6(Alk$_{3,6}$)** was prepared on the various resins using published protocols (ESI for details).[6] We used [SIMesCu(4,7Cl-Phen)Cl][‡‡] in a mixture of methanol and dichloromethane (2/8) to keep a good swelling of the resin in presence of a proton source that is essential for the catalysis. In these conditions, the outcome is strongly dependant of the type of resin. A total lack of reactivity was observed using 2-chlorotrityl resin with 20 mol-% catalyst or more as demonstrate by the recovery of the hexamer **II-6(Alk$_{3,6}$)** in 95% yield after cleavage. In addition, the colour of the solution stays reddish,

[a] *Université Clermont Auvergne, CNRS, Clermont Auvergne INP, ICCF, F-63000 Clermont–Ferrand, France.*
[b] *Université Clermont Auvergne, CNRS, ICCF, F-63000 Clermont–Ferrand, France.*
Electronic Supplementary Information (ESI) available: [details of any supplementary information available should be included here]. See DOI: 10.1039/x0xx00000x

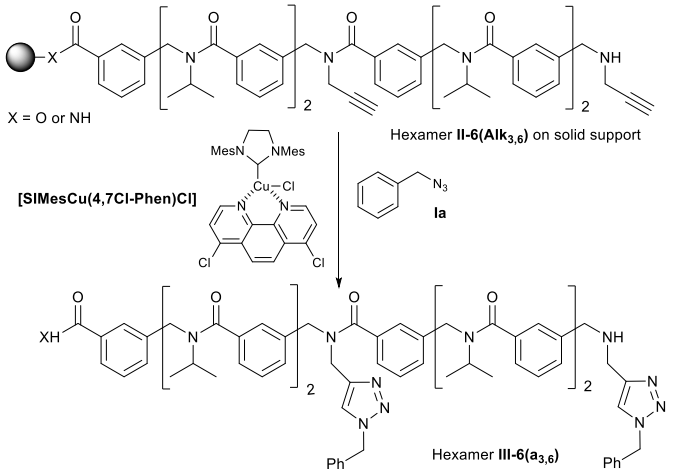

Scheme 1. Model reaction to study the on-resin click chemistry process

However, HPLC-mass spectroscopy proved that the products consist in a mixture of mono- and double-clicked compounds in a ratio 7/3. Increasing the temperature to 50°C allows to obtain a total conversion of the two propargyl groups after 2h. Regardless the temperature, in all cases a 50% purity measured by HPLC was observed after cleavage, hampering the use of the trityl-OH ChemMatrix® as solid support. Using Rink acid resin and performing the CuAAC reaction at 50°C during 3h, we were pleased to obtain full conversion and acceptable crude HPLC purity (>70%) for **III-6($a_{3,6}$)** (X = O) but in low yields (ranging from 20 to 50%). We also noticed that the reaction colour turns rapidly from red to greenish, suggesting a fast destruction of the catalyst and the production of copper(II). By analysis of the reaction mixture and the washing solvent, we found that partial cleavage of the arylopeptoid oligomer occurred during the click step, explaining low yields obtained. Decreasing the temperature to RT doesn't improve the results (80% conversion after 18h but cleavage from the resin still occurring). Thus, we concluded that a partial cleavage occurs competitively with the CuAAC reaction. From these first tests, the CuAAc reaction using copper(I)-*N*-heterocyclic carbene [SIMesCu(4,7Cl-Phen)Cl] proved to be difficult to efficiently access functionalised arylopeptoid oligomers with a *C*-terminal acid group. By contrast, using Rink Amide resin, we were delighted to find a lack of cleavage, a total conversion to **III-6($a_{3,6}$)** featuring a C-terminal primary amide (X = NH) with good reproducibility, crude purity > 80% (Figure 2) and yield after 5 hours at room temperature using 20 mol-% catalyst. Importantly, the solution stays reddish, suggesting a good stability of the catalyst. At 50°C, we were also able to decrease the reaction time to 1 h without alteration of yield and purity and reach the same results using only 1 mol-% of catalyst after 7 h. For comparison, the more classical conditions[15] using CuI catalyst (5 mol%) in presence of ascorbic acid (8 mol-%) and Hünig base (15 mol-%) in DMF/piperidine (7/3) at 50°C affords a low conversion (30%) to an equimolar mixture of mono- and bis-triazole after 3h.

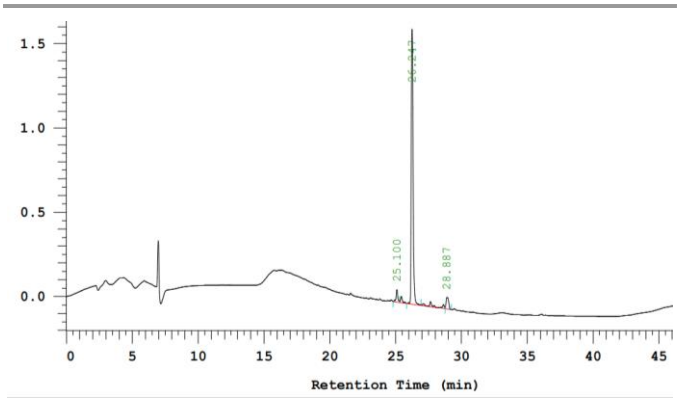

Figure 2. HPLC chromatogram of crude **III-6($a_{3,6}$)**.

In view of these results, to continue this work we decided to use only Rink Amide resin-bound oligomers and to perform on support CuAAc reaction with 5 mol-% of [SIMesCu(4,7Cl-Phen)Cl] as catalyst at 50°C in presence of four equivalents of azides per alkyne. Using these optimized conditions, a set of functionalized azides (**Ia-e**) were tested on **II-3(Alk_2)**, **II-4($Alk_{2,4}$)** and **II-6($Alk_{2,4,6}$)** resin-bound oligomers (Scheme 2). The collection of azides contains benzyl (**Ia**), cyclohexyl (**Ib**), *tert*-butyl carboxylic ester (**Ic**), Boc-protected amine (**Id**), and alcohol (**Ie**) groups.

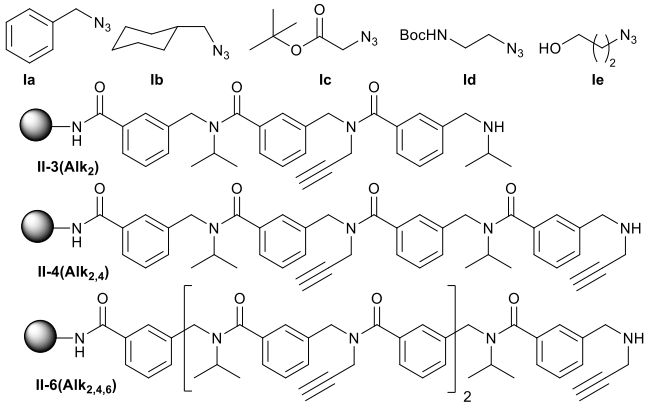

Scheme2. Collection of azides and resin-bound starting materials.

We were glad to obtain good yields and purities regardless the number and the position(s) of the alkyne(s) (table 1). In all cases, a total conversion was observed by LCMS associated with good crude purities. Therefore, a large range of functionalized triazoles could be introduced efficiently at different positions of the arylopeptoids.

Table 1: Clicked arylopeptoid from **II-3(Alk_2), II-4($Alk_{2,4}$) and II-6($Alk_{2,4,6}$)**

Arylopeptoid	Isolated yield (%)	Isolated purity (%)[a]
III-3(a_2)	98	98
III-3(b_2)	85	85
III-3(c_2)	97	96
III-3(d_2)	85	97
III-3(e_2)	90	99
III-4($a_{2,4}$)	85	87
III-4($b_{2,4}$)	75	95
III-4($c_{2,4}$)	85	81
III-4($d_{2,4}$)	77	95

III-4($e_{2,4}$)	98	97
III-6($a_{2,4,6}$)	78	88
III-6($b_{2,4,6}$)	76	91
III-6($c_{2,4,6}$)	67	95
III-6($d_{2,4,6}$)	70	93
III-6($e_{2,4,6}$)	82	98

[a] Purity determined by analytical HPLC.

In order to increase the chemical diversity, we have explored the possibility to build a small combinatorial library. A major issue in this field is to obtain a homogeneous distribution of the products. Therefore, we estimate the relative reaction rate of the different azides **Ia-e** in solution toward propargyl alcohol, as depicted in Scheme 3, using microcalorimetry.

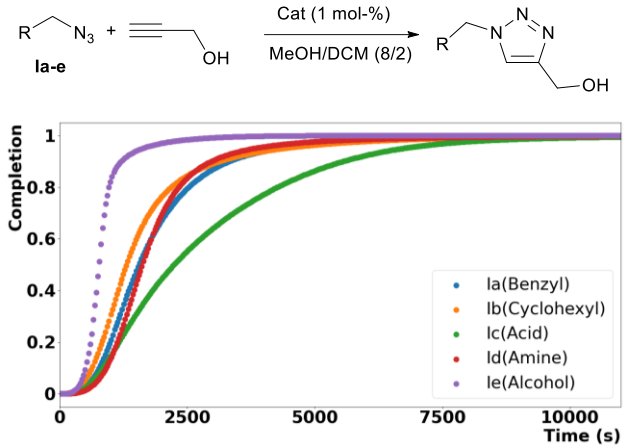

Scheme 3. Completion vs time for azides **Ia-e** in solution.

Interestingly, the completion versus time curves present all a sigmoid shape, the alcohol **Ie** being the more reactive and the protected acid **Ic** the less. This shape is relevant of a non-classical rate law, probably due to either a slow generation of the catalyst from an inactive species or an activation by the product.

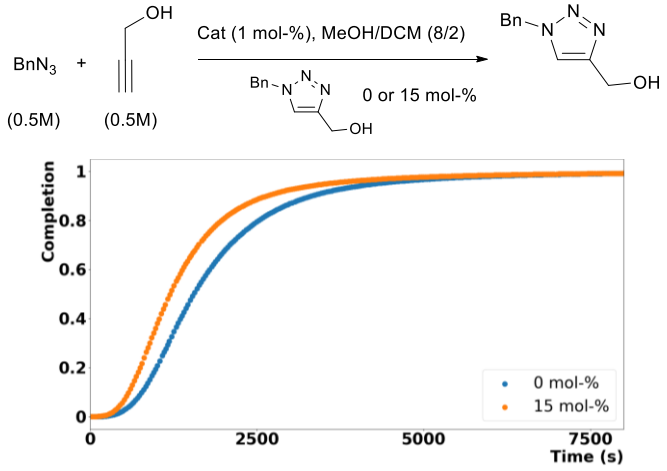

Scheme 4. Completion vs time in presence of 0 or 15 mol-% of added product

To determine if the reaction is activated by the product, we compared the reaction of benzyl azide with propargyl alcohol in solution in absence or presence of a small amount of triazole product (15 mol-%, Scheme 4). The addition of 15 mol-% of the product produces a shorten of the inductive period and an increase of rate, typical of an activation by the product. This observation is important to build our combinatorial library because it suggests that a reaction can be accelerated by the product of another one that occurs faster and simultaneously. Therefore, the products repartition will not reflect the relation of rates anymore. We confirm this hypothesis by reacting the protected amine **Id** and the alcohol **Ie** with the supported tetramer **II-4(Alk$_{2,4}$)** using 5 mol-% of catalyst (Figure 3).

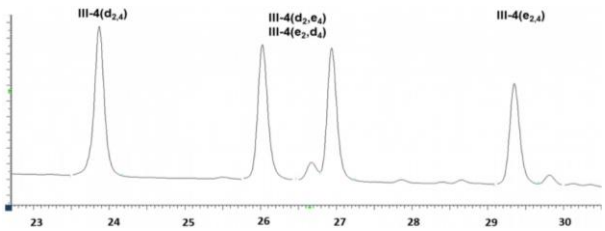

Figure 3. HPLC chromatogram showing repartition of products **III-4-(e,d)(2,4)**.

After cleavage, we observe the presence of the four products (identified by LC-MS) in comparable amount determined by HPLC (28, 25, 24 and 19% area), demonstrating that no strong preference occurs. Therefore, couples of azides from the pool **Ia-e** were selected for building the combinatorial libraries from resin-bound tetramer **II-4(Alk$_{2,4}$)** and hexamer **II-6(Alk$_{2,4,6}$)** containing two and three alkynes respectively. The combination should afford n^m possible compounds (where n: number of azides and m: number of alkynes), thus four and eight different oligomers are expected. As shown in Table 2, total conversions were observed with good isolated yields and purities. For entries 1-5, as expected, a mixture of four arylopeptoids were obtained, containing two identical triazoles and two positional isomeric compounds identified by LC-MS. For entries 6-10, HPLC separable signals were obtained. However, difficult separation was sometime obtained giving peaks overlapping. Figure 4 depicts the eight diversely functionalised arylopeptoids **III-6(a,c)(2,4,6)** (entry 7). The first and last peaks were identified as **III-6($c_{2,4,6}$)** and **III-6($a_{2,4,6}$)** respectively (comparison with authentic samples, Table 1). The regioisomers containing two acids/one benzyl or two benzyl/one acid were identified (LC-MS and HPLC) as two distinct subsets (retention times of 41-43 and 47-50 minutes, respectively).

Table2. Combinatorial CuAAc on resin-bound **II-4(Alk$_{2,4}$)** or **II-6(Alk$_{2,4,6}$)**

Entry	Products[a]	Isolated yield (%)	Purity (%)[b]
1	**III-4(a,b)(2,4)**	76	90
2	**III-4(a,d)(2,4)**	92	97
3	**III-4(b,d)(2,4)**	99	95
4	**III-4(c,d)(2,4)**	68	96
5	**III-4(d,e)(2,4)**	85	84
6	**III-6(b,c)(2,4,6)**	82	97
7	**III-6(a,c)(2,4,6)**	68	98
8	**III-6(b,d)(2,4,6)**	82	95
9	**III-6(a,d)(2,4,6)**	80	98
10	**III-6(d,e)(2,4,6)**	81	99

[a] Double bracket notation refers for all positional isomers.[‡] [b] Purity determined by analytical HPLC.

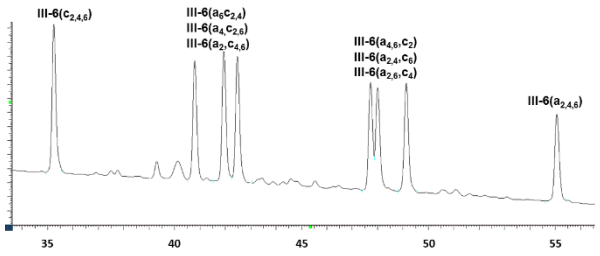

Figure 4. HPLC chromatogram of **III-6(a,c)(2,4,6)**.

This point out the problem of the identification of a specific compound from a mixture of regioisomers. Therefore, a sequential approach was developed to access oligomers with various triazoles at well-defined positions. Thus, the oligomer should continue to grow-up on the solid support after click reaction. We performed a back synthesis of **III-4(d$_2$,e$_4$)** and **III-4(e$_2$,d$_4$)** (Figure 3) and all the regioisomers of **III-6(a,c)(2,4,6)** appearing between 40-50 minutes (Figure 4). For the tetramers, two synthetic pathways were explored (scheme 5). Path A starts with **III-3(Alk$_2$)** which was clicked with **Id**. We were pleased to see that elongation occurs efficiently to afford **III-4(d$_2$,Alk$_4$)**. Final post-functionalization using **1e** affords the expected product (82 % yield, 92% HPLC purity). Path B describes the synthesis of the second regioisomer which occurs by i) cycloaddition with **1e**, ii) elongation, iii) CuAAC with **Id** and iv) cleavage. **III-4(e$_2$,d$_4$)** was obtained in 79% isolated yield (87% HPLC purity) for 11 steps. Interestingly, elongation occurs on the alcohol **III-3(e$_2$)** without any side reactions (*i.e*. esterification).

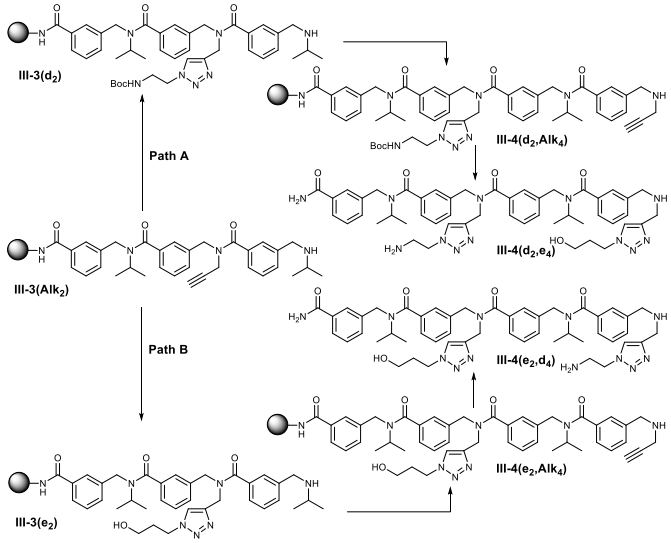

Scheme 5. Back synthesis of **III-4(d$_2$,e$_4$)** and **III-4(e$_2$,d$_4$).**

Following identical strategies (see ESI), hexamers **III-6(a$_2$,c$_{4,6}$), III-6(a$_4$,c$_{2,6}$)** and **III-6(a$_6$,c$_{2,4}$)** for first subset (Figure 4) were synthetized in 84, 93 and 67% isolated yield respectively (85, 97 and 87% HPLC purity); the second subset **III-6(a$_{4,6}$,c$_2$)**, **III-6(a$_{2,6}$,c$_4$)** and **III-6(a$_{2,4}$,c$_6$)** being isolated in 83, 84 and 90% yield respectively (92, 92.5 and 83% HPLC purity). This combination of sequential post-functionalization by click and growing sequence allows an efficient back synthesis of each of the mixture components allowing each peak displayed in schemes 5 and 6 to be attributed using the pure samples (table S1 in ESI).

In conclusion, we report for the first time the use of Cu(I)-NHC for poly-functionalisation by CuAAc reaction on resin. This efficient and mild process performed on rink amide resin-bound oligomers with a panel of azides was applied to access a small library of functionalized *meta*-arylopeptoid trimers, tetramers and hexamers. To increase the chemical diversity, a combinatorial approach was efficiently developed. Finally, a sequential approach has enabled the synthesis of specific oligomers containing various triazole groups at well-defined positions demonstrating the versatility of this on support click chemistry process using [SIMesCu(4,7Cl-Phen)Cl] as catalyst.

Notes and references

‡: **I** stand for azides, **II** for resin-bound arylopeptoid oligomers containing alkyne(s) and **III** for arylopeptoid oligomers containing triazole(s). A single bracket notation stands for a single regioisomer, i.e. **III-3(a$_2$)** refers to a trimer containing a benzyl triazole at position 2. Notation with two brackets refers to a mixture of compounds from combinatorial library, first bracket stands for the triazole's substituents and the second for the positions.

‡‡: SIMes: 1,3-Bis(2,4,6-trimethylphenyl)-4,5-dihydroimidazol-2-ylidene; 4,7Cl-Phen : 4,7-dichloro-1,10-phenanthroline.

1 A. Akhdar, A. Gautier, T. Hjelmgaard and S. Faure, *ChemPlusChem*, 2021, **86**, 298.

2 I. Huc, *Eur. J. Org. Chem.,* 2004, 17; D.-W. Zhang, X. Zhao, J.-Li Hou and Z.-T. Li, *Chem. Rev.,* 2012, **112**, 5271.

3 T. Hjelmgaard, O. Roy, L. Nauton, M. El-Ghozzi, D. Avignant, C. Didierjean, C. Taillefumier and S. Faure, *Chem. Commun*., 2014, **50**, 3564; T. Tsuzuki, H. Katagiri, Y. Kitamura, Y. Kitade and M. Ikeda, Tetrahedron, 2016, **72**, 6886.

4 T. Hjelmgaard, S. Faure, D. Staerk, C. Taillefumier and J. Nielsen, *Eur. J. Org. Chem.,* 2011, 4121.

5 M. A. Kline, L. Guo and R. N. Zuckermann in *Sequence-Controlled Polymers,* (Ed.: J.-F. Lutz), Wiley-VCH, Weinheim, **2018**, 183; R. N. Zuckermann, D. A. Goff, S. Ng, K. Spear, B. O. Scott, A. C. Sigmund, R. A. Goldsmith, C. K. Marlowe, Y. Pei, L. Richter and R. Simon, *US005877278A*, 1999.

6 T. Hjelmgaard, S. Faure, E. De Santis, D. Staerk, B. D. Alexander, A. A. Edwards, C. Taillefumier and J. Nielsen, *Tetrahedron,* 2012, **68**, 4444.

7 M. Ikeda, K. Horio, T. Tsuzuki, R. Torii, A. Shibata, Y. Kitamura, H. Katagiri and Y. Kitade, *Tetrahedron Lett.,* 2015, **56**, 6726.

8 J. E. Rasmussen, M. M. Boccia, J. Nielsen, C. Taillefumier, S. Faure and T. Hjelmgaard, *Tetrahedron Lett.*, 2014, **55**, 5940.

9 M. Mammen, S. K. Choi and G. M. Whitesides, *Angew. Chem. Int. Ed.,* 1998, **37**, 2754; J. E. Gestwicki, C. W. Cairo, L. E. Strong, K. A. Oetjen and L. L. Kiessling, *J. Am. Chem. Soc.,* 2002, **124**, 14922.

10 For a review on combinatorial chemistry of peptoids, see: C.N. Herlan, D. Feser, U. Schepers and S. Bräse, *Chem. Commun.,* 2021, **57**, 11131.

11 V. Castro, H. Rodríguez and F. Albericio, *ACS Comb. Sci.*, 2016, **18**, 1.

12 V. Hong, S. I. Presolski, C. Ma and M. G. Finn, *Angew. Chem. Int. Eds*, 2009, **48**, 9879.

13 S. Li, H. Cai, J. He, H. Chen, S. Lam, T. Cai, Z. Zhu, S. J. Bark and C. Cai, *Bioconjugate Chem.* 2016, **27**, 2315.

14 C. Gaulier, A. Hospital, B. Legeret, A. F. Delmas, V. Aucagne, F. Cisnetti and A. Gautier, *Chem. Commun.*, 2012, **48**, 4005; P. Bruyat, A. Gautier, L. Jean and P-Y Renard *J. Org. Chem.,* 2018, **83**, 21, 13515.

15 H. Jang, A. Fafarman, J. M. Holub and K. Kirshenbaum, *Org. Lett.,* 2005, **7**, 1951; T. Zabrodski, M. Baskin, P. J. Kiniraj and G. Maayan, *Synlett*, 2015, **26**, 461.

III.C. Discussion.

III.C.1. Description of the equipment.

The synthesis of the arylopeptoids was done using a bench top shaker purchase from Serlabo. This machine could hold up to 6 reactors (Figure III.1.a), allowing to work in parallel. In order to obtain reproducible results, we used jacketed reactors purchased from VLC company (Issoire) in which a water flux surrounds the reaction chamber (Figure III.1.b). Indeed, as the laboratory's 'room temperature' fluctuates between 38°C in summer and 12°C in winter, this equipment is of paramount importance. The jacketed system is connected through a fish water pump (Eheim compactON 600, 4L/min) to two thermostated water batches (Xtemp, XT5618B8: cold batch, Lauda: hot batch) (Figure III.2.a). The cold bath was fixed at 25°C and the hot one at 45°C. By changing the position of the pump fish, the temperature inside the reactor could switch very rapidly (2 minutes) and in a reproducible manner. Finally, reactors were connected to a pump (KIF LABOPORT) to drain down the reaction solvent into a receiver container (elimination of the solvent takes 1-2 seconds).

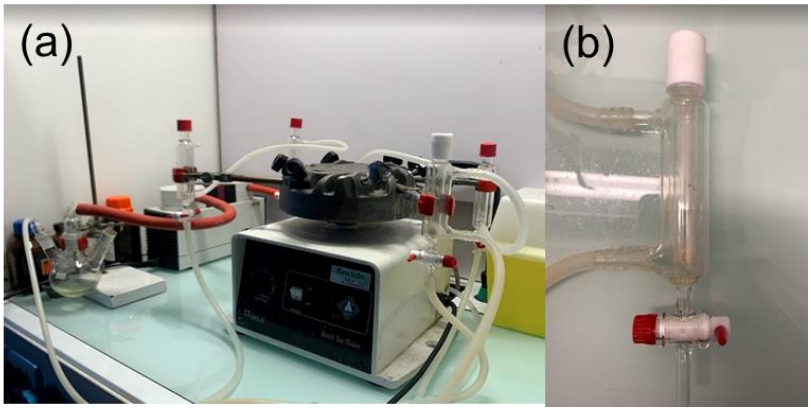

Figure III.I. The jacketed reactor, shaking machine and pump.

Importantly, we find out that if normal toppers are working well for the initial and iterative steps, they are destroyed during the final cleavage which use the corrosive trifluoroacetic acid. A strong contamination of the product by unknown polymeric compounds were detected. Therefore, for this step only we replace the usual toppers by those in Teflon made by our colleague Marc Nivoix at the 'Institut Pascal', UCA (Figure III.2.b).

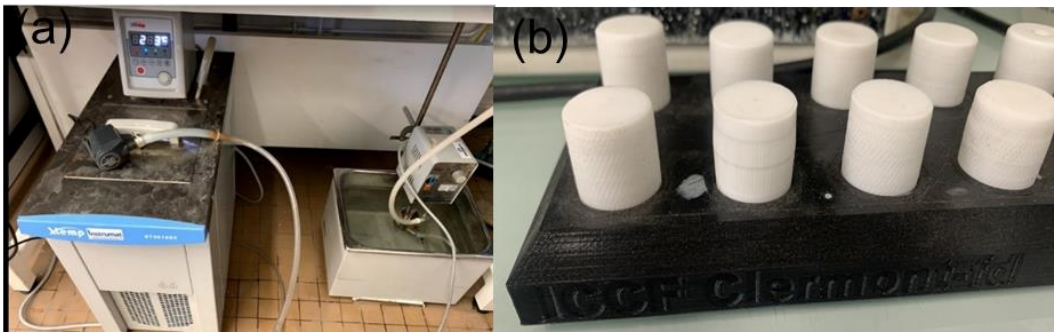

Figure III.2. The thermostatic machines and the Teflon's toppers.

III.C.2. Methodological study: process and optimization.

As shown in the publication, we've faced several problems arising from the nature of the resin and the catalytic step.

III.C.2.a. Starting material

As we discussed in chapter I, the optimized method of the synthesis of the arylopeptoids uses benzoyl chloride instead of DICs activation of benzoic acids. It should be noted that *meta* and *para* compounds are cheap and easily synthetized from the corresponding benzoyl alcohol using $SOCl_2$ (Scheme III.2).[185]

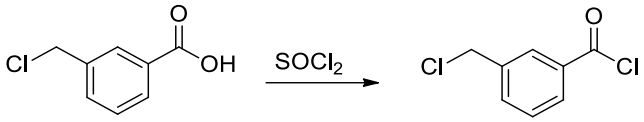

Scheme III.2 Synthesis of 3-chloromethyl benzoyl chloride.

Oppositely to the *meta* and *para* regioisomers, the *ortho* chloromethyl benzoyl chloride is a relatively expensive reagent. Indeed, it is synthetized from *ortho*-toluic acid or phthalide using noxious reagent and harsh conditions (Scheme III.3).[186] Many other synthetic routes could be found in literature, all based on dangerous conditions. Therefore, we decide to buy this compound.

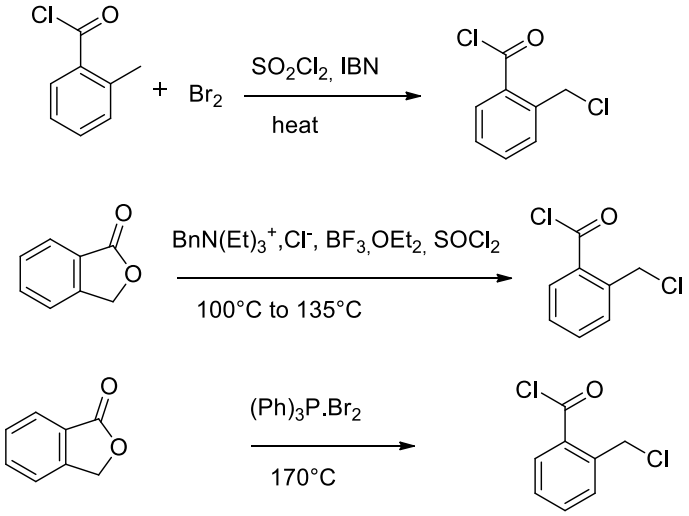

Scheme III.3 Synthesis of *ortho*- benzoyl chloride starting material.

Arylopeptoid oligomers are accessible in high yields and purities on solid support using the solid-phase submonomer synthesis, as shown by Hjelmgaard *et al*.[106]

[185] Arnaud, S. P.; Wu, L.; Wong Chang, M-A.; Comefrod, J. W.; Farmer, T. J.; Schmid, M.; Chang, F.; Li, Z.; Mascal M. *Faraday Discuss.* **2017**, *202*, 61-77.

[186] Kalugin, V. E.; Shestopalov, A. M. *Russ. Chem. Bull., Int. Ed.* **2019**, 68, 588-596. (b) Gotsch, E.; Jenny, C-J.; Reinld, P.; Ricklin, F. *Helv. Chim. Acta*. **1996**, *79*, 2219-2234.

III-C.2.b. The choice of the resin

We used 2-chlorotrityl resin (100-200 mesh, 1% DVB, loading 1.71 mmol/g), Chemmatrix (trityl-OH resin, 35-100 mesh, loading 0.33 mmol/g, aldrich), Rink acid (100-200 mesh, loading 0.6 mmol/g, Novabiochem) and Rink amide (100-200 mesh, loading 0.62 mmol/g, Novabiochem,). At first, we tested the synthesis of *meta*-arylopeptoid hexamers incorporating isopropyl and propargyl side chains. We find out that all resins except the Chemmatrix, work well on 200 mg scale (usually 90% crude yield and 90% purity; Figure III.3).

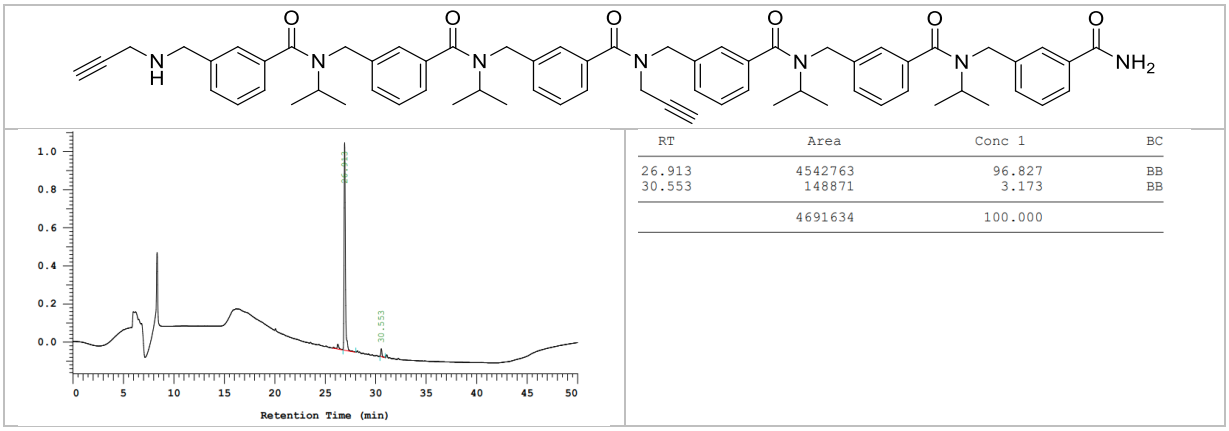

Figure III.3. Example of model *meta*-arylopeptoid hexamer made on 2-chlorotrityl resin and its HPLC trace.

Regarding the Chemmatrix resin, the classical protocol starts with the trityl-OH linker which is supposed to react with the 3-chloromethyl benzoyl chloride in presence of Hunig's base in CH_2Cl_2. However, observed yields and purities were very low (5%). To circumvolve this problem, we activate the resin through the transformation of the trityl-OH into trityl-Cl using $SOCl_2$. The first step consists now in the introduction of the 3-chloromethyl benzoic acid in presence of Hunig's base in CH_2Cl_2 with an overnight reaction at room temperature for the first acylation. After elongation, the cleavage with TFA/DCM (50/50), occurs smoothly but purity of the product was 30-50% (Figure III.4.a). We therefore add a carbocation scavenger (triisopropyl silane TIS) in a mixture TFA/H_2O/TIS (95:2.5:2.5) which leads to a better result in terms of purity 80%. Overall, to our delight, we observed good yield and purity which increase up to 80% (Figure III.4.b).

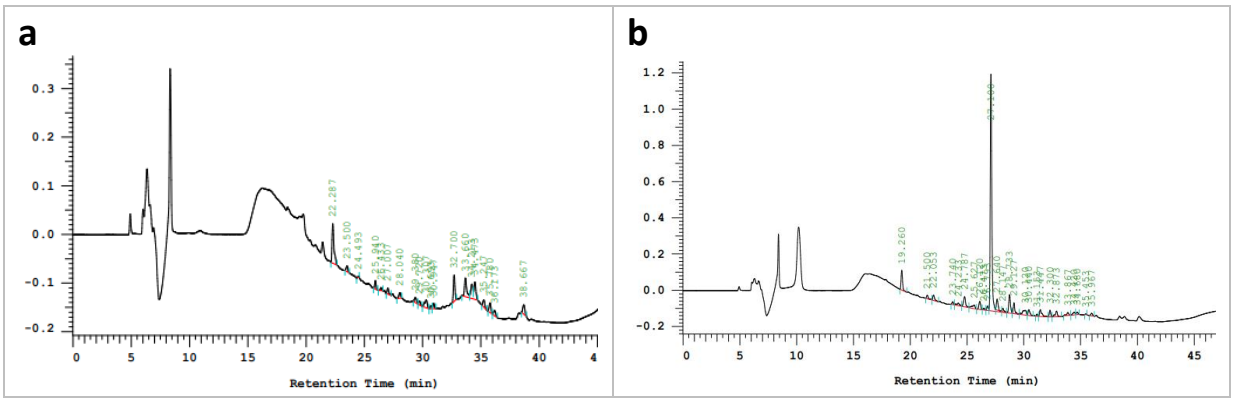

Figure III.4. HPLC traces of the crude hexamer obtained using chemmatrix resin: First studied protocol (a) and optimized protocol (b).

III-C.2.c. Optimization of the CuAAC reaction on support

We started to conduct the "click" experiments on a model hexamer carrying two propargyl side chain on 2-chlorotrityl resin in the presence of an excess of benzyl azide (6 equiv.) and 20 mol% catalyst **A** at 50°C. Failure of the CuAAC was observed in both MeOH and MeOH/CH_2Cl_2 as solvents (Scheme III.4). Indeed, after cleavage only oligomers containing alkynes and no triazole compounds were observed by HPLC and LCMS. The reason of this total failure is unknown and this reaction needs more investigations.

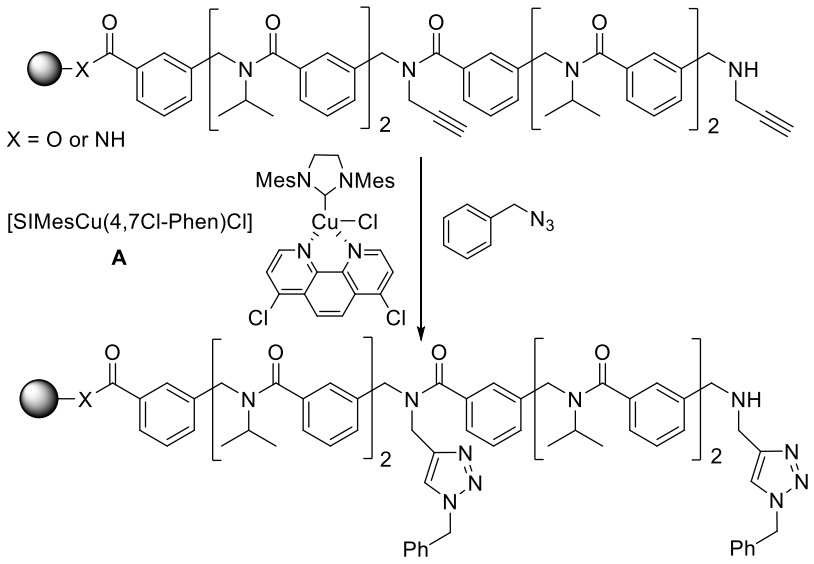

Scheme III.4. Model reaction for the CuAAC optimization

Regarding Chemmatrix resin, we observed better results (Table III.2). The cleaved mixture shows 80% conversion of the starting material and as products, 65% of mono-triazole and 35% of bis-triazole when using 10 mol% catalyst per triple bond at RT for 16h in CH_2Cl_2/MeOH (2/8). Increasing again the temperature to 50°C during 1.5h reaction time, the conversion was increased up to 90%. The amount of bis-triazole oligomer increases to 80%. Finally, a full conversion was observed when the catalyst was increased up to 20 mol% per triple bond in only 2h at 50°C, leading to 100% of bis-triazoles oligomer in this case.

T (°C)	Time (h)	%mol catalyst/ triple bond	Conversion (%)	Mono-triazole (%)	Bis-triazole (%)	Crude purity of bis-triazole
25	1	10	60	75	25	50%
25	16	10	80	65	35	75%
50	1.5	20	90	20	80	60%
50	2	20	100	0	100	45%

Table III.2. Optimization of CuAAC on chemmatrix.

The chemmatrix resin shows a very good conversion and yields, but we face a purity problem after cleavage of the resin (Figure III.5). Indeed, undefined compounds of high molecular masses

appear, probably arising from the resin decomposition. This was expected as many problems were already found with the cleavage of the starting material from the Chemmatrix resin.

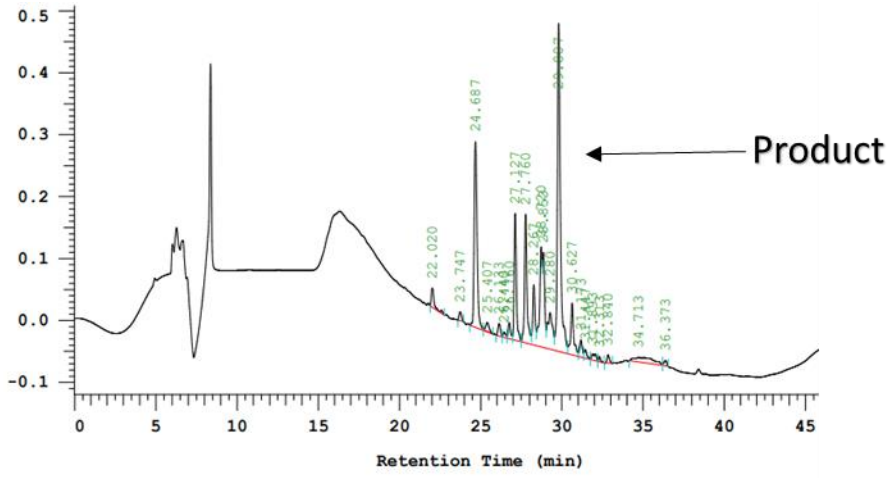

Figure III.5. HPLC chromatogram of the crude hexamer (expected compound at 29.007 min) after cleavage from Chemmatrix resin.

We take advantage of the best conditions found for Chemmatrix resin to be applied on the Rink Acid resin. As mentioned in the publication, our results show a full conversion to the bis-triazoles after 2h, but with a low yield (20%). The drained solution of the CuAAC reaction shows the presence of the bis-triazoles product in this solution, which imply that a cleavage was occurring during the reaction probably due to the sensitivity of the Rink Acid resin to Lewis acidity. Indeed, the Rink Acid linker is a methylene biphenyl in which the formation of a positive charge is facilitated by the presence of the electro-donating groups. Therefore, presence of copper(II), a stronger Lewis acid than copper(I) could easily explain the cleavage during the click reaction.

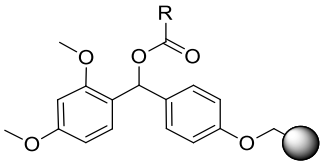

Figure III.6. Structure of the Rink Acid resin linker.

This hypothesis is supported by the poor stability of our catalyst in these conditions as the solution turns rapidly from blood red to green, indicative of the formation of copper (II). The reason of the instability of our catalyst in the presence of Rink Acid resin is not known. More studies showed a trend of destruction of catalyst as temperature increases, which leads to even more cleavage from the resin during the reaction.

Finally, we switch to Rink Amide resin as amides are known to be more stable than esters. To our delight, it shows more robustness than Rink Acid in click reaction, as >99% conversion could be achieved in less than 2 h without facing any cleavage problems. Gratifying, the catalyst shows high stability with the rink amide, the color of the reaction staying bloody red after 5 h at 50°C.

The crude product shows a rather good purity (84%) and after purification the isolated yield of the bis-triazoles hexamer was 85% yield with 95% purity (Figure III.7).

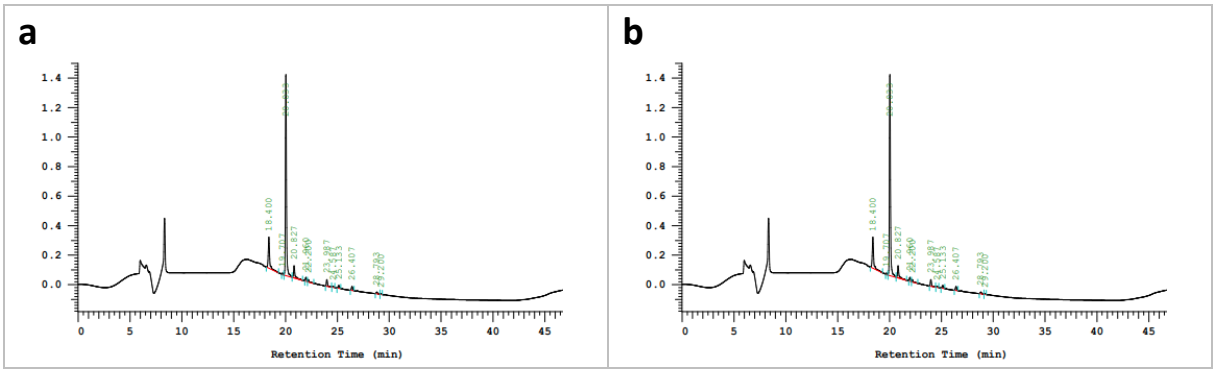

Figure III.7. The HPLC chromatograms of crude hexamer (a) and pure hexamer (b) after CuAAC with BnN_3.

Optimization and kinetic study of the on-resin reaction (*meta*-arylopeptoids on Rink Amide resin)

After the selection of Rink Amide (RA) as the resin to continue our studies with, the optimization of the on-resin reaction was studied on the model reaction of the trimer synthesized on RA resin with the benzyl azide at 50°C in a mixture CH_2Cl_2/MeOH (8/2) (Scheme III.5). The optimization of the amount of catalyst was studied at 50°C using 1 ml of solvent and 4 equiv. of benzyl azide (Table III.3).

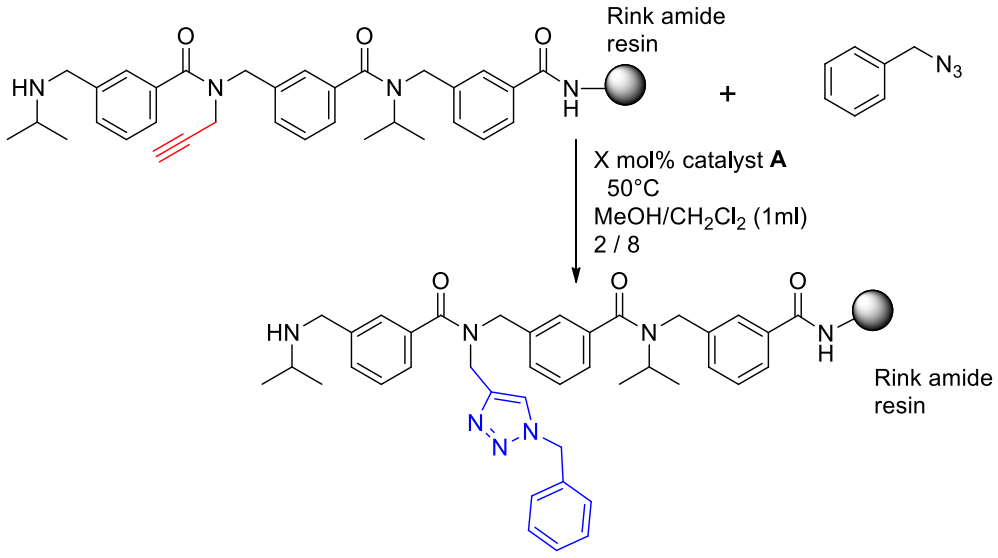

Scheme III.5. Model reaction for conditions optimization.

At first, 20 mol% of catalyst was added giving full conversion after 1 h. Decreasing the amount to 10 mol% increases the reaction time to 2 h and with a catalyst loading of 0.5 mol-% 3 h are necessary. The reaction was completed in 7 h using only 1 mol% catalyst **A**.

Entry	% Catalyst	Time for full conversion (h)
1	20	1
2	10	2
3	5	3
4	1	7

Tableau III.3. Optimization of the catalyst % and time of the reaction.

After optimization of the catalyst amount, the completion on solid support was studied using 1 mol% catalyst at 50°C. The experiments were done on 100 mg scale of resin (100-200 mesh, 0.54 mmol/g) and the stock solution of 10 ml (of the catalyst) was prepared directly before the reactions to ensure more accuracy of the study and 1 ml was taken by a Hamilton syringe also for best accuracy. After studying the conversion of the reactions using HPLC, the graph below was obtained. This graph shows the existence of a small inductive period (30 minutes) after what the conversion seems to increase linearly, reaching 100% after 7h.

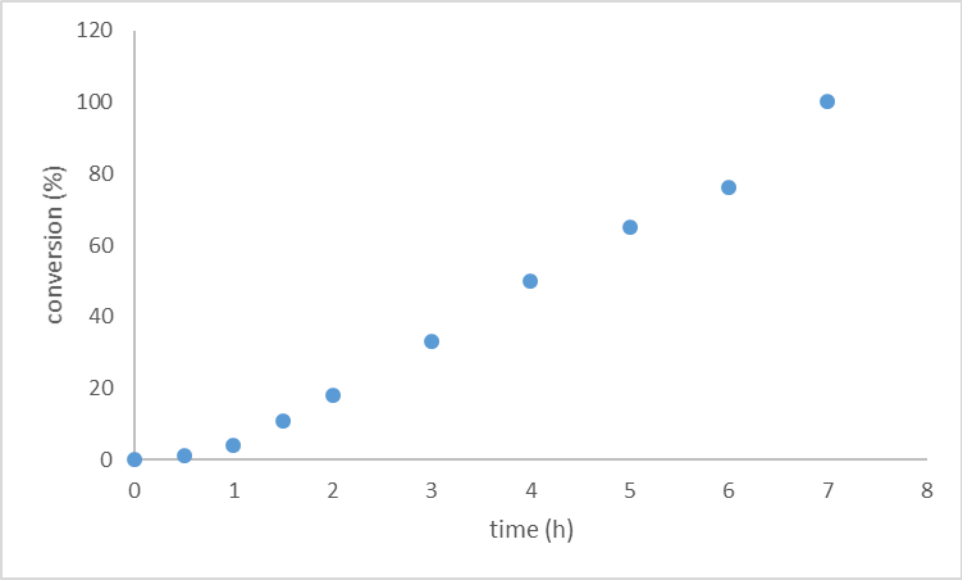

Graph III.1. Completion of the CuAAC reaction on resin with 1 mol% catalyst.

III.C.2.d. Combinatorial and back reaction on resin.

The reaction is efficient enough to allow combinatorial chemistry. As written in the publication, we showed that the reaction occurs with intervention of the product in the reaction rate which imply that a roughly equal amount of each product in the combinatorial process is produced. Our main challenge was therefore the resynthesis of a specific compound that could contain different triazoles. Indeed, we succeed to elongate the chain after the click reaction without affecting the crude yields and purity. Thus, the catalyst NHC-Cu(I) catalyst gratifyingly not perturbate the synthesis.

III.C.3. Unpublished results.

III.C.3.a Combinatorial Library extension.

We wish here to report unpublished results regarding combinatorial library. We successfully applied the CuAAC reaction with 3 different azides to the hexamer (containing 3 triple bonds) which should mathematically furnish 3^3=27 compounds. It is important to note that all yields related to a combinatorial mixture are calculated based on the average of the molecular weight of all the compounds present according to the fact that equal proportions are formed.

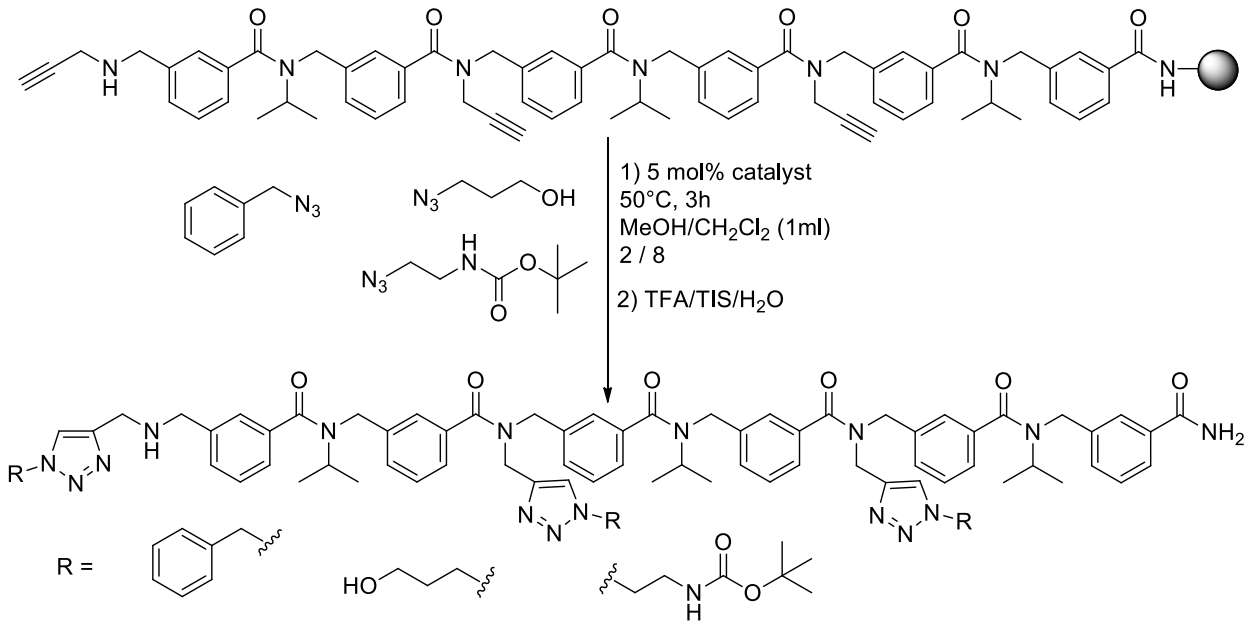

Scheme III.6. Combinatorial reaction with three different azides.

However, we notice that the different regioisomers are overlapping for some of them. This was proved by changing the HPLC methods and making it longer, which affords a better separation (Figure III.8).

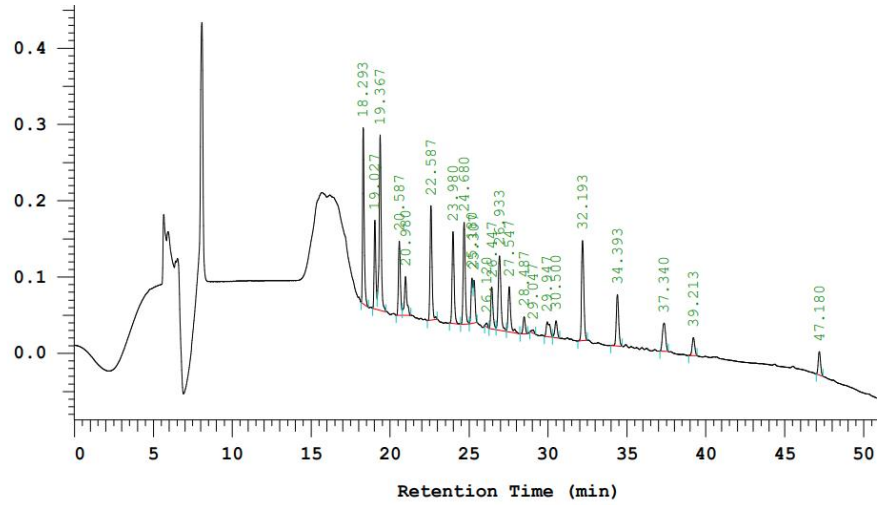

Figure III.8. HPLC diagram of the crude of the combinatorial process with 3 azides.

However, only 22 peaks among the 27 expected were found, probably still due to overlapping. Based on HPLC chromatogram of pure compounds already synthetized, the peaks at 18.29, 22.59 and 47.18 are attributed to the oligomers carrying three amines, three alcohols and three cyclohexyl substituted triazoles, respectively. Proof of this identification is re-enforced by the LC-HRMS. The appearance order of the product's peaks corresponds to the hydrophilicity of the side chains: protonated amines appear first, followed by alcohols and then cyclohexyl groups as the most hydrophobic side chains. Indeed, all the possible combinations that we expect were found: combinations of amine and alcohol side-chains appears from 18 to 23 minutes, then comes combination of the three different side-chains: amine, alcohol and cyclohexyl (retention time from 23 to 30), followed by cycloxyl and alcohol combination (30-40 minutes) and ending with the oligomer carrying only cyclohexyl substituent at 47 min.

Range of retention time (min)	Products
18.293	Triamine
19-22.6	Mixture of amine and alcohol triazoles
23-32	Mixture of amine, alcohol and cyclohexyl
32-40	Mixture of alcohol and cyclohexyl
47.18	Tri-cyclohexyl

Tableau III.4. Combinatorial library distribution according to the nature of the triazoles.

III.C.3.b. Extension to meta-heptamers.

The synthesis of heptamers in the *meta*-arylopeptoid series was also explored on RA resin (Figure III.9). The heptamer **III.1** with 4 propargyl side-chains, synthetized using the submonomer method, was obtained with 84% isolated yield and 95% purity after Buchi LC.

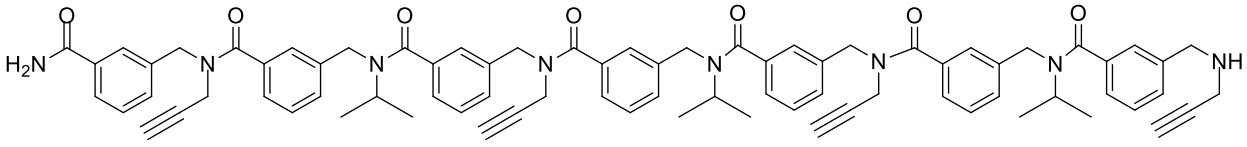

III.1

isolated yield = 84%
isolated purity =95%

Figure III.9. The *meta*-arylopeptoid heptamer synthesized on rink amide.

The optimized CuAAC reaction conditions show full conversion to the desired triazoles, in high isolated yield and purities (Figure III.10). The *meta*-heptamer triazole **III.2**, containing the cyclohexyl substituent, was isolated in 82% yield and 93% purity. **III.3**, containing aminopropyl substituent, was isolated in 78% yield and 95% purity.

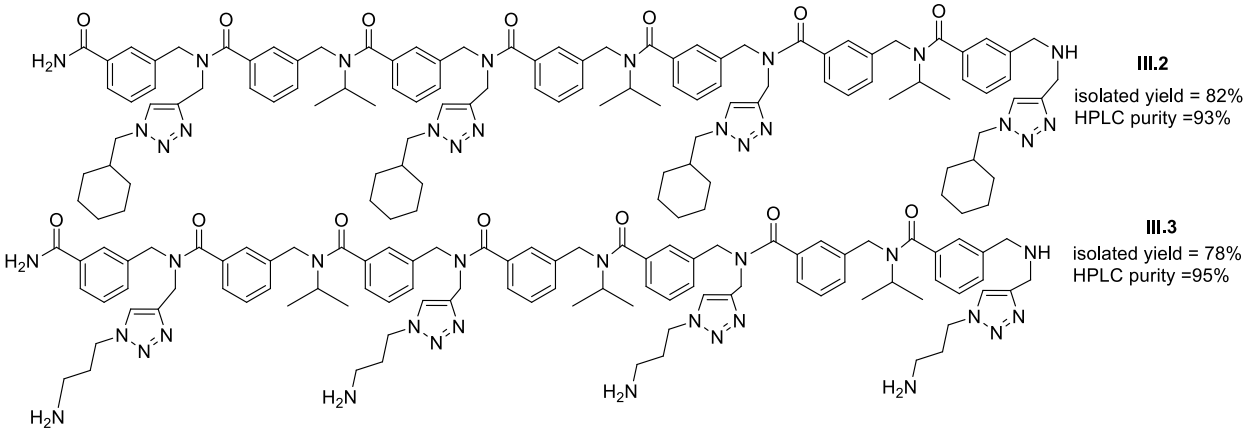

Figure III.10. The triazoles formed from *meta*-arylopeptoids heptamer **III.1**.

Therefore, these results indicated that our methodology could be extended to longer oligomers. The application of these arylopeptoids will be presented in chapter IV.

III.C.4. Extension of the methodology to *ortho*-arylopeptoids.

After succeeding in the CuAAC on meta-arylopeptoids, a logical extension is to perform CuAAC reaction on the *ortho* series. As previously reported, the synthesis of *ortho*-oligomers is more challenging that those of *meta*- and *para*-arylopeptoids. Therefore, several modifications in the protocol were necessary. Both the acylation and substitution reactions of the *ortho*-arylopeptoids were done at room temperature to prevent hydrolysis (Scheme III.3).[156] It is important to mention that the first substitution of the amine should be the isopropyl amine since the addition of the propargyl amine shows a very low yield, due to formation of the corresponding isoindolinone as previously observed.[156] Besides, the nucleophilic parameters (N and s) in Mayer's scale are 12.29, 0.59 and 13.8, 0.7, for propargyl and isopropyl amines respectively.[187] This observed parameter probably comes from the strong inductive effect of the triple bond; ι parameter in Inamoto scale is 3.074 for propargyl amine and 2.493 for isopropyl (note that ι parameter for CF_3 is 2.985).[188]After the first monomer completion, no problems with the substitution steps were observed and synthesis with alternating propargyl amine and isopropyl amine could be done. The *ortho*-arylopeptoids were synthesized on Rink Acid resin with high crude yield (up to 90%) and high crude purity (more than 95% by LCMS).

[187] Mayr's Database Of Reactivity Parameters - N-Nucleophiles (lmu.de)

[188] Inamoto, N.; Masuda, S. *Chem. Lett.* **1982**, *11*, 1003-1006.

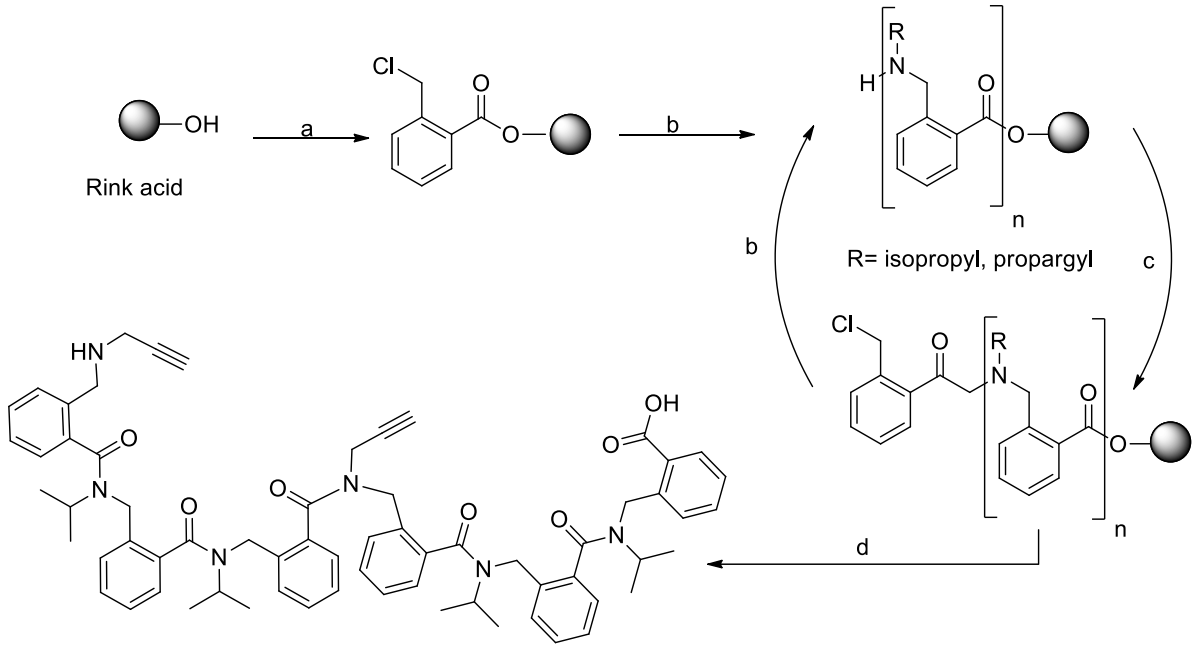

Scheme III.7. Solid phase submonomer synthesis on Rink Acid resin with an acid at the *C*-terminus. (a) $ClCH_2ArCOCl$ (3.0 equiv., 0.5 M), DIPEA (3.0 equiv.), DMAP (3 equiv.), CH_2Cl_2, RT, 10 min (b) R-NH_2 (20 equiv., 2.0 M), DMSO, RT, 1h (c) $ClCH_2ArCOCl$ (3.0 equiv., 0.5 M), DIPEA (6.0 equiv.), CH_2Cl_2, RT, 10 min (d) TFA/TIS/H_2O 95/2.5/2.5, RT, 30 min.

The click chemistry was then applied on Rink Acid-supported oligomer using the optimized CuAAC conditions of *meta*-arylopeptoids. More than 95% of conversion was observed, but some cleavage from the resin occurs during the reaction which decreases the crude yield to 20%. This cleavage was not unexpected in the view of what was observed in the *meta* series. For this reason, we adapted the synthesis of *ortho*-arylopeptiods on Rink Amide resin. The synthesis of *ortho*-arylopeptoid was performed using the submonomer synthesis on RA resin using the same procedure. The propargyl amine could be added on the first monomer on this resin thanks to its high stability that decreases the risk of aminolysis and/or isoindolinone formation.[156]

We synthesized three different series of *ortho*-arylopeptoids in high crude yield (90%) and high crude purity (90% by HPLC) (Figure III.11). Purification led to oligomers with excellent isolated yields. The *ortho*-tetramer **III.4** was isolated in 75% yield and 96% HPLC purity. **III.5** was isolated in 85% yield and 97% HPLC purity. **III.6** was isolated in 79% yield and 99% HPLC purity.

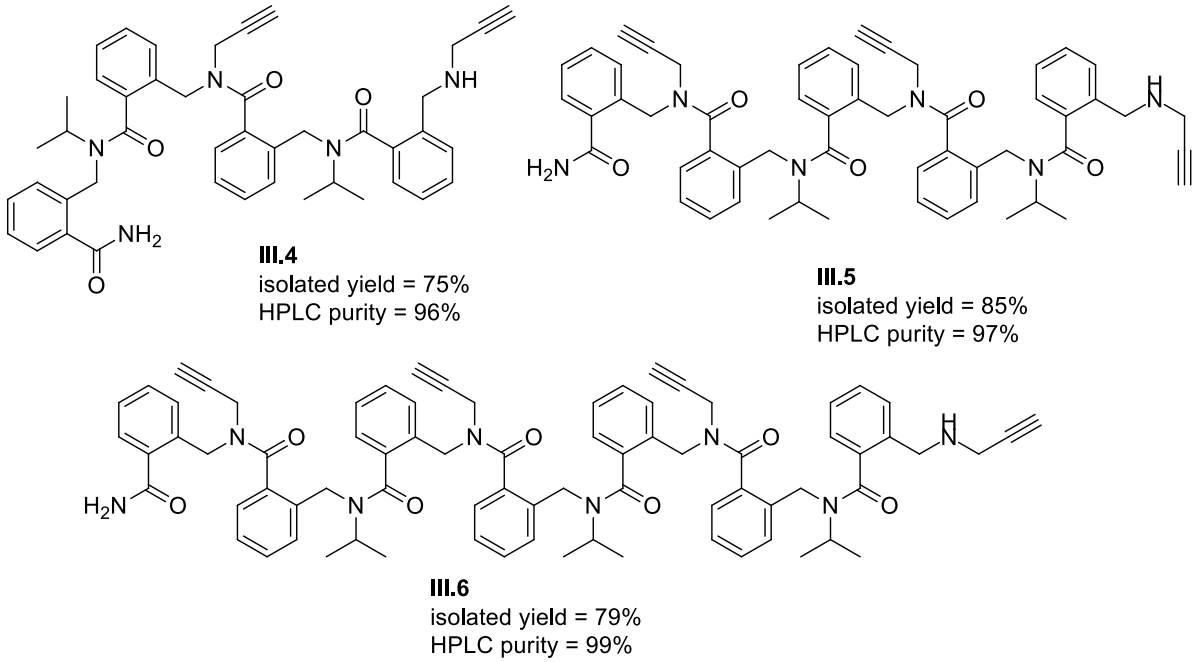

Figure III.11 Structures of different oligomers (4 to 6 residues) of *ortho*-arylopeptoids synthesized.

Using the optimal CuAAC conditions found before, full conversion, high isolated yields and purities were obtained with 3-azidopropan-1-amine (after cleavage of the Boc protection) and (azidomethyl)cyclohexane azides. The isolated yields and purities of all the *ortho*-triazolyl arylopeptoids are shown in table III.5.

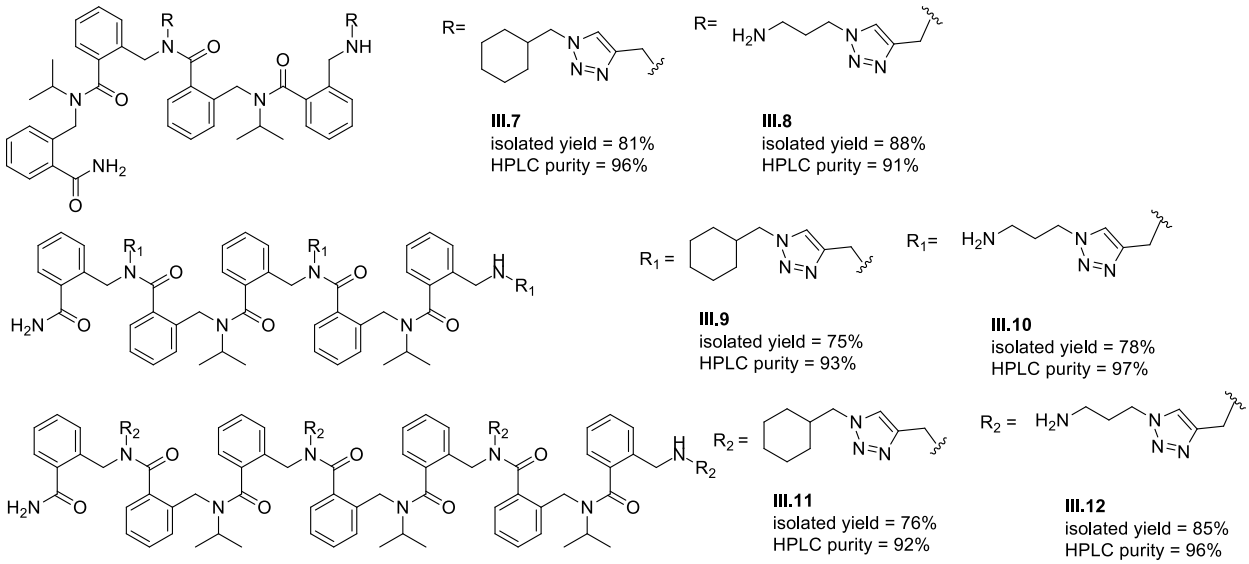

Figure III.12. *Ortho*-arylopeptoids with triazole side-chains synthezised.

Ortho-Arylopeptoid	Isolated yield (%)	Isolated HPLC purity (%)[a]
III.7	81	96
III.8	88	91
III.9	75	93
III.10	78	97
III.11	76	92
III.12	85	96

Table III.5. Isolated yields and HPLC purities of clicked *ortho*-arylopeptoids.

Combinatorial click was also applied on the *ortho*-arylopeptoids by the catalyzed cycloaddition upon addition of a mixture of *N*-Boc protected 3-azidopropan-1-amine and (azidomethyl)cyclohexane at the same time to pentamer **III.5**. This should afford 2^3 =8 compounds. Indeed, this reaction led to approximately equal ratios of the eight desired products (identified by LCMS) that appears in the same order that those obtained in the *meta* series and discussed above.

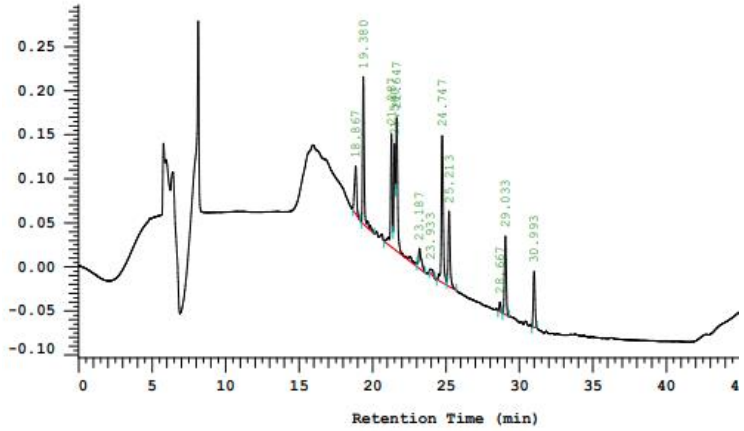

Figure III.13. HPLC chromatogram of the mixture of oligomers obtained through combinatorial CuAAC on pentamer **III.5**.

Overall, these results indicate that the combinatorial methodology could be extended to the *ortho* series.

III.C.5. Advantage of this on-support click process using NHC-Cu(I) catalyst.

In this chapter, we reported several advantages of using [SIMesCu(4,7-Cl_2-Phen)]Cl as catalyst for the CuAAC reaction. It allows to lower the amount of copper(I) compared to literature precedent that could reach 40 equivalents in the case of copper iodide. Indeed, full conversion could be obtained with only 1 mol% of the NHC-Cu(I) catalyst. Moreover, the procedure does not need additives such as sacrificial reducing agents. Regarding the yields, the protocol on Rink Amide resin shows high efficiency (70 to 90%) with very good purity (>90%). Moreover, this method proves its efficiency with different functionalized azides, as we have used 5 azides without affecting the yields or purities. Moreover, we proved the efficiency of this method on *ortho*-arylopeptoids that results in good purities and yields. For the composition of the combinatorial, the mixture consists in a quasi-equimolar amount of products. The back synthesis of specific oligomers carrying different type of triazole side-chains is possible in good isolated yields and purities. This methodology could be useful to synthesize triazoliums containing oligomers and

build up several libraries. This will be discussed in the following chapter as well as the biological activity associated to the triazolium-based arylopeptoids.

Chapter IV: Synthesis of triazolium-based arylopeptoids and their antibacterial activities.

I would like to acknowledge Romane Freitas (BTS, Lycée Paul Constant, Montluçon) for the help she provided for the formation of part of the triazolium-based arylopeptoids that will be presented in this chapter (Series A and B).

IV.A. Introduction.

We were interested in the finding of new type of oligomers possessing antibacterial activities. Indeed, the microbial resistance is increasing nowadays due to the high usage of antibiotics for treatment, which in turn is causing more than 700.000 of death a year from the drug-resistant diseases. Antimicrobial peptides (AMPs) have gained attention due to their broad-spectrum activities with low emergence of resistance; but their therapeutic use is hampered by unwanted toxicity, poor pharmacokinetics and high cost. This makes the development of peptidomimetic strategies attractive in order to overcome the resistance of the bacteria. For this reason, many peptidomimetics were developed and show great advances to combat antibioresistance. Peptoids represent a promising class of antimicrobial peptide mimics, especially for its diversity, low cost and protease stability. Parameters such as the oligomer length, hydrophobicity, chirality, charge and side chain nature were studied for their influence on the antimicrobial activity, in addition to their selectivity for bacteria *versus* mammalian cells. As first example, Barron and co-workers reported that the threefold PPI-type structure of α-peptoids mimics the helical amphipathic structure of *magainins* (class of AMPs found in the African clawed frog *Xenopus laevis*), which give a special interest for peptoids antimicrobial activity. In these structures, the (*S*)-phenylethyl side chain (peptoid residue *N*spe) helps to form the helical PPI-type structure and provide hydrophobic faces whereas the cationic side chains are introduced every 3 residues to generate amphipathic character. The dodecamer (*N*Lys-*N*spe-*N*spe)$_4$ (Figure IV.1) showed an excellent broad-spectrum antibacterial activity (MIC *E.coli* (µM) = 3.5–14, MIC *M. tuberculosis* (µM) = 14.2, MIC *S. aureus (µM) = 2*) but also displayed potent cytotoxicity against carcinoma (LC_{50} (prostate cancer) (µM) = 5; LC_{50} (ovarian cancer) (µM) = 6).[189]

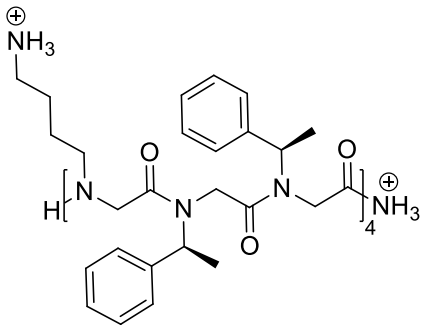

Figure IV.1. The dodecamer (*N*Lys-*N*spe-*N*spe)$_4$ developed by Barron.

[189] Huang, W.; Seo, J.; Willingham, S.B.; Czyzewski, A.M.; Gonzalgo, M.L.; Weissman, I.L.; Barron, A.E. *PLoS ONE* **2014**, *9*, e90397.

Our group was interested in the synthesis of peptoid oligomers bearing triazolium side chains instead of lysine equivalent (*N*Lys) to provide cationic charge necessary to create the amphipathic character. Indeed, it has been shown that a strong n→ π* electronic interaction take place between the oxygen non-bonded doublet of the carbonyl and the electronic deficient azolium favoring the *cis* conformation of the amide carrying the 1,2,3-triazolium-type side chain (Figure IV.4).[115a] Therefore, this *cis* preference promotes PPI-type helical folding of the peptoids. The use of this cationic side chain involved in the stabilization of the amphipathic helix has led to short amphiphilic oligomers with interesting antimicrobial properties.

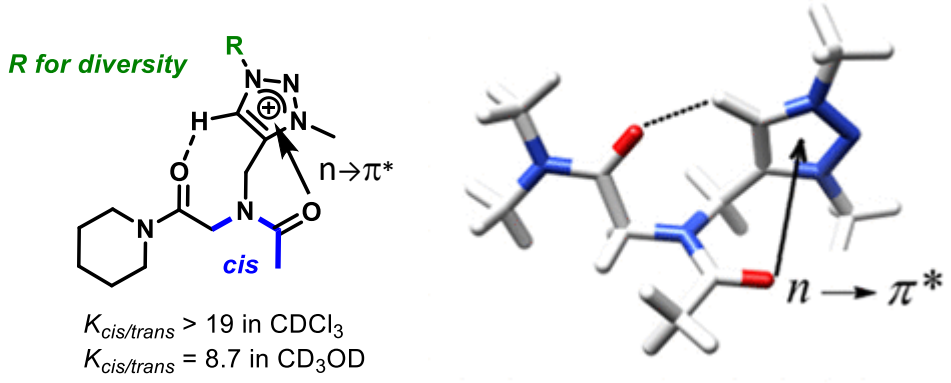

Figure IV.2. n→ π* electronic interactions in peptoid model carrying triazolium side chain.

In 2017, the first solid-phase synthesis of peptoids carrying 1,2,3-triazolium-based side chains was reported (Figure IV.2).[190] The three series reported were studied for their antibacterial efficiency against both Gram positive and Gram negative bacterial strains. The nonamers bearing cyclohexylmethyl substituent (*N*chtm$^+$) and benzyl substituent (*N*btm$^+$) on the triazolium side chain shows a potent activity (MIC ≤ 3 μM) against *S. aureus* and *E. faecalis* bacteria and good selectivity (Table IV.1).

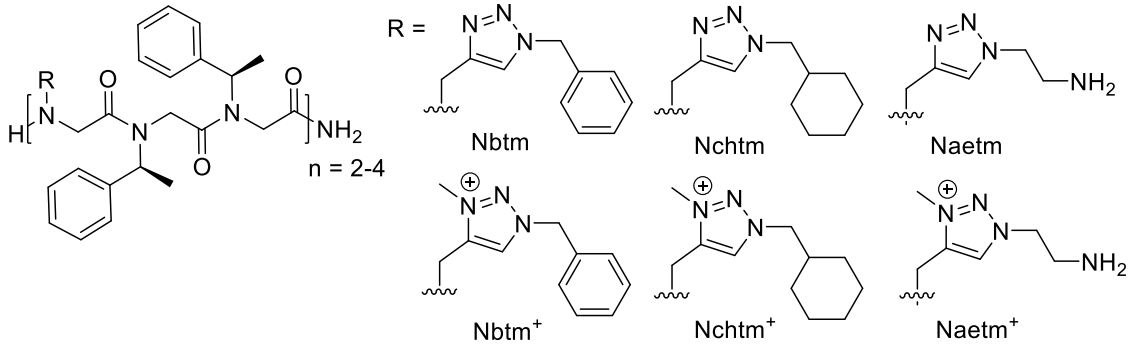

Figure IV.3. The 1,2,3-triazole-type and 1,2,3-triazolium-type side chains synthesized by our team.

[190] Shyam, R.; Charbonnel, N.; Jobe, A.; Blavignac, C.; Forestier, C.; Taillefumier, C.; Faure, S. *ChemMedChem.* **2018**, *13*, 1513-1516.

Peptoid oligomers	*E. coli* JM109		*P. aeruginosa* ATCC27853		*S. aureus* CIP 6525		*E. faecalis* ATCC29212	
	MIC	MBC	MIC	MBC	MIC	MBC	MIC	MBC
H-(*N*btm$^+$-*N*spe-*N*spe)$_2$-NH_2	100	100	-	-	**3.2**	3.2	50	100
H-(*N*aetm$^+$-*N*spe-*N*spe)$_2$-NH_2	>200	>200	>200	>200	>200	>200	>200	>200
H-(*N*btm$^+$-*N*spe-*N*spe)$_3$-NH_2	**12.5**	25	>200	>200	**1.6**	3.2	**1.6**	3.2
H-(*N*aetm$^+$-*N*spe-*N*spe)$_3$-NH_2	25	50	>200	>200	50	100	50	100
Melittin	6.3	12.5	12.5	25	3.1	6.3	6.3	12.5

Table IV.1. Minimum inhibitory concentration (MIC) and Minimum bactericidal concentration (MBC) in μM for a selection of triazolium-based peptoid oligomers.

It is important to mention that, to the best of our knowledge, literature do not report anti-bacterial activities of arylopeptoids but the potential of cationic arylamides as antimicrobial was early shown. In 2002, Degrado reported a series of facially amphiphilic arylamide oligomers that could be able to mimic the essential features of a large class of antimicrobial peptides and proteins.[191] These polymers were interesting for their low cost and easy synthesis presented, and their promising antibacterial efficiency. Degrado and Tew developed arylamide oligomers and studied their antibacterial activity over the years, which results in oligomers with outstanding antibacterial activity and selectivity (Figure IV.3).[192] Also, Degrado studied their mechanisms of action showing that the bacterial membrane is the target of these arylamide foldamers.[193]

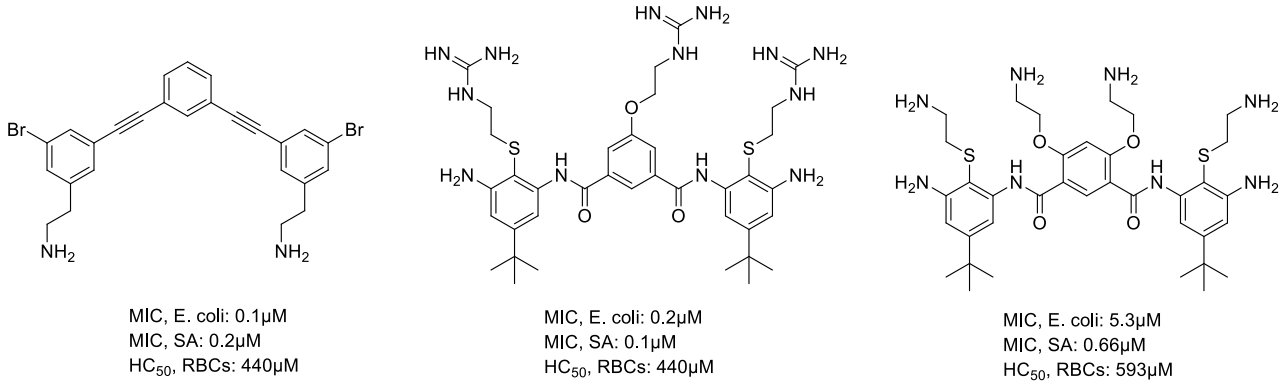

Figure IV.3. Examples of antimicrobial arylamide oligomers, their minimum inhibitory concentration (MIC) against *E. coli* and *S. aureus* (SA) and the concentration required to cause 50% lysis of a suspension of red blood cells (HC_{50}, RBCs).

[191] Tew, G. N.; Liu, D.; Chen, B.; Doerksen, R. J.; Kaplan, J.; Carroll, P. J.; Klein, M. L.; DeGrado, W. F. *Proc. Natl. Acad. Sci.* **2002**, *99*, 5110.5114.

[192] Tew, G. N.; Scott, R. W.; klein, M. L.; DeGrado, W. F. *Acc. Chem. Res.* **2010**, *43*, 30–39.

[193] Mensa, B.; Kim, Y. H.; Choi, S.; Scott, S.; Caputo, G. A.; DeGrado, W. F. *Antimicrob. Agents Chemother.* **2011**, *55*, 5043-5053.

The positive charge is an essential factor responsible of bacterial activity in AMPs.[194] For example, the positively charged AMPs destabilize the membrane of Gram-negative bacteria which enables the peptide to pass into the cell causing depolarization and pore formation that results in the cell death.[195] For this reason, we were interested in introducing cationic side chains along arylopeptoids to obtain new type of cationic amphipathic structures. We thought that triazolium-based arylopeptoids would be of particular interest due to previous antimicrobial activities obtained by our group. The 1,2,3-triazolium-type side-chains is not innocent as it presents a great importance in conformational preferences of *N,N*-disubstituted amides and might also stabilized conformation of arylopeptoids in solution.

To generate library of cationic amphipathic arylopeptoids, an efficient and facile method of synthesis is needed. Thus, the problem resumes to the discovery of a valuable synthetic way providing rapidly a large range of possible candidates. Therefore, after finding an efficient and adaptable synthetic strategy to introduce the triazole-type side chains (and the diversity embedded within) presented in chapter III, we will now focus on the formation of triazolium-containing oligomers and the evaluation of their antibacterial properties.

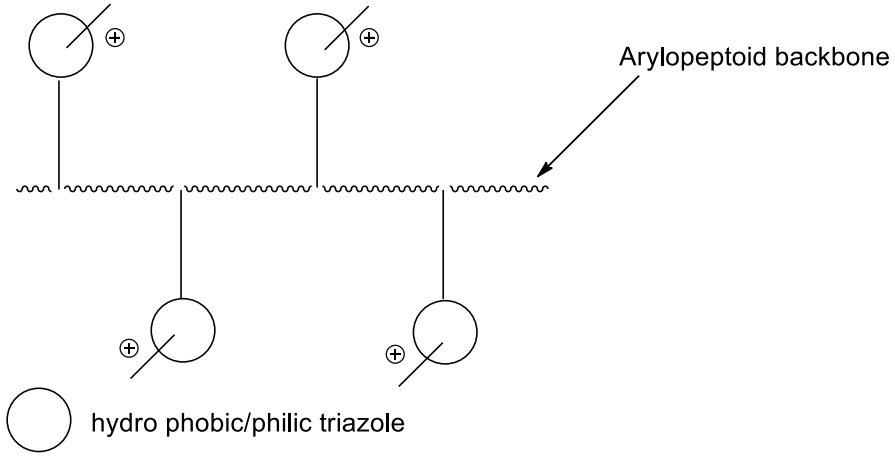

Scheme IV.1. Model of the targeted triazolium-based arylopeptoids.

IV.B. Discussion.

IV.B.1. Solid-phase synthesis of triazolium-based arylopeptoids.

Triazoliums are classically obtained by alkylation at the N3 position of the triazole group. Usual alkylating reagents comprise methyl iodide, methyl triflates or Meerwein's salts (trimethyloxonium tetrafluoroborate).[196] As we will work on solid support, acidity due to partial decomposition of the alkylating reagents have to be taken into account in order to avoid cleavage from the resin. Thus, we discarded methyl triflate and Meerwein's salts and focused only on methyl iodide that already have proven its efficiency on solid support.[190]

[194] Takahashi, D.; Shukla, S.K.; Prakash, O.; Zhang, G. *Biochimie* **2010**, *92*, 1236–1241.
[195] Clifton, L.A.; Skoda, M.W.; Le Brun, A.P.; Ciesielski, F.; Kuzmenko, I.; Holt, S.A.; Lakey, *Langmuir* **2015**, *31*, 404–412.
[196] Curphey, T. J. *Org. Synth.* **1971**, *51*, 142.

After performing click reaction using the optimized protocol with Rink Amide resin described in chapter III, the *N*-terminal amine was protected with a Boc group to prevent its methylation. We then used methyl iodide as published previously to obtain full conversion of the triazoles at 45°C (the reaction time was extended to 24h to secure a full conversion).[190] The cationic oligomer was cleaved from the resin and then purified using C18 column chromatography to isolate the product with more than 90% purity and more than 80% yield. In the following part, we will discuss the synthesis of 7 different series of linear triazolium-based arylopeptoids using this standard procedure, depicted in scheme IV.1. The 7 series that we synthesized were divided into 4 series of *meta*-arylopeptoids (A-D) and 3 series of *ortho*-arylopeptoids (E-G) with different length of oligomers (trimers to heptamers) and with different triazolium side chains (carrying alcohol, amine or cyclohexyl substituents). The synthetic method is exemplified for **IV.2** in the scheme below:

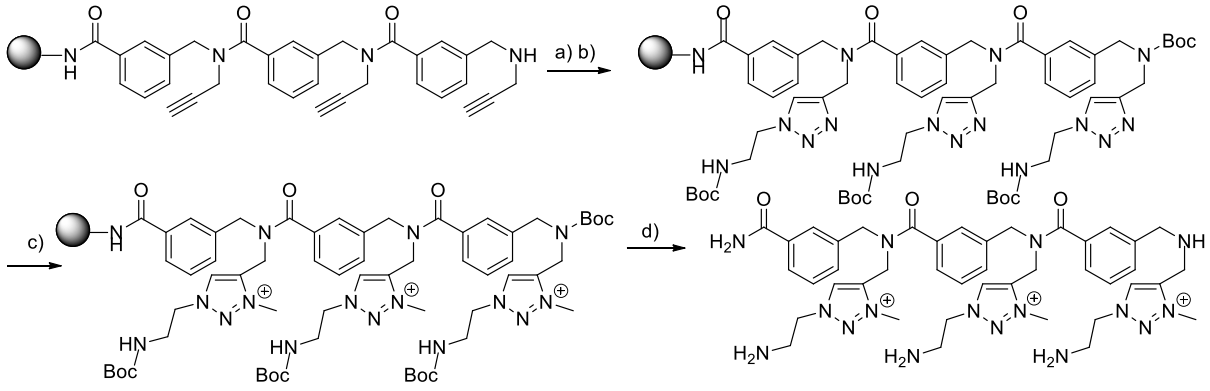

Scheme IV.2. Example of the route to triazolium-based arylopeptoids.

IV.B.1.1. Series A

The first series of triazolium-based arylopeptoids contains *meta*-trimers with three triazolium-type side chains. First, the trimer containing 3 consecutives propargyl amine side chains **IV.1** was synthesized on Rink Amide resin. **IV.1** was not isolated, and it was used to synthesized Series A.

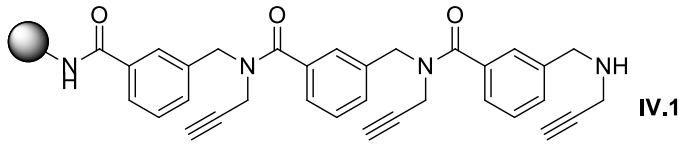

Figure IV.5. On-support trimer with three consecutive propargyl side chains.

The standard procedure was applied to obtain the cationic trimers (Figure IV.6.a) containing alcohol, amine and cyclohexyl substituents on the triazoliums. Product **IV.2**, containing alcohol substituents, was isolated in 95% yield and 97% purity after column chromatography. Product **IV.3**, containing the ammonium substituent, was isolated in 82% yield and 99% purity. Product **IV.4**, containing the cyclohexyl substituent was isolated in 74% yield and 90% purity.

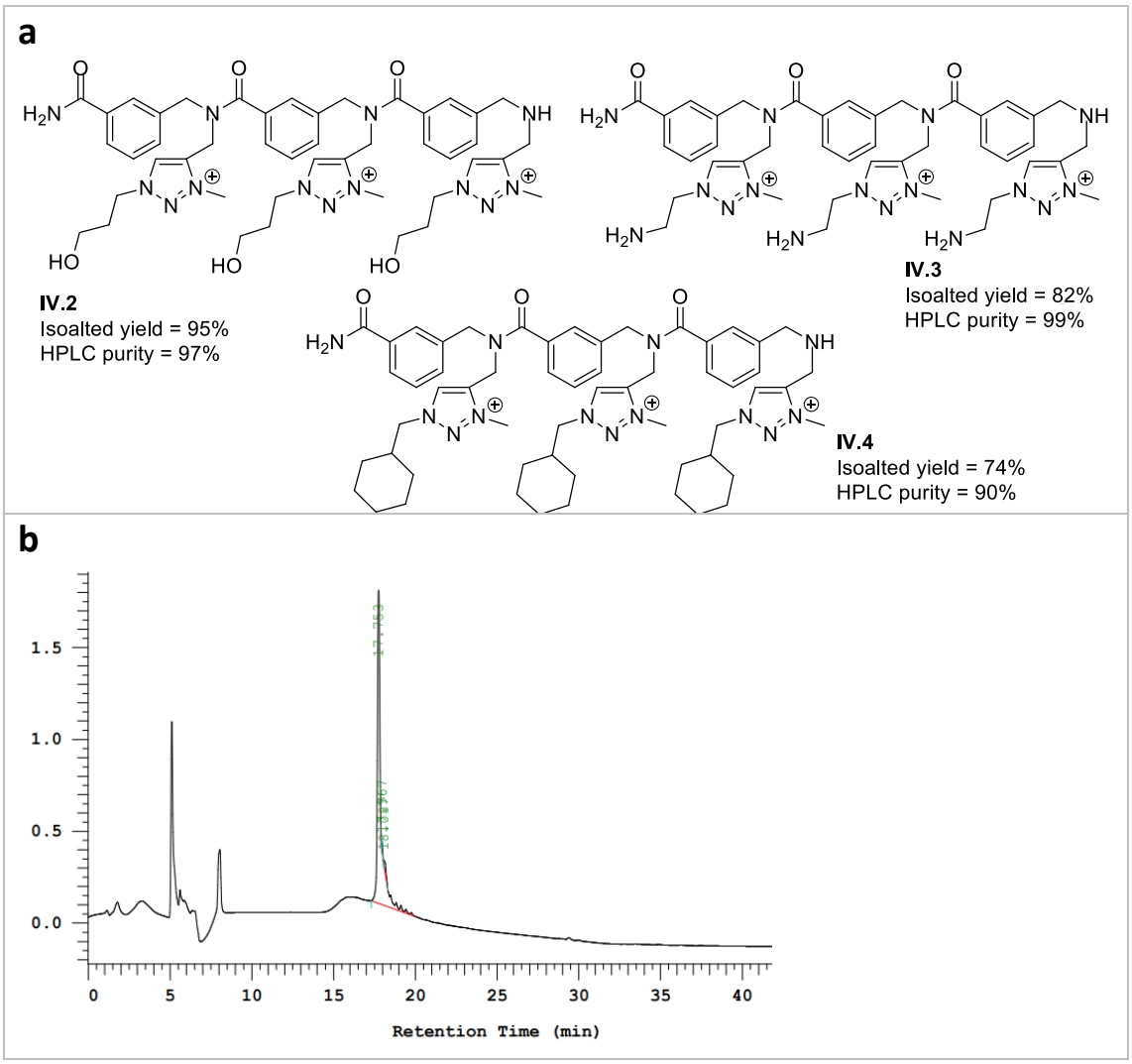

Figure IV.6. (a) Triazolium-based triarylopeptoids obtained with the standard procedure using one azide. (b) Example of HPLC chromatogram (220 nm): purified oligomer **IV.2**.

The standard procedure also applied well to form a combinatorial library with two substituents described before using two azides for the CuAAC reaction step. Thus, we combined alcohol-cyclohexyl, amine-cyclohexyl and amine-alcohol substituents. In each case a theoretical maximum of 2^3=8 compounds should be synthetized (Scheme IV.7.a). HRMS shows the presence of all the expected masses, however, several overlapping in HPLC chromatograms were observed using the standard method of separation (Figure IV.7.b). We didn't try to find a better separation method. In all cases, average to good yields and good HPLC purities were observed: the combinatorial library **IV.5** (alcohol and cyclohexyl) were obtained in 87% yield and 97% purity, combinatorial **IV.6** (ammonium and cyclohexyl) in 67% yield and 90% purity and combinatorial **IV.7** (alcohol and cyclohexyl) in 92% yield and 98% purity.

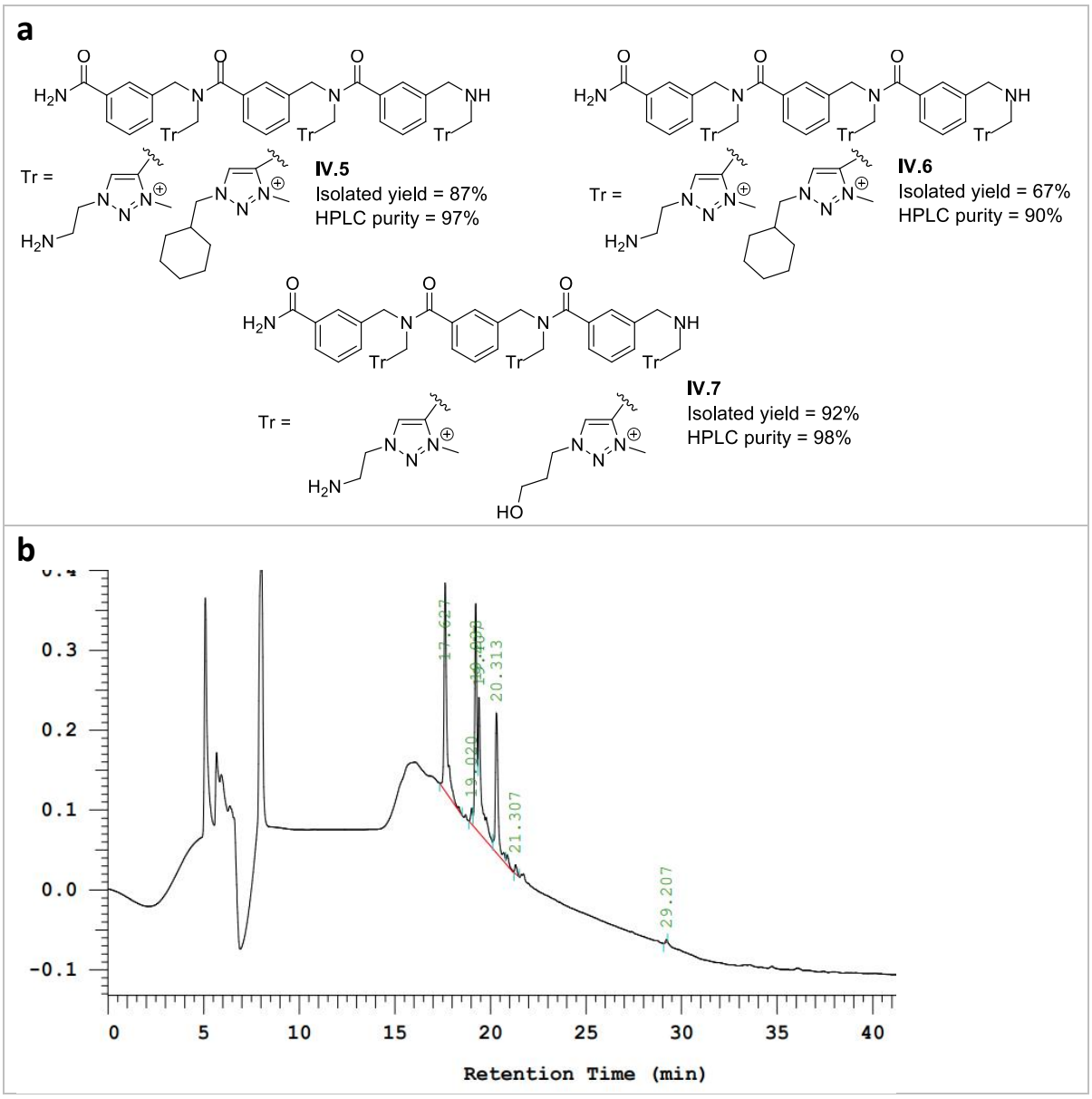

Figure IV.7. (a) Cationic combinatorial libraries obtained with the standard procedure using two azides. (b) Example of HPLC chromatogram (220 nm): oligomers mixture **IV.7**.

The appearance order of the product's peaks of triazolium-based oligomers in HPLC corresponds to the same order of that of related triazole-based oligomers (chapter III). This order is dependent on the hydrophilicity of the side chains: ammoniums appear first followed by alcohols and then cyclohexyls as the most hydrophobic side chains. This applies for all the triazolium-based oligomers described, with the fact that triazolium compounds appears before triazole ones thanks to the positively charged triazoliums.

IV.B.1.2. Series B

The second series of triazolium-based arylopeptoids contains the meta-tetramers with two triazolium side chains at various positions in the sequence. First, the tetramer containing two propargyl groups located at the second residue and terminus, was synthesized on Rink amide resin

in 72 % yield and 96 % purity (Figure IV.8). This product was described in the publication associated with chapter III).

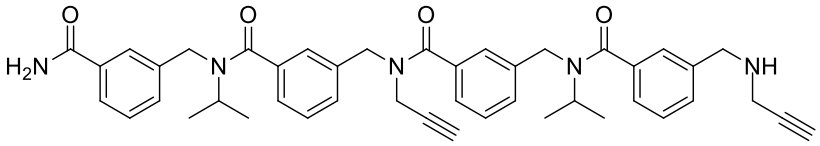

Figure IV.8. Tetramer with two propargyl side chains.

The standard procedure was applied to obtain the triazolium groups shown in Figure IV.9.a containing alcohol, amine and cyclohexyl substituents. Good yields and HPLC purity were observed, product IV.8, containing alcohol substituents, was isolated in 78% yield and 94% purity, product IV.9 (ammonium substituents) in 88% yield and 95% and the product IV.10 (cyclohexyl substituents) was isolated in 71% yield and 97% purity.

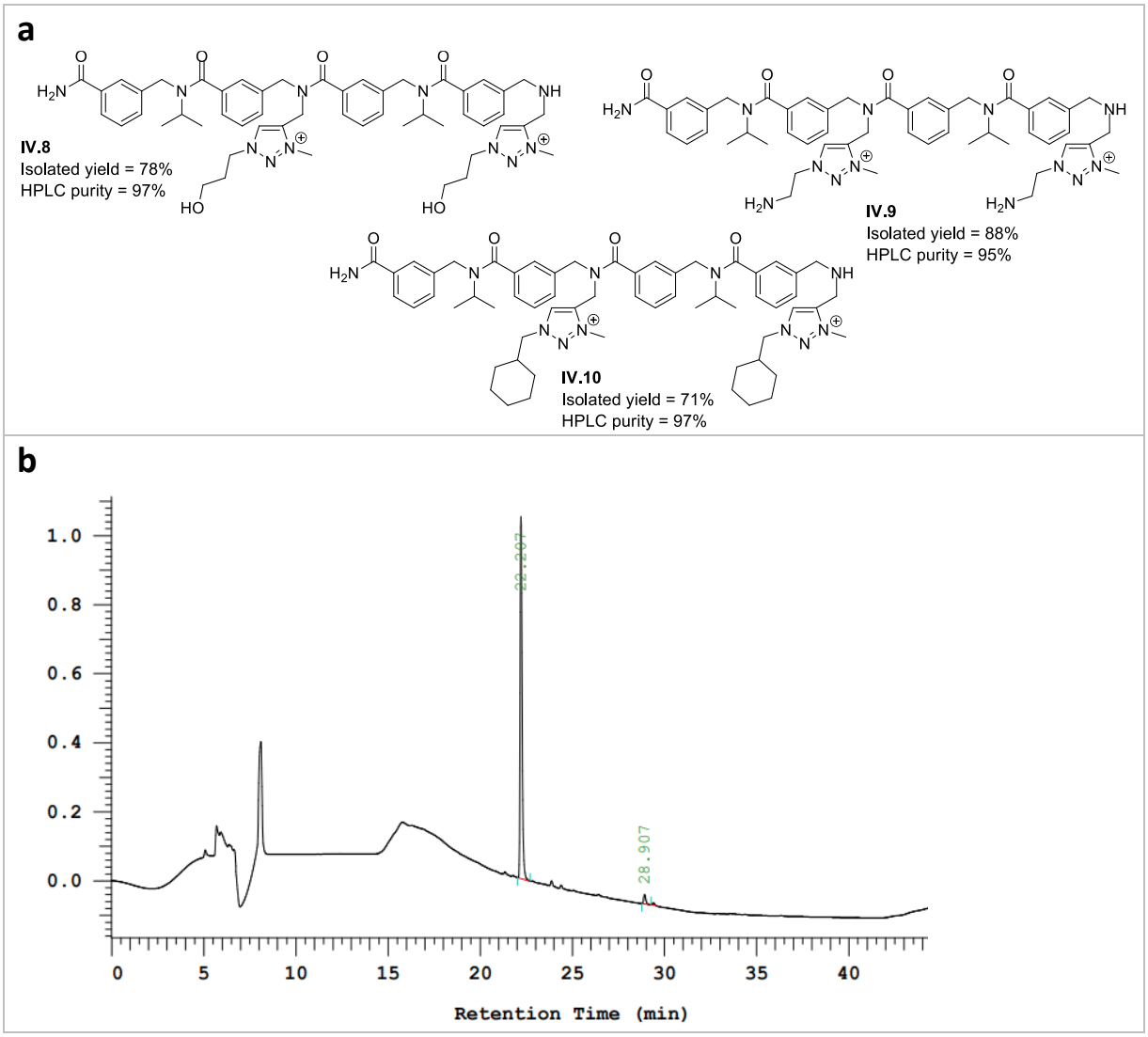

Figure IV.9. (a) Triazolium-based arylopeptoids (series B) obtained with the standard procedure using one azide. (b) Example of HPLC chromatogram (220 nm): purified oligomer **IV.10**.

Our standard procedure was also applied to form a combinatorial library using two different azides. Here again, we combined alcohol-cyclohexyl, amine-cyclohexyl, amine-alcohol which should afford a theoretical maximum of 2^2=4 compounds for each subset. HRMS shows the presence of all the expected mass and absence of overlapping were observed in HPLC (Figure IV.10.b). The combinatorial library **IV.11** (alcohol and cyclohexyl) was obtained in 99% yield and 86% purity, **IV.12** (ammonium and cyclohexyl) in 78% yield and 94% purity and **IV.13** (alcohol and cyclohexyl) in 56% yield and 97% purity.

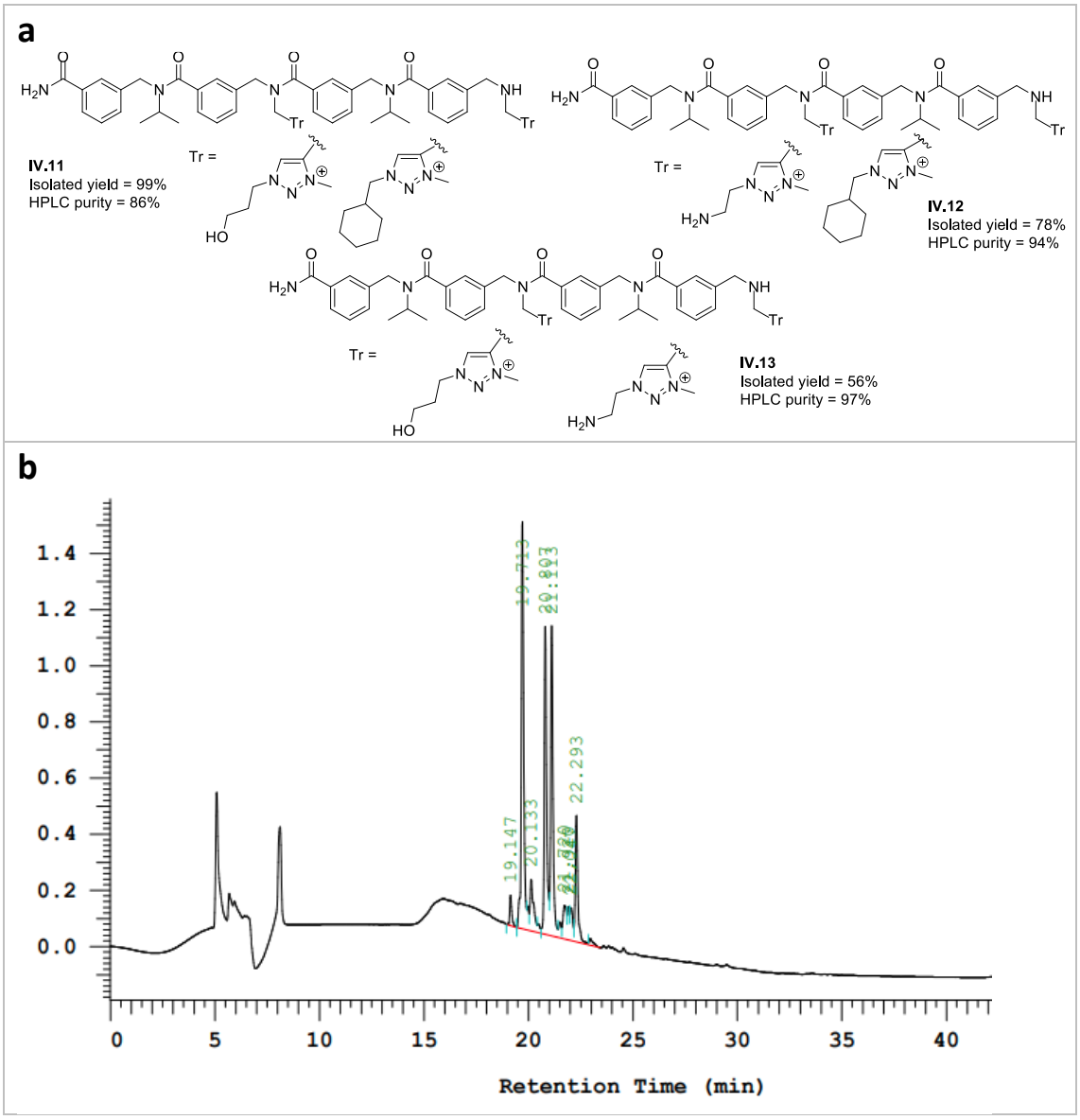

Figure IV.10. (a) Combinatorial triazolium-based libraries obtained with the standard procedure using two azides. (b) HPLC chromatogram (220 nm) of the purified oligomers mixture **IV.11**.

The appearance order of the compounds was the same as we mentioned above, with the amine appearing first, followed by the alcohol and finally the cyclohexyl substituents.

IV.B.1.3. Series C

The third series of triazolium-based arylopeptoids contains the *meta*-pentamers with three triazolium-type side chains. First the *meta*-pentamer **IV.14** containing three alternating propargyl amine side chains were synthesized on Rink Amide resin. **IV.1** was not isolated, and it was used to synthesized Series C.

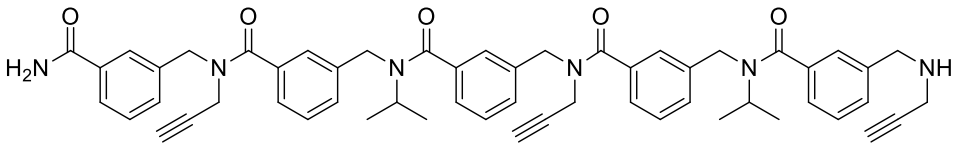

Figure IV.11. *meta*-Pentamer with three propargyl groups **IV.14**.

The standard procedure was applied to obtain the triazolium-based pentamers depicted in Figure IV.12a that contain alcohol, ethylamine, propylamine and cyclohexyl substituents on triazoliums.

Yields are averaged to good and no problem was found to purify the arylopeptoids using C18 column chromatography. Product **IV.15**, containing alcohol groups, was isolated in 55% yield and 90% purity; **IV.16**, containing ethylamine substituents, isolated in 92% yield and 99% purity; **IV.17**, containing cyclohexyl substituents, in 96% yield and 95% purity and **IV.18**, containing propylamine substituents, in 93% yield and 99% purity.

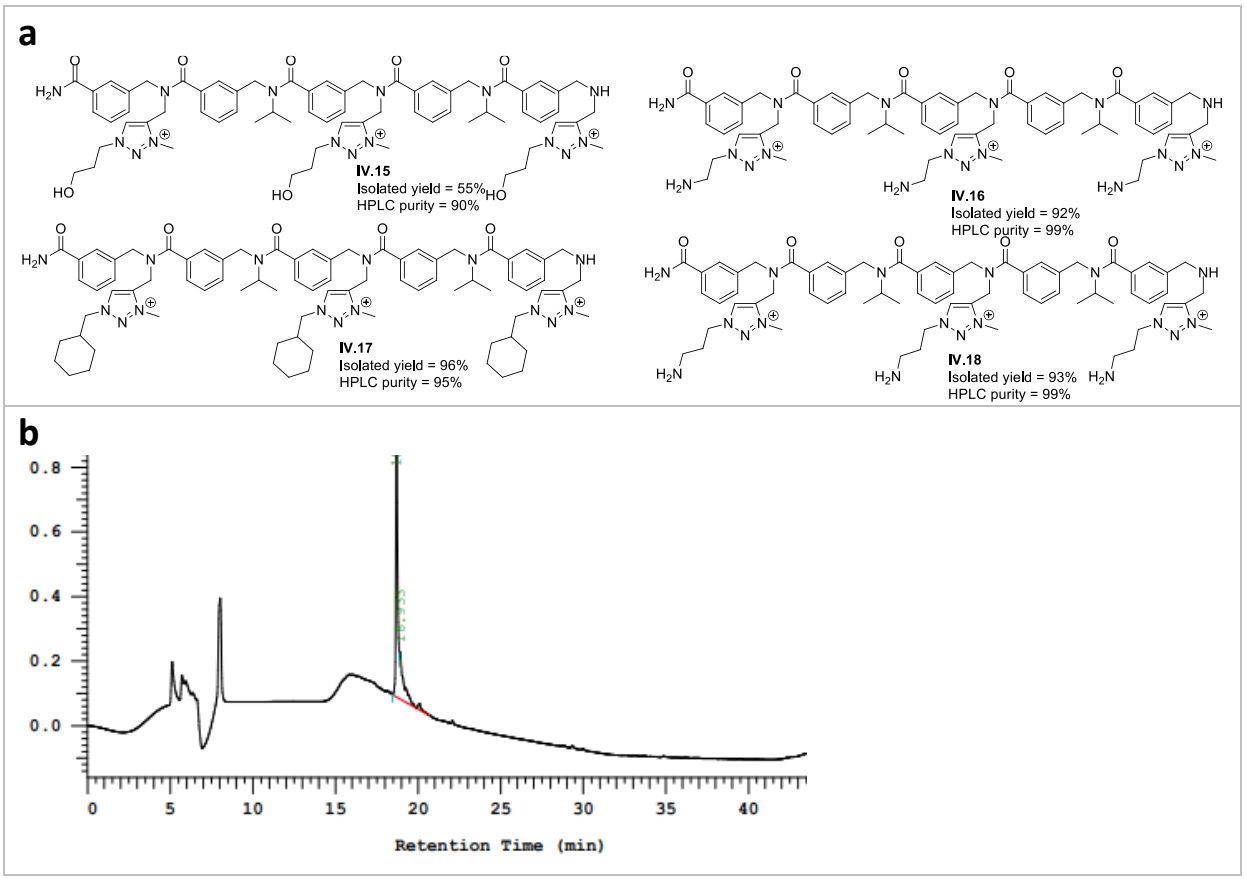

Figure IV.12. (a) Triazolium-based arylopeptoids obtained with the standard procedure using one azide. (b) HPLC chromatogram (220 nm) of pure **IV.18**.

The standard procedure was also applied well to form a combinatorial library with three of the side chains described before. Thus, alcohol and cyclohexyl, ethylamine and cyclohexyl, ethylamine and alcohol were combined giving three libraries. As mentioned before we expect a theoretical maximum of 2^3=8 compounds (Figure IV.13.a). HRMS shows the presence of all the expected masses. However, as mentioned before, the overlapping of several peaks in HPLC chromatograms was observed using the standard method of separation (Figure IV.13.b).

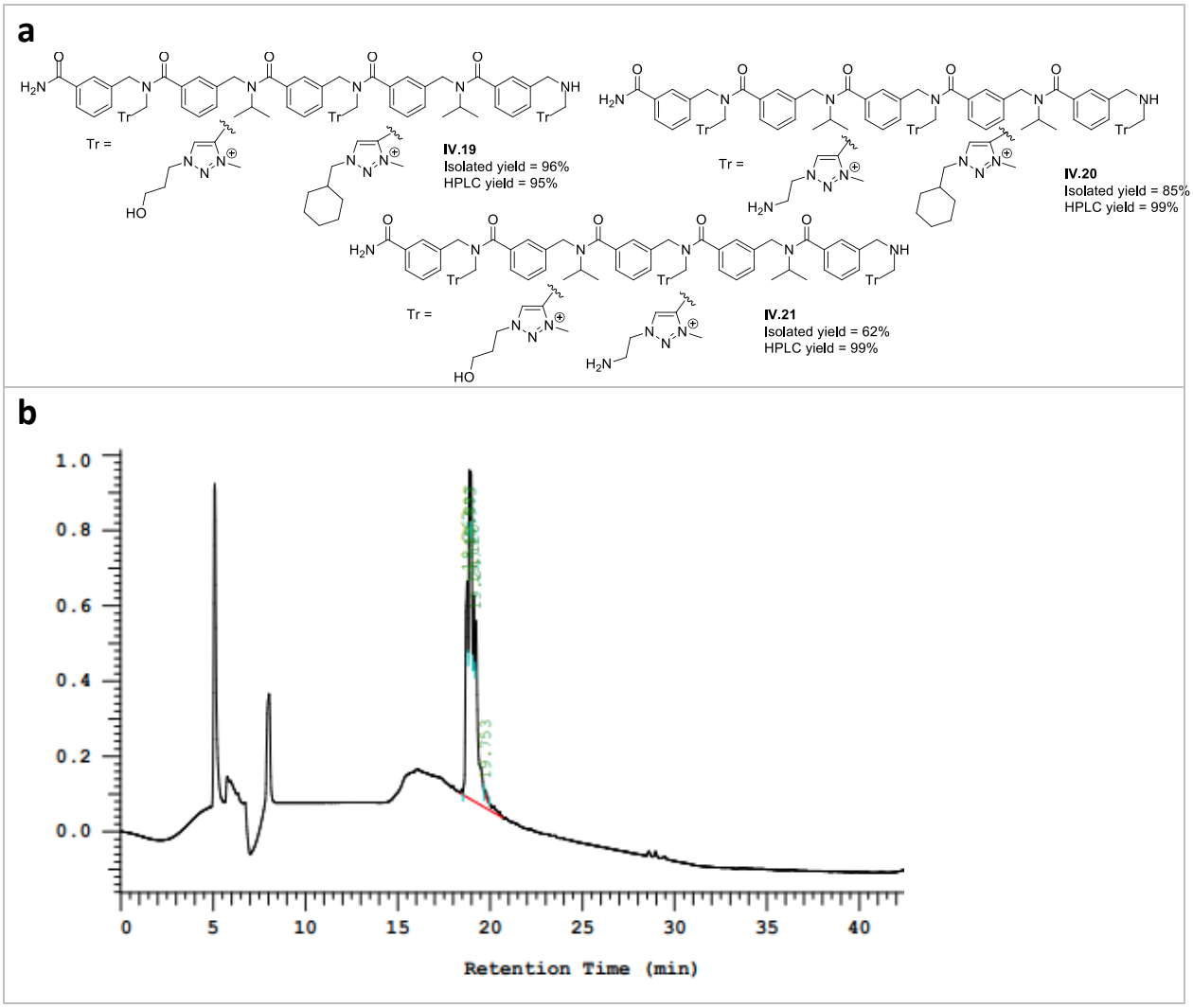

Figure IV.13. (a) Combinatorial triazolium-based arylopeptoid libraries obtained with the standard procedure using two azides. (b) HPLC chromatogram (220 nm) of the purified oligomers mixture **IV.21**.

The combinatorial products **IV.19** (alcohol and cyclohexyl) were obtained in 96% yield and 95% purity; **IV.20** (ethylamine and cylohexyl) in 85% yield and 99% purity and **IV.21** (alcohol and ethylamine) in 62% yield and 99% purity.

IV.B.1.4. Series D

A new series of triazolium-based arylopeptoids containing the meta-heptamers with four triazolium side chains was prepared. The meta-heptamer containing four alternating propargyl-

isopropyl side chains III.1 was synthesized on Rink amide resin in 84 % yield and 95 % purity (Figure IV.14).

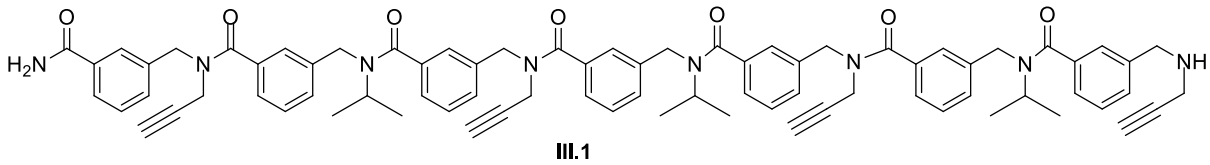

III.1

Figure IV.14. *meta*-heptamer with four propargyl side chains.

The standard procedure was applied to obtain the triazolium-containing heptamers shown in Figure IV.15 containing amine and cyclohexyl side chains. Product **IV.22**, containing propylamine (ammonium) substituent, was isolated in 78% yield and 96% purity and product **IV.23**, containing cyclohexyl substituent, in 87% yield and 95% purity.

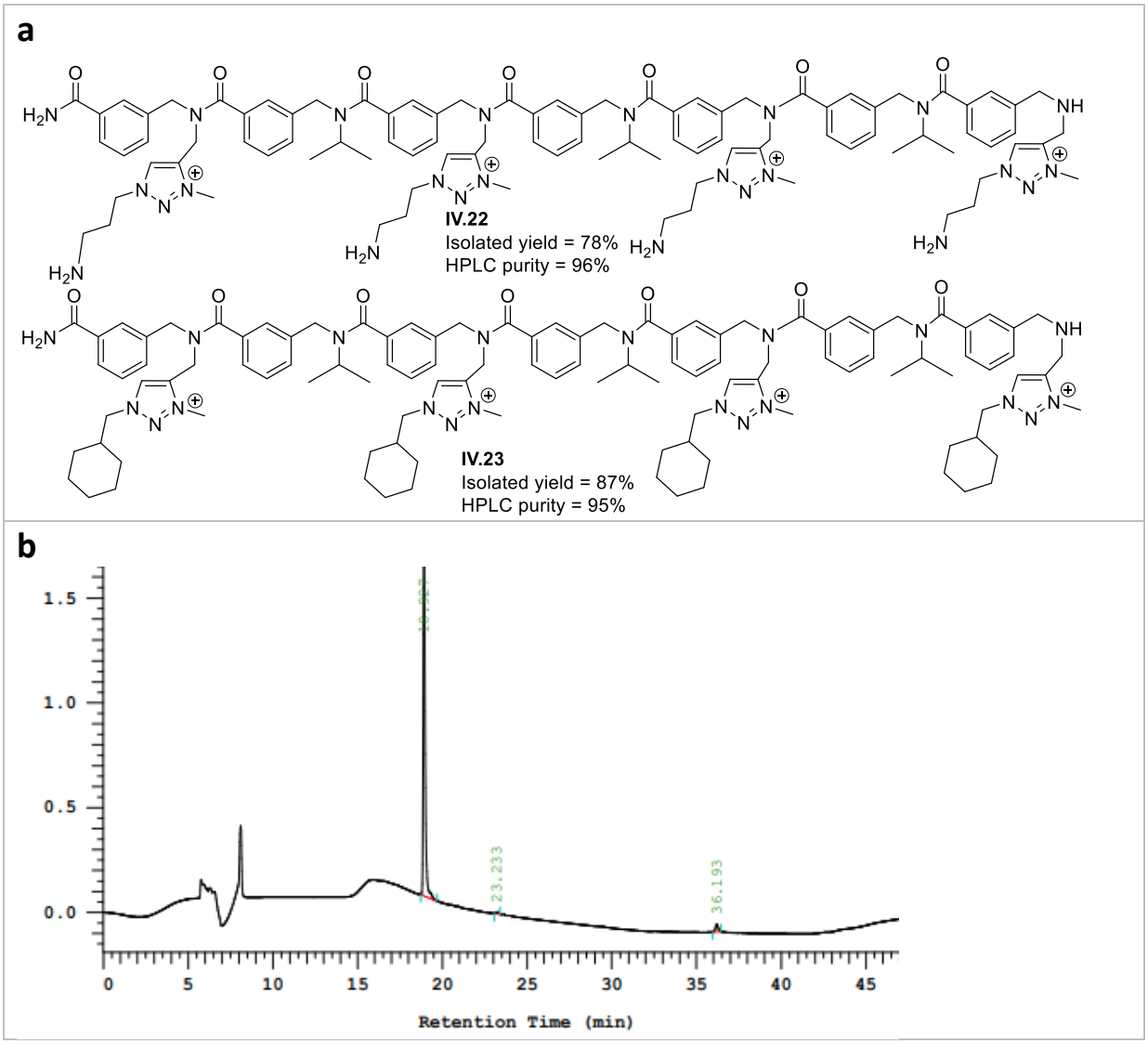

Figure IV.15. (a) Triazolium-based heptameric arylopeptoids obtained with the standard procedure using one azide. (b) HPLC chromatogram (220 nm) of purified oligomer **IV.22**.

The standard procedure was also applied well to form a combinatorial library with the two azides described before. Thus, propylamine and cyclohexyl, were combined giving a library of triazolium-containing heptamers. The overlapping of several peaks in HPLC was observed using the standard method of separation (Figure IV.16.b).

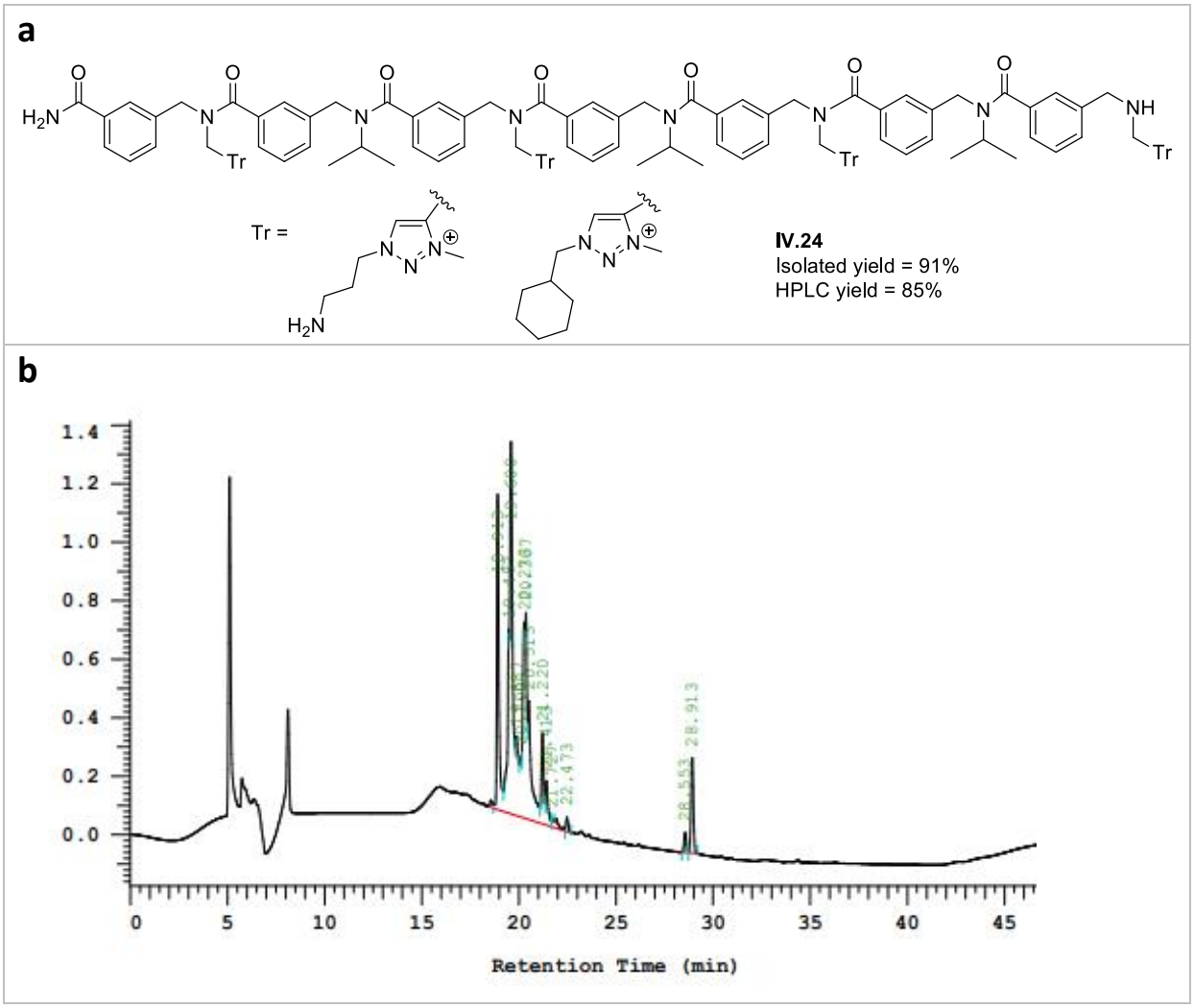

Figure IV.16 (a) Triazolium-based heptameric arylopeptoids mixture obtained with the standard procedure using two azides. (b) HPLC chromatogram (220 nm) of the purified heptamers mixture **IV.24**.

IV.B.1.5. Series E

After the synthesis of four different series of meta-arylopeptoids with triazolium side chains, we have naturally extended the synthesis to ortho-arylopeptoids for which the synthesis of triazoles side chains has been already described in chapter III. Here, we will introduce the synthesis of three different series of linear ortho-arylopeptoids. As previously mentioned, the ortho-backbone might be more constrained than the meta-one.

The first ortho-series contains ortho-tetramers with two triazolium side chains. First the ortho-tetramer containing two alternating propargyl amine side chains **III.4** was synthesized on Rink Amide resin in 75 % yield and 96 % purity (Figure IV.17).

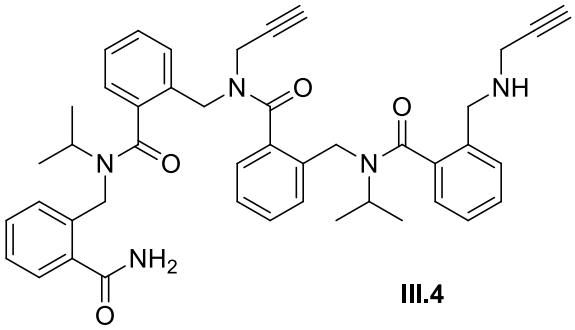

Figure IV.17. Structure of the *ortho*-tetramer **III.4** with two propargyl side chains.

The standard procedure was applied to obtain the triazolium-containing tetramers shown in Figure IV.18 carrying amine and cyclohexyl substituents. Product **IV.25**, containing propylamine substituent, was isolated in 80% yield and 99% HPLC purity and **IV.26**, containing cyclohexylmethyl substituent, was isolated in 86% yield and 98% HPLC purity.

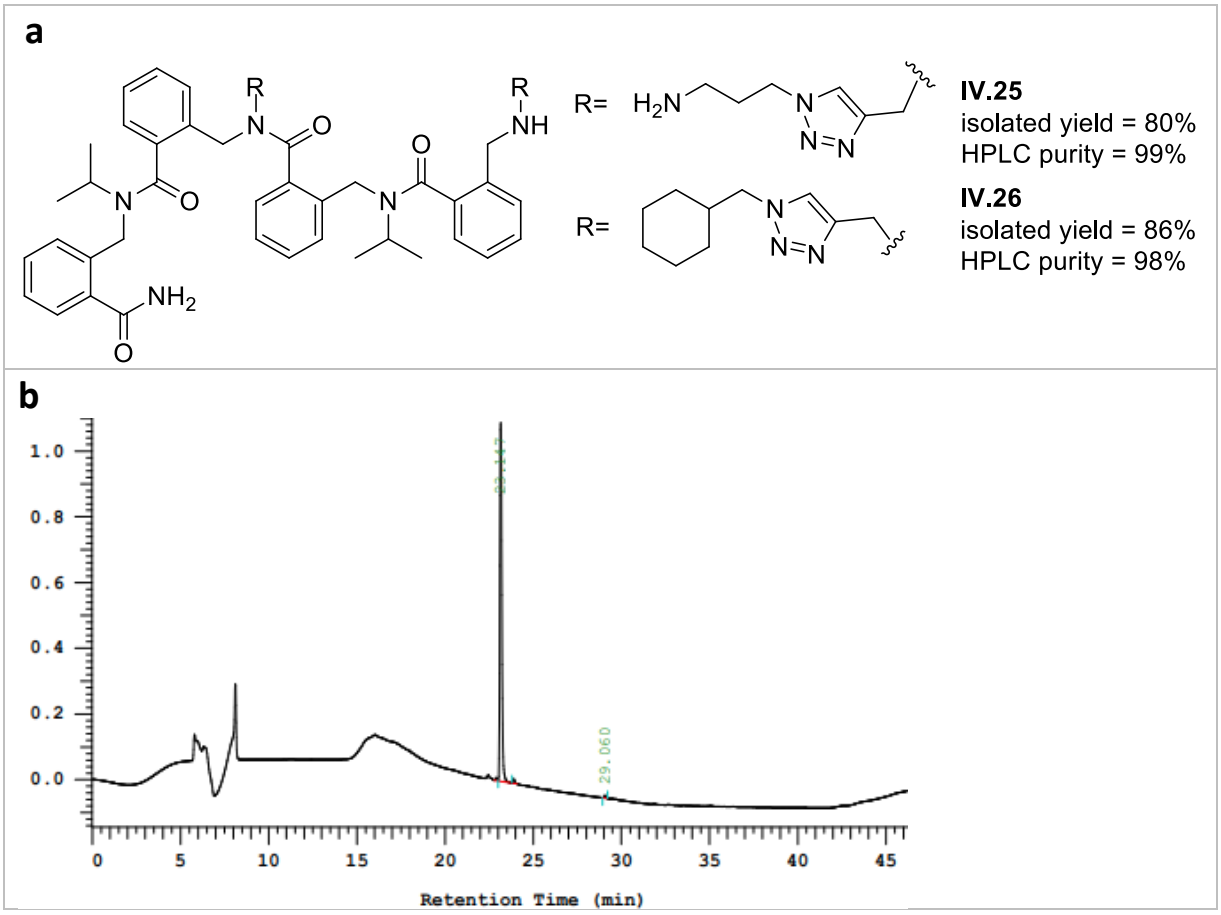

Figure IV.18. (a) Triazolium-based ortho-tetramers obtained with the standard procedure using one azide. (b) HPLC chromatogram (220 nm) of purified arylopeptoid **IV.25**.

IV.B.1.6. Series F

We also introduced the ortho-pentamers with three triazolium side chains for which the starting material containing three alternating propargyl side chains **III.5** was synthesized on Rink Amide resin in 85 % yield and 967 % purity (Figure IV.19).

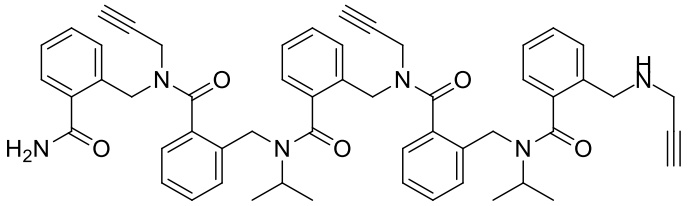

Figure IV.19. Structure of *ortho*-pentamer **III.5** with three propargyl side chains.

The standard procedure was applied to obtain the triazolium-containing pentamers shown in Figure **IV.20** containing amine and cyclohexyl groups. Product **IV.27**, containing cyclohexylmethyl substituents, was isolated in 82% yield and 95% purity and **IV.28**, containing propylamine substituent, was isolated in 86% yield and 97%.

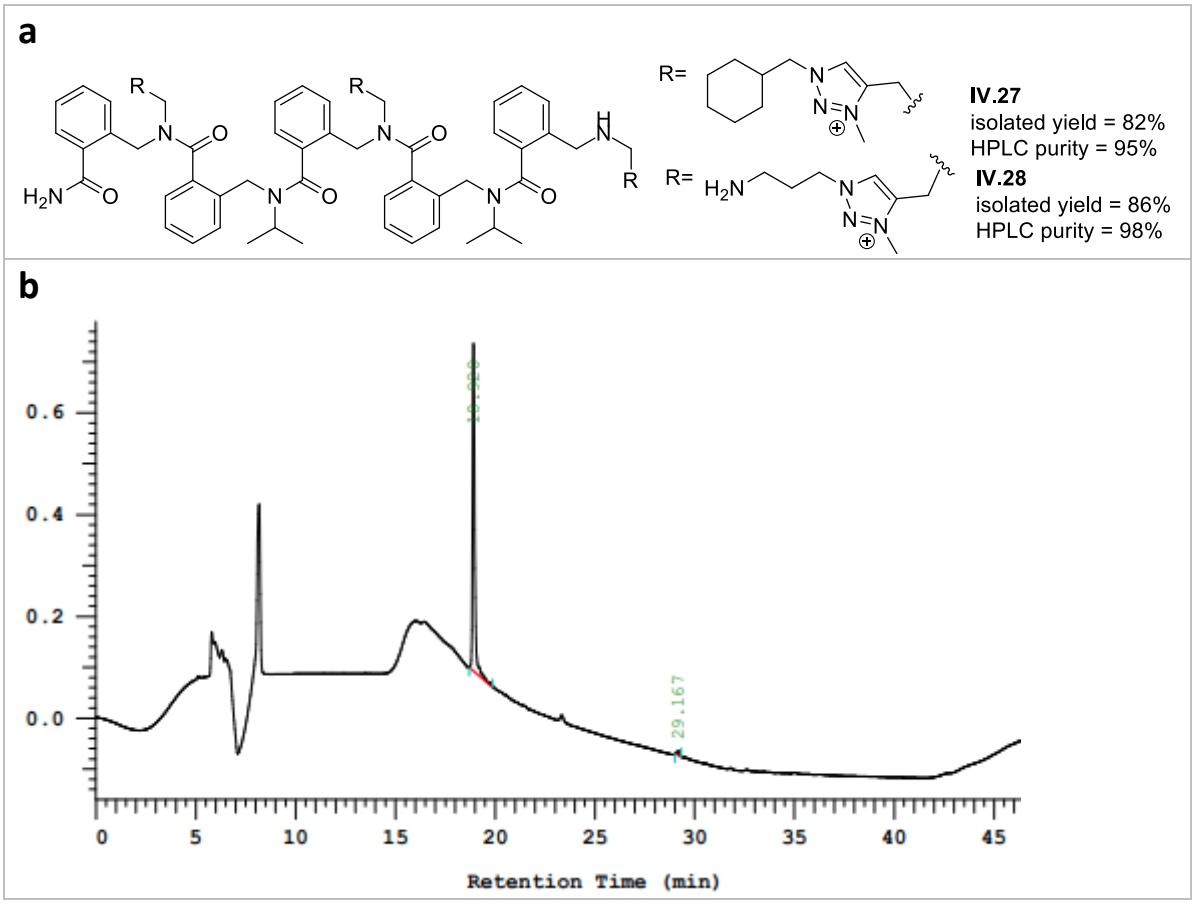

Figure IV.20. (a) Triazolium-containing *ortho*-pentamers obtained with the standard procedure using one azide. (b) HPLC chromatogram (220 nm) of purified *ortho*-pentamer **IV.28**.

The standard procedure was also applied well to form a combinatorial library with two different azides described before that should afford 23=8 compounds. We combined aminopropyl and

cyclohexyl methyl azides. (Scheme IV.21.a). HRMS shows the presence of all the expected masses, and HPLC shows the 8 expected different products although overlapping occurs, Figure IV.21.b. The combinatorial **IV.29** was obtained in 95% yield and 96% purity.

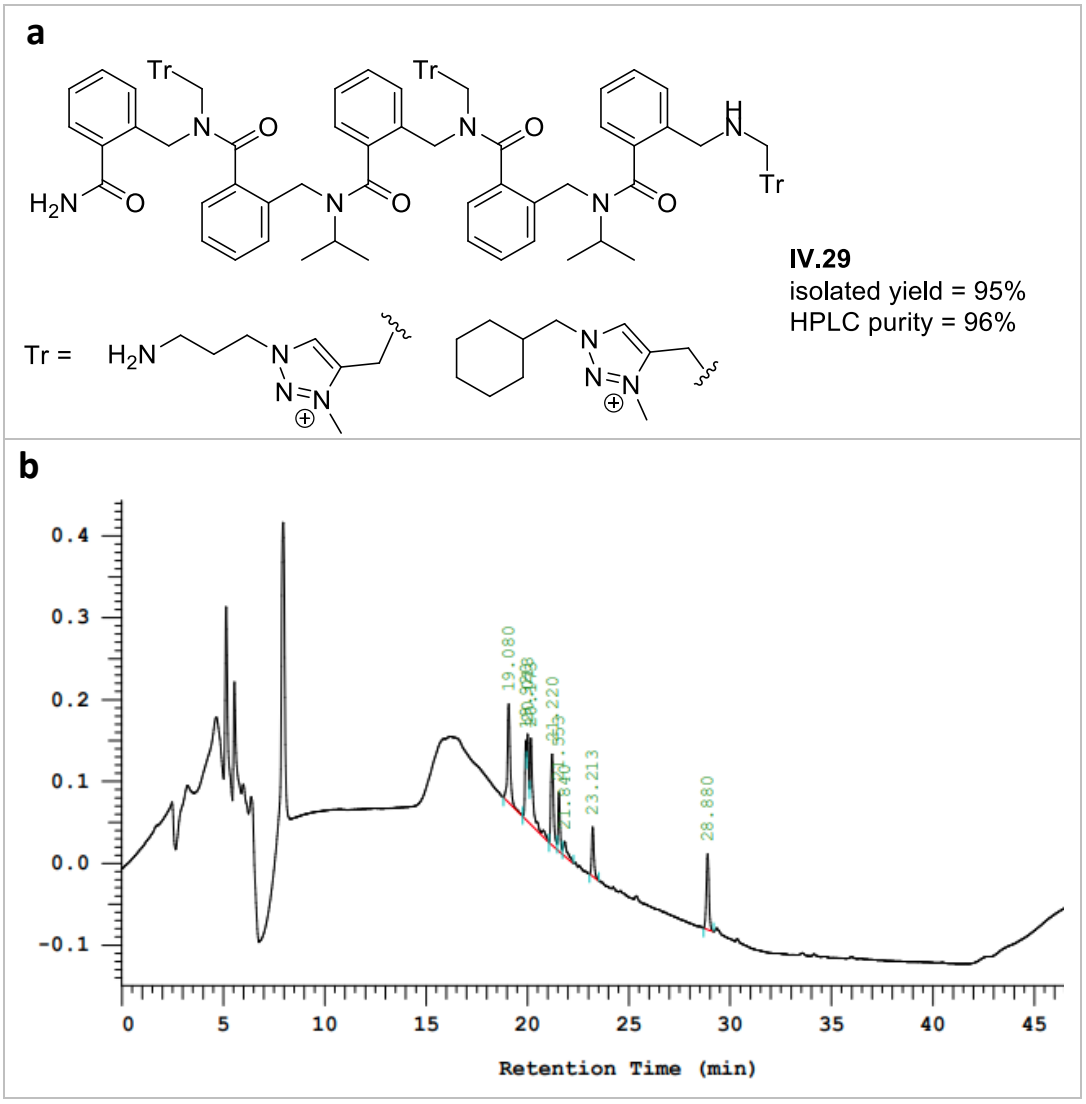

Figure IV.21. a) Triazolium-containing pentamers obtained with the standard procedure using two azides. (b) HPLC chromatogram (220 nm) of purified pentamers mixture **IV.29**.

IV.B.1.7. Series G

We extended to the ortho-heptamer containing four triazolium side chains. The ortho-heptamer containing four alternating propargyl side chains **III.6** was synthesized on Rink Amide resin in 79 % yield and 99 % purity (Figure IV.22).

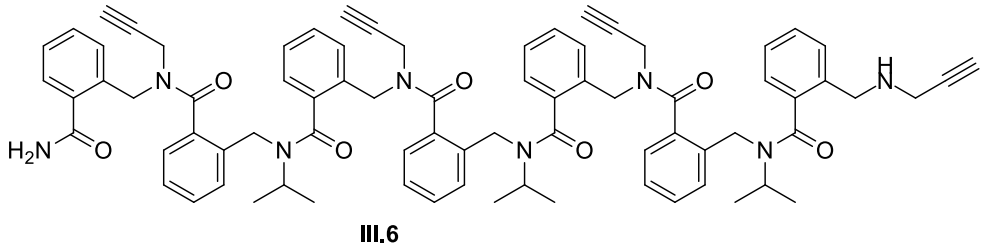

III.6

Figure IV.22. Structure of *ortho*-heptamer III.6 with four propargyl side chains.

The standard procedure was applied to obtain the triazolium-based heptamers shown in Figure IV.23 containing amine and cyclohexylmethyl substituents. Product **IV.30**, containing cyclohexylmethyl side chain, was isolated in 89% yield and 92% purity and **IV.31**, containing propylamine side chain, in 95% yield and 98% purity.

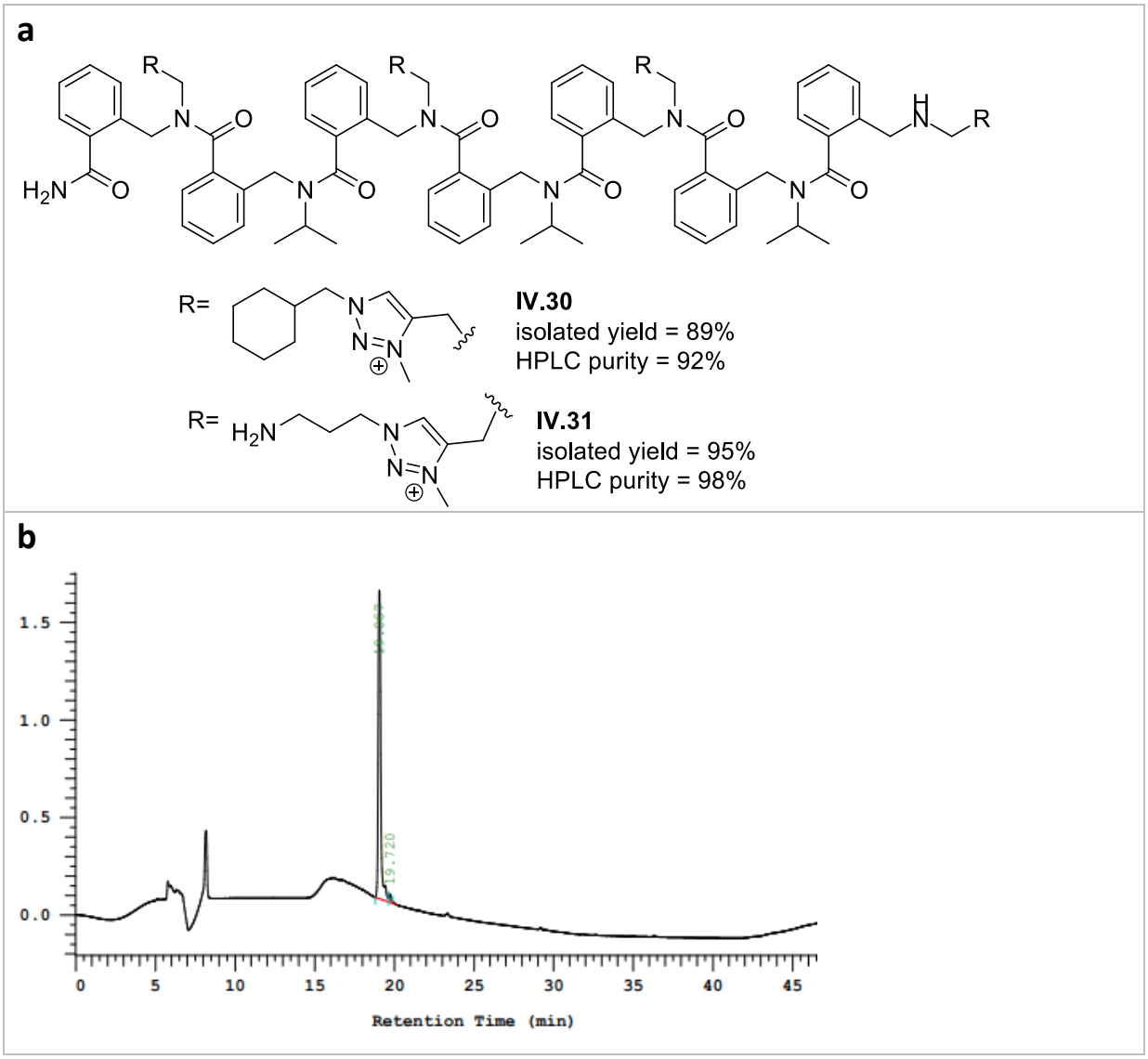

Figure IV.23. (a) Triazolium-containing *ortho*-heptamers obtained with the standard procedure using one azide. (b) HPLC chromatogram (220 nm) of purified heptamer **IV.30**.

IV.B.2. Conformational study

Our team has reported the effect of triazolium side chains on inducing *cis* amide conformation through a strong n→ π* electronic interaction in peptoids (Figure IV.4).[115a] To explore the behavior of this side chain in arylopeptoids, we synthesized two models *meta*-arylopeptoid **IV.32** and **IV.33** containing a triazole and a triazolium side chains, respectively. These models refer to previous conformational studies performed on arylopeptoids (see Chapter I section I.B.3.1.2). After the synthesis of the first monomer with propargyl side chain, the acylation with 3-methylbenzoyl chloride was performed, followed with the click reaction, under the optimized conditions described above, in the presence of benzyl azide (Scheme IV.3). **IV.32** was produced with 85 % yield and 95 % purity after cleavage from the resin. **IV.33** was produced with 89 % yield and 98 % purity after exposing the supported triazole to methyl iodide followed by the cleavage from the resin (Scheme IV.3).

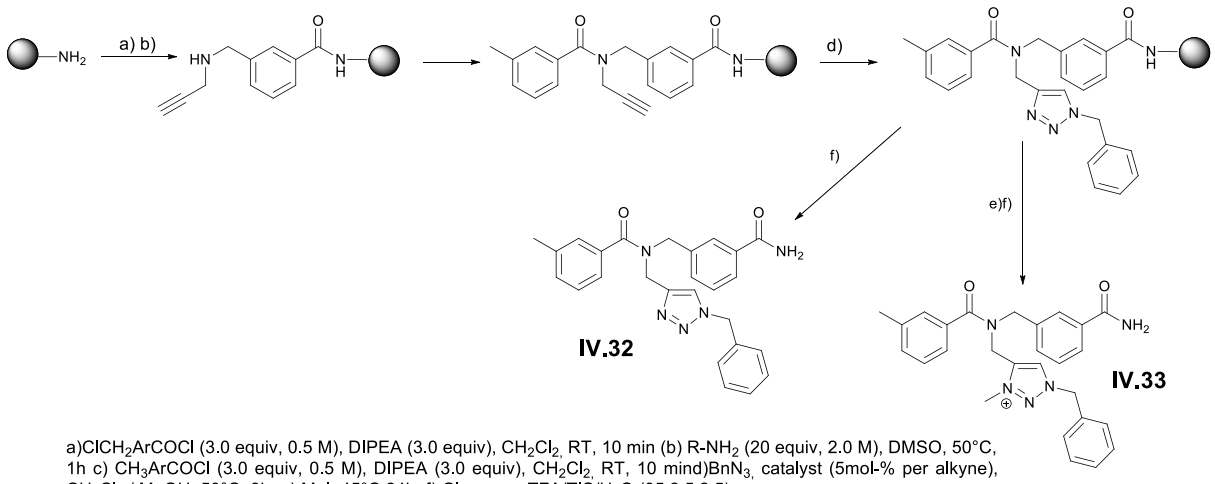

a)$ClCH_2ArCOCl$ (3.0 equiv, 0.5 M), DIPEA (3.0 equiv), CH_2Cl_2, RT, 10 min (b) R-NH_2 (20 equiv, 2.0 M), DMSO, 50°C, 1h c) $CH_3ArCOCl$ (3.0 equiv, 0.5 M), DIPEA (3.0 equiv), CH_2Cl_2, RT, 10 mind)BnN_3, catalyst (5mol-% per alkyne), CH_2Cl_2 / MeOH; 50°C, 3h; e) MeI, 45°C,24h; f) Cleavage: TFA/TIS/H_2O (95:2.5:2.5).

Scheme IV.3. Synthesis of model compounds **IV.32** and **IV.33**.

High sensitivity of the cis/trans conformation of arylopeptoids toward the bulkiness of the side chains was proved before.[106] Thus, confirmation preferences of these two models were studied by NMR. The variable temperature ^{1}H-NMR studies of **IV.32**, in CD_3CN, revealed the presence of two conformers in 60/40 proportion (Figure IV.24). At room temperature, broad signals were observed indicative of coalescence phenomena. Indeed, at low temperature two subsets of signals appeared in proportion 60:40. However, only a single set of sharp signals were observed in ^{1}H-NMR spectra of variable temperature study of **IV.33** in CD_3CN (Figure IV.24).

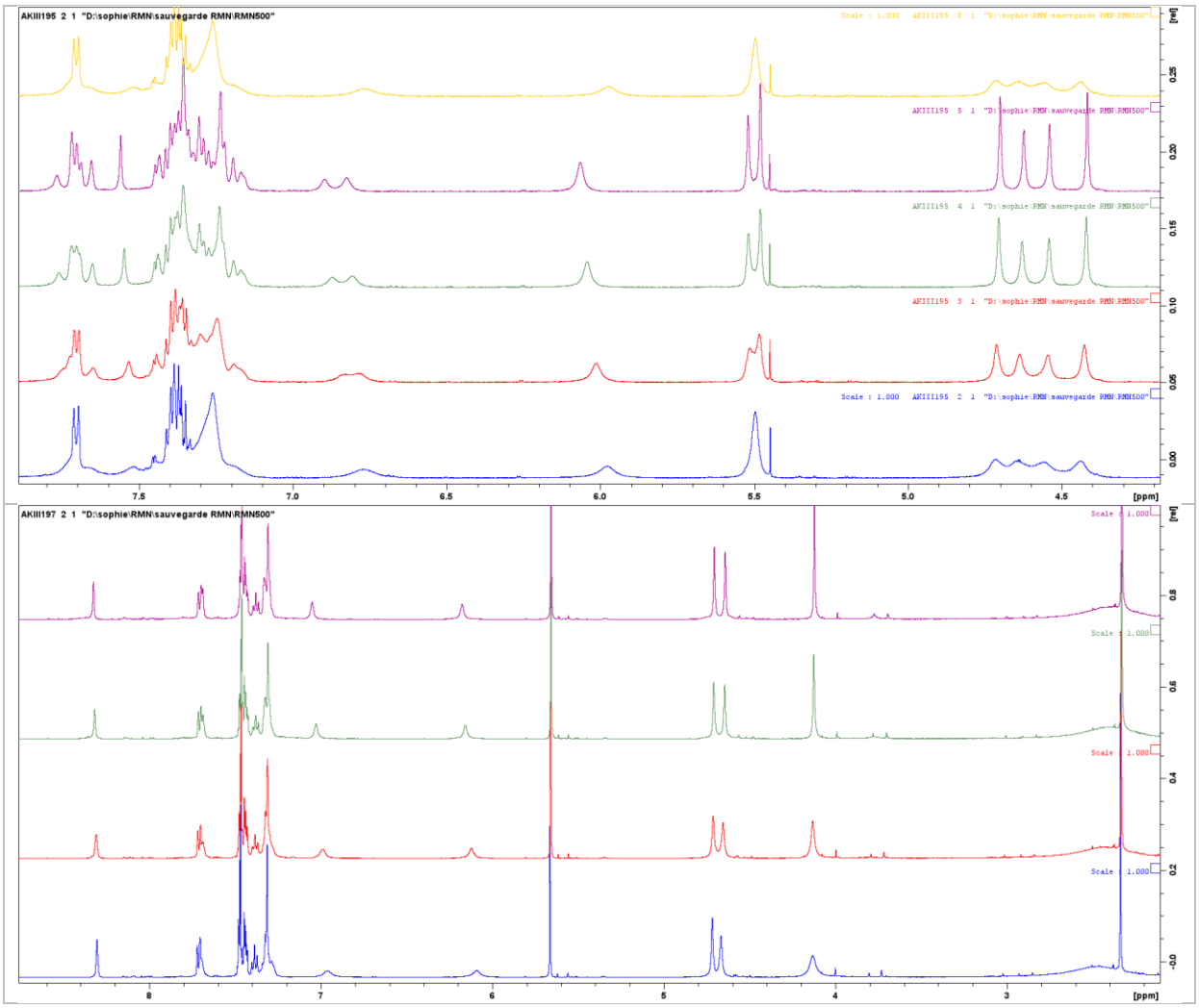

Figure IV.24. Variable temperature study of **IV.32** (a) and **IV.33** (b) in CD_3CN (4-8 ppm region): 298 K (blue curve), 288K (red curve), 278 K (green curve), 273 K (purple curve), 298 K at the end of the study (yellow curve).

Thanks to 2D-NMR experiments (COSY, HSQC and HMBC), signals assignation was performed. However, some signals overlapping in the aromatic region were observed and not all aromatic CHs were attributable (Figure IV.25.b). Then, NOESY experiment was performed at 278 K to determine the conformer present in solution (CD_3CN). All the correlations that we observed in the NOESY eperiments are listed in table IV.2. Unfortunately, due to aromatic CHs overlapping, it was not possible to conclude on the amide conformation conformation in *cis* or *trans* but it was possible to deduce the triazolium side chain positioning. Indeed, the NOESY correlations indicated that the triazolium proton H**a** is close to methylene CH_2 **c** and aromatic CH**g**. By contrast, the methyl group CH_3 **e** from triazolium didn't see the protons **c**. According to the NOESY results, we were able to conclude on the position of the triazolium with respect to the aromatic $ArCONH_2$ and we hypothesized two possible conformers: one with the *cis* amide and the other with the *trans* amide as shown in the Figure IV.25.a.

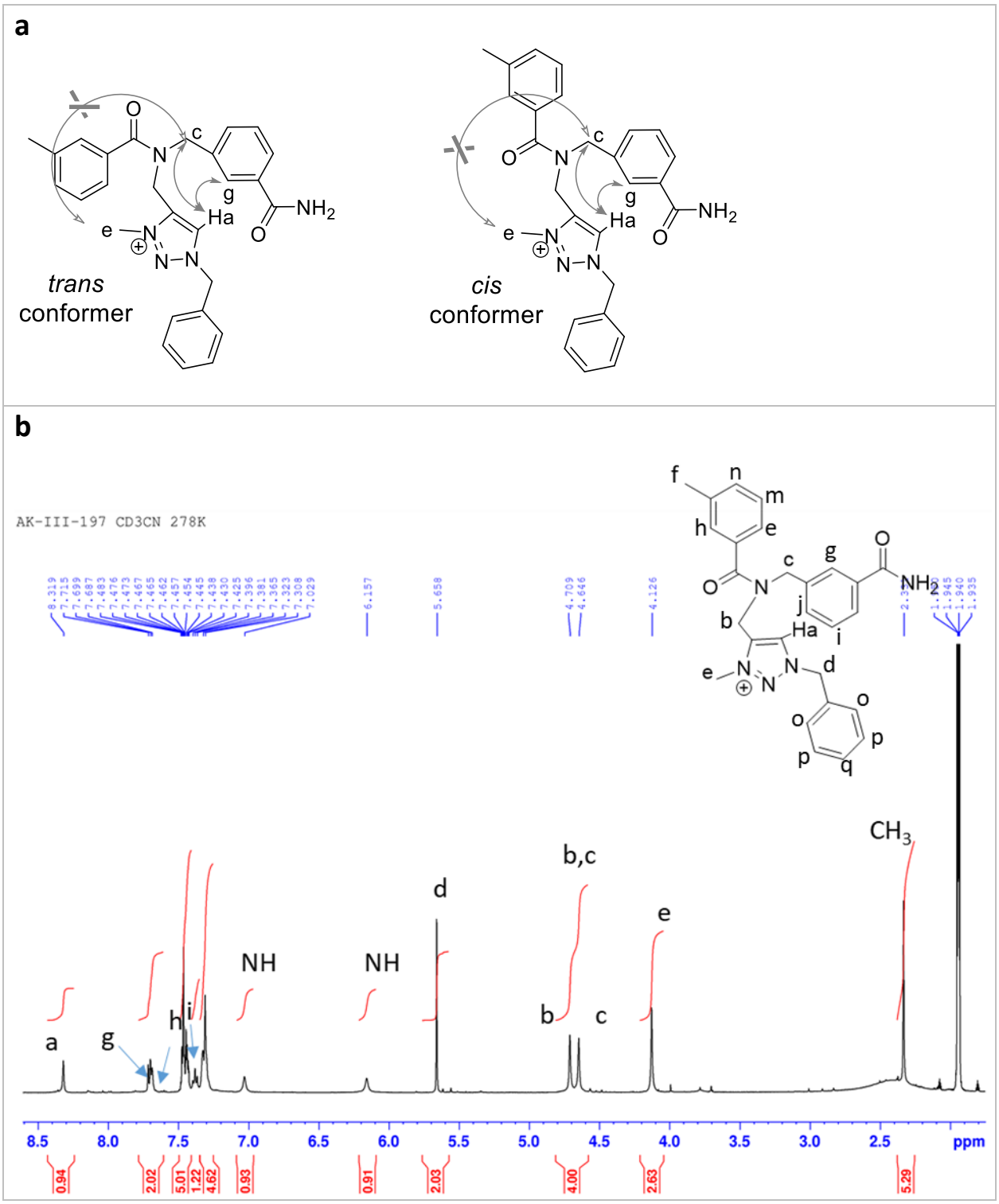

Figure IV.25. (a) ^{1}H-NMR of **IV.33** in CD_3CN at room temperature. (b) Structures of the two possible conformers hypothesized from the NOESY experiment at 278K.

Protons	Correlations
a to **b**	strong
a to **c**	weak
a to **d**	strong
a to **g**	weak
a to **h**	Not found
a to **i**	Not found
b to **g**	strong
b to **e**	strong
e to **c**	Not found
c to **g**	strong
d to **o** & **o'**	strong
d to **a**	strong

Table IV.2. Correlations obtained by NMR studies.

Computational calculation was performed in order to evaluate which conformer cis or trans is lower in energy than the other.

A scan of the energy of the molecule in gas phase along the dihedral amide bond (360° rotations with a 10° step) was performed by Gaussian software, using density functional theory (DFT) at the 6-31g level (the rest of the molecule was freely optimized). The resulting energetic diagram is depicted in Figure IV.26.

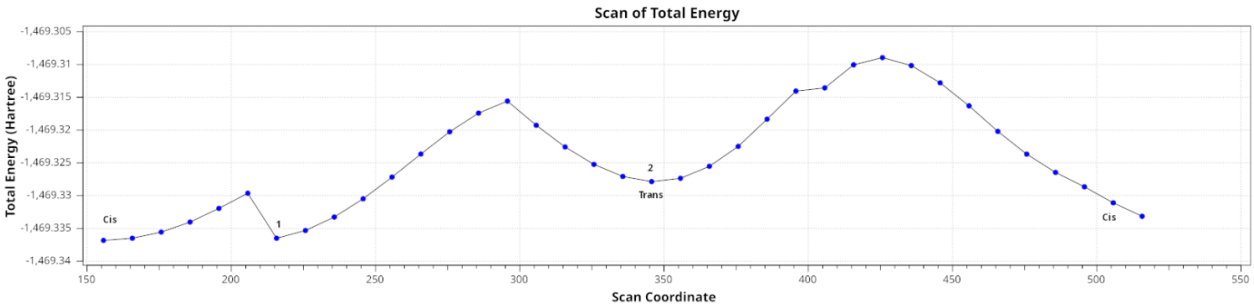

Figure IV.26. Energetic profile of compound **IV.33**.

This optimization shows two local minima, 1 and 2, corresponding to the *cis* and the *trans* amide conformations respectively. Each of these conformations were further freely optimized with thermodynamic correction at 20°C. It results that the *cis* conformation is positioned at 6.7 kcal (Gibbs energy, ΔG) below the *trans* conformer. Supposing that an equilibrium occurs only between these two conformers (*cis* to *trans*), we could easily calculate the percentage of the minor *trans* conformer.

$$K = \frac{[Trans]}{[Cis]} = e^{-\Delta G/R.T} = e^{-\frac{6.7}{8.314.(273+20)}} = 9.10^{-6}$$

Therefore, the percentage of *trans* conformer is less than 1%.

These calculations support that the *cis* conformer is the only detectable compound in the NMR study. Therefore, introduction of the triazolium in the side chain locks the *N*,*N*-disubstituted amide in the *cis* conformation (Figure IV.27).

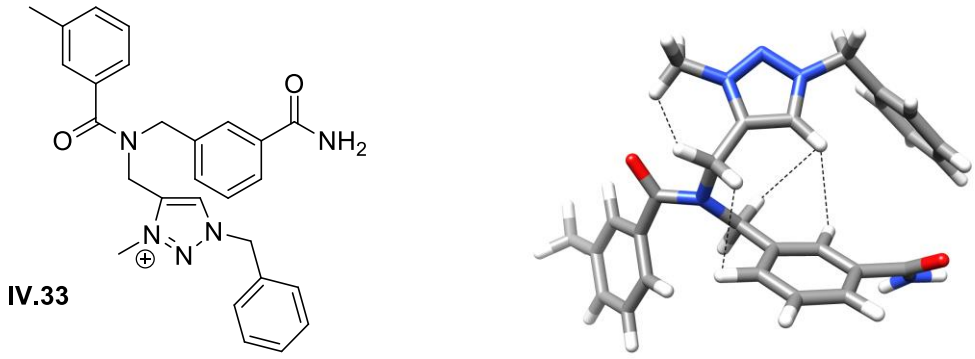

Figure IV.27. Conformation of lowest energy found by calculation.

The effect of the triazolium side chains on conformational preferences of linear oligomers is more difficult to access due to the presence of several conformers in solution. However, ^{1}H NMR spectra showed less coalescence after the conversion of triazoles into triazoliums.

IV.B.3. Biological tests.

The main goal of the synthesis of the triazolium-containing arylopeptoids was to test their antimicrobial activities. Indeed, the previous studies on peptoids with triazolium side chains in our group, in addition to the successful antimicrobial activities of arylamides was encouraging to start such studies on these novel cationic *N*-substituted aromatic oligoamides.

The evaluation of the antimicrobial activity was first conducted on selected compounds from Series: A, B and C in collaboration with Christiane Forestier from LMGE (Laboratoire Microorganisms: Génome Environment) at Université Clermont Auvergne. This study was carried out as part of the ANR project AmphiPep. All experiments have been performed by Mélodie Malige from LMGE. We first selected 11 *meta*-arylopeptoids with different side chains, length (trimer to pentamer) and charge (+2 to +6) to start the antibacterial studies on 4 different bacterial strains (*E.coli* JM109, *E. coli* ATCC25922, *P. aeruginosa* ATCC27853, and *S. aureus* CIP6525) (Table IV.1). The Minimal Inhibitory Concentrations (MICs) were determined as recommended by the Clinical and Laboratory Standards Institute. MBCs were determined by sub-culturing broth dilutions of the MIC assay on Trypticase Soy agar.

			E.coli JM109	E.coli ATCC25922	P.aeruginosa ATCC27853	S.aureus CIP6525
Code	**Series**	**Réf**	**MIC/MBC**	**MIC / MBC**	**MIC / MBC**	**MIC / MBC**
D1	**B**	**IV.10**	100/>100	50/>100	>100/>100	**12,5/25**
D2	**B**	**IV.9**	>100/>100	>100/>100	>100/>100	>100/>100
D3	**B**	**IV.12**	>100/>100	>100/>100	>100/>100	>100/>100
D4	**C**	**IV.18**	**50/50**	**25/>100**	>100/>100	100/>100
D5	**C**	**IV.16**	>100/>100	>100/>100	>100/>100	>100/>100
D6	**C**	**IV.17**	50/>100	50/>100	>100/>100	**6,25/6,25**
D7	**C**	**IV.21**	>100/>100	>100/>100	>100/>100	>100/>100
D8	**C**	**IV.20**	>100/>100	>100/>100	>100/>100	>100/>100
D9	**A**	**IV.3**	>100/>100	>100/>100	>100/>100	>100/>100
D10	**A**	**IV.4**	100/>100	50/>100	>100/>100	>100/>100
D11	**A**	**IV.6**	>100/>100	>100/>100	>100/>100	>100/>100

Table IV.3 Antibacterial activities of different compounds from series A, B and C. Minimum Inhibitory Concentration (MIC) and Minimum Bactericidal Concentration (MBC) are determined in μM and are representative of three independent experiments.

From this first screening, only three arylopeptoids show an activity on Gram positive or Gram negative bacteria. These identified oligomers contain only two type of side chains which are triazoliums with cyclohexylmethy and aminopropyl substituents. Tetramer **IV.10** and pentamer **IV.17** carrying exclusively cyclohexylmethyl substituents show activities against *S. aureus*, with the longer oligomer **IV.17** showing better activity (MIC 6.25 versus 12.5 μM) and a modest effect on *E. coli* (MIC 50 μM). The pentamer **IV.18** with propylammonium substituents shows a small effect against *E. coli* (MIC 25 and 50 μM) while the same pentamer **IV.16** with ethyl ammonium has no activity. This suggest that addition of a supplementary methylene between the ammonium and the triazolium is beneficial.

The results from this first screening were consistent with trends in antimicrobial activities of triazolium-based peptoids with cyclohexyl and ammonium substituents. After having the results from series A, B and C, a second generation of arylopeptoids was designed and synthesised. Our choice was to continue only using cyclohexylmethyl and propylamine substituent on triazolium side chains. Also, another important factor was deduced from this study, the alternating between triazolium side chain (as hydrophilic) and the isopropyl amine (as a hydrophobic side chain). This alternating was expected to be affecting the antimicrobial activity, as the hydrophobicity is highly correlated with the antimicrobial activity and increasing the hydrophobicity to a certain level

improves antimicrobial activity.[197] So we decided to elongate the chain length, keeping the alternating of between triazolium and isopropyl amine side chains. We also decided to develop *ortho*-arylopeptoids analogues to study the influence of the backbone on activity. Indeed, in the *ortho*-series the backbone will be more constrained and different orientations of the side chains will be obtained compared to the meta-series. With the aim to identify more potent arylopeptoids, series D, E, F and G have been prepared and were tested against the same panel of bacterial strains (Table IV.3).

			***E.coli* JM109**	***E.coli* ATCC25922**	***P.aeruginosa* ATCC27853**	***S.aureus* CIP6525**
Code	**Series**	**Réf**	**MIC/MBC**	**MIC/MBC**	**MIC/MBC**	**MIC/MBC**
E1	**D**	**IV.23**	3,2/6,25	3,2/100	>100/>100	1,6/12,5-50->100
E2	**D**	**IV.22**	3,2/3,2	6,25/50 or >100	>100/>100	>100/>100
E3	**D**	**IV.24**	3,2/3,2	6,25/>100	25/100	25/100
E4	**E**	**IV.26**	>100/>100	>100/>100	>100/>100	25/100
E5	**E**	**IV.25**	>100/>100	>100/>100	>100/>100	>100/>100
E6	**F**	**IV.27**	100/100	100/>100	>100/>100	6,25/100
E7	**F**	**IV.28**	25/50	50/>100	>100/>100	>100/>100
E8	**F**	**IV.29**	50/50	100/>100	>100/>100	100/100
E9	**G**	**IV.30**	6,25/12,5-6,25-25	6,25/>100	>100/>100	1,6/12,5
E10	**G**	**IV.31**	12,5/25-12,5-50	25/50 or >100	>100/>100	>100/>100

Table IV.4. Antibacterial activities of series D, E, F and G. Minimum Inhibitory Concentration (MIC) and Minimum Bactericidal Concentration (MBC) are determined in μM and are representative of three independent experiments.

Series D (*meta*-arylopeptoid heptamers) proved to be active against bacteria with better activity than that of series C. The heptamer triazolium **IV.23** directly comparable with **IV.17** (same side chains, heptamer versus pentamer and charge +4 versus +3) is more potent on *S. aureus* (1.6 versus 6.25 μM) and really active against the two *E. coli* (3.2 and 3.2 versus 100 and 50 μM). Also, the heptamer triazolium **IV.22** directly comparable with **IV.18** (same side chains, heptamer versus pentamer and charge +4 versus +3) is more active against the two *E. coli* (3.2 and 6.5 versus 50 and 25 μM). Surprisingly, the combinatorial mixture **IV.24** was the only product active against the four bacteria strains although modest on *P. aeruginosa* and *S. aureus*. We suppose that one of the isomers could be active against *P.aeruginosa* or that a synergic effect is obtained by association of different oligomers as it was observed for AMPs.198This increase of activity between series D and C was attributed to the increase of the sequence length together with the cationic charge. The

[197] (a) Wang, J.; Dou, X.; Song, J.; Lyu, Y.; Zhu, X.; Xu, L.; Li, W.; Shan, A. *Med. Res. Rev.* **2019**, *39*, 831–859. (b) Takahashi, D.; Shukla, S.K.; Prakash, O.; Zhang, G. *Biochimie* **2010**, *92*, 1236–1241.

[198] Bechinger, B.; Salinikov, E. S. *Chem. Phys. Lipids* **2012**, *165*; 282–301.

results of the *ortho*-series (E, F and G) were similar to that from the *meta*-series. The tetramer **IV.26** from series E shows slight activity only on *S. aureus*, and an increased activity was obvious with series F (pentamers). The *ortho*-heptamers from series G proved to be the most active among the ortho-arylopeptoids we prepared. The most potent in the *ortho*-series is heptamer **IV.30** (cyclohexylethyl triazolium, charge +4) with MIC 6.25 µM on E. coli strains and MIC 1.6 µM on S. aureus. These results were consistent with the *meta*-heptamers results from series D. If we compare oligomers with same design from meta and *ortho* series (**IV.23** versus **IV.30** and **IV.22** versus **IV.31**) we observe the same selectivity profile and a slightly better activity for oligomers of the *meta* series. The conformational restriction may have also influence on the selectivity between bacterial and mammalian cells. The cytotoxicity of the active compounds is currently under study at LMGE.

IV.C. Conclusion.

In this chapter, we reported the synthesis of triazolium-based arylopeptoids after synthesizing the triazoles in the CuAAC method we used in chapter III. Also, we studied the conformational preferences and proved that the amide conformation is locked in *cis* in the presence of triazolium as a side chain. Moreover, the antibacterial activity of 7 different series of triazolium-based *meta*- and *ortho*-arylopeptoids was studied, revealing the potent effect of several compounds, especially with the ammonium and cyclohexylethyl substituents. The selectivity towards bacteria *versus* mammalian cells will give insight on the potential of these oligomers as antibacterial agents. After the encouraging antibacterial results, we start to think about synthesizing new series of triazolium-based arylopeptoids with longer chain length in addition to triazolium-based cycloarylopeptoids.

Chapter V: Crown-like 3D-structures from constrained cyclic *ortho*- and *meta*-arylopeptoids.

I would like to acknowledge Cristina Ionete, Erasmus exchange Master II student from University of Bucarest, Roumania, for the help she provides regarding the synthesis of the starting materials and the cyclisation procedure that will be presented below. A work that was unfortunately stopped by the COVID-19 arrival. I also thank Teodor Cucuiet, Erasmus exchange Master II student from Babeș-Bolyai University, Cluj-Napoca, Roumania who helped exploring the formation of the unusual linked bis-triazole structures.

V.A. Introduction.

The nature has been always a great inspiration in finding solutions for research. For example, nature produces cyclic peptides to attain more conformational rigidity in peptides, in addition to a wide range of potent biological activity including antibacterial activity gained.[199] The synthesis of a wide range of synthetic peptides and peptidomimetics, with the cyclisation as a strategy to enhance proteolytic resistance and cell penetration was reported by many researchers.[200] This cyclization strategy was also studied in peptoids.[201] The conformational heterogeneity of linear peptoids is mainly arising from the *cis-trans* isomerization around the amide bond.[202] Indeed, cyclisation of the linear peptoids restricts the amide backbone isomerism, reducing the number of possible confirmations and increasing their rigidity. These conformational restrictions could improve biological activity and selectivity. For example, according to reported studies, cyclic peptoids show better antimicrobial activity in addition to improved cell penetration compared to linear precursors.[203]

V.A.1. Macrocyclization.

This section will focus on previous work on the macrocyclization of peptoids and arylopeptoids, and conformational behavior of these macrocycles.

---

[199] a) Finger, S.; Kerth, A.; Dathe, M.; Blume, A. *Biochimica et Biophysica Acta* **2015**, *1848*, 2998-3006. b) Kling, A.; Lukat, P.; Almeida, D. V.; Bauer, A.; Fontaine, E.; Sordello, S.; Zaburannyi, N.; Herrmann, J.; Wenzel, S. C.; Kçnig, C.; Ammerman, N. C.; Barrio, M.B.; Borchers, K.; Bordon-Pallier, F.; Brçnstrup, M.; Courtemanche, G.; Gerlitz, M.; Geslin, M.; Ham-mann, P.; Heinz, D. W.; Hoffmann, H.; Klieber, S.; Kohlmann, M.; Kurz, M.; Lair, C.; Matter, H.; Nuermberger, E.; Tyagi, S.; Fraisse, L.; Grosset, J. H.; La-grange, S. ; Müller, R. *Science* **2015**, *348*, 1106-1112; c) Bionda, N.; Fleeman, R. M.; de la Fuente-NfflÇez, C.; Rodriguez, M. C.; Reffuveille, F.; Shaw, L. N.; Pastar, I.; Davis, S.C.; Hancock, R. E. W.; Cudic, P. *Eur.J.Med. Chem.* **2016**, *108,* 354-363. d) Claro, B.; Peon, A.; Gonzalez-Freire, E.; Goormaghtigh, E.; Amorin, M.; Granja, J. R.; Garcia-Fandino, R.; Bastos, M. *Colloids Surf. B* **2021**, *208*, 112086. e) Liu, Y.; Liu, Y.; Li, Z. *Food Chem.* **2022**, *385*, 132715.

[200] a) Shin, S. B. Y.; Yoo, B.; Todaro, L. J.; Kirshenbaum, K. *J. Am.Chem.Soc.* **2007**, *129*, 3218-3225. b) Ban´kowski, K.; Witkowska, E.; Michalak, O. M.; Sidoryk, K.; Szymanek, E.; Antkowiak, B.; Paluch, M.; Filip, K. E.; Cebrat, M.; Setner, B.; Szewczuk, Z.; Stefanowicz, P.; Cmoch, P.; Izdebski, J. *Eur.J.Med.Chem.* **2013**, *63*,457-467 c) Nischan, N.; Herce, H. D.; Natale, F.; Bohlke, N.; Budisa, N.; Cardoso, M. C.; Hackenberger, C.P.R. *Angew.Chem.Int. Ed.* **2015**, *54*, 1950-1953. d) Sayers, E. J.; Barlow, V. L.; Tsai, Y-H.; Jones, A. T. *Methods Mol Biol.* **2022**, 2383, 211-228.

[201] Webster, A. M.; Cobb, S. L.; *Chem.Eur.J.* **2018**, *24*, 7560 -7573.

[202] Kalita, D.; Sahariah, B.; Mookerje, S. P.; Sarma, K. *Chem Asian J.* **2022**, *17*, e202200149.

[203] Huang, M. L.; Shin, S. B. Y.; Benson, M. A.; Torres, V. J.; Kirshenbaum, K. *ChemMedChem* **2012**, *7*,114–122.

In 2007, Kirshenbaum reported the first synthesis of cyclic α-peptoids using head-to-tail cyclisation strategy.[200a] In order to determine the optimal chain length for cyclization, linear peptoids, cleaved from 2-chlorotrityl resin, were synthesized. The results showed that hexamers are the minimum optimal length to be cyclized in good yields. The linear hexamer was cyclized in DMF in the presence of PyBOP as coupling reagent and DIPEA leading to the cyclohexamer in 97% HPLC yield after 5 minutes at room temperature (Scheme V.1).

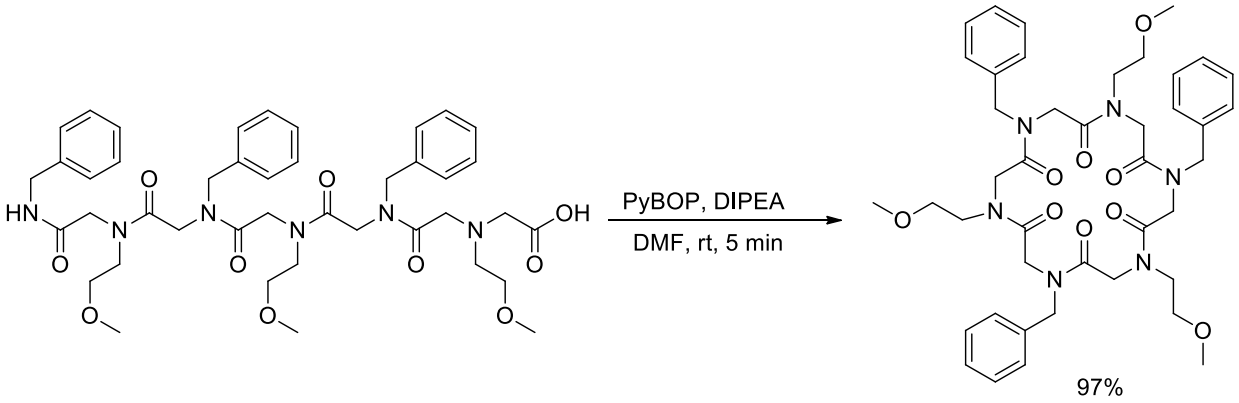

Scheme V.1. Cyclization of linear peptoids *via* head-to-tail strategy.

The head-to-tail cyclization strategy proved to be efficient to cyclize linear peptoids with length up to 20 mers giving up to 97% HPLC yield in concentration ranging from 0.6 to 3 mM. The cyclic hexamer was crystallized and the crystals revealed that the hydrophobic phenyl side chains are oriented on one face, while the methoxy ethyl side chains are oriented on the other face of the ring (Figure V.1). This ordering of the side chains due to a *cis-cis-trans-cis-cis-trans* arrangement of the backbone amides, suggests the possibility to obtain ordered amphiphilic structure.

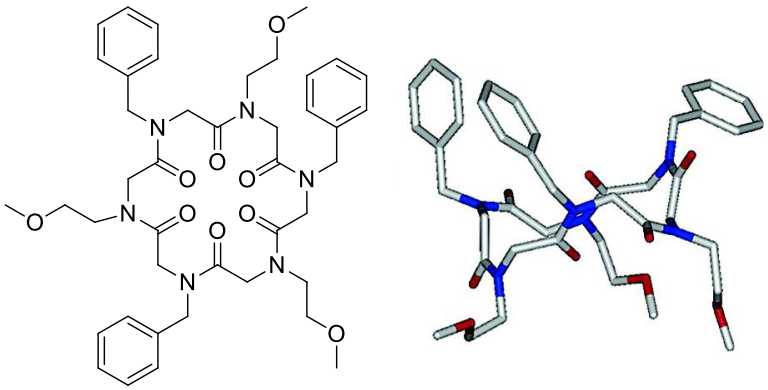

Figure V.1. Crystal structure of a cyclic peptoid hexamer showing segregation of polar and apolar side chains on opposing faces of the macrocycle.

Since these pioneer works, macrocycles made from α-, β- or α,β-peptoids have been studied extensively and reviewed. [201,204]

In the field of *N*-alkylated aromatic oligoamides, it was reported that macrocyclic *N*-alkylated *para*-cyclophanamides, with a long hydrophobic side chain, could act as hosts for various guest and artificial enzymes.[205] However, these cyclophanamide-based macrocycles are exclusively synthesized by one-pot polymerization that restricts the side chain diversity, ring size and backbone types. Our group reported the cyclisation of arylopeptoids which form shape persistent structures in solution and high order nano-tubular structures in solid state.[206] As we mentioned in chapter I, linear arylopeptoids can be efficiently synthesized, with high diversity in terms of side chains and backbone type, and can undergo head-to-tail cyclisation to form well-defined structures similar to *N*-alkylated *para*-cyclophanamides.

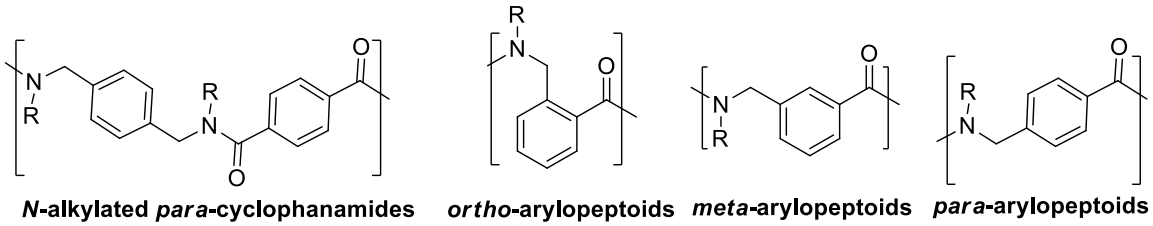

Figure V.9. Repeating units of *N*-alkylated *para*-cyclophanamides and arylopeptoids.

An interesting strategy to obtain cyclic structures consist in a prerequisite dimerization of short oligomer followed by a cyclization as depicted in Scheme V.2. It has been found that when the length and/or the conformational behavior of the starting material do not permit a rapid cyclization, a dimerization occurs providing an arylopeptoid that will cyclize smoother.

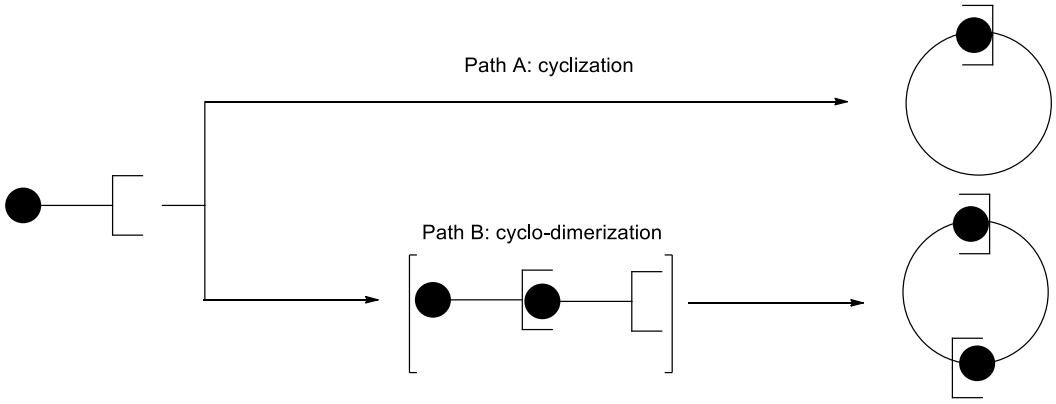

Scheme V.2. Two different paths for cyclisation.

[204] A) D'Amato, A. *Eur. J. Org. Chem.* **2022**, e202200665. b) Yoo, B.; Shin, S. B. Y.; Huang, M. L.; Kirshenbaum, K. *Chem. Eur. J.* **2010**, *16*, 5528 – 5537

[205] a) Murakami, Y.; Kikuchi, J.-i.; Suzuki, M.; Matsuura, T. *J. Chem. Soc. Perkin Trans.* **1988,** *1*, 1289-1299. b) Murakami, Y.; Kikuchi, J.-i.; Hisaeda, Y.; Hayashida, O. *Chem. Rev.* **1996**, *96*, 721–758.

[206] Hjelmgaard, T.; Roy, O.; Nauton, L.; El-Ghozzi, M.; Avignant, D.; Didier-jean, C.; Taillefumier, C.; Faure, S. *Chem.Commun.* **2014**, *50*, 3564-3567.

This strategy was exploited to prepare macrocycles from the trimeric linear arylopeptoids (*ortho*-, *meta*- and *para*-) containing isopropyl or ethyl side chains, synthesized as described by Hjelmgaard *2et al*. The cyclisation procedure reported for α,β-cyclopeptoids was applied.[104,206] The linear arylopeptoids were cyclized in the presence of HATU and DIPEA in CH_2Cl_2/DMF (4:1) after the deprotection of the *tert*-butyl group in TFA/CH_2Cl_2 (Scheme V.3).

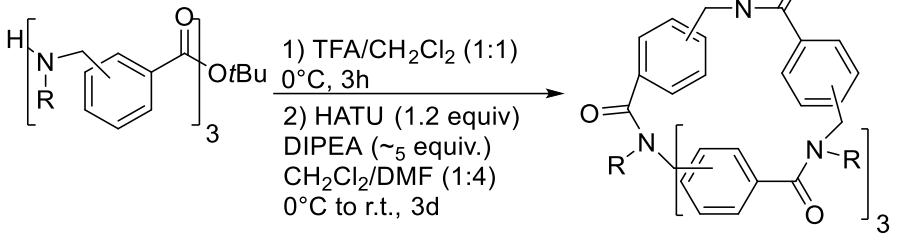

	R	Cyclo-trimer (%)	Cyclo-hexamer (%)
Para	*i*Pr	-	61
Para	Et	-	57
Meta	*i*Pr	88	-
Meta	Et	83	-
Ortho	*i*Pr	4	33
Ortho	Et	48	45

Scheme V.3. Cyclisation of *ortho*-, *meta*- and *para*-arylopeptoids.

The cyclisation of *para*-trimers was challenging due to its rigid backbone. The cyclisation was disfavored as the cyclotrimers were not obtained, instead, the cyclodimerisation occurred (Scheme V.2, Path B). Cyclohexamers were obtained with good yield (57-61%) with both side chains (Scheme V.3). By contrast, *meta*-trimers undergo direct macrocyclisation (Scheme V.2, Path A) to form the cyclotrimers in high yields (83-88%). The *ortho*-trimers cyclisation was more dependent on the nature of the side chains. In case of *ortho*-trimer with ethyl side chain, the cyclic hexamer and cyclic trimer were obtained in similar amounts with a total yield of more than 90% (Figure V.3), undergoing both paths A and B (Scheme V.2). While for the *ortho*-trimer with *iso*propyl side chain, the total yield of cyclisation decreased to 37%, with a majority of cyclohexamer (Path B, Scheme V.2) that counts for 33% (Figure V.3). This decrease in the yield and favoring of cyclohexamer in *ortho*-trimers was attributed to the increase congestion of the backbone which disfavors the direct ring closure.

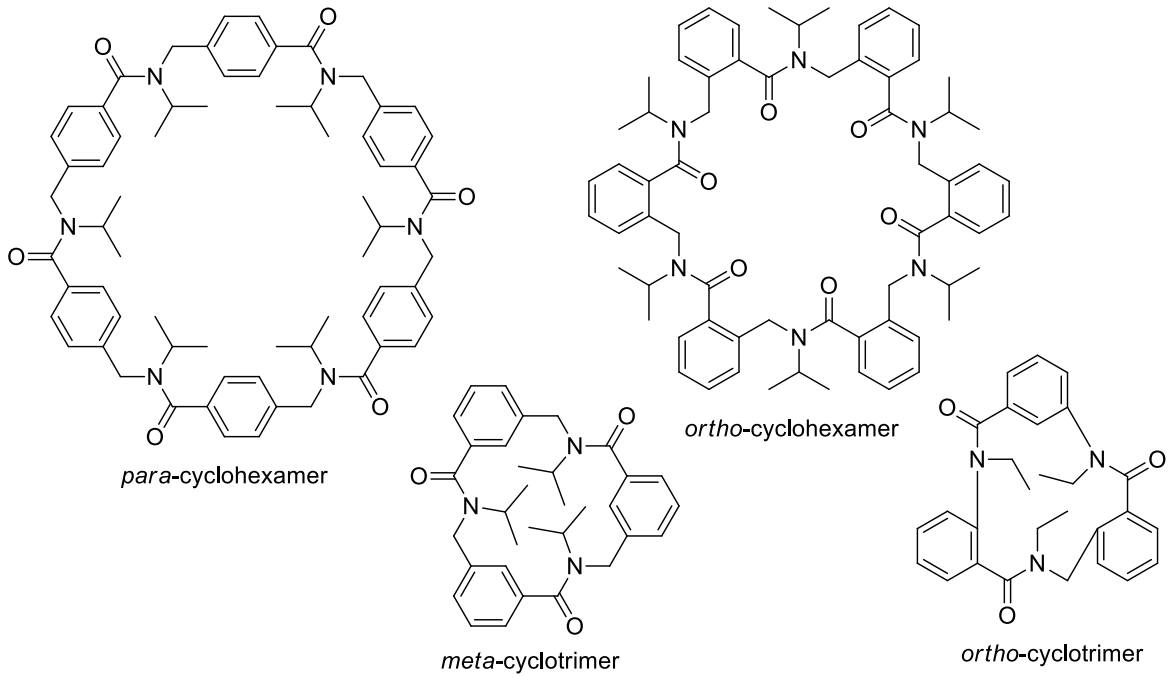

Figure V.3. Cyclotrimers and cyclohexamers produced.

The *meta*-cyclotrimer formed a needlelike crystal from EtOAc, which was the first arylopeptoid suitable for X-ray diffraction (Figure V.4.a). The molecules stack on top of each other to form a tubular assembly as a result of van der Waals interaction. Also, a nanoscale hollow tube consisting of six parallel tube-like structures form a second organization based on aromatic π-π stacking. Also, the *ortho*-cyclotrimer with the ethyl side chains forms a crystal suitable for X-ray diffraction (Figure V.4.b) which revealed a *cis-trans-trans* arrangement of the backbone amides. According to DFT calculations performed with B3LYP functional and 6-31G(d,p) bases set , the *cis-trans-trans* conformation is the lowest in energy in solution. The *cis* amide bond is deviated by 20° from the planarity to release the strain, which could explain the difficulty for cyclisation in the *ortho*-series. The *ortho*-cyclohexamer, with isopropyl side chains, forms single crystals in acetonitrile. Interestingly, one acetonitrile molecule in an interior cavity was found. This X-ray structure revealed that the macrocycles stack and form a tubular array bridged by additional water molecules (Figure V.4.c).

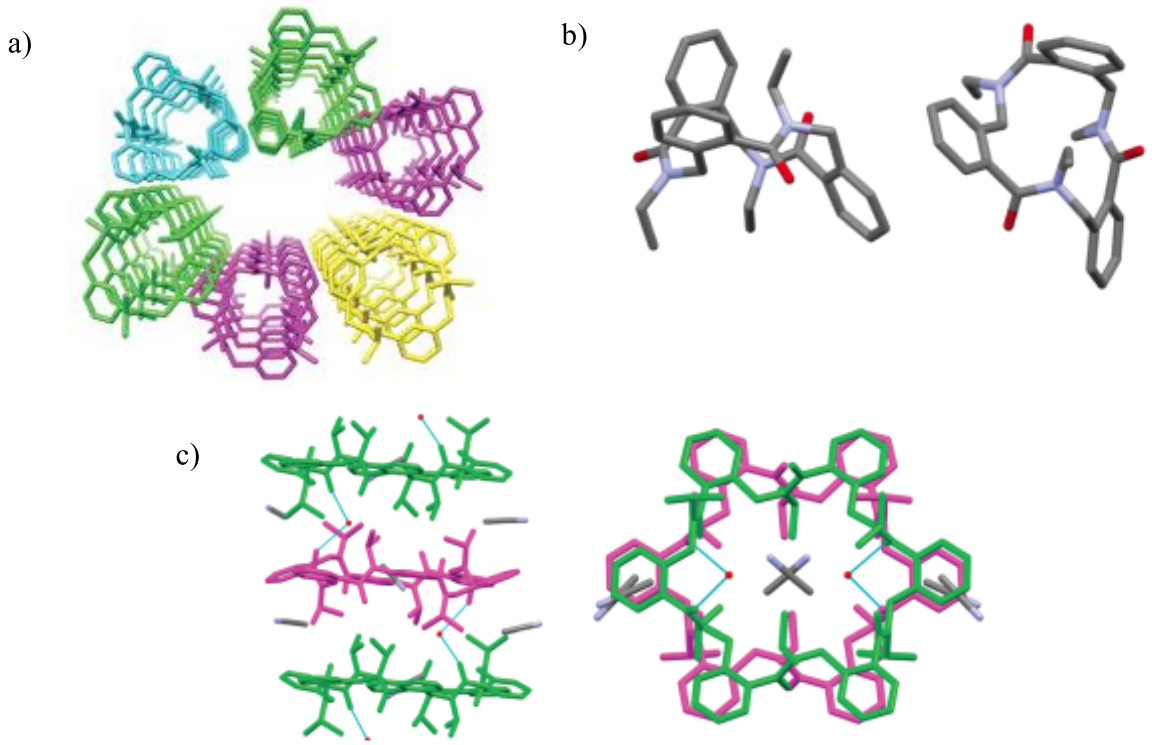

Figure V.4. X-ray structures of *meta*- and *ortho*-cyclotrimers and *ortho*-cyclohexamer.

In 2018, Faure's group reported the synthesis of macrocycles with diverse shape and sizes.[207] First, the linear precursors containing combined *N*-substituted *ortho*-, *meta*- and *para*-aminobenzamide subunits were synthesized on solid-phase using submonomer protocol. COMU was selected as a coupling reagent after the optimization of the macrocyclization process. The *para*-tetramer cyclisation was problematic, as it results in a mixture of cyclotetramer and cyclooctamer to be the only compound encountering cyclodimerization in this study. The cyclisation of the other 11 precursors in the study was efficient and yields more than 50% of the desired macrocycle. Notably, it was deduced that the efficiency of the macrocyclization is dependent on the sequence pattern in the linear precursors. For example, the yield of the cyclotetramer derived from *meta-para-meta-para* linear tetramer was 10 % more than that derived from *para-meta-para-meta* linear tetramer. However, the NMR study of the two macrocycles produced were superimposable indicating that cyclization step has no influence on the conformational preference of the final macrocycle. The conformational study by ^{1}H-NMR ($CDCl_3$) indicates a flexibility of the structure. Indeed, coalescent signals for most of them are found, except for the *para*-cyclotetramer. in addition to the alternating *para-ortho* and *meta-ortho*-cylotetramers which showed different spectra.

The conformational structures of these macrocycles were studied in solution and in the solid state. For example, ^{1}H-NMR of *meta-ortho*-cyclotetramer revealed the existence of two stable conformations at room temperature, with coalescence observation upon heating. The

[207] Hjelmgaard, T.; Nauton, L.; De Riccardis, F.; Jouffret, L.; Faure, *S. Org. Lett.* **2018**, *20*, 268-271

crystallization of this compound in CH_3CN revealed an extended zigzag arrangement of the backbone with an all *trans* conformation of backbone amides (Figure V.5).

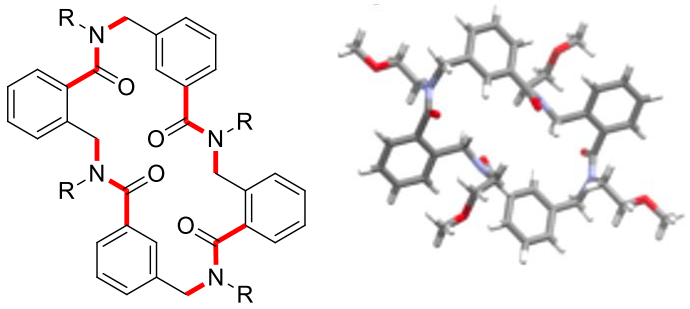

Figure V.5. Chemical structure showing amides conformation and X-ray crystal structure of the *ortho,meta,ortho,meta*-cyclotetramer.

Ikeda reported the synthesis of *para*-cycloarylopeptoids and also studied their conformational behavior.[208] After the synthesis of linear *para*-arylopeptoids using the procedure developed by our group, exploration of the macrocyclization using HBTU, PyBOP and DIC was done. PyBOP and HBTU showed the same efficiency and PyBOP was finally selected as standard reagent. The effect of the length revealed that trimer cyclodimerizes to furnish the corresponding hexamer macrocycle, as already explored by our group, while the tetramers and hexamers are cyclized in the same yield. The efficiency of the macrocyclization was improved when the linear arylopeptoids were added slowly *via* a syringe pump to sustain the high dilution, as the isolated yield increased up to 92% with 50 µL h^{-1} addition. The cyclization was efficient on a range of *para*-tetraarylopeptoids containing different side chains, with more than 72% yield.

The crystals of tetramer macrocycle containing hexyl side chain was obtained in isopropanol and the one containing alternating iBt and mBzl side chains was obtained in chloroform. The crystals were studied by X-ray diffraction revealing different structures (Figure V.6). The four amide bonds in the first macrocycle adopts *cis-trans-cis-trans* conformation. However, the second macrocycle adopted all-*cis* confirmation referred as open confirmation providing a cavity to accommodate one chloroform molecule. The ^{1}H-NMR studies using different solvents suggested that conformational exchange among *ctct*, *cccc* and other *cis/trans* isomerism of amide bond confirmations. Further ^{1}H-NMR studies under various solvent conditions suggested that tetrameric macrocycles adopt an open all-*cis* conformation in apolar media, which was also supported by DFT calculations.

[208] Hayakawa, M.; Ohsawa, A.; Takeda, K.; Torii, R.; Kitamura, Y.; Katagiri, H.; Ikeda, M. *Org. Biomol. Chem.* **2018**, *16*, 8505-8512.

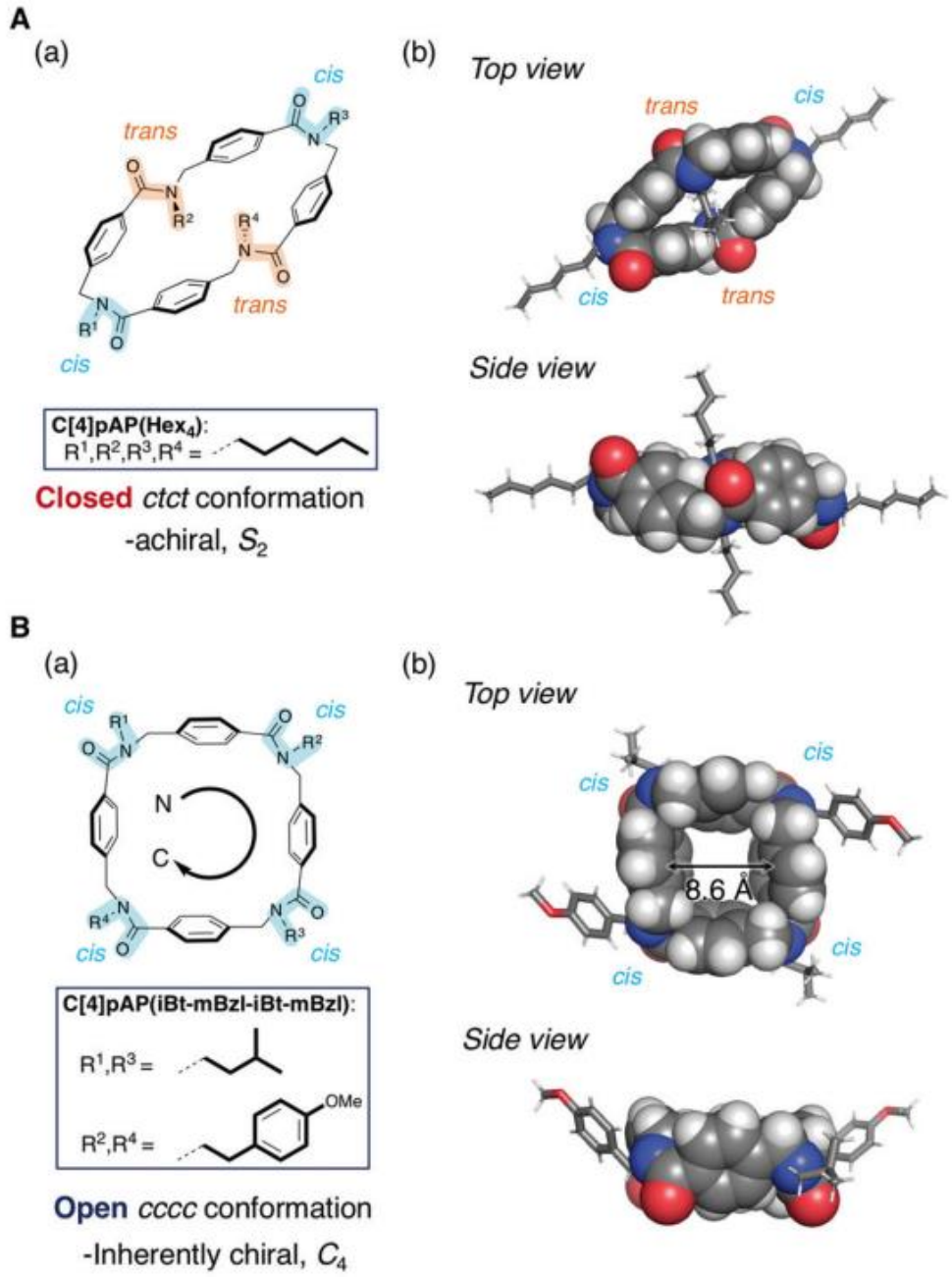

Figure V.5. Open and Closed confirmations of macrocycles and their X-ray diffraction structures.

Cyclic arylopeptoids has proved to adopt well-defined architectures in solution. Also, some macrocycles such as *ortho*-hexamer proved to have an interior cavity that is large enough to accommodate guest molecules. This class of cyclic oligoamides could prove its application in different field such as chemical biology or supramolecular chemistry.

V.A.2. Bicyclic compounds by CuAAC.

In the following chapter, the synthesis of *meta*- and *ortho*- linear and macrocyclic arylopeptoids are discussed. We use CuAAC reaction (catalyzed by our copper(I)-NHC complex) to synthesize

crown-like and tube-like architectures made from arylopeptoid macrocycles. A crystal structure of one of these macrocycles is also presented.

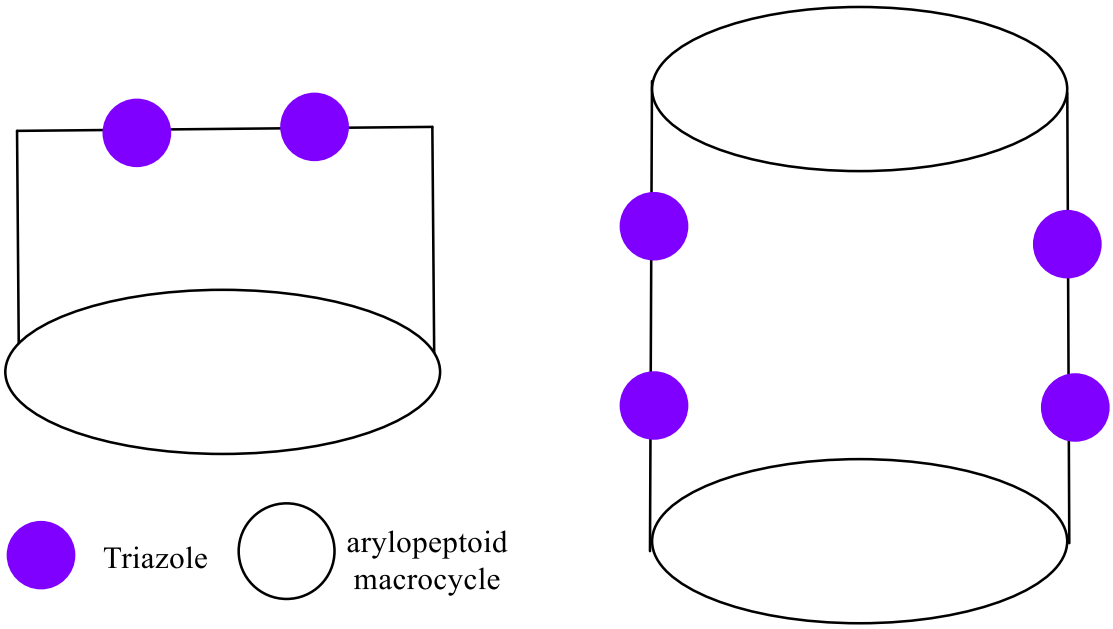

Scheme V.4. Schematic structure of targeted crown-like and tube-like structures

Crown-like 3D-structures from constrained cyclic arylopeptoids

Ayman Akhdar,[a] Lionel Nauton,[b] Laurent Jouffret,[b] Sophie Faure*[b] and Arnaud Gautier*[b]

The access to crown-like or tube-like structures from *ortho*- and *meta*-arylopeptoid macrocycles was explored through CuAAC reaction using a partially flexible bis(azide) and Cu^{I}-*N*-heterocyclic carbene as catalyst.

Molecular containers presenting cavities that can accommodate guests have been the focus of a growing interest in the past decades for their potential use in small molecule separation, in gas storage and biomimetic catalysis.[1] Numerous three-dimensional ordered structures have been constructed by mean of non-covalent interactions, such as hydrogen bonding[2] and metal–ligand coordination.[3] In comparison, covalent assembly to build molecular containers and cages is less studied probably due to the synthetic challenge.[4] A significant advance was made in this field, with the introduction of dynamic covalent chemistry which relies on reversible covalent reactions to access the thermodynamically most favored species.[5] However, the 2D and 3D molecular architectures thus constructed may suffer from a lack of stability and structural diversity. Shape-persistent organic containers such as cyclodextrins, cyclophanes and calixarenes with great potential for host-guest chemistry, have indeed been intensively studied. Considerable efforts have been made to enlarge ring sizes, backbone types and functional diversity of these synthetic receptors. We are interested in the design of organic 3D structures made by covalent assembly of macrocyclic oligoamides to build molecular containers with structural and functional features giving rise to a particular kind of chemical behavior.[6] Indeed, Kubik unveiled the potential of bis(cyclopeptide) covalently connected as molecular anion containers.[7] Recently, macrocyclic peptidomimetics processing *N*,*N*-disubstituted backbone amides instead of secondary amides, *i.e.* cyclopeptoids, were advantageously used to access crown- and tube-like 3D-structures by Kirshenbaum and Bräse groups. Herein, we present an efficient route to access crown-like structures made from cyclic *N*-substituted aminomethyl benzamide oligomers, *i.e.* cycloarylopeptoids,[8] through double CuAAC process using a stable source of Cu(I) (Figure 1).

Literature reveals two strategies based on Copper(I)-catalyzed azide-alkyne cycloaddition (CuAAC) reaction (8 equivalent of $Cu(MeCN)_4,PF_6$ catalyst) were employed (Figure 1). Kirshenbaum and co-workers use a cyclic peptoid containing an azide and an alkyne to access crown and tube-like structures in 27% and 4% isolated yield, respectively.[9] To avoid homodimerization yielding tube-like compound, the reaction was conducted at high dilution. To favour the formation of tube-like structure, Bräse group uses two cyclic peptoids containing each two azides and two alkynes.[10] The CuAAC process leds to compounds in yields ranging from 6 to 7%.

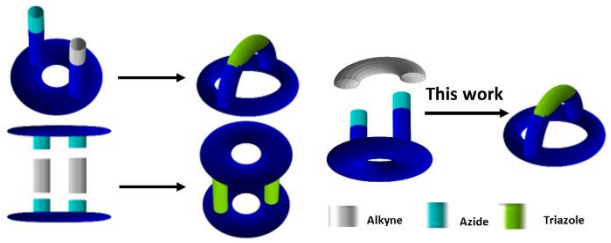

Figure 1. Strategies to access crown- and tube-like 3D-structures.

We hypothesized that selectivity and reactivity could be improved by using a pre-organized cyclic structure including a proper choice of the distances between the alkynes connecting groups, and an oxidation resistant Cu^{I} catalyst. To construct the pre-organised macrocycles, we selected arylopeptoids (*i.e. N*-alkylated aminomethyl benzamide oligomers) which are peptoid-inspired aromatic oligomamides.[11] Arylopeptoid macrocycles were shown to adopt well-defined conformation in solution; particularly in the *ortho* series.[12] Therefore, we selected for the present study, cyclic *ortho*- and *meta*- hexaarylopeptoids **IIa,b** available through cyclization of their linear counterpart **Ia,b** and catalyst (**III**), a Cu^{I}-*N*-Heterocyclic carbene recognized to be stable for years where exposed to air (Figure 2).[13]

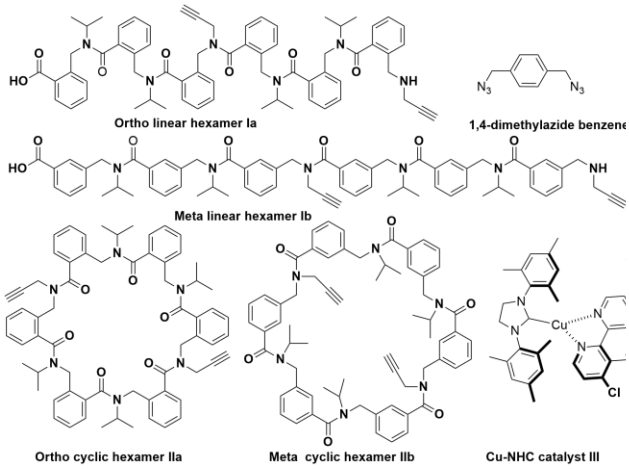

Figure 2. Structures of linear and cyclic arylopeptoids, azide and Cu(I) catalyst used.

The conformational studies of these cyclic hexamers have been reported for a full substitution by isopropyl side chains.[12] The cyclic *ortho*-hexamer displays a well-defined conformation in solution with a 6-fold rotational symmetry and a full *trans* arrangement of the backbone amides whereas the *meta* parent shows a high conformational flexibility. As partner for the CuAAC reaction, we use the partially flexible 1,4-dimethylazide benzene because the azides inter distance (7.1 Å between the two N1) seems compatible with the cavity size in **IIa,b**. Linear arylopeptoids were synthetized on rink acid resin for **Ia** (*ortho* series) and 2-chloro trityl resin for **Ib** (*meta* series),[14] using a submonomer strategy in 90 and 93% yield, respectively and HPLC purity > 96% (see ESI for details). Cyclisation using HATU as coupling reagent in presence of DIPEA affords **IIa** and **IIb** in 70 and 81% yields. Unexpectedly, **IIa** crystallizes spontaneously at room temperature from the chromatographic eluent MeOH/Water/TFA 80:20:1 (despite an exhaustive screening of solvents and techniques, single crystal of **IIb** suitable for X-ray diffraction could not be obtained). Compound **IIa** crystallized in the space group C2/c and displays an all *trans* conformation of the backbone amides with isopropyl and propynyl side-chains pointing alternatively up and down of the plan of the ring (Figure 3). The crystal contains 3 molecules of water that are involved in the crystal packing (ESI for details). The distance between the two internal carbons of the alkyne groups is 12.7 Å. We also examined the NMR spectra of the two cyclic hexamers. As expected, ^{1}H NMR of **IIb** (*meta* series) in a large range of solvent (Chloroform-d, acetone-d_6, acetonitrile-d_3, methanol-d_4, dmso-d_6) furnishes only broad signals, indicative of the presence of several conformations interconverting

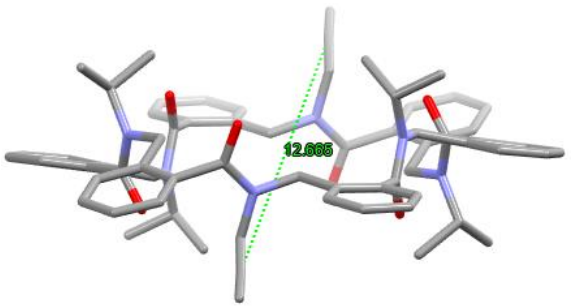

Figure 3. X-ray structure of cycloarylopeptoid **IIa**.

at the NMR precession rate. Regarding **IIa** (*ortho* series), the replacement of two isopropyl by the less bulky propargyl side-chains furnishes ^{1}H NMR spectra reflecting a conformational flexibility in acetone-d_6, acetonitrile-d_3, methanol-d_4 or dmso-d_6 but better resolved spectrum is observed in $CDCl_3$, suggesting the existence of conformational preferences. At low temperature (268 K), the number of AB systems from backbone methylene and the 8 signals corresponding to the methyl from isopropyl side chains suggest one non-symmetric preferred conformation (ESI). Therefore, we tackled a conformational analyse study using the NAMD program complemented with the field force cgenff36 for which dynamics were all conducted at 400K during 10 ns.[15] We took advantage of the X-ray structure as starting point and explored another similar structure in which the two propargyl groups are placed on the same face (Figure 4).

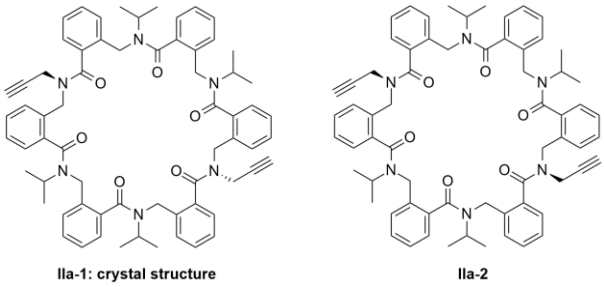

Figure 4. Representation of the two all-*trans* conformers studied.

Results show that the cyclic *ortho*-arylopeptoid core is rigid, keeping its all-*trans* amide arrangement all along the dynamics (ESI). For each of them, we have selected 2 or 3 possible structures which were minimized using Gaussian 16 at the density functional theory level and with 6-31g(d,p) basis set in methanol.[16] Overall, we found that the two conformers are positioned in a tiny energetic gap (Table 1). The energetic gap between the two conformers is very low which permit a full interconversion process between these species during the CuAAC reaction. Examination of the C2 alkyne/alkyne distance in **IIa-1** is relatively small, 10 Å, a value compatible with the inter azide distance in 1,4-bis(azidomethyl)benzene favouring the crown-like structure formation (Figure 5).

Table 1. Energetic placement of studied conformers of **IIa**.

Conformations	Relative free Gibbs energy (kCal/mol)
IIa-1	0.13
IIa-2	0

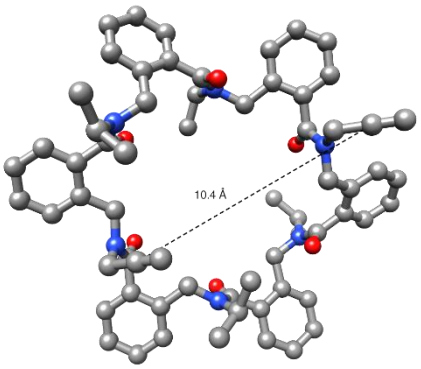

Figure 5: Gaussian optimized structure of *ortho*-arylopeptoid macrocycle **IIa-1**.

Regarding the *meta* series, the procedure highlights that the cyclic core is more flexible and in perpetual rearrangement without preferred conformations.

The CuAAC reaction between *ortho*-macrocycle **IIa** and 1,4-bis(azidomethyl)benzene was first catalysed with 100 mol% of $Cu(MeCN)_4,PF_6$ furnishing 20% isolated overall yield of **IVa** and **Va** (8:2 ratio; Figure 6) in agreement with literature concerning peptoid macrocycles.[ref-1] We observed a total disappearance of the starting material and formation of insoluble, white unidentifiable material that could result from polymerisation.[10] The same reaction was then catalysed using 10 mol-% of catalyst **III** at 0.5 mM in methanol for 2 days.‡ To our delight, the reaction went to completion and afforded the crown-like structure **IVa** as major compound (78% isolated yield) and only traces amount of tube-like structure **Va** (<3%) (Figure 6).‡‡ Impressively, the concentration could be increased from 5.10^{-4} M to 10^{-1} M keeping good yield (70%) and surprisingly without affecting the ratio between crown- and tube-like adducts. Gaussian optimisation reveals that the structure of **IVa**, presents an inter triazoles distance of 9.6 Å, close to the inter alkynes distance in the lower energetic conformer of **IIa**. It is noteworthy that the bridging does not lead to a deformation of the cyclic core. Moreover, gaussian optimization highlights the existence of a H-bonding between the triazole's hydrogen and the oxygen of an amide bond (2.2 Å), the second triazole staying a pure hydrophobic environment (Figure 7).

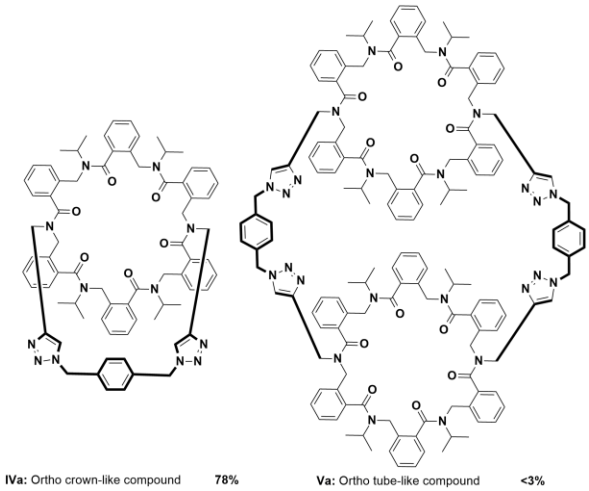

Figure 6. Bicyclic and tricyclic compounds obtained by CuAAC of *ortho*-macrocycle **IIa** with 1,4-bis(azidomethyl)benzene.

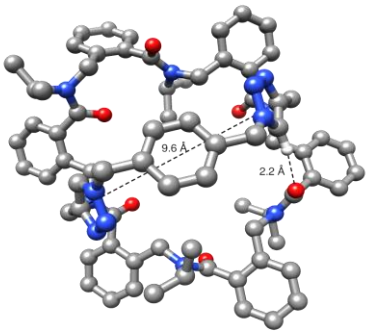

Figure 7. Gaussian optimized structure of bicycle **IVa** from the *ortho* series.

The CuAAC reaction proceeded differently using the cyclic *meta*-hexaarylopeptoid **IIb**. Using $Cu(MeCN)_4,PF_6$ catalyst (100 mol-% at 0.5 mM), although the starting material was totally consumed, the reaction afforded a mixture of bicyclic compound (**IVb**) and tricyclic compound (**Vb**) in a 3:7 ratio in 35% overall yield. Gratifying, the use of catalyst **III** (10 mol-% at 0.5 mM) increased the overall yield to 82%, albeit the ratio **IVb**/**Vb** is switched down to ≈ 1:1 based on isolated pure compounds (Figure 8). As for the *ortho* series, the proportion stayed constant when increasing the concentration to 10^{-1} M.

These new 1,2,3-triazole-containing structures might be of interest as confined receptors for anion recognition through C-H…anion bond interactions.[17] To further enhance the H-bond donor capability and potentially favour anion-π interaction, the triazoles could be converted into triazoliums.[18] Therefore, the synthetized triazoles were treated with excess of methyl iodide in MeCN at 70°C for 24h. For tube-like **Vb**, the expected compounds were detected by HPLC-HRMS but exhaustive decomposition occured during the methylation either using methyl iodide or methyl triflate at room temperature. Oppositely, the

crown-like structures **IVa,b** afforded stable triazolium-based **VIa** and **VIb** in quantitative yields (Figure 9).

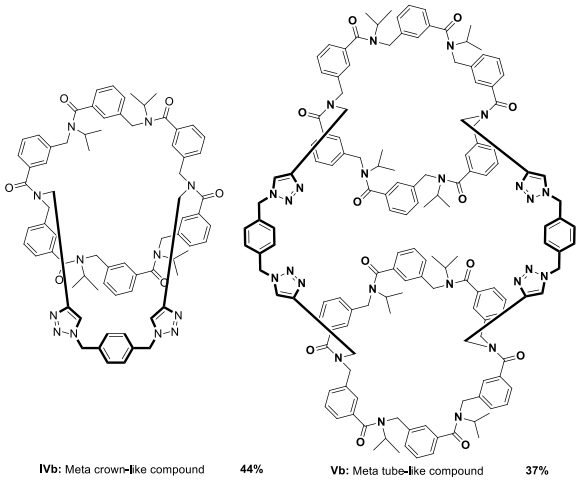

Figure 8. Bicyclic and tricyclic compounds obtained by CuAAC of *meta*-macrocycle **IIb** with 1,4-bis(azidomethyl)benzene.

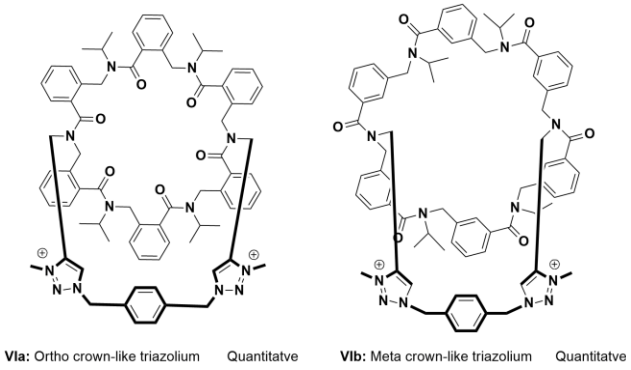

Figure 9: Triazolium-based bicyclic compounds in the *ortho*- and *meta*-series.

In conclusion, we reported an efficient access to crown-like structure in the arylopeptoid series. As hypothesized, the spatial preorganization of the cyclic core - responsible of the selectivity displayed by *ortho*-arylopeptoids - and proper choice of the NHC catalyst **III** that outperforms the classical $[Cu^{I}(MeCN)_4]^+$ are key factors that should be considered. Further application of this 3-dimensional constrained structure will be reported in due course.

Conflicts of interest

In accordance with our policy on Conflicts of interest please ensure that a conflicts of interest statement is included in your manuscript here. Please note that this statement is required for all submitted manuscripts. If no conflicts exist, please state that "There are no conflicts to declare".

Notes and references

‡ Protic solvents are preferred as proton source to free the triazole from the copper(I)-triazolyl. Indeed, blank experiments show that no reaction occurs in pure CH_2Cl_2 and $CHCl_3$ and in absence of catalyst III after one week.
‡‡ The proof of the total linkage cannot be obtained by HRMS as single and double CuAAC reactions afford compounds of identical mass. A proof is given by the lack of the strong azide band at 2100 cm^{-1} in infra-red spectra for compounds **IVa,b** and **Vb**.
‡‡‡ Due to the low solubility of **IIa** in methanol a CH_2Cl_2/MeOH mixture was used.

1 P. Ballester, M. Fujita and J. Rebek, *Chem. Soc. Rev.*, 2015, **44**, 392.
2 *M. Morgan Conn and J. Rebek, Chem. Rev.* 1997, **97**, 1647.
3 R. Chakrabarty, P. S. Mukherjee and P. J. Stang, *Chem. Rev.* 2011, **111**, 6810.
4 S.-L. Huang, G.-X. Jin, H.-K. Luo and T. S. A. Hor, *Chem. Asian J.* 2015, **10**, 24; G. Montà-González, F. Sancenón, R. Martínez-Máñez and V. Martí-Centelles, *Chem. Rev.* 2022, **122**, 13636.
5 Y. Jin, Q. Wang, P. Taynton and W. Zhang, *Acc. Chem. Res.* 2014 **47**, 1575.
6 W. Liu and J. Fraser Stoddart, *Chem*. 2021, **7**, 919.
7 T. Fiehn, R. Goddard, R. W. Seidel and S. Kubik, *Chem. Eur. J.* 2010, **16**, 7241; S. Kubik, *Acc. Chem. Res.* 2017, **50**, 2870.
8 A. Akhdar, A. Gautier, T. Hjelmgaard and S. Faure, *ChemPlusChem*, 2021, **86**, 298.
9 S. B. L. Vollrath, S. Bräse and K. Kirshenbaum, *Chem. Sci*., 2012, **3**, 2726.
10 C. N. Herlan, K. Sommer, P. Weis, M. Nieger and S. Bräse, *Molecules* 2021, **26**, 150.
11 D. J. Combs and R. S. Lokey, *Tetrahedron Lett.*, 2007, **48**, 2679; T. Hjelmgaard, S. Faure, D. Staerk, C. Taillefumier and J. Nielsen, *Eur.J. Org. Chem.*, 2011, 4121.
12 T. Hjelmgaard, O. Roy, L. Nauton, M. El-Ghozzi, D. Avignant, C. Didierjean, C. Taillefumier and S. Faure *Chem. Commun.* 2014, **50**, 3564. T. Hjelmgaard, L. Nauton, F. De Riccardis, L. Jouffret, and S. Faure *Org. Lett.*, 2018, **20**, 268. M. Hayakawa, A. Ohsawa, K. Takeda, R. Torii, Y. Kitamura, H. Katagiri and M. Ikeda, *Org. Biomol. Chem.*, 2018, **16**, 8505.
13 M.-L. Teyssot, A. Chevry, M. Traïkia, M. El-Ghozzi, D. Avignat and A. Gautier, *Chem-Eur. J.* 2009, **15**, 6322. M.-L. Teyssot, L. Nauton, J.-L. Canet, F. Cisnetti, A. Chevry and A. Gautier*, Eur. JOC.*, 2010, **18**, 3507. P. Bruyat, A. Gautier, L. Jean, and P-Y Renard, *J. Org. Chem*. 2018, 83, 21, 13515. d) A. Akhdar, S. Faure and A. Gautier, *Org. Biomol. Chem*., 2022,**20**, 2402.
14 T. Hjelmgaard, S. Faure, E. De Santis, D. Staerk, B. D. Alexander, A. A. Edwards, C. Taillefumier and J. Nielsen, *Tetrahedron*, 2012, **68**, 4444.
15 ref NAMD and field force cgenff36
16 ref Gaussian
17 R. Peng, Y. Xu and Q. Cao, *Chinese Chem. Lett.* 2018, **29**, 1465.
18 A. Kumar and P. S. Pandey, *Org. Lett.* 2008, **10**, 165; A. Caballero, F. Zapata, L. González, P. Molina, I. Alkorta and J. Elguero, *Chem. Commun.*, 2014, **50**, 4680.

V.C. Discussion.

V.C.1. Optimization of the CuAAC reaction.

The linear hexamer *meta*-arylopeptoids from 2-chlorotrityl resin is obtained with 93% yield (96% HPLC purity) using the classical submonomer method described before.[155] The cyclisation of hexamer *meta*-arylopeptoids provides the macrocycle in 81% yield and 95% purity using the procedure developed by our group with a slight modification (See ESI for details).[206]

We start to study the CuAAC reaction with benzyl azide. The macrocycle is dissolved in MeOH, in the presence of 2.2 equiv. of the azide and 20 mol% of the Cu-NHC catalyst. After stirring overnight at room temperature another 20 mol% of catalyst was added to ensure the complete conversion of the starting material. The CuAAC reaction in this case results in the formation of two compounds **V.1** and **V.2** in 70% yield and 70:30 proportion (Scheme V.5).

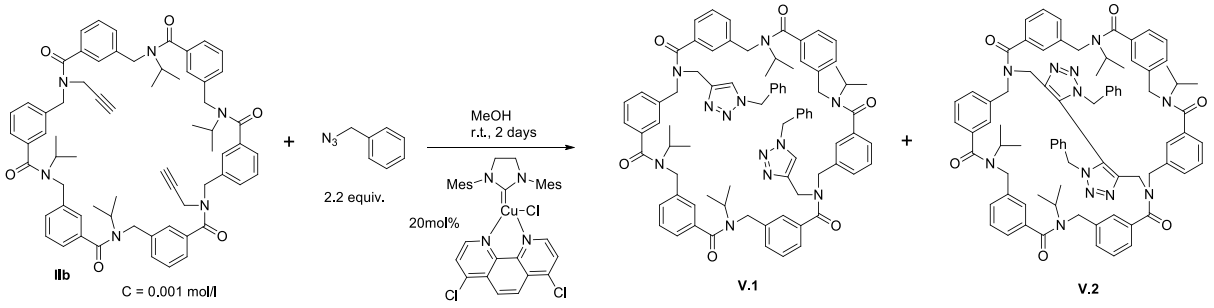

Scheme V.5. CuAAC reaction of the *meta*-macrocycle with benzyl azide.

Interestingly, the linked bis-triazole **V.2** was an unexpected product in this reaction. However, 5,5'-bistriazoles were already reported as byproducts of CuAAC reactions. [209] Bis-triazoles are most likely obtained through an oxidative coupling of the triazolide intermediates formed during the reaction. The synthesis of these linked bis-triazoles was studied as the main product of the CuAAC reaction by modifying the Cu^{I} source, ligand and base added. Several examples were reported for the synthesis of the bis-triazoles with a yield up to 95%.

An optimization of the reaction was studied in order to obtain the bis-triazole **V.2** as main product. We therefore variate the solvents, catalysts (Figure V.6) and catalyst amount (Table V.1). A total lake of reactivity was observed in CH_2Cl_2. The reaction shows full conversion with 10 mol% catalyst **A** in MeOH and EtOH, ratio **V.1**/**V.2**=7/3. Keeping MeOH as a solvent, the amount of **A** was increased to 50% which shows a small increase in **V.1** (80%). With 100 mol% and 200 mol% of **A**, ratio of compound **V.1** reach 92 and 98% respectively.

A more crowded and slower catalyst, **B**, was also used.[210] We selected this catalyst because we want to explore the effect of a slower reaction rate that could keep a carbon-copper bond for a longer time in the reaction sequence (unpublished result from the lab). With 10 mol% of **B** in methanol, 70 mol% conversion was observed with a **V.1** /**V.2** ratio 65:35. Full conversion with the same ratio was obtained with 40 mol% of catalyst **B**.

[209] (a) Angell, Y.; Burgess, K. *Angew. Chem. Int. Ed.* **2007**, *46*, 3649-3651. (b) Teyssot, M. L.; Nauton, L.; Canet, J. L.; Cisnetti, F.; Chevry, A.; Gautier, A. *Eur. J. Org. Chem.* **2010**, 3507-3515. (c) Brassard, C. J.; Zhang, X.; Brewer, C. R.; Liu, P.; Clark, R. J.; Zhu, L. *J. Org. Chem.* **2016**, *81*, 12091-12105.

[210] Ibrahim, H.; Guillot, R.; Cisnetti, F.; Gautier, A. *Chem. Commun.* **2014**, *50*, 7154-7156.

As previously observed with catalyst **A**, increasing the catalyst to 100 mol% led to an increase of the proportion of clicked compound **V.1** (95%) while decreasing the conversion to 55%. Finally, copper iodide was used as catalyst at 200 mol% with the addition of Hünig base (DIPEA) according to literature conditions.[211] These conditions lead selectively to the clicked compound **V.1** with full conversion and only traces amount of the linked compound **V.2.** The mechanism responsible for the formation of compound **V.2** stay unexplained at the moment and more experiments should be undertaken to optimize the formation of this compound.

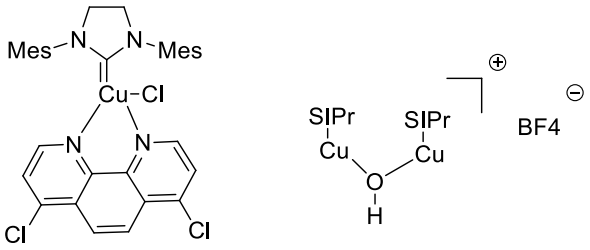

Figure V.6. Catalysts **A** and **B** used for the optimization study.

Catalyst	**Solvent**	**% Catalyst /compound**	**% Conversion**	**% Bistriazole V.1**	**% Linked bistriazole V.2**
A	EtOH	10	99%[a]	70	30
A	MeOH	10	99%[a] [b]	70	30
A	CH_2Cl_2	10	0[a]	0	0
A	CH_3CN	200	50%[a]	90	10
A	MeOH	50	99%[a]	80	20
A	MeOH	100	90[a] [b]	92	8
A	MeOH	200	80[a]	98	2
B	MeOH	10	70[a]	65	35
B	MeOH	40	99[b]	65	35
B	MeOH	100	55[b]	95	5
B	MeOH	200	80[b]	97	3
CuI, DIPEA	CH_3CN	200	100[b]	99	1

Table V.1. The reaction time was 48 hr at room temp and 2,2 equiv. of phenyl azide, the crude product yield was analyzed by LCMS [a] or HPLC [b], [**IIb**] = 1 mM except for CuI :10 mM

Unfortunately, we were not able to form selectively the bis-triazoles linked compound **V.2**. It was thus decided to focus on normal clicked product in the *meta* and *ortho* series.

From the previous study, methanol was selected as a solvent with 10 mol% catalyst **A**. In order to extend the study, we synthesized the hexamer *ortho* macrocycle. We know from previous work that *ortho*-cyclohexamer carrying isopropyl side chains adopts a shape persistent structure in solution with an all *trans* conformation of the backbone amides. We found the same arrangement for **IIa** in solid state (see publication in section V.B). This macrocycle was synthesized in the same way used for the synthesis of *meta*-macrocycle (See ESI for details).

[211] Oladeinde, O. A.; Hong, S. Y.; Holland, R. J.; Maciag, A. E.; Keefer, L. K.; Saavedra, J. E.; Nandurdikar, R. S. *Org. Lett.* **2010**, *12*, 4256-4259.

The linear *ortho*-arylopeptoids was obtained in 90% yield (96% HPLC purity) on Rink Acid resin, and the corresponding macrocycle was obtained in 70% yield (95% HPLC purity). The optimized conditions were used on the *ortho*-macrocycle to provide selectively compound **V.3** in 90% yield and 93% purity, without the presence of the bicyclic product (Scheme V.6).

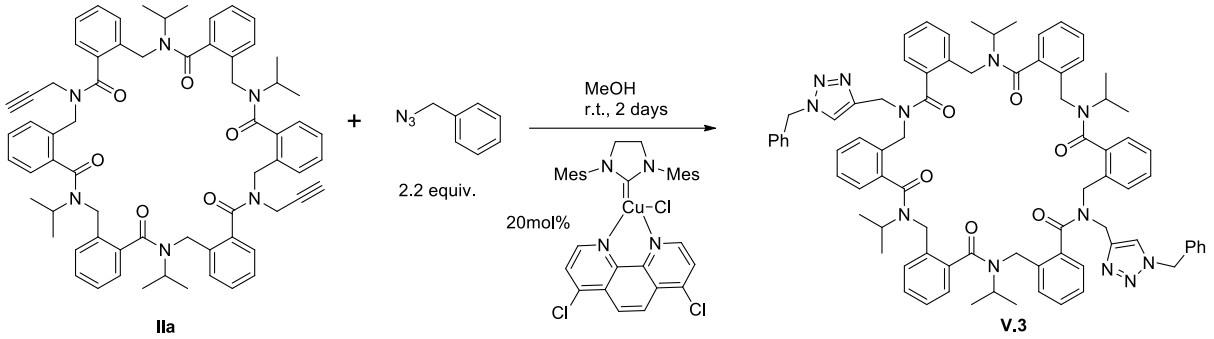

Scheme V.6. CuAAC reaction of the *ortho*-macrocycle with benzyl azide.

V.C.2. Optimization of the CuAAC reaction with bis-azide.

The work reported with 1,4-bis(azidomethyl)benzene in the publication was also extended to 9,10-bis(azidomethyl)anthracene. Indeed, we observed that this compound presents interesting fluorescence properties: this bis-azide is non-fluorescent while a strong fluorescence appears (λ_{ex} = 315 nm) after click reaction. This facilitates the purification of the compounds which are difficult to detect on TLC. It also presents the same or very close chromatographic behavior than the compounds synthetized with 1,4-bis(azidomethyl)benzene. Finally, 9,10-bis(azidomethyl)anthracene was selected in the hope of getting X-ray suitable crystals.

The *meta*-macrocycle **IIb** was reacted with 2.2 equivalents of 9,10-bis(azidomethyl)anthracene in presence of 10 mol% catalyst per alkyne group at room temperature in methanol for 48h. The reaction provides two main products, the crown-like **V.4** or the tube-like **V.5** that are isolated in approximately equal proportions (Scheme V.7).

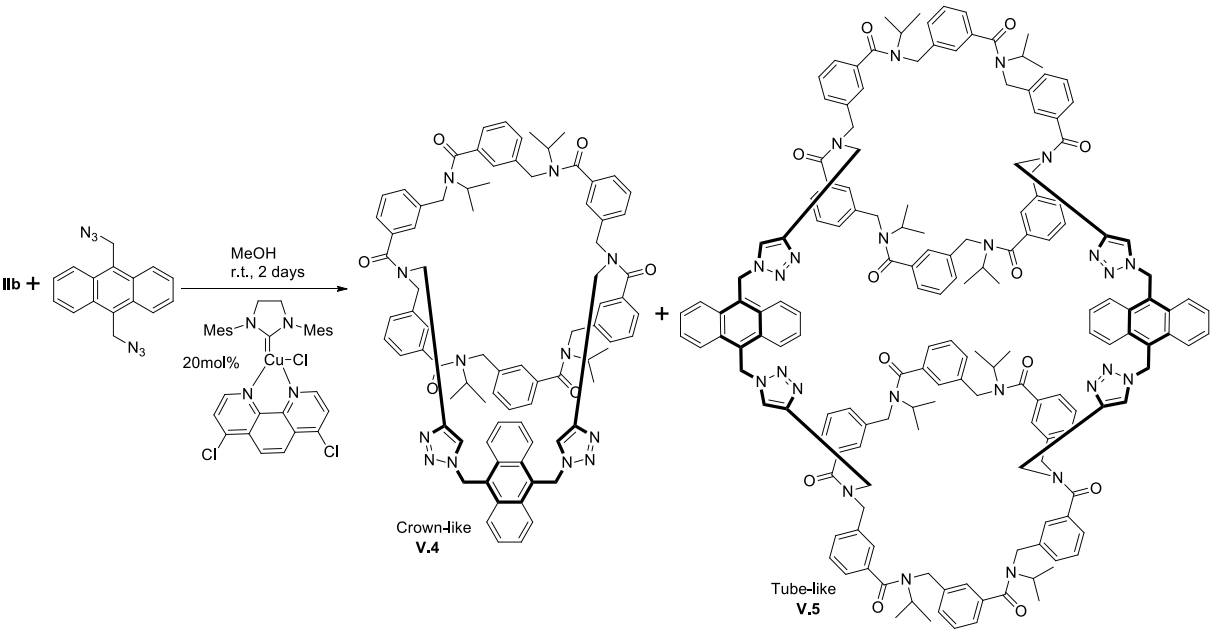

Scheme V.7. CuAAC reaction of the *meta*-macrocycle with bis(azidomethyl)anthracene.

Entry 1 (Table V.2) shows the full conversion of **IIb** in 48 h in the presence of 10 mol% catalyst per alkyne group at 1 mM concentration, and 1.2 equivalents of 9,10-bis(azidomethyl)anthracene at room temperature, resulting in 55% of **V.4** and 45% of **V.5**. The decrease of concentration to 0.5 mM with the same conditions provides a slight increase in the proportion of **V.4** to reach 60% (Table V.2, Entry 2). Then, the concentration was decreased to 0.25 mM, which results in decrease of conversion to 50% after 48h, with more increase in the amount of crown-like **V.4** to become 75%, with 25% of **V.5**. Addition of another portion of the catalyst (10 mol%) after 48h, results in the increase of the conversion to 80%, with the same proportions. After 72h, a 3rd addition of the catalyst results in 95% conversion with 70% of **V.4** (Table V.2, entry 5). The conditions of Entry 2 were selected to continue this study and perform the work using 1,4-bis(azidomethyl)benzene **C** described in the above publication

Entry	[**IIb**] (mM)	Bis-azide (equiv.)	Catalyst loading / triple bond (mol%)	time (h)	Conversion of **IIb** (%)	% **V.4**	% **V.5**
1	1	1.2	10	48	100	55	45
2	0.5	1.2	10	48	100	60	40
3	0.25	1.2	10	48	50	75	25
4	0.25	1.2	20	72	80	75	25
5	0.25	1.2	30	96	95	70	30

Table V.2. Optimization of the CuAAC reaction in solution at room temperature.

The reaction of *meta*-macrocycle **IIb** with 9,10-bis(azidomethyl)anthracene under the optimized conditions yields 74% of a crown-like and tube-like products. Crown-like **V.4** was obtained with 38% yield and 96% HPLC purity and tube-like **V.5** with 36% yield. Also, the same conditions were applied using the *ortho*-macrocycle **IIa**, which yields 57% of the crown-like **V.6** and traces of tube-like **V.7** (less than 3% that were not able to be isolated) (Scheme V.8).

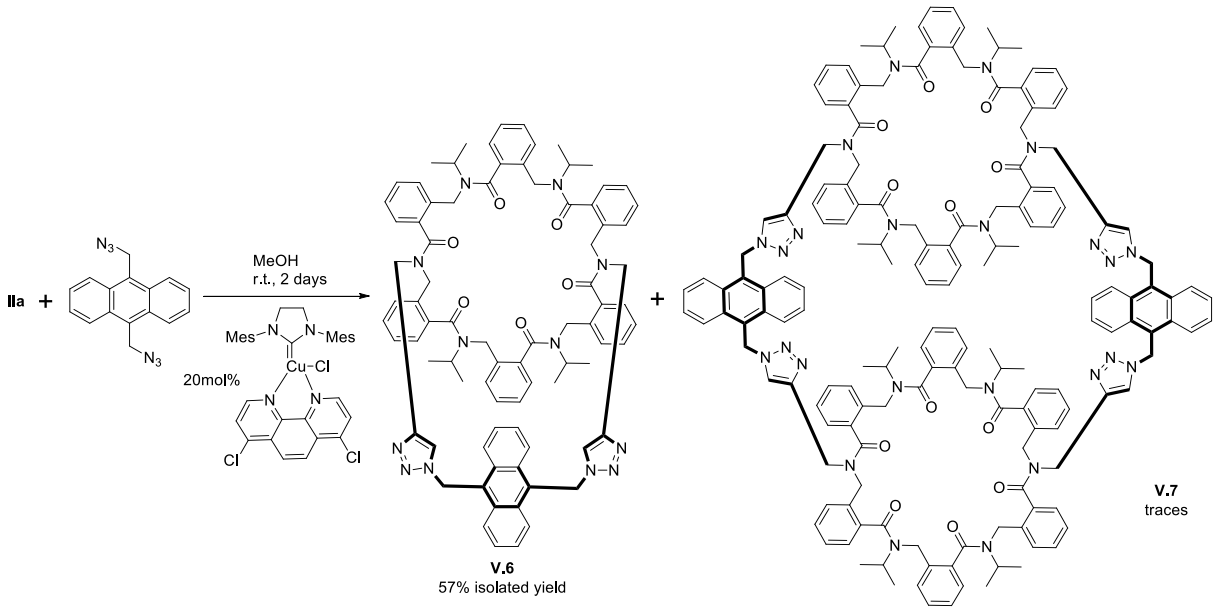

Scheme V.8. CuAAC reaction of the *ortho*-macrocycle with bis(azidomethyl)anthracene.

Unfortunately, all attempts to crystallize the compounds containing the anthracene moiety were unsuccessful.

V.C.3. Methylation

The post-modification of triazoles into triazoliums was studied with the clicked cycloarylopeptoids from *meta* and *ortho* series using methyl iodide in the same conditions that we described in the publication.

The methylation of clicked cycloarylopeptoids **V.1** and **V.3** was performed in ace pressure tube in pure MeI at 70°C (Scheme V.9) and produces the double methylated products **V.8** and **V.9**, respectively, in quantitative yields.

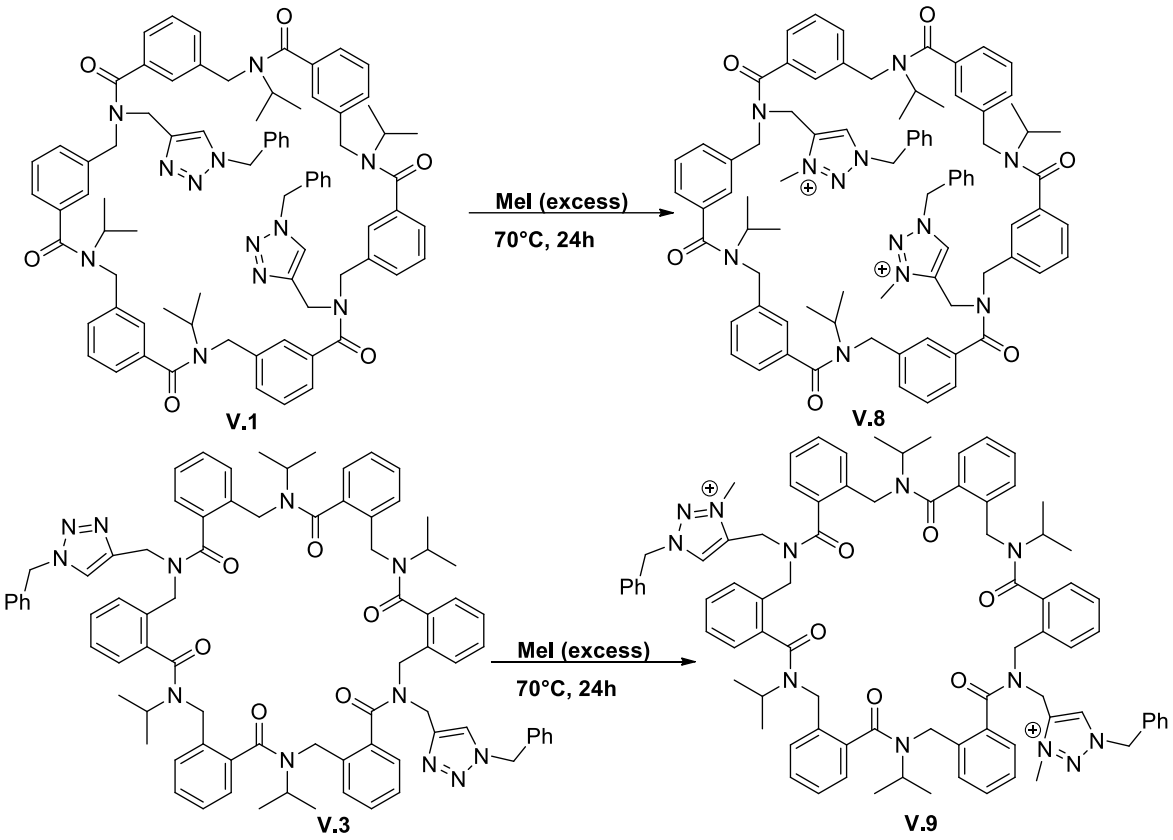

Scheme V.9. Methylation of **V.1** and **V.3**.

However, regarding the linked compound **V.2** and the crown-like and tube-like compounds containing anthracene **V.4, V.5** and **V.6**, decomposition occurs during the reaction as detected by LCMS. Concomitant with the formation of the expected compounds, an exhaustive decomposition occurs during the course of the methylation. We tried to overcome this degradation by using methyltriflate at room temperature, but the degradation still occurs.

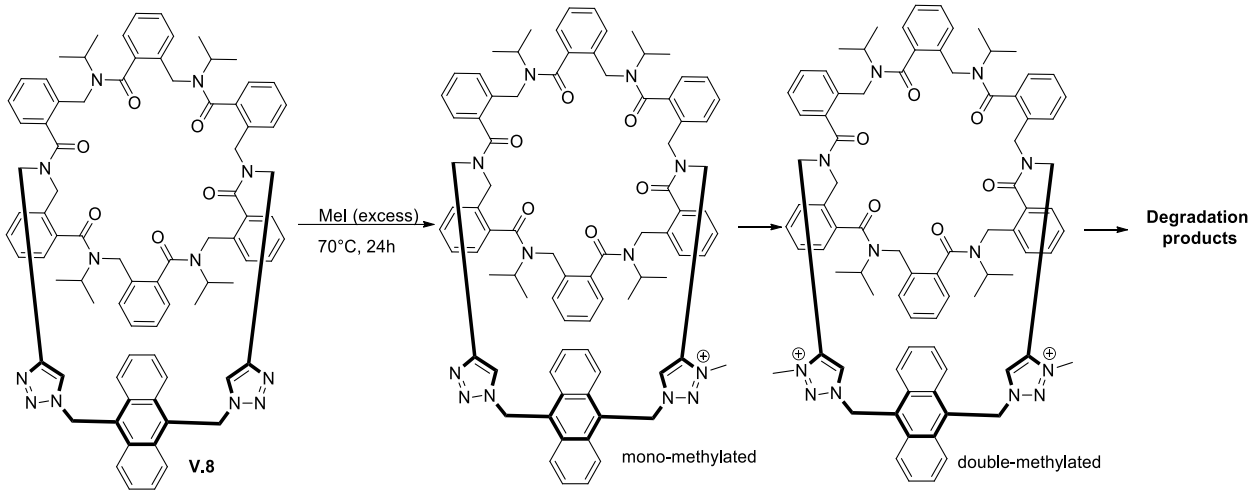

Scheme V.10. Triazoliums formation of the crown-like anthracene derivative.

V.C.4. Limitation of the catalyst for poly-functionalization.

We found some limitations of our catalyst when we applied it to hexameric macrocycles containing 4 and 6 propargyl side chains. We start with the synthesis of three new macrocycles according the same procedure used above. The *meta*-macrocycle with four propargyl side chains **V.13** was obtained with 68% yield and 96% HPLC purity, the *meta*-macrocycle **V.14** (six propargyl) was obtained with 74% yield and 96% HPLC purity and the *ortho*-macrocycle **V.15** (four propargyl) was obtained with 70% yield and 99% HPLC purity.

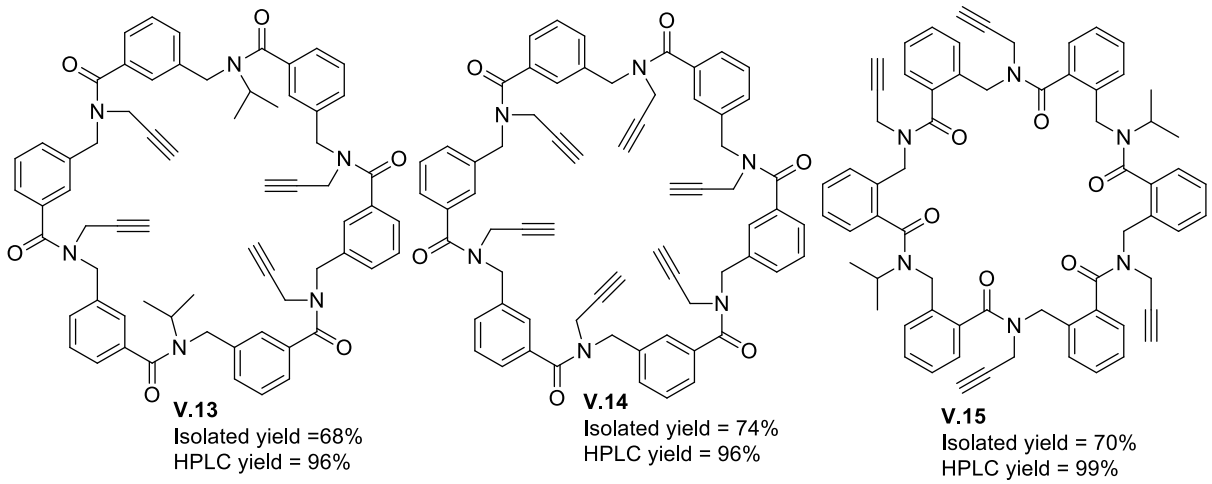

Figure V.7. The new cycloarylopeptoids synthesized.

CuAAc reaction was performed on these three new macrocycles cyclohexylmethyl azide (Scheme V.11). In all cases, a total consumption of the starting materials was observed, but the reaction didn't reach completion. For example, for the product of **V.13**, CuAAC reaction furnish a mixture of compounds containing 3 and 4 triazoles. Addition of catalyst or more amount of azide in order to 'push' the reaction did not give any improvement. The incompletion of the last click (formation of the 4th triazole in **V.13** and **V.15**, and 6th triazole in **V.14**) was attributed to the steric hindrance obtained, which was supposed as a limitation of our catalyst. The same problem was faced in the CuAAC reaction of **V.14** and **V.15**.

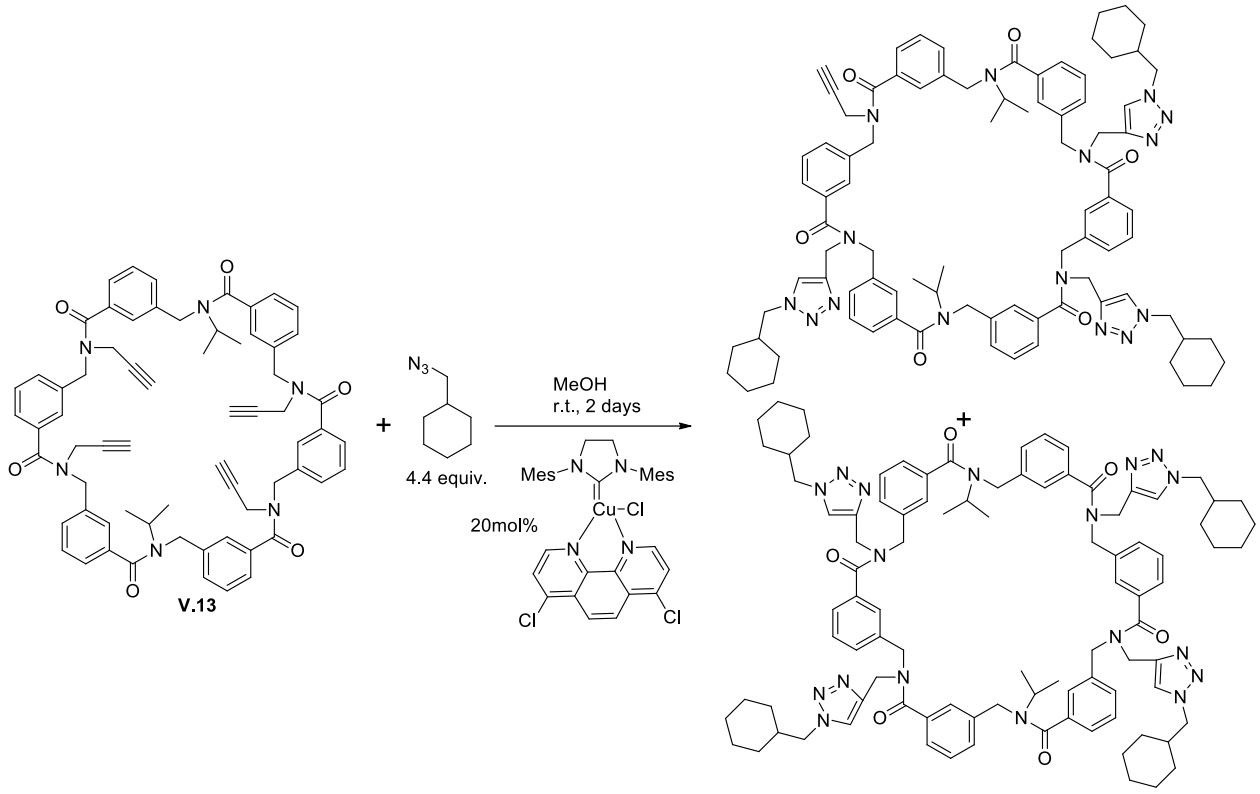

Scheme V.11. CuAAC reaction of *meta*-cycloarylopeptoid hexamer **V.13**.

We also tried using the less sterically hindered Boc-protected aminopropyl azide, but the problem was not solved and a mixture of products was obtained.

V.C.5. Conclusion

The catalyst proved its efficiency to perform CuAAC reactions on macrocyclic arylopeptoids in solution. The *ortho*-arylopeptoid cyclohexamer affords exclusively crown-like structures, a feature unreported in the literature. By contrast, the *meta*-cyclohexamer leads to crown-like and tube-like structures in proportion on average 1:1. Importantly, the yield and selectivity of the reaction is not affected by the increase of the concentration (up to 0.1M), providing the same products with both anthracene and benzyl bis(azide). This suggests the selectivity is due to the shape of the starting macrocycle. This study opens the way to easier synthesis at larger scale for crown-like compounds. Despite the limitation, probably caused by the steric hindrance, it is possible to efficiently produce poly-triazoles using as low as 10 mol% per alkyne group without the use of additives. More studies should be conducted in order to achieve fully-clicked compounds of **V.13**, **V.14** and **V.15**. The triazoliums could also be synthesized from these molecules in order to test their biological activity.

Chapter VI: H-shaped bis-triazoles

I would like to acknowledge my colleague Zein Chamas, UCA, for the help during the synthesis of many of the compounds described below.

VI.A.1. Linking two arylopeptoids on support

As chapter III was devoted to multiple click on solid support, it seems logical to explore the possibility to realize an intramolecular linkage by on-resin CuAAC reaction using bis-azides. This would afford an alternative synthetic path to cyclic structures. Indeed, this closure methodology have been reported by Kirshenbaum in the case of oligomers containing azide and alkyne in a peptoid carrying chiral α-methyl benzyl side chains.[212] In this case, a mixture of two cyclic structures from intramolecular and intermolecular processes (corresponding to cyclodimérisation) were obtained in averaged yields using copper iodide, DIPEA and ascorbic acid) (Scheme VI.1). Interestingly, the ratio cyclodimer/cyclic compound is dependant of the distance (position) between the reactive functions. A preorganization of the peptoid in PPI-type helix allows to obtain the best ratio in favour of the cyclic compound at i and i+3 positions because of proximal effect of azide and alkyne on the same face of the helix.

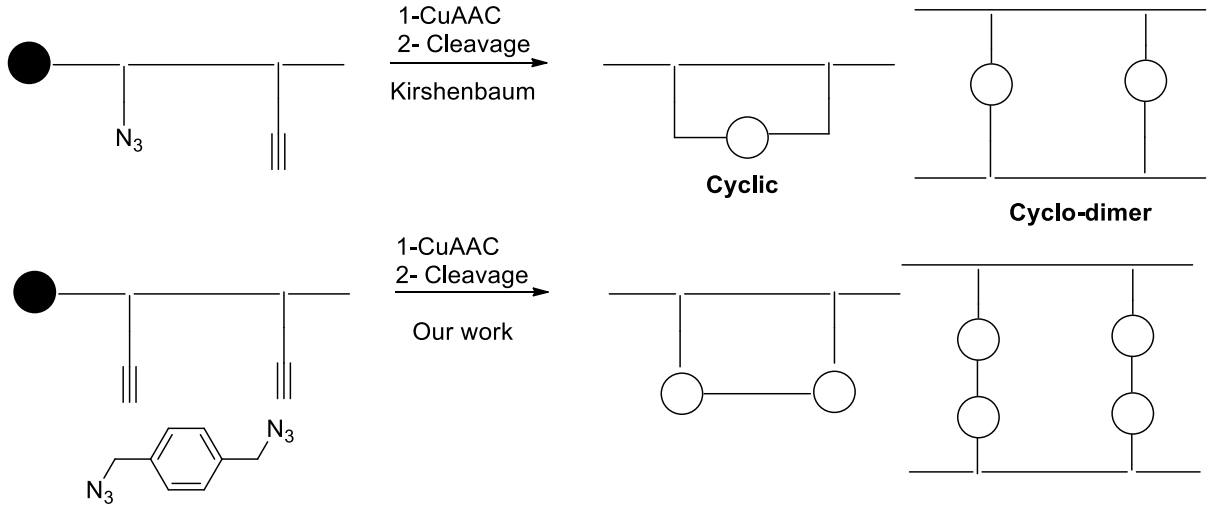

Scheme VI.1. Model synthesis of cyclic and cyclo-dimeric compounds: Kirshenbaum work on peptoids (top) and this work on arylopeptoids (bottom).

Based on this precedent and on our results from chapter V (crown-like and tube-like structures), it was encouraging to test our bis(azides) on supported linear arylopepoid containing two alkynes to provide cyclic compounds. We therefore used the 1,4-dimethylazide benzene already described in chapter V for the tube- and crown-like structures and our starting material was the supported *meta*-tetramer **II-4-(Alk2,4)** containing two propargyl side chains (Scheme VI.2, see publication in chapter III). We added 1.1 equivalent of diazide and catalysed with 10 mol-% of [(SIMesCu)(Cl_2-Phen)Cl] **A** in 2/8 methanol-dichloromethane mixture at 50°C (4 hours). We obtain the cycloarylopeptoid **VI.1** as minor component and one arising from a double linkage **VI.2** of two oligomers as major compound (detected by HRMS and HPLC). Other polymeric

[212] Holub, J. M.; Jang, H.; Kirshenbaum, K. Org. Lett **2007**, *9*, 3275-3278.

compounds were also detected. Besides, two regioisomers could be formed by the double intermolecular linkage as shown in Scheme VI.2.

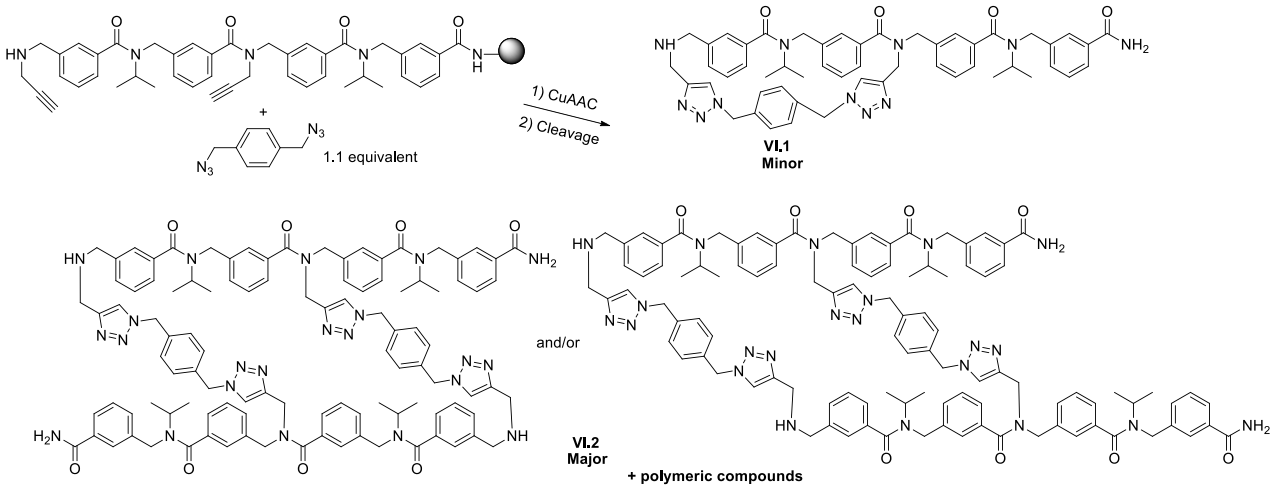

Scheme VI.2. Cyclic products obtained from on-resin CuAAC using bis-azide

This results shows that new cyclic structures could be easily obtained on solid support in a manner similar to Kirshenbaum's. Unfortunately, the major compound was difficult to purify as it appears within the polymeric compounds. Therefore, based on our observation, we start to explore the possibility of making a single linkage between two backbones. Indeed, this would afford new type of structures and shortcuts the time needed for synthesis as compounds could be obtained by dimerization. Besides, if elongation could be performed after the first link, a second link might be performed regioselectivity. This pathway would avoid the problem of regioselectivity encountered in the above strategy.

VI.A.2. H-shaped arylopeptoids

At first, the simplest starting material containing only one alkyne on a trimer (synthesized in the publication of chapter III) was engaged in the reaction with 0.55 equivalent of 1,4-dimethylazide benzene to furnish expected H-shaped **VI.3** in 84 % and 90% HPLC purity (Scheme VI.3).

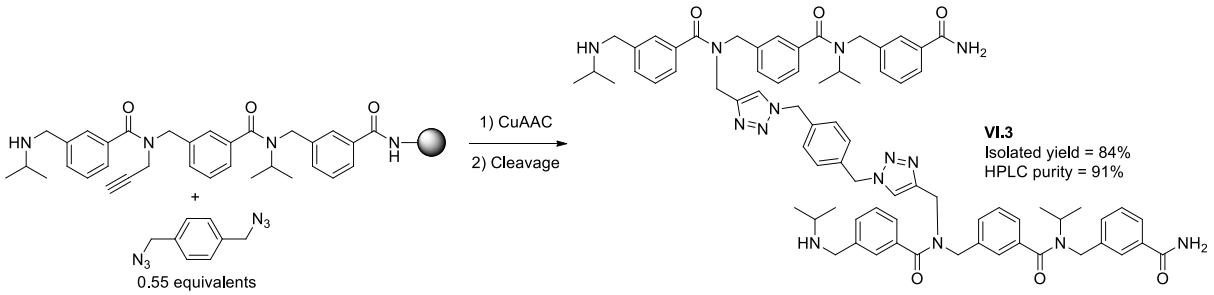

Scheme VI.3. H-shape arylopeptoids by on resin CuAAC.

This first experiment shows that dimerization occurs as expected giving a H-shape type structure, but here, as no polymerization occurs, the compound is purified easily.

In order to study the selectivity of the reaction, excess of 1,4-dimethylazide benzene (8 equivalents) were added. This reaction produces a mixture of the mono-clicked linear

arylopeptoid **VI.4** and the dimeric compound **VI.3** in 8:1 proportion (Scheme VI.4). **VI.4** was isolated with 78% yield and 98% HPLC purity.

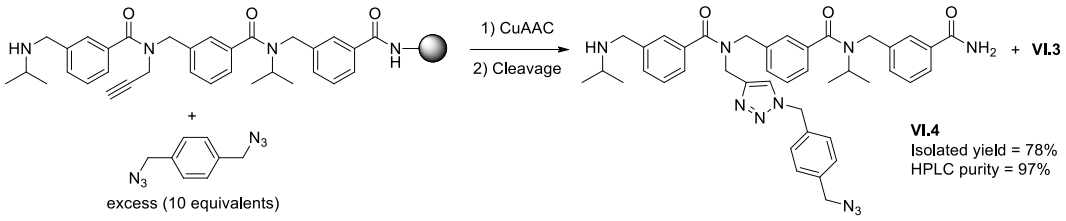

Scheme VI.4. Synthesis of mono-clicked arylopeptoid.

This observation, although it was not explored further, pave the way for the introduction of new functionalities, such as linkage between *meta*- and *ortho*- or *para*-arylopeptoids.

Elongation of the on-support linked hexamer is possible but using harder conditions. Large excess of 3-chloromethyl benzoyl chloride (6 equivalents) should be used and an extended time (1h) to introduce the chlorine intermediate **VI.5** whereas only 10 min were required for the non-linked compound (chapter III). Moreover, this step should be repeated two times to reach completion. After this first step, usual conditions could be used to continue the elongation of the backbone.

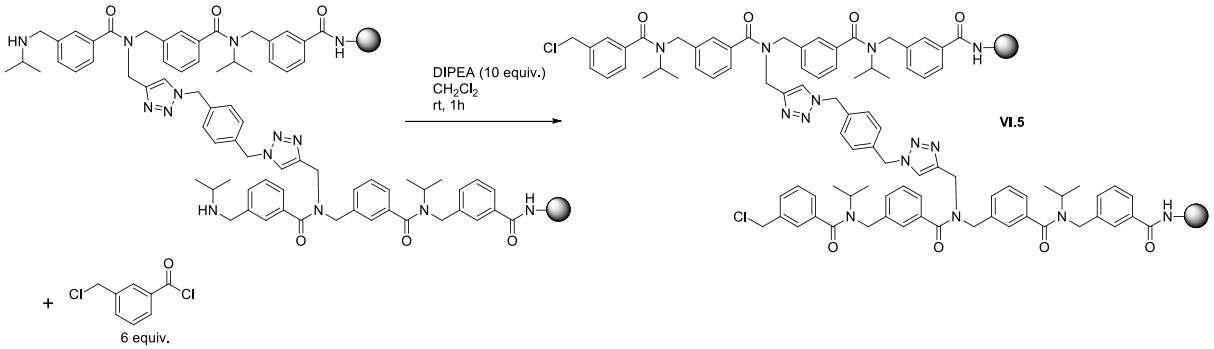

Scheme VI.5. Elongation of the backbone after linkage of the arylopeptoids.

We hypothesized that the problematic acylation post-linkage is due to a congestion in/on the support after linkage and thus steric hindrance around reactive positions. To circumvolve this matter, we examined the possibility of performing the CuAAC reaction on the benzyl chloride intermediate **VI.5**. Gratifyingly, we found out that the click reaction occurs smoothly without producing side products. Therefore, the synthesis could be continued more easily using our standard protocol as depicted in the following scheme:

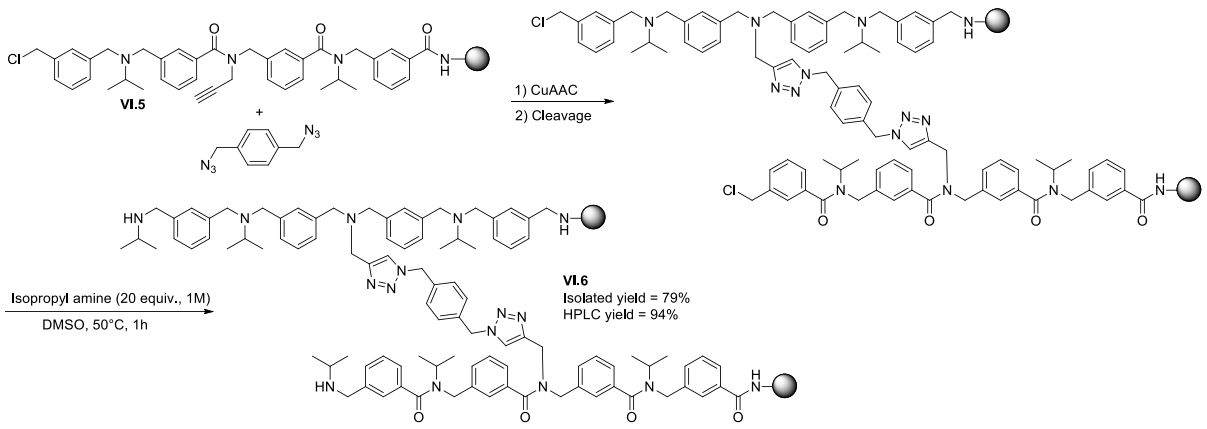

Scheme VI.6. On-resin CuAAC reaction on the chloride intermediate

To our delight, the elongation with isopropyl amine side chains was repeated sequentially up to four times giving structures as long as a 14-mers (Figure VI.1).

Figure VI.1. The series of linked arylopeptoids obtained.

We found out that the elongation is not limited to isopropyl amine side chains but propargyl amine could be also introduced. This open the possibility of adding a terminal closure, as depicted in scheme VI.7.

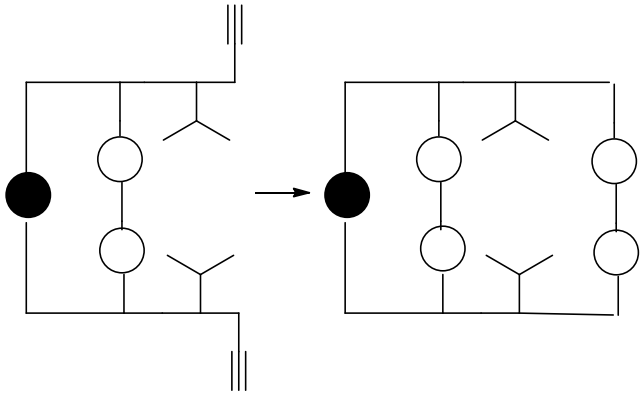

Scheme VI.7. Terminal closure of H-shaped products.

Unfortunately, experiments showed that exhaustive formation of polymeric compounds occured.

However, our strategy could still be applied to oligomer containing multiple alkynes with a mono-functional azide. Thus, performing these CuAAC reactions on the solid support will afford the possibility of introducing more diversity. The following scheme depicts this strategy:

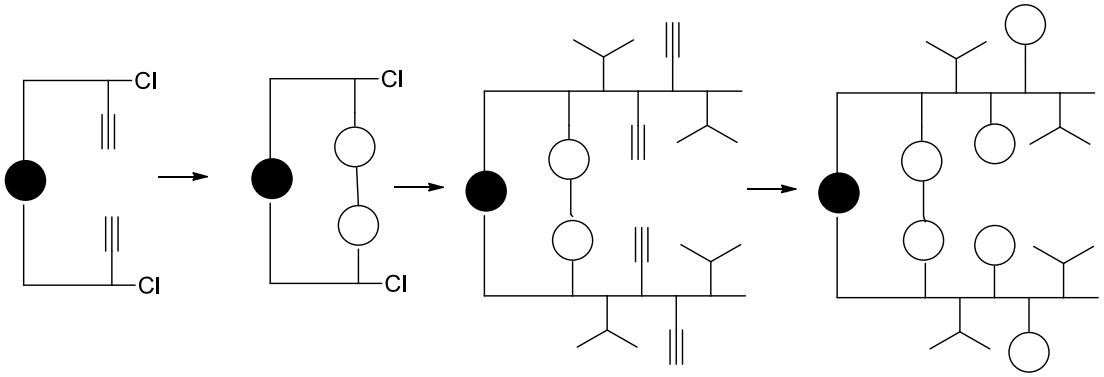

Scheme VI.8. Linkage of arylopeptoids followed by elongation and post-functionalisation by click.

The trimer was synthetized, then clicked and two elongation rounds allowed to obtain the supported oligomer containing four alkynes.

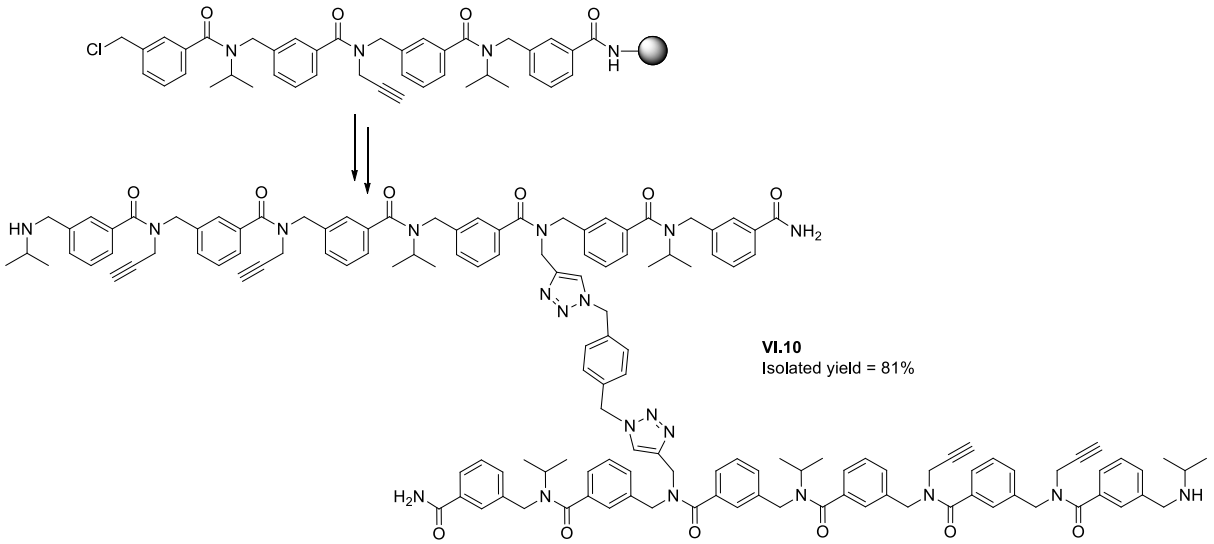

Scheme VI.9. Linked arylopeptoids with 4 alkyne groups.

A second CuACC reaction was engaged with benzyl azide and cyclohexyl methyl azide. The expected compounds were obtained in good yields around 70%, after Buchi LC purification (Figure VI.2). However, the HPLC analysis of the compounds revealed not possible using classical methods, probably due to the hydrophobicity and big size of these arylopeptoids preventing its passage in the C18 column.

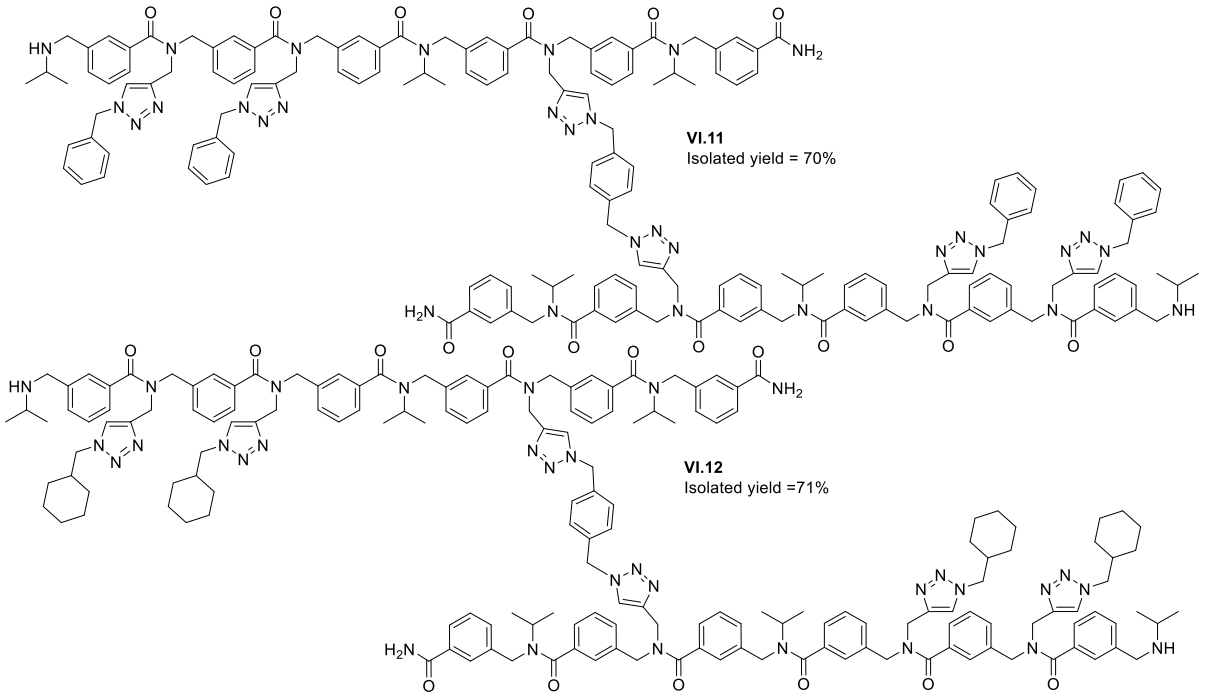

Figure VI.2. Linked arylopeptoids through bis-triazole linker

It is important to note that this shortcut allows to obtain a 12-mers and 14 steps.

VI.A.3. Conclusion.

In conclusion, we reported here, that the catalyst [(SIMes)Cu(Cl_2-Phen)]Cl, allows the dimerization of arylopeptoids on the solid support to form H-shaped compounds. All yields and purity are good to excellent compared to literature. The better reactivity seems here also be due

to the resistance of our catalyst to oxidation. We thus obtained structures up to 14-mers using a short time synthesis. Also, hetero H-shaped oligomers linked between *meta*- and *ortho/para* arylopeptoids might be constructed starting from the compound **VI.4**. This preliminary work paves the way to the extension and exploration of a combinatorial library of H-shaped compounds. Further work is necessary to circumvent the problem of regioselectivity and polymerisation encountered when performing intermolecular click at two positions simultaneously. In a perspective of application, the formation of triazolium-based oligomers as potential antibacterials should be considered.

Perspectives.

The objective of my thesis work was the synthesis of arylopeptoids and their modification through CuAAC reactions using Cu-carbene based catalysts in order to form triazoles structures.

To start with, we synthesized the Cu^{I}-NHC catalyst using the published procedures by our group. The purity of the catalyst synthesized was 96%, as calculated using the qNMR we developed.

Then, we introduced an efficient method to synthesize triazoles-based arylopeptoids using as less as 1 mol% of [SIMesCu(4,7-Cl_2-Phen)]Cl as a catalyst, on solid phase. Gratifyingly, the CuAAC reactions was efficient without the need of additives such as reducing agents. Using this catalyst, we build up combinatorial libraries containing up to 27 compounds in quasi equal amounts. We succeeded to convert the triazoles_ into triazoliums on support. Conformational studies based on NMR and quantum optimizations revealed the backbone amides carrying triazolium in arylopeptoids have a locked *cis* conformation. Moreover, potent antibacterial activity was observed for several triazolium-based oligomers.

We offered a route for the synthesis of crown- and tube-like macrocycles. The use of our carbene based catalyst afforded the desired products without any effect of concentration. These 3 dimentional structures were produced with good yield and purities after in solution click reaction using bis(azide).

We also synthesized the interesting H-shaped compounds, in which we succeeded to link the arylopeptoids on-resin. These branched oligomers were produced with excellent yields compared to literature.

In conclusion, my thesis project affords a new strategy to apply CuAAC reactions in solution and on solid support, to produce triazole-based arylopeptoids. Although some limitations of the catalyst were faced, especially for the poly-functionalization of **V.13**, **V.14**, and **V.15** macrocycles. To access this type of poly-triazolyl macrocycles, we will study a new catalyst for the CuAAC reaction or introduce another route of synthesis.

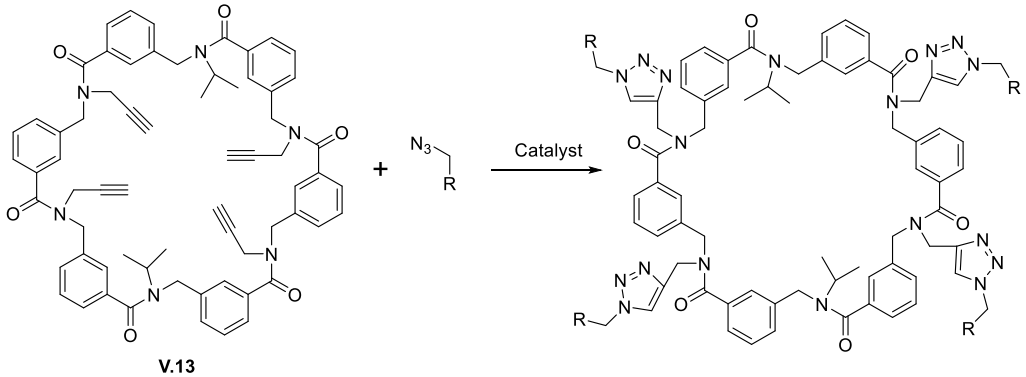

Scheme 1. CuAAC in solution using other catalyst.

Another route for example could be the application of click chemistry on solid support (2-chlorotrityl resin). Then after cleavage, the macrocyclization using the procedure applied in chapter V to obtain the poly-triazolyl macrocycles (Scheme 2). The synthesis of the triazolium

based macrocycles would be expected after the treatment with methyl iodide. This could introduce more diversity and achieve higher yields of the desired products.

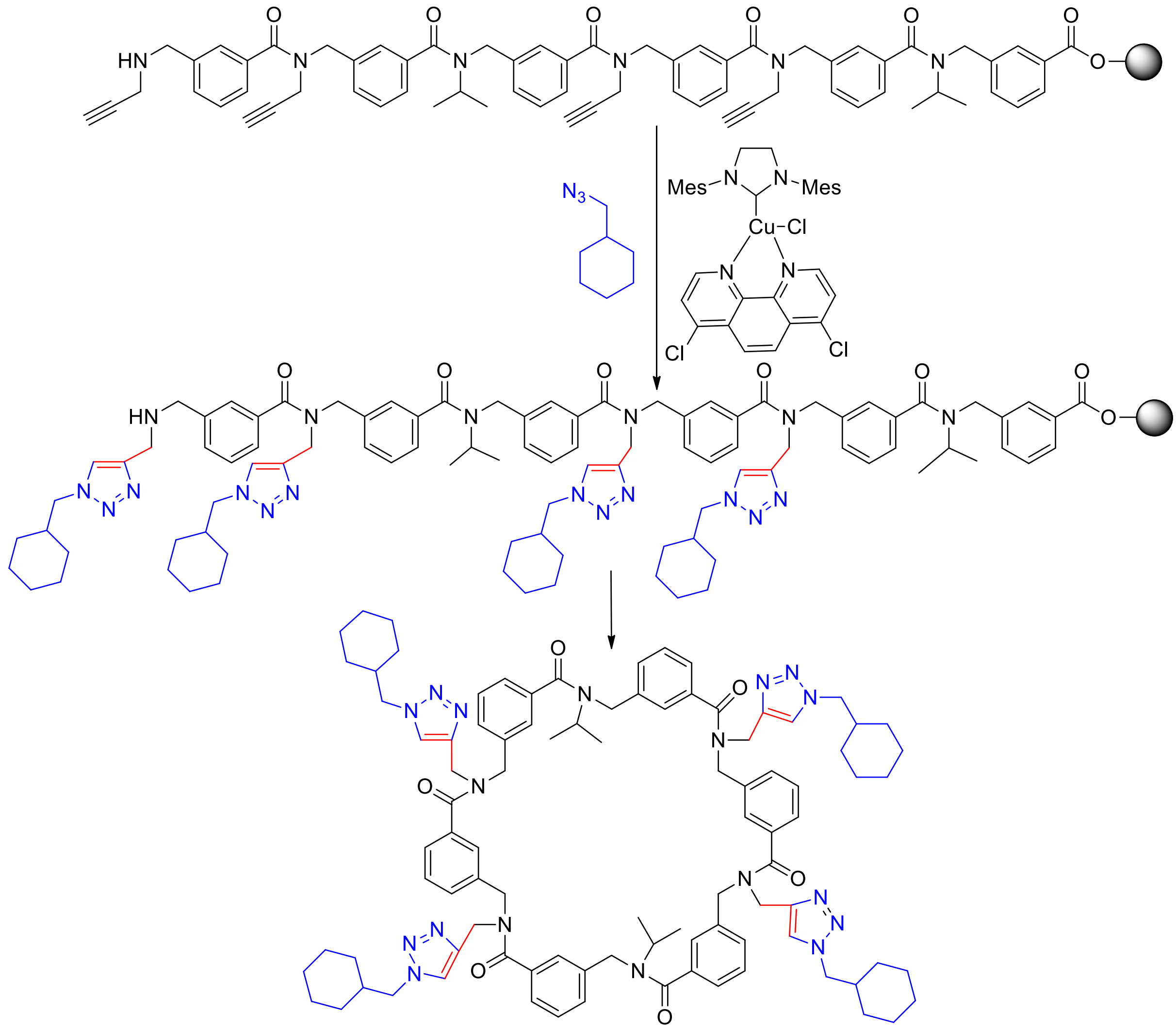

Scheme 2. Synthesis of cyclic triazole arylopeptoids.

Moreover, the synthesis of triazolium-based macrocycles with various combinations (*ortho*, *meta* and *para*) would be interesting to study. These various combinations could be tested for their antibacterial activity and as guest-host molecules.

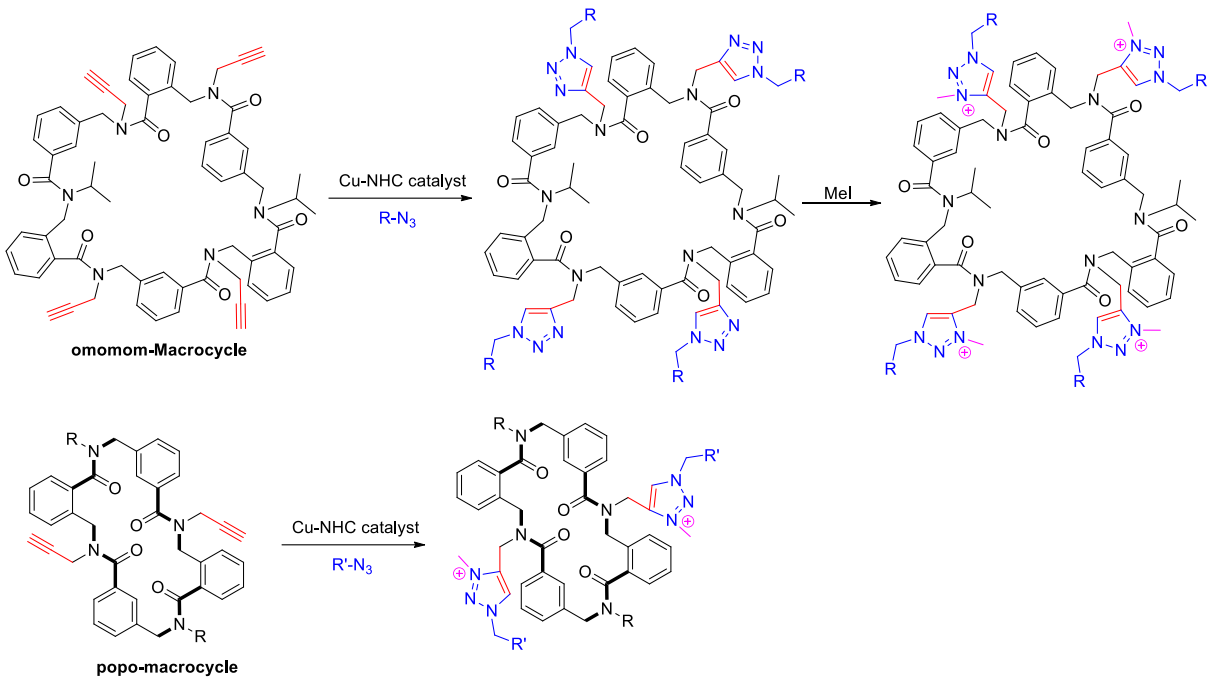

Scheme 3. Cyclic triazoles of various aromatic combinations.

Finally, the exploration of H-shaped compounds will be continued by the team and their triazoliums will be synthesized and tested for their antibacterial activities.

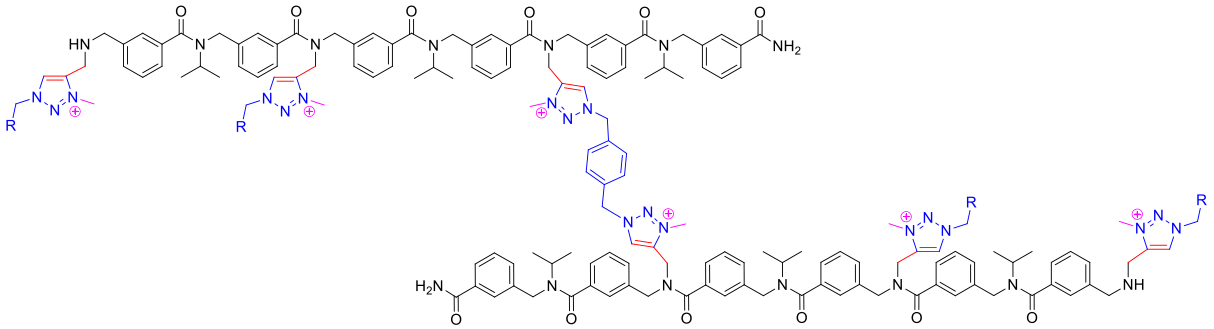

Scheme 4. H-shaped triazoliums

Experimental Section

Chapter II

S1. Generals.

All ligands and complexes were analyzed by ^{1}H and $\{1H\}^{19}F$ NMR spectroscopy on a Bruker advance 400 spectrometer. $CDCl_3$ was neutralized over anhydrous K_2CO_3 prior to use. The water content was measured using a coulometric Karl Fischer titrator (MettlerToledo, DL32).

Sample Preparation: The sample and the standard are weighed using a Mettler Toledo balance (0.01 mg accuracy) into a single Eppendorf, then solvent was added and the recipient was gently shaken to ensure a total dissolution. The solution was transferred into a 3 mm standard NMR tube for analysis.

Pulse Program: Sample Temperature: 19 °C (regulated ± 0.1 K), single pulse, without carbon decoupling ('zg' with 90° pulse). Data Points (acquired): 64 K. NS=64. Relaxation delay: D1=60s. Acquisition Time: 4s. Spectral window for proton: SW=30 ppm and O1: 7.5 ppm; for fluorine, PF_6: SW=120 ppm and O_1=90 ppm, BF_4: SW=-130 ppm and O1=100 ppm.

Post-Acquisition Processing was performed with ACDLABS software (1.2, academic version). Zero Filling: to 256K. Line Broadening: LB = 0.1 Hz. Phasing: manually. Baseline Correction, for ^{1}H NMR: 6^{th} order polynomial. For each signal measured a ratio signal/noise>100 is verified.

S2. Structures

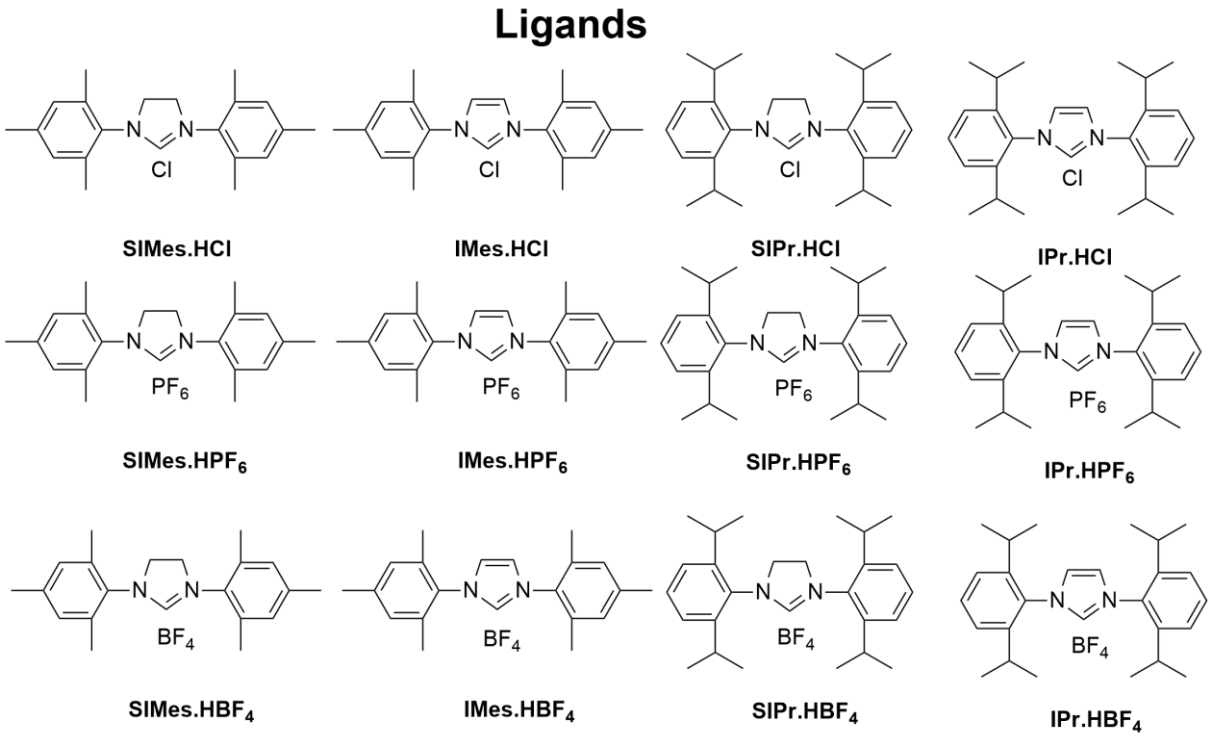

Complexes

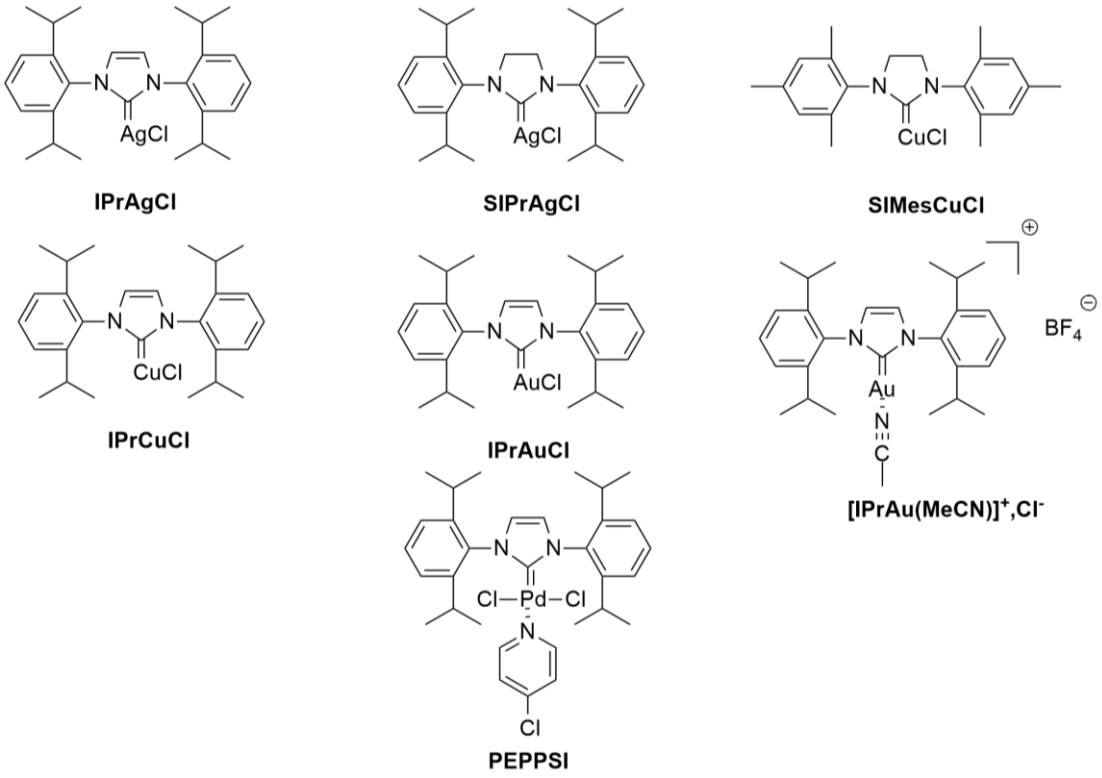

Purity Determination

S3. Determination of the purity of 1,4 DMB standard.

Purity was determined as the average of 6 independent measurements in dmso_d_6 from maleic acid gold standard trace certified (Aldrich) as primary standard.

Example of spectrum

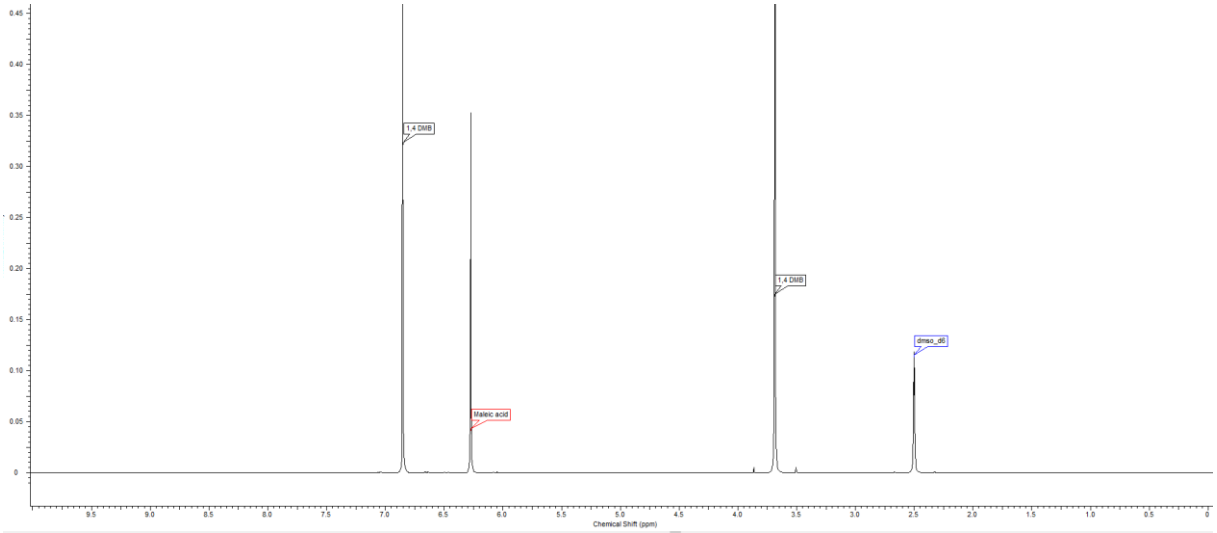

Purity is calculated as the ratio of the number of mol of 1,4-DMB determined by qNMR divided by the number of mol of 1,4-DMB weighted, taking into account of the primary standard purity (99.98 +/- 0.13 %).

Exp	1	2	3	4	5	6

Purity	99.32	98.39	98.91	99.56	100.00	100.04
Average	99.48 %					
Standard deviation	+/- 0.06%					

The linearity of the response in the range 10 to 25 mg (0.08 to 0.17 mmol) was verified:

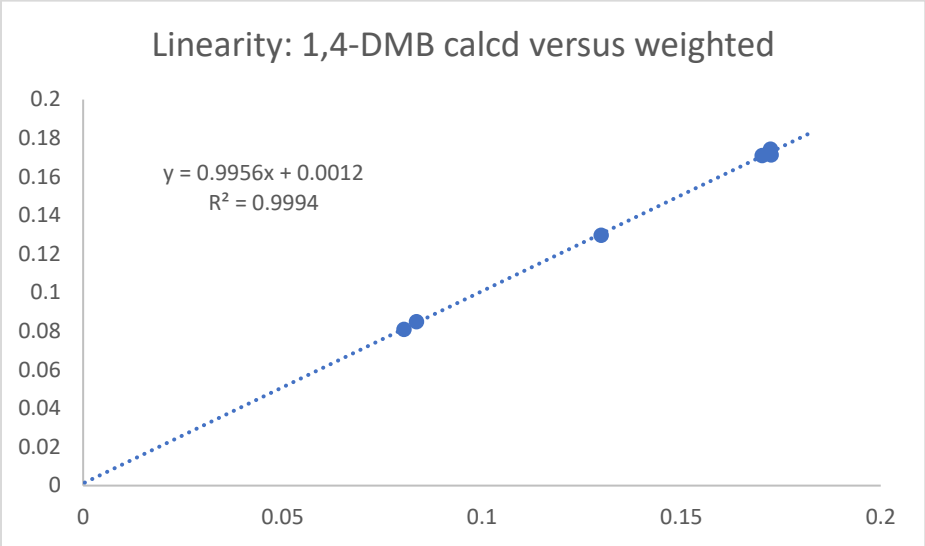

S4. ^{19}F NMR spectra of SIPr.HPF$_6$

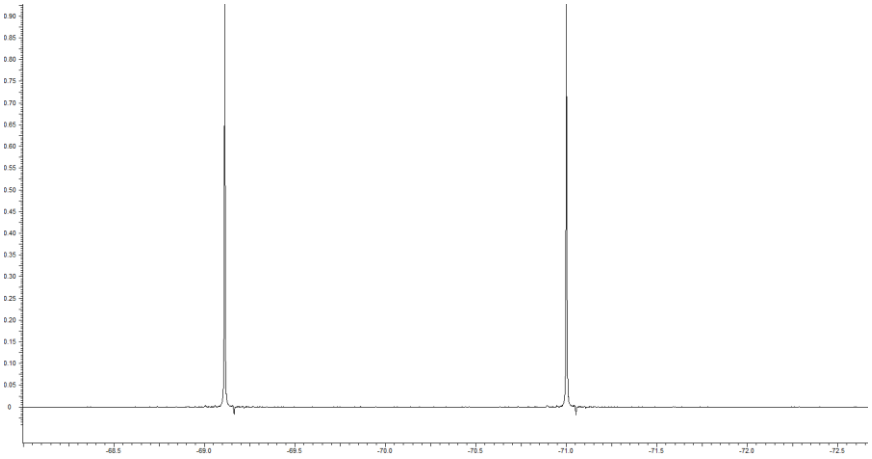

S5. ^{19}F NMR spectra of SIPr.HBF$_4$

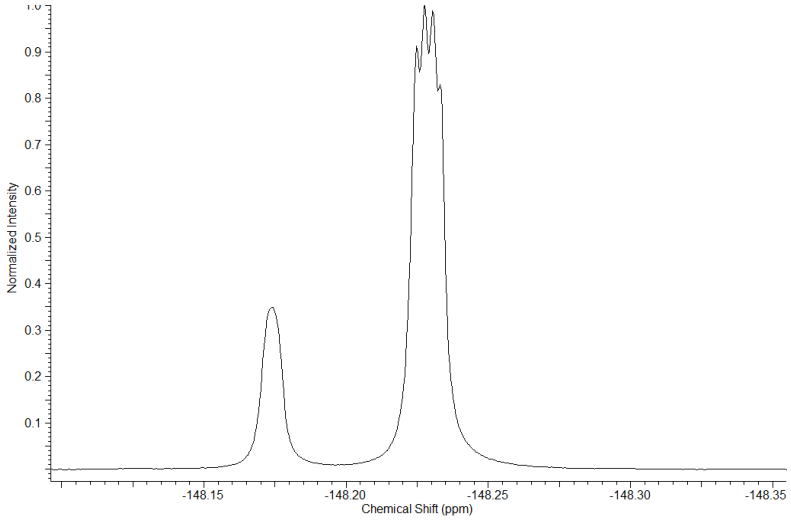

S6. SIMes.HCl 0.5H_2O

Zero filling	LB	Phase	Baseline
256K	0.1	Manual	6Th order

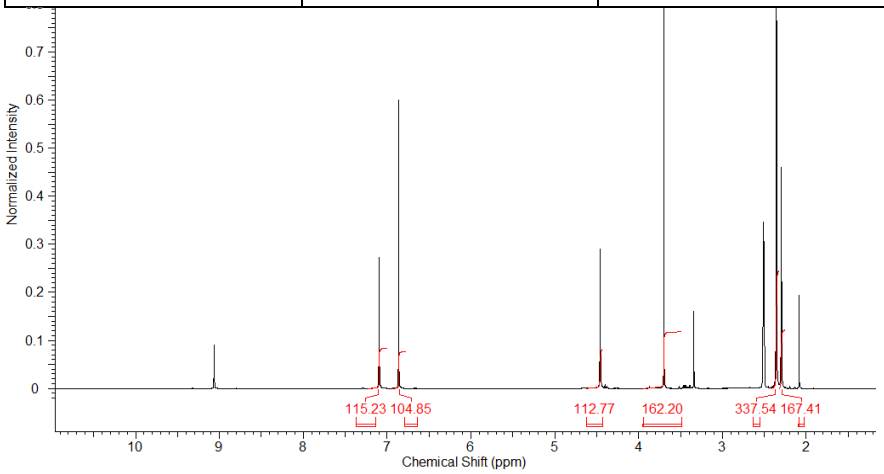

Masse sample (mg)	Masse Standard (mg)	Solvent: dmso-d_6
36.61	12.52	

Signals standard (ppm)	6.86	3.7		
Integration	104.8	162.2		
Signals sample (ppm)	7.1	4.45	2.35	2.3
Integration	115.2	112.7	337.5	167.4

Somme of the integral: sample, 732.8; standard, 267.

Number of protons: sample, 26; standard, 10.

Molecular weight: sample, 351.9; standard, 138.2.

Mass of: sample, 36.61; standard: 12.52.

$$P_s = \frac{I_s}{I_{std}} . \frac{N_{std}}{N_s} . \frac{M_s}{M_{std}} . \frac{m_{std}}{m_s} . P_{std} = \frac{732.8}{267} . \frac{10}{26} . \frac{351.9}{138.2} . \frac{12.52}{36.61} . 0.995 \ = 0.914$$

Purity: 91%

S7. IMes.HCl, 1H_2O ^{1}H qNMR

Zero filling	LB	Phase	Baseline
256K	0.1	Manual	6Th order

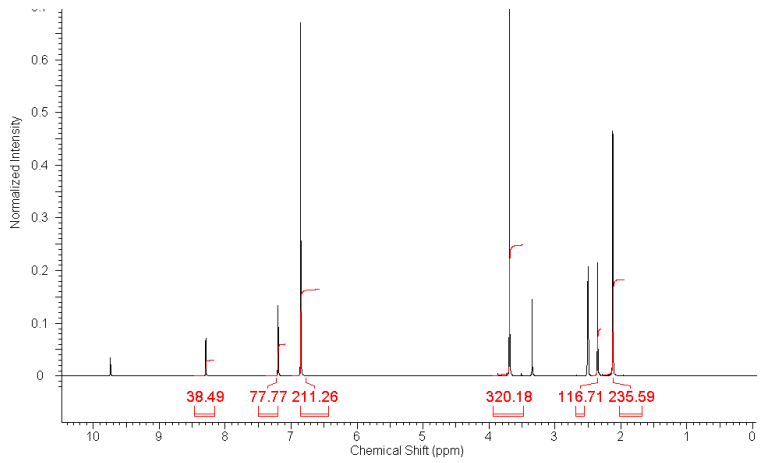

Masse sample (mg)	Masse Standard (mg)	Solvent: dmso-d_6
13.48	13.96	

Signals standard (ppm)	6.86	3.7		
Integration	211.3	320.2		
Signals sample (ppm)	8.3	7.2	2.4	2.1
Integration	38.5	77.7	116.7	235.6

Somme of the integral: sample, 468.5; standard, 531.5.

Number of protons: sample, 24; standard, 10.

Molecular weight: sample, 358.9; standard, 138.2.

Mass of: sample, 13.48; standard: 13.96.

$$P_s = \frac{I_s}{I_{std}} . \frac{N_{std}}{N_s} . \frac{M_s}{M_{std}} . \frac{m_{std}}{m_s} . P_{std} = \frac{468.5}{531.5} . \frac{10}{24} . \frac{358.9}{138.2} . \frac{13.96}{13.48} . 0.995 \ = 0.983$$

Purity: 98%

S8. SIPr.HCl, $0H_2O$ ^1H qNMR

Zero filling	LB	Phase	Baseline
256K	0.1	Manual	6^{Th} order

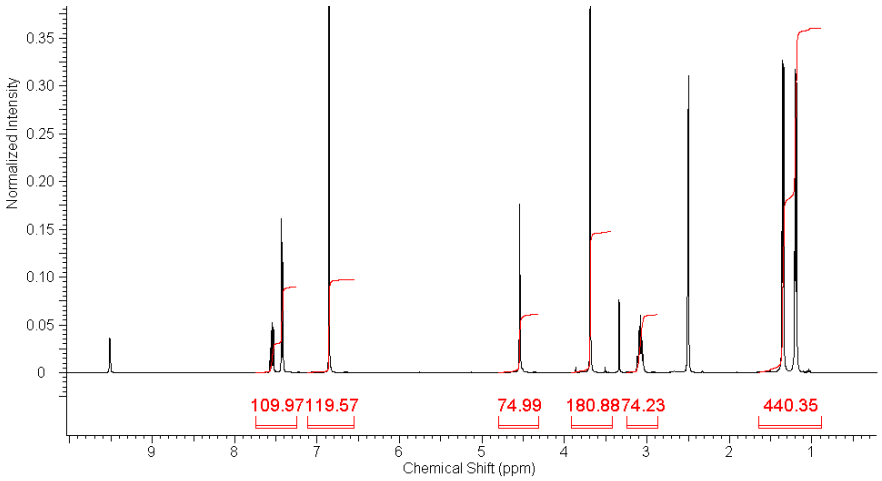

Masse sample (mg)	Masse Standard (mg)	Solvent: dmso-d_6
31.98	15.53	

Signals standard (ppm)	6.86	3.7		
Integration	119.6	180.9		
Signals sample (ppm)	7.5	4.5	3.1	2.3
Integration	110	75	74.2	440.4

Somme of the integral: sample, 699.6; standard, 300.5.

Number of protons: sample, 40; standard, 10.

Molecular weight: sample, 445.1; standard, 138.2.

Mass of: sample, 31.98; standard: 15.53.

$$P_s = \frac{I_s}{I_{std}} . \frac{N_{std}}{N_s} . \frac{M_s}{M_{std}} . \frac{m_{std}}{m_s} . P_{std} = \frac{699.6}{300.5} . \frac{10}{40} . \frac{445.1}{138.2} . \frac{15.53}{31.98} . 0.995 \ = 0.906$$

Purity: 91%

S9. IPr.HCl, 0.5H_2O ^1H qNMR

Zero filling	LB	Phase	Baseline
256K	0.1	Manual	6Th order

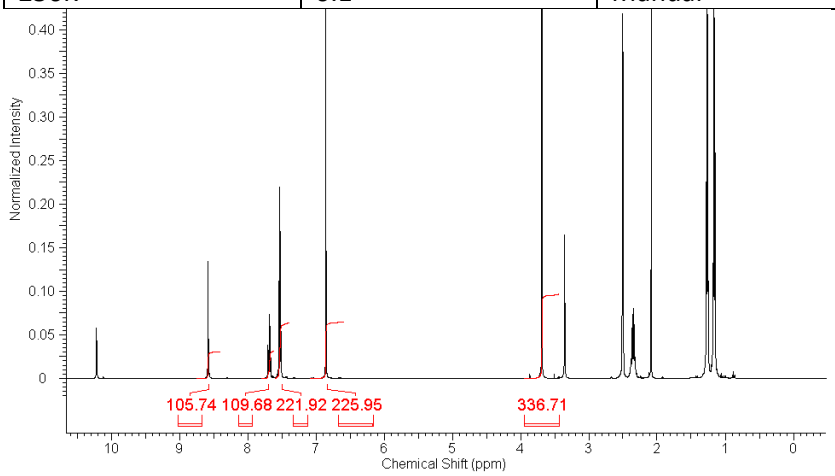

Masse sample (mg)	Masse Standard (mg)	Solvent: dmso-d_6
31.75	11.27	

Signals standard (ppm)	6.86	3.7	
Integration	226	336.7	
Signals sample (ppm)	8.6	7.7	3.7
Integration	105.7	109.7	221.9

Somme of the integral: sample, 437.3; standard, 562.7.

Number of protons: sample, 8; standard, 10.

Molecular weight: sample, 434.1; standard, 138.2.

Mass of: sample, 31.75; standard: 11.27.

$$P_s = \frac{I_s}{I_{std}} . \frac{N_{std}}{N_s} . \frac{M_s}{M_{std}} . \frac{m_{std}}{m_s} . P_{std} = \frac{552.1}{562.7} . \frac{10}{8} . \frac{434.1}{138.2} . \frac{11.27}{31.75} . 0.995 \ = 0.96$$

Purity: 96%

S10. SIMes.HPF_6 ^1H qNMR

Zero filling	LB	Phase	Baseline
256K	0.1	Manual	6Th order

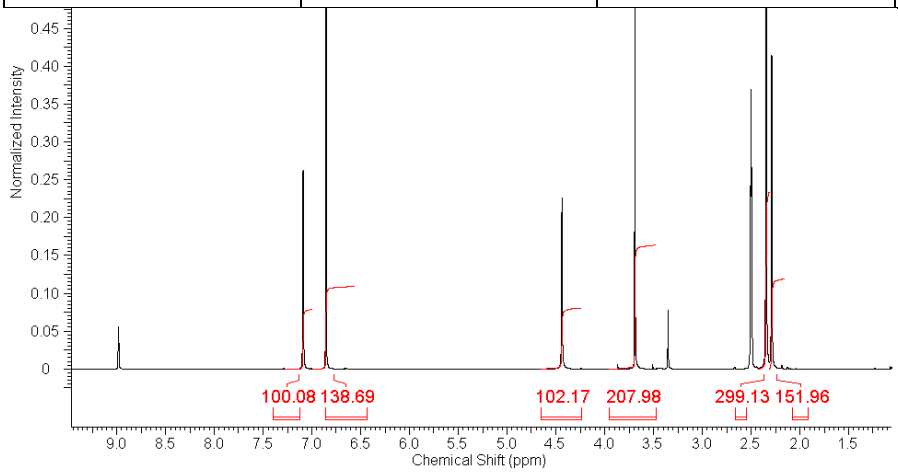

Masse sample (mg)	Masse Standard (mg)	Solvent: dmso-d_6
31.00	12.98	

Signals standard (ppm)	6.86	3.7		
Integration	138.7	208		
Signals sample (ppm)	7.1	4.43	2.34	2.29
Integration	100.1	102.7	299.1	152

Somme of the integral: sample, 653.9; standard, 346.7.

Number of protons: sample, 26; standard, 10.

Molecular weight: sample, 452.4; standard, 138.2.

Mass of: sample, 30.00; standard: 12.98.

$$P_s = \frac{I_s}{I_{std}} . \frac{N_{std}}{N_s} . \frac{M_s}{M_{std}} . \frac{m_{std}}{m_s} . P_{std} = \frac{653.9}{346.7} . \frac{10}{26} . \frac{452.4}{138.2} . \frac{12.98}{31} . 0.995 = 0.98$$

Purity: 98%

S11. SIMes.HPF$_6$ ^{19}F qNMR

Zero filling	LB	Phase	Baseline
256K	0.1	Manual	6Th order

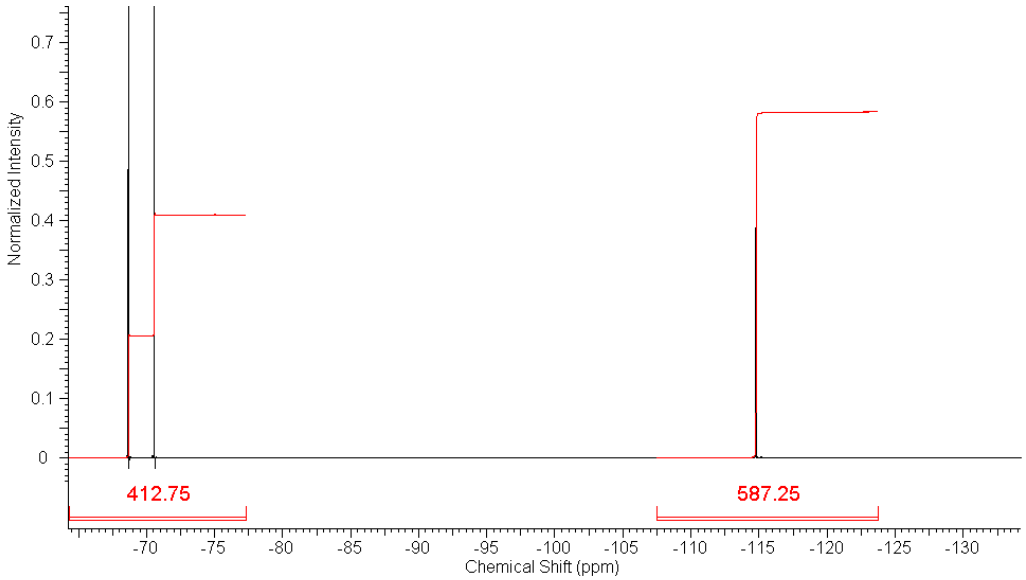

Masse sample (mg)	Masse Standard (mg)	Solvent: dmso-d_6
10.64	28.14	

Signals standard (ppm)	-115
Integration	587.3
Signals sample (ppm)	-70
Integration	412.8

Somme of the integral: sample, 412.8; standard, 587.3.

Number of fluorine: sample, 6; standard, 1.

Molecular weight: sample, 453.4; standard, 144.6.

Mass of: sample, 10.64; standard: 28.4.

$$P_s = \frac{I_s}{I_{std}} . \frac{N_{std}}{N_s} . \frac{M_s}{M_{std}} . \frac{m_{std}}{m_s} . P_{std} = \frac{412.8}{587.3} . \frac{1}{6} . \frac{453.4}{144.6} . \frac{28.4}{10.64} . 0.996 \ = 0.96$$

Purity: 96%

S12. IMes.HPF$_6$ ^{1}H qNMR

Zero filling	LB	Phase	Baseline
256K	0.1	Manual	6Th order

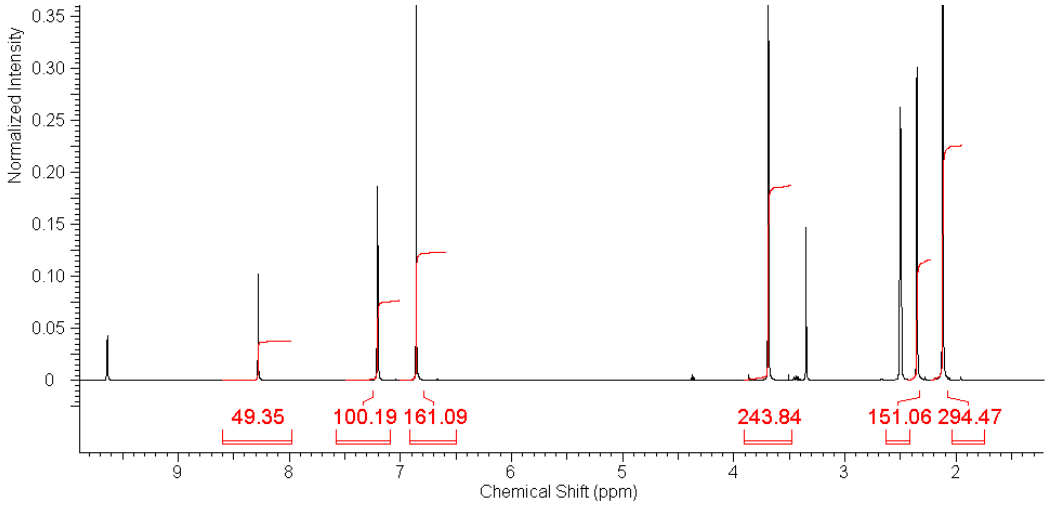

Masse sample (mg)	Masse Standard (mg)	Solvent: dmso-d$_6$
31.51	15.25	

Signals standard (ppm)	6.86	3.7		
Integration	161.1	243.8		
Signals sample (ppm)	8.28	7.2	2.34	2.12
Integration	49.35	100.2	151.1	294.5

Somme of the integral: sample, 595.2; standard, 404.9.

Number of protons: sample, 24; standard, 10.

Molecular weight: sample, 450.4; standard, 138.2.

Mass of: sample, 31.51; standard: 15.25.

$$P_s = \frac{I_s}{I_{std}} . \frac{N_{std}}{N_s} . \frac{M_s}{M_{std}} . \frac{m_{std}}{m_s} . P_{std} = \frac{595.2}{404.9} . \frac{10}{24} . \frac{450.4}{138.2} . \frac{15.25}{31.51} . 0.995 \ = 0.96$$

Purity: 96%

S13. IMes.HPF$_6$ ^{19}F qNMR

Zero filling	LB	Phase	Baseline
256K	0.1	Manual	6Th order

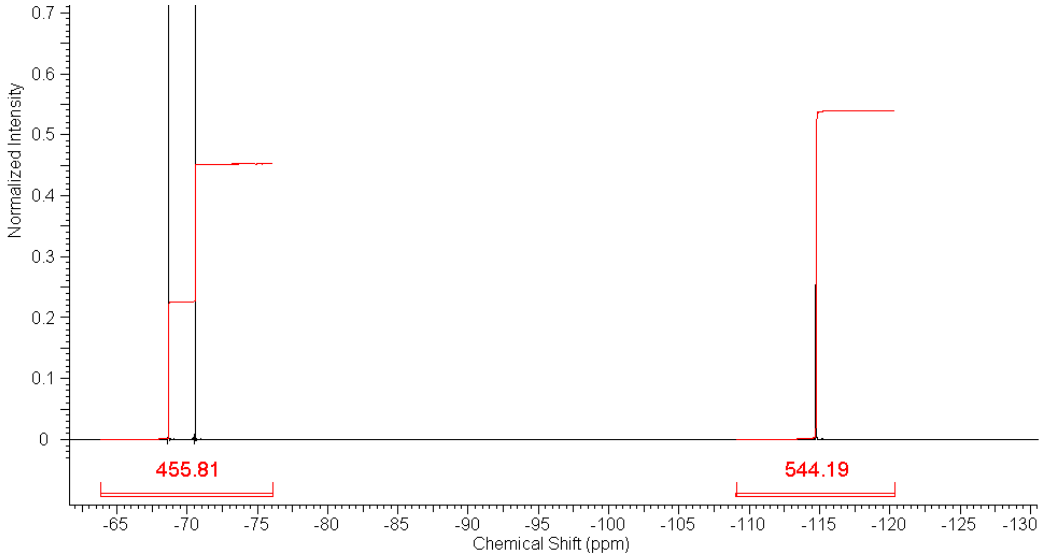

Masse sample (mg)	Masse Standard (mg)	Solvent: dmso-d_6
11.27	25.82	

Signals standard (ppm)	-115
Integration	544.2
Signals sample (ppm)	-70
Integration	455.8

Somme of the integral: sample, 455.8; standard, 544.2.

Number of fluorine: sample, 6; standard, 1.

Molecular weight: sample, 450.4; standard, 144.6.

Mass of: sample, 11.27; standard: 25.82.

$$P_s = \frac{I_s}{I_{std}} \cdot \frac{N_{std}}{N_s} \cdot \frac{M_s}{M_{std}} \cdot \frac{m_{std}}{m_s} \cdot P_{std} = \frac{455.8}{544.2} \cdot \frac{1}{6} \cdot \frac{450.4}{144.6} \cdot \frac{25.82}{11.27} \cdot 0.996 \ = 0.99$$

Purity: 99%

S14. SIPr.HPF$_6$ ^{1}H qNMR

Zero filling	LB	Phase	Baseline
256K	0.1	Manual	6Th order

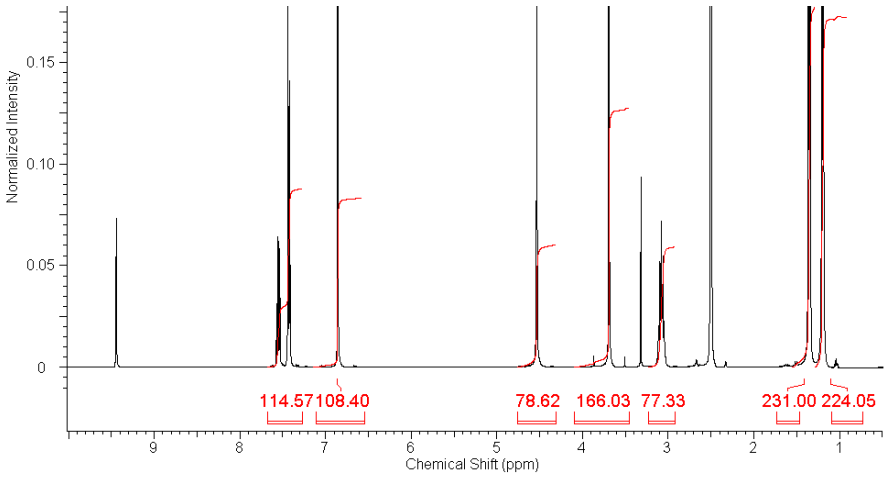

Masse sample (mg)	Masse Standard (mg)	Solvent: dmso-d_6
32.09	11.51	

Signals standard (ppm)	6.86	3.7			
Integration	108.4	166			
Signals sample (ppm)	7.49	4.54	3.1	11.35	1.19
Integration	114.6	78.6	77.3	231	224.1

Somme of the integral: sample, 725.6; standard, 274.4.

Number of protons: sample, 38; standard, 10.

Molecular weight: sample, 536.6; standard, 138.2.

Mass of: sample, 32.09; standard: 11.51.

$$P_s = \frac{I_s}{I_{std}} . \frac{N_{std}}{N_s} . \frac{M_s}{M_{std}} . \frac{m_{std}}{m_s} . P_{std} = \frac{725.6}{274.4} . \frac{10}{38} . \frac{536.6}{138.2} . \frac{11.51}{32.09} . 0.995 \ = 0.96$$

Purity: 96%

S15. SIPr.HPF$_6$ ^{19}F qNMR

Zero filling	LB	Phase	Baseline
256K	0.1	Manual	6Th order

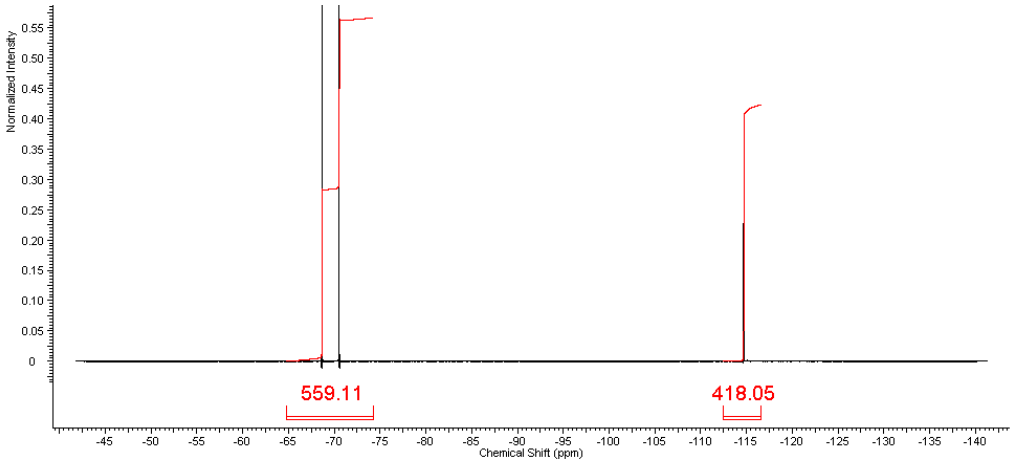

Masse sample (mg)	Masse Standard (mg)	Solvent: dmso-d_6
11.56	13.6	

Signals standard (ppm)	-115
Integration	418.1
Signals sample (ppm)	-70
Integration	559.1

Somme of the integral: sample, 559.1; standard, 418.1.

Number of fluorine: sample, 6; standard, 1.

Molecular weight: sample, 534.6; standard, 144.6.

Mass of: sample, 11.56; standard: 13.6.

$$P_s = \frac{I_s}{I_{std}} . \frac{N_{std}}{N_s} . \frac{M_s}{M_{std}} . \frac{m_{std}}{m_s} . P_{std} = \frac{559.1}{418.1} . \frac{1}{6} . \frac{534.6}{144.6} . \frac{13.6}{11.56} . 0.996 \ = 0.97$$

Purity: 97%

S16. IPr.HPF$_6$ ^{1}H qNMR

Zero filling	LB	Phase	Baseline
256K	0.1	Manual	6Th order

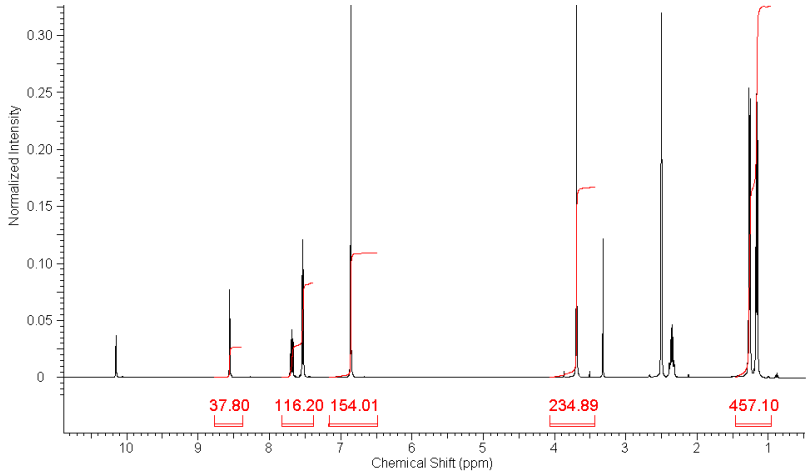

Masse sample (mg)	Masse Standard (mg)	Solvent: dmso-d$_6$
41.33	20.79	

Signals standard (ppm)	6.86	3.7	
Integration	154.0	234.9	
Signals sample (ppm)	8.56	7.61	1.21
Integration	37.8	116.2	457.1

Somme of the integral: sample, 611.1; standard, 388.9.

Number of protons: sample, 32; standard, 10.

Molecular weight: sample, 536.6; standard, 138.2.

Mass of: sample, 41.33; standard: 20.79.

$$P_s = \frac{I_s}{I_{std}} . \frac{N_{std}}{N_s} . \frac{M_s}{M_{std}} . \frac{m_{std}}{m_s} . P_{std} = \frac{611.1}{388.9} . \frac{10}{32} . \frac{536.6}{138.2} . \frac{20.79}{41.33} . 0.995 \ = 0.95$$

Purity: 95%

S17. IPr.HPF$_6$ ^{19}F qNMR

Zero filling	LB	Phase	Baseline
256K	0.1	Manual	6Th order

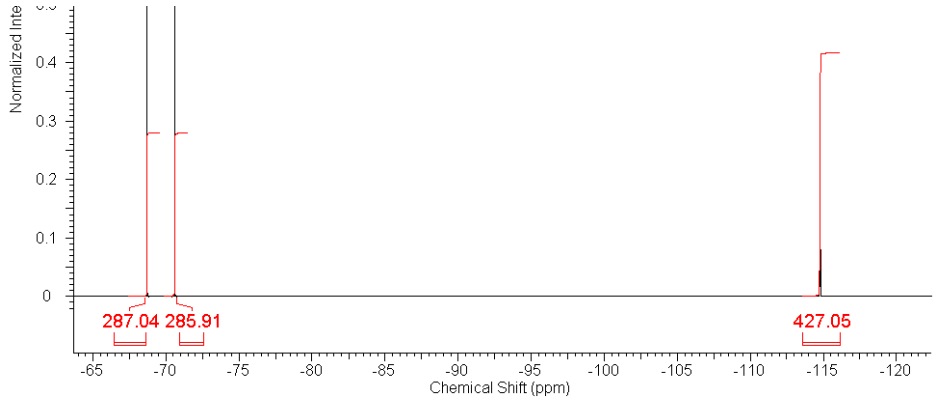

Masse sample (mg)	Masse Standard (mg)	Solvent: dmso-d_6
12.80	14.98	

Signals standard (ppm)	-115	
Integration	427	
Signals sample (ppm)	-70	-70
Integration	287	285.9

Somme of the integral: sample, 572.9; standard, 427.

Number of fluorine: sample, 6; standard, 1.

Molecular weight: sample, 534.6; standard, 144.6.

Mass of: sample, 12.8; standard: 14.98.

$$P_s = \frac{I_s}{I_{std}} . \frac{N_{std}}{N_s} . \frac{M_s}{M_{std}} . \frac{m_{std}}{m_s} . P_{std} = \frac{572.9}{427} . \frac{1}{6} . \frac{534.6}{144.6} . \frac{14.98}{12.8} . 0.996 \ = 0.96$$

Purity: 96%

S18. SIMes.HBF$_4$ ^{1}H qNMR

Zero filling	LB	Phase	Baseline
256K	0.1	Manual	6Th order

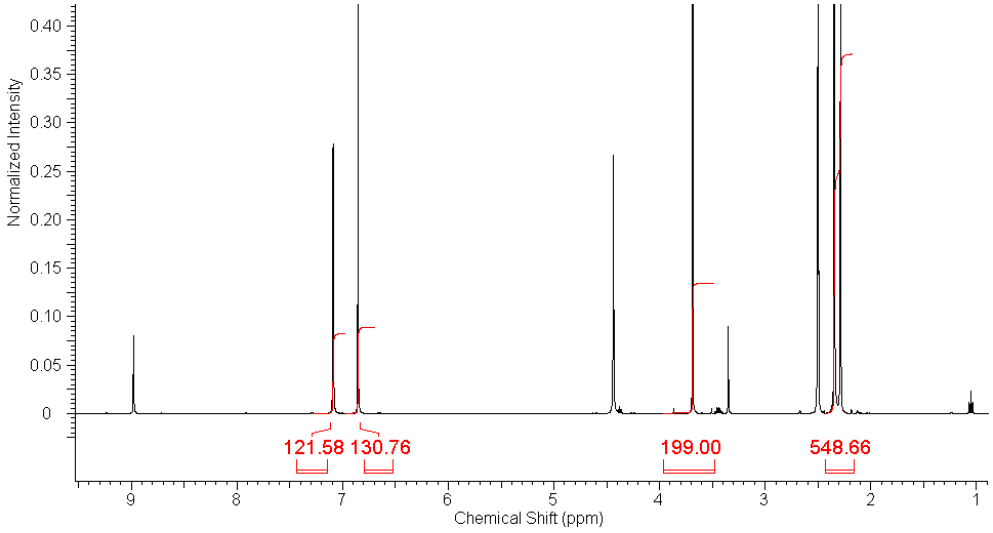

Masse sample (mg)	Masse Standard (mg)	Solvent: dmso-d_6
31.18	11.75	

Signals standard (ppm)	6.86	3.7
Integration	130.8	199
Signals sample (ppm)	7.09	2.32
Integration	121.6	548.7

Somme of the integral: sample, 670.3; standard, 329.8.

Number of protons: sample, 22; standard, 10.

Molecular weight: sample, 394.3; standard, 138.2.

Mass of: sample, 31.18; standard: 11.75.

$$P_s = \frac{I_s}{I_{std}} \cdot \frac{N_{std}}{N_s} \cdot \frac{M_s}{M_{std}} \cdot \frac{m_{std}}{m_s} \cdot P_{std} = \frac{670.3}{329.8} \cdot \frac{10}{22} \cdot \frac{394.3}{138.2} \cdot \frac{11.75}{31.18} \cdot 0.995 = 0.98$$

Purity: 98%

S19. SIMes.HBF$_4$ ^{19}F qNMR

Zero filling	LB	Phase	Baseline
256K	0.1	Manual	6Th order

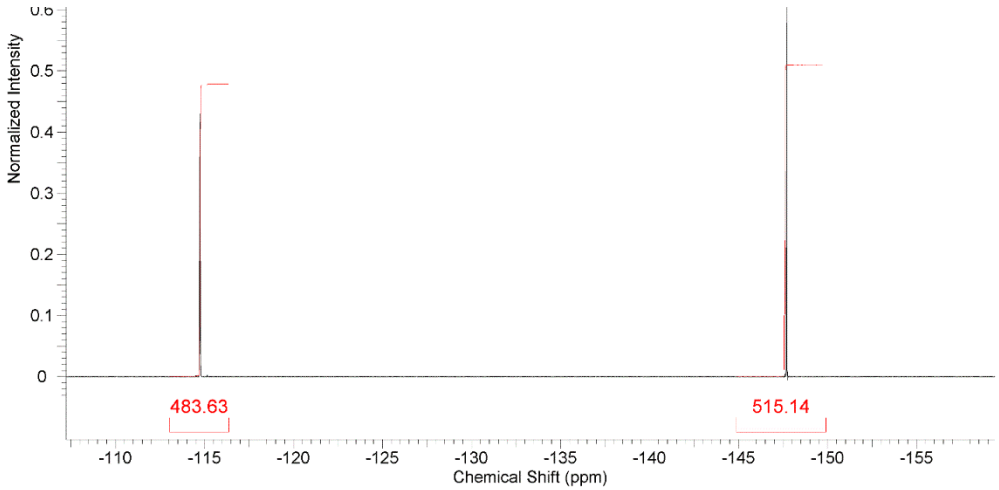

Masse sample (mg)	Masse Standard (mg)	Solvent: dmso-d$_6$
10.62	14.58	

Signals standard (ppm)	-115
Integration	484
Signals sample (ppm)	-148
Integration	515

Somme of the integral: sample, 515; standard, 484.

Number of fluorine: sample, 4; standard, 1.

Molecular weight: sample, 394.2; standard, 144.6.

Mass of: sample, 10.62; standard: 14.58.

$$P_s = \frac{I_s}{I_{std}} \cdot \frac{N_{std}}{N_s} \cdot \frac{M_s}{M_{std}} \cdot \frac{m_{std}}{m_s} \cdot P_{std} = \frac{515}{484} \cdot \frac{1}{4} \cdot \frac{394.2}{144.6} \cdot \frac{14.58}{10.62} \cdot 0.996 = 0.99$$

Purity: 99%

S20. IMes.HBF$_4$ ^{1}H qNMR

Zero filling	LB	Phase	Baseline
256K	0.1	Manual	6Th order

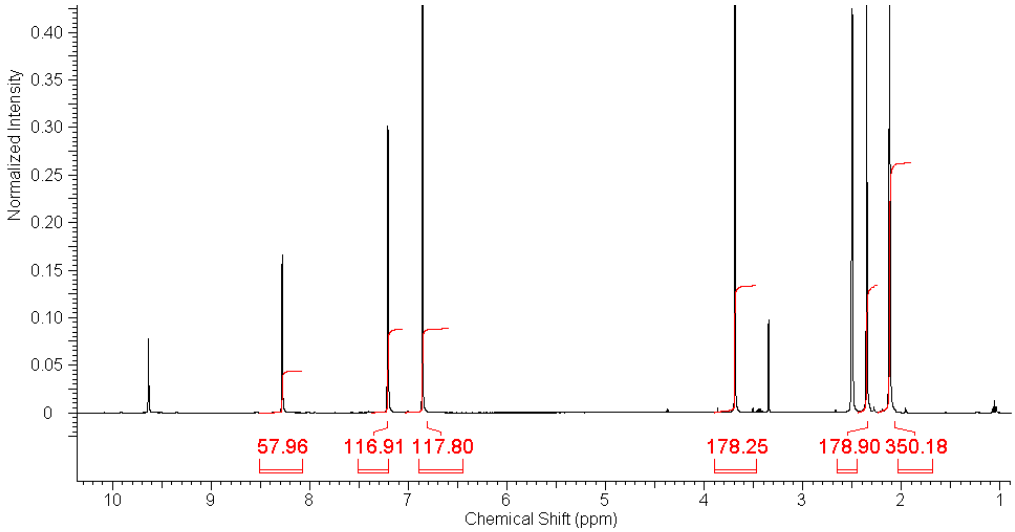

Masse sample (mg)	Masse Standard (mg)	Solvent: dmso-d_6
35.55	12.02	

Signals standard (ppm)	6.86	3.7		
Integration	117.8	178.3		
Signals sample (ppm)	8.3	7.2	2.4	2.1
Integration	58	116.9	178.9	350.2

Somme of the integral: sample, 704; standard, 296.1.

Number of protons: sample, 24; standard, 10.

Molecular weight: sample, 392.2; standard, 138.2.

Mass of: sample, 35.55; standard: 12.02.

$$P_s = \frac{I_s}{I_{std}} . \frac{N_{std}}{N_s} . \frac{M_s}{M_{std}} . \frac{m_{std}}{m_s} . P_{std} = \frac{704}{296.1} . \frac{10}{24} . \frac{392.2}{138.2} . \frac{12.02}{35.55} . 0.995 \ = 0.94$$

Purity: 94%

S21. IMes.HBF$_4$ ^{19}F qNMR

Zero filling	LB	Phase	Baseline
256K	0.1	Manual	6Th order

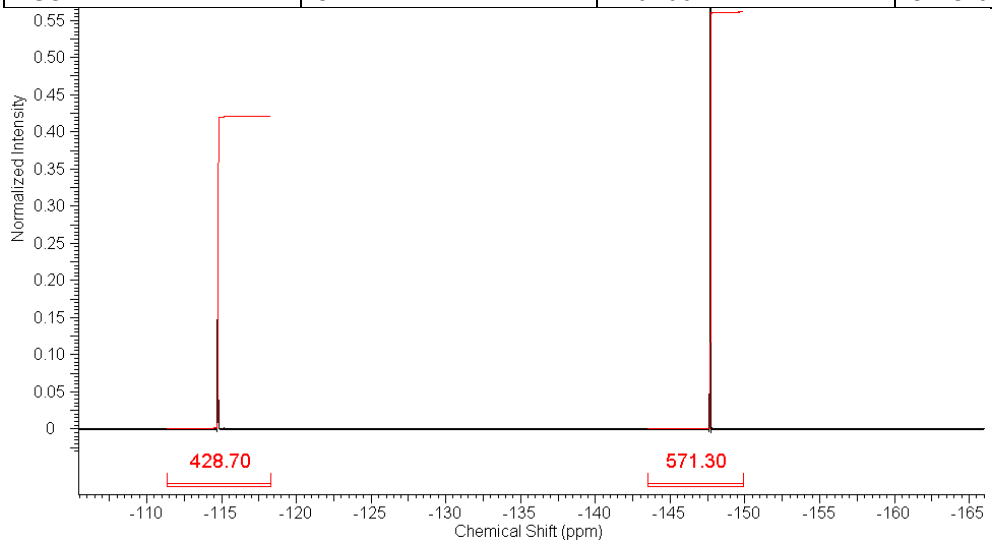

Masse sample (mg)	Masse Standard (mg)	Solvent: dmso-d_6
11.18	12.1	

Signals standard (ppm)	-115
Integration	429
Signals sample (ppm)	-148
Integration	571

Somme of the integral: sample, 571; standard, 429.

Number of fluorine: sample, 4; standard, 1.

Molecular weight: sample, 392.2; standard, 144.6.

Mass of: sample, 11.18; standard: 12.1.

$$P_s = \frac{I_s}{I_{std}} . \frac{N_{std}}{N_s} . \frac{M_s}{M_{std}} . \frac{m_{std}}{m_s} . P_{std} = \frac{571}{429} . \frac{1}{4} . \frac{392.2}{144.6} . \frac{12.1}{11.18} . 0.996 \ = 0.97$$

Purity: 97%

S22. SIPr. HBF_4 ^1H qNMR

Zero filling	LB	Phase	Baseline
256K	0.1	Manual	6Th order

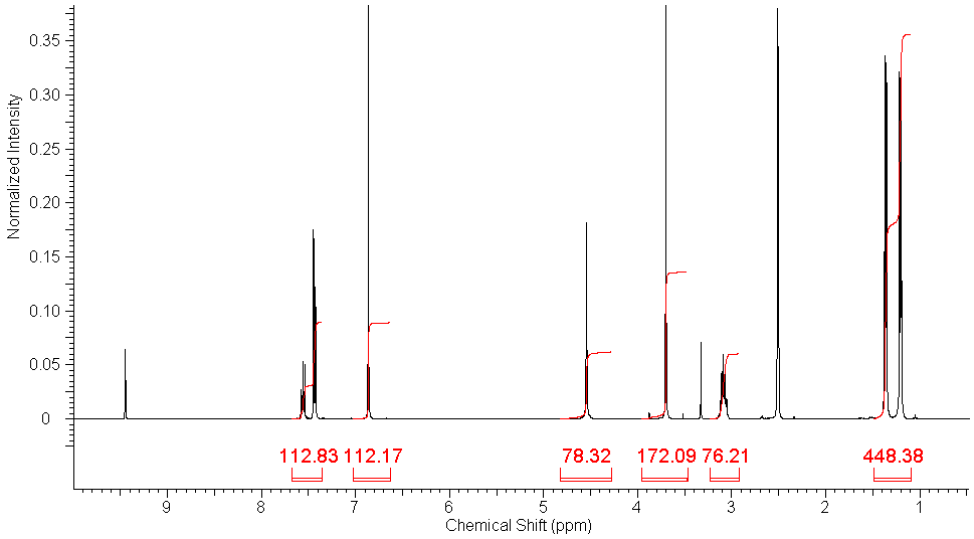

Masse sample (mg)	Masse Standard (mg)	Solvent: dmso-d_6
30.8	12.92	

Signals standard (ppm)	6.86	3.7		
Integration	112.2	172.2		
Signals sample (ppm)	7.5	4.6	3.1	1.29
Integration	112.8	78.3	76.2	448.4

Somme of the integral: sample, 715.7; standard, 284.4.

Number of protons: sample, 38; standard, 10.

Molecular weight: sample, 478.4; standard, 138.2.

Mass of: sample, 30.8; standard: 12.92.

$$P_s = \frac{I_s}{I_{std}} . \frac{N_{std}}{N_s} . \frac{M_s}{M_{std}} . \frac{m_{std}}{m_s} . P_{std} = \frac{715.7}{284.4} . \frac{10}{38} . \frac{478.4}{138.2} . \frac{12.92}{30.8} . 0.995 \ = 0.95$$

Purity: 95%

S23. SIPr. HBF_4, ^{19}F qNMR

Zero filling	LB	Phase	Baseline
256K	0.1	Manual	6Th order

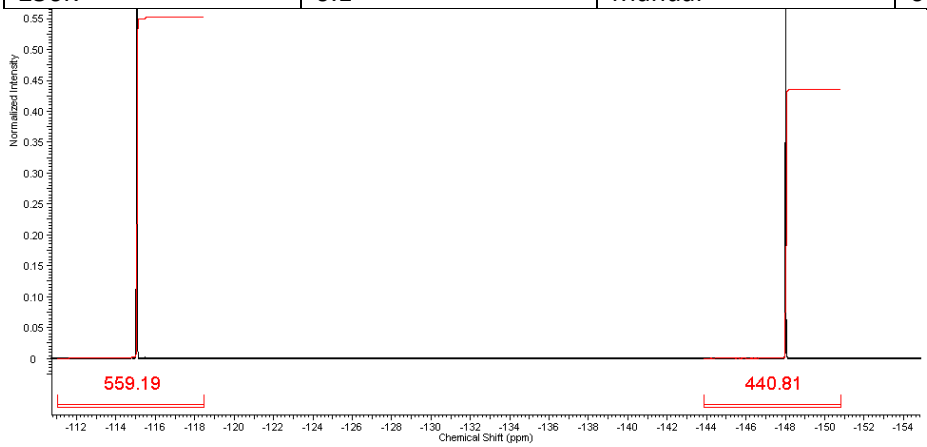

Masse sample (mg)	Masse Standard (mg)	Solvent: dmso-d_6
10.1	15.2	

Signals standard (ppm)	-115
Integration	559.2
Signals sample (ppm)	-148
Integration	440.8

Somme of the integral: sample, 440.8; standard, 559.2.

Number of fluorine: sample, 4; standard, 1.

Molecular weight: sample, 478.4; standard, 144.6.

Mass of: sample, 10.1; standard: 15.2.

$$P_s = \frac{I_s}{I_{std}} . \frac{N_{std}}{N_s} . \frac{M_s}{M_{std}} . \frac{m_{std}}{m_s} . P_{std} = \frac{440.8}{559.2} . \frac{1}{4} . \frac{478.4}{144.6} . \frac{15.2}{10.1} . 0.996 = 0.97$$

Purity: 97%

S24. IPr. HBF_4, ^1H qNMR

Zero filling	LB	Phase	Baseline
256K	0.1	Manual	6Th order

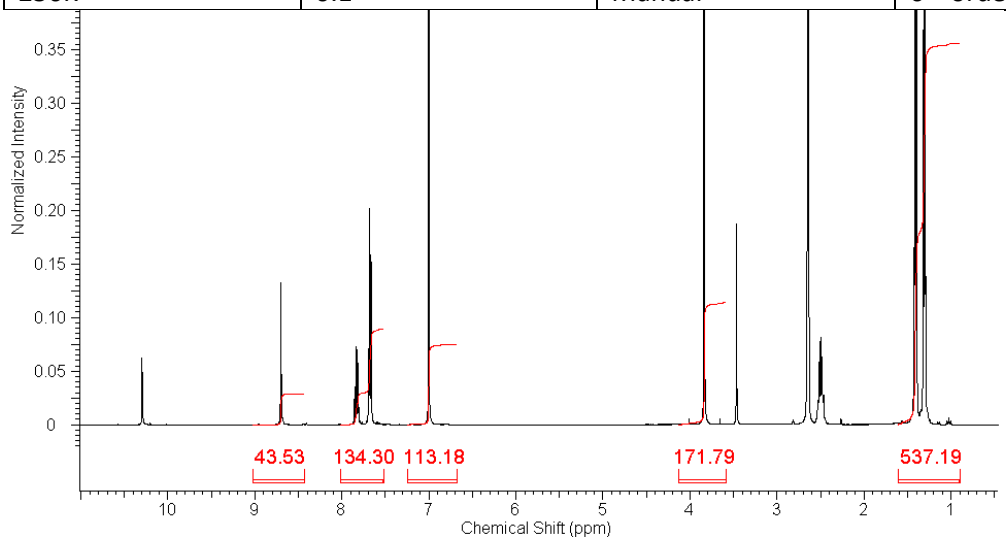

Masse sample (mg)	Masse Standard (mg)	Solvent: dmso-d_6
31.58	10.96	

Signals standard (ppm)	6.86	3.7	
Integration	113.2	171.8	
Signals sample (ppm)	8.7	7.8	1.4
Integration	45.53	134.3	537.2

Somme of the integral: sample, 717.3; standard, 285.

Number of protons: sample, 32; standard, 10.

Molecular weight: sample, 476.4; standard, 138.2.

Mass of: sample, 31.58; standard: 10.96.

$$P_s = \frac{I_s}{I_{std}} . \frac{N_{std}}{N_s} . \frac{M_s}{M_{std}} . \frac{m_{std}}{m_s} . P_{std} = \frac{717.3}{285} . \frac{10}{32} . \frac{476.4}{138.2} . \frac{10.96}{31.58} . 0.995 \ = 0.93$$

Purity: 93%

S25. IPr. HBF_4, ^{19}F qNMR

Zero filling	LB	Phase	Baseline
256K	0.1	Manual	6Th order

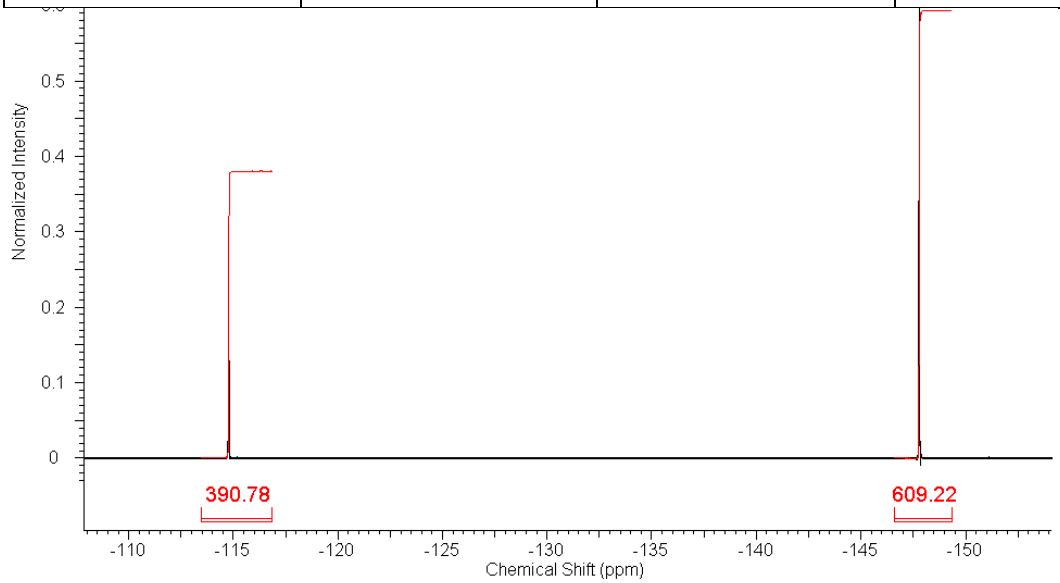

Masse sample (mg)	Masse Standard (mg)	Solvent: dmso-d_6
14.9	11.2	

Signals standard (ppm)	-115
Integration	390.8
Signals sample (ppm)	-148
Integration	609.2

Somme of the integral: sample, 609.2; standard, 390.8.

Number of fluorine: sample, 4; standard, 1.

Molecular weight: sample, 476.4; standard, 144.6.

Mass of: sample, 14.9; standard: 11.12.

$$P_s = \frac{I_s}{I_{std}} . \frac{N_{std}}{N_s} . \frac{M_s}{M_{std}} . \frac{m_{std}}{m_s} . P_{std} = \frac{609.2}{390.8} . \frac{1}{4} . \frac{476.4}{144.6} . \frac{11.12}{14.9} . 0.996 \ = 0.95$$

Purity: 95%

S26. IMesAgCl, ^1H qNMR

Zero filling	LB	Phase	Baseline
256K	0.1	Manual	6Th order

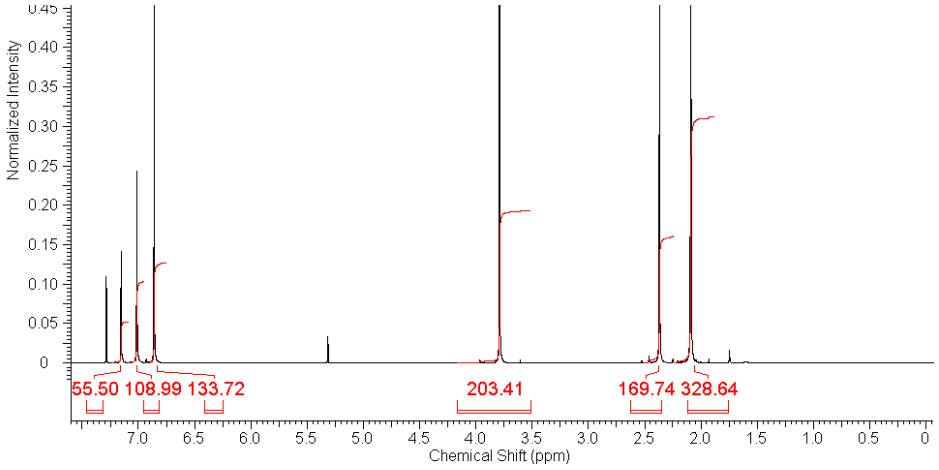

Masse sample (mg)	Masse Standard (mg)	Solvent: $CDCl_3$
41.72	14.9	

Signals standard (ppm)	6.86	3.7		
Integration	133.72	203.4		
Signals sample (ppm)	7.14	7.0	2.36	2.07
Integration	55.5	109	169.7	328.6

Somme of the integral: sample, 662.8; standard, 327.1.

Number of protons: sample, 24; standard, 10.

Molecular weight: sample, 449.7; standard, 138.2.

Mass of: sample, 41.72; standard: 14.9.

$$P_s = \frac{I_s}{I_{std}} . \frac{N_{std}}{N_s} . \frac{M_s}{M_{std}} . \frac{m_{std}}{m_s} . P_{std} = \frac{662.8}{337.4} . \frac{10}{24} . \frac{449.7}{138.2} . \frac{14.9}{41.72} . 0.995 \ = 0.97$$

Purity: 97%

S27. SIMesAgCl, ^1H qNMR

Zero filling	LB	Phase	Baseline
256K	0.1	Manual	6Th order

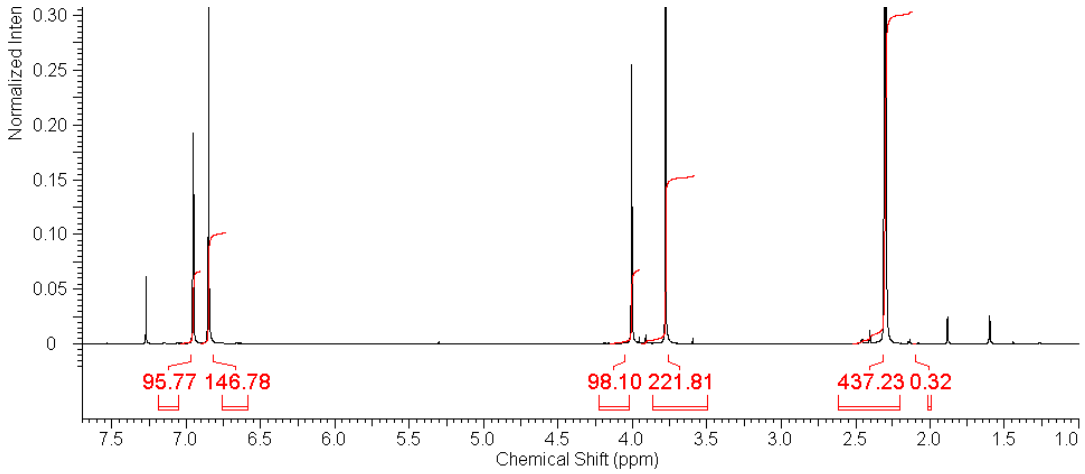

Masse sample (mg)	Masse Standard (mg)	Solvent: $CDCl_3$
28.79	12.74	

Signals standard (ppm)	6.86	3.7	
Integration	146.8	221.8	
Signals sample (ppm)	6.95	4	2.3
Integration	95.8	98.1	437.2

Somme of the integral: sample, 631.1; standard, 368.6.

Number of protons: sample, 26; standard, 10.

Molecular weight: sample, 449.8; standard, 138.2.

Mass of: sample, 28.79; standard: 12.74.

$$P_s = \frac{I_s}{I_{std}} . \frac{N_{std}}{N_s} . \frac{M_s}{M_{std}} . \frac{m_{std}}{m_s} . P_{std} = \frac{631.1}{368.7} . \frac{10}{26} . \frac{449.8}{138.2} . \frac{12.74}{28.79} . 0.995 \ = 0.95$$

Purity: 95%

S28. IPrAgCl, ^1H qNMR

Zero filling	LB	Phase	Baseline
256K	0.1	Manual	6Th order

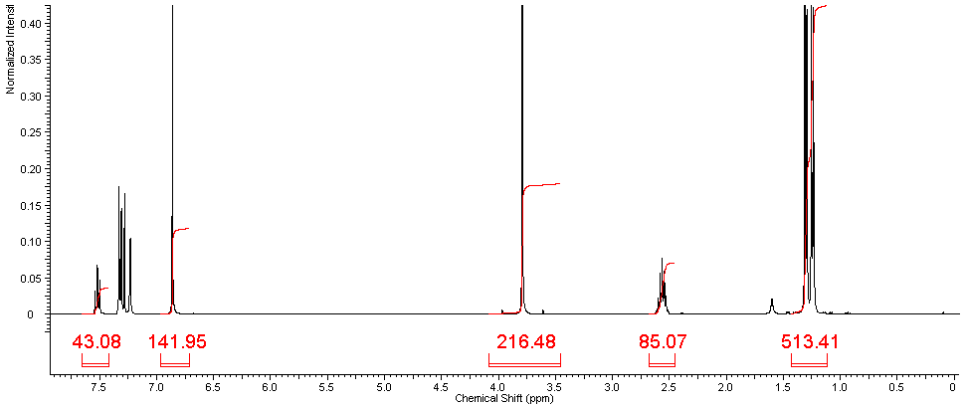

Masse sample (mg)	Masse Standard (mg)	Solvent: $CDCl_3$
23.89	10.20	

Signals standard (ppm)	6.86	3.7	
Integration	142.0	216.5	
Signals sample (ppm)	7.7	7.5	7.4
Integration	43.1	85.1	513.4

Somme of the integral: sample, 641.6; standard, 358.5.

Number of protons: sample, 30; standard, 10.

Molecular weight: sample, 531.9 standard, 138.2.

Mass of: sample, 23.89; standard: 10.2.

$$P_s = \frac{I_s}{I_{std}} . \frac{N_{std}}{N_s} . \frac{M_s}{M_{std}} . \frac{m_{std}}{m_s} . P_{std} = \frac{641.6}{358.5} . \frac{10}{30} . \frac{531.9}{138.2} . \frac{10.2}{23.89} . 0.995 \ = 0.97$$

Purity: 97%

S29. SIPrAgCl ^1H qNMR

Zero filling	LB	Phase	Baseline
256K	0.1	Manual	6Th order

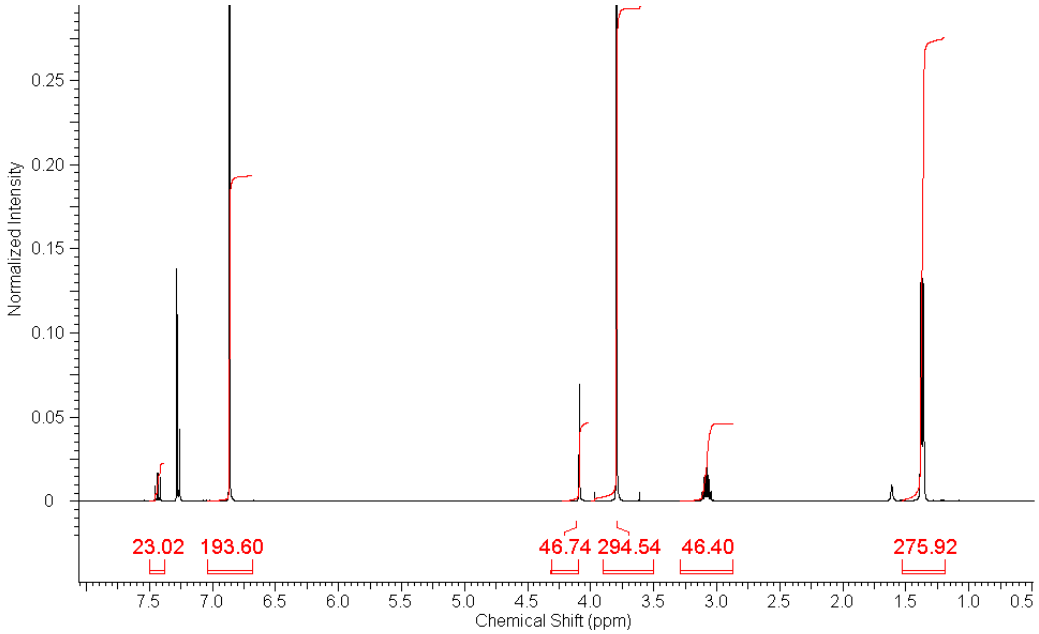

Masse sample (mg)	Masse Standard (mg)	Solvent: $CDCl_3$
11.86	12.83	

Signals standard (ppm)	6.86	3.7		
Integration	193.6	294.5		
Signals sample (ppm)	7.43	4.1	3.1	1.4
Integration	23.0	46.7	46.4	275.9

Somme of the integral: sample, 392; standard, 488.1.

Number of protons: sample, 34; standard, 10.

Molecular weight: sample, 533.9; standard, 138.2.

Mass of: sample, 11.86; standard: 12.83.

$$P_s = \frac{I_s}{I_{std}} . \frac{N_{std}}{N_s} . \frac{M_s}{M_{std}} . \frac{m_{std}}{m_s} . P_{std} = \frac{392}{488.1} . \frac{10}{34} . \frac{533.9}{138.2} . \frac{12.83}{11.86} . 0.995 = 0.98$$

Purity: 98%

S30. SIMesCuCl, ^1H qNMR

Zero filling	LB	Phase	Baseline
256K	0.1	Manual	6Th order

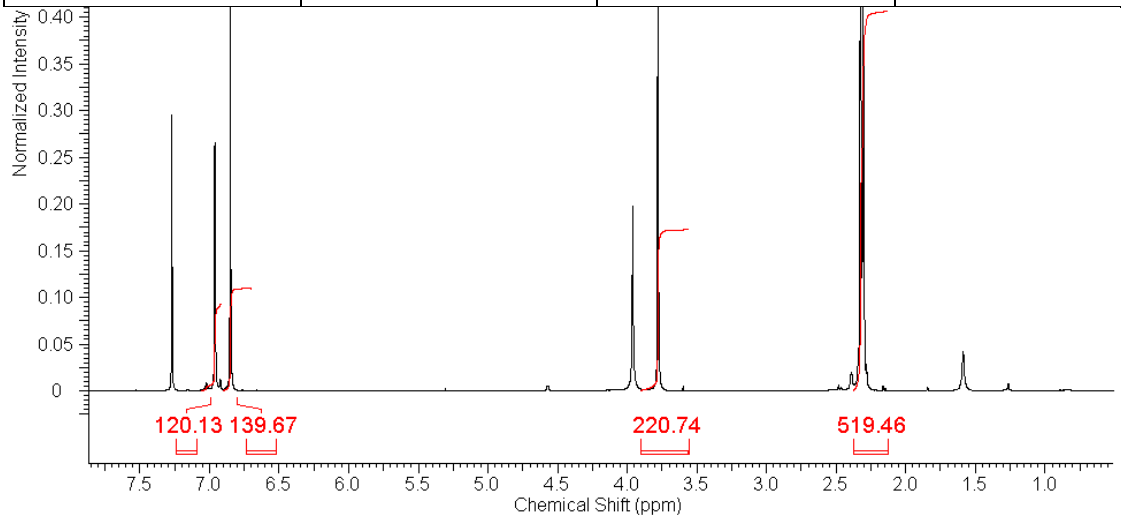

Masse sample (mg)	Masse Standard (mg)	Solvent: CDCl3
33.25	13.18	

Signals standard (ppm)	6.86	3.7
Integration	139.7	220.7
Signals sample (ppm)	7.0	2.3
Integration	120.1	519.5

Somme of the integral: sample, 639.6; standard, 360.4.

Number of protons: sample, 22; standard, 10.

Molecular weight: sample, 405.4; standard, 138.2.

Mass of: sample, 33.25; standard: 13.18.

$$P_s = \frac{I_s}{I_{std}} . \frac{N_{std}}{N_s} . \frac{M_s}{M_{std}} . \frac{m_{std}}{m_s} . P_{std} = \frac{639.6}{360.4} . \frac{10}{22} . \frac{405.4}{138.2} . \frac{13.18}{33.25} . 0.995 \ = 0.93$$

Purity: 93%

S31. IPrCuCl, ^{1}H qNMR

Zero filling	LB	Phase	Baseline
256K	0.1	Manual	6Th order

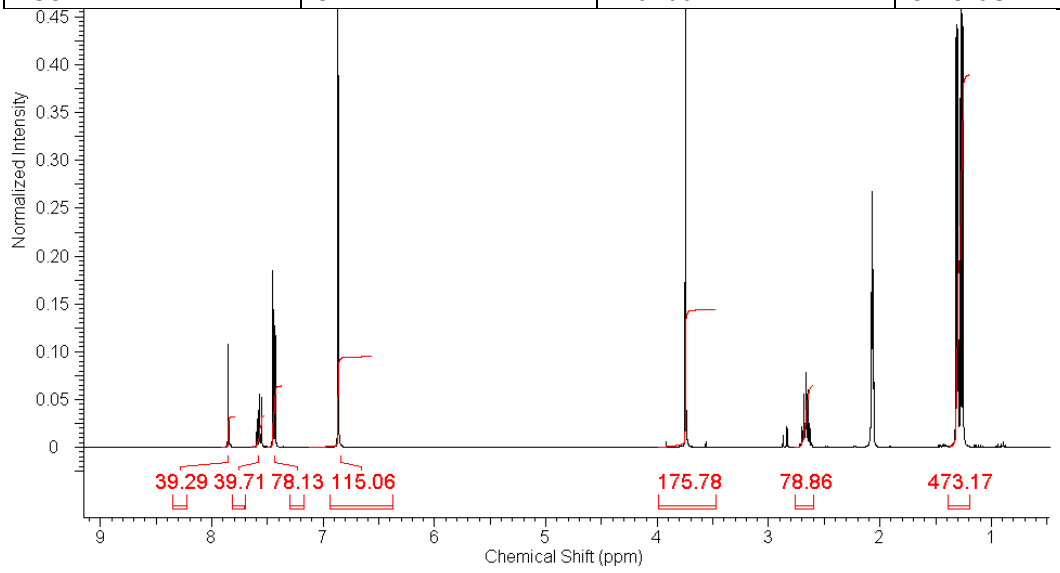

Masse sample (mg)	Masse Standard (mg)	Solvent: Acetone-d$_6$
31.38	13.00	

Signals standard (ppm)	6.86	3.7			
Integration	115.1	175.8			
Signals sample (ppm)	7.9	7.6	7.4	2.7	1.3
Integration	39.3	39.7	78.1	78.9	473.2

Somme of the integral: sample, 709.2; standard, 290.9.

Number of protons: sample, 36; standard, 10.

Molecular weight: sample, 489.6; standard, 138.2.

Mass of: sample, 31.38; standard: 13.00.

$$P_s = \frac{I_s}{I_{std}} . \frac{N_{std}}{N_s} . \frac{M_s}{M_{std}} . \frac{m_{std}}{m_s} . P_{std} = \frac{709.2}{290.9} . \frac{10}{36} . \frac{489.6}{138.2} . \frac{13.00}{31.38} . 0.995 \ = 0.98$$

Purity: 98%

S32. IPrAuCl, ^{1}H qNMR

Zero filling	LB	Phase	Baseline
256K	0.1	Manual	6Th order

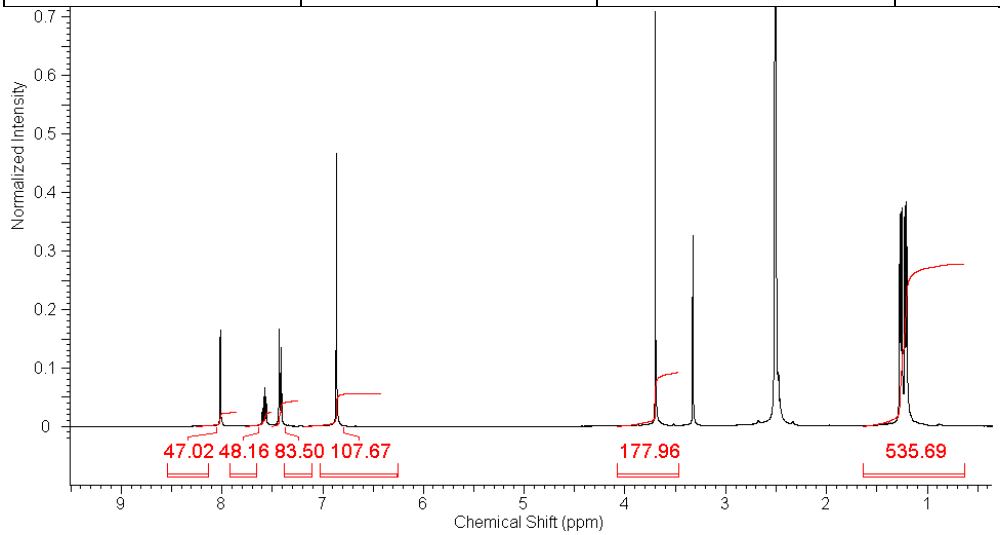

Masse sample (mg)	Masse Standard (mg)	Solvent: dmso-d$_6$
50.83	13.52	

Signals standard (ppm)	6.86	3.7		
Integration	107.7	178.0		
Signals sample (ppm)	8.0	7.6	7.4	1.2
Integration	47	48.2	83.5	535.7

Somme of the integral: sample, 714.4; standard, 285.7.

Number of protons: sample, 32; standard, 10.

Molecular weight: sample, 621; standard, 138.2.

Mass of: sample, 50.83; standard: 13.52.

$$P_s = \frac{I_s}{I_{std}} . \frac{N_{std}}{N_s} . \frac{M_s}{M_{std}} . \frac{m_{std}}{m_s} . P_{std} = \frac{714.4}{285.7} . \frac{10}{32} . \frac{621.0}{138.2} . \frac{13.52}{50.83} . 0.995 \ = 0.92$$

Purity: 92%

S33. [IPrAu,MeCN], BF$_4$,^{1}H qNMR

Zero filling	LB	Phase	Baseline
256K	0.1	Manual	6Th order

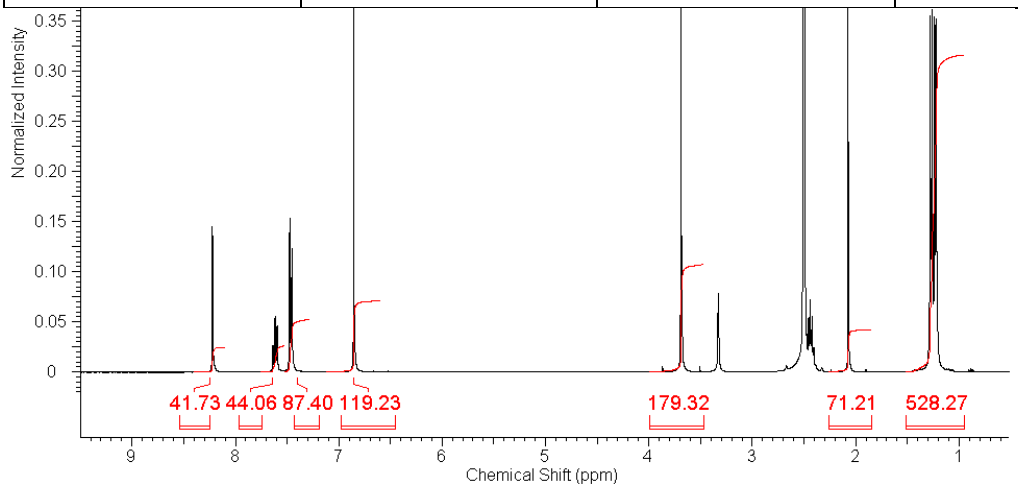

Masse sample (mg)	Masse Standard (mg)	Solvent: dmso-d_6
49.3	12.21	

Signals standard (ppm)	6.86	3.7			
Integration	119.2	179.3			
Signals sample (ppm)	8.2	7.6	7.5	2.0	1.3
Integration	41.7	44.1	87.4	71.2	528.3

Somme of the integral: sample, 772.71; standard, 289.5.

Number of protons: sample, 35; standard, 10.

Molecular weight: sample, 713.4; standard, 138.2.

Mass of: sample, 49.3; standard: 12.21.

$$P_s = \frac{I_s}{I_{std}} . \frac{N_{std}}{N_s} . \frac{M_s}{M_{std}} . \frac{m_{std}}{m_s} . P_{std} = \frac{772.7}{289.5} . \frac{10}{35} . \frac{713.4}{138.2} . \frac{12.21}{49.3} . 0.995 \ = 0.93$$

Purity: 93%

S34. [IPrAu,MeCN], BF_4, ^{19}F qNMR

Zero filling	LB	Phase	Baseline
256K	0.1	Manual	FID reconstruction

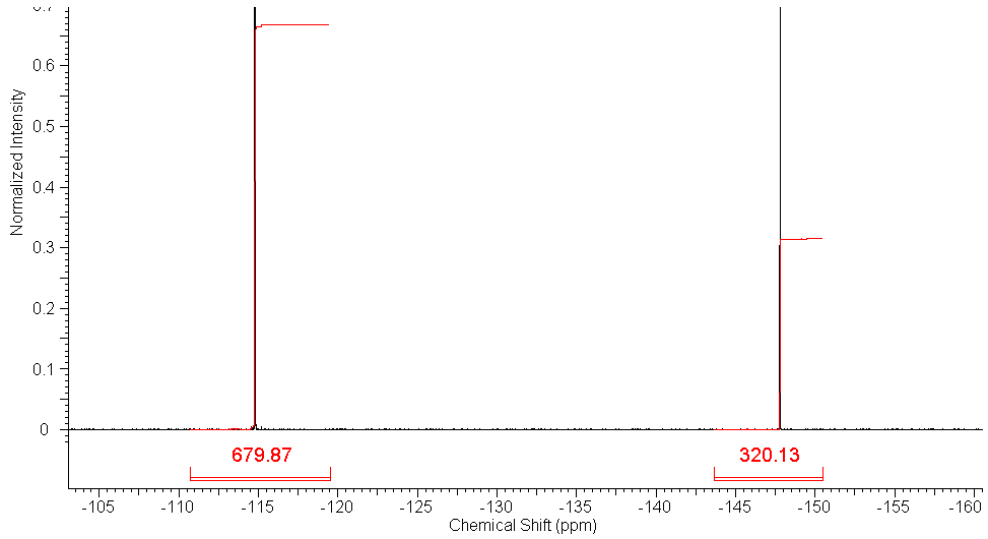

Masse sample (mg)	Masse Standard (mg)	Solvent: dmso-d_6
16.74	26.74	

Signals standard (ppm)	-115
Integration	679.9
Signals sample (ppm)	-148
Integration	320.1

Somme of the integral: sample, 320.1; standard, 679.9.

Number of fluorine: sample, 4; standard, 1.

Molecular weight: sample, 713.4; standard, 144.6.

Mass of: sample, 16.74; standard: 26.74.

$$P_s = \frac{I_s}{I_{std}} . \frac{N_{std}}{N_s} . \frac{M_s}{M_{std}} . \frac{m_{std}}{m_s} . P_{std} = \frac{320.1}{679.9} . \frac{1}{4} . \frac{713.4}{144.6} . \frac{26.74}{16.74} . 0.996 \ = 0.95$$

Purity: 95%

S35. PEPSSI. 0.8 CH_2Cl_2, ^1H qNMR

Zero filling	LB	Phase	Baseline
256K	0.1	Manual	6Th order

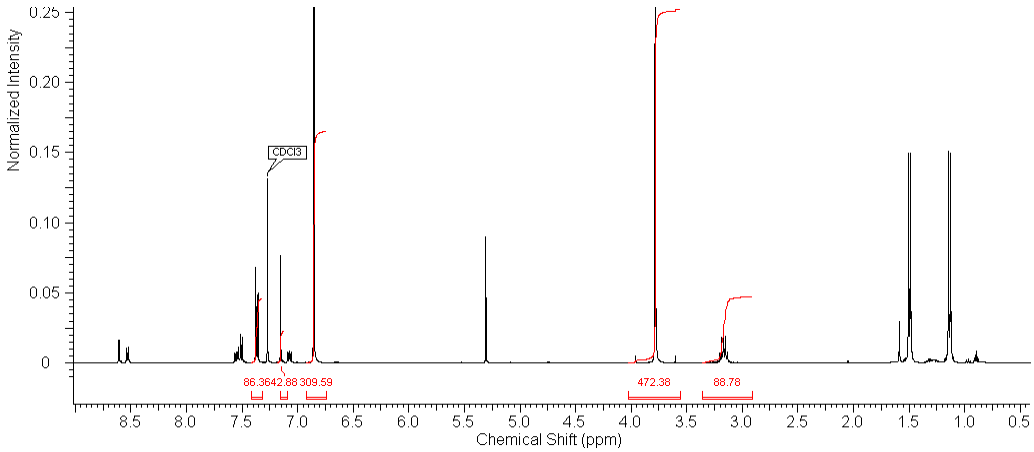

Masse sample (mg)	Masse Standard (mg)	Solvent: $CDCl_3$
19.73	13.43	

Signals standard (ppm)	6.7	3.7	
Integration	309.6	472.4	
Signals sample (ppm)	7.37	7.15	3.16
Integration	86.4	42.9	88.8

Somme of the integral: sample, 307.1; standard, 782.

Number of protons: sample, 14; standard, 10.

Molecular weight: sample, 745; standard, 138.2.

Mass of: sample (0.8 dcm), 19.73; standard: 12.43.

$$P_s = \frac{I_s}{I_{std}} . \frac{N_{std}}{N_s} . \frac{M_s}{M_{std}} . \frac{m_{std}}{m_s} . P_{std} = \frac{307}{782} . \frac{10}{14} . \frac{745}{138.2} . \frac{12.43}{19.73} . 0.995 \ = 0.96$$

Purity: 96%

Chapter III.

1-General information

Chemicals: Rink amine resin (0.62mmol/g loading) was obtained from Novabiochem, piperidine and dichloromethane from Carlo Erba; 3-chloromethylbenzoylchloride, TFA, DIPEA, isopropyl, and propargyl amines from TCI; *N*-methylpyrrolidone from Alfa Aesar and DMSO from Acros. Benzyl azide (**1a**), (azidomethyl)cyclohexane (**1b**), *tert*-butyl azido acetate (**1c**), *tert*-butyl (2-azidoethyl)carbamate (**1d**) and 3-azido propane-1-ol (**1e**) were synthetized according to literature procedures. 10 mL jacketed reactors were purchased from Kamush and thermo-regulated using a Lauda thermostat. NMR was recorded on Bruker advance 400 spectrometer. Purification was performed on a Buchi Pure Chromatography system.

Analytical HPLC was recorded on an Hitachi liquid chromatograph (Oven 5310, 30°C; Pump 5160; DAD detector 5430) equipped with a C18 Acclaim column (4.6mm×250mm, 5µm, 120Å). Detection wavelength was 240nm or 280nm and flow rate 0.5mL/min. Gradient elution used (A) water/0.1% TFA; (B) methanol according Method A: (Solvents A/B: 0 to 5 minutes isocratic at 95/5; 5 to 25 minutes gradient to 5/95; 25 to 35 minutes isocratic at 5/95; 35 to 45 minutes gradient to 95/5; 45 to 50 minutes 95/5) or Method B (Solvents A/B: 0 to 5 minutes isocratic at 95/5; 5 to 10 minutes gradient to 75/25; 10 to 50 minutes gradient to 40/60; 50 to 65 minutes gradient to 5/95; 65 to 70 minutes isocratic at 5/95; 70 to 80 minutes gradient to 95/5).

Reactions kinetics were carried out in a THT Micro Reaction Calorimeter, which allows continuous monitoring of the instantaneous enthalpy exchanged by the reactor. The sample vessel consists in a 1.5 ml septum-cap vial equipped with a magnetic stirrer. The system operates by comparing the heat exchanged (q) in the reaction sample vessel compared with that from a reference compartment.

Fraction conversion is given by the:

$$\%(t) = \frac{\int_0^t q.dt}{\int_0^\infty q.dt}$$

Integrations were determined using a house build python programme using the trapezoid method. Time constant of the system was measured to $50s^{-1}$ and was not used for correction. A typical example for heat flow (mW) versus time is given below (figure left) ($C_{proparyl\ alcohol}$= 0.5M, $C_{benzyl\ azide}$ = 0.5M Catalyst: 1mol-%). The integration method affords the following conversion versus time curve (Figure right). Conversion determined from the heat flow integration method was compared to conversions measured by NMR.

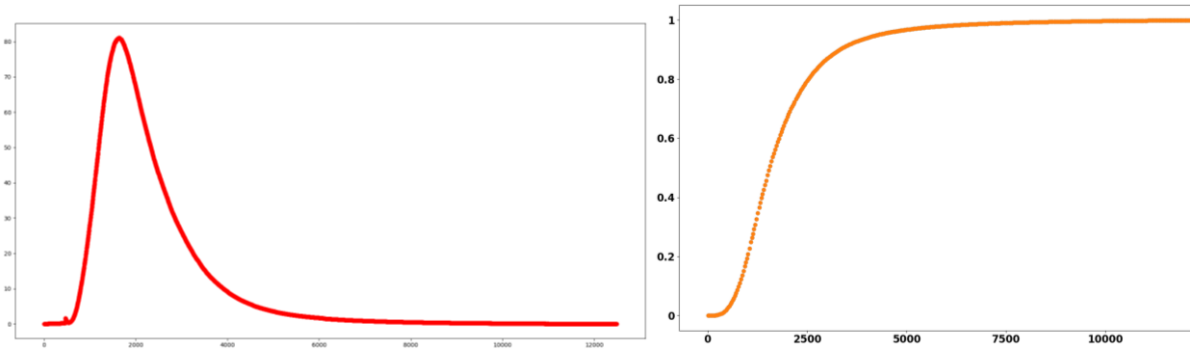

2.General procedures

2.1- Synthesis of alkyne substituted peptoids (General procedure A)

The synthesis of the *meta*-arylopeptoid hexamer was performed according to the submonomer synthesis using Rink amide resin (100-200 mesh, loading 0.54 mmol/g, novabiochem, 8.55001.0005, Batch no. S7816901016).

1-For 100mg of resin, swelling: 2 ml of CH_2Cl_2 at RT for 10 min

2- Fmoc Deprotection: resin was washed with NMP (N-Methyl-2-pyrrolidone) (5x2ml), then piperidine/NMP 1:4 (1ml) was added and agitated for 2 min and then drained. Further piperidine/NMP 1:4 (1.0 mL) was added and the resin was agitated for 15 min, drained and washed with NMP (5x2 mL) and CH_2Cl_2 (5x2 mL)

3- 3-chloromethylbenzoylchloride (3 equiv. per mmol loading) and DIPEA (6 equiv. per mmol loading) dissolved in 1 mL CH_2Cl_2 were added at RT, shaken 10 minutes, then washed with CH_2Cl_2 (5x2ml), then with DMSO (5x2ml).

4- Isopropyl or propargyl amine (20 equiv per mmol loading) dissolved in 0.5 mL of DMSO was added. The temperature was raised to 50°C for 1h then the resin was washed with DMSO (5x2ml), then with CH_2CL_2 (5x2ml).

Steps 2 and 3 were repeated to grow the targeted arylopeptoid oligomer until the expected sequence length.

2.2. Click reaction on support: general procedure B.

Resin-bound arylopeptoid obtained from 100 mg of resin were introduced in a reactor containing 1 mL of CH_2Cl_2/MeOH mixture (v/v = 8:2). Azides (4.0 equiv. per alkyne) and 5 mol-% of catalyst per alkyne were added. The reactor is gently shaken for 3h at 50°C. The resin was washed with MeOH (5x2ml) at 50°C and then with CH_2Cl_2 (5x2ml) at room temperature. Cleavage was performed by gently shaking in a 1 mL solution of TFA/TIS/H_2O (95:2.5:2.5) for 10 min at RT. The solution was drained out and evaporated to dryness under reduced pressure. The foam was dissolved in a minimum amount of CH_2Cl_2 (≈0.4 mL), then 30 volumes (≈ 12 mL) of diethyl ether were added. The white precipitate formed was isolated after centrifugation.

3.Synthesis and Characterization data of arylopeptoid trimers

*3.1. meta-arylopeptoid trimer **III-3(Alk$_2$).***

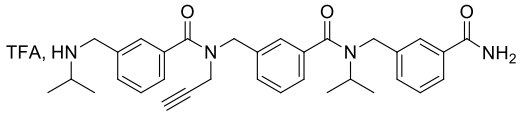

Trimer **III-3(Alk$_2$)** was synthesised according general procedure A using 50 mg of RA resin (0.027mmol).

m_{crude}= 30 mg (purity 85%), crude yield 170%

m_{pure}= 17 mg (purity 100%), isolated yield 98%

HRMS (TOF MS ES+): *m/z* calcd for $C_{33}H_{39}N_4O_3$ $[M+H]^+$: 539.30167; found: 539.3013 (-0.74 ppm).

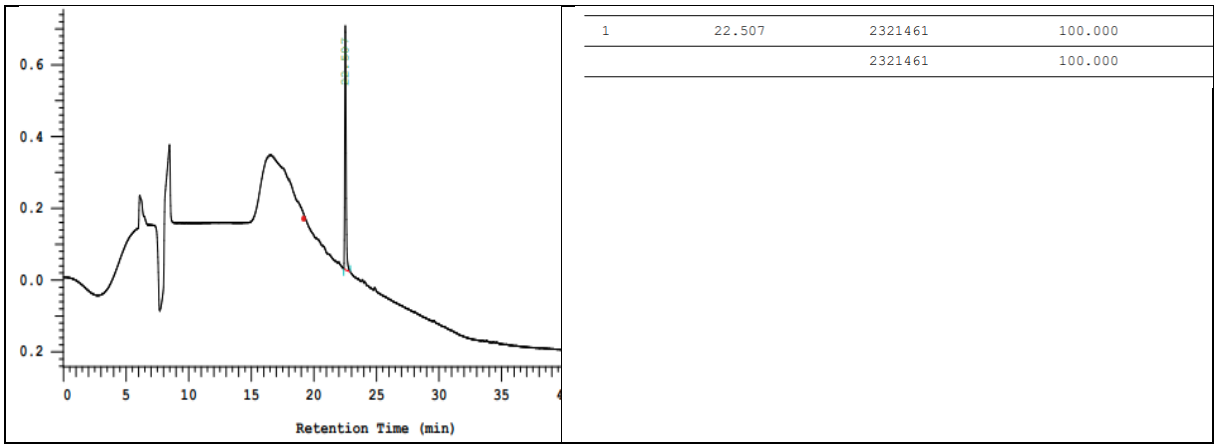

1	22.507	2321461	100.000
		2321461	100.000

*Figure S10 HPLC chromatogram of purified **III-3(Alk$_2$)**.*

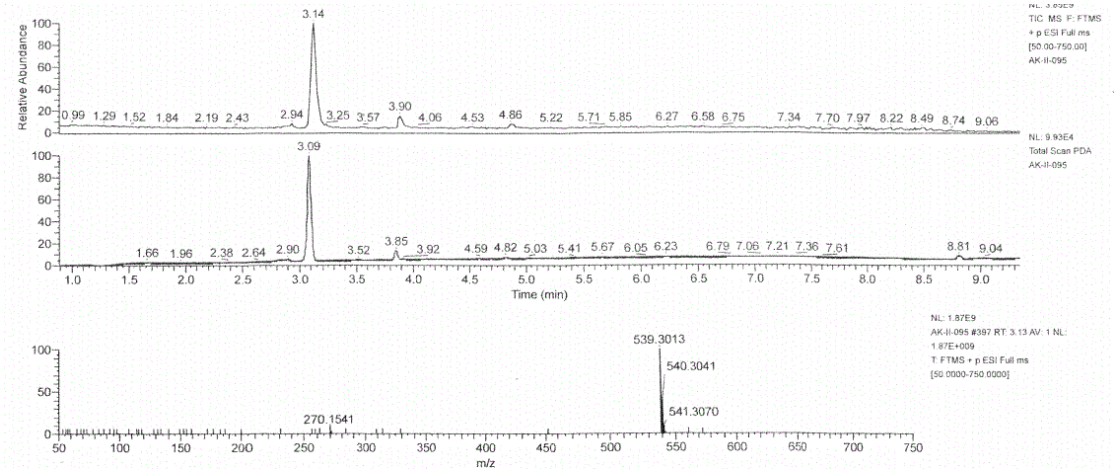

*Figure S11 LCMS spectra of **III-3(Alk$_2$)**.*

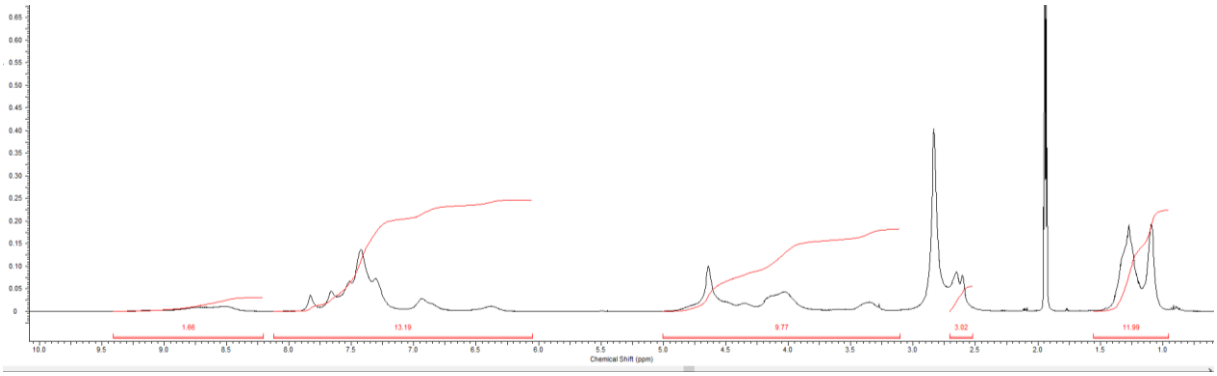

*Figure S12 ^{1}H-NMR spectra in CD_3CN of **III-3(Alk$_2$)**.*

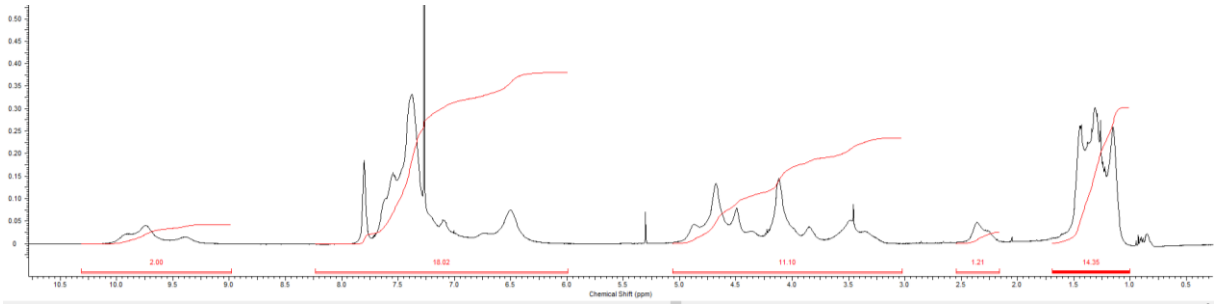

*Figure S13 ^{1}H-NMR spectra in $CDCl_3$ of **III-3(Alk$_2$)**.*

*3.2. meta-arylopeptoid trimer **III-3(a$_2$).***

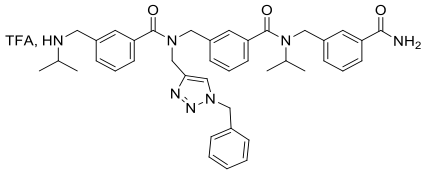

Trimer **III-3(a$_2$)** was synthesised according general procedure A then general procedure B using 50 mg of RA resin (0.027mmol).

m_{crude}= 33 mg (purity 85%), 155% crude yield
m_{pure}= 20.8 mg (purity 98%), 98% isolated yield
HRMS (TOF MS ES+): *m/z* calcd for $C_{40}H_{46}N_7O_3$ $[M+H]^+$: 672.36566; found: 672.3645 (-1.73 ppm).

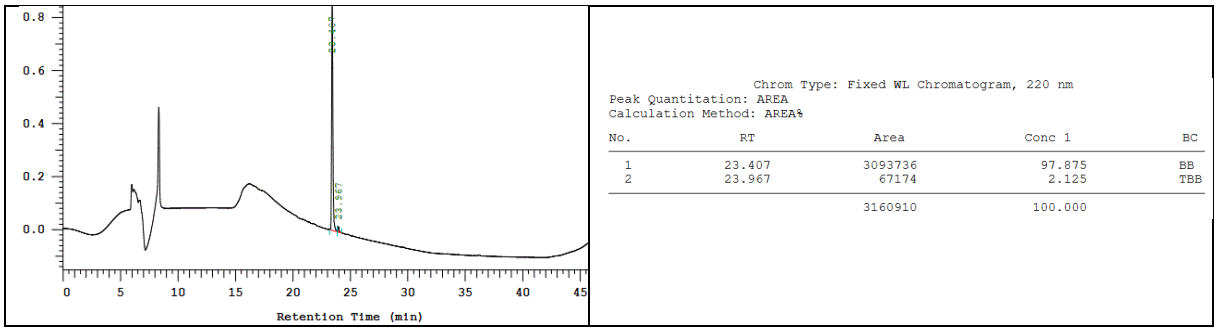

*Figure S14 HPLC chromatogram of purified **III-3(a$_2$).***

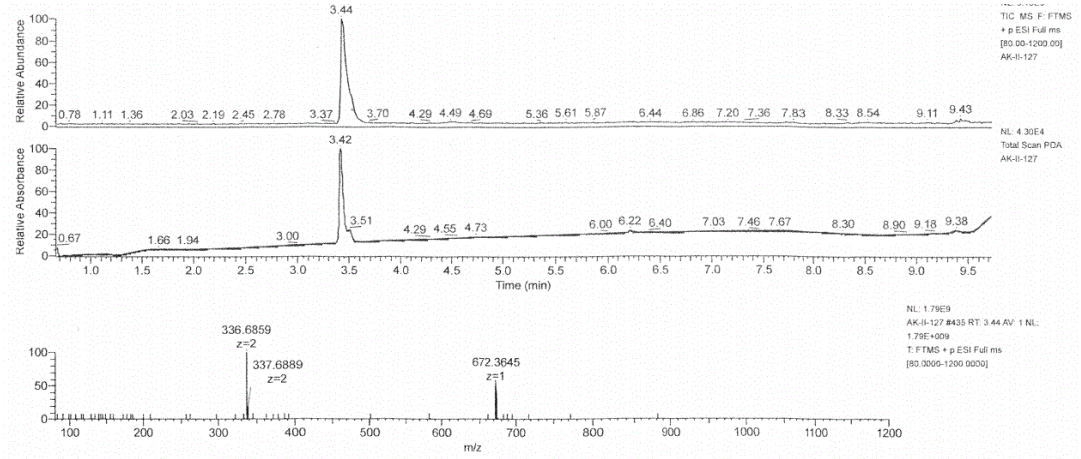

*Figure S15 LCMS spectra of **III-3(a$_2$).***

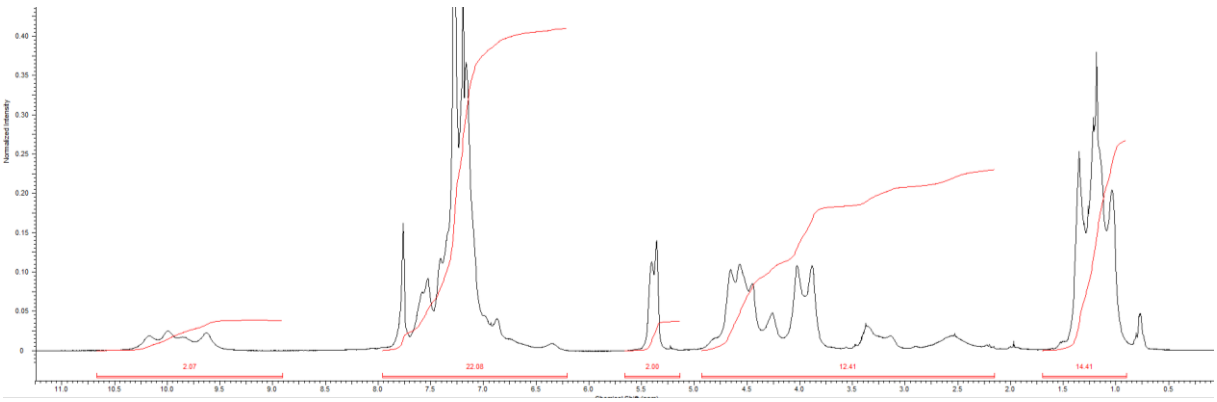

*Figure S16 ^{1}H-NMR spectra in $CDCl_3$ of **III-3(a$_2$).***

*3.3. meta-arylopeptoid trimer, **III-3(b_2).***

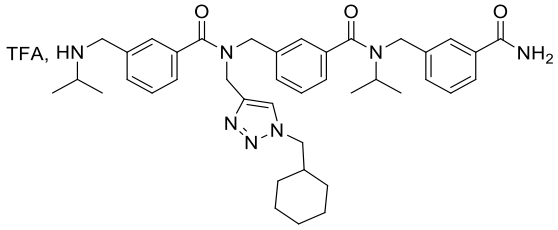

Trimer **III-3(b_2)** was synthesised according general procedure A then general procedure B using 100 mg of RA resin (0.054 mmol).

m_{crude}= 46.2 mg (purity 83%), crude yield 112%
m_{pure}= 30 mg (purity 85%), isolated yield 85%
HRMS (TOF MS ES+): *m/z* calcd for $C_{40}H_{52}N_7O_3$ $[M+H]^+$: 678.41261; found: 678.4128 (0.24 ppm).

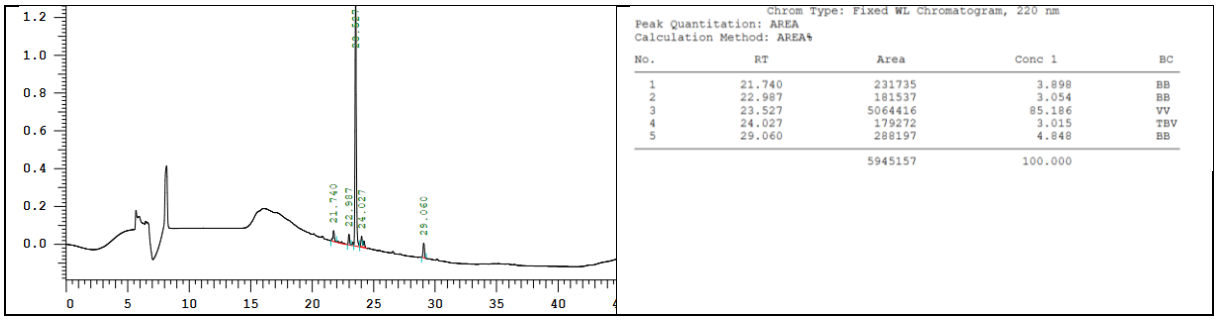

*Figure S17 HPLC chromatogram of purified **III-3(b_2)***

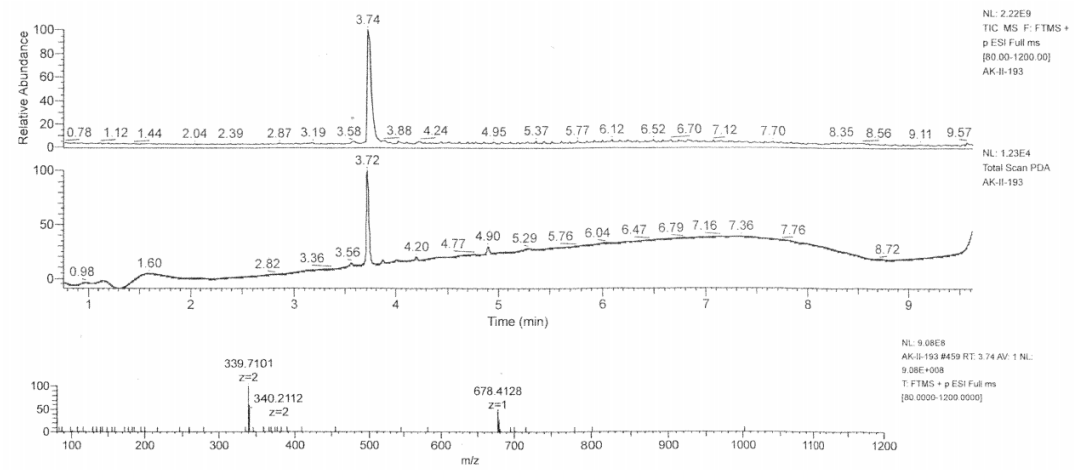

*Figure S18 LCMS spectra of **III-3(b_2)***

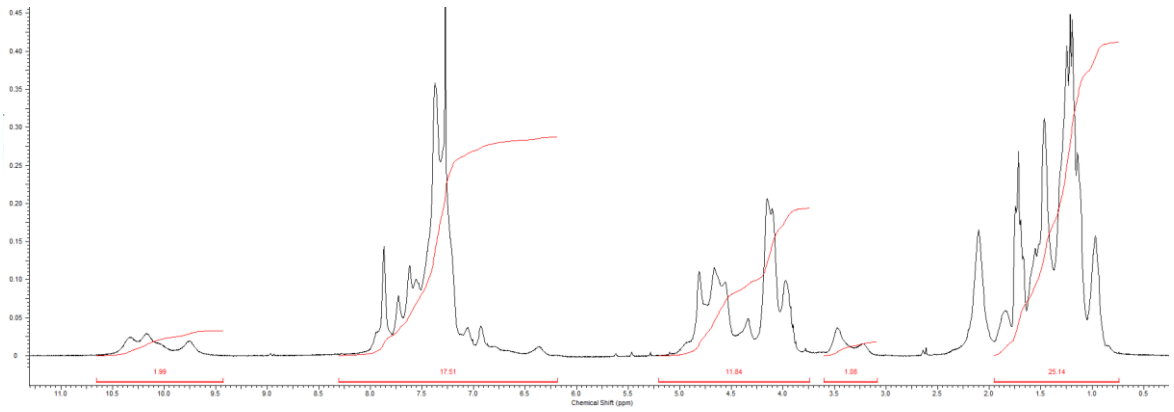

*Figure S19 ^{1}H-NMR spectra in $CDCl_3$ of **III-3(b_2).***

3.4.meta-arylopeptoid trimer, ***III-3(c_2).***

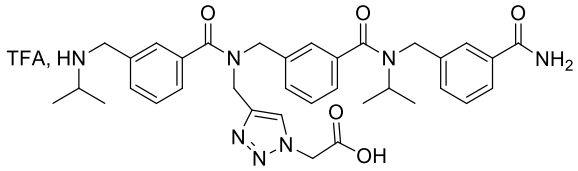

Trimer **III-3(c_2)** was synthesised according to general procedure A then general procedure B using 50 mg of RA resin (0.027mmol). After cleavage from the resin, the acid group was deprotected by treatment in 3ml TFA/CH_2Cl_2 (2/8) solution at room temperature overnight.

m_{crude}= 30mg (purity 85%), crude yield 147%
m_{pure}= 20 mg (purity 96%), isolated yield 97%
HRMS (TOF MS ES+): *m/z* calcd for $C_{35}H_{42}N_7O_5$ $[M+H]^+$: 640.32419; found: 640.3235 (-1.1 ppm).

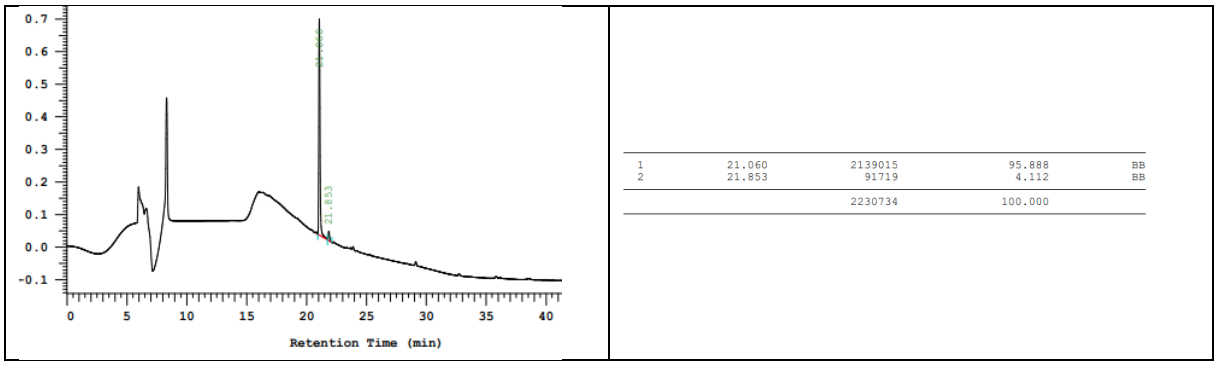

*Figure S20 HPLC chromatogram of purified **III-3(c_2)***

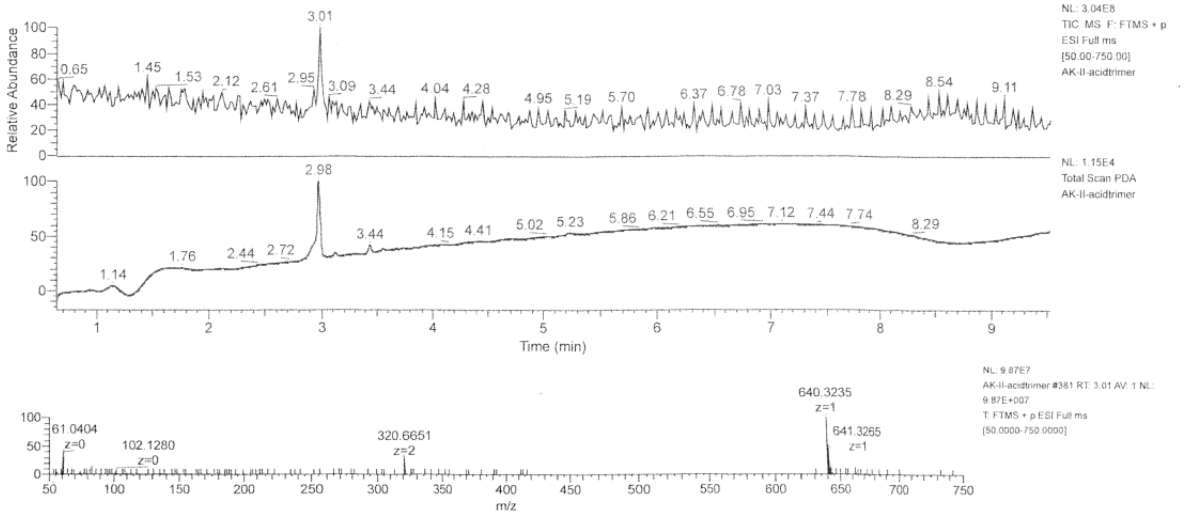

*Figure S21 LCMS spectra of **III-3(c_2)***

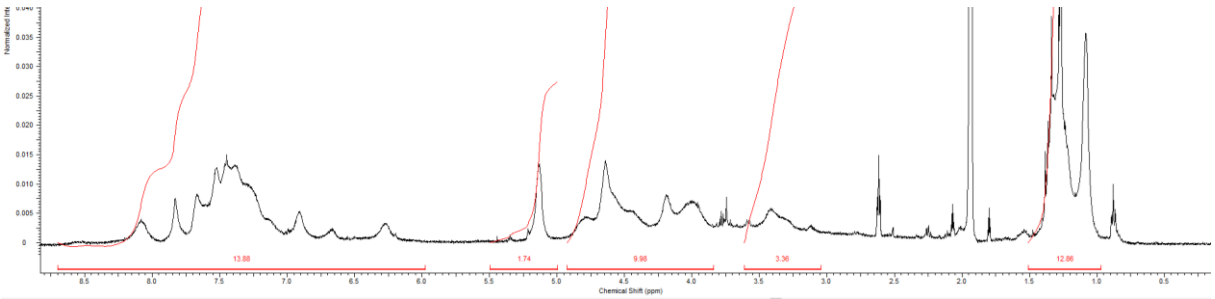

*Figure S22 ^{1}H-NMR spectra in CD_3CN of **III-3(c_2).***

3.5. *meta*-arylopeptoid trimer, ***III-3(d$_2$)***.

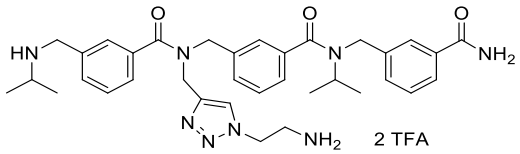

Trimer **III-3(d$_2$)** was synthesised according general procedure A then general procedure B using 250 mg of RA resin (0.135mmol).

m_{crude}= 139 mg (purity 87%), crude yield 120%
m_{pure}= 98 mg (purity 97%), isolated yield 85%
HRMS (TOF MS ES+): *m/z* calcd for $C_{35}H_{45}N_8O_3$ $[M+H]^+$: 625.36091; found: 625.3611 (0.27 ppm).

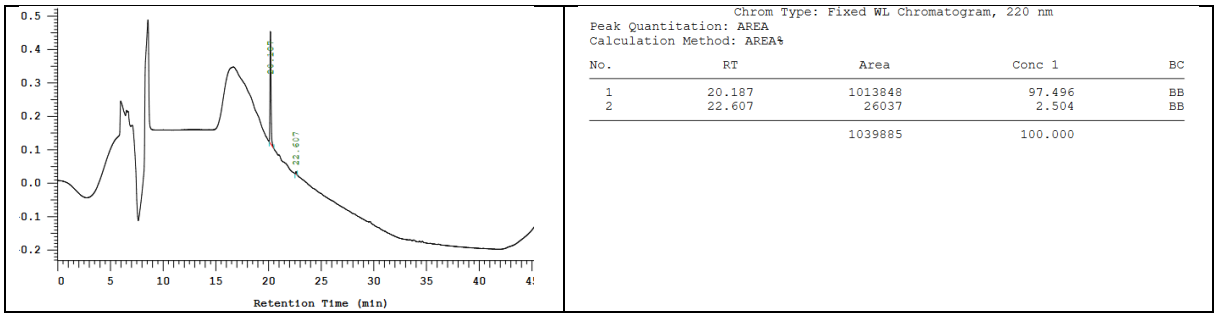

*Figure S23 HPLC chromatogram of purified **III-3(d$_2$)**.*

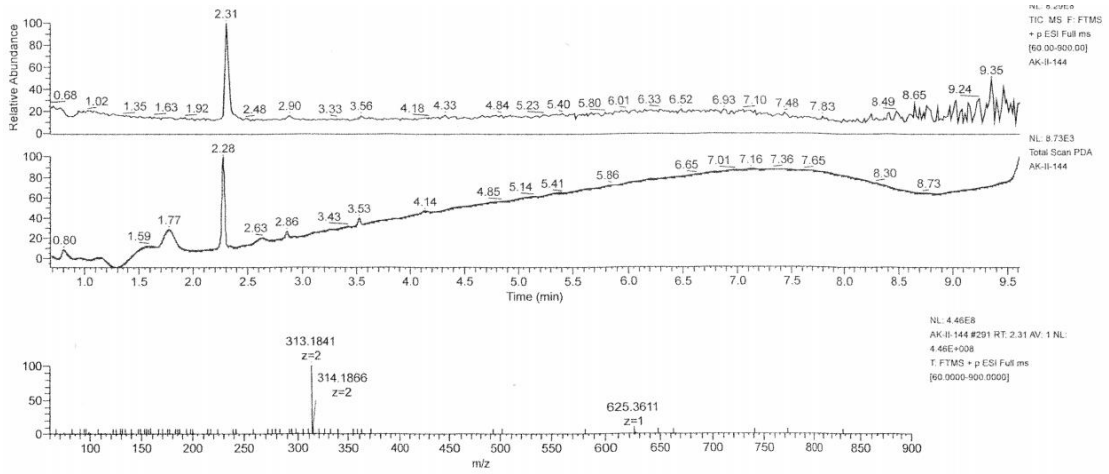

*Figure S24 LCMS spectra of **III-3(d$_2$)**.*

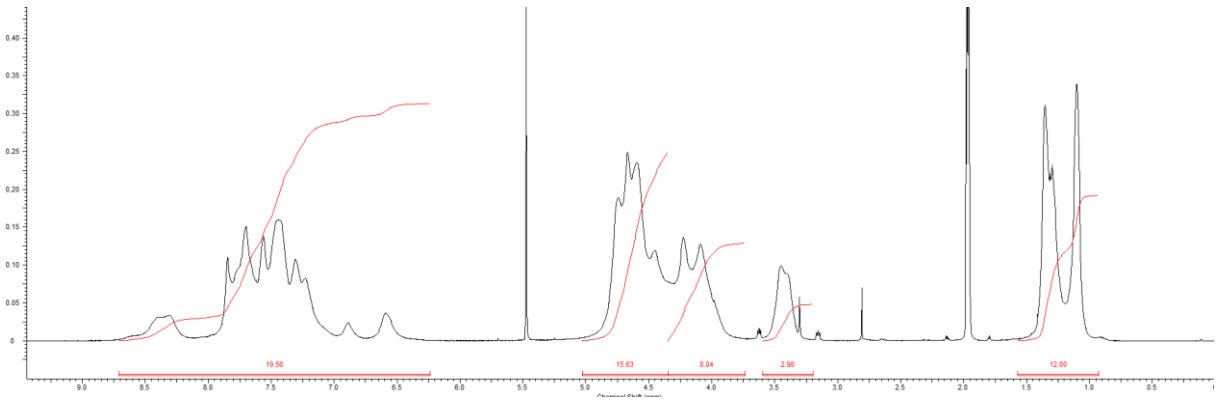

*Figure S25 ^{1}H-NMR spectra in CD_3CN of **III-3(d$_2$)**.*

*3.6. meta-arylopeptoid trimer, **III-3(e$_2$).***

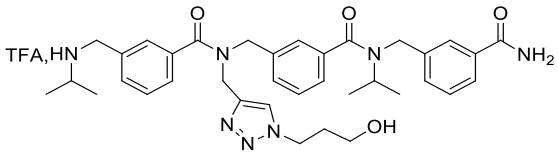

Trimer **III-3(e$_2$)** was synthesised according general procedure A then general procedure B using 100 mg of RA resin (0.054 mmol).

m_{crude}= 72 mg (purity 80%), crude yield 120%
m_{pure}= 30 mg (purity 99%), isolated yield 90%
HRMS (TOF MS ES+): *m/z* calcd for $C_{36}H_{46}N_7O_4$ $[M+H]^+$: 640.36058; found: 640.3593 (-1.98 ppm).

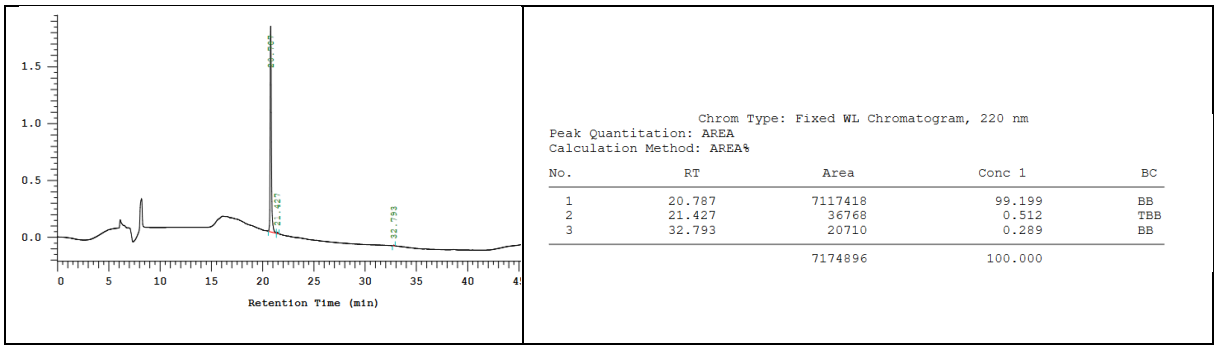

*Figure S26 HPLC chromatogram of purified **III-3(e$_2$)***

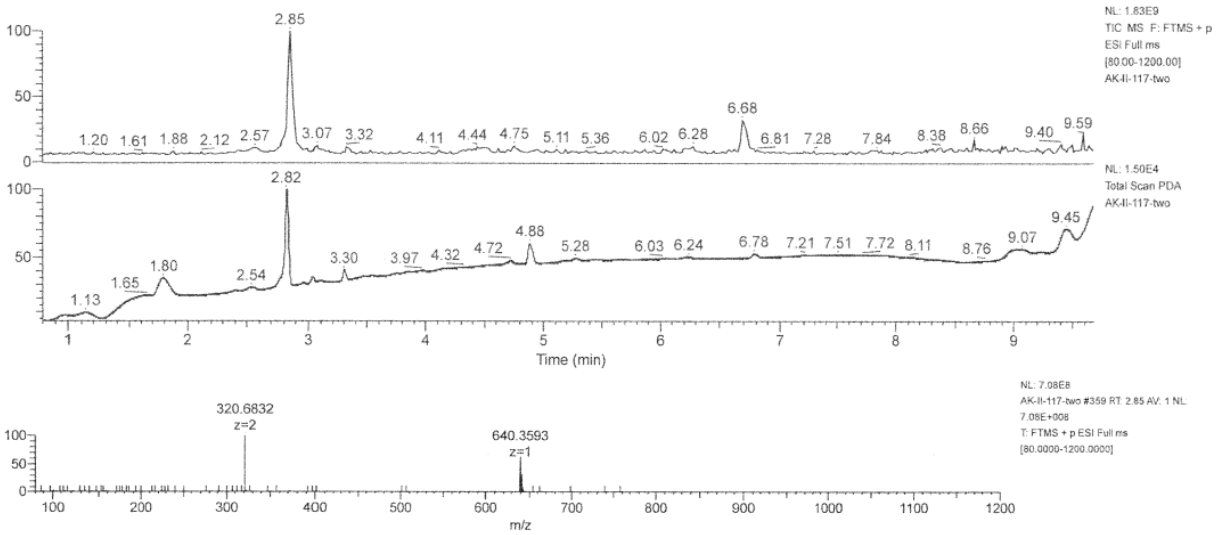

*Figure S27 LCMS spectra of **III-3(e$_2$).***

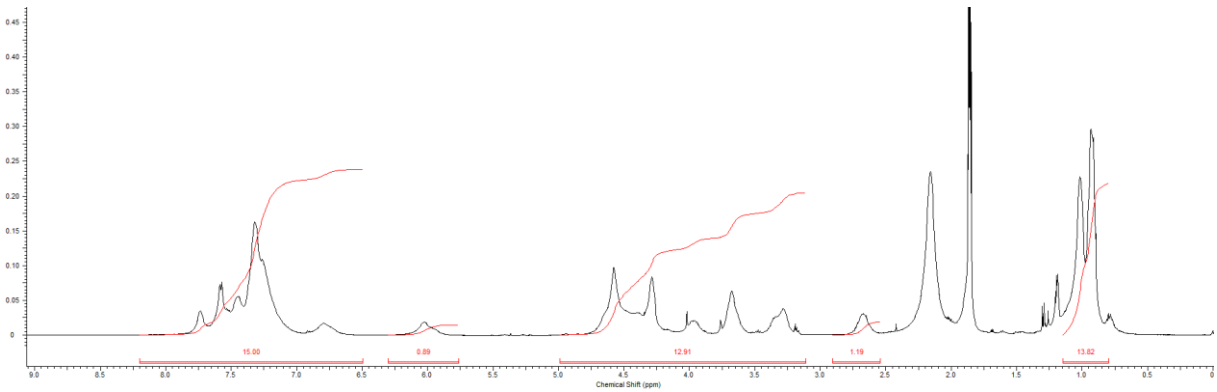

*Figure S28 ^{1}H-NMR spectra in CD_3CN of **III-3(e$_2$).***

4. Synthesis and Characterization data of arylopeptoid tetramers.

*4.1. meta-arylopeptoid tetramer, **II-4-(Alk$_{2,4}$)**.*

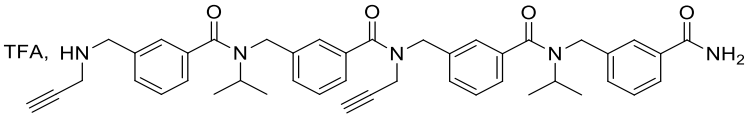

Tetramer **II-4-(Alk$_{2,4}$)** was synthesised according to general procedure A using 100 mg of RA resin (0.054 mmol), then cleavage by gently shaking a solution of TFA/TIS/H_2O (95:2.5:2.5, 1mL) for 10 min at RT.

m_{crude}= 50mg (purity 80%), crude yield 112%
m_{pure}= 32 mg (purity 96%), isolated yield 72%
HRMS (TOF MS ES+): *m/z* calcd for $C_{44}H_{48}N_5O_4$ $[M+H]^+$: 710.37008; found: 710.3702 (0.14 ppm).

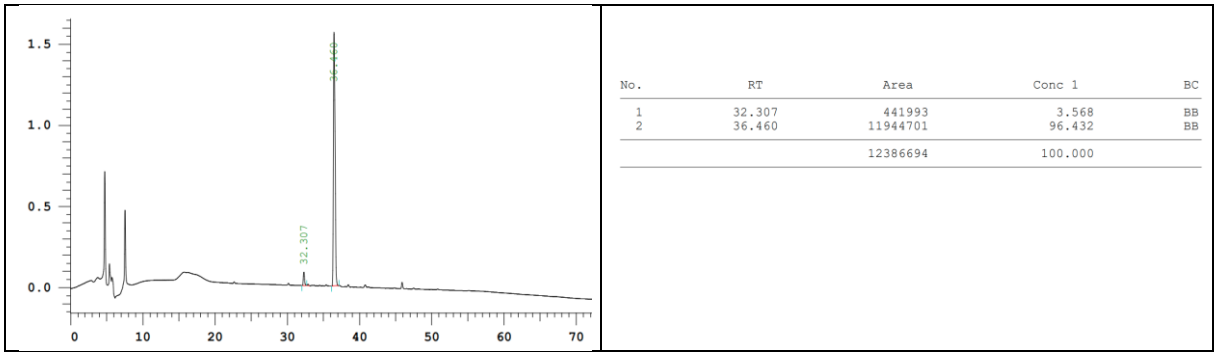

*Figure S29 HPLC chromatogram of purified **II-4-(Alk$_{2,4}$)**.*

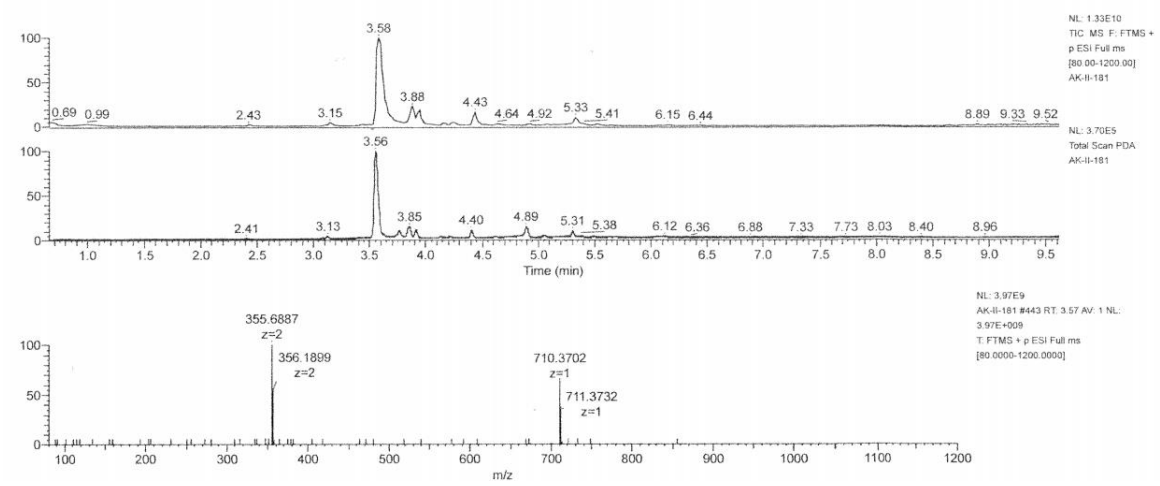

*Figure S30 LCMS spectra of **II-4-(Alk$_{2,4}$)**.*

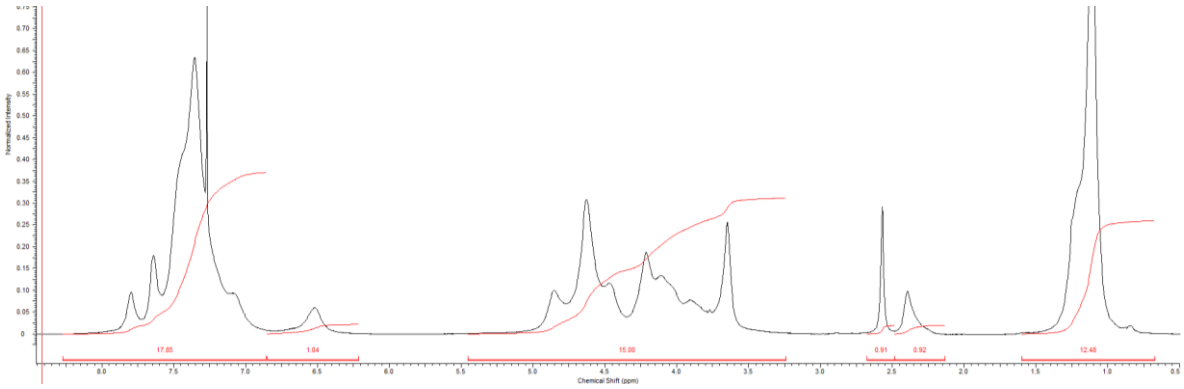

*Figure S31 ^{1}H-NMR spectra in CD_3Cl_3 of **II-4-(Alk$_{2,4}$)**.*

4.2. Homo clicked arylopeptoids

*4.2.1. meta-arylopeptoid tetramer, **III-4($a_{2,4}$).***

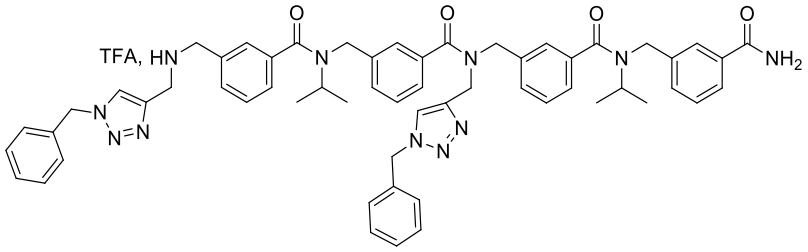

Tetramer **III-4($a_{2,4}$)** was synthesised according general procedure A then general procedure B using 100 mg of RA resin (0.054 mmol)

m_{crude}= 68 mg (purity 82%), crude yield 115%
m_{pure}= 44 mg (purity 87%), isolated yield 85%
HRMS (TOF MS ES+): *m/z* calcd for $C_{58}H_{62}N_{11}O_4$ $[M+H]^+$: 976.49808; found: 976.4974 (-0.72 ppm).

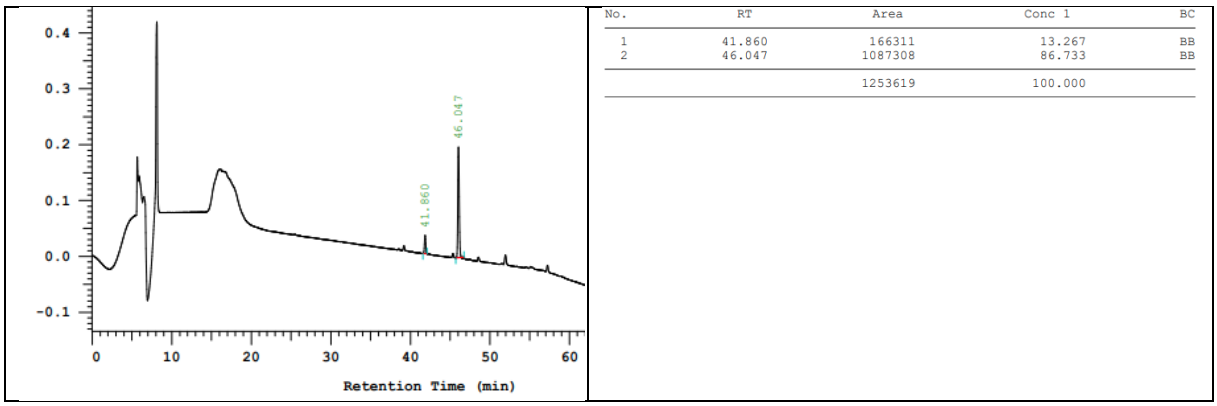

No.	RT	Area	Conc 1	BC
1	41.860	166311	13.267	BB
2	46.047	1087308	86.733	BB
		1253619	100.000	

*Figure S32 HPLC chromatogram of purified **III-4($a_{2,4}$).***

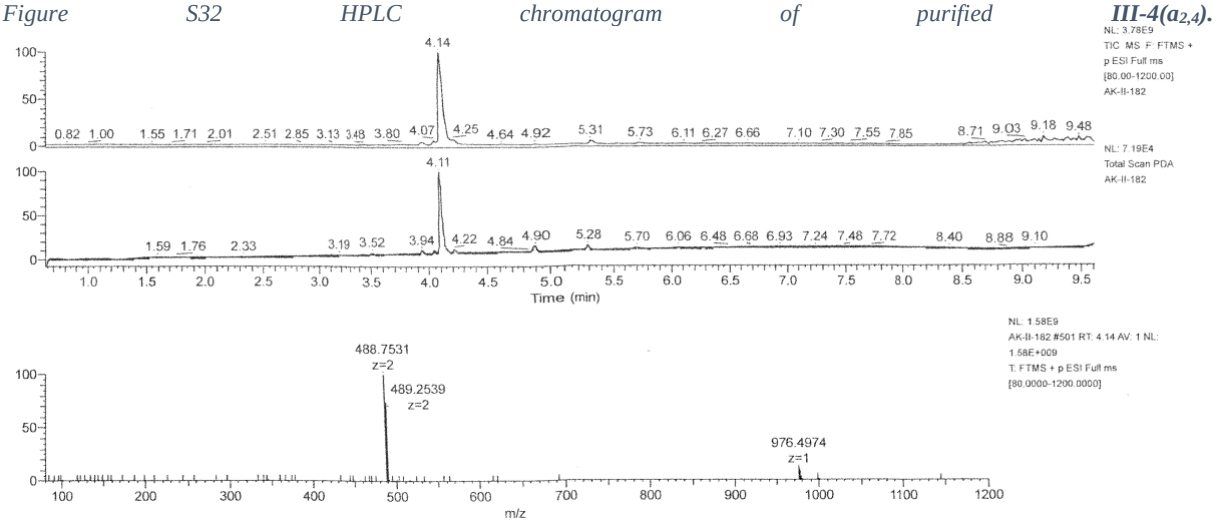

*Figure S33 LCMS spectra of **III-4($a_{2,4}$).***

4.2.2. meta-arylopeptoid tetramer, ***III-4($b_{2,4}$)***

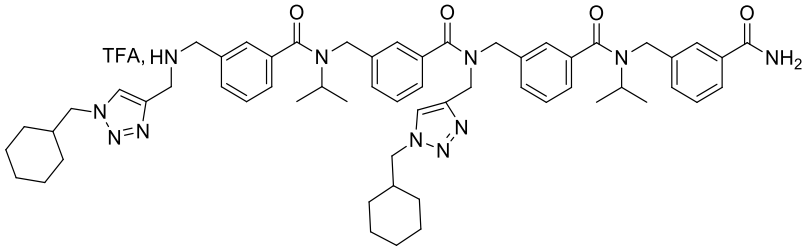

Tetramer **III-4($b_{2,4}$)** was synthesised according general procedure A then general procedure B using 100 mg of RA resin (0.054 mmol)

m_{crude}= 73 mg (purity 85%), crude yield 124%

m_{pure}= 40 mg (purity 95%), isolated yield 75%

HRMS (TOF MS ES+): *m/z* calcd for $C_{58}H_{74}N_{11}O_4$ $[M+H]^+$: 988.59198; found: 988.5907 (-1.29 ppm).

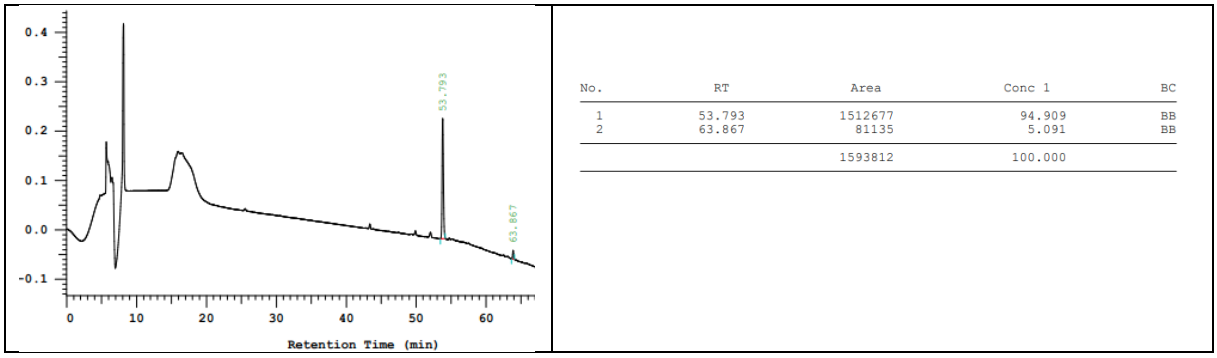

*Figure S34 HPLC chromatogram of purified **III-4($b_{2,4}$)**.*

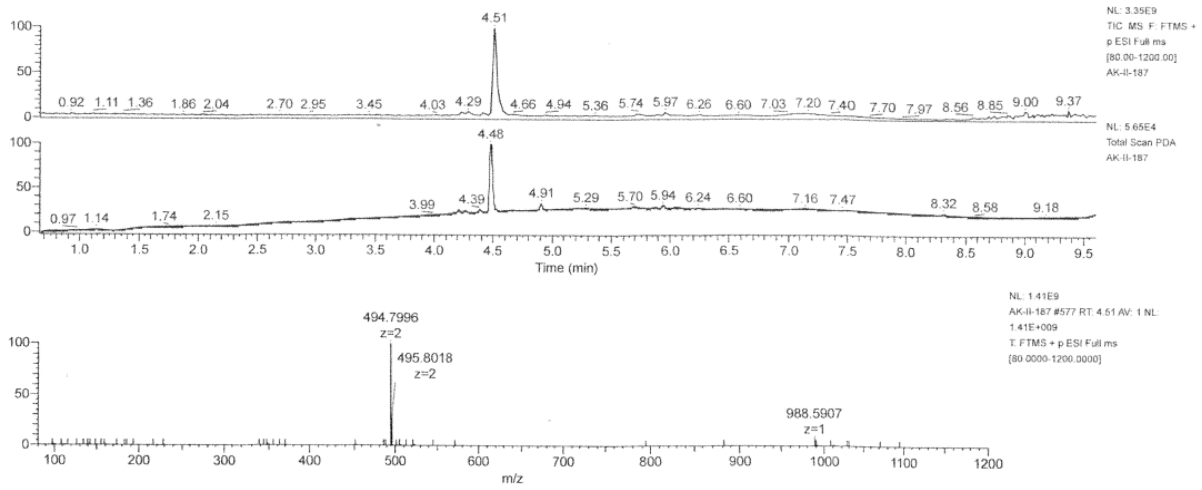

*Figure S35 LCMS spectra of **III-4($b_{2,4}$)**.*

4.2.3. meta-arylopeptoid tetramer, ***III-4($c_{2,4}$)***.

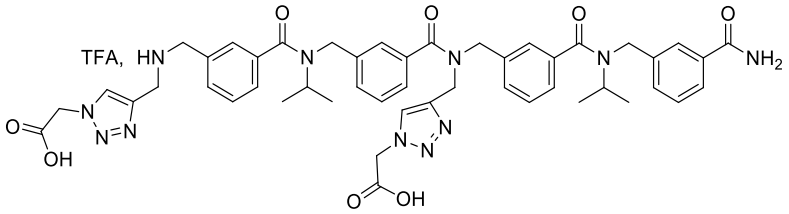

Tetramer **III-4($c_{2,4}$)** was synthesised according general procedure A then general procedure B using 100 mg of RA resin (0.054 mmol).

m_{crude}= 73mg (purity 78%), 131% crude yield
m_{pure} = 44mg (purity 81%), 85% isolated yield
HRMS (TOF MS ES+): *m/z* calcd for $C_{48}H_{55}N_{11}O_8$ $[M+2H]^{2+}$: 456.71121; found: 456.7113 (0.22 ppm).

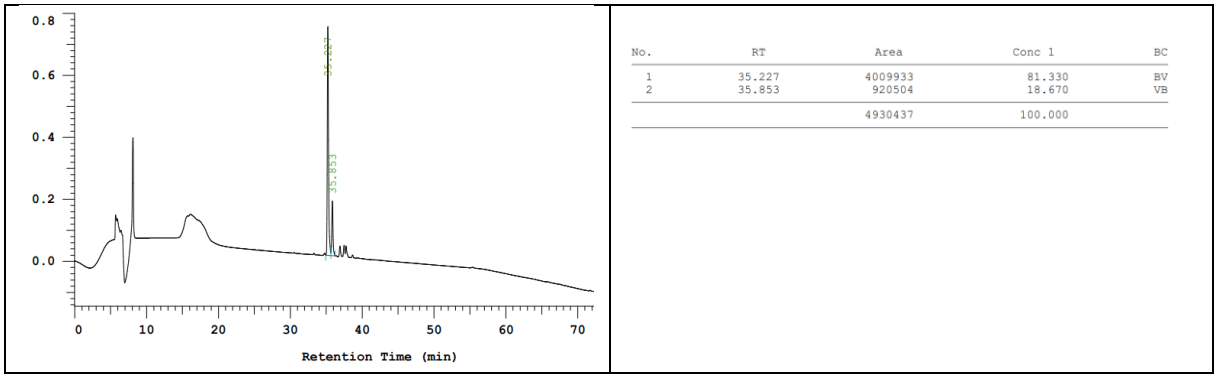

*Figure S36 HPLC chromatogram of purified **III-4($c_{2,4}$)**.*

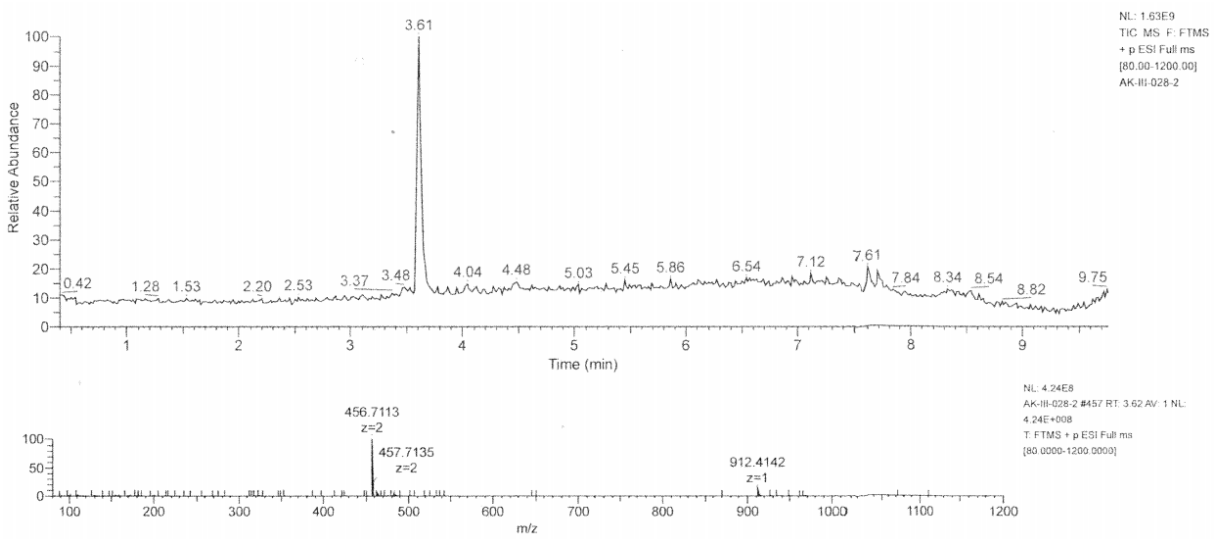

*Figure S37 LCMS spectra of **III-4($c_{2,4}$)**.*

4.2.4. meta-arylopeptoid tetramer, III-4($d_{2,4}$).

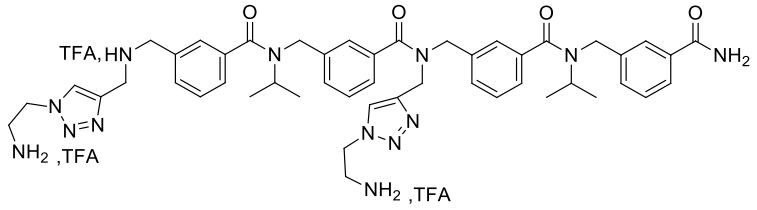

Tetramer **III-4($d_{2,4}$)** was synthesised according general procedure A then general procedure B using 100 mg of RA resin (0.054 mmol)

m_{crude}= 73mg (purity 80%), crude yield 110%
m_{pure}= 36mg (purity 95%), isolated yield 77%
HRMS (TOF MS ES+): *m/z* calcd for $C_{48}H_{62}N_{13}O_4$ $[M+3H]^{3+}$: 294.83438; found: 294. 8345 (0.33 ppm).

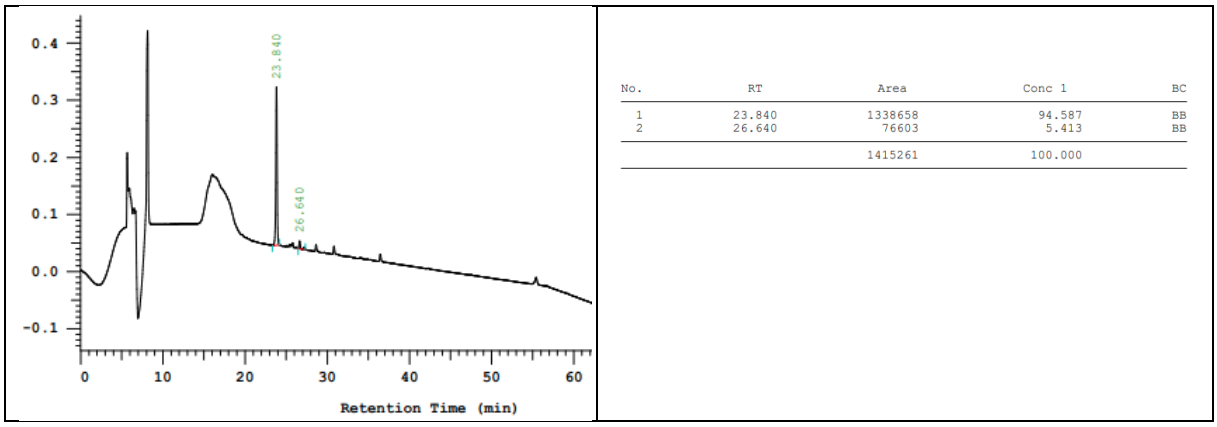

No.	RT	Area	Conc 1	BC
1	23.840	1338658	94.587	BB
2	26.640	76603	5.413	BB
		1415261	100.000	

Figure S38 HPLC chromatogram of purified ***III-4(d$_{2,4}$).***

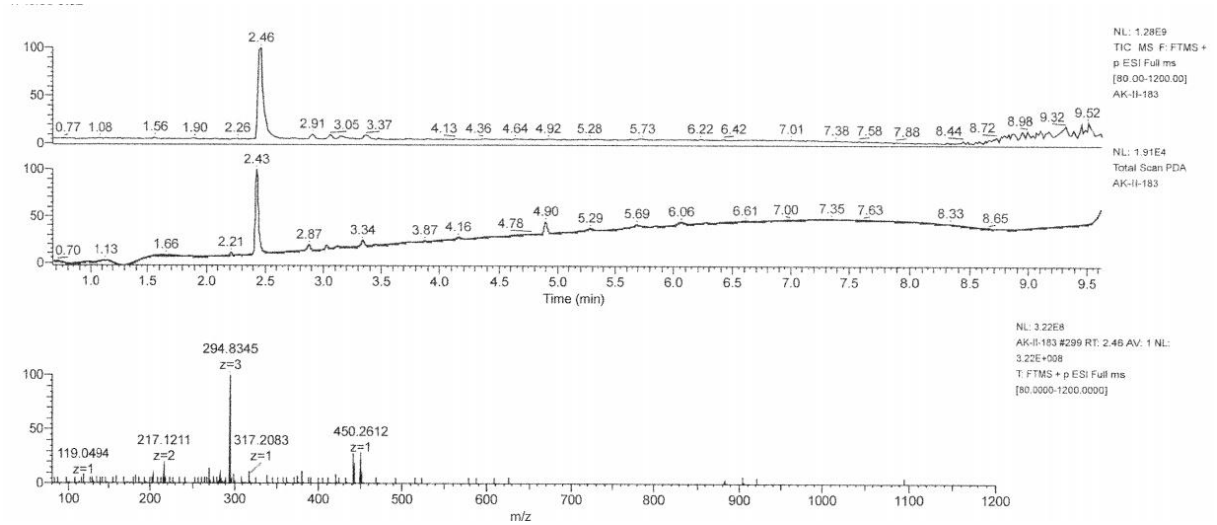

Figure S39 LCMS spectra of ***III-4(d$_{2,4}$).***

4.2.5. meta-arylopeptoid tetramer, ***III-4(e$_{2,4}$).***

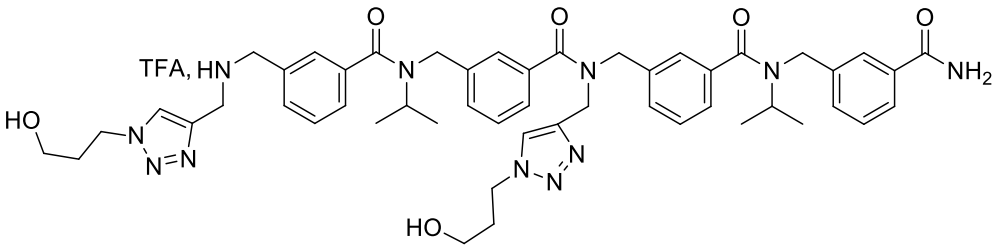

Tetramer **III-4(e$_{2,4}$)** was synthesised according general procedure A then general procedure B using 125 mg of RA resin (0.0775 mmol)

m_{crude}= 101 mg (purity 85%), crude yield 148%

m_{pure}= 70 mg (purity 97 %), isolated yield 98%

HRMS (TOF MS ES+): *m/z* calcd for $C_{50}H_{62}N_{11}O_6$ $[M+H]^+$: 912.48791; found: 912.4866 (-1.46 ppm).

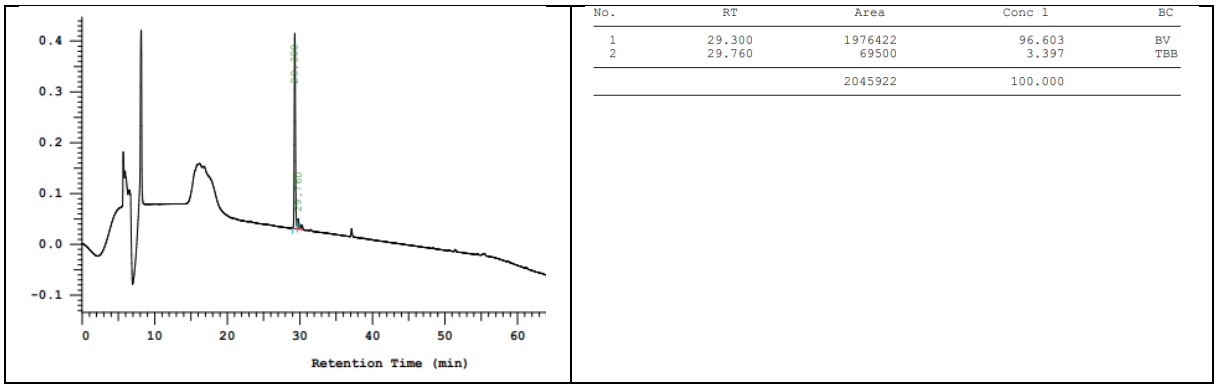

No.	RT	Area	Conc 1	BC
1	29.300	1976422	96.603	BV
2	29.760	69500	3.397	TBB
		2045922	100.000	

Figure S40 HPLC chromatogram of purified ***III-4(e2,4)***

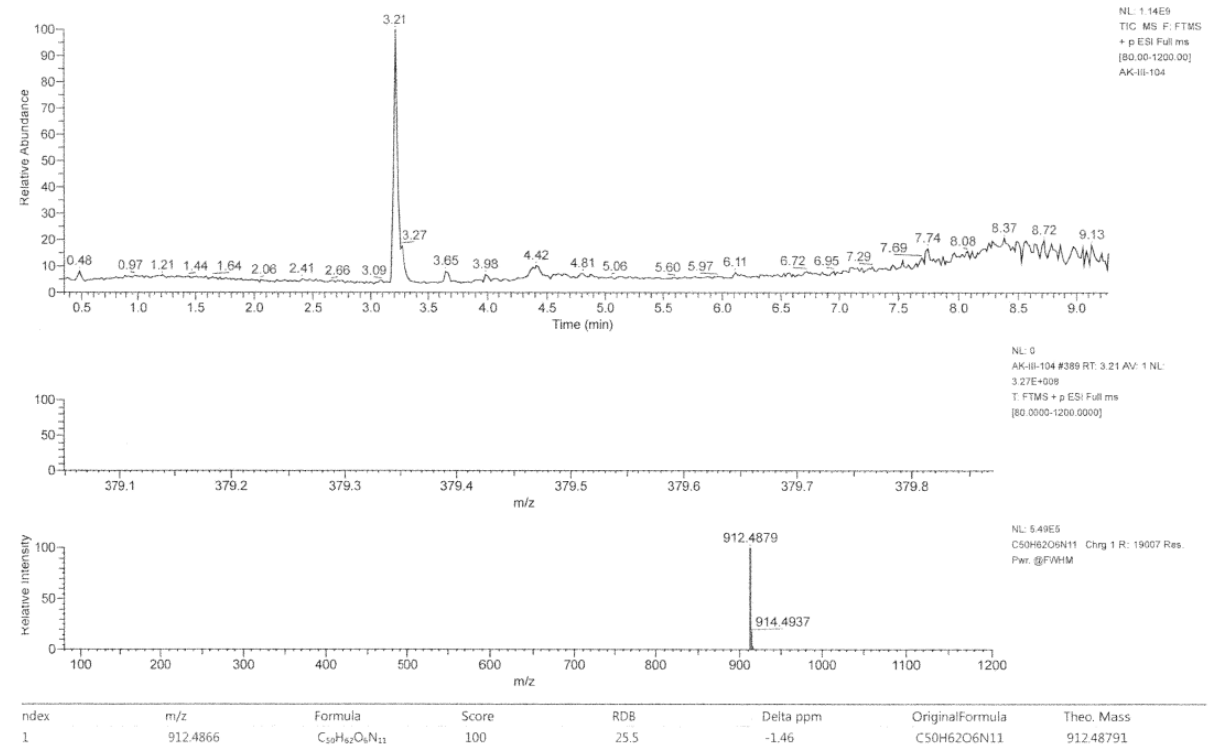

ndex	m/z	Formula	Score	RDB	Delta ppm	OriginalFormula	Theo. Mass
1	912.4866	$C_{50}H_{62}O_6N_{11}$	100	25.5	-1.46	C50H62O6N11	912.48791

Figure S41 LCMS spectra of ***III-4(e2,4)***

4.3. Combinatorial on arylopeptoid tetramers

4.3.4. meta-arylopeptoid tetramer, III-4(a,b)(2,4).

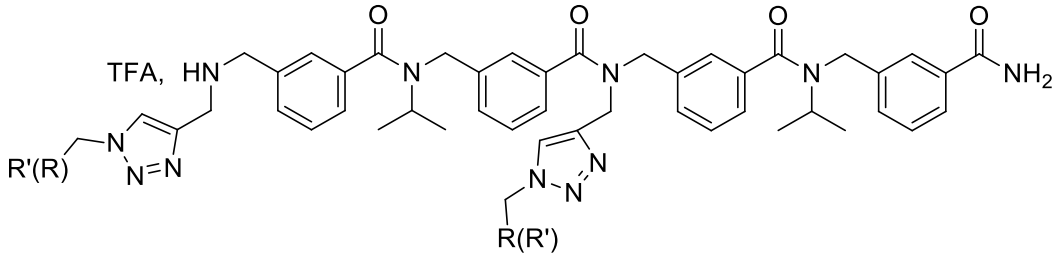

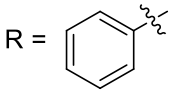

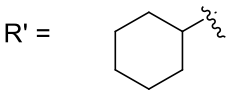

Tetramer **III-4(a,b)(2,4)** was synthesised according general procedure A then general procedure B using 100 mg of RA resin (0.054 mmol)

m_{crude}= 74 mg (purity 81%), crude yield 121%
m_{pure}= 50 mg (purity 97 %), isolated yield 82%
LCMS pic at 4.16 min: HRMS (TOF MS ES+): *m/z* calcd for $C_{58}H_{62}N_{11}O_4$ $[M+H]^+$: 976.49808 found: 976.4979 (-0.15 ppm).
LCMS pic at 4.33 min: HRMS (TOF MS ES+): *m/z* calcd for $C_{58}H_{68}N_{11}O_4$ $[M+H]^+$: 982.54503; found: 982.545 (0.02 ppm).
LCMS pic at 4.52 min: HRMS (TOF MS ES+): *m/z* calcd for $C_{58}H_{75}N_{11}O_4$ $[M+2H]^{2+}$: 494.79963; found: 494.8005 (1.84 ppm).

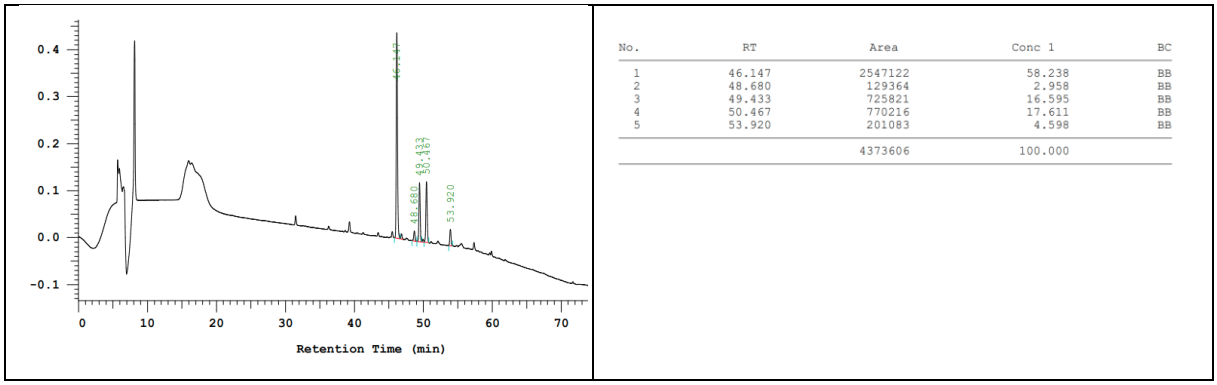

No.	RT	Area	Conc 1	BC
1	46.147	2547122	58.238	BB
2	48.680	129364	2.958	BB
3	49.433	725821	16.595	BB
4	50.467	770216	17.611	BB
5	53.920	201083	4.598	BB
		4373606	100.000	

Figure S42 HPLC chromatogram of purified ***III-4(a,b)(2,4).***

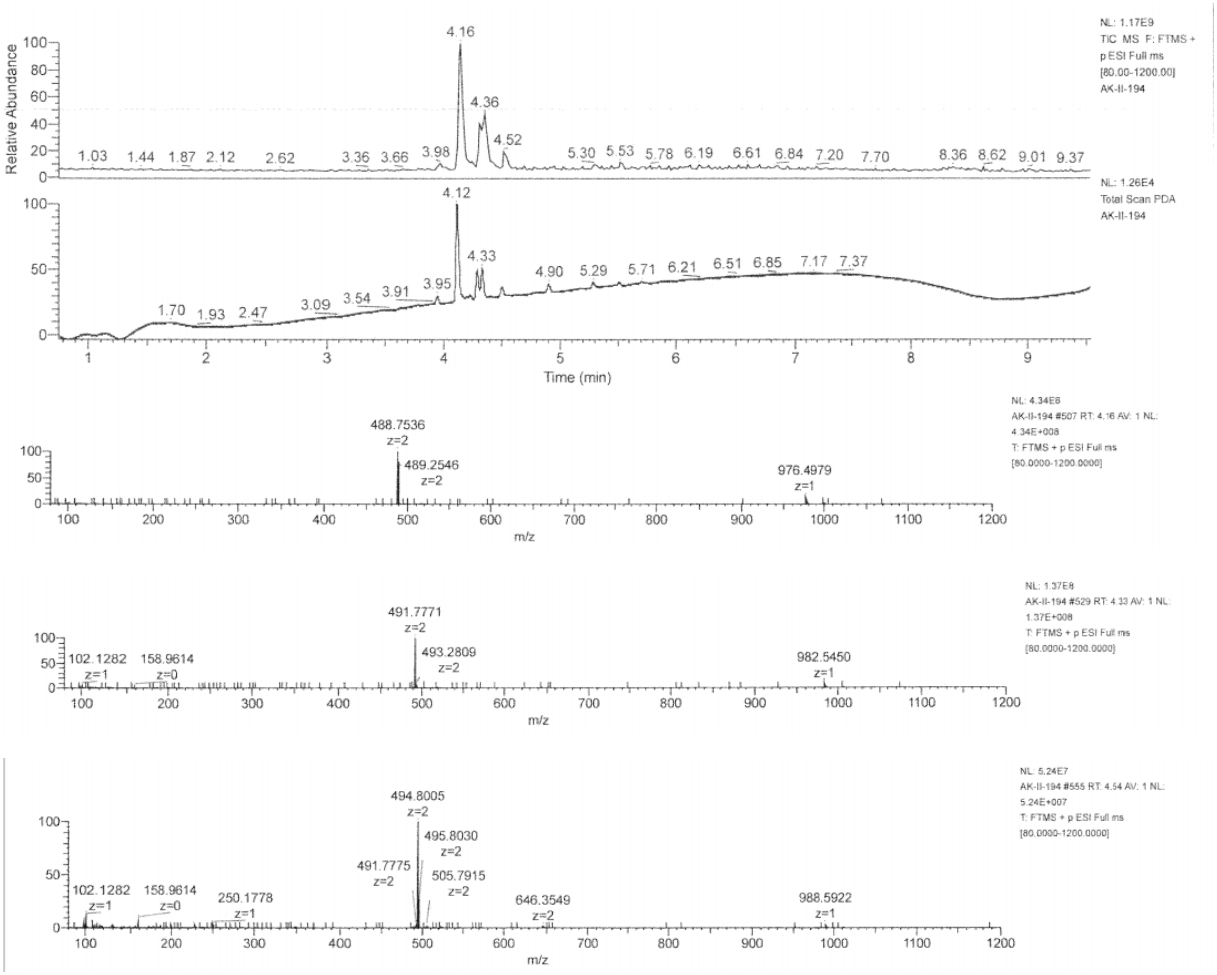

Figure S43 LCMS spectra of ***III-4(a,b)(2,4).***

*4.3.2. meta-arylopeptoid tetramer **III-4(a,d)(2,4)**.*

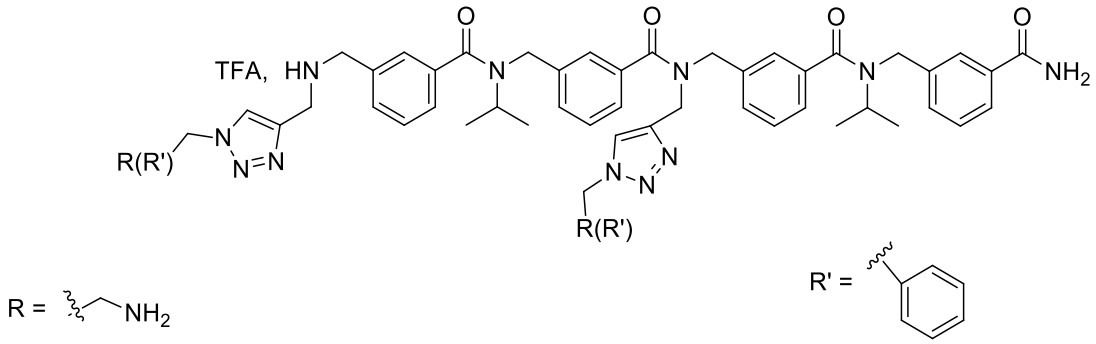

Tetramer **III-4(a,d)(2,4)** was synthesised according general procedure A then general procedure B using 100 mg of RA resin (0.054 mmol)

m_{crude}= 71mg (purity 79%), crude yield 116%
m_{pure}= 46 mg (purity 93%), isolated yield 91%
LCMS pic at 4.12 min: HRMS (TOF MS ES+): *m/z* calcd for $C_{58}H_{63}N_{11}O_4$ $[M+2H]^{2+}$: 488.75268; found: 488.753 (0.58 ppm).
LCMS pic at 3.14 min: HRMS (TOF MS ES+): *m/z* calcd for $C_{53}H_{62}N_{12}O_4$ $[M+2H]^{2+}$: 465.2503; found: 465.2506 (0.67 ppm).
LCMS pic at 3.27 min: HRMS (TOF MS ES+): *m/z* calcd for $C_{53}H_{62}N_{12}O_4$ $[M+2H]^{2+}$: 465.2503; found: 465.2505 (0.4 ppm).
LCMS pic at 2.46 min: HRMS (TOF MS ES+): *m/z* calcd for $C_{48}H_{61}N_{13}O_4$ $[M+2H]^{2+}$: 441.74793 found: 441.748 (0.21 ppm).

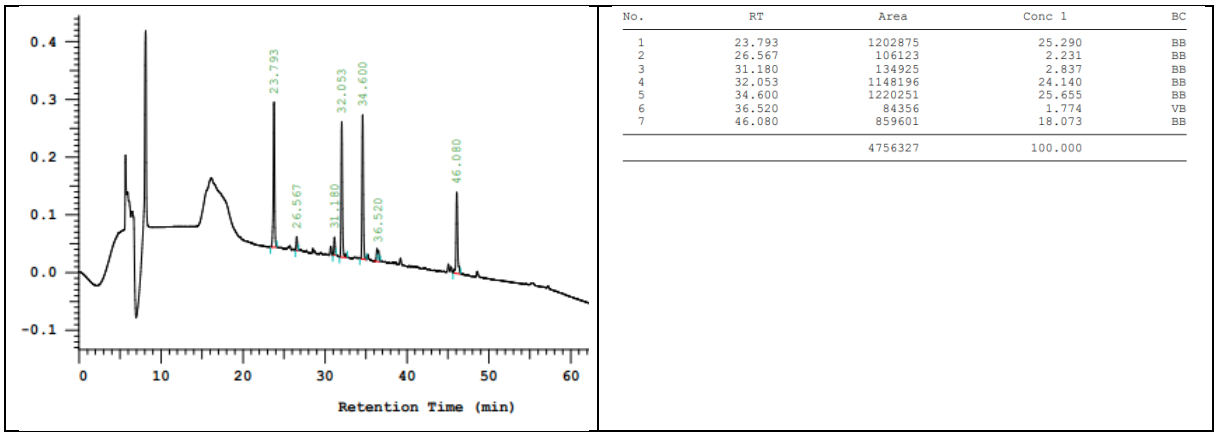

No.	RT	Area	Conc 1	BC
1	23.793	1202875	25.290	BB
2	26.567	106123	2.231	BB
3	31.180	134925	2.837	BB
4	32.053	1148196	24.140	BB
5	34.600	1220251	25.655	BB
6	36.520	84356	1.774	VB
7	46.080	859601	18.073	BB
		4756327	100.000	

*Figure S44 HPLC chromatogram of purified **III-4(a,d)(2,4)**.*

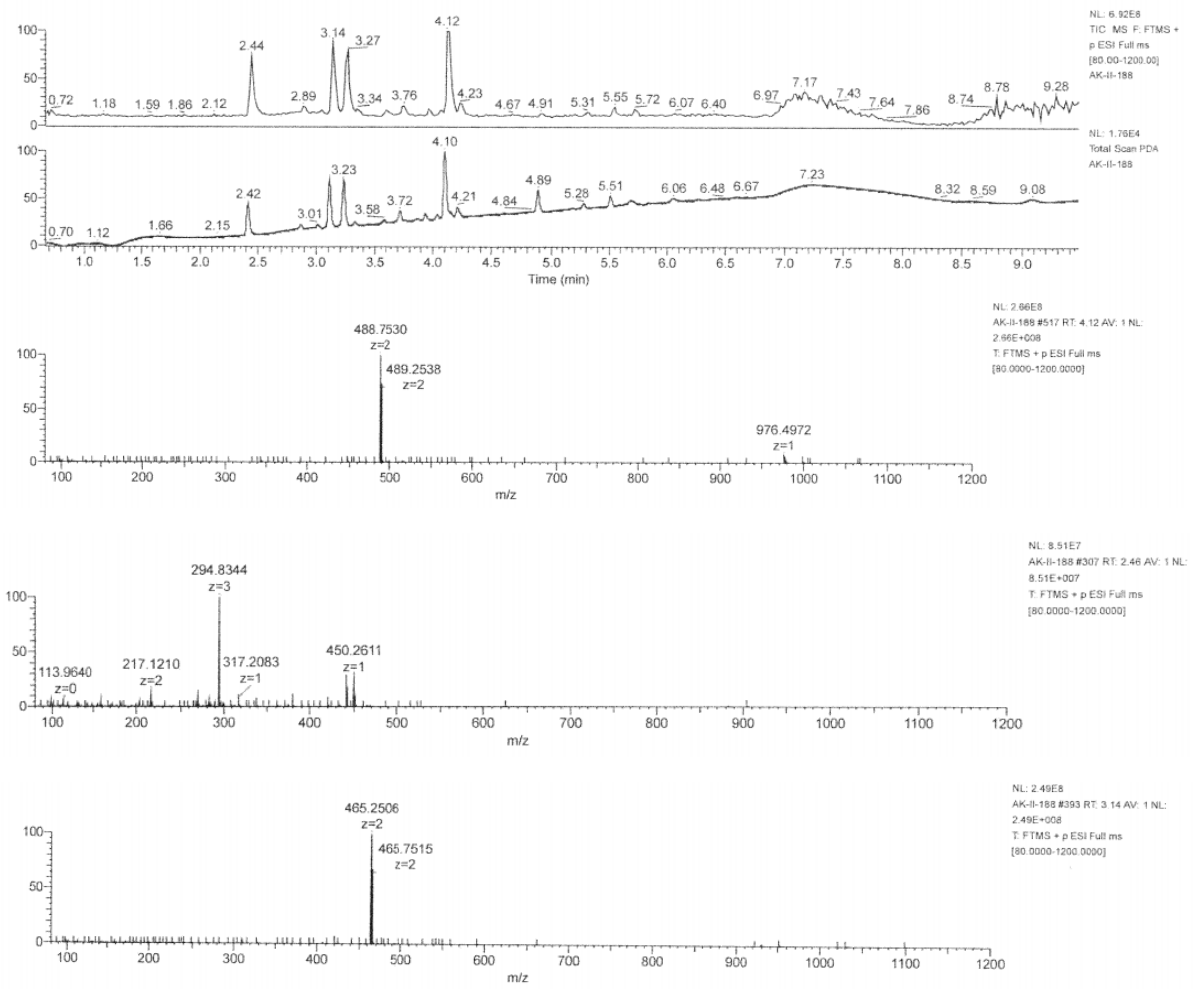

Figure 45 LCMS spectra of ***III-4(a,d)(2,4)***

4.3.3. meta-arylopeptoid tetramer ***III-4(b,c)(2,4)***.

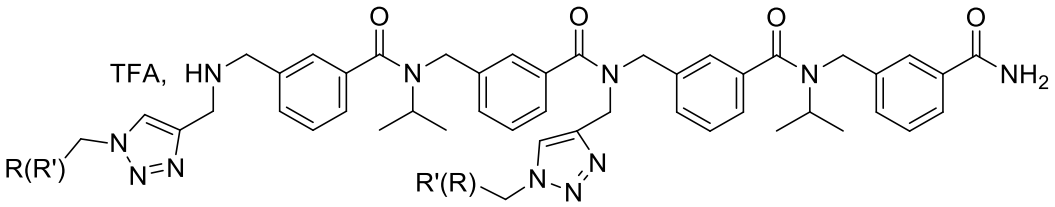

R = 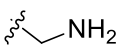 R' = 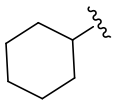

Tetramer **III-4(b,c)(2,4)** was synthesised according general procedure A then general procedure B using 100 mg of RA resin (0.054 mmol)

m_{crude}= 74mg (purity 81%), crude yield 121%
m_{pure}= 46 mg (purity 92%), isolated yield 82%
LCMS pic at 2.45 min: HRMS (TOF MS ES+): *m/z* calcd for $C_{48}H_{62}N_{13}O_4$ $[M+3H]^{3+}$: 294.83438 found: 294.8346 (0.64 ppm)
LCMS pic at 3.30 min: HRMS (TOF MS ES+): *m/z* calcd for $C_{53}H_{68}N_{12}O_4$ $[M+2H]^{2+}$: 468.27378; found: 468.274 (0.52 ppm).

LCMS pic at 3.45 min: HRMS (TOF MS ES+): *m/z* calcd for $C_{53}H_{68}N_{12}O_4$ $[M+2H]^{2+}$: 468.27378; found: 468.274 (0.58 ppm).
LCMS pic at 4.51 min: HRMS (TOF MS ES+): *m/z* calcd for $C_{58}H_{75}N_{11}O_4$ $[M+2H]^{2+}$: 494.79963; found: 494.7999 (0.48 ppm)

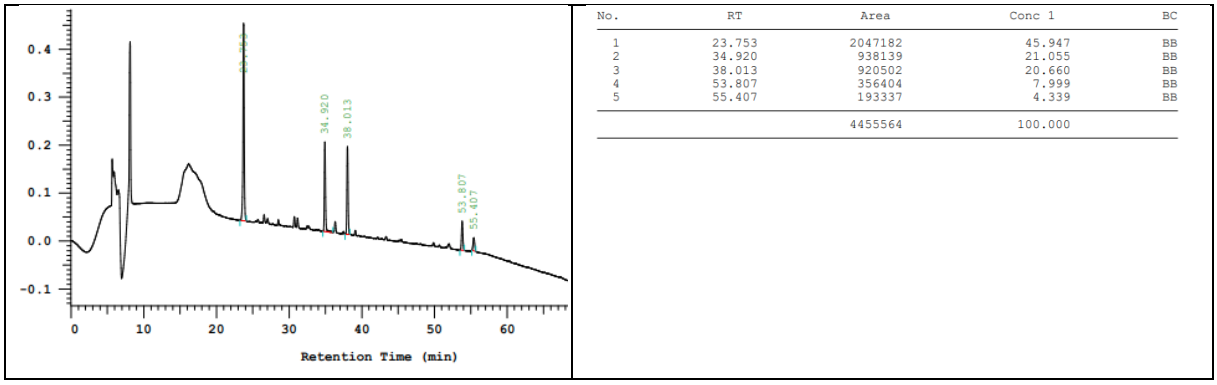

No.	RT	Area	Conc 1	BC
1	23.753	2047182	45.947	BB
2	34.920	938139	21.055	BB
3	38.013	920502	20.660	BB
4	53.807	356404	7.999	BB
5	55.407	193337	4.339	BB
		4455564	100.000	

Figure S46 HPLC chromatogram of purified ***III-4(b,c)(2,4)***

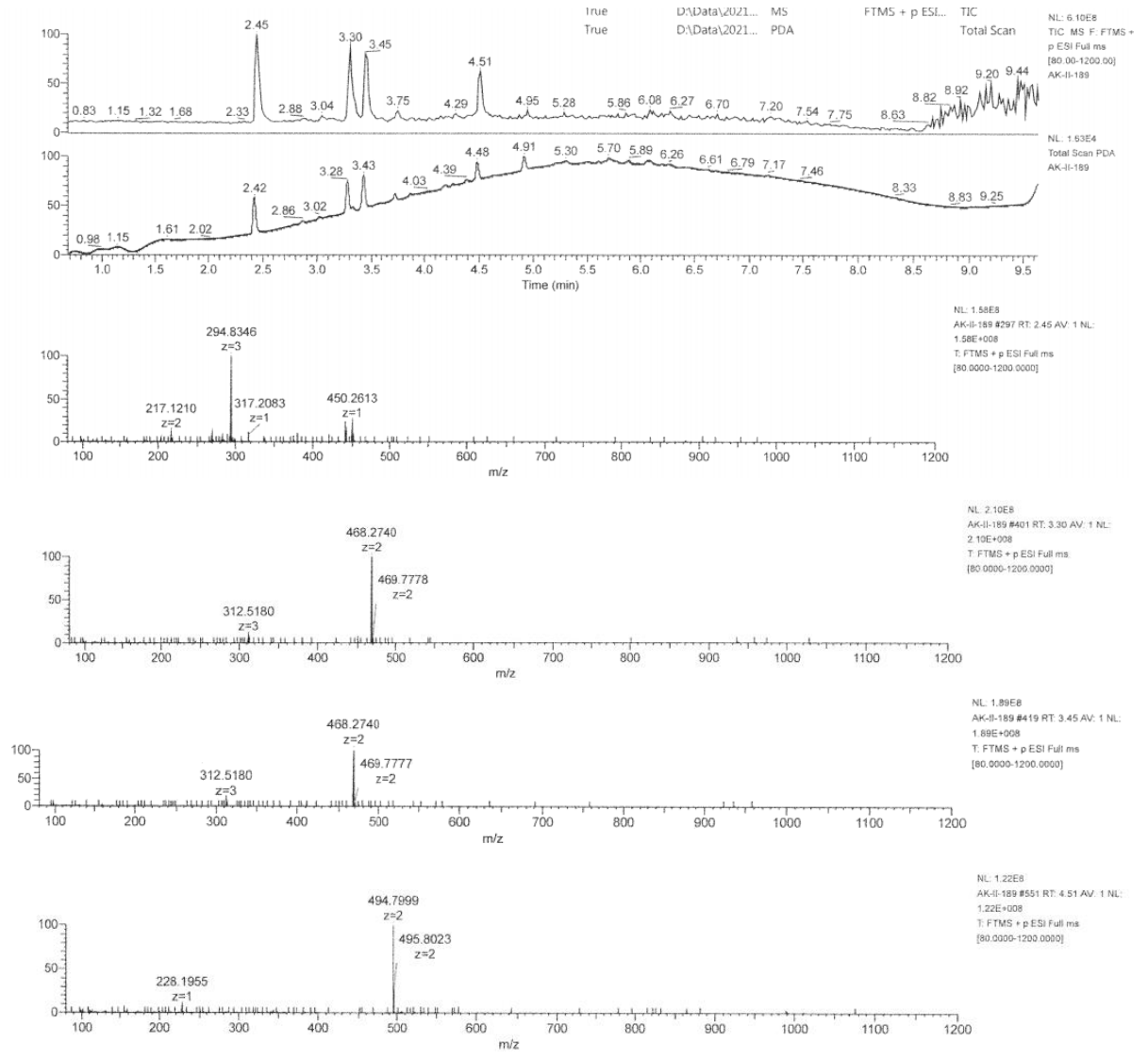

Figure S47 LCMS spectra of ***III-4(b,c)(2,4).***

*4.3.1. meta-arylopeptoid tetramer **III-4(c,d)(2,4).***

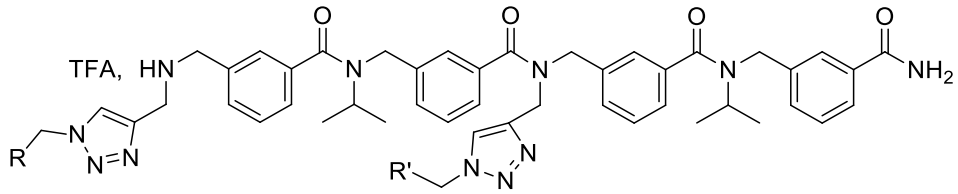

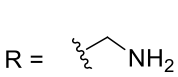

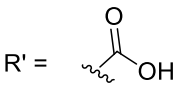

Tetramer **III-4(c,d)(2,4)** was synthesised according general procedure A then general procedure B using 100 mg of RA resin (0.054 mmol)
m_{crude}= 78mg (purity 87%), crude yield 119%
m_{pure}= 50mg (purity 91%), isolated yield 68%

LCMS pic at 2.42 min: HRMS (TOF MS ES+): *m/z* calcd for $C_{48}H_{62}N_{13}O_4$ $[M+3H]^{3+}$: 294.8343 found: 294.8342 (-0.71 ppm).
LCMS pic at 2.96 min: HRMS (TOF MS ES+): *m/z* calcd for $C_{48}H_{58}N_{12}O_6$ $[M+2H]^{2+}$: 449.2296; found: 449.22957 (0.18 ppm).
LCMS pic at 3.02 min: HRMS (TOF MS ES+): *m/z* calcd for $C_{48}H_{58}N_{12}O_6$ $[M+2H]^{2+}$: 449.2296; found: 449.22957 (-0.03 ppm).
LCMS pic at 3.60 min: HRMS (TOF MS ES+): *m/z* calcd for $C_{48}H_{55}N_{11}O_8$ $[M+2H]^{2+}$: 456.7112; found: 456.71121 (0.01 ppm).

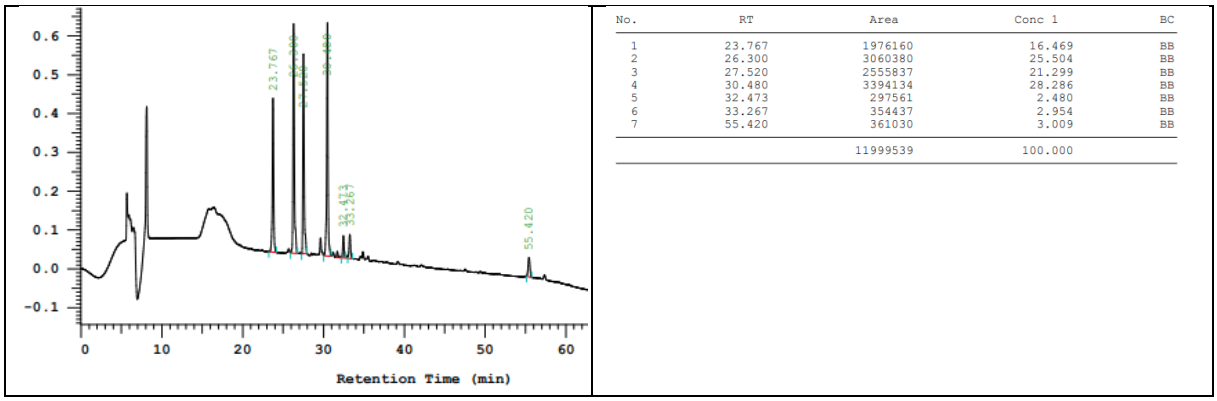

No.	RT	Area	Conc 1	BC
1	23.767	1976160	16.469	BB
2	26.300	3060380	25.504	BB
3	27.520	2555837	21.299	BB
4	30.480	3394134	28.286	BB
5	32.473	297561	2.480	BB
6	33.267	354437	2.954	BB
7	55.420	361030	3.009	BB
		11999539	100.000	

*Figure S48 HPLC chromatogram of purified **III-4(c,d)(2,4).***

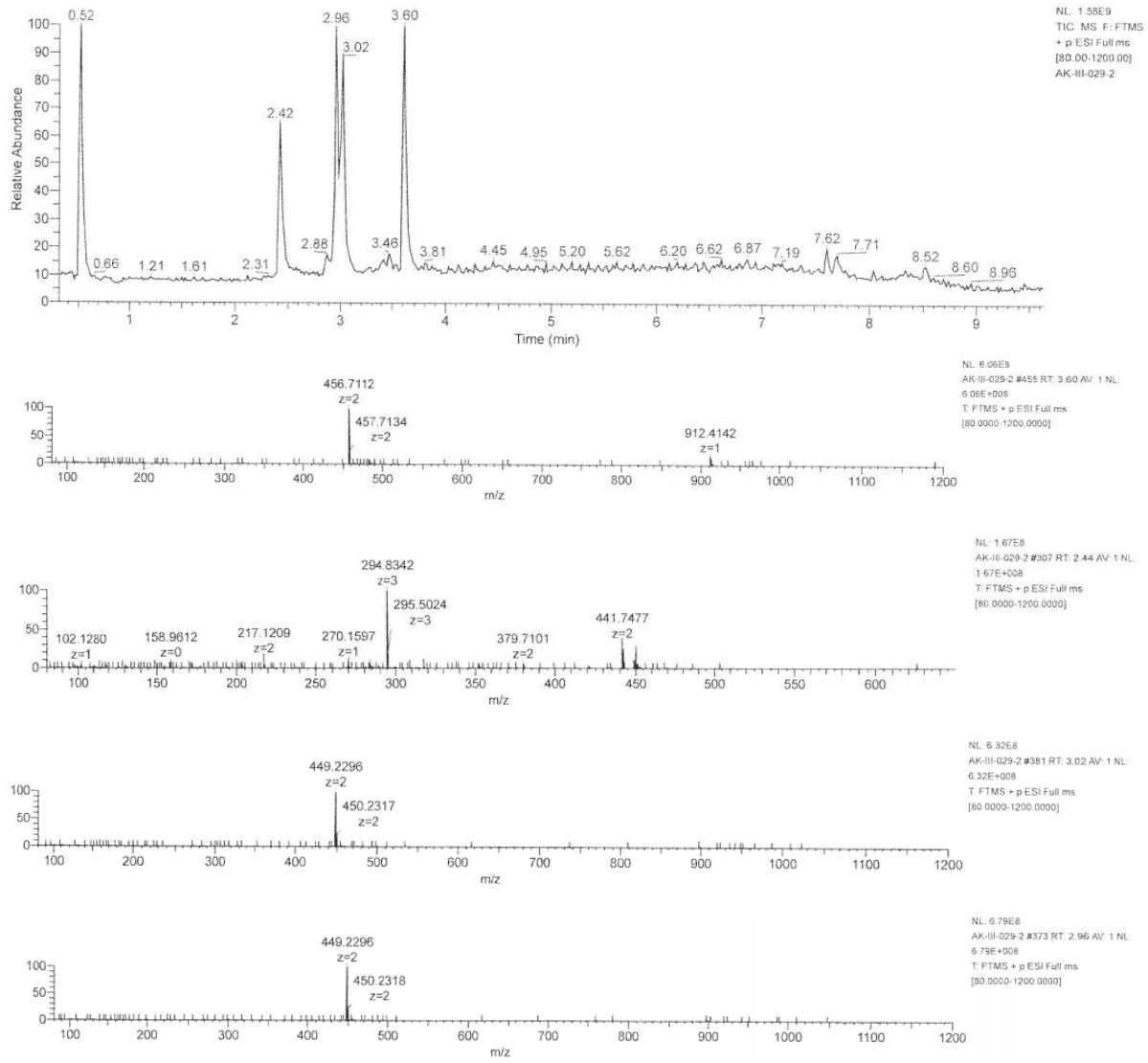

Figure S49 LCMS spectra of ***III-4(c,d)(2,4).***

4.3.4. meta-arylopeptoid tetramer, III-4(d,e)(2,4).

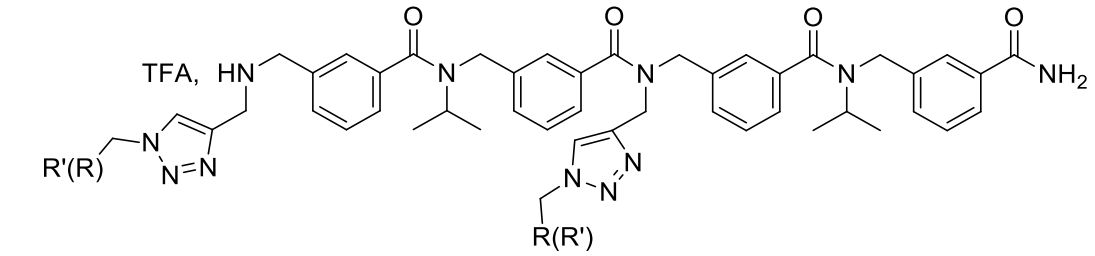

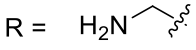

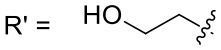

Tetramer **III-4(d,e)(2,4)** was synthesised according general procedure A then general procedure B using 25 mg of RA resin (0.0155 mmol)

m_{crude}= 25mg (purity 81%), crude yield 118%
m_{pure}= 17.8 mg (purity 97%), isolated yield 84%

LCMS pic at 3.2 min: HRMS (TOF MS ES+): *m/z* calcd for $C_{50}H_{63}N_{11}O_6$ $[M+2H]^{2+}$: 456.74759; found: 456.747 (-1.21 ppm).
LCMS pic at 2.76 min: HRMS (TOF MS ES+): *m/z* calcd for $C_{49}H_{62}N_{12}O_4$ $[M+2H]^{2+}$: 449.24776; found: 449.2473 (-0.99 ppm).
LCMS pic at 2.74 min: HRMS (TOF MS ES+): *m/z* calcd $C_{49}H_{61}N_{12}O_5$ $[M+2H]^{2+}$: 897.48824; found: 897.4871 (-1.31 ppm).
LCMS pic at 2.44 min: HRMS (TOF MS ES+): *m/z* $C_{48}H_{61}N_{13}O_4$ $[M+2H]^{2+}$: 441.74793; found: 441.7474 (-1.11 ppm).

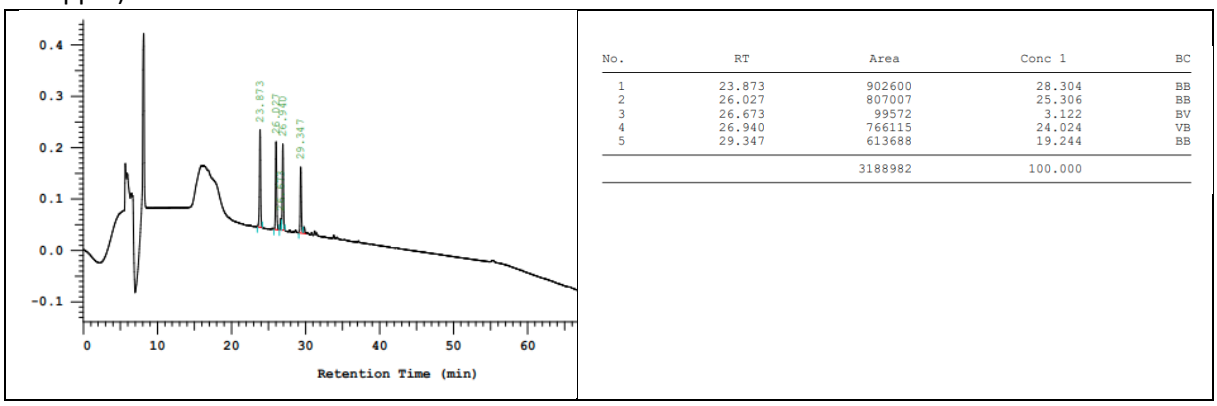

No.	RT	Area	Conc 1	BC
1	23.873	902600	28.304	BB
2	26.027	807007	25.306	BB
3	26.673	99572	3.122	BV
4	26.940	766115	24.024	VB
5	29.347	613688	19.244	BB
		3188982	100.000	

Figure S50 HPLC chromatogram of purified ***III-4(d,e)(2,4)***.

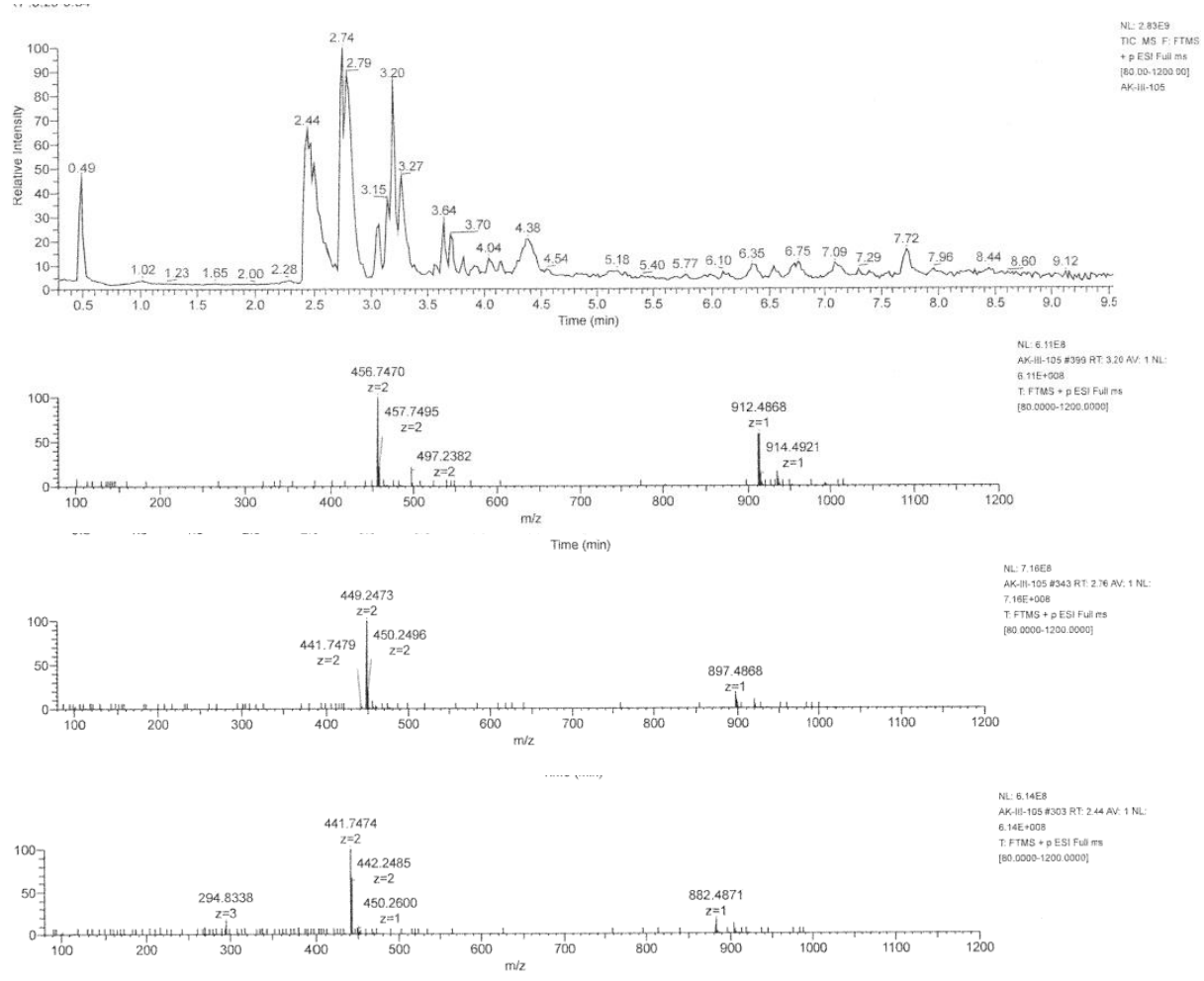

Figure S51 LCMS spectra of ***III-4(d,e)(2,4)***.

5. Hexamers

5.1.1. meta-arylopeptoid hexamer, III-6(Alk$_{3,6}$).

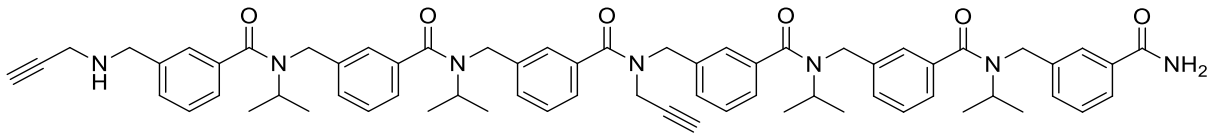

Hexamer **III-6(Alk$_{3,6}$)** was synthesised according to general procedure A using 50 mg of RA resin (0.027 mmol), then cleavage by gently shaking a solution of TFA/TIS/H_2O (95:2.5:2.5, 1mL) for 10 min at RT.

m_{crude}= 33 mg, crude yield 118%
m_{pure}= 24 mg (purity 94%), isolated yield 84%
HRMS (TOF MS ES+): *m/z* calcd for $C_{66}H_{74}N_7O_6$ $[M+H]^+$: 1060.56951; found: 1060.5684 (-1.08 ppm).

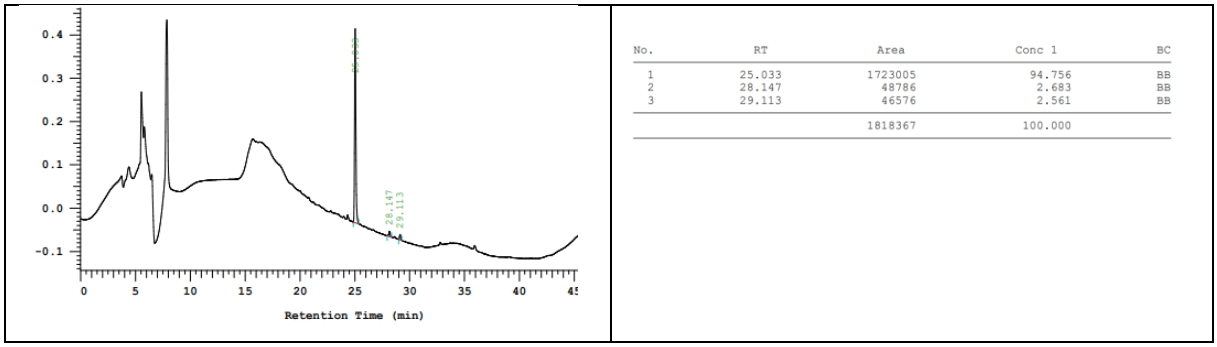

*Figure S52 HPLC chromatogram of purified **III-6(Alk$_{3,6}$).***

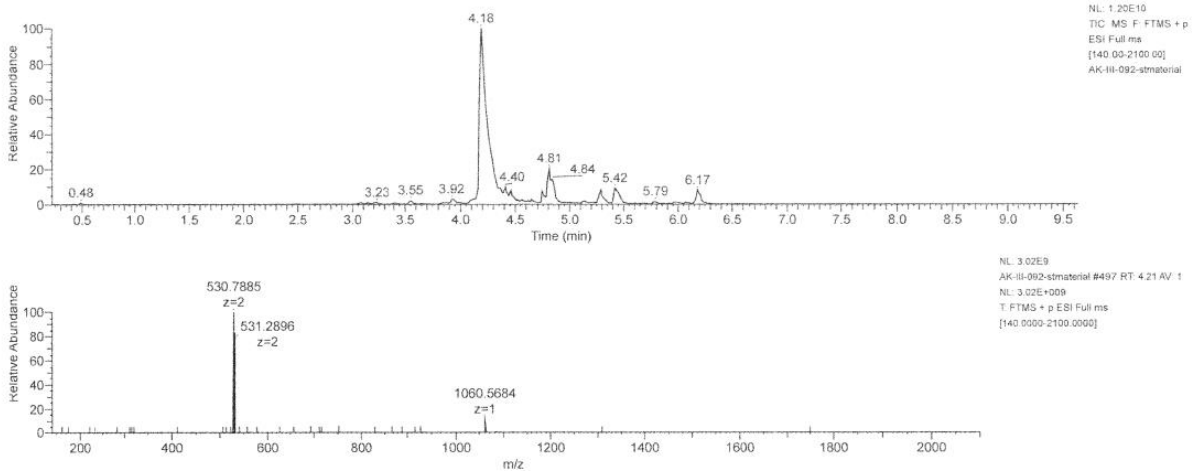

*Figure S53 LCMS spectra of **III-6(Alk$_{3,6}$).***

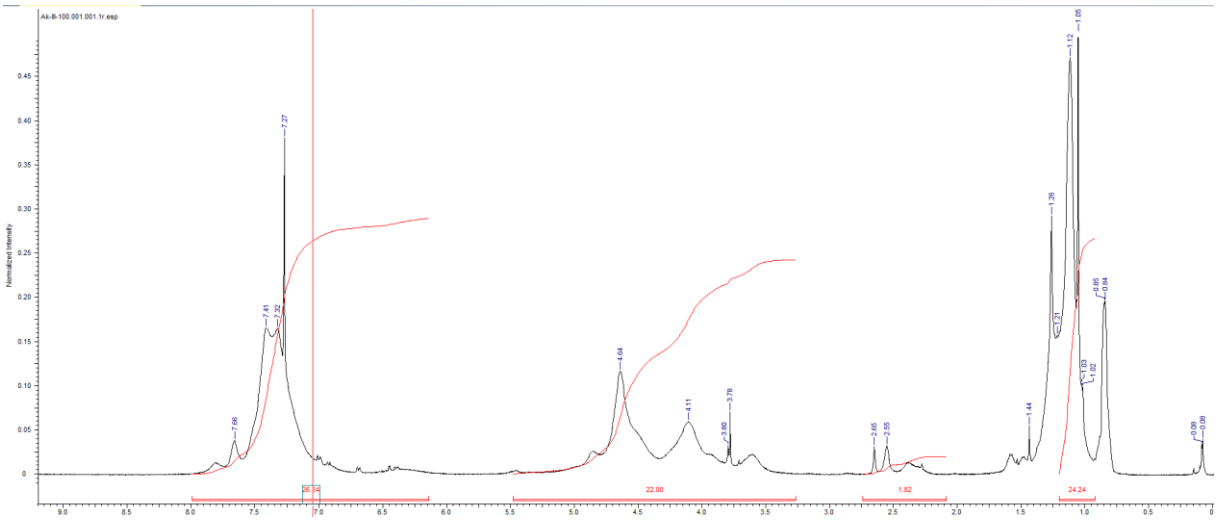

*Figure 54 ^{1}H-NMR in $CDCl_3$ of **III-6(Alk3,6)***

*5.2. meta-arylopeptoid hexamer, **III-6($a_{3,6}$).***

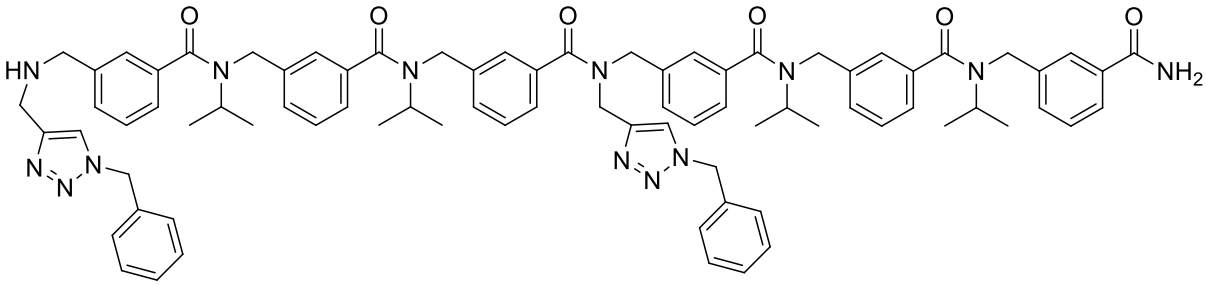

Hexamer **III-6($a_{3,6}$)** was synthesised according general procedure A then general procedure B using 50 mg of RA resin (0.027 mmol)

m_{crude}= 42 mg (purity 84%), crude yield 117%
m_{pure}= 28.2 mg (purity 94%), isolated yield 85%
HRMS (TOF MS ES+): *m/z* calcd for $C_{80}H_{88}N_{13}O_6$ $[M+H]^+$: 1326.6975; found: 1326.6975 (0 ppm).

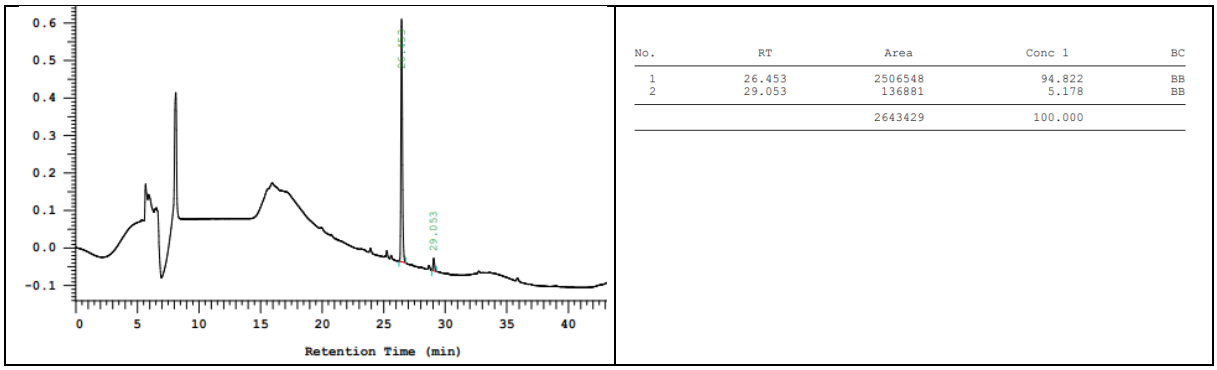

No.	RT	Area	Conc 1	BC
1	26.453	2506548	94.822	BB
2	29.053	136881	5.178	BB
		2643429	100.000	

*Figure S55 HPLC chromatogram of purified **III-6($a_{3,6}$).***

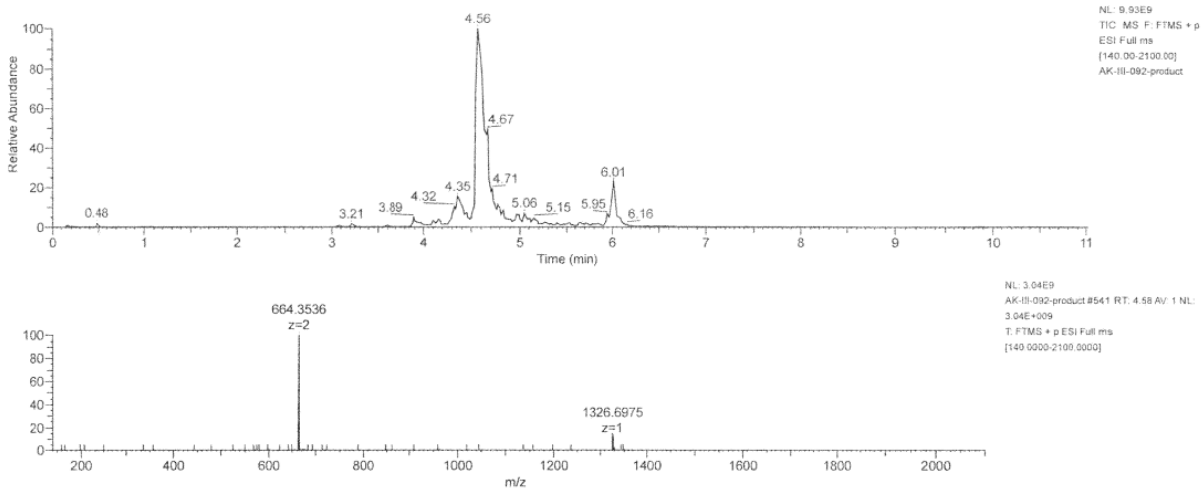

Figure S56 LCMS spectra of ***III-6($a_{3,6}$).***

5.2. Starting material, *III-6($Alk_{2,4,6}$).*

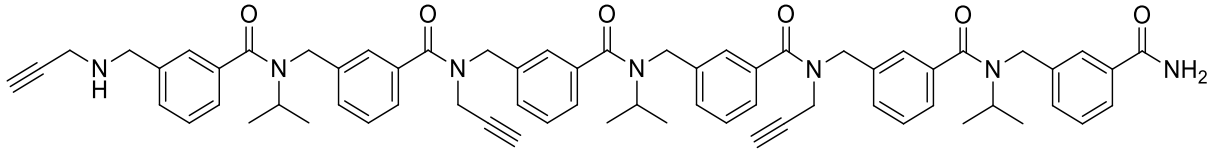

Hexamer **III-6($Alk_{2,4,6}$)** was synthesised according to general procedure A using 100 mg of RA resin (0.054 mmol), then cleavage by gently shaking a solution of TFA/TIS/H_2O (95:2.5:2.5, 1mL) for 10 min at RT.

m_{crude}= 77mg (purity 85%), crude yield 121%
m_{pure} = 50.2mg (purity 97%), isolated yield 87%
HRMS (TOF MS ES+): *m/z* calcd for $C_{80}H_{88}N_{13}O_6$ $[M+H]^+$: 1056.53821; found: 1056.5367 (-1.39ppm).

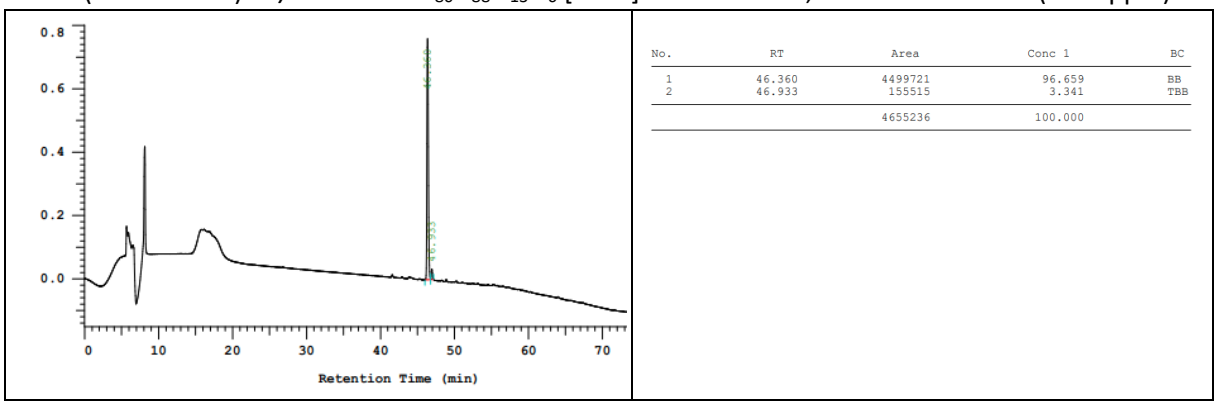

No.	RT	Area	Conc 1	BC
1	46.360	4499721	96.659	BB
2	46.933	155515	3.341	TBB
		4655236	100.000	

Figure S57 HPLC chromatogram of purified ***III-6($Alk_{2,4,6}$)***

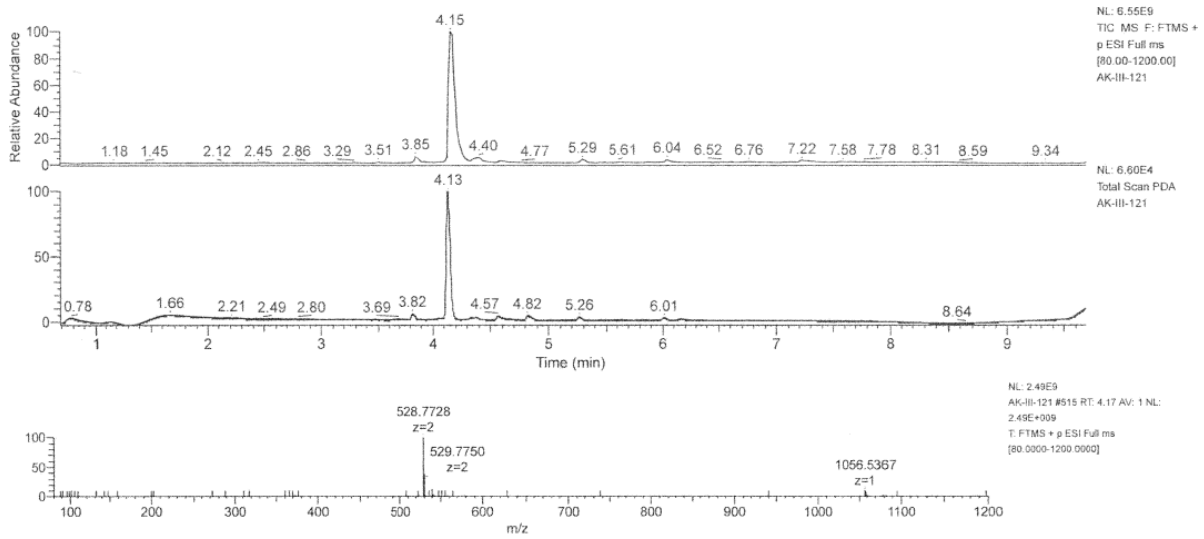

Figure S58 LCMS spectra of ***III-6(Alk$_{2,4,6}$).***

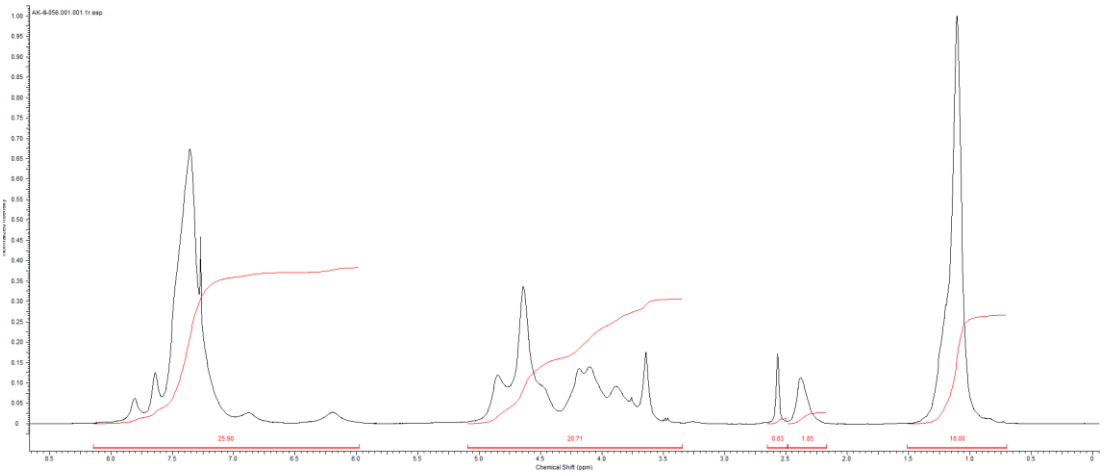

Figure S59 ^{1}H-NMR spectra in $CDCl_3$ of ***III-6(Alk$_{2,4,6}$)***

5.2. Homo clicked peptoides

5.2.1. meta-arylopeptoid Hexamer, ***III-6(a$_{2,4,6}$).***

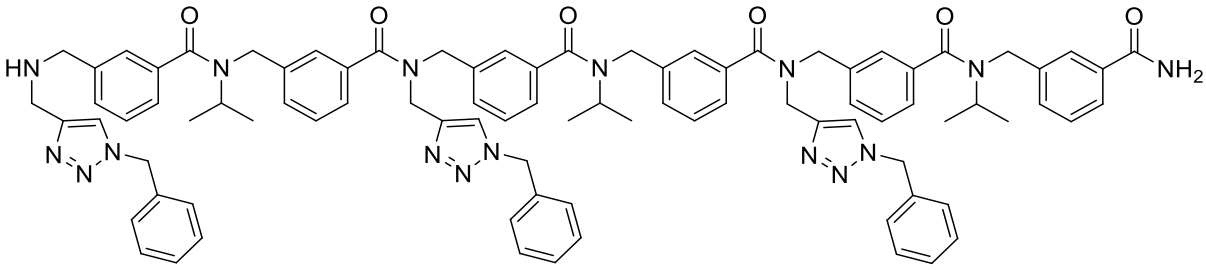

Hexamer **III-6(a$_{2,4,6}$)** was synthesised according general procedure A then general procedure B using 100 mg of RA resin (0.054 mmol)

m_{crude}= 116 mg (purity 87%), crude yield 137%
m_{pure}= 64 mg (purity 88%), isolated yield 78%
HRMS (TOF MS ES+): *m/z* calcd for $C_{87}H_{91}N_{16}O_6$ $[M+H]^+$: 1455.7302; found: 1455.7341 (2.7 ppm).

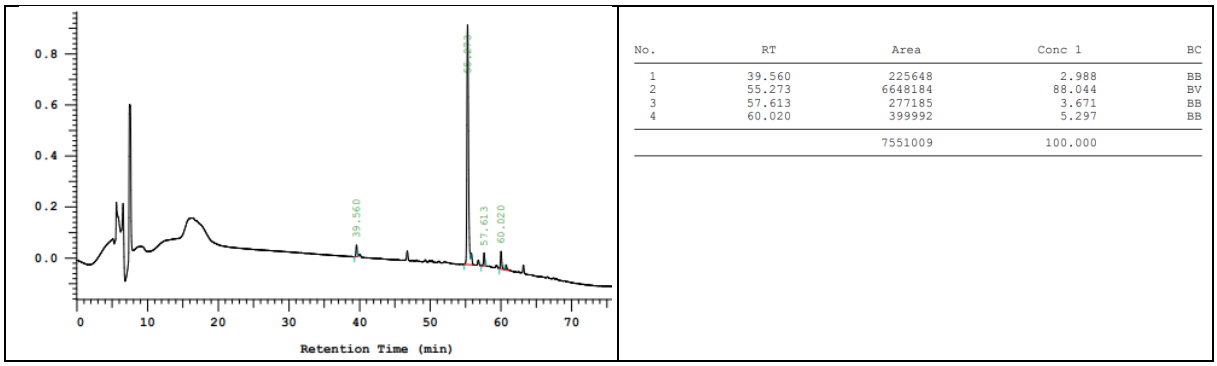

No.	RT	Area	Conc 1	BC
1	39.560	225648	2.988	BB
2	55.273	6648184	88.044	BV
3	57.613	277185	3.671	BB
4	60.020	399992	5.297	BB
		7551009	100.000	

Figure S60 HPLC chromatogram of purified ***III-6(a$_{2,4,6}$).***

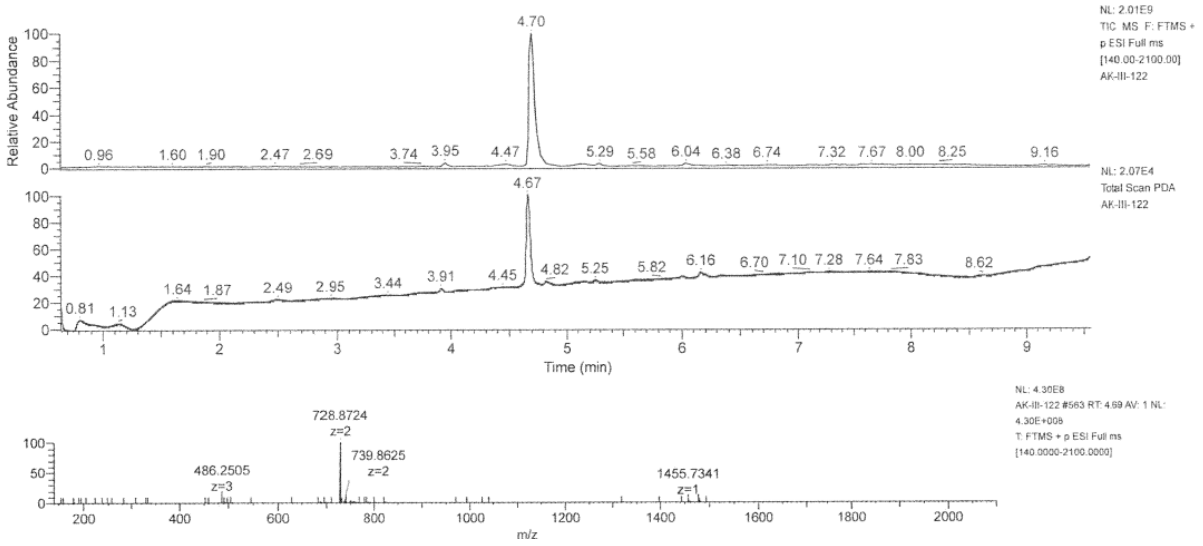

Figure S61 LCMS spectra of ***III-6(a$_{2,4,6}$).***

5.2.2. meta-arylopeptoid Hexamer, ***III-6(b$_{2,4,6}$).***

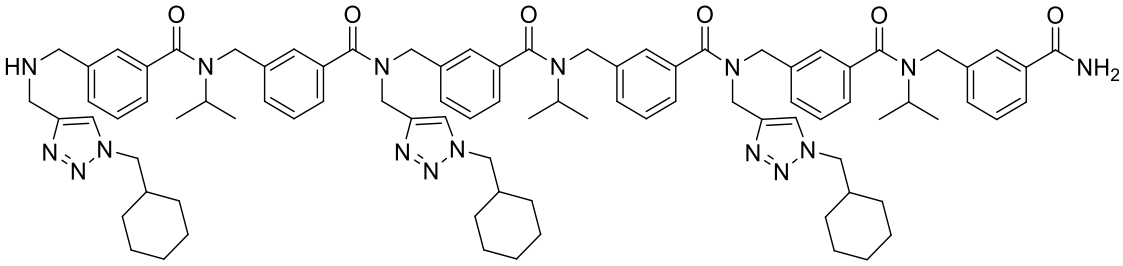

Hexamer **III-6(b$_{2,4,6}$)** was synthesised according general procedure A then general procedure B using 50 mg of RA resin (0.027 mmol)

m_{crude}= 38 mg (purity 86%), crude yield 96%
m_{pure}= 30 mg (purity 91%), isolated yield 76%
HRMS (TOF MS ES+): *m/z* calcd for $C_{87}H_{110}N_{16}O_6$ $[M+H]^{2+}$: 737.43916; found: 737.4398 (0.81 ppm).

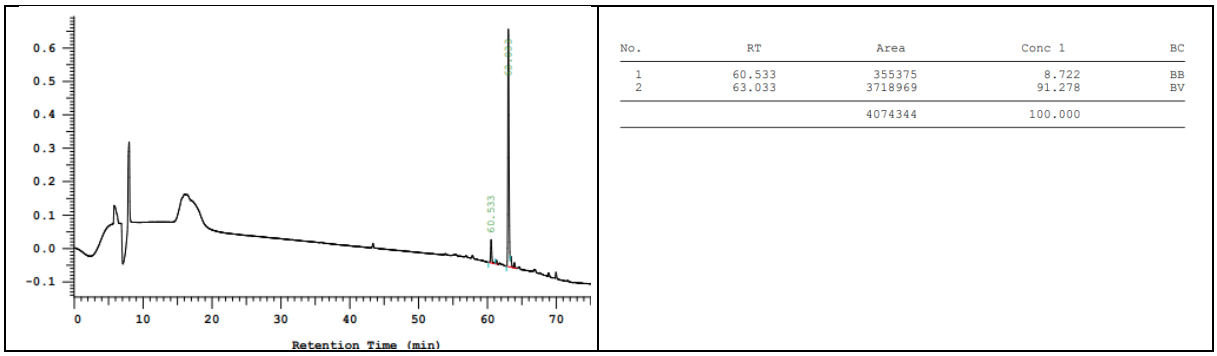

No.	RT	Area	Conc 1	BC
1	60.533	355375	8.722	BB
2	63.033	3718969	91.278	BV
		4074344	100.000	

Figure S62 HPLC chromatogram of purified ***III-6(b$_{2,4,6}$).***

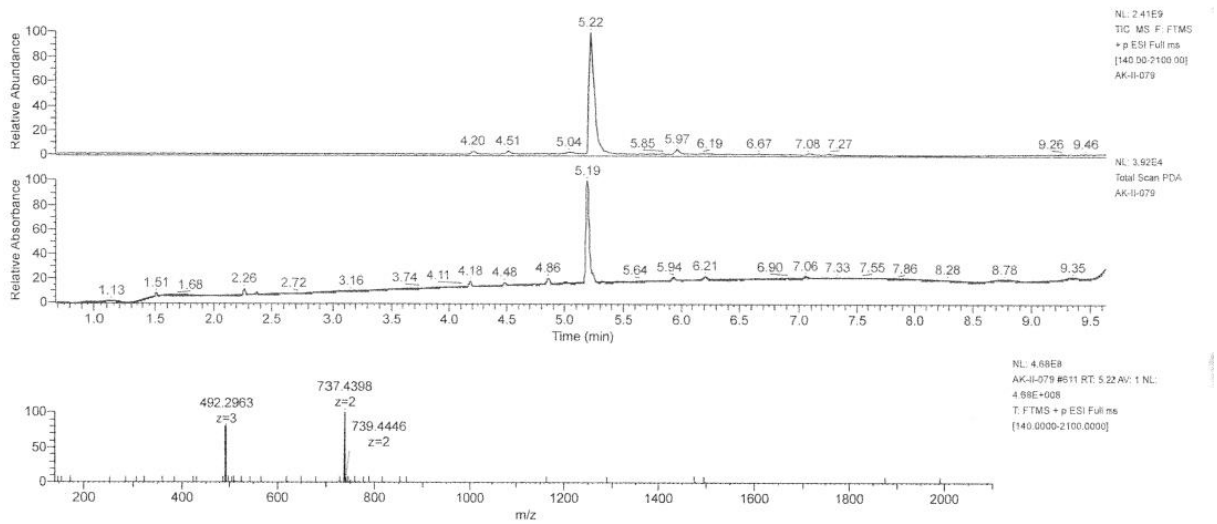

Figure S63 LCMS spectra of ***III-6(b$_{2,4,6}$).***

5.2.3. meta-arylopeptoid Hexamer, III-6(c$_{2,4,6}$).

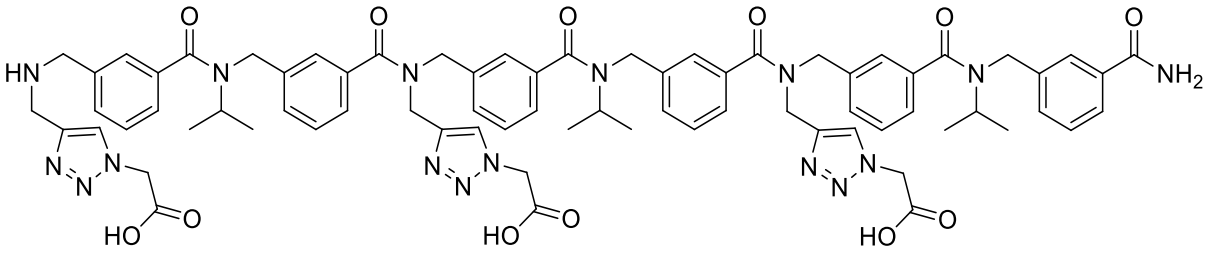

Hexamer **III-6(c$_{2,4,6}$)** was synthesised according general procedure A then general procedure B using 100 mg of RA resin (0.054 mmol)

m_{crude}= 90 mg (purity 85%), crude yield 113%

m_{pure}= 49 mg (purity 94%), isolated yield 68%

HRMS (TOF MS ES+): *m/z* calcd for $C_{72}H_{80}N_{16}O_{12}$ $[M+2H]^{2+}$: 680.30653; found: 680.3074 (1.33 ppm).

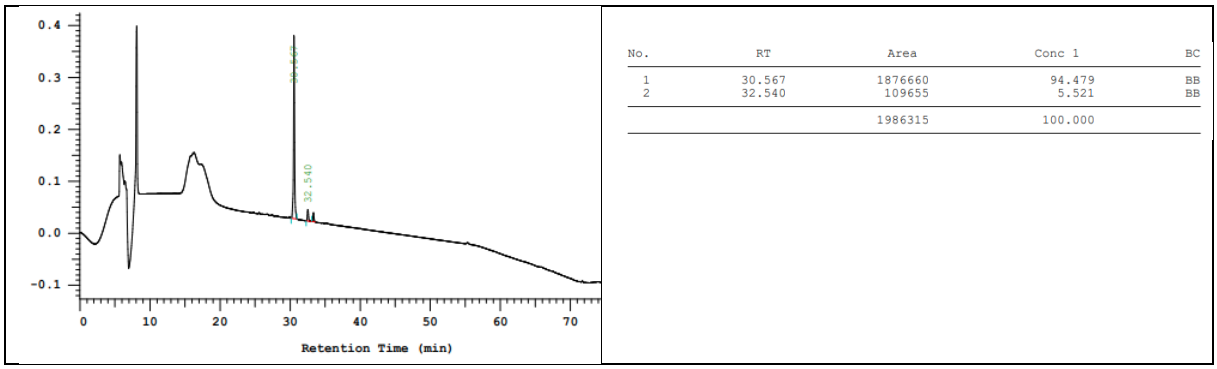

No.	RT	Area	Conc 1	BC
1	30.567	1876660	94.479	BB
2	32.540	109655	5.521	BB
		1986315	100.000	

Figure 64 HPLC chromatogram of purified ***III-6(c2,4,6).***

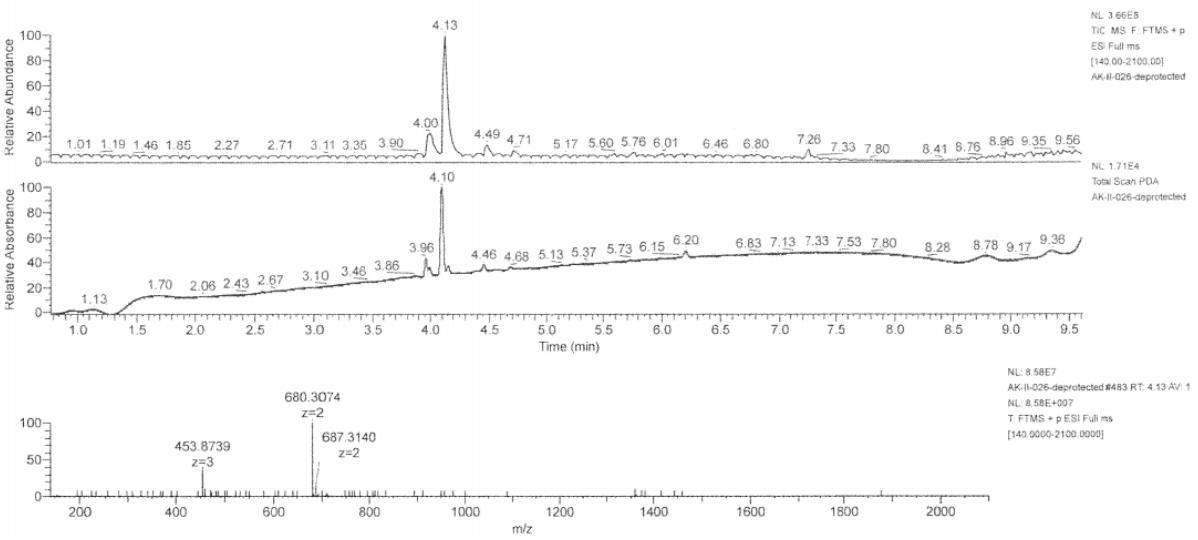

Figure 65 LCMS spectra of ***III-6(c2,4,6).***

5.2.4. meta-arylopeptoid Hexamer, III-6(d2,4,6).

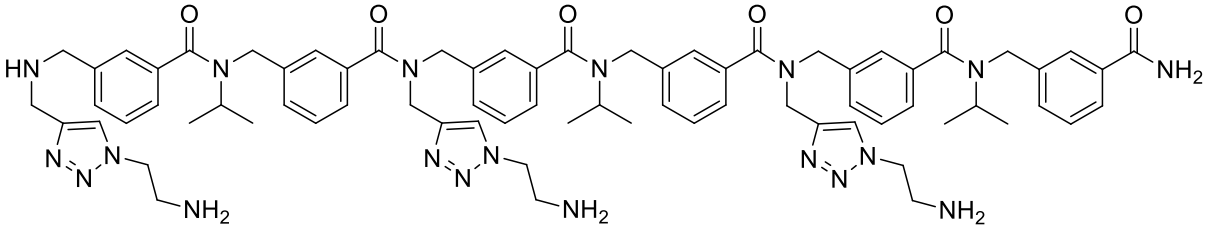

Hexamer **III-6(d$_{2,4,6}$)** was synthesised according general procedure A then general procedure B using 100 mg of RA resin (0.054 mmol)

m_{crude}= 116 mg (purity 86%), crude yield 98%
m_{pure}= 64 mg (purity 93%), isolated yield 70%
HRMS (TOF MS ES+): *m/z* calcd for $C_{72}H_{90}N_{19}O_{12}$ $[M+3H]^{3+}$: 438.91017; found: 438.9101 (-0.09ppm).

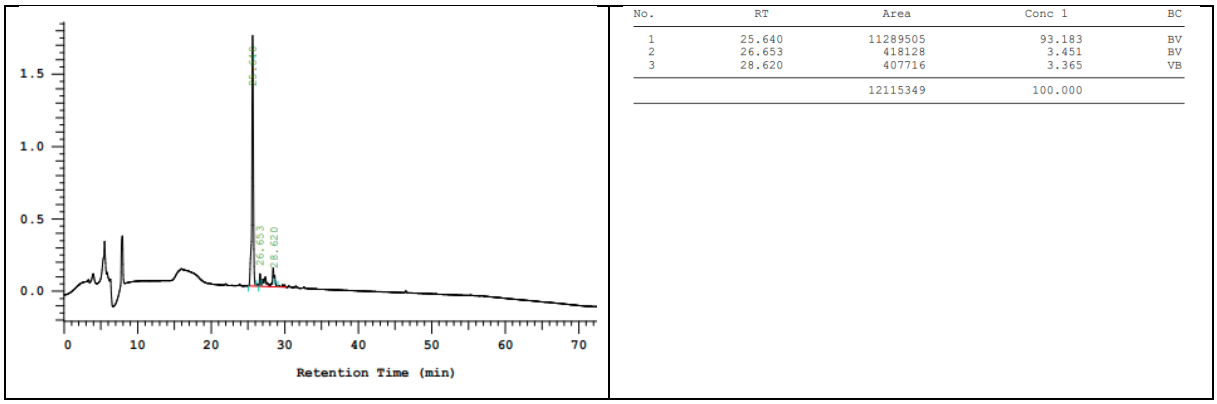

No.	RT	Area	Conc 1	BC
1	25.640	11289505	93.183	BV
2	26.653	418128	3.451	BV
3	28.620	407716	3.365	VB
		12115349	100.000	

Figure 66 HPLC chromatogram of purified ***III-6(d$_{2,4,6}$).***

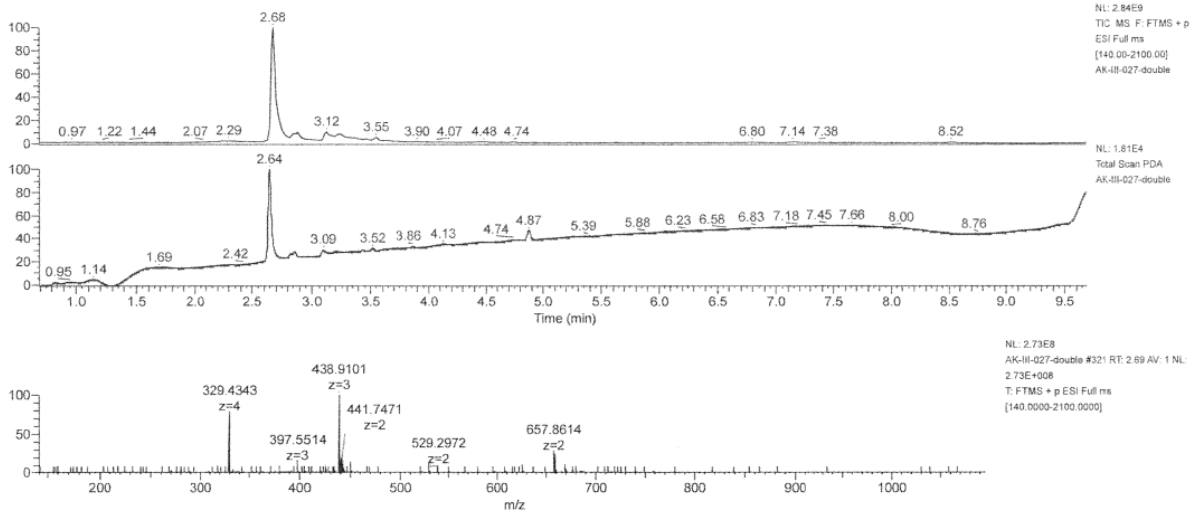

Figure 67 LCMS spectra of ***III-6(d$_{2,4,6}$).***

5.2.5. meta-arylopeptoid Hexamer, ***III-6(e$_{2,4,6}$).***

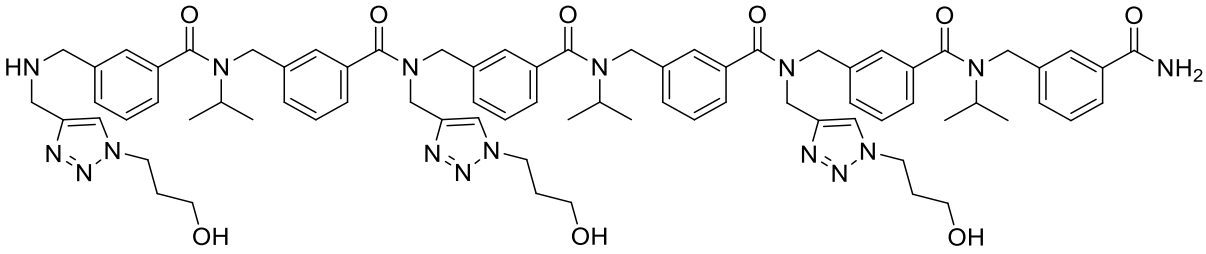

Hexamer **III-6(e$_{2,4,6}$)** was synthesised according general procedure A then general procedure B using 50 mg of RA resin (0.027 mmol)

m_{crude}= 46 mg (purity 86%), crude yield 116%
m_{pure}= 33.80 mg (purity 100%), isolated yield 82%
HRMS (TOF MS ES+): *m/z* calcd for $C_{75}H_{92}N_{16}O_9$ $[M+2H]^{2+}$: 680.36111; found: 680.3602 (-1.38 ppm).

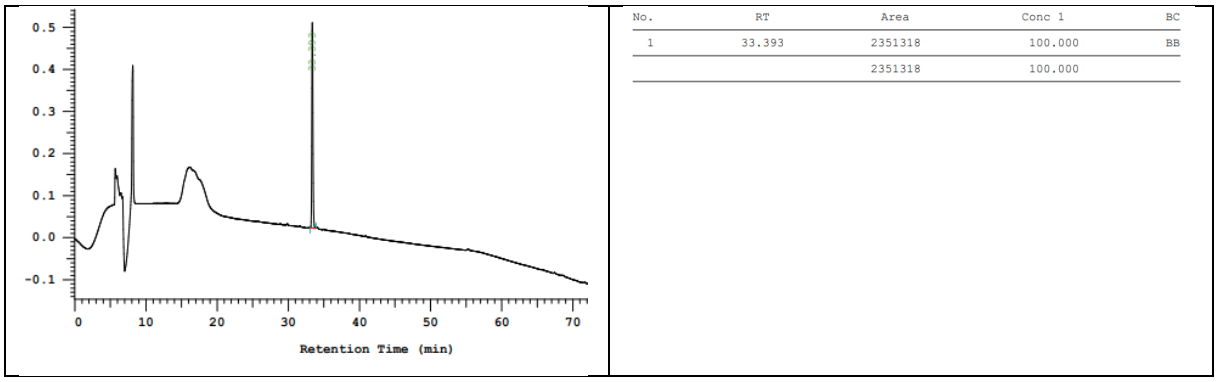

Figure 68 HPLC chromatogram of purified ***III-6(e2,4,6).***

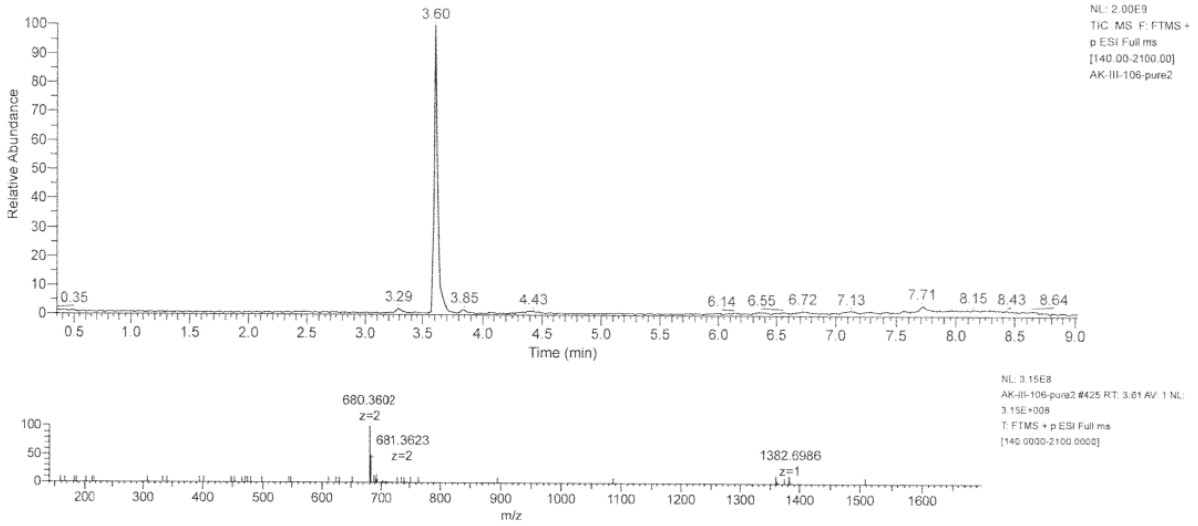

Figure S69 LCMS spectra of ***III-6(e$_{2,4,6}$).***

5.3. Combinatorial on hexamer

5.3.1. Meta-arylopeptoid Hexamer III-6(a,c)(2,4,6).

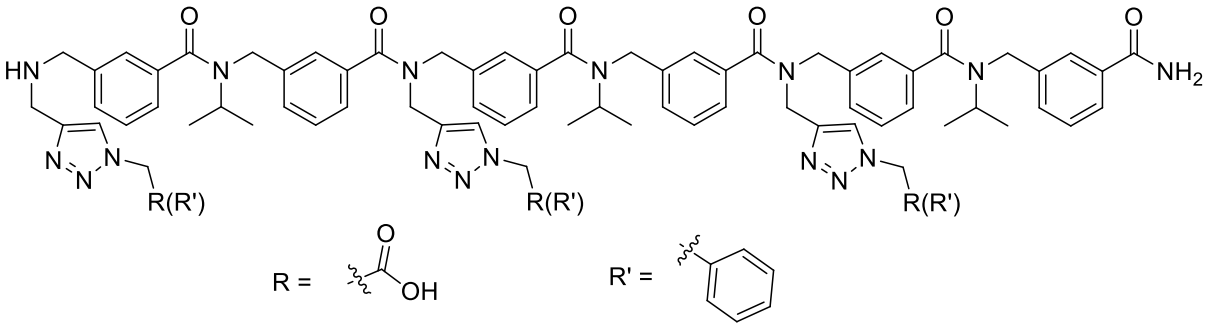

Hexamer **III-6(a,c)(2,4,6)** was synthesised according general procedure A then general procedure B using 100 mg of RA resin (0.054 mmol)

m_{crude}= 122 mg (purity 89%), crude yield 159%
m_{pure}= 51 mg (purity 98%), isolated yield 67%
LCMS pic at 4.12 min: HRMS (TOF MS ES+): *m/z* calcd for $C_{72}H_{80}N_{16}O_{12}$ $[M+2H]^{2+}$: 680.30653 found: 680.3069 (0.52 ppm)
LCMS pic at 4.27 min: HRMS (TOF MS ES+): *m/z* calcd for $C_{77}H_{84}N_{16}O_{10}$ $[M+2H]^{2+}$: 696.32727 found: 696.3272 (-0.08 ppm)

LCMS pic at 4.42 min: HRMS (TOF MS ES+): *m/z* calcd for $C_{77}H_{84}N_{16}O_{10}$ $[M+2H]^{2+}$: 696.32727 found: 696.3273 (0.09 ppm)
LCMS pic at 4.73 min: HRMS (TOF MS ES+): *m/z* calcd for $C_{77}H_{90}N_{16}O_{10}$ $[M+2H]^{2+}$: 699.35074 found: 699.3508 (0.05 ppm)
LCMS pic at 4.5 min: HRMS (TOF MS ES+): *m/z* calcd for $C_{77}H_{84}N_{16}O_{10}$ $[M+2H]^{2+}$: 696.32727 found: 696.3275 (0.27 ppm)
LCMS pic at 4.5 min: HRMS (TOF MS ES+): *m/z* calcd for $C_{82}H_{88}N_{16}O_8$ $[M+2H]^{2+}$: 712.348 found: 712.3472 (-1.09 ppm)
LCMS pic at 4.59 min: HRMS (TOF MS ES+): *m/z* calcd for $C_{82}H_{88}N_{16}O_8$ $[M+2H]^{2+}$: 712.348 found: 712.3477 (-0.4 ppm)
LCMS pic at 4.72 min: HRMS (TOF MS ES+): *m/z* calcd for $C_{82}H_{88}N_{16}O_8$ $[M+2H]^{2+}$: 712.348 found: 712.3477 (-0.4 ppm)
LCMS pic at 4.72 min: HRMS (TOF MS ES+): *m/z* calcd for $C_{87}H_{92}N_{16}O_6$ $[M+2H]^{2+}$: 728.36874 found: 728.368 (-1.04 ppm)

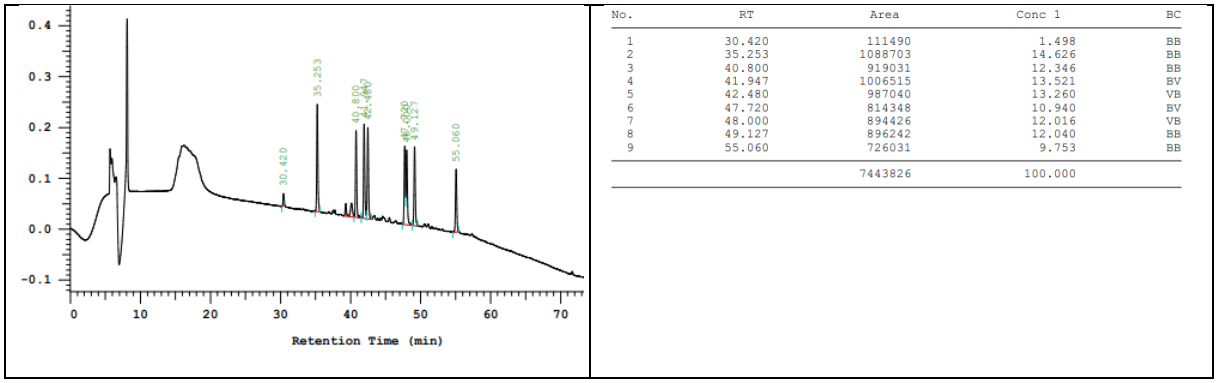

No.	RT	Area	Conc 1	BC
1	30.420	111490	1.498	BB
2	35.253	1088703	14.626	BB
3	40.800	919031	12.346	BB
4	41.947	1006515	13.521	BV
5	42.480	987040	13.260	VB
6	47.720	814348	10.940	BV
7	48.000	894426	12.016	VB
8	49.127	896242	12.040	BB
9	55.060	726031	9.753	BB
		7443826	100.000	

Figure S70 HPLC chromatogram of purified ***III-6(a,c)(2,4,6)***

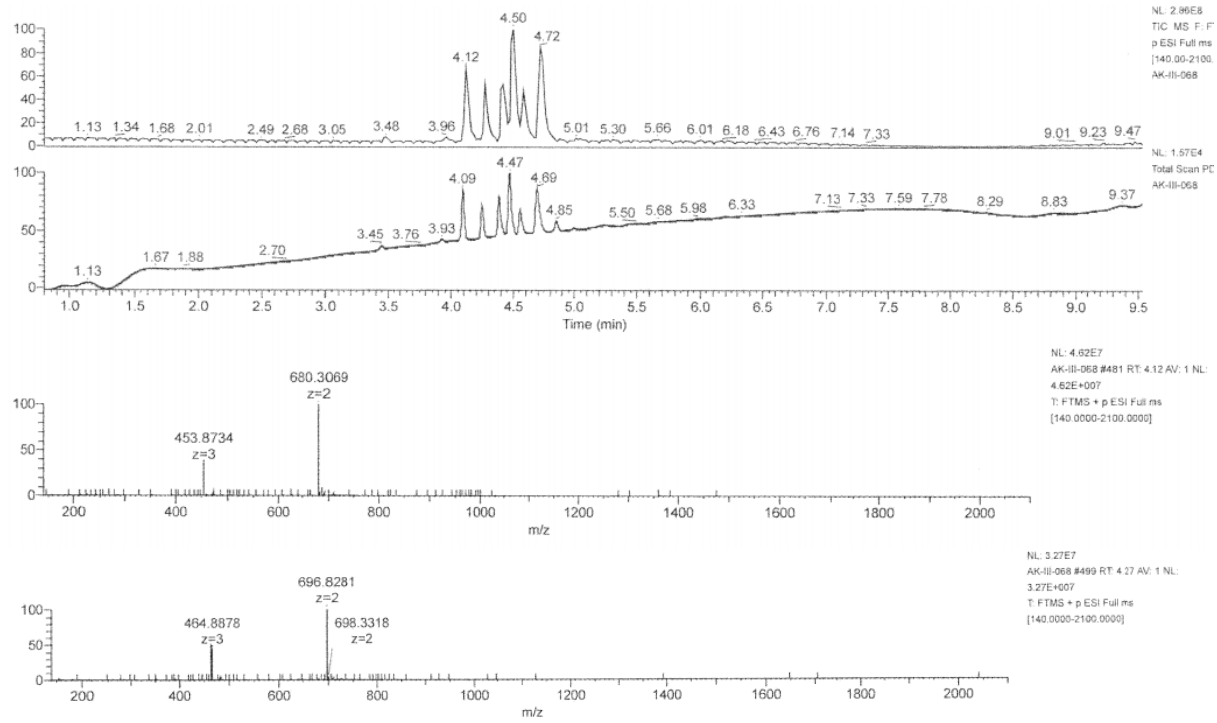

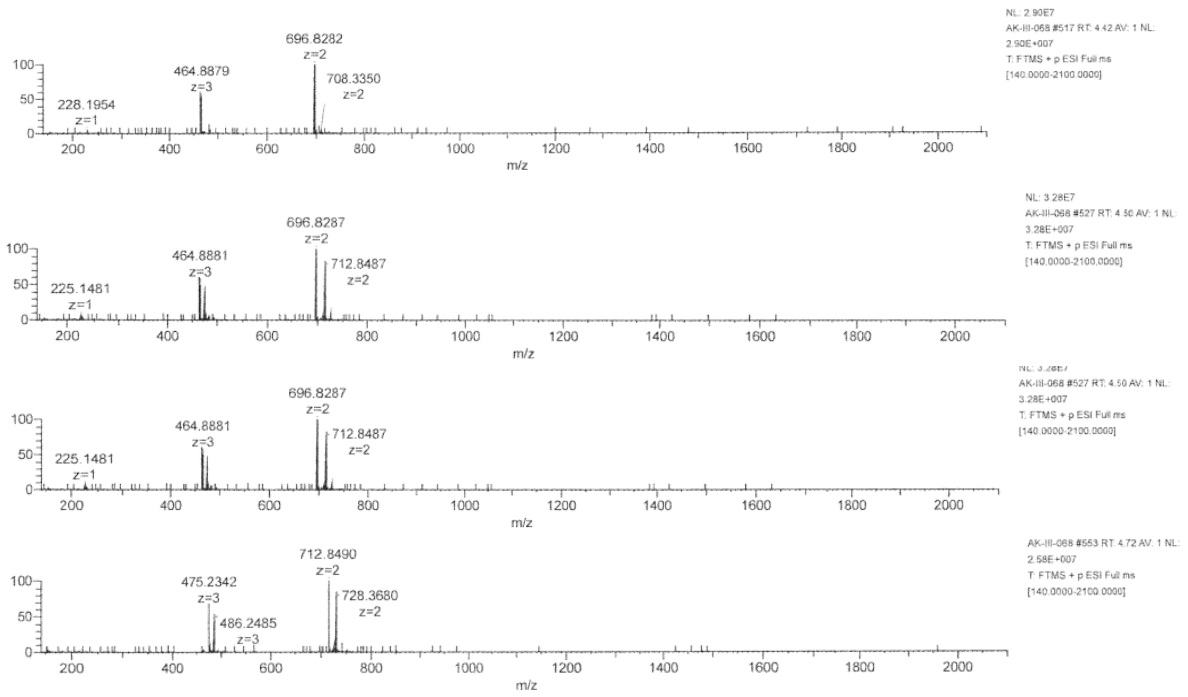

Figure S71 LCMS spectra of ***III-6(a,c)(2,4,6).***

5.3.2. meta-arylopeptoid Hexamer, ***III-6(a,d)(2,4,6).***

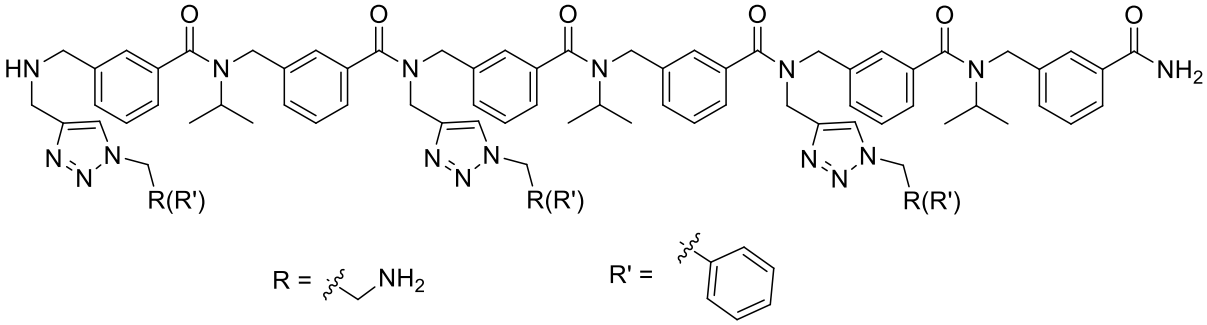

Hexamer **III-6(a,d)(2,4,6)** was synthesised according general procedure A then general procedure B using 50 mg of RA resin (0.031 mmol)

m_{crude}= 58 mg (purity 89%), crude yield 150%
m_{pure}= 30 mg (purity 95%), isolated yield 80%
LCMS pic at 3.13 min: HRMS (TOF MS ES+): *m/z* calcd for $C_{72}H_{89}N_{19}O_6$ $[M+2H]^{2+}$: 657.86161 found: 657.8621 (0.68 ppm).
LCMS pic at 3.29 min: HRMS (TOF MS ES+): *m/z* calcd for $C_{77}H_{90}N_{18}O_6$ $[M+2H]^{2+}$: 681.36399 found: 681.3641 (0.22 ppm).
LCMS pic at 3.76 min: HRMS (TOF MS ES+): *m/z* calcd for $C_{82}H_{91}N_{17}O_6$ $[M+2H]^{2+}$: 704.86636 found: 704.8671 (1 ppm)
LCMS pic at 3.76 min: HRMS (TOF MS ES+): *m/z* calcd for $C_{82}H_{91}N_{17}O_6$ $[M+2H]^{2+}$: 704.86636 found: 704.8671 (1 ppm)
LCMS pic at 4.09 min: HRMS (TOF MS ES+): *m/* calcd for $C_{82}H_{91}N_{17}O_6$ $[M+2H]^{2+}$: 704.86636 found: 704.8668 (0.56 ppm)
LCMS pic at 4.66 min: HRMS (TOF MS ES+): *m/z* $C_{87}H_{92}N_{16}O_6$ $[M+2H]^{2+}$: 728.36874 found: 728.3690 (0.3 ppm)

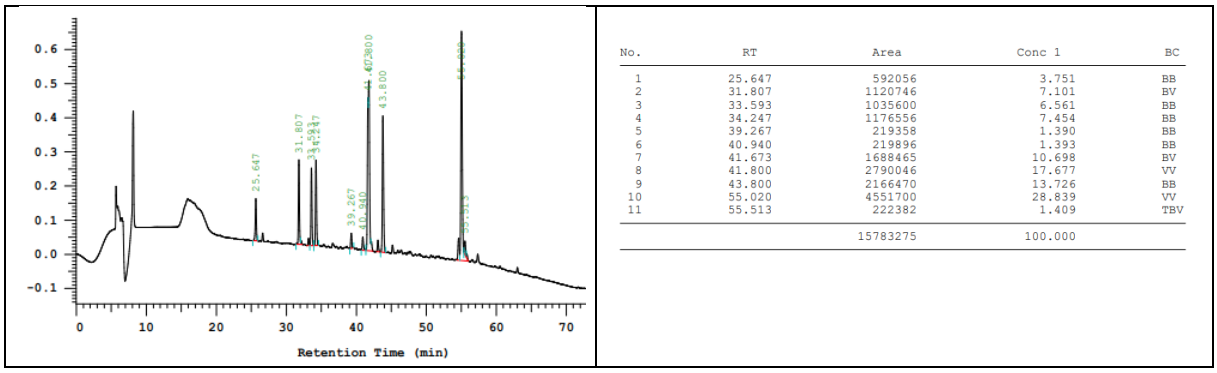

No.	RT	Area	Conc 1	BC
1	25.647	592056	3.751	BB
2	31.807	1120746	7.101	BV
3	33.593	1035600	6.561	BB
4	34.247	1176556	7.454	BB
5	39.267	219358	1.390	BB
6	40.940	219896	1.393	BB
7	41.673	1688465	10.698	BV
8	41.800	2790046	17.677	VV
9	43.800	2166470	13.726	BB
10	55.020	4551700	28.839	VV
11	55.513	222382	1.409	TBV
		15783275	100.000	

*Figure S72 HPLC chromatogram of purified **III-6(a,d)(2,4,6)**.*

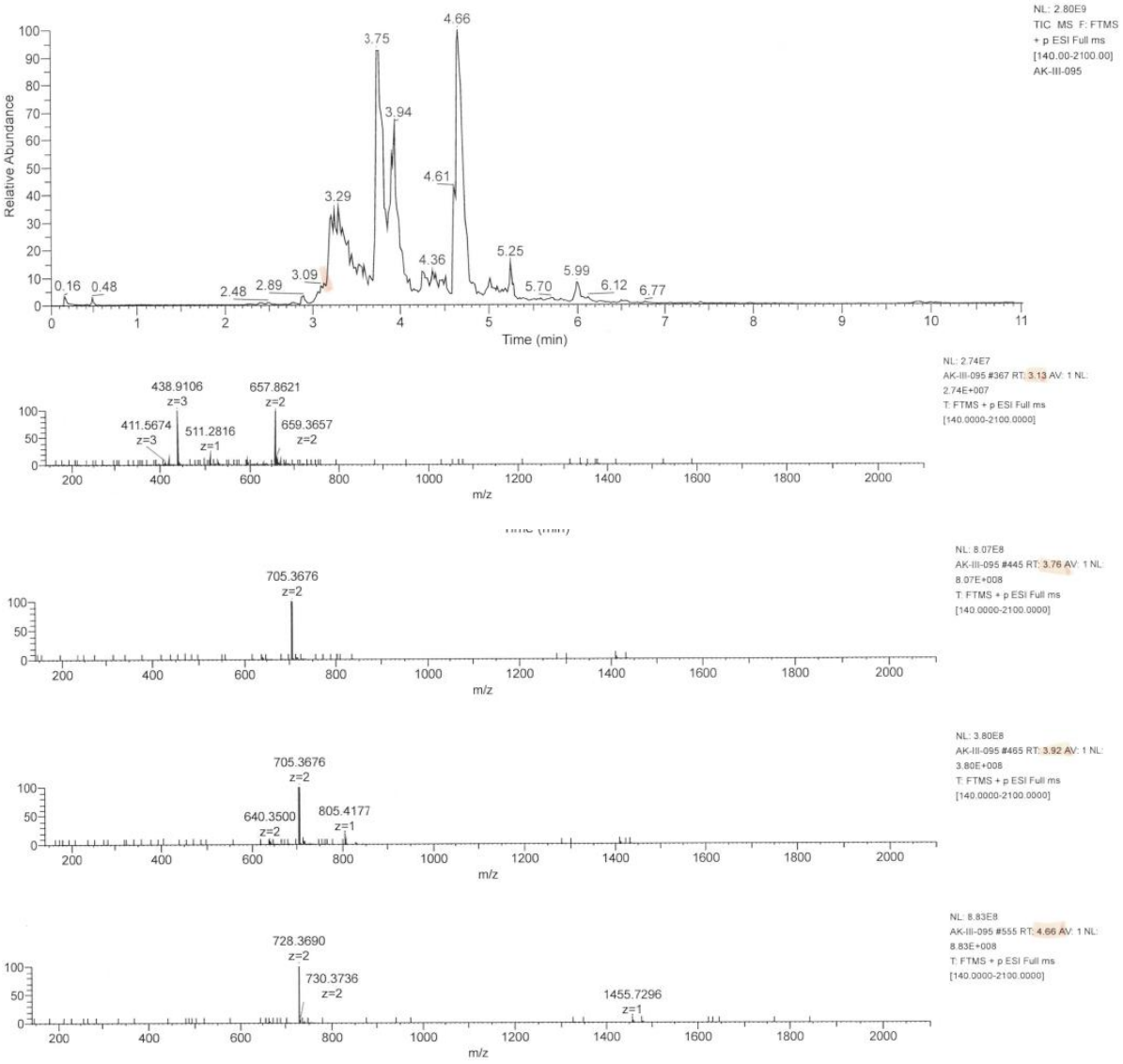

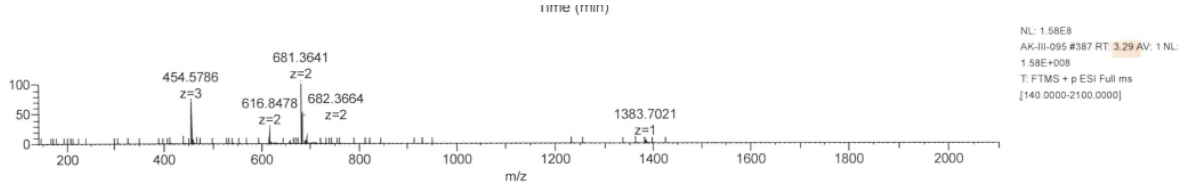

Figure S73 LCMS spectra of ***III-6(a,d)(2,4,6)****.*

5.3.3. meta-arylopeptoid Hexamer, ***III-6(b,c)(2,4,6)****.*

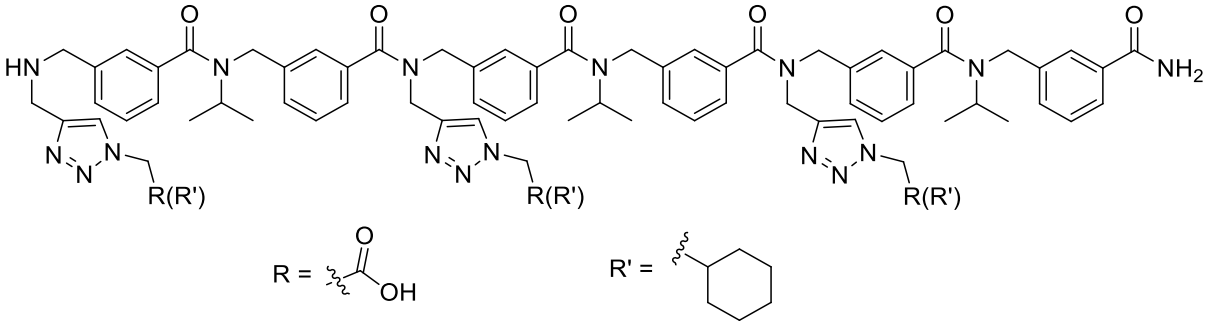

Hexamer **III-6(b,c)(2,4,6)** was synthesised according general procedure A then general procedure B using 100 mg of RA resin (0.054 mmol)

m_{crude}= 112 mg (purity 80%), crude yield 137%
m_{pure}= 62 mg (purity 88%) isolated yield 82%
LCMS pic at 4.12 min: HRMS (TOF MS ES+): *m/z* calcd for $C_{72}H_{80}N_{16}O_{12}$ $[M+2H]^{2+}$: 680.30653 found: 680.3065 (-0.11 ppm).
LCMS pic at 4.46 min: HRMS (TOF MS ES+): *m/z* calcd for $C_{77}H_{90}N_{16}O_{10}$ $[M+2H]^{2+}$: 699.35074 found: 699.3507 (-0.05 ppm)
LCMS pic at 4.63 min: HRMS (TOF MS ES+): *m/z* calcd for $C_{77}H_{90}N_{16}O_{10}$ $[M+2H]^{2+}$: 699.35074 found: 699.3507 (-0.05 ppm)
LCMS pic at 4.73 min: HRMS (TOF MS ES+): *m/z* calcd for $C_{77}H_{90}N_{16}O_{10}$ $[M+2H]^{2+}$: 699.35074 found: 699.3508 (0.05 ppm)
LCMS pic at 4.85 min: HRMS (TOF MS ES+): *m/* calcd for $C_{82}H_{100}N_{16}O_8$ $[M+2H]^{2+}$: 718.39495 found: 718.3951 (0.18 ppm)
LCMS pic at 4.94 min: HRMS (TOF MS ES+): *m/* calcd for $C_{82}H_{100}N_{16}O_8$ $[M+2H]^{2+}$: 718.39495 found: 718.395 (0.01 ppm)
LCMS pic at 5.12 min: HRMS (TOF MS ES+): *m/* calcd for $C_{82}H_{100}N_{16}O_8$ $[M+2H]^{2+}$: 718.39495 found: 718.395 (0.09 ppm)
LCMS pic at 5.24 min: HRMS (TOF MS ES+): *m/z* calcd for $C_{87}H_{110}N_{16}O_6$ $[M+2H]^{2+}$: 737.43916 found: 737.4392 (0.06 ppm)

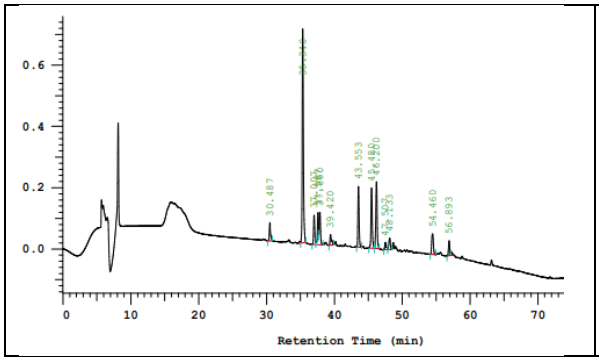

No.	RT	Area	Conc 1	BC
1	30.487	351964	3.238	BB
2	35.340	3829201	35.224	BB
3	37.007	497540	4.577	BV
4	37.587	575907	5.298	VV
5	37.860	585930	5.390	VB
6	39.420	250522	2.304	BB
7	43.553	1066193	9.808	BB
8	45.480	1150864	10.586	BB
9	46.200	1323972	12.179	BB
10	47.507	161316	1.484	BB
11	48.133	253709	2.334	BB
12	54.460	545957	5.022	BB
13	56.893	278025	2.557	BB
		10871100	100.000	

Figure S74 HPLC of purified ***III-6(b,c)(2,4,6)****.*

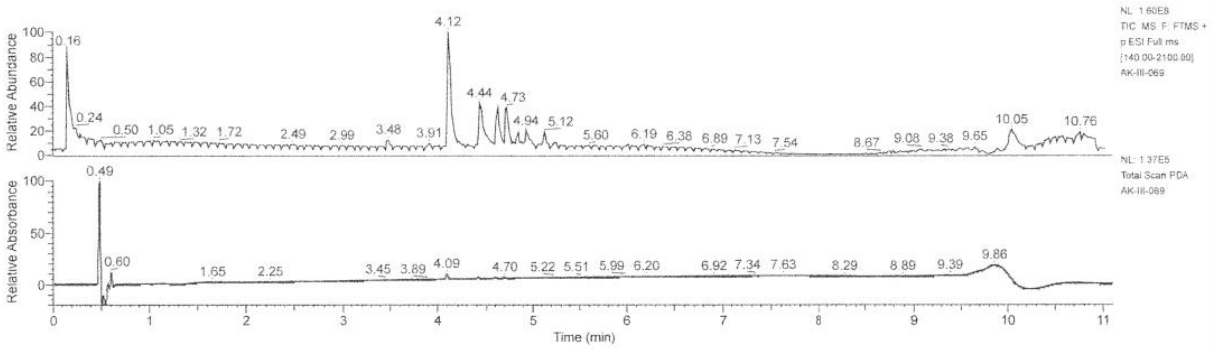
NL: 1.60E8
TIC MS F: FTMS + p ESI Full ms [140.00-2100.00] AK-III-069
Relative Abundance
0.16
0.24
0.50
1.05
1.32
1.72
2.49
2.99
3.48
3.91
4.12
4.44
4.73
4.94
5.12
5.60
6.19
6.38
6.89
7.13
7.54
8.67
9.08
9.38
9.65
10.05
10.76
NL: 1.37E5
Total Scan PDA AK-III-069
Relative Absorbance
0.49
0.60
1.65
2.25
3.45
3.89
4.09
4.70
5.22
5.51
5.99
6.20
6.92
7.34
7.63
8.29
8.89
9.39
9.86
Time (min)

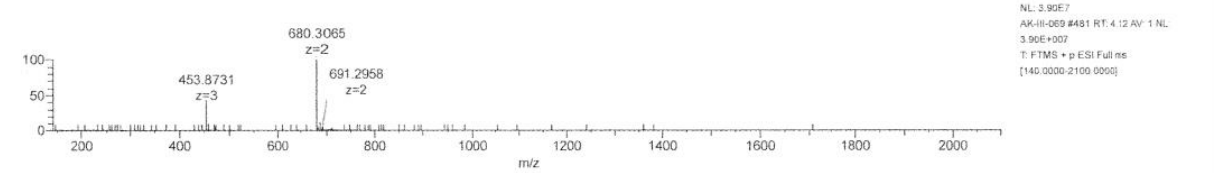
NL: 3.90E7
AK-III-069 #481 RT: 4.12 AV: 1 NL: 3.90E+007
T: FTMS + p ESI Full ms [140.0000-2100.0000]
680.3065 z=2
453.8731 z=3
691.2958 z=2
m/z

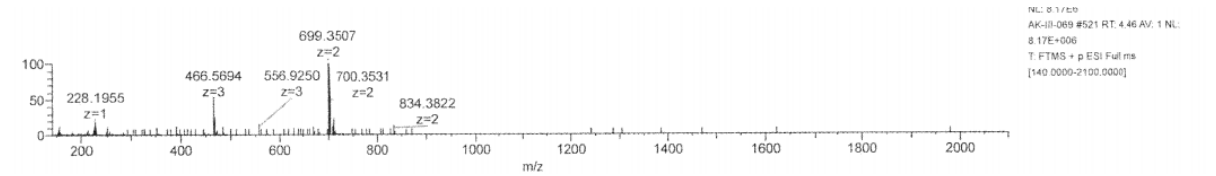
AK-III-069 #521 RT: 4.46 AV: 1 NL: 8.17E+006
T: FTMS + p ESI Full ms [140.0000-2100.0000]
699.3507 z=2
466.5694 z=3
556.9250 z=3
700.3531 z=2
228.1955 z=1
834.3822 z=2
m/z

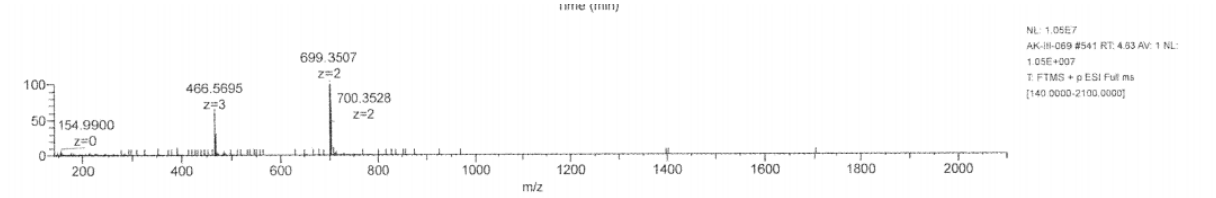
NL: 1.05E7
AK-III-069 #541 RT: 4.63 AV: 1 NL: 1.05E+007
T: FTMS + p ESI Full ms [140.0000-2100.0000]
699.3507 z=2
466.5695 z=3
700.3528 z=2
154.9900 z=0
m/z

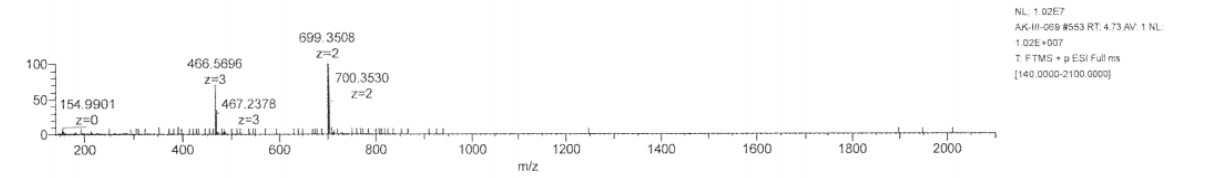
NL: 1.02E7
AK-III-069 #553 RT: 4.73 AV: 1 NL: 1.02E+007
T: FTMS + p ESI Full ms [140.0000-2100.0000]
699.3508 z=2
466.5696 z=3
700.3530 z=2
154.9901 z=0
467.2378 z=3
m/z

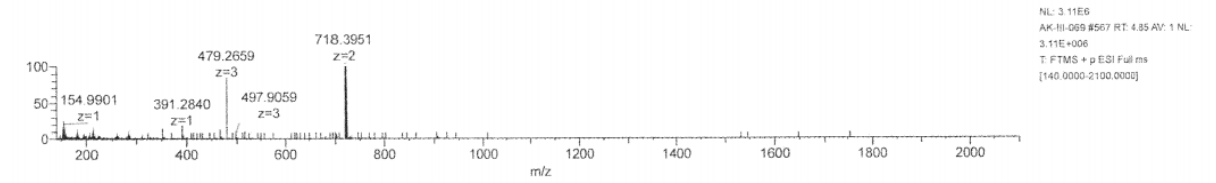
NL: 3.11E6
AK-III-069 #567 RT: 4.85 AV: 1 NL: 3.11E+006
T: FTMS + p ESI Full ms [140.0000-2100.0000]
718.3951 z=2
479.2659 z=3
154.9901 z=1
391.2840 z=1
497.9059 z=3
m/z

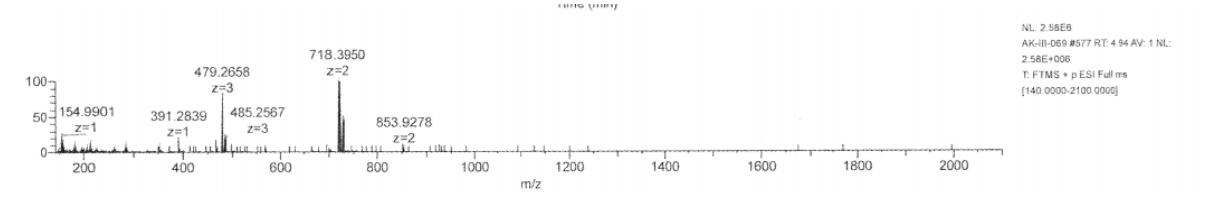
NL: 2.58E6
AK-III-069 #577 RT: 4.94 AV: 1 NL: 2.58E+006
T: FTMS + p ESI Full ms [140.0000-2100.0000]
718.3950 z=2
479.2658 z=3
154.9901 z=1
391.2839 z=1
485.2567 z=3
853.9278 z=2
m/z

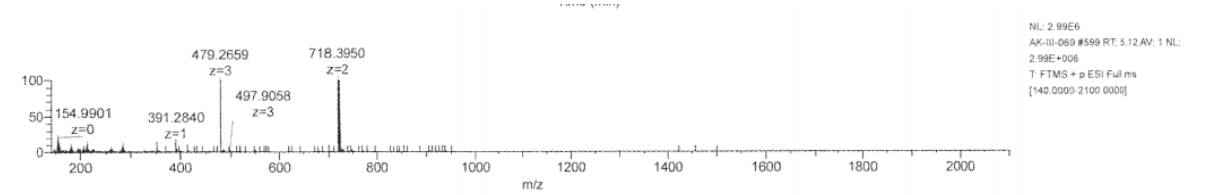
NL: 2.99E6
AK-III-069 #599 RT: 5.12 AV: 1 NL: 2.99E+006
T: FTMS + p ESI Full ms [140.0000-2100.0000]
718.3950 z=2
479.2659 z=3
497.9058 z=3
154.9901 z=0
391.2840 z=1
m/z

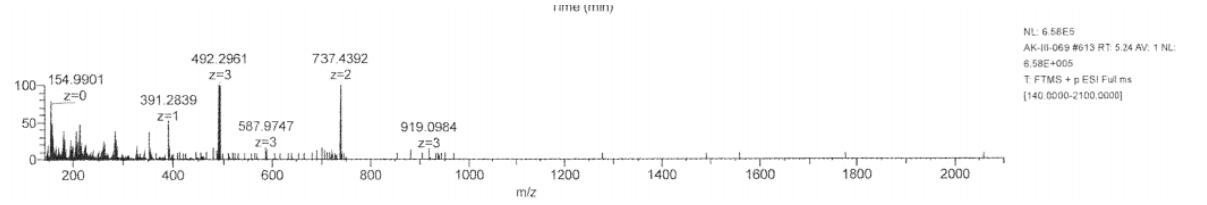

Figure S75 LCMS spectra of ***III-6(b,c)(2,4,6)****.*

5.3.3. meta-arylopeptoid Hexamer, III-6(b,d)(2,4,6).

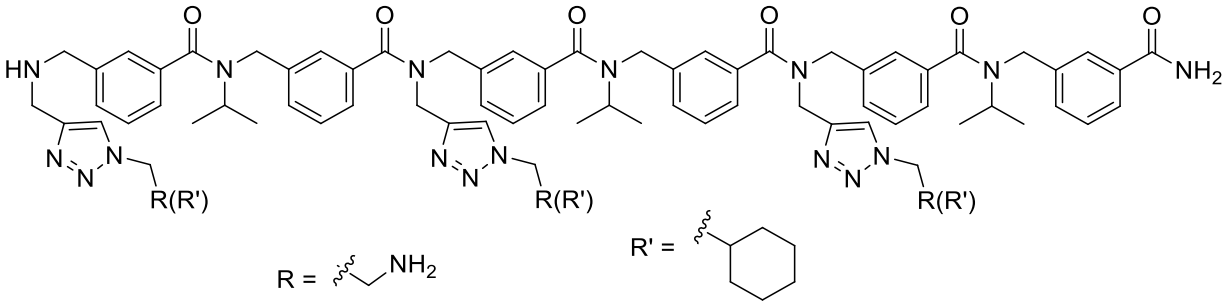

Hexamer **III-6(b,d)(2,4,6)** was synthesised according general procedure A then general procedure B using 100 mg of RA resin (0.054 mmol)

m_{crude}= 74 mg (purity 81%), crude yield 88%
m_{pure}= 62 mg (purity 96%), isolated yield 82%
LCMS pic at 3.64 min: HRMS (TOF MS ES+): *m/z* calcd for $C_{72}H_{90}N_{19}O_6$ $[M+3H]^{3+}$: 438.91017 found: 438.9103 (0.39 ppm)
LCMS pic at 3.8 min: HRMS (TOF MS ES+): *m/z* calcd for $C_{77}H_{97}N_{18}O_6$ $[M+3H]^{3+}$: 456.59407 found: 456.5945 (1.04 ppm)
LCMS pic at 4.26 min: HRMS (TOF MS ES+): *m/z* calcd for $C_{82}H_{103}N_{17}O_6$ $[M+2H]^{2+}$: 710.91331 found: 710.9135 (0.2 ppm)
LCMS pic at 4.51 min: HRMS (TOF MS ES+): *m/z z* calcd for $C_{82}H_{103}N_{17}O_6$ $[M+2H]^{2+}$: 710.91331 found: 710.9135 (0.2 ppm)
LCMS pic at 4.09 min: HRMS (TOF MS ES+): *m/* calcd for $C_{82}H_{91}N_{17}O_6$ $[M+2H]^{2+}$: 704.86636 found: 704.8668 (0.56 ppm)
LCMS pic at 4.66 min: HRMS (TOF MS ES+): *m/z* calcd for $C_{87}H_{110}N_{16}O_6$ $[M+2H]^{2+}$: 737.43916 found: 737.4396 (0.64 ppm)

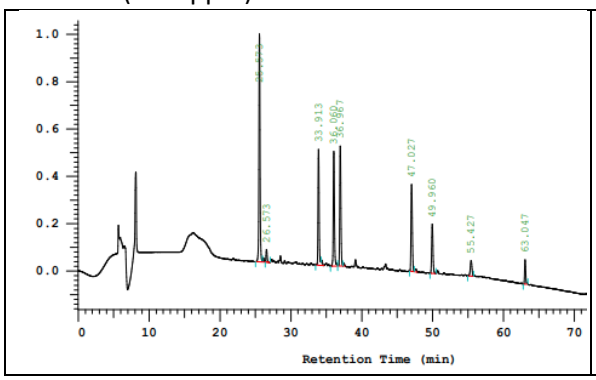

No.	RT	Area	Conc 1	BC
1	25.573	4684919	28.033	BV
2	26.573	244364	1.462	TBB
3	33.913	2392303	14.315	BV
4	36.060	2474881	14.809	BB
5	36.967	2582955	15.455	BB
6	47.027	2119784	12.684	BB
7	49.960	1220859	7.305	BB
8	55.427	498947	2.986	BB
9	63.047	493299	2.952	BB
		16712311	100.000	

Figure S76 HPLC chromatogram of purified ***III-6(b,d)(2,4,6)***

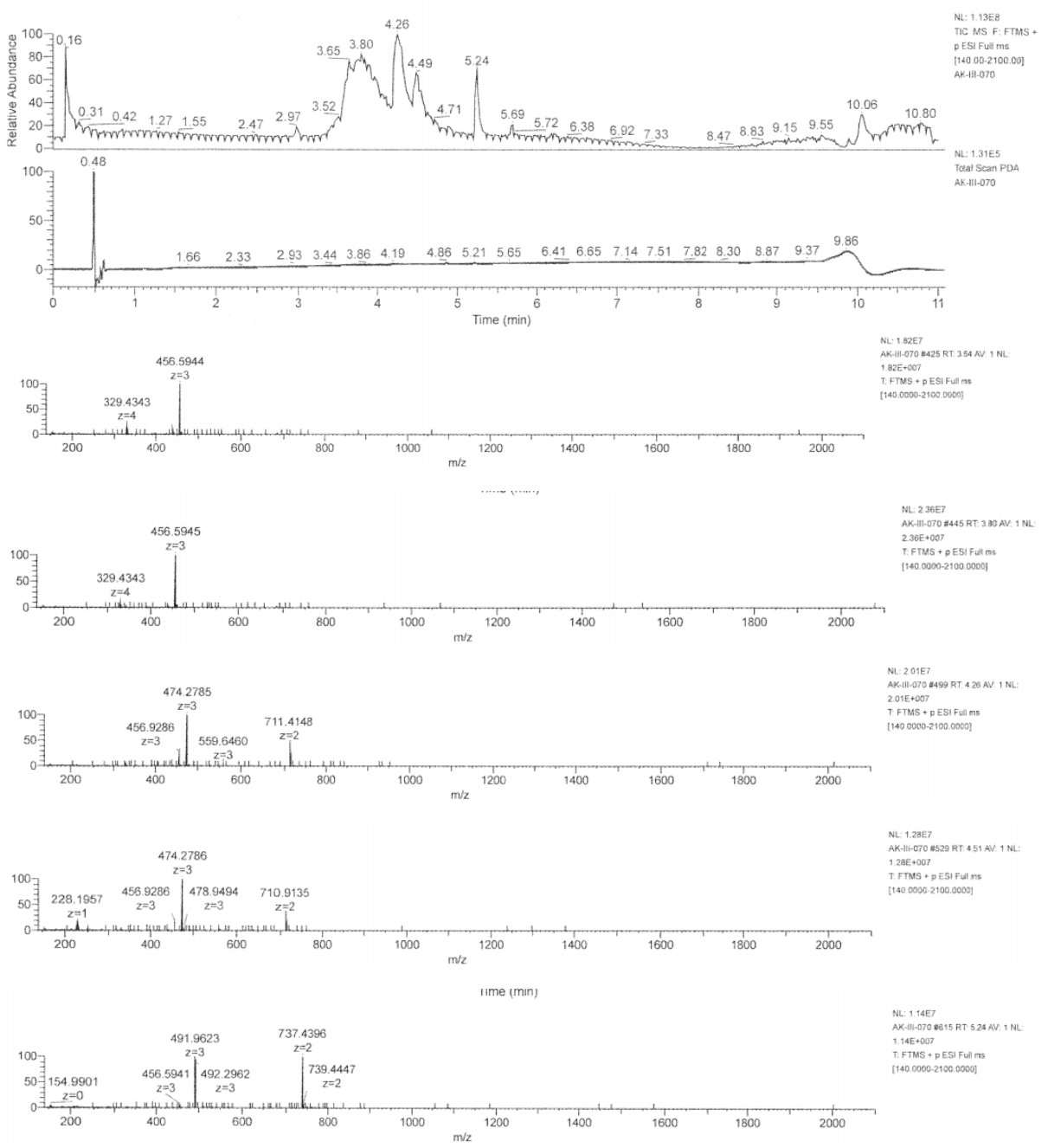

Figure S77 LCMS spectra of ***III-6(b,d)(2,4,6).***

5.3.4. meta-arylopeptoid Hexamer, III-6(c,d)(2,4,6).

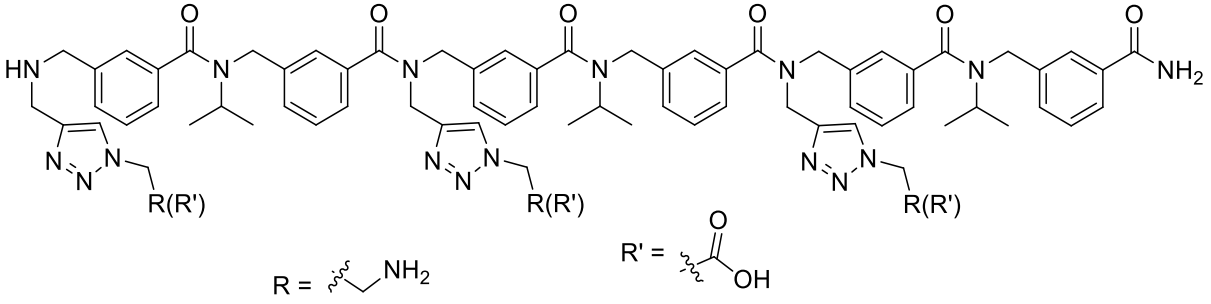

Hexamer **III-6(c,d)(2,4,6)** was synthesised according general procedure A then general procedure B using 50 mg of RA resin (0.031 mmol)

m_{crude}= 46 mg (purity 86%), crude yield 110%
m_{pure}= 33.8 mg (purity 97.8%), isolated yield 81%
LCMS pic at 3.29 min: HRMS (TOF MS ES+): *m/z* calcd for $C_{72}H_{87}N_{18}O_8$ $[M+3H]^{3+}$: 443.89793 found: 443.8988 (1.97 ppm).
LCMS pic at 3.19 min: HRMS (TOF MS ES+): *m/z* calcd for $C_{72}H_{87}N_{18}O_8$ $[M+3H]^{3+}$: 443.89793; found: 443.8989 (-2.11 ppm).
LCMS pic at 3.56 min: HRMS (TOF MS ES+): *m/z* calcd $C_{72}H_{83}N_{17}O_{10}$ $[M+2H]^{2+}$: 672.82489; found: 672.8253 (0.63 ppm).
LCMS pic at 4.13 min: HRMS (TOF MS ES+): *m/z* $C_{72}H_{80}N_{16}O_{12}$ $[M+2H]^{2+}$: 680.30653; found: 680.3075 (1.42 ppm).

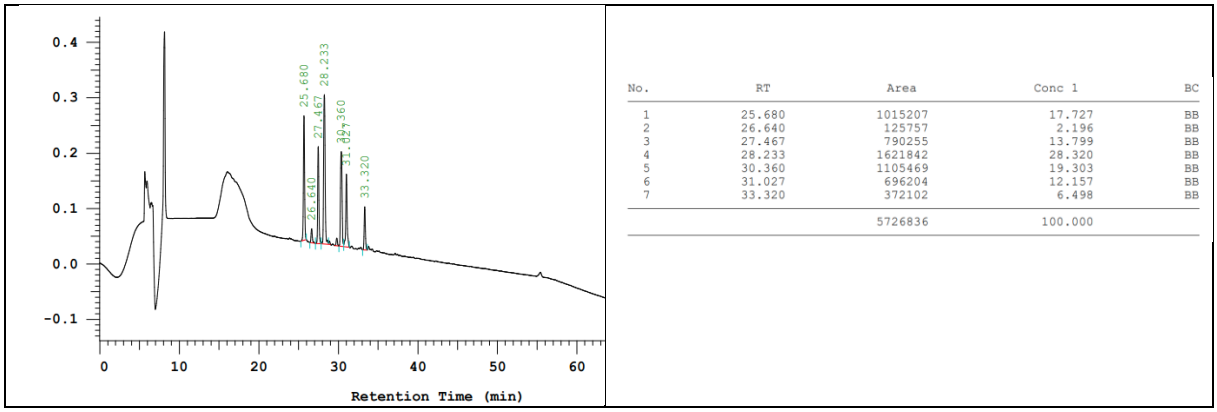

No.	RT	Area	Conc 1	BC
1	25.680	1015207	17.727	BB
2	26.640	125757	2.196	BB
3	27.467	790255	13.799	BB
4	28.233	1621842	28.320	BB
5	30.360	1105469	19.303	BB
6	31.027	696204	12.157	BB
7	33.320	372102	6.498	BB
		5726836	100.000	

Figure S78 HPLC chromatogram of purified ***III-6(c,d)(2,4,6)****.*

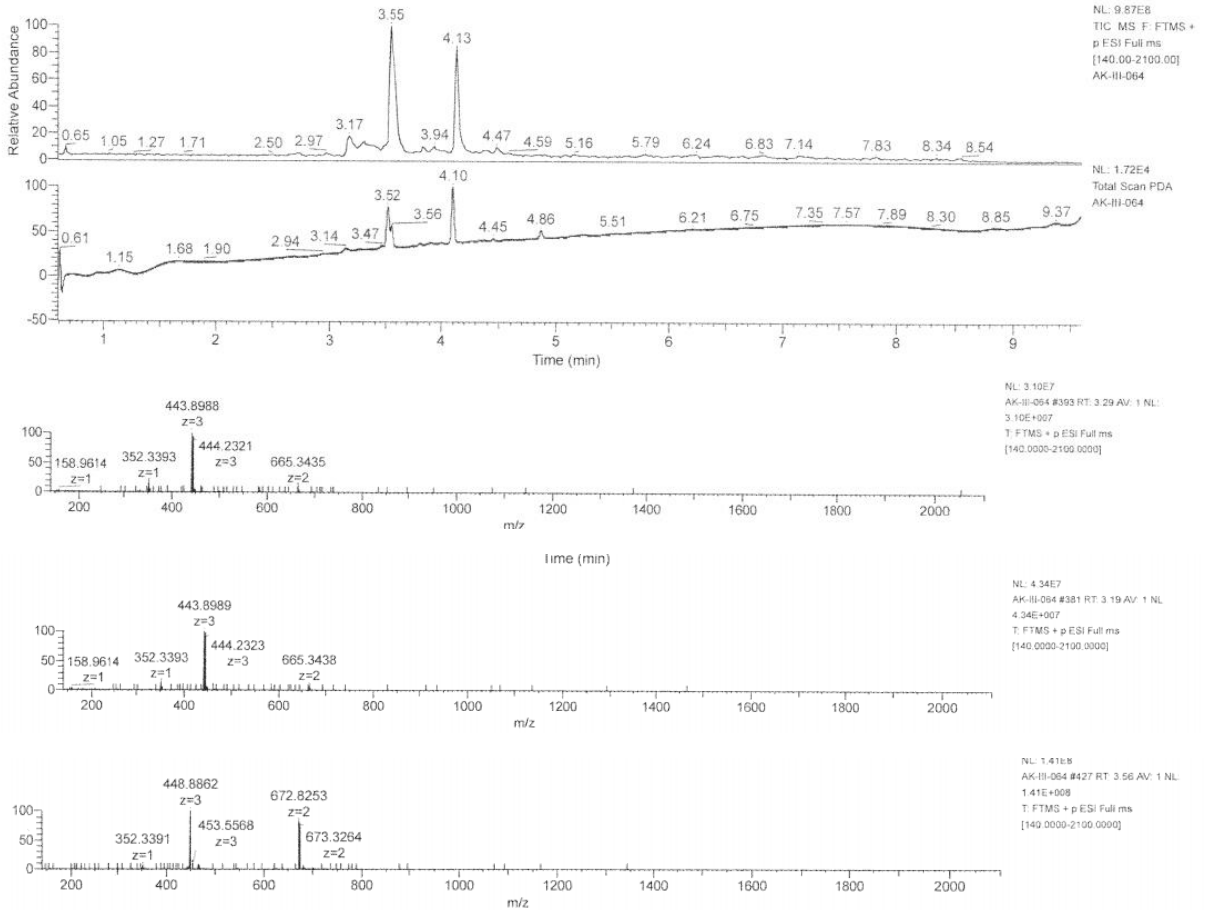

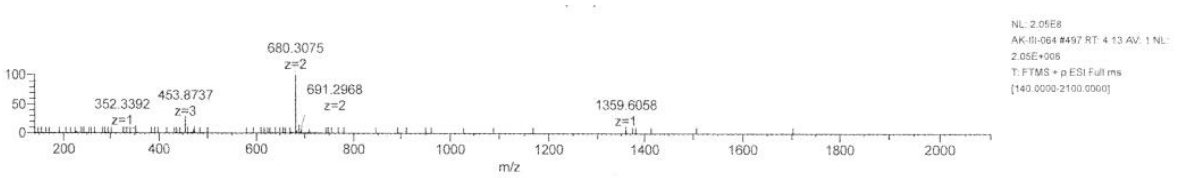

Figure S79 LCMS spectra of ***III-6(c,d)(2,4,6)****.*

5.3.5. Meta-arylopeptoid Hexamer, ***III-6(d,e)(2,4,6)****.*

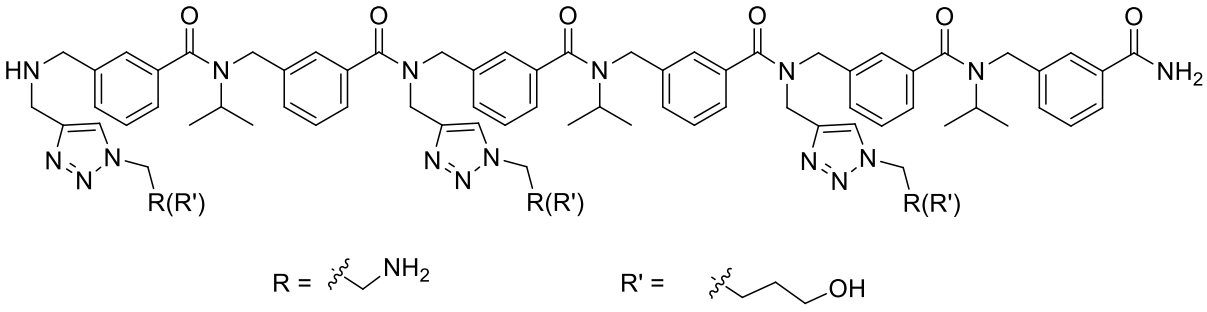

Hexamer **III-6(d,e)(2,4,6)** was synthesised according general procedure A then general procedure B using 50 mg of RA resin (0.031 mmol)

m_{crude}= 46 mg (purity 89%), crude yield 111%

m_{pure}= 33.8 mg (purity 98%), isolated yield 81%

LCMS pic at 2.77 min: HRMS (TOF MS ES+): *m/z* calcd for $C_{72}H_{89}N_{16}O_6$ $[M+2H]^{2+}$: 657.86161 found: 657.8613 (-0.52 ppm)

LCMS pic at 2.89 min: HRMS (TOF MS ES+): *m/z* calcd for $C_{73}H_{90}N_{18}O_7$ $[M+2H]^{2+}$: 665.36145 found: 665.3611 (-0.54 ppm)

LCMS pic at 3.18 min: HRMS (TOF MS ES+): *m/z* calcd for $C_{74}H_{91}N_{17}O_8$ $[M+2H]^{2+}$: 672.86128 found: 672.8617 (0.62 ppm)

LCMS pic at 3.58 min: HRMS (TOF MS ES+): *m/z* calcd for $C_{75}H_{92}N_{16}O_9$ $[M+2H]^{2+}$: 680.36111 found: 680.3611 (0.05 ppm)

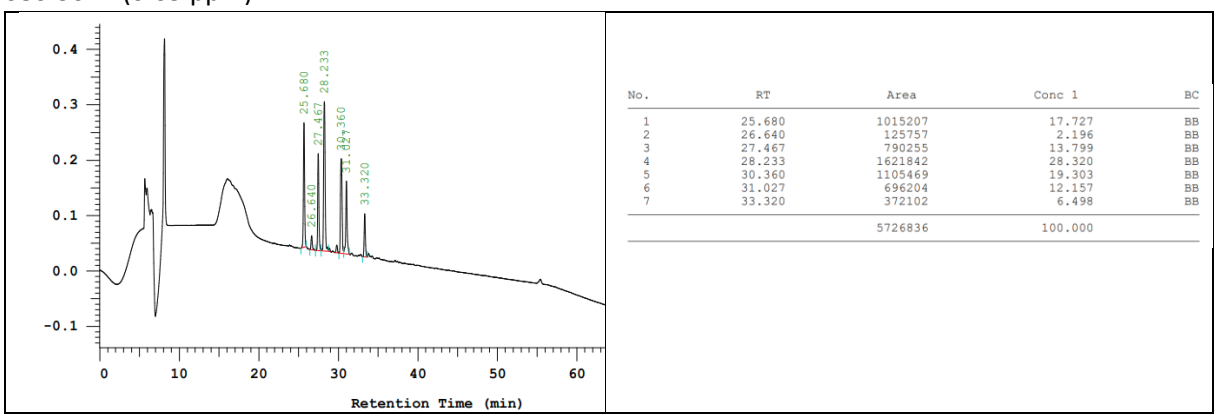

No.	RT	Area	Conc 1	BC
1	25.680	1015207	17.727	BB
2	26.640	125757	2.196	BB
3	27.467	790255	13.799	BB
4	28.233	1621842	28.320	BB
5	30.360	1105469	19.303	BB
6	31.027	696204	12.157	BB
7	33.320	372102	6.498	BB
		5726836	100.000	

Figure S80 HPLC chromatogram of purified ***III-6(d,e)(2,4,6).***

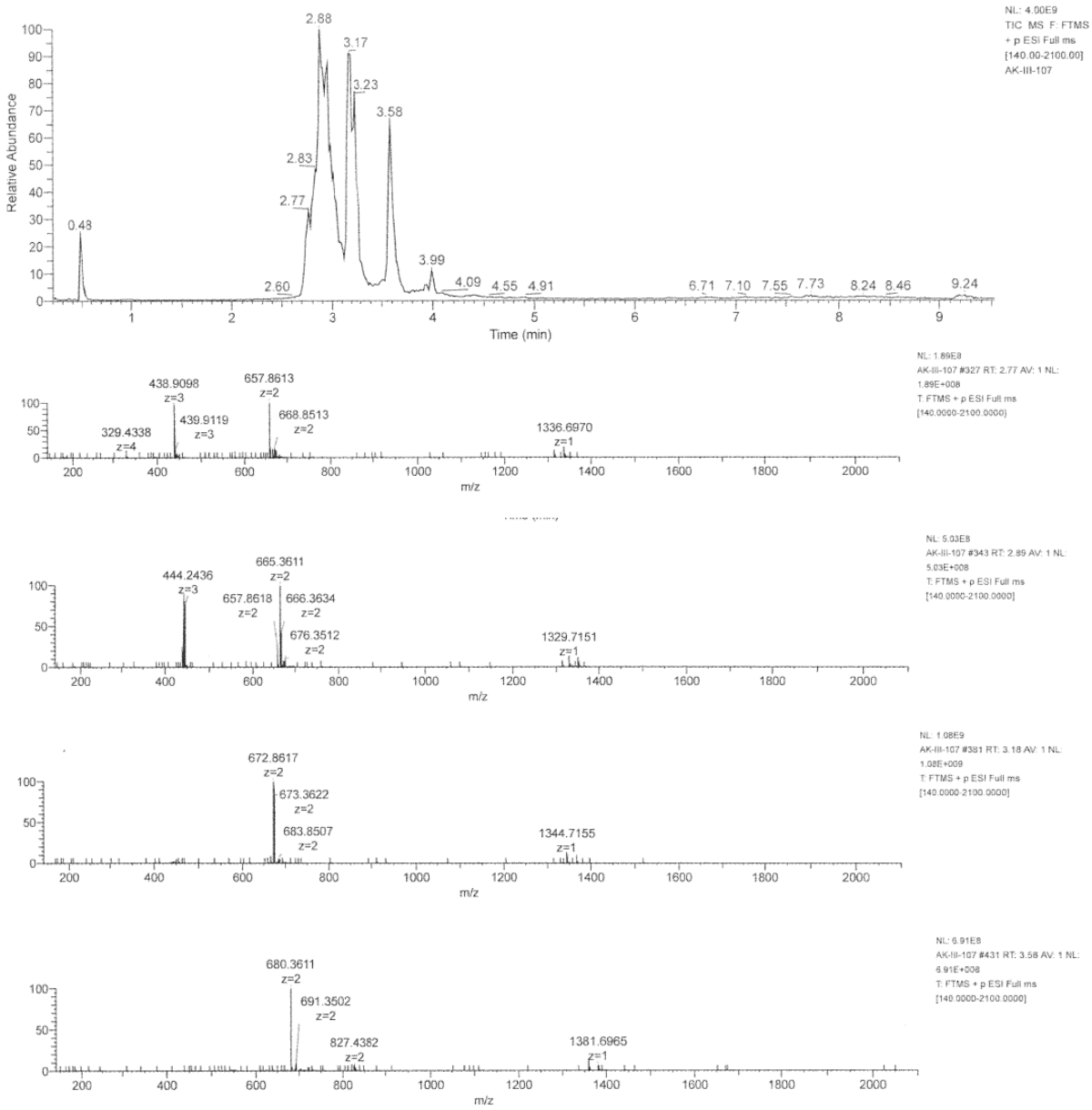

Figure S81 LCMS spectra of ***III-6(d,e)(2,4,6)***.

6.Sequential click for regioisomers

6.1. Synthetic paths

6.1.1. Synthetic path for ***III-6(a_2,$c_{4,6}$)***

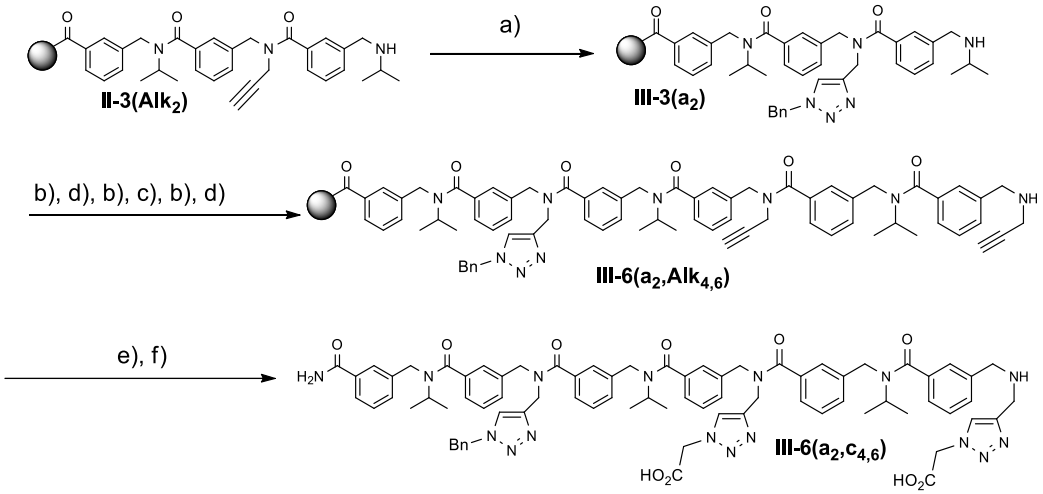

a) DCM/MeOH (*v*/*v*=8/2), Cata (5mol-%), **Ia**, 50°C. b) 3-(chloromethyl)-benzoyl chloride, DIPEA, DCM, RT. c) *iso*propyl amine, dmso, 50°C. d) Propargyl amine, dmso, 50°C. e) DCM/MeOH (*v*/*v*=8/2), Cata (5mol-%), **Ic**, 50°C. f) TFA/H_2O/tri *iso*propyl silane (95/2.5/2.5).

6.1.2. Synthetic path for **III-6(a_4,$c_{2,6}$)**

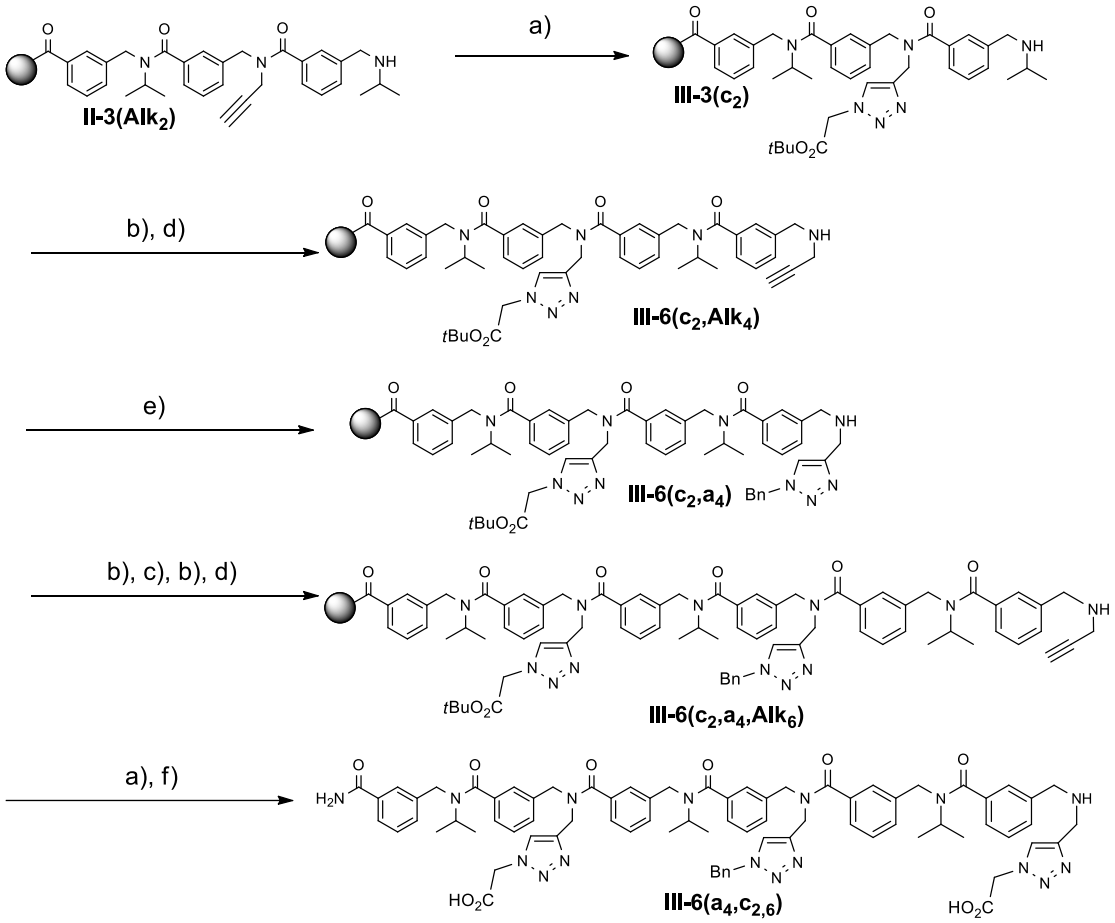

a) DCM/MeOH (*v*/*v*=8/2), Cata (5mol-%), **Ic**, 50°C. b) 3-(chloromethyl)-benzoyl chloride, DIPEA, DCM, RT. c) *iso*propyl amine, dmso, 50°C. d) Propargyl amine, dmso, 50°C. e) DCM/MeOH (*v*/*v*=8/2), Cata (5mol-%), **Ia**, 50°C. f) TFA/H_2O/tri *iso*propyl silane (95/2.5/2.5).

6.1.3. Synthetic path for *III-6-(a_6,$c_{2,4}$)*

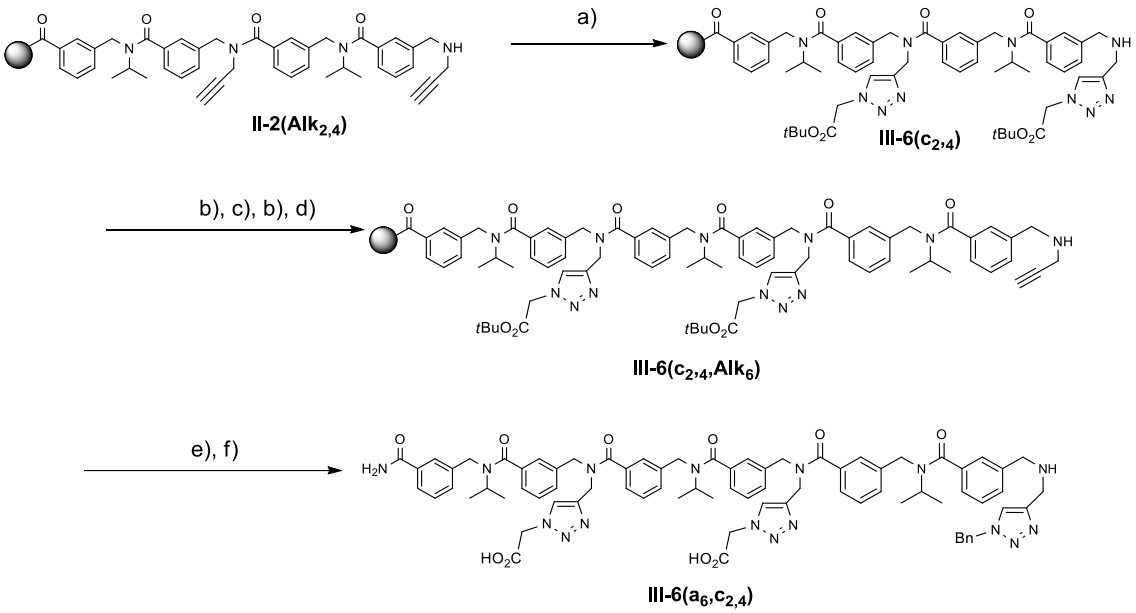

a) DCM/MeOH (*v*/*v*=8/2), Cata (5mol-%), **Ic**, 50°C. b) 3-(chloromethyl)-benzoyl chloride, DIPEA, DCM, RT. c) *iso*propyl amine, dmso, 50°C. d) Propargyl amine, dmso, 50°C. e) DCM/MeOH (*v*/*v*=8/2), Cata (5mol-%), **Ia**, 50°C. f) TFA/H_2O/tri *iso*propyl silane (95/2.5/2.5).

6.1.4. Synthetic path for *III-6-($a_{2,4}$,c_6)*

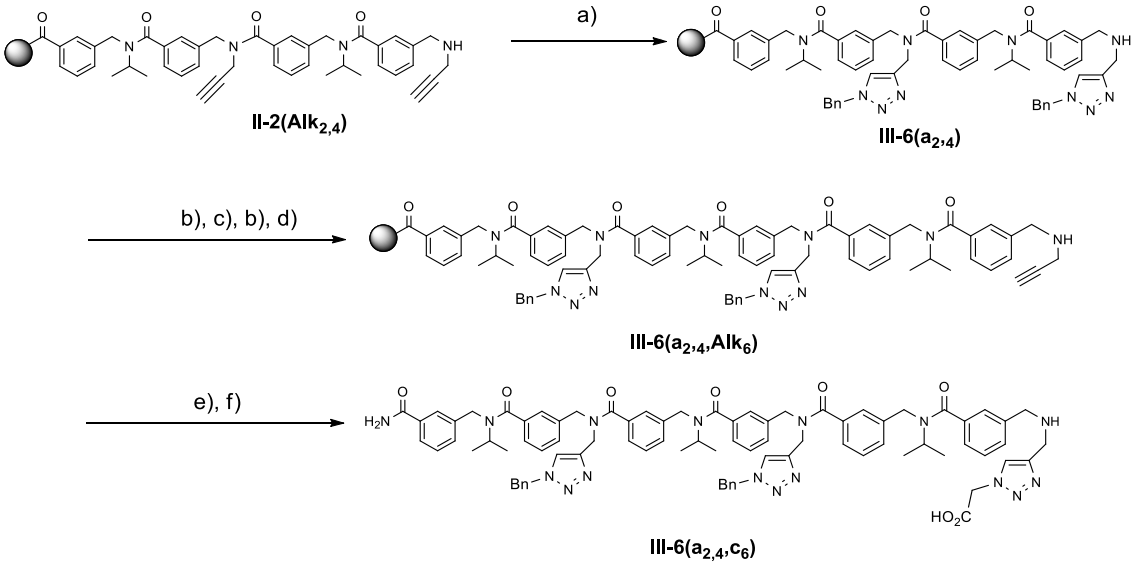

a) DCM/MeOH (*v*/*v*=8/2), Cata (5mol-%), **Ia**, 50°C. b) 3-(chloromethyl)-benzoyl chloride, DIPEA, DCM, RT. c) *iso*propyl amine, dmso, 50°C. d) Propargyl amine, dmso, 50°C. e) DCM/MeOH (*v*/*v*=8/2), Cata (5mol-%), **Ic**, 50°C. f) TFA/H_2O/tri *iso*propyl silane (95/2.5/2.5).

6.1.5. Synthetic path for **III-6-($a_{4,6}$,c_2)**

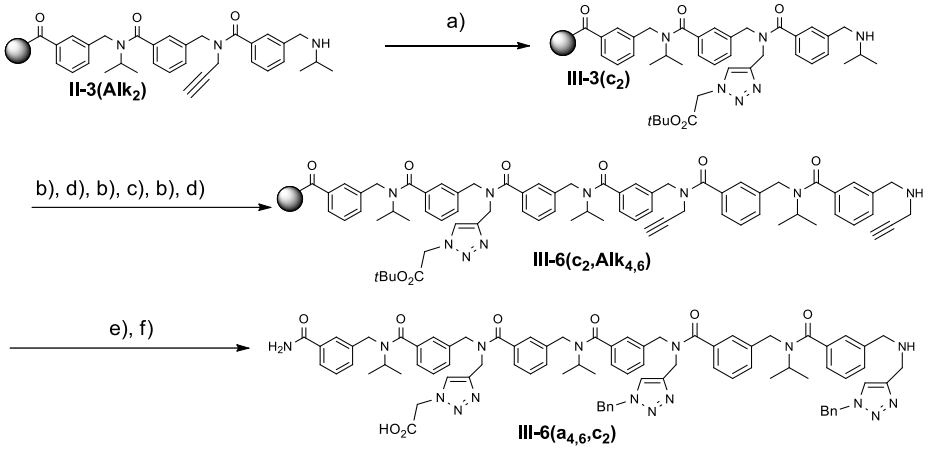

a) DCM/MeOH (*v*/*v*=8/2), Cata (5mol-%), **Ic**, 50°C. b) 3-(chloromethyl)-benzoyl chloride, DIPEA, DCM, RT. c) *iso*propyl amine, dmso, 50°C. d) Propargyl amine, dmso, 50°C. e) DCM/MeOH (*v*/*v*=8/2), Cata (5mol-%), **Ia**, 50°C. f) TFA/H_2O/tri *iso*propyl silane (95/2.5/2.5).

6.1.6. Synthetic path for **III-6-($a_{2,6}$,c_4)**

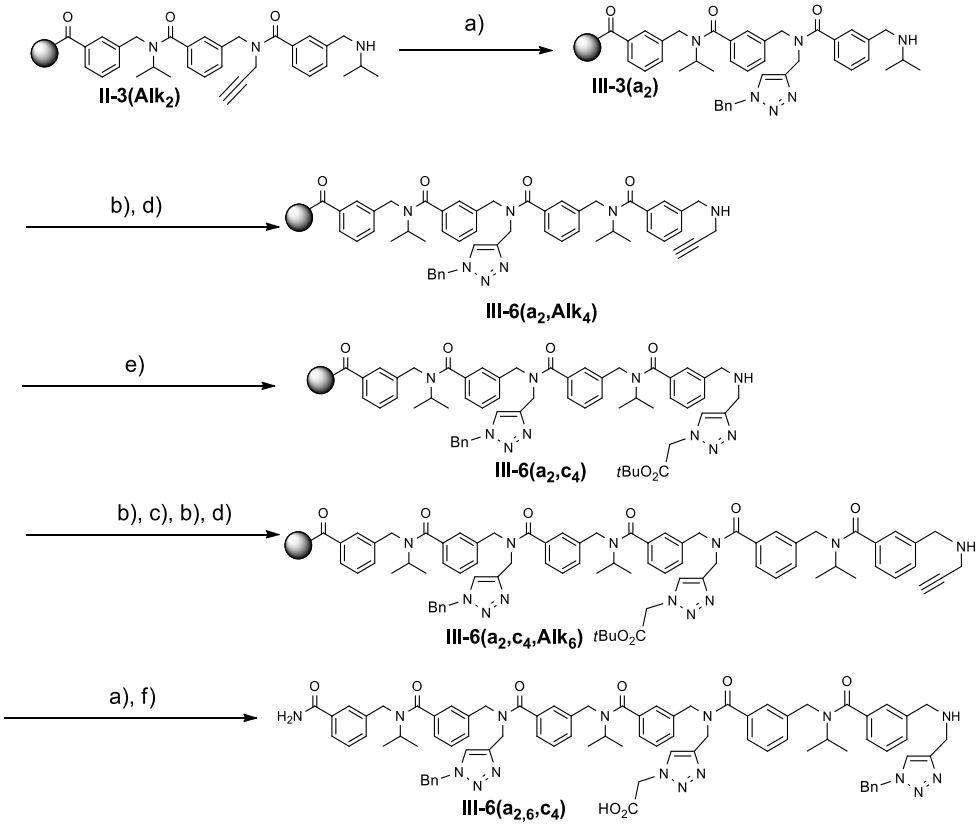

a) DCM/MeOH (*v*/*v*=8/2), Cata (5mol-%), **Ia**, 50°C. b) 3-(chloromethyl)-benzoyl chloride, DIPEA, DCM, RT. c) *iso*propyl amine, dmso, 50°C. d) Propargyl amine, dmso, 50°C. e) DCM/MeOH (*v*/*v*=8/2), Cata (5mol-%), **Ic**, 50°C. f) TFA/H_2O/tri *iso*propyl silane (95/2.5/2.5).

6.2. Analysis

*6.2.1. Synthesis of meta-arylopeptoid Hexamer, **III-6-(a_2,$c_{4,6}$):***

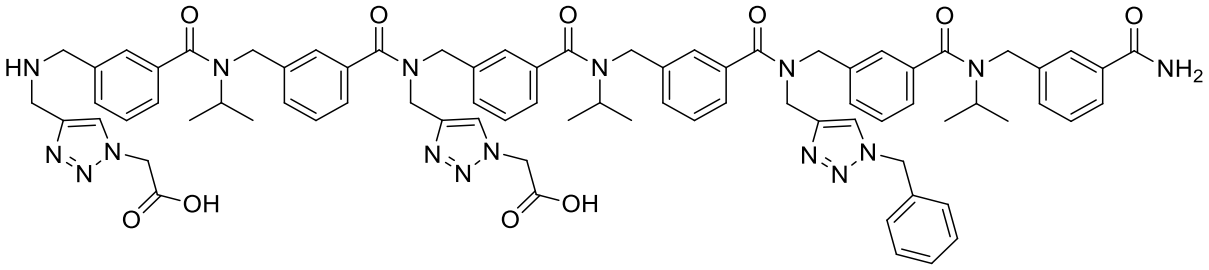

m_{crude} = 118 mg (purity 81%), crude yield 157%

m_{pure}= 63 mg, (purity 85%), isolated yield 84%

HRMS (TOF MS ES+): *m/z* calcd for $C_{77}H_{83}N_{16}O_{10}$ $[M+H]^+$: 1391.64726 found: 1391.6487 (1.02 ppm)

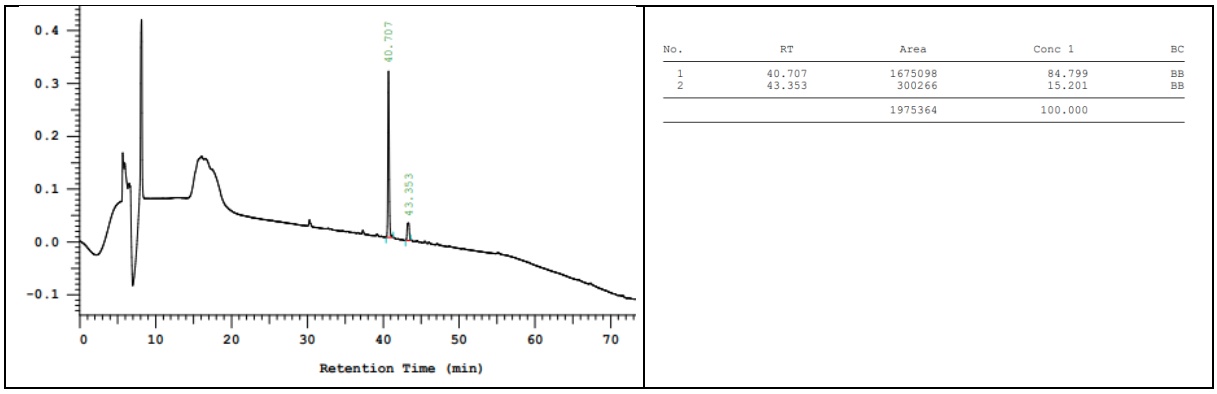

*Figure S82 HPLC chromatogram of purified **III-6-(a_2,$c_{4,6}$)**.*

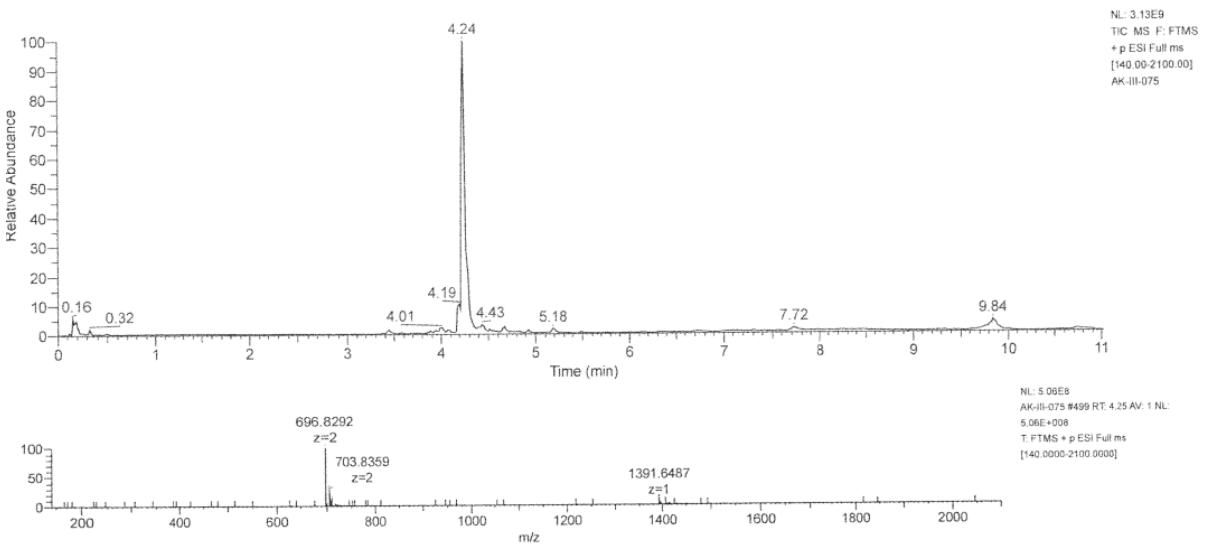

*Figure S83 LCMS spectra of **III-6-(a_2,$c_{4,6}$)**.*

6.2.2.Synthesis of meta-arylopeptoid Hexamer, ***III-6-($a_4c_{2,6}$):***

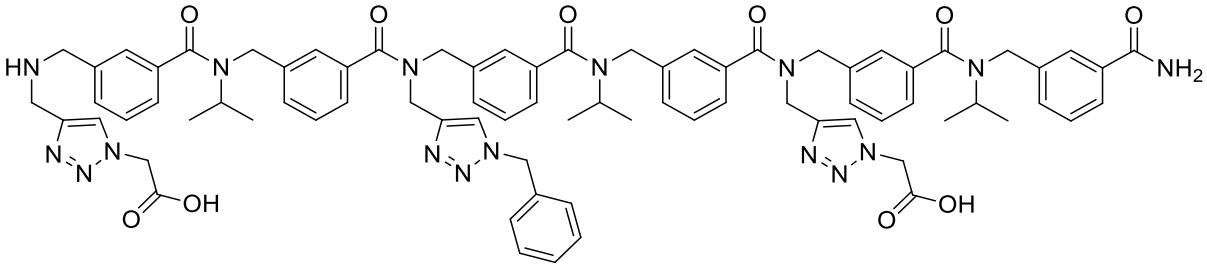

m_{crude} = 109 mg, (Purity 85%), crude yield 145%

m_{pure}= 70 mg, (Purity 97%), isolated yield 93%

HRMS (TOF MS ES+): *m/z* calcd for $C_{77}H_{83}N_{16}O_{10}$ $[M+H]^+$: 1391.64726 found: 1391.6487 (1.02 ppm)

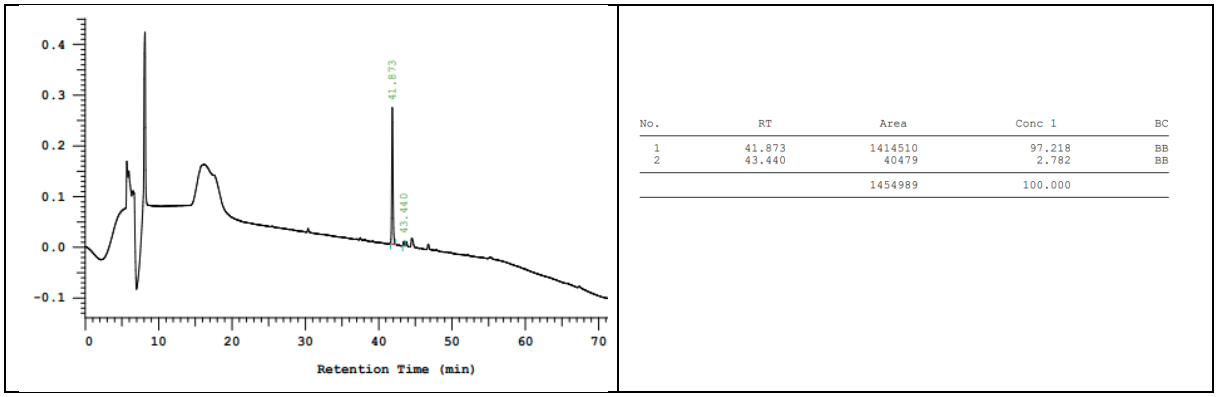

Figure S84 HPLC chromatogram of purified ***III-6-($a_4c_{2,6}$).***

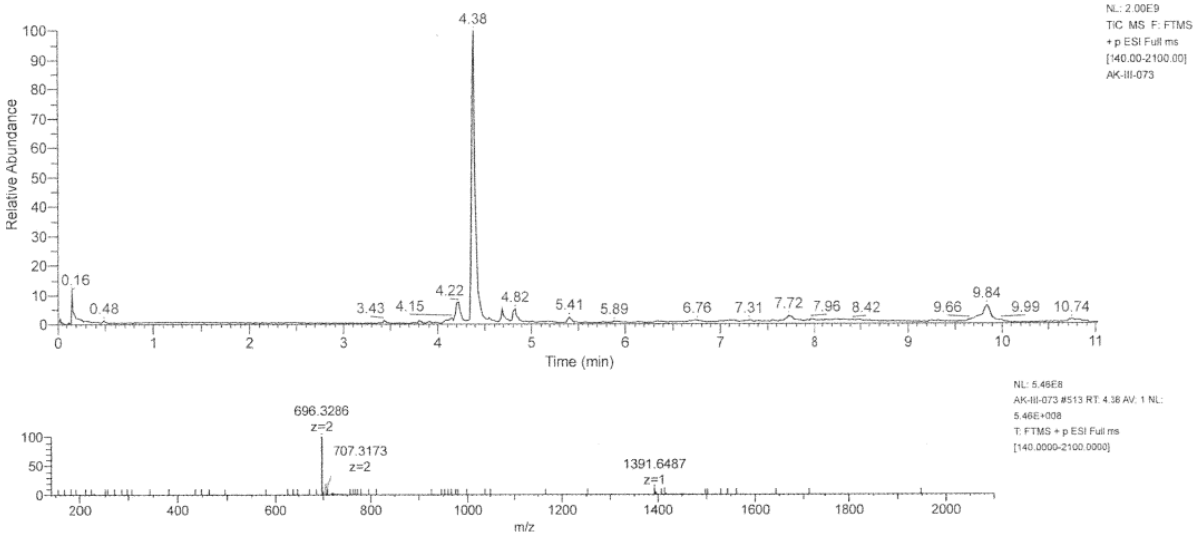

Figure S85 LCMS spectra of purified ***III-6-($a_4c_{2,6}$).***

6.2.3. Synthesis of meta-arylopeptoid Hexamer, ***III-6-($a_6c_{2,4}$):***

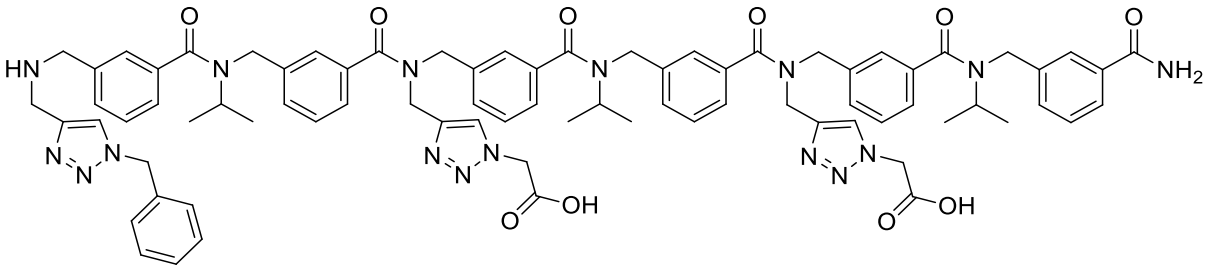

m_{crude} = 112 mg, (Purity 69%), crude yield 149%

m_{pure}= 50 mg, (Purity 87%), isolated yield 67%

HRMS (TOF MS ES+): *m/z* calcd for $C_{77}H_{83}N_{16}O_{10}$ $[M+H]^+$: 1391.64726 found: 1391.6487 (1.02 ppm)

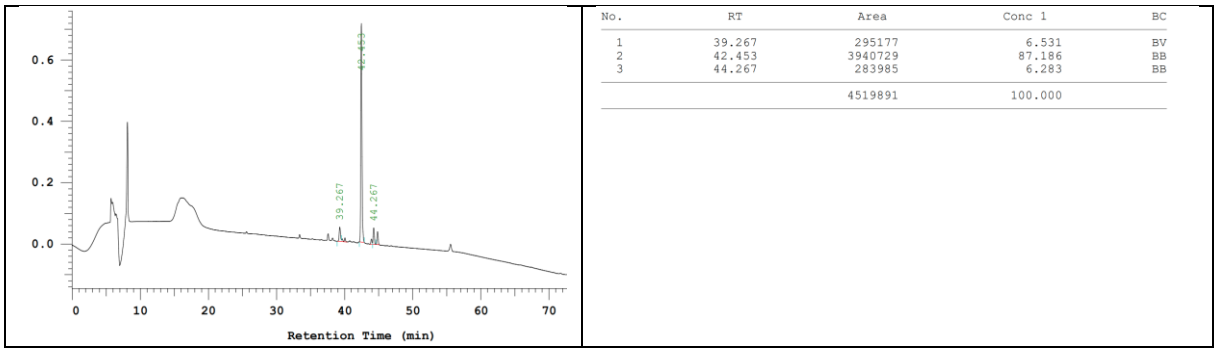

No.	RT	Area	Conc 1	BC
1	39.267	295177	6.531	BV
2	42.453	3940729	87.186	BB
3	44.267	283985	6.283	BB
		4519891	100.000	

Figure S86 HPLC chromatogram of purified ***III-6-(a_6,$c_{2,4}$).***

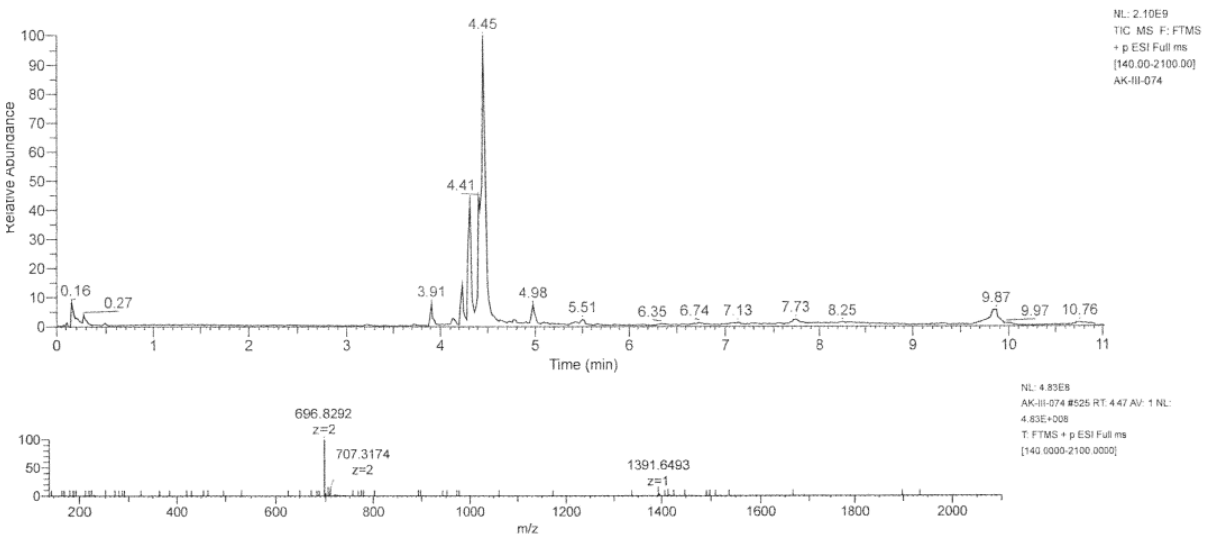

Figure S87 LCMS spectra of ***III-6-(a_6,$c_{2,4}$).***

6.2.4. Synthesis of meta-arylopeptoid Hexamer, ***III-6-($a_{2,4}$,c_6):***

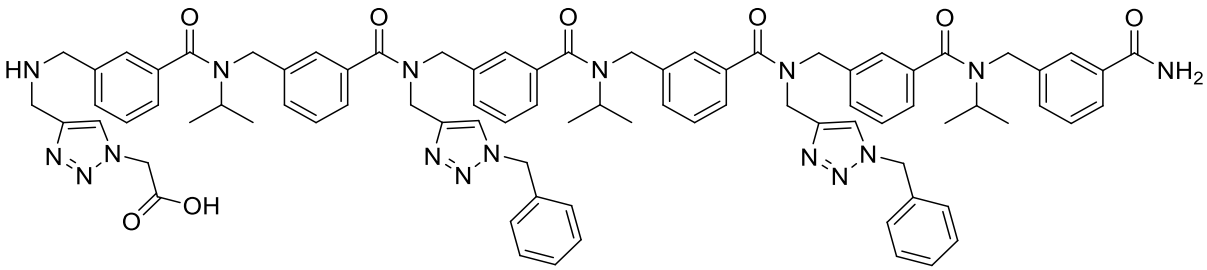

m_{crude} = 23.65 mg, (Purity 78%), crude yield 105%

m_{pure}= 20.1 mg, (purity 83%), isolated yield 90%.

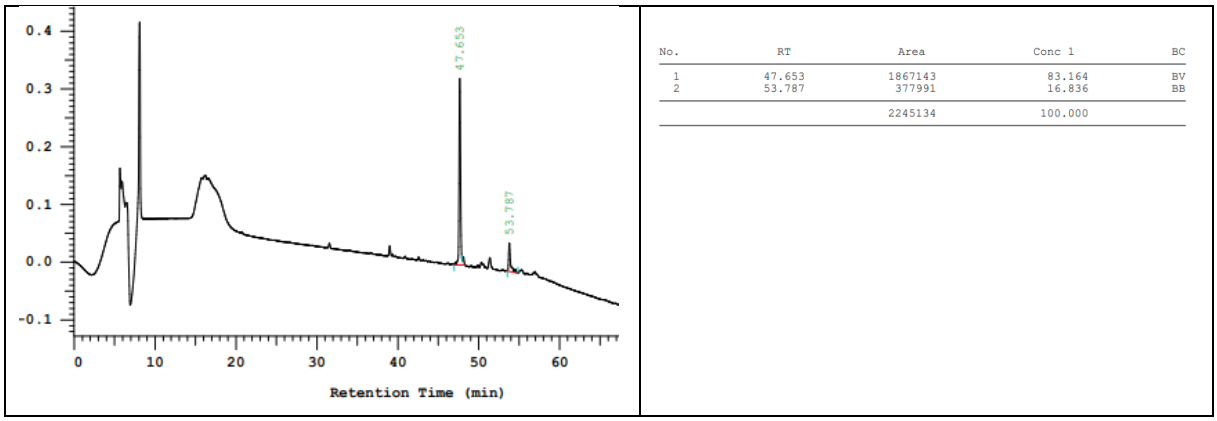

No.	RT	Area	Conc 1	BC
1	47.653	1867143	83.164	BV
2	53.787	377991	16.836	BB
		2245134	100.000	

Figure S88 HPLC chromatogram of purified ***III-6-($a_{2,4}c_6$).***

6.2.5. Synthesis of meta-arylopeptoid Hexamer, III-6-($a_{4,6}c_2$):

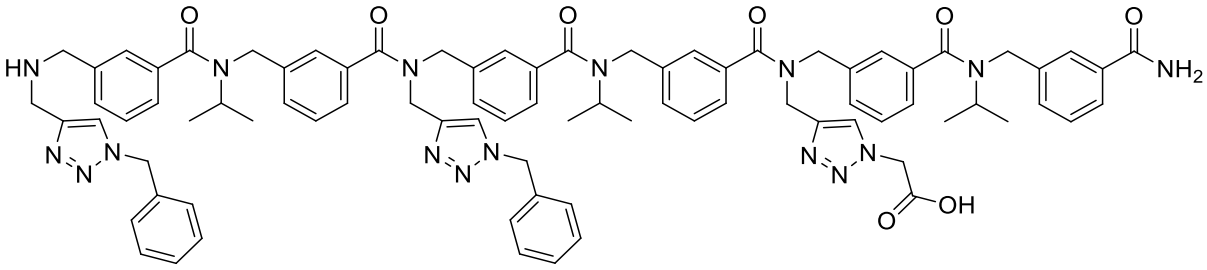

m_{crude} = 24.6 mg, (purity 82%), crude yield 109 %
m_{pure}= 18.6 mg (purity 92%), isolated yield 83%

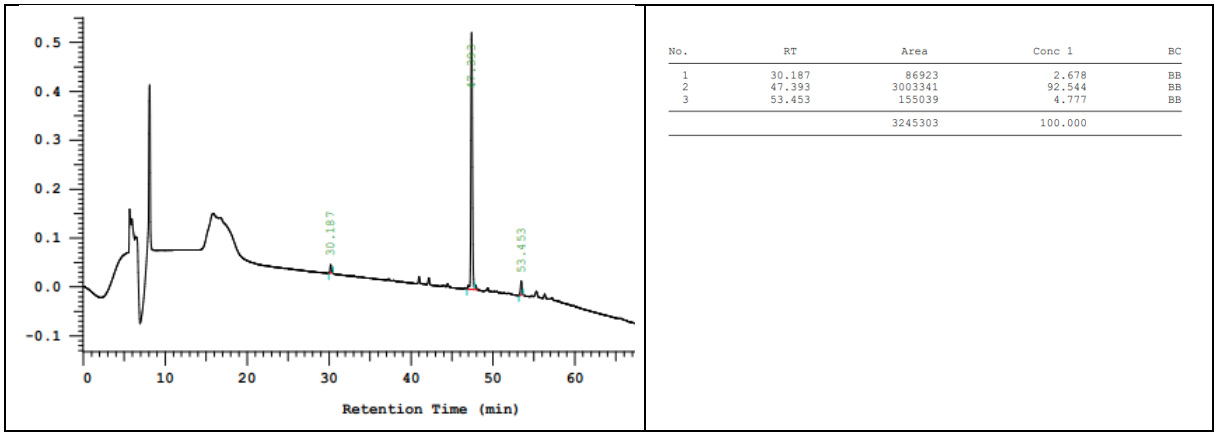

No.	RT	Area	Conc 1	BC
1	30.187	86923	2.678	BB
2	47.393	3003341	92.544	BB
3	53.453	155039	4.777	BB
		3245303	100.000	

Figure S89 HPLC chromatogram of purified ***III-6-($a_{4,6}c_2$).***

6.2.6. Synthesis of meta-arylopeptoid Hexamer, III-6-($a_{2,6}c_4$):

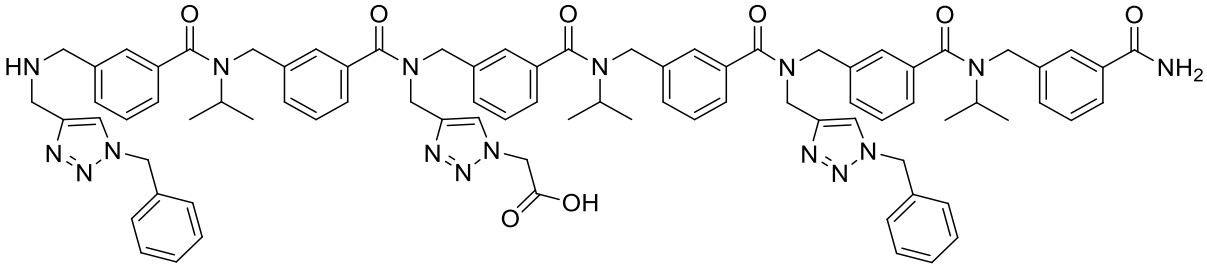

m_{crude} = 25 mg (purity 87%), crude yield 111%
m_{pure}= 19 mg (purity 93%), isolated yield 84%

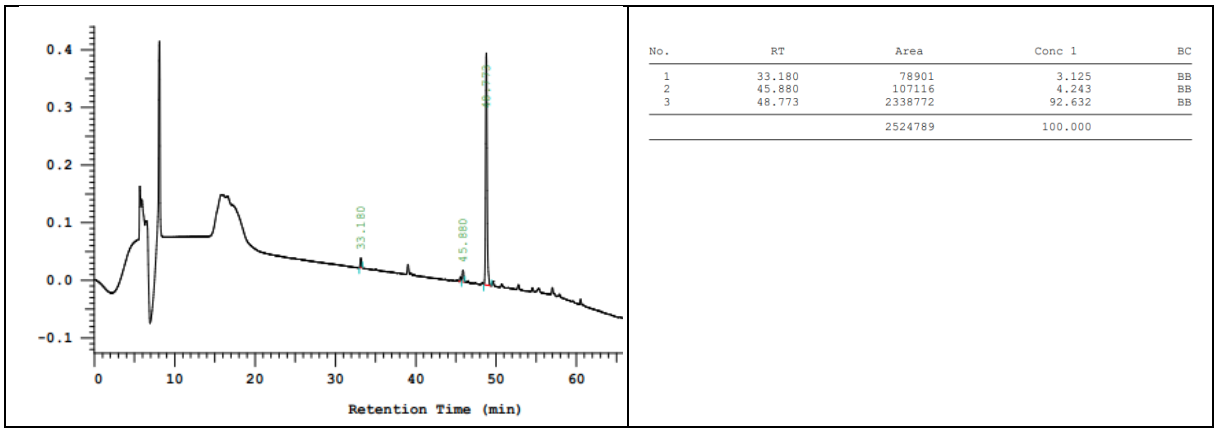

No.	RT	Area	Conc 1	BC
1	33.180	78901	3.125	BB
2	45.880	107116	4.243	BB
3	48.773	2338772	92.632	BB
		2524789	100.000	

Figure S90 HPLC chromatogram of purified ***III-6-($a_{2,6}$,c_4)***

6.2.7. Synthesis of meta-arylopeptoid Hexamer, III-4(d_2,e_4):

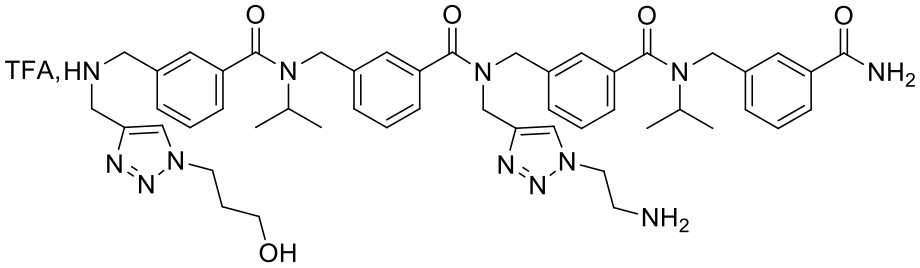

m_{crude} = 16.7 mg (purity 87%), crude yield 117%
m_{pure}= 11.6 mg (purity 92%), isolated yield 82%

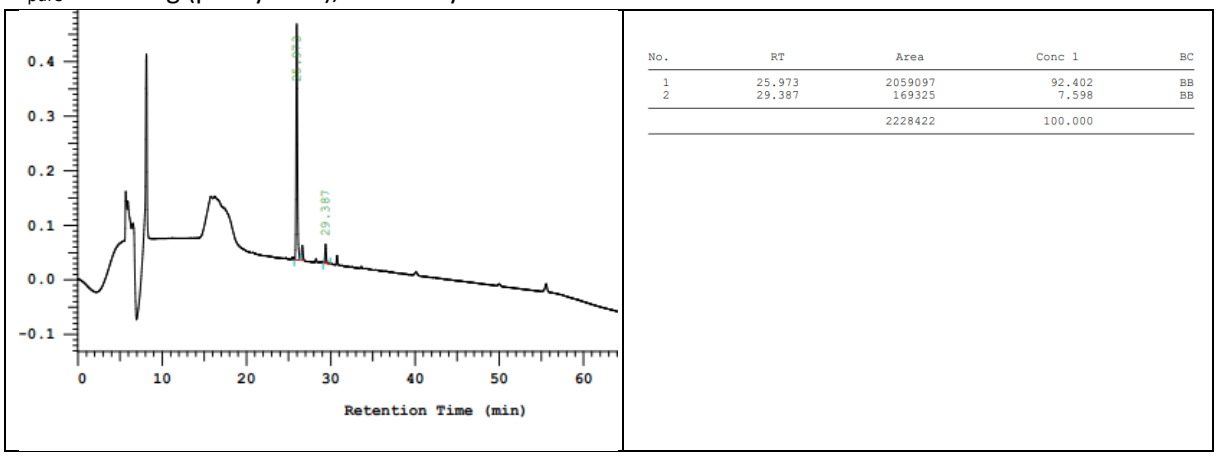

No.	RT	Area	Conc 1	BC
1	25.973	2059097	92.402	BB
2	29.387	169325	7.598	BB
		2228422	100.000	

Figure S91 HPLC chromatogram of purified ***III-4(d_2,e_4).***

6.2.8. Synthesis of meta-arylopeptoid Hexamer, III-4(e_2,d_4):

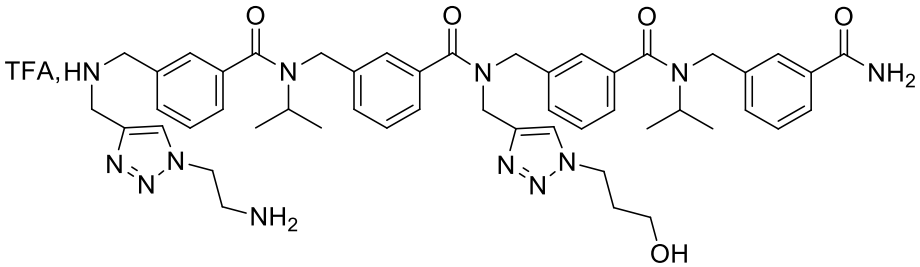

m_{crude} = 17.2 mg, (purity 83%) crude yield 121%
m_{pure}= 11.2 mg, (purity 87%), isolated yield 79%

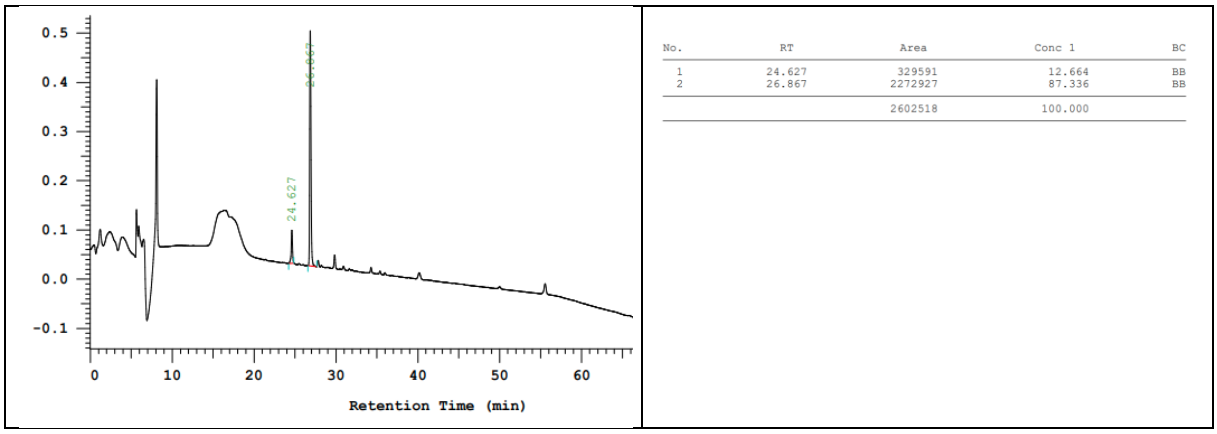

No.	RT	Area	Conc 1	BC
1	24.627	329591	12.664	BB
2	26.867	2272927	87.336	BB
		2602518	100.000	

Figure S92 HPLC chromatogram of purified ***III-4(e_2,d_4).***

7.Table of retention times.

Arylopeptoid	Retention time	Identification
III-4-(e,d)(2,4)	26.0	**III-4(d_2,e_4)**
	26.9	**III-4(d_4,e_2)**
III-6(a,c)(2,4,6)	40.8	**III-6-(a_2)($c_{4,6}$)**
	41.8	**III-6-(a_4)($c_{2,6}$)**
	42.5	**III-6-(a_6)($c_{2,4}$)**
	47.7	**III-6-(c_2)($a_{4,6}$)**
	48	**III-6-(c_6)($a_{2,4}$)**
	49.1	**III-6-(c_4)($a_{2,6}$)**

8.Heptamers

8.1.1. meta-arylopeptoid Heptamers, ***III.1****.*

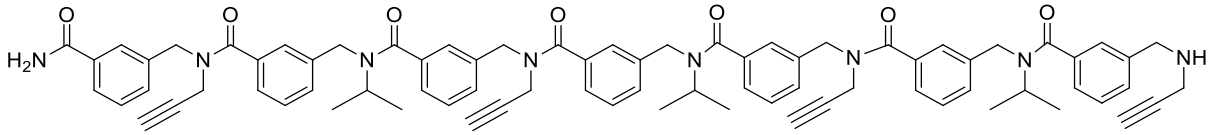

m_{pure}= 32mg (purity 92%), 84% isolated yield

HRMS (TOF MS ES+): *m/z* calcd for $C_{77}H_{80}N_8O_7$ $[M+2H]^{2+}$: 614.30695; found: 614.3069 (-0.11 ppm).

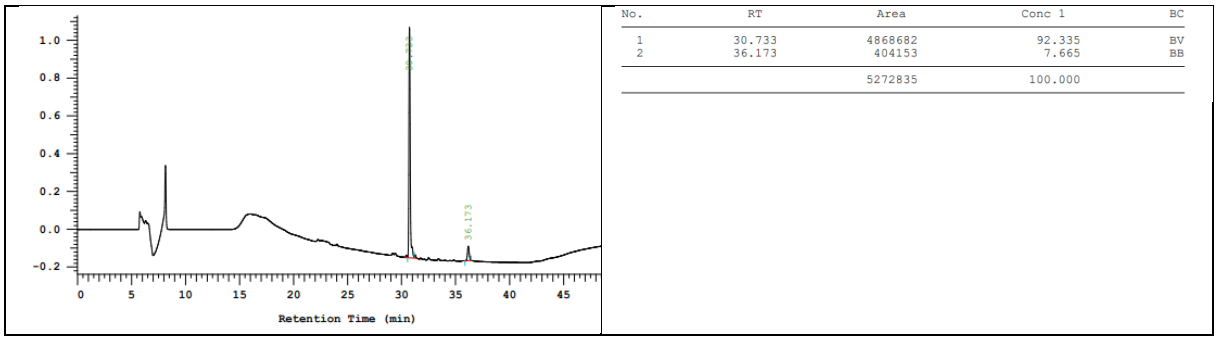

No.	RT	Area	Conc 1	BC
1	30.733	4868682	92.335	BV
2	36.173	404153	7.665	BB
		5272835	100.000	

Figure S93 HPLC chromatogram of the purified ***III.1****.*

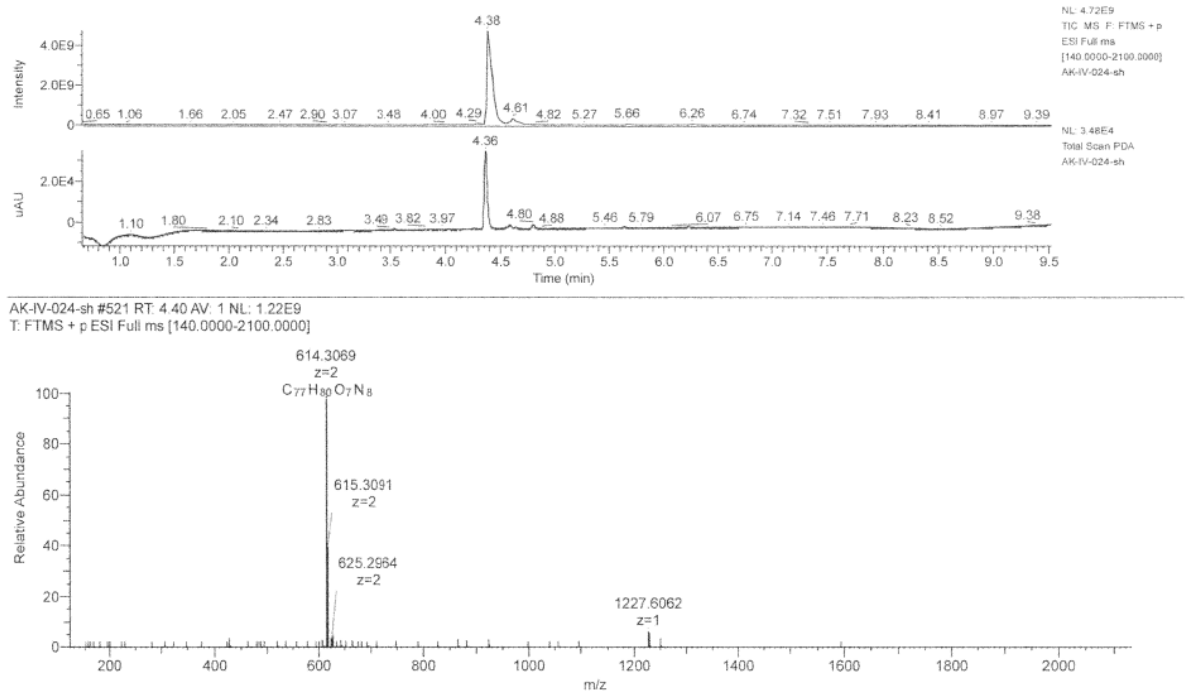

Figure S94. LCMS of crude ***III.1****.*

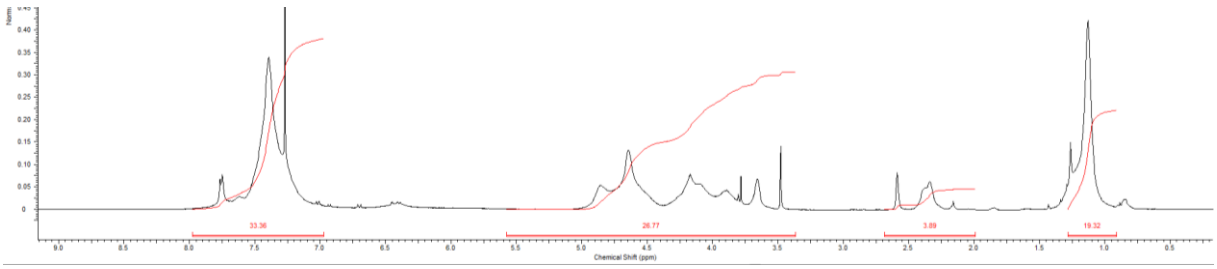

Figure S95 [1]H-NMR of pure ***III.1****.*

8.2.Homo clicked arylo-peptoides

8.2.1.Meta-arylopeptoids heptamer, ***III.2****.*

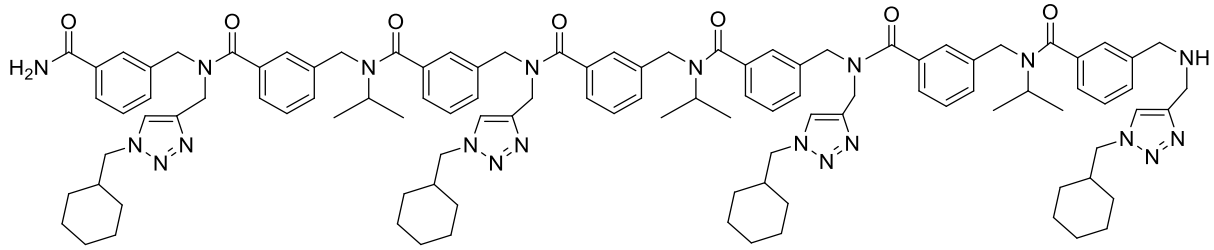

m_{pure}= 45.3 mg (purity 93%), 82% isolated yield

HRMS (TOF MS ES+): *m/z* calcd for $C_{105}H_{130}N_{20}O_7$ $[M+2H]^{2+}$: 892.52884; found: 892.5278 (-1.13 ppm).

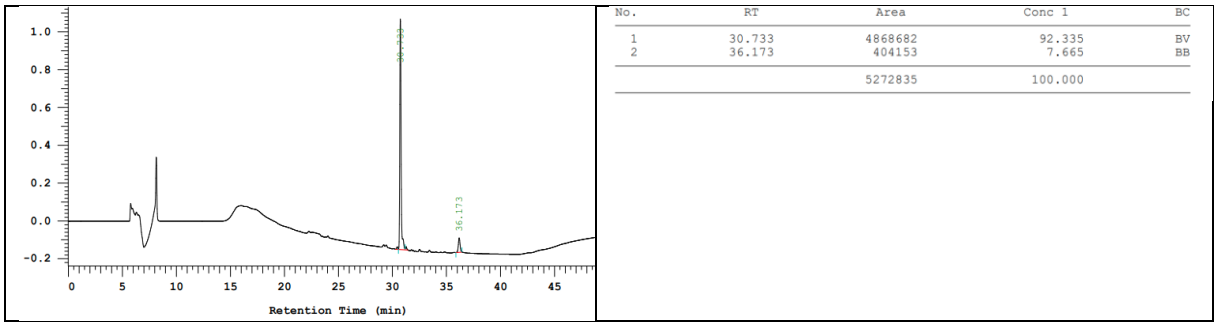

No.	RT	Area	Conc 1	BC
1	30.733	4868682	92.335	BV
2	36.173	404153	7.665	BB
		5272835	100.000	

*Figure S96 HPLC chromatogram of the purified **III.2**.*

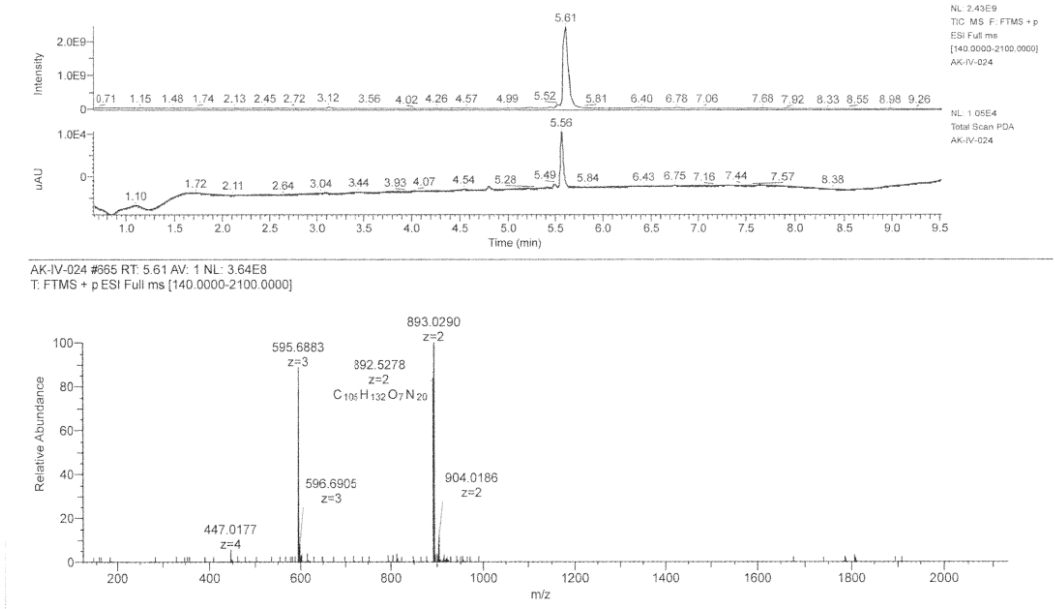

*Figure S97 LCMS of the crude **III.2**.*

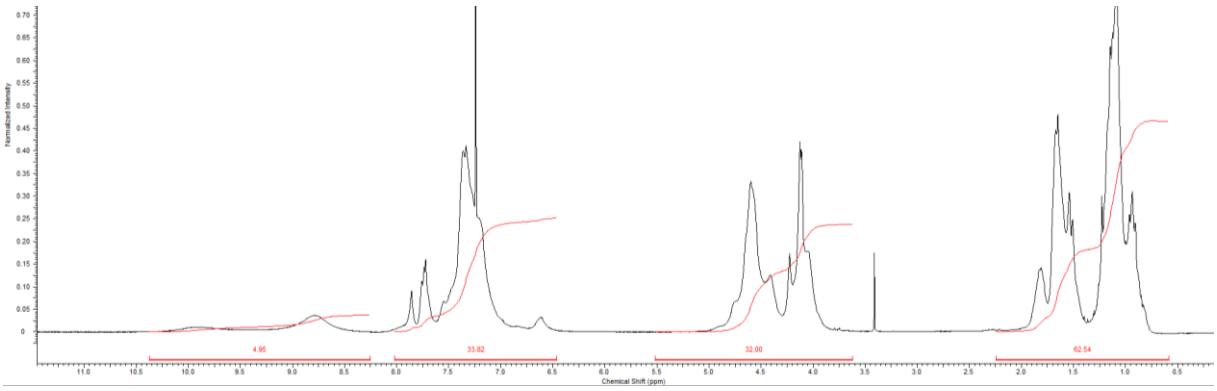

*Figure S98 ^{1}H-NMR of the pure **III.2**.*

8.2.2.Meta-arylopeptoids heptamer, III.3.

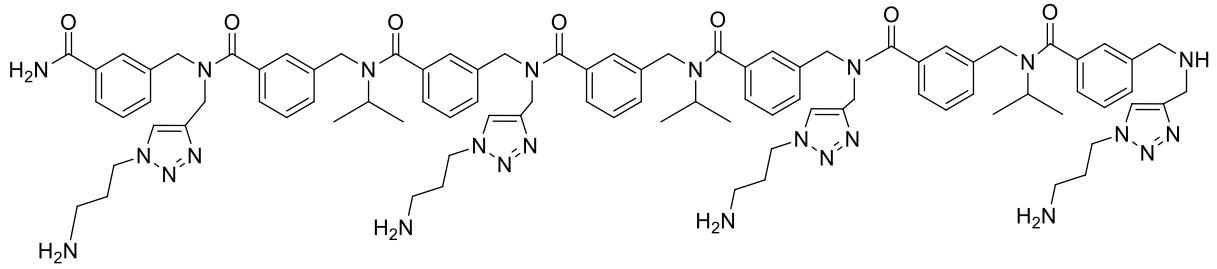

m_{pure}= 55 mg (purity 95%), 78% isolated yield
HRMS (TOF MS ES+): *m/z* calcd for $C_{89}H_{114}N_{24}O_7$ $[M+4H]^{2+}$: 407.73201; found: 407.7320 (0.04 ppm).

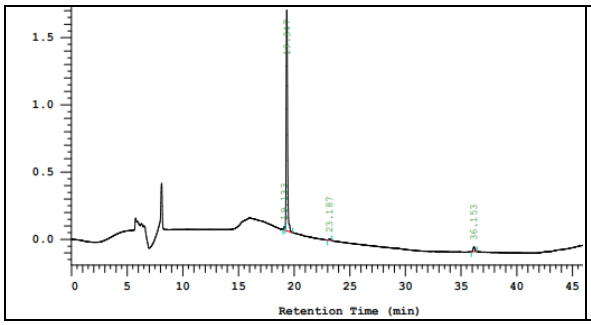

No.	RT	Area	Conc 1	BC
1	19.133	80563	1.196	BV
2	19.347	6409401	95.153	VB
3	23.187	50965	0.757	BB
4	36.153	194991	2.895	BB
		6735920	100.000	

*Figure S99 HPLC chromatogram of the purified **III.3**.*

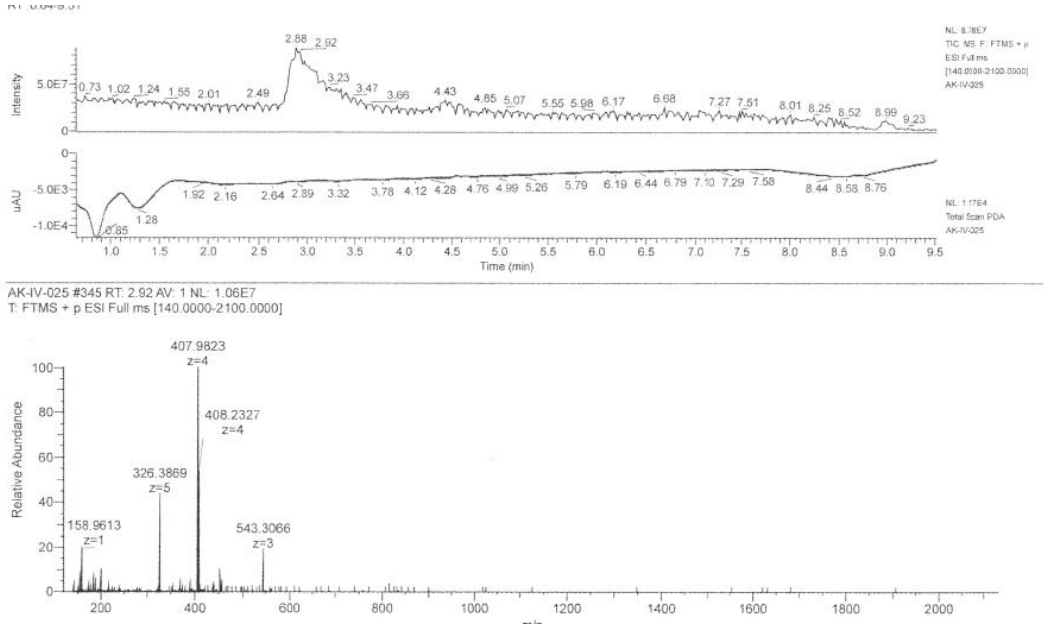

*Figure S100 LCMS of the crude **III.3**.*

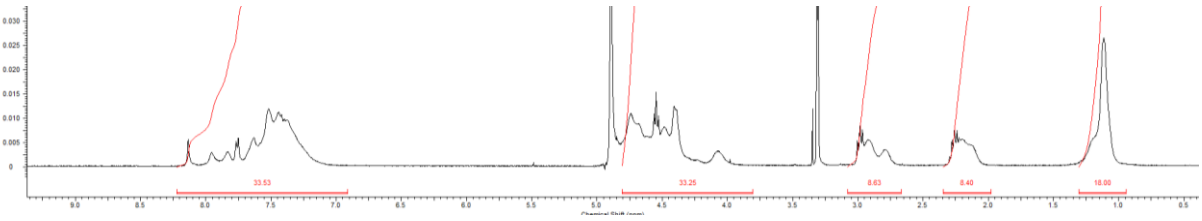

*Figure S101 ^{1}H-NMR in MeOD of the pure **III.3**.*

9.*Ortho* arylopeptoids Tetramers.

*9.1. Ortho arylopeptoids starting material **III.4**.*

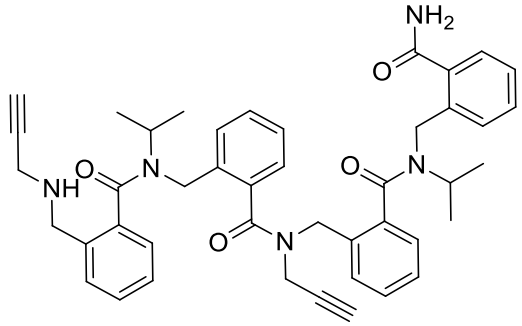

m_{pure}= 19.8 mg (purity 96%), 75% isolated yield
HRMS (TOF MS ES+): *m/z* calcd for $C_{44}H_{48}N_5O_4$ $[M+H]^+$: 710.37008; found: 710.3702 (0.22 ppm).

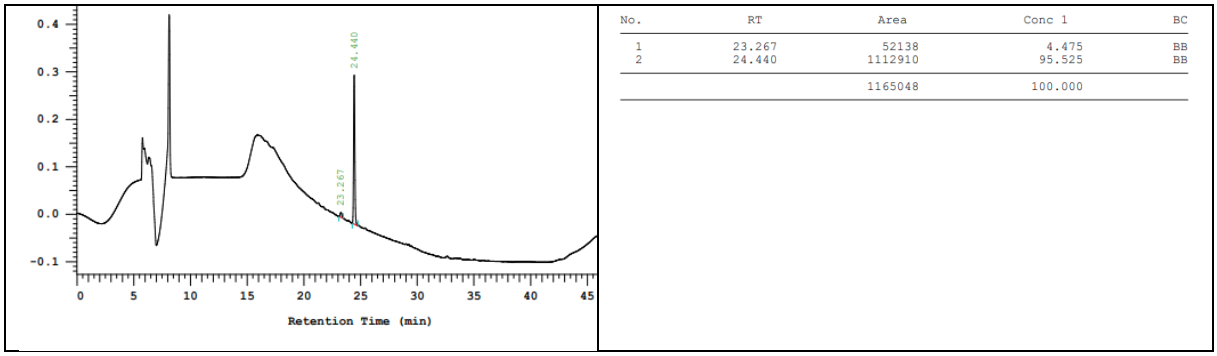

No.	RT	Area	Conc 1	BC
1	23.267	52138	4.475	BB
2	24.440	1112910	95.525	BB
		1165048	100.000	

*Figure S102 HPLC of the purified **III.4**.*

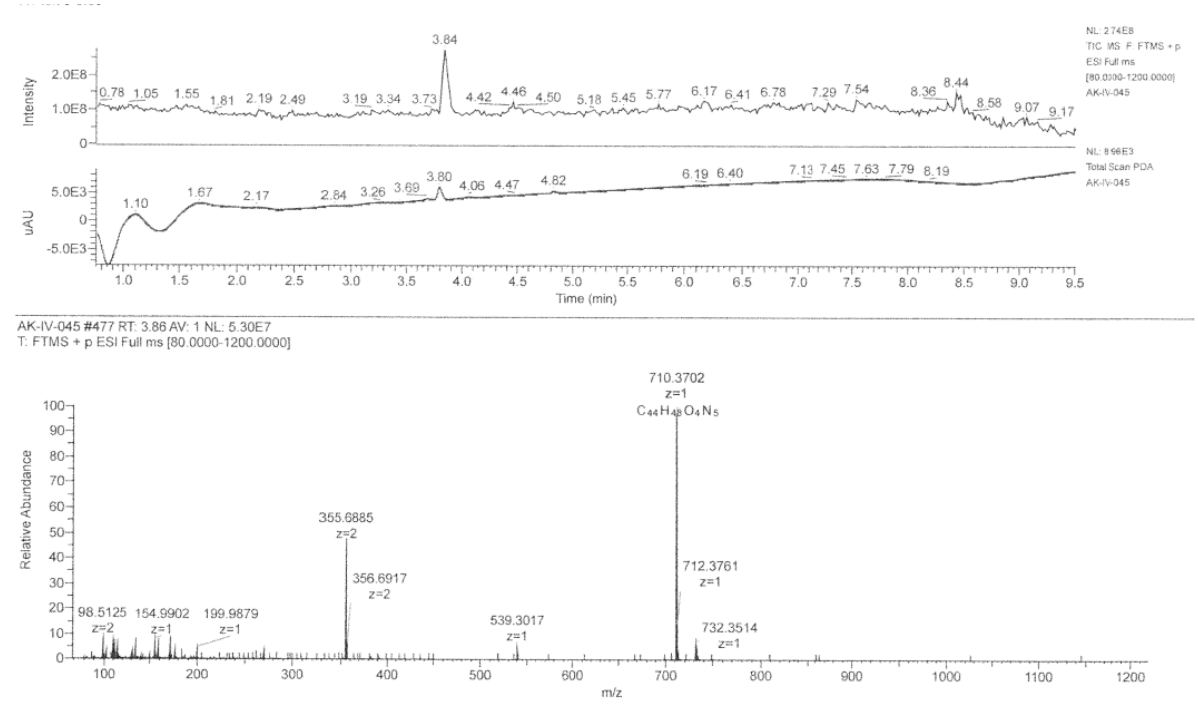

*Figure S103 LCMS of the crude **III.4**.*

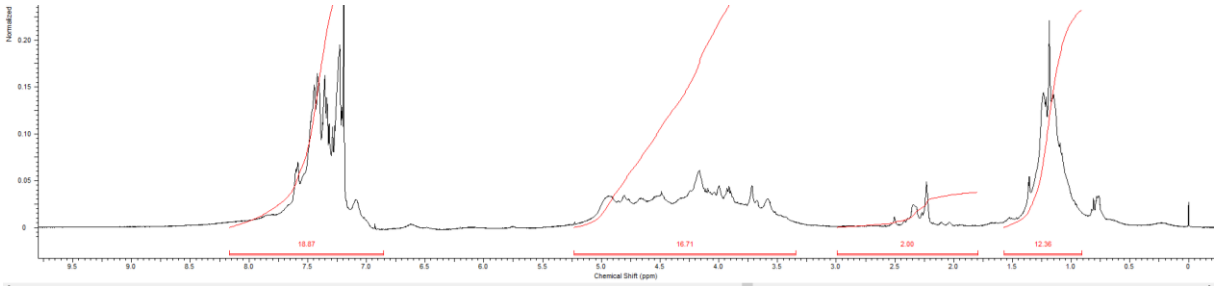

*Figure S104 ^{1}H-NMR of the pure **III.4**.*

*9.2. Ortho arylopeptoids starting material **III.7**.*

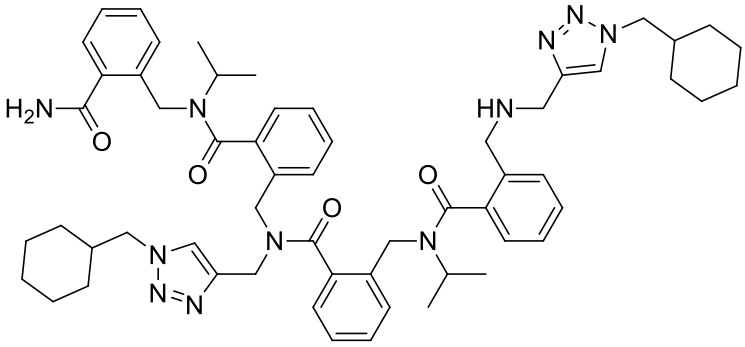

m_{pure}= 10 mg (purity 96%), 81% isolated yield (starting from 20 mg resin)
HRMS (TOF MS ES+): *m/z* calcd for $C_{58}H_{75}N_{11}O_4$ $[M+2H]^{2+}$: 494.79963; found: 494.8001 (1.04 ppm).

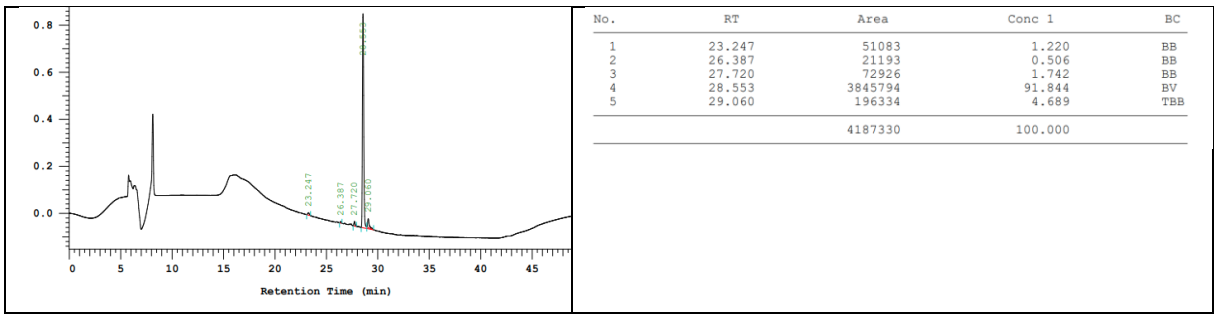

No.	RT	Area	Conc 1	BC
1	23.247	51083	1.220	BB
2	26.387	21193	0.506	BB
3	27.720	72926	1.742	BB
4	28.553	3845794	91.844	BV
5	29.060	196334	4.689	TBB
		4187330	100.000	

*Figure S105 HPLC of the purified **III.7**.*

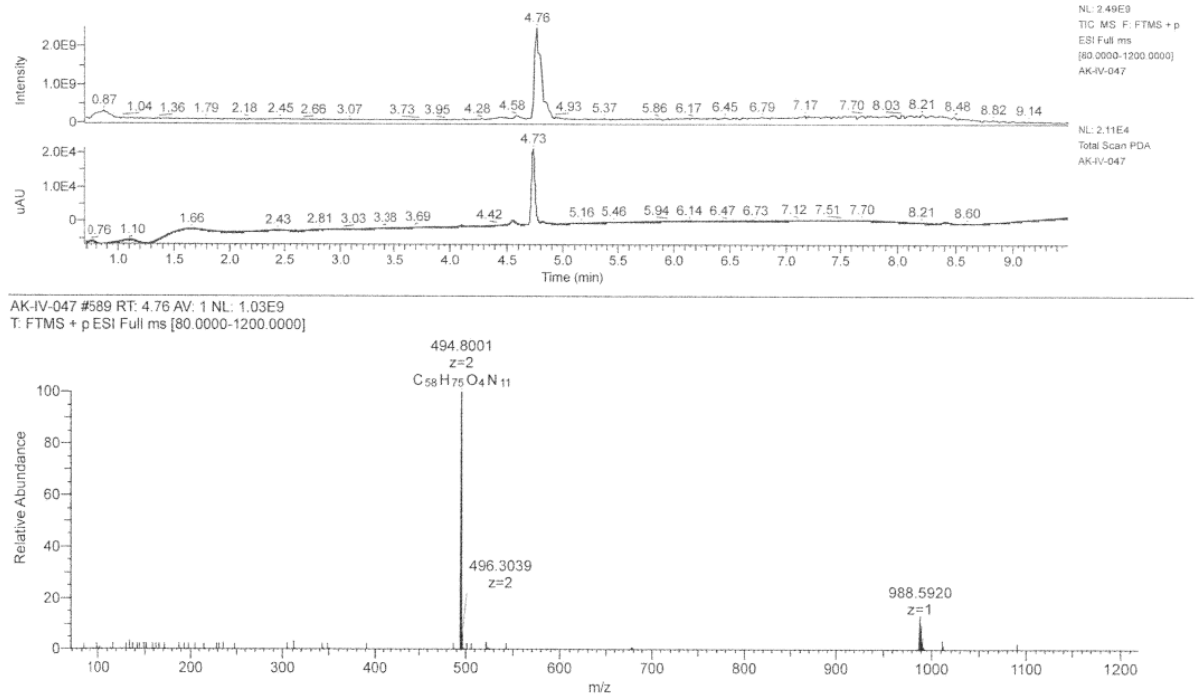

*Figure S106 LCMS of the crude **III.7**.*

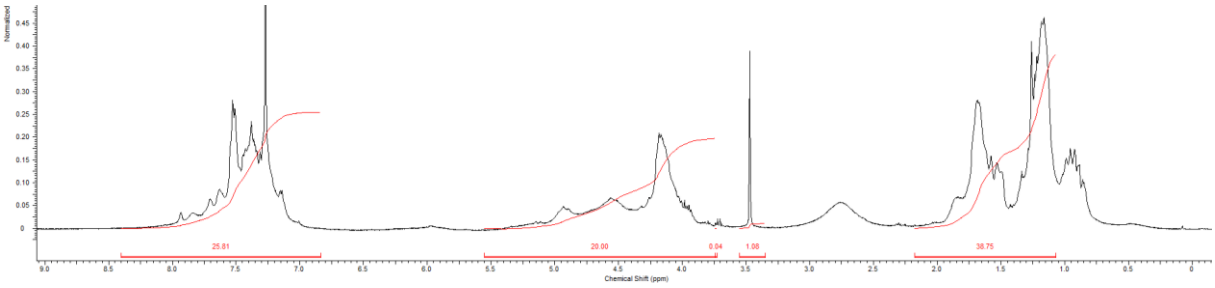

*Figure S107 ^{1}H-NMR of the pure **III.7**.*

*9.3. Ortho arylopeptoids starting material, **III.8**.*

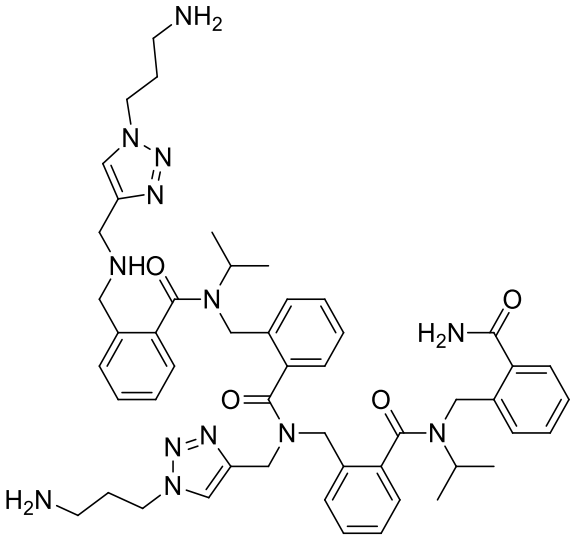

m_{pure}= 9.8 mg (purity 91%), 88% isolated yield (starting from 20 mg resin)
HRMS (TOF MS ES+): *m/z* calcd for $C_{50}H_{65}N_{13}O_4$ $[M+2H]^{2+}$: 455.76358; found: 455.7632 (-0.79 ppm).

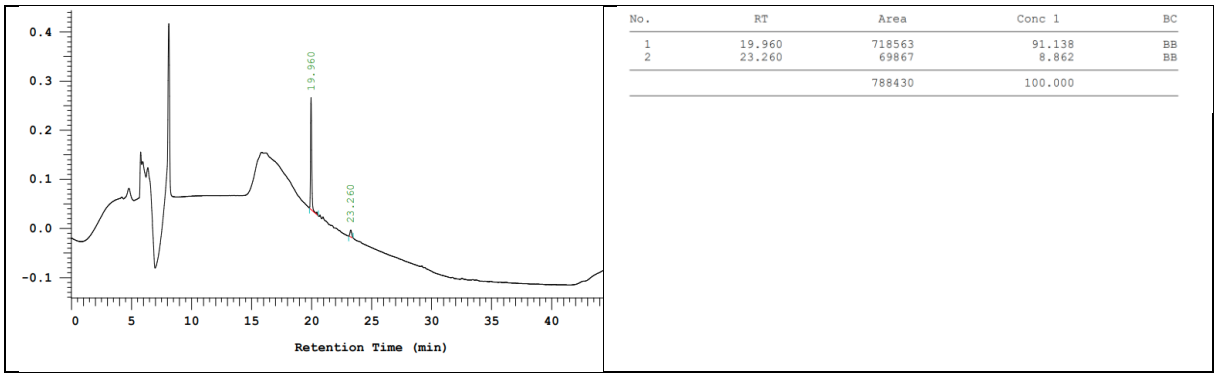

No.	RT	Area	Conc 1	BC
1	19.960	718563	91.138	BB
2	23.260	69867	8.862	BB
		788430	100.000	

*Figure S108 HPLC of the puyrified **III.8**.*

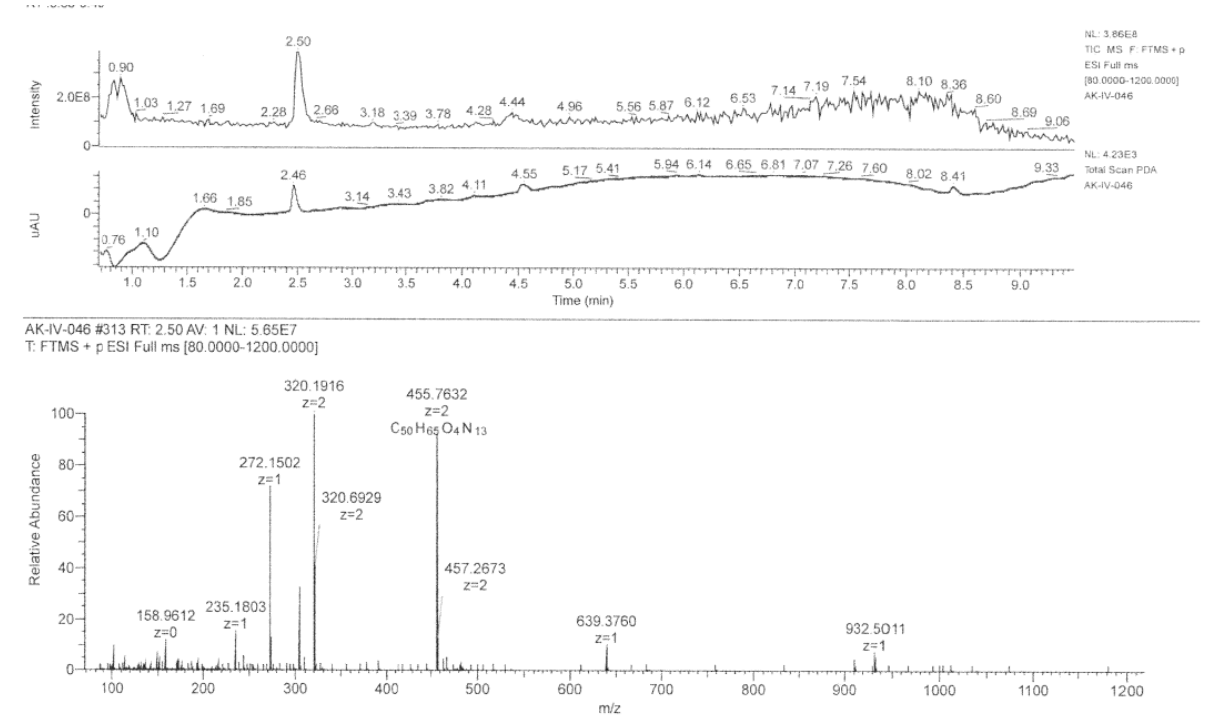

*Figure S109 LCMS of the crude **III.8**.*

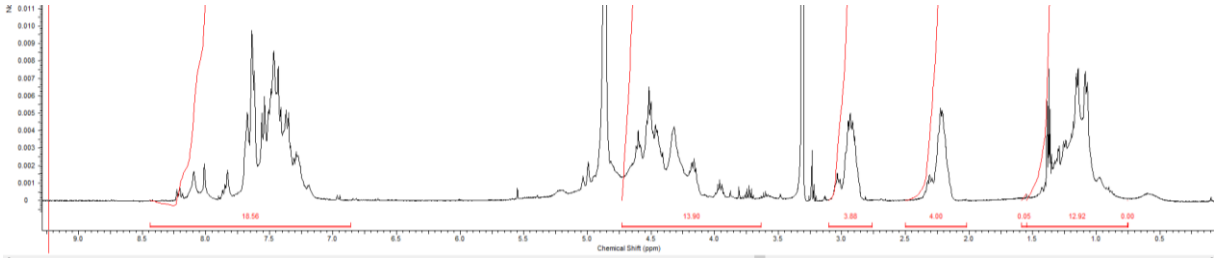

*Figure S110 ^{1}H-NMR of the pure **III.8**.*

10.*Ortho* arylopeptoids Pentamers

10.1. Ortho arylopeptoids starting material, ***III.5***.

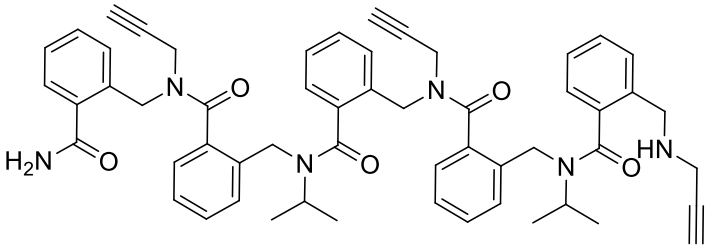

m_{pure}= 23.1 mg (purity 97%), 85% isolated yield (starting from 50 mg resin)
HRMS (TOF MS ES+): *m/z* calcd for $C_{55}H_{57}N_6O_5$ $[M+H]^+$: 881.4385; found: 881.4388 (0.39 ppm).

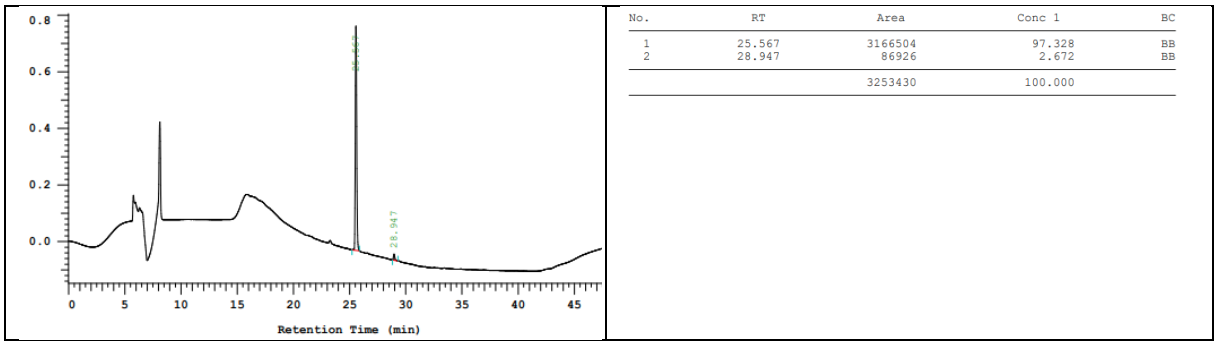

No.	RT	Area	Conc 1	BC
1	25.567	3166504	97.328	BB
2	28.947	86926	2.672	BB
		3253430	100.000	

Figure S111 HPLC of the puyrified ***III.5***.

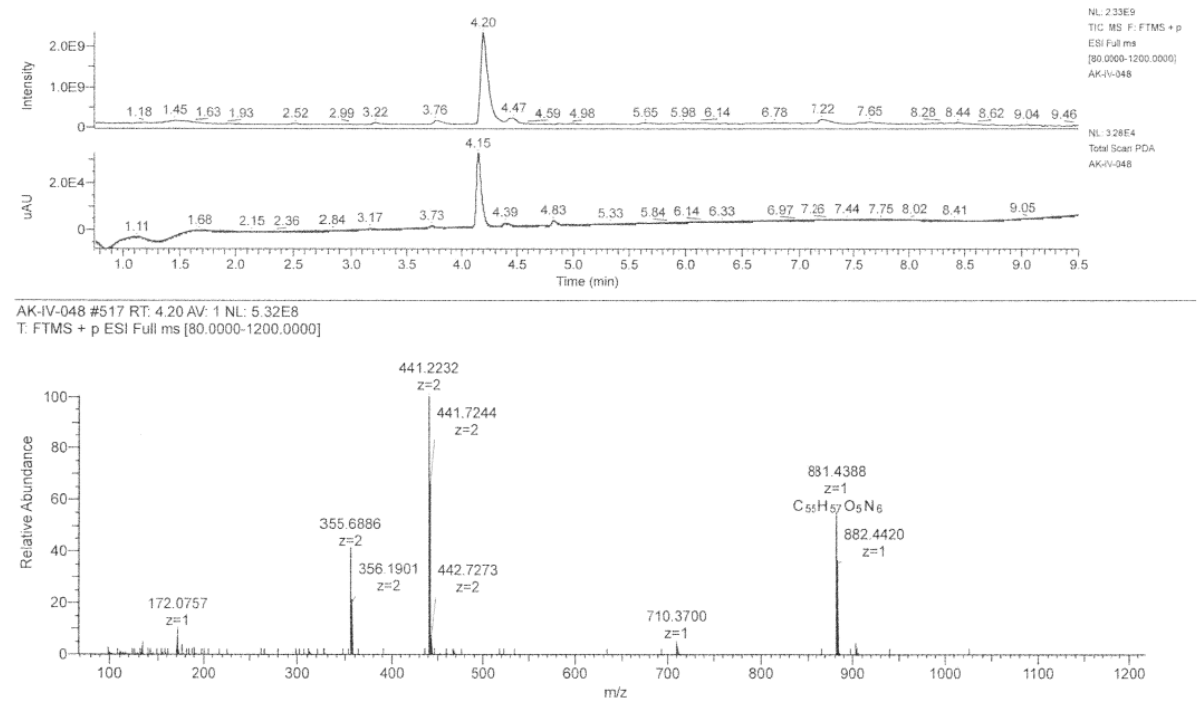

Figure S112 LCMS of the crude ***III.5****.*

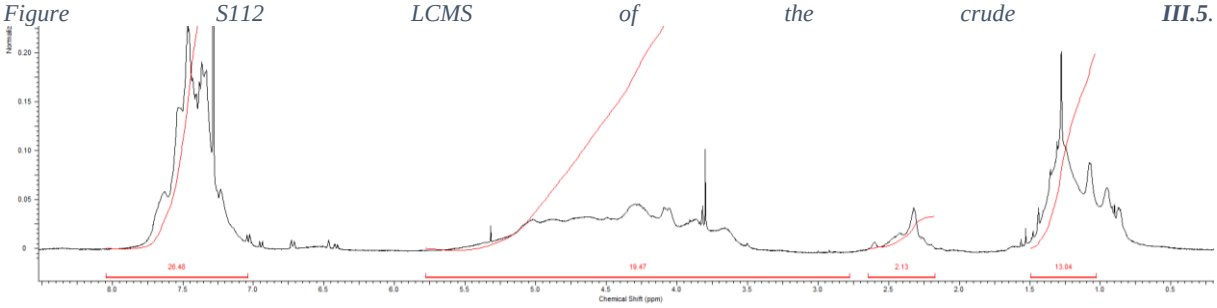

Figure S113 $_1$H-NMR in $CDCl_3$ of the pure ***III.5****.*

10.2.1. Click of Ortho-arylopeptoids pentamers, ***III.9****.*

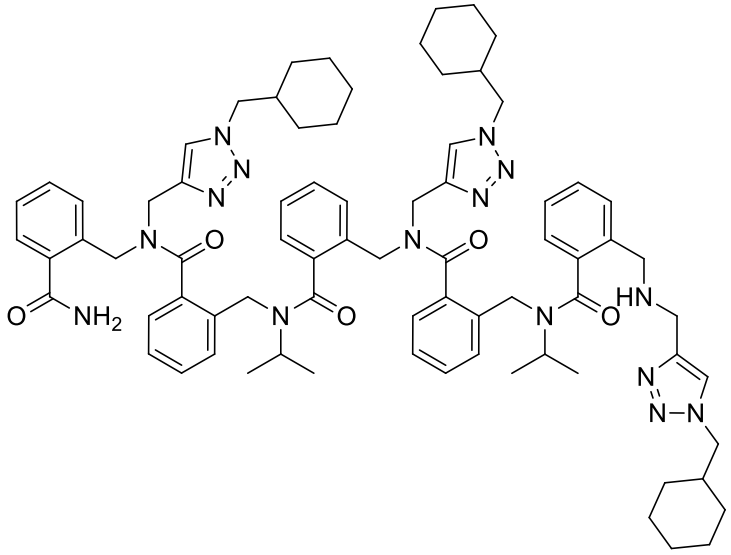

m_{pure}= 9 mg (purity 93%), 75% isolated yield (starting from 15 mg resin)

HRMS (TOF MS ES+): *m/z* calcd for $C_{76}H_{97}N_{15}O_5$ $[M+2H]^{2+}$: 649.88931; found: 649.8891 (-0.32 ppm).

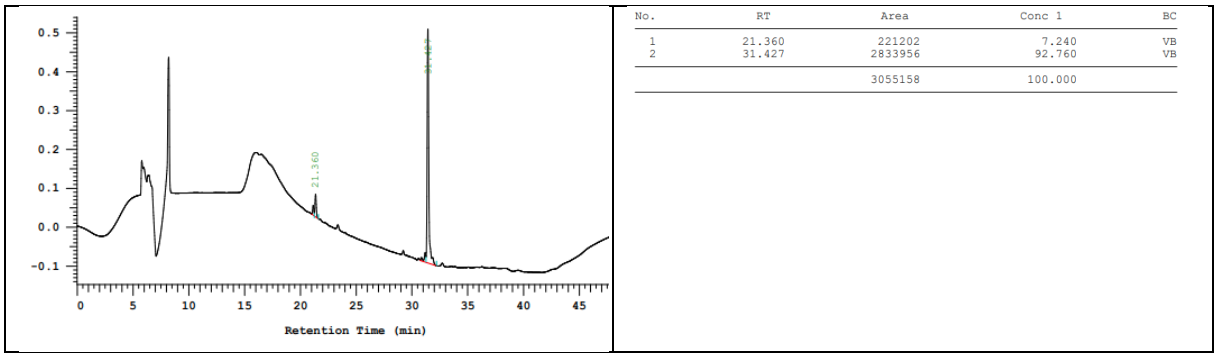

No.	RT	Area	Conc 1	BC
1	21.360	221202	7.240	VB
2	31.427	2833956	92.760	VB
		3055158	100.000	

*Figure S114 HPLC of the purified **III.9.***

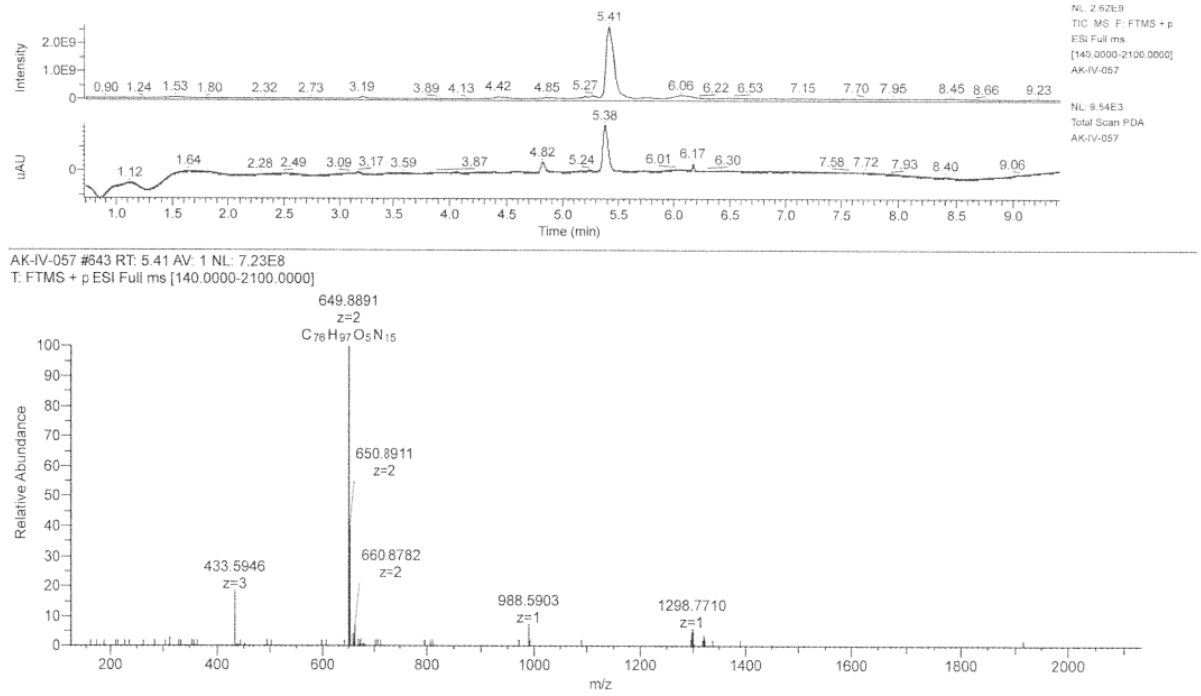

*Figure S115 LCMS of the crude **III.9.***

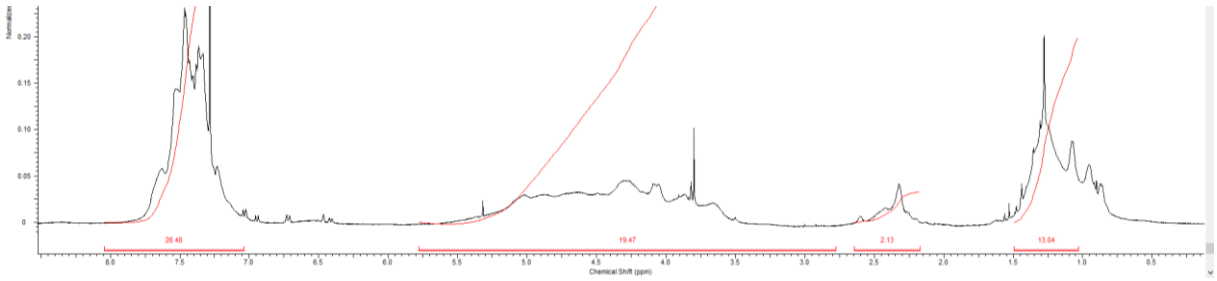

*Figure S116 ^{1}H-NMR in $CDCl_3$ of the pure **III.9.***

*10.2.2 Click of Ortho-arylopeptoids pentamers, **III.10**.*

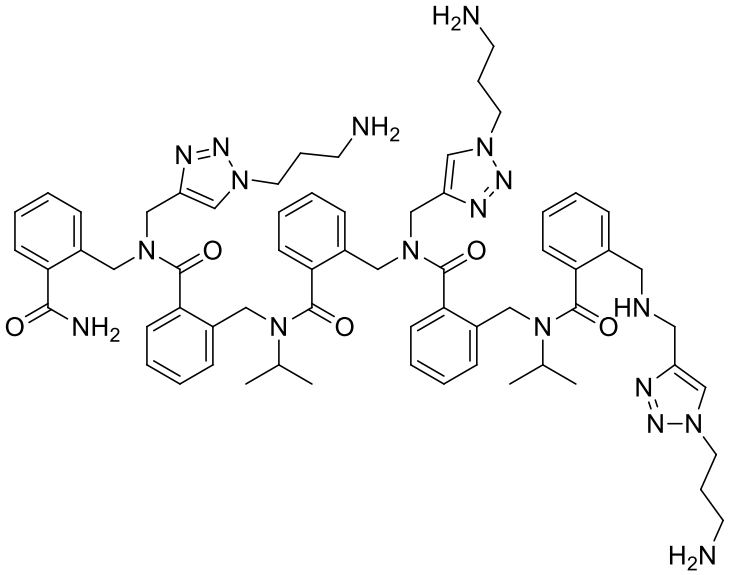

m_{pure}= 8.5 mg (purity 97%), 78% isolated yield (starting from 15 mg resin)
HRMS (TOF MS ES+): *m/z* calcd for $C_{64}H_{83}N_{18}O_5$ $[M+3H]^{3+}$: 394.55925; found: 394.5589 (-0.80 ppm).

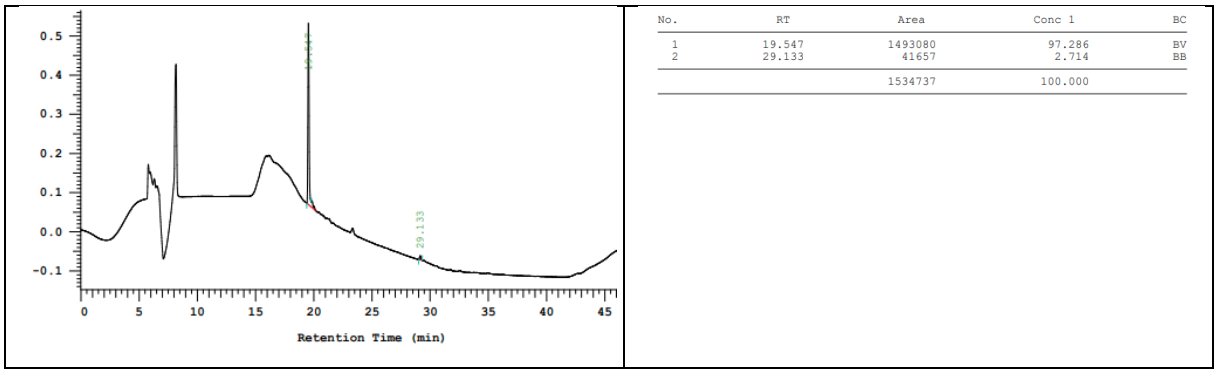

No.	RT	Area	Conc 1	BC
1	19.547	1493080	97.286	BV
2	29.133	41657	2.714	BB
		1534737	100.000	

*Figure S117 HPLC of the purified **III.10**.*

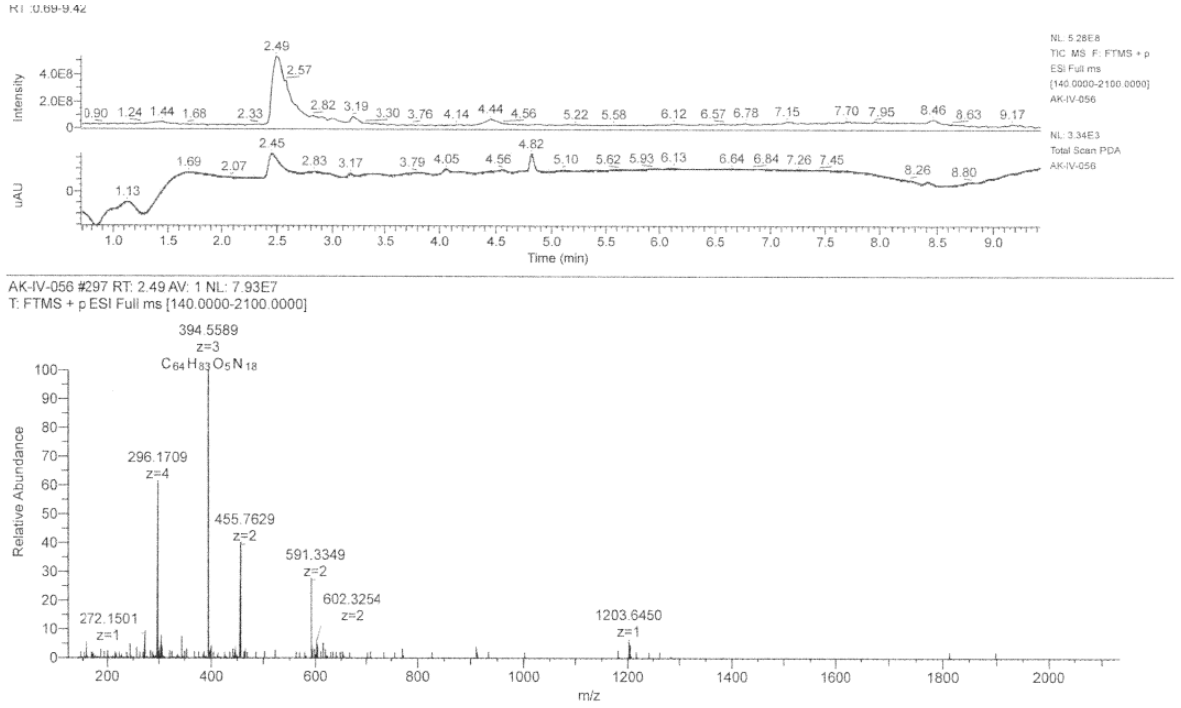

*Figure S118 LCMS of the crude **III.10**.*

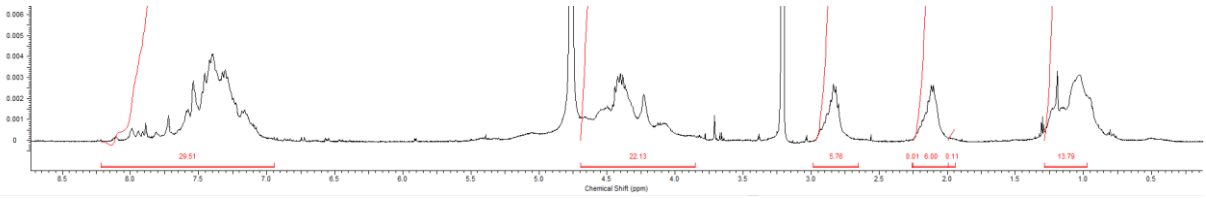

*Figure S119 ^{1}H-NMR in MeOD of the pure **III.10**.*

*10.2.3. Combinatorial Click of Ortho-arylopeptoids pentamers, **III.13**.*

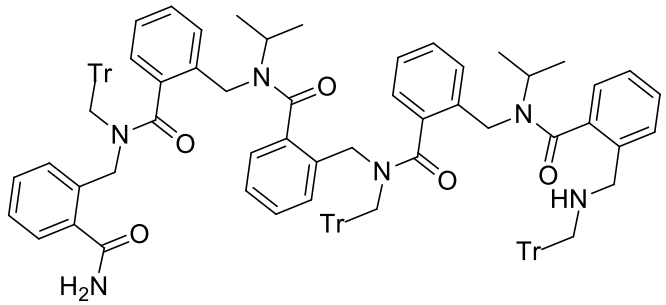

Tr = 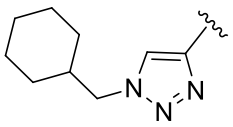 or 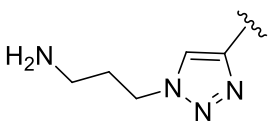

m_{pure}= 11 mg (purity 92%), 72% isolated yield (starting from 20 mg resin)

HRMS (TOF MS ES+) pic at 5.41: *m/z* calcd for $C_{76}H_{97}N_{15}O_5$ $[M+2H]^{2+}$: 649.88931; found: 649.8893 (-0.04 ppm).

HRMS (TOF MS ES+) pic at 4.11: *m/z* calcd for $C_{72}H_{92}N_{16}O_5$ $[M+2H]^{2+}$: 630.37128; found: 630.3710 (-0.49 ppm).

HRMS (TOF MS ES+) pic at 4.21: *m/z* calcd for $C_{72}H_{92}N_{16}O_5$ $[M+2H]^{2+}$: 630.37128; found: 630.3712 (-0.10 ppm).

HRMS (TOF MS ES+) pic at 3.34: *m/z* calcd for $C_{68}H_{87}N_{17}O_5$ $[M+2H]^{2+}$: 610.85326; found: 610.853 (-0.47 ppm).
HRMS (TOF MS ES+) pic at 2.59: *m/z* calcd for $C_{64}H_{83}N_{18}O_5$ $[M+2H]^{2+}$: 591.33523; found: 591.3353 (0.16 ppm).

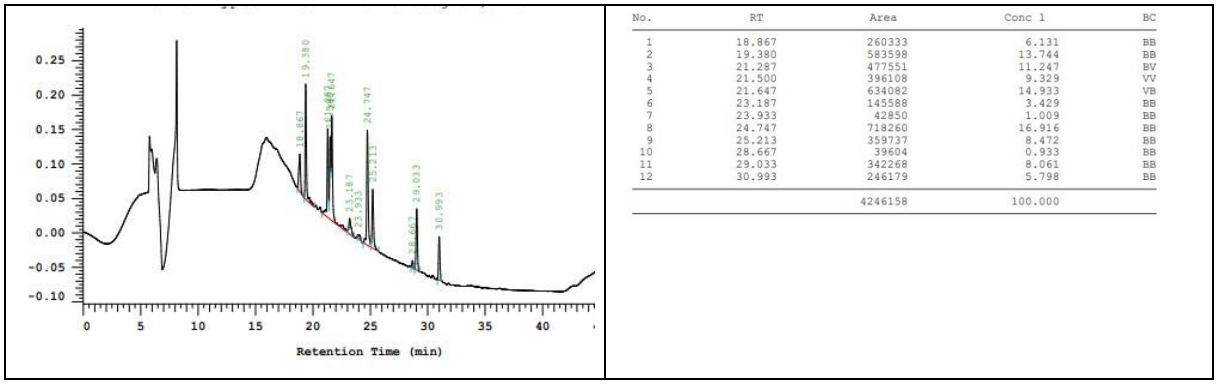

No.	RT	Area	Conc 1	BC
1	18.867	260333	6.131	BB
2	19.380	583598	13.744	BB
3	21.287	477551	11.247	BV
4	21.500	396108	9.329	VV
5	21.647	634082	14.933	VB
6	23.187	145588	3.429	BB
7	23.933	42850	1.009	BB
8	24.747	718260	16.916	BB
9	25.213	359737	8.472	BB
10	28.667	39604	0.933	BB
11	29.033	342268	8.061	BB
12	30.993	246179	5.798	BB
		4246158	100.000	

*Figure S120 HPLC of the **III.13**.*

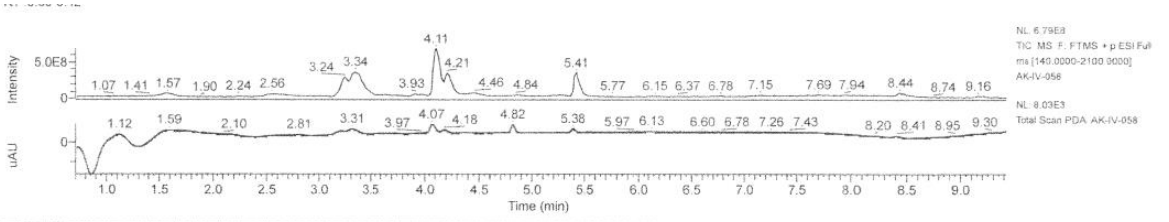

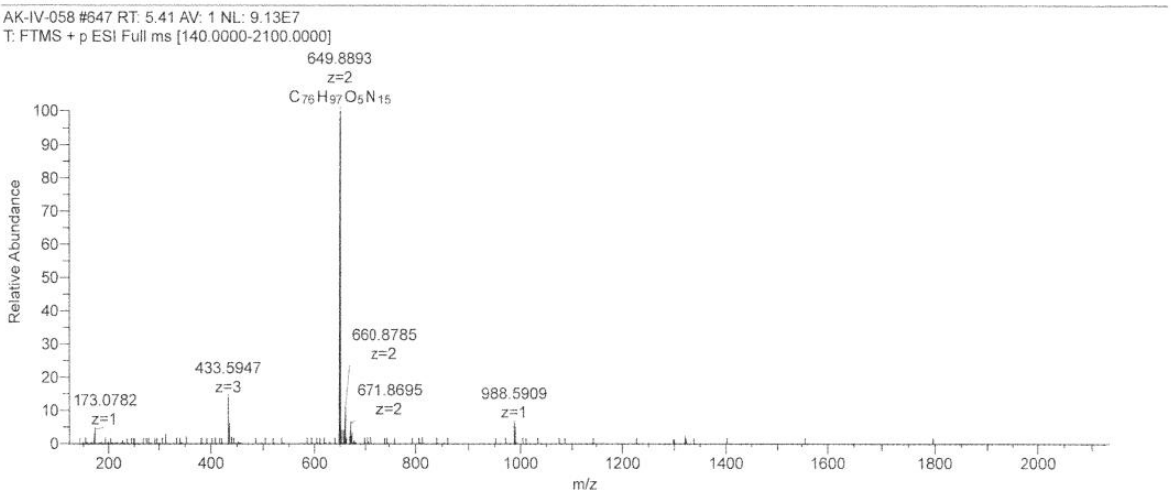

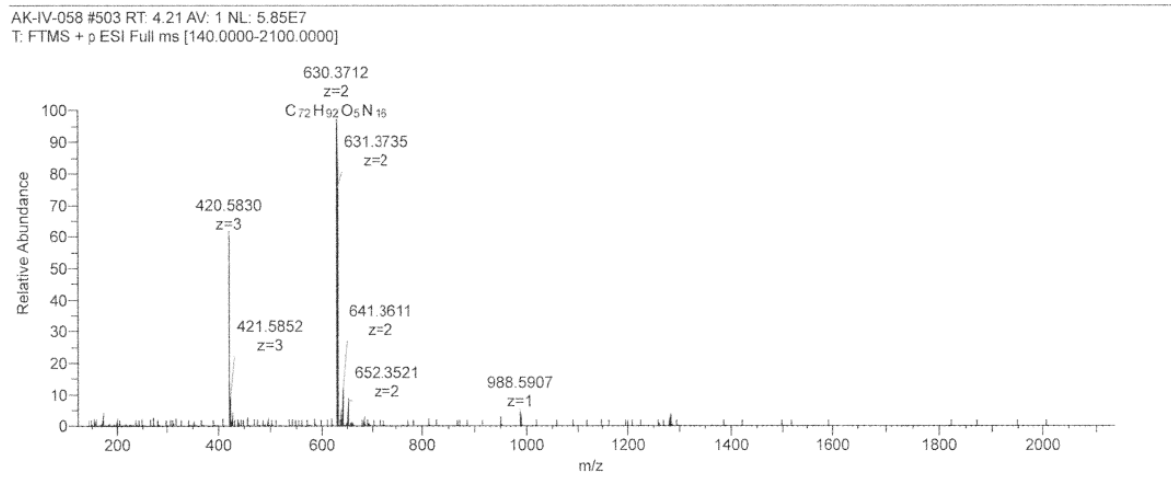

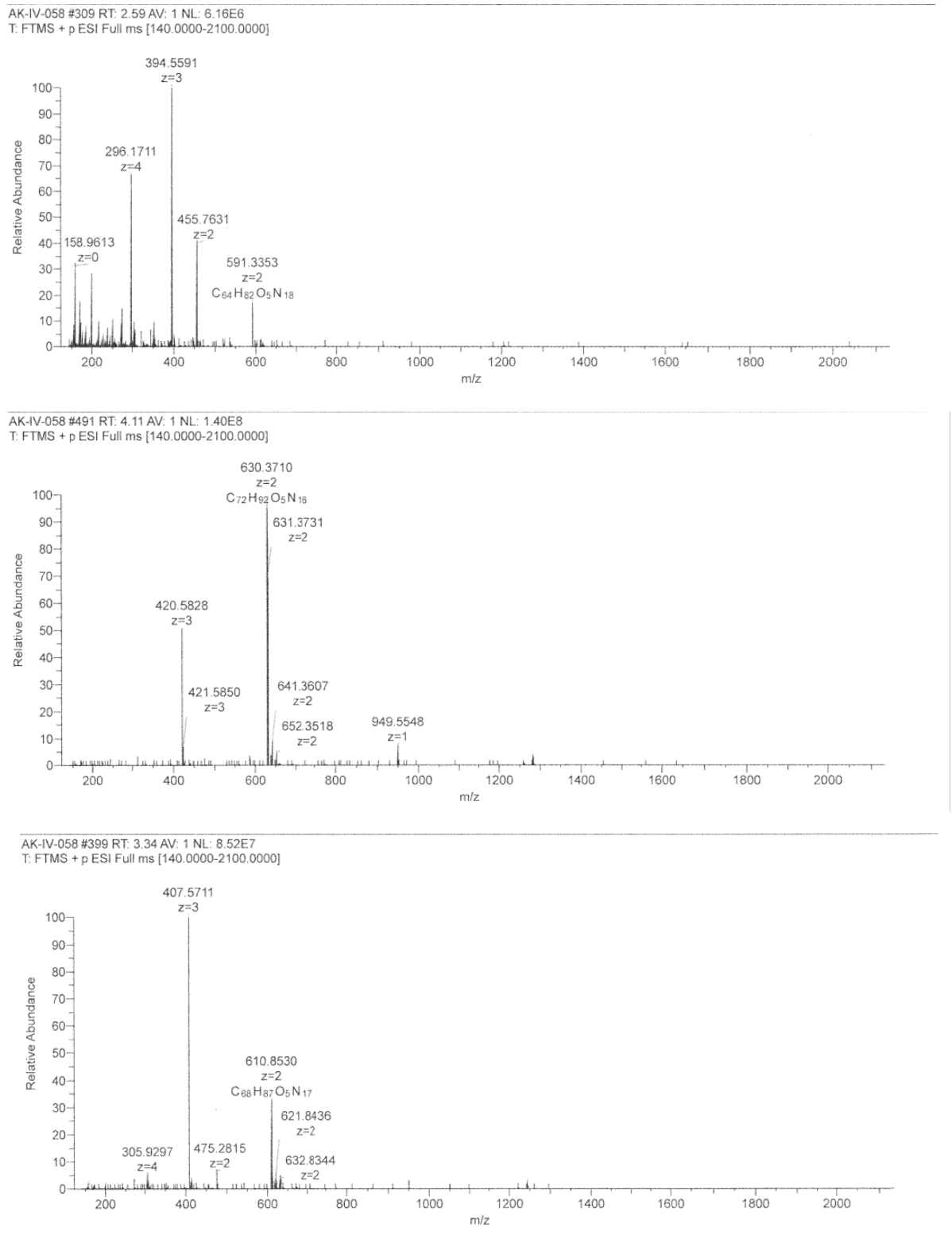

*Figure S121 LCMS of the crude **III.13**.*

11.*Ortho* arylopeptoids Pentamers

*11.1. Ortho-arylopeptoids starting material **III.6**.*

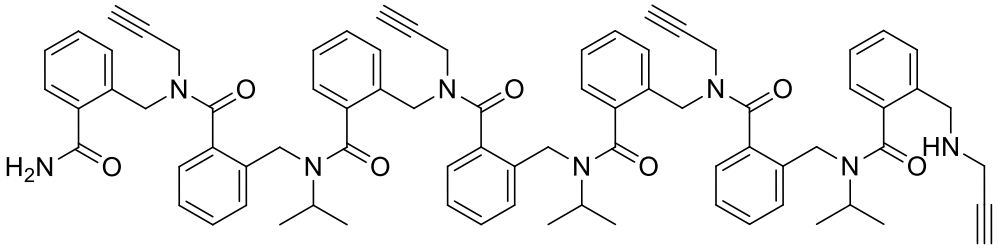

m_{pure}= 30 mg (purity 99%), 79% isolated yield (starting from 50 mg resin)
HRMS (TOF MS ES+): *m/z* calcd for $C_{77}H_{80}N_8O_5$ $[M+2H]^{2+}$: 614.30695; found: 614.3071 (0.19 ppm).

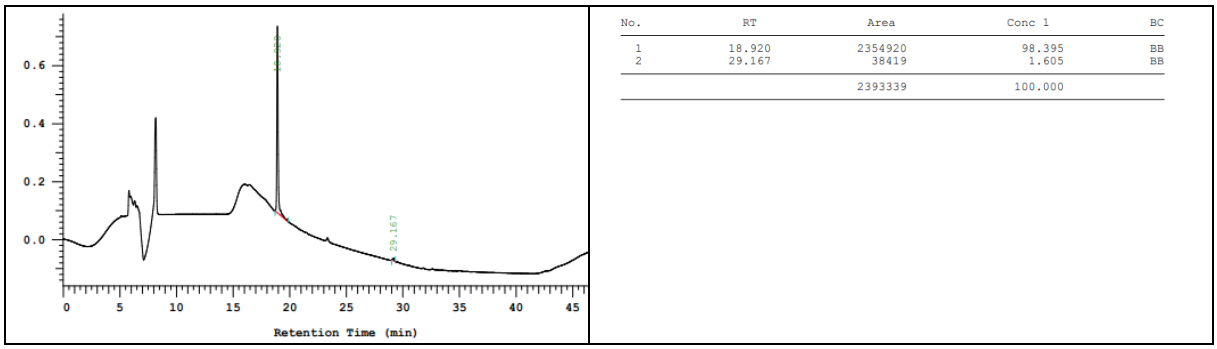

*Figure S122 HPLC of the pure **III.6.***

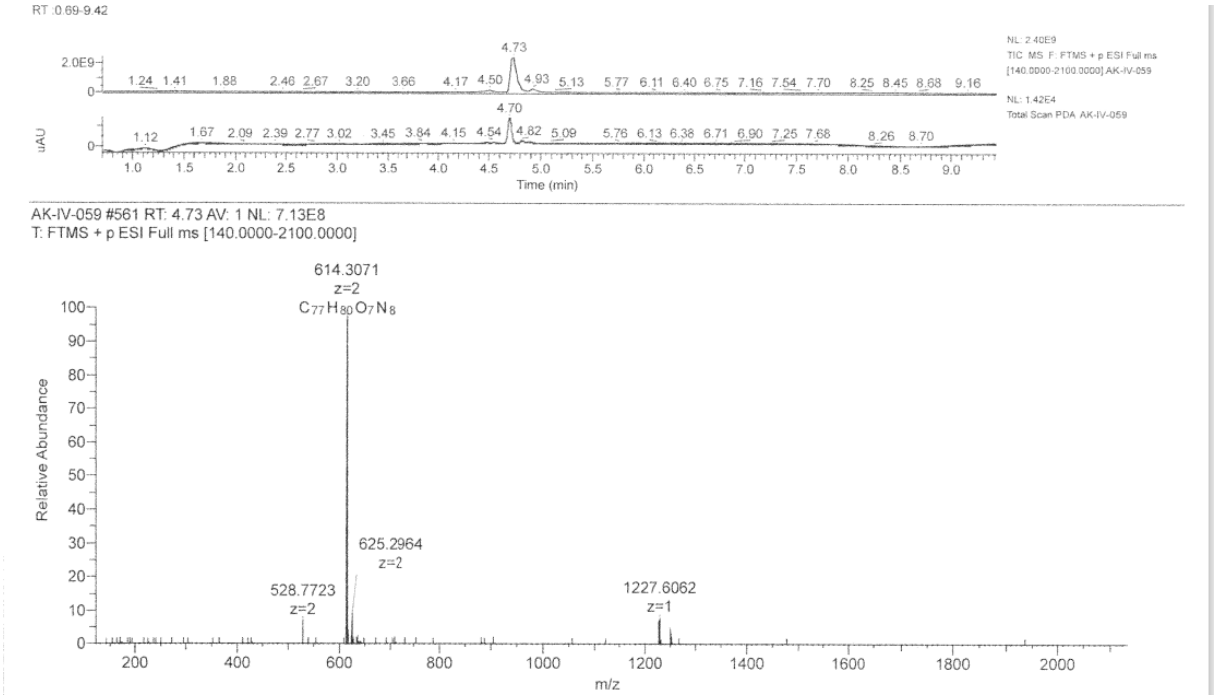

*Figure S123 LCMS of the crude **III.6.***

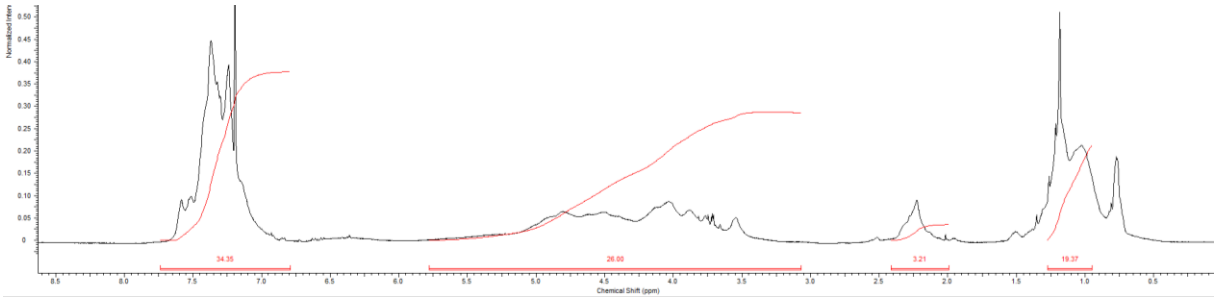

*Figure S124 ^{1}H-NMR in $CDCl_3$ of the pure **III.6.***

*11.2.1. Ortho-arylopeptoids clicked, **III.11**.*

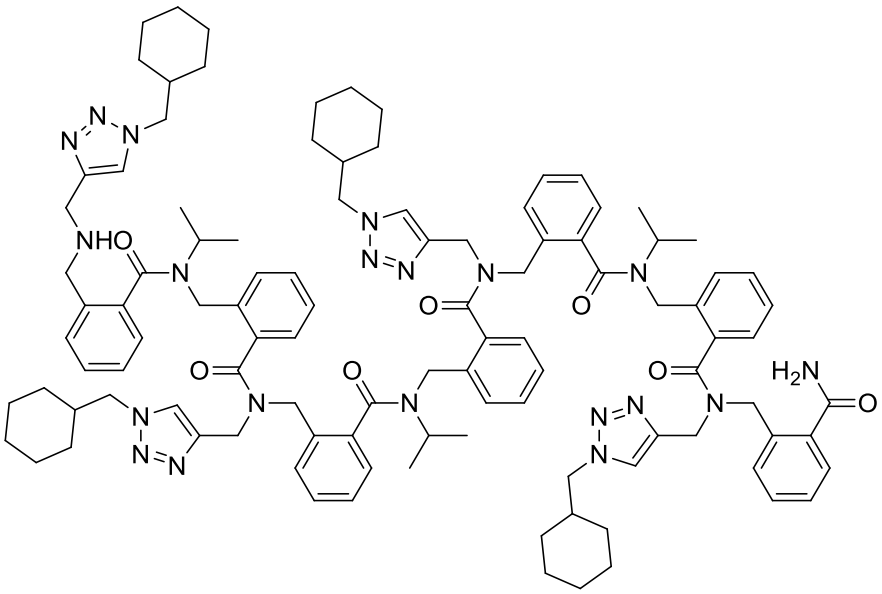

m_{pure}= 16.8 mg (purity 92%), 76% isolated yield (starting from 20 mg resin)
HRMS (TOF MS ES+): *m/z* calcd for $C_{105}H_{132}N_{20}O_7$ $[M+2H]^{2+}$: 892.52884; found: 892.5289 (0.03 ppm).

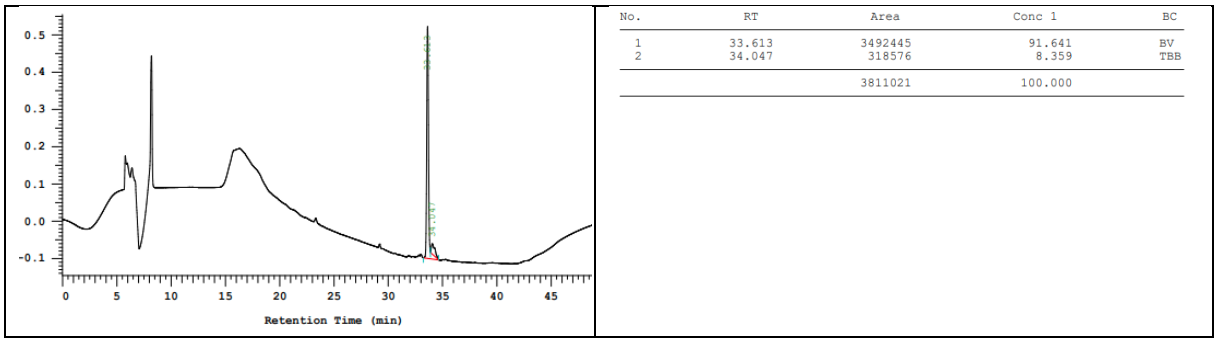

No.	RT	Area	Conc 1	BC
1	33.613	3492445	91.641	BV
2	34.047	318576	8.359	TBB
		3811021	100.000	

*Figure S125 HPLC of the pure **III.11**.*

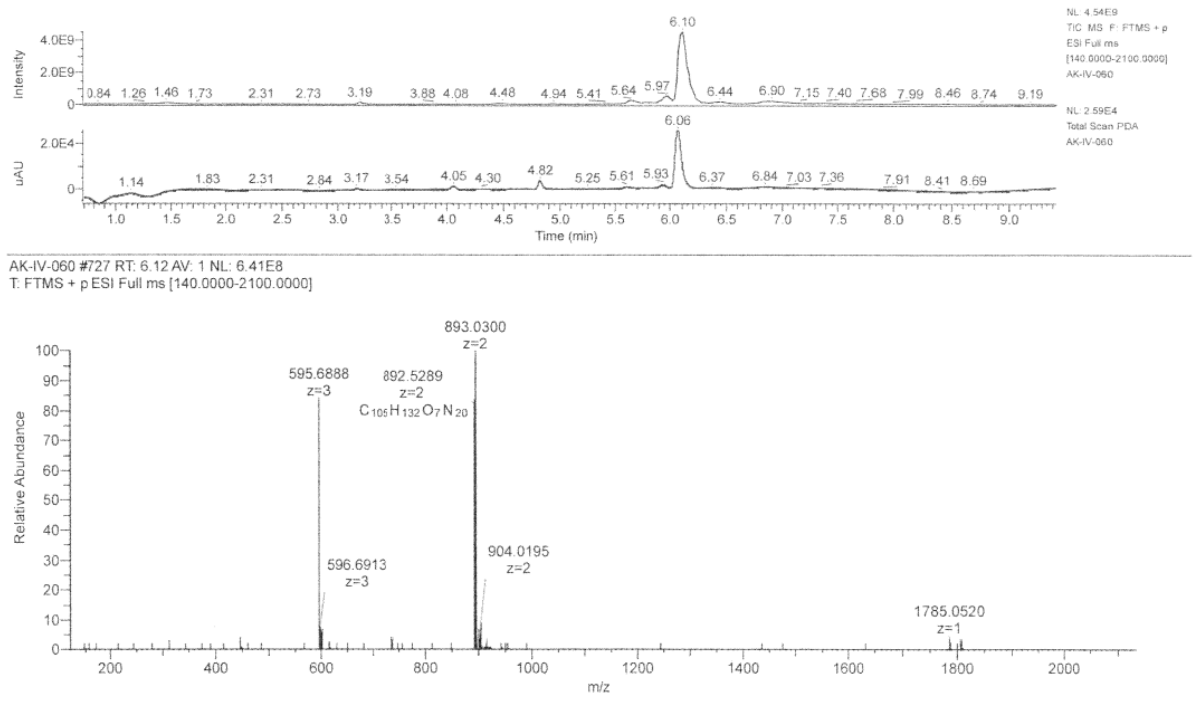

*Figure S126 LCMS of the crude **III.11**.*

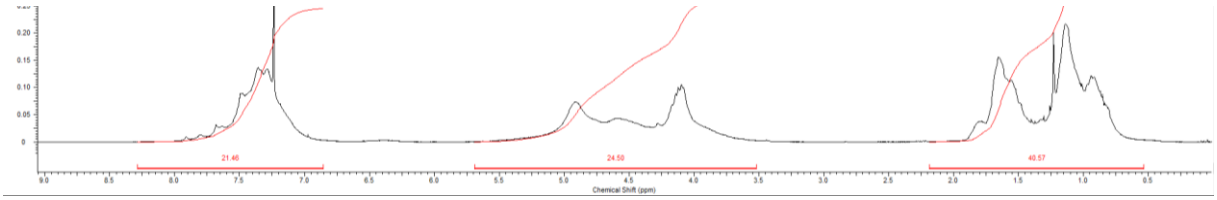

*Figure S127 ^{1}H-NMR in $CDCl_3$ of the pure **III.11**.*

*11.2.2 Ortho-arylopeptoids clicked, **III.12**.*

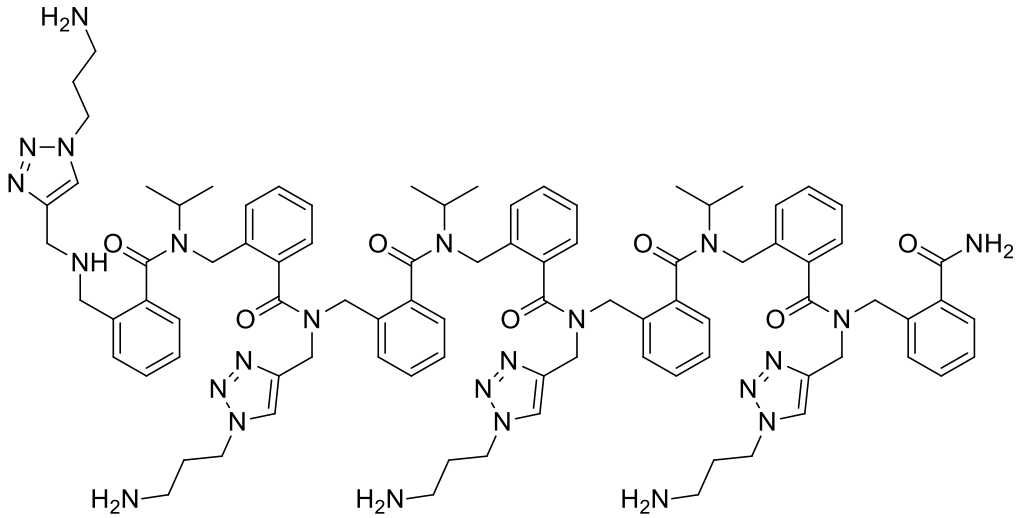

m_{pure}= 17.2 mg (purity 96%), 85% isolated yield (starting from 20 mg resin)
HRMS (TOF MS ES+): *m/z* calcd for $C_{89}H_{112}N_{24}O_7$ $[M+2H]^{2+}$: 814.45674; found: 814.4553 (-1.74 ppm).

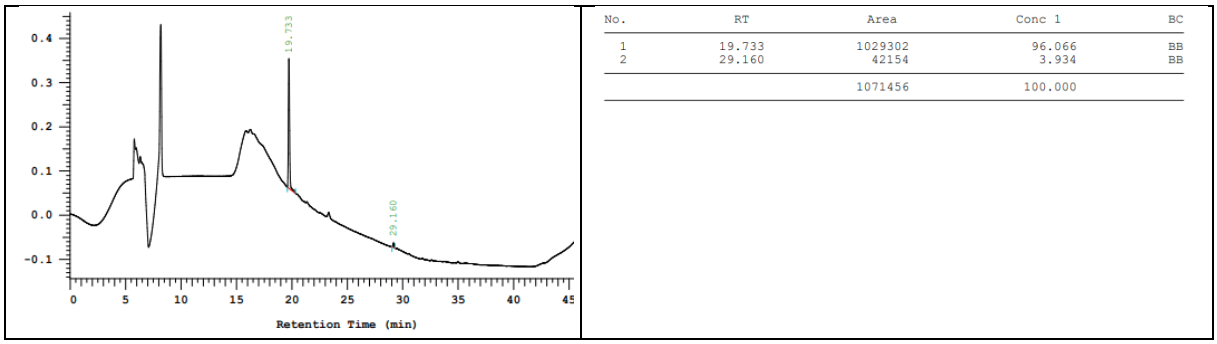

No.	RT	Area	Conc 1	BC
1	19.733	1029302	96.066	BB
2	29.160	42154	3.934	BB
		1071456	100.000	

*Figure S128 HPLC of the pure **III.12**.*

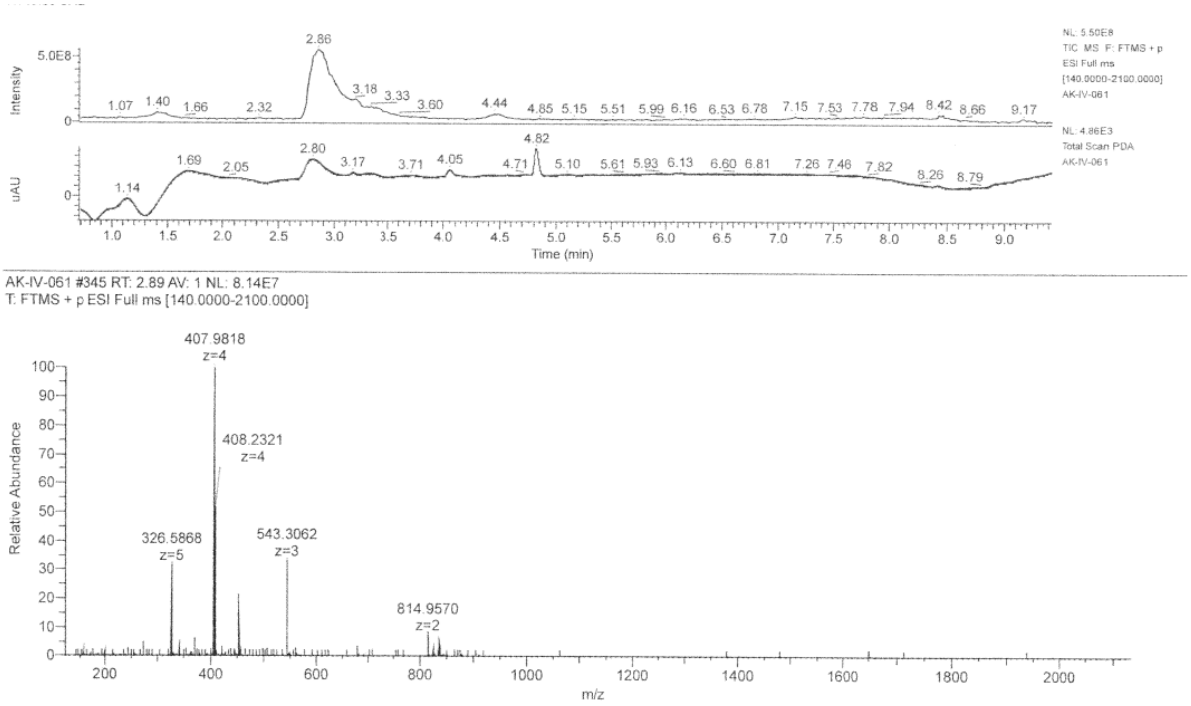

*Figure S129 LCMS of the crude **III.12**.*

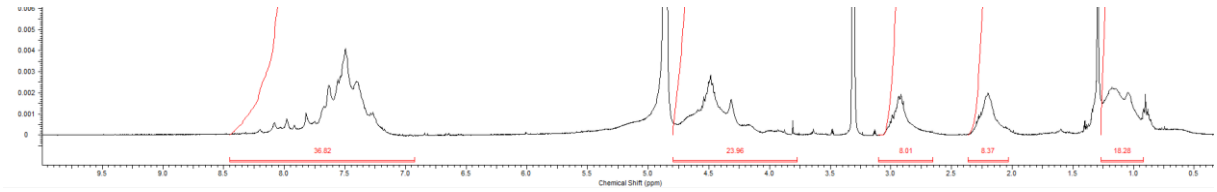

*Figure S130 ^{1}H-NMR in MeOD of the pure **III.12**.*

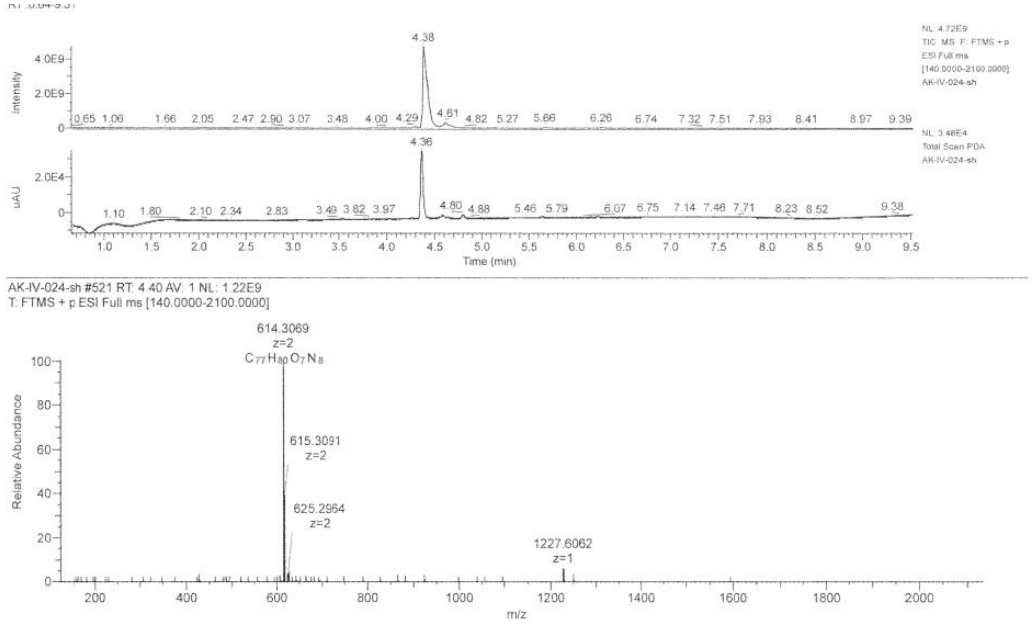

*Figure S131 LCMS of the crude **III.12**.*

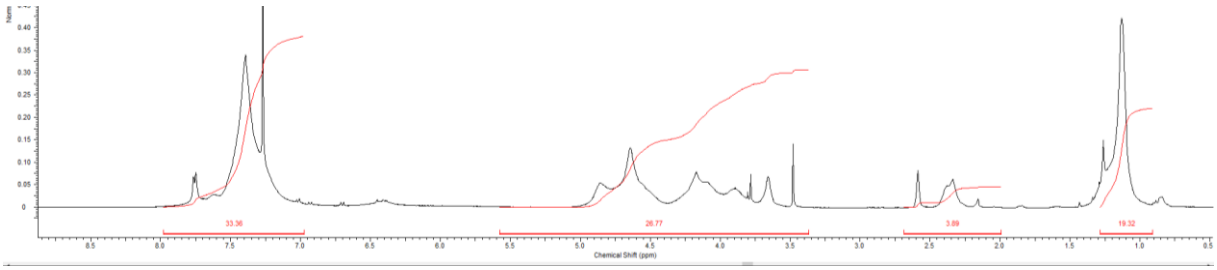

*Figure S132 ^{1}H-NMR spectra in $CDCl_3$ of **III.12**.*

Chapter IV.

IV.1. Synthesis of triazolium

Standard procedure: First, the synthesis of the desired length of the peptoids, and click reaction using the optimized protocol described in chapter III is performed on the rink amide resin (100 mg, loading 0.62 mmol/g). The resin is rinsed with CH_2Cl_2 (5x2 ml), then to a solution of di-tert-butyl dicarbonate (40 mg, 0.183 mmol, 3 equiv.) in CH_2Cl_2 (1 ml) at rt DIPEA (0.063 mL, 0.366 mmol, 6 equiv.). The solution was added to the resin and the resulting mixture was agitated for 1h at rt. The resin was drained and washed with CH_2Cl_2 (5x2 mL). Then, pure MeI (2 ml) was added. After shaking for 24 hours at 45°C, the solution was drained and washed with CH_2Cl_2 (8×2 ml) to yield the crude triazolium product. Finally, the triazoliums based arylopeptoids were cleaved from the resin, by treatment with 1 mL of TFA/triisopropylsilane/water (95:2.5:2.5 by volume) for 15 min. The cleavage mixture was then diluted with CH_2Cl_2 (5×2 ml) and evaporated under reduced pressure to get rid of TFA.

1.Series A

1.1. IV.2.

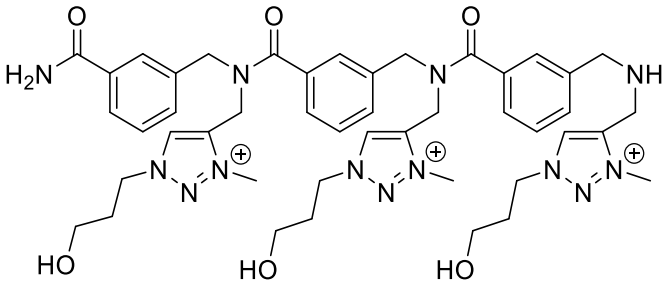

IV.2

Trimer **IV.2** was synthesised according to the standard procedure using 150 mg of Rink Amide resin (loading 0.62 mmol/g).

m_{crude}= 126 mg, 153% crude yield

m_{pure}= 78 mg (95% isolated yield, HPLC purity 97%),

HRMS (TOF MS ES+): *m/z* calcd for $C_{45}H_{60}N_{13}O_6$ $[M]^{3+}$: 292.82577; found: 292.8260 (0.86 ppm).

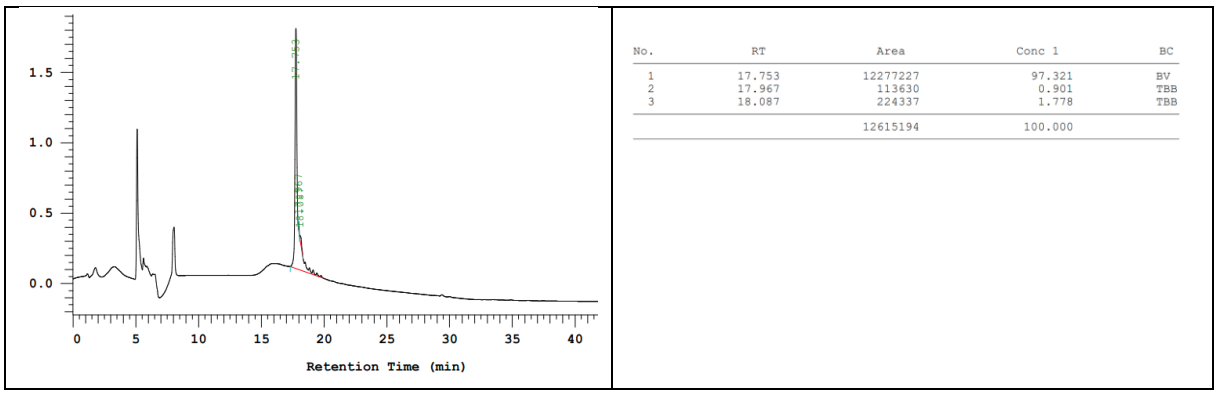

No.	RT	Area	Conc 1	BC
1	17.753	12277227	97.321	BV
2	17.967	113630	0.901	TBB
3	18.087	224337	1.778	TBB
		12615194	100.000	

Figure S133. HPLC chromatogram (220 nm) of purified **IV.2**.

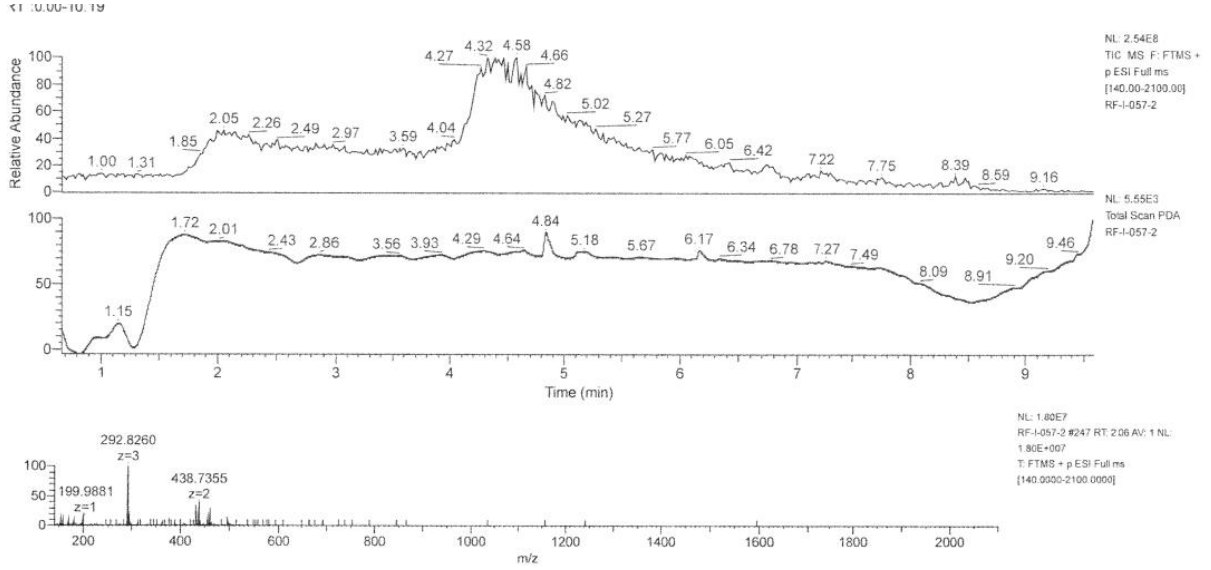

Figure S134. LCMS spectrum of **IV.2.**

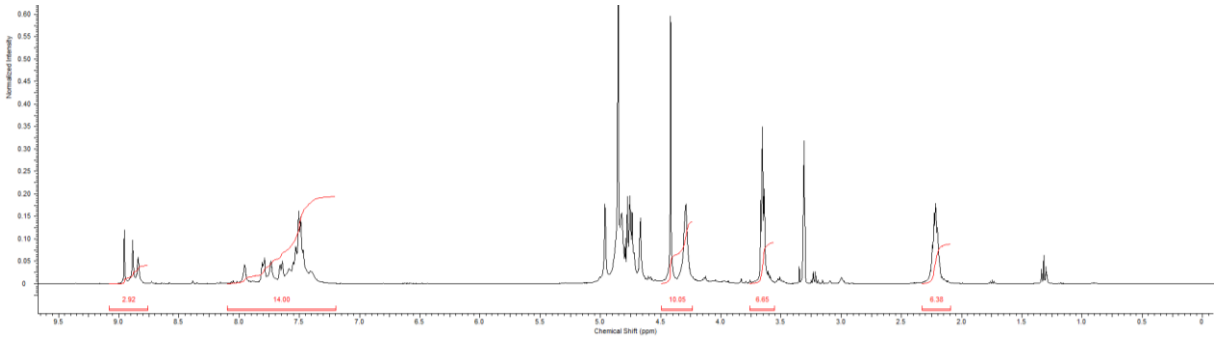

Figure S135. ^{1}H-NMR spectrum in MeOD of **IV.2**.

1.2. IV.3.

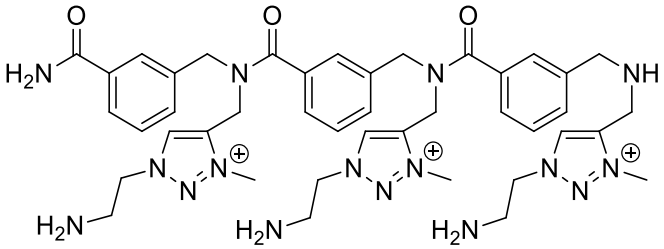

IV.3

Trimer **IV.3** was synthesised according to the standard procedure using 100 mg of Rink Amide resin (loading 0.62 mmol/g).

m_{crude}= 61 mg, 118% crude yield

m_{pure}= 42 mg (82% isolated yield, HPLC purity 99%)

HRMS (TOF MS ES+): *m/z* calcd for $C_{42}H_{57}N_{16}O_3$ $[M]^{3+}$: 277.82610; found: 277.8257 (-1.4 ppm).

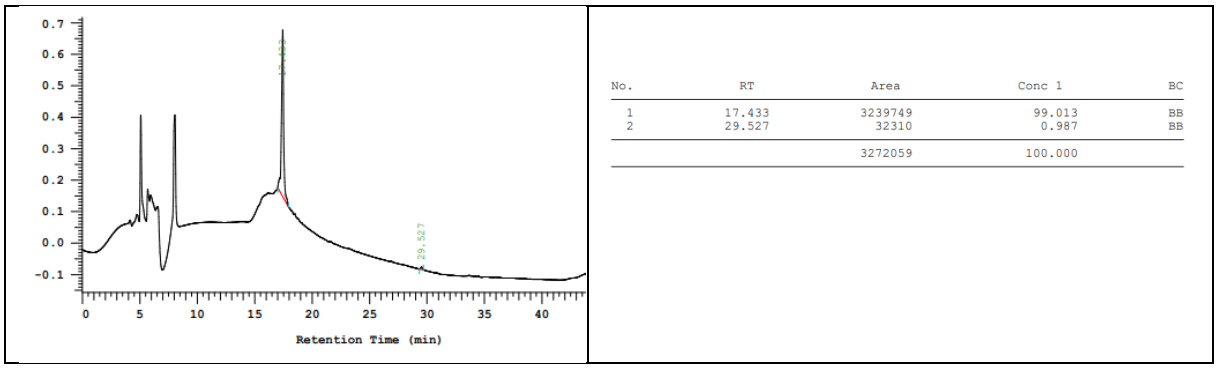

No.	RT	Area	Conc 1	BC
1	17.433	3239749	99.013	BB
2	29.527	32310	0.987	BB
		3272059	100.000	

Figure S136. HPLC chromatogram (220 nm) of purified **IV.3**.

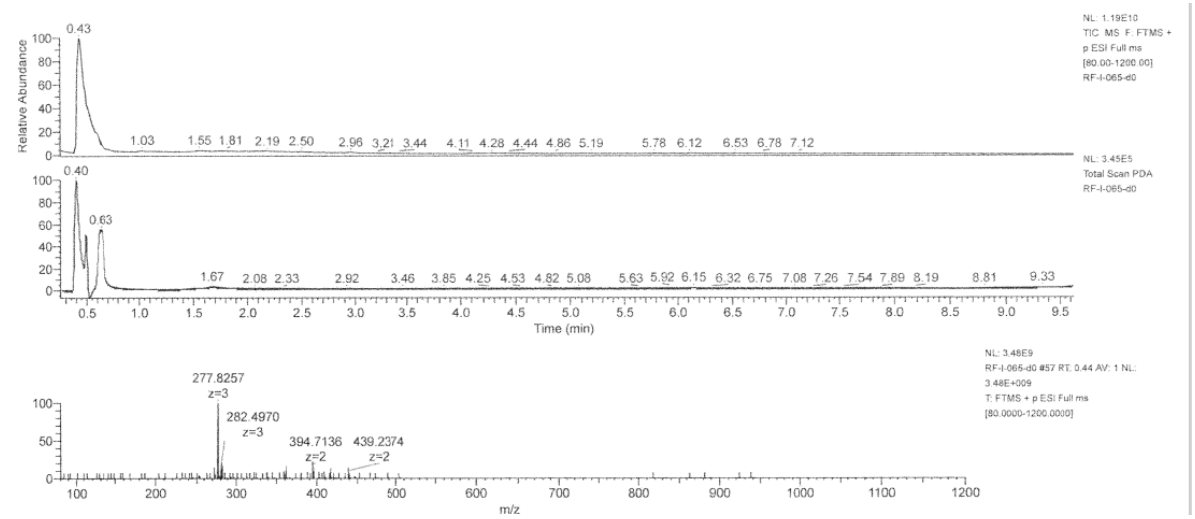

Figure S137. LCMS spectra of purified **IV.3**.

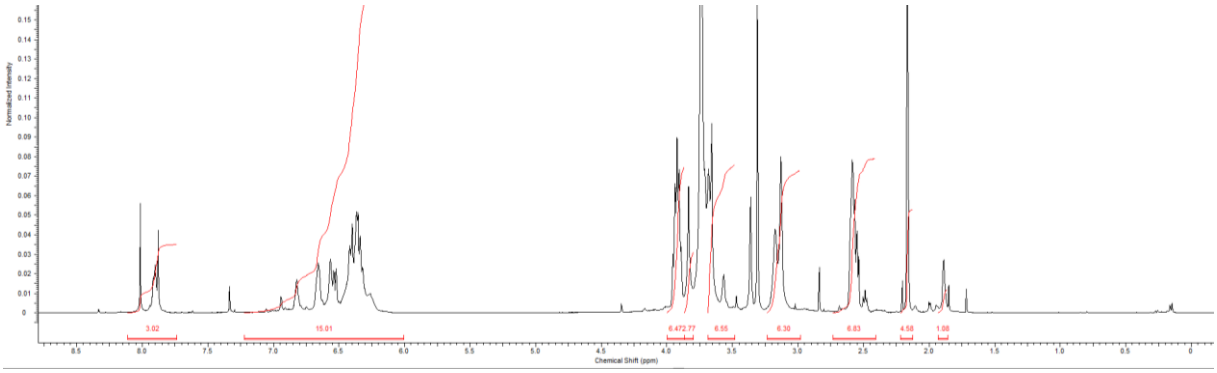

Figure S138. ^{1}H-NMR spectra in MeOD of **IV.3**.

1.3. IV.4.

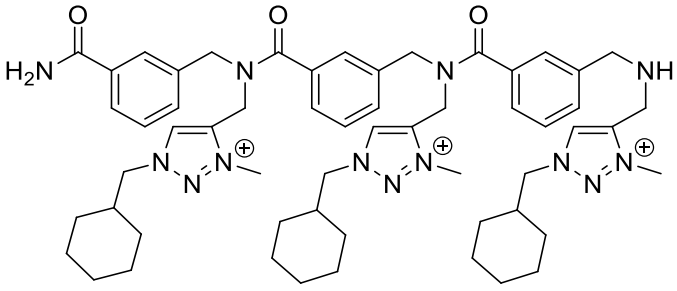

IV.4

Trimer **IV.4** was synthesised according to the standard procedure using 150 mg of Rink amide resin (loading 0.62 mmol/g).

m_{crude}= 131 mg, 184% crude yield

m_{pure}= 68 mg (74% isolated yield, HPLC purity 90%)

HRMS (TOF MS ES+): *m/z* calcd for $C_{57}H_{78}N_{13}O_3$ $[M]^{3+}$: 330.87780; found: 330.8782 (1.3 ppm).

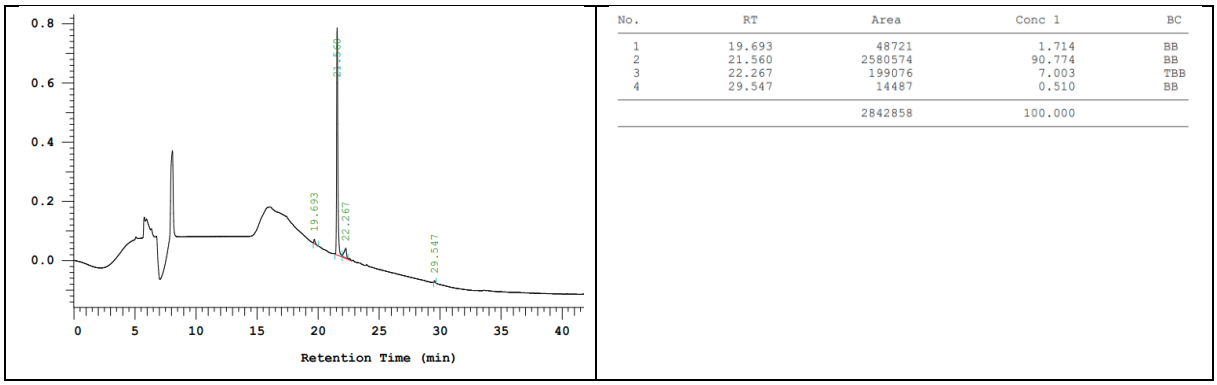

No.	RT	Area	Conc 1	BC
1	19.693	48721	1.714	BB
2	21.560	2580574	90.774	BB
3	22.267	199076	7.003	TBB
4	29.547	14487	0.510	BB
		2842858	100.000	

Figure S139. HPLC chromatogram (220 nm) of purified **IV.4**.

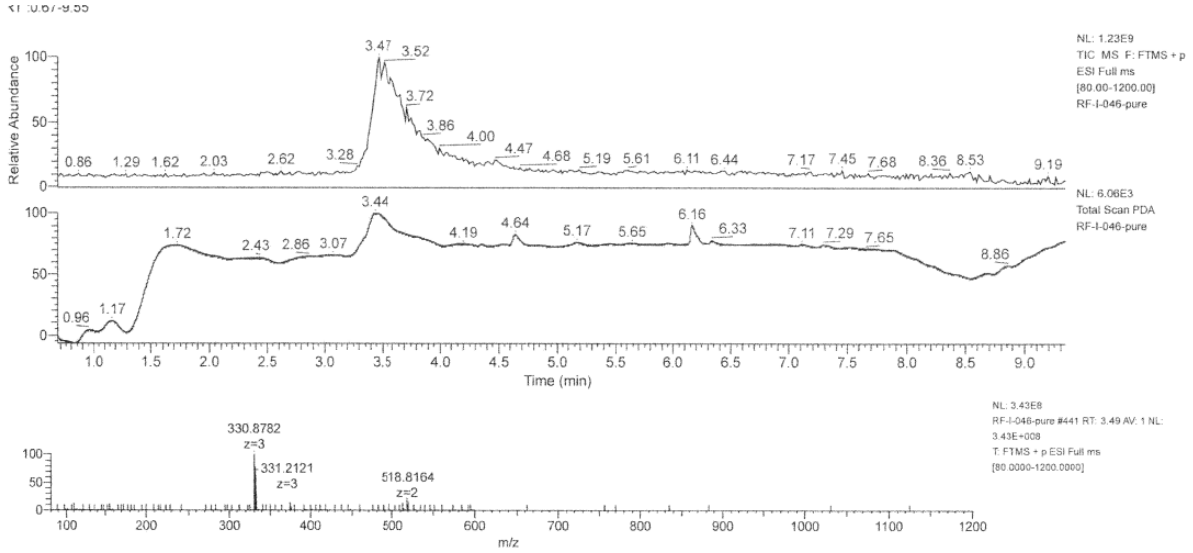

Figure S140. LCMS spectrum of **IV.4**.

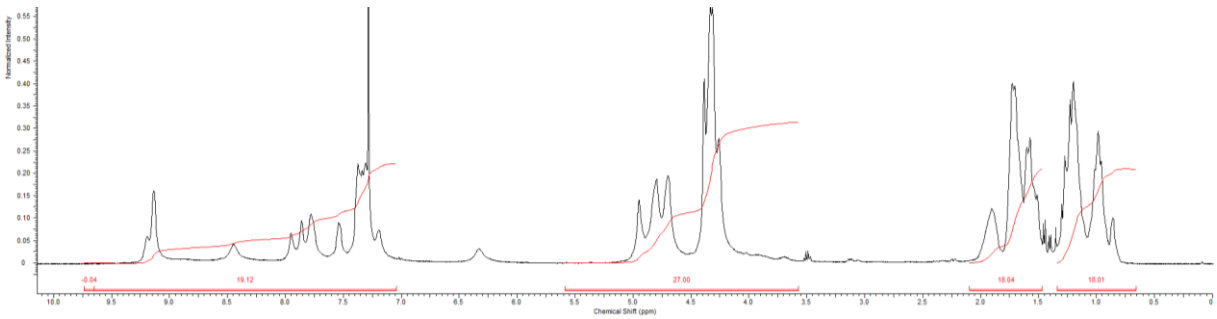

Figure S141. ^{1}H-NMR spectra in $CDCl_3$ of **IV.4**.

1.4. *IV.5.*

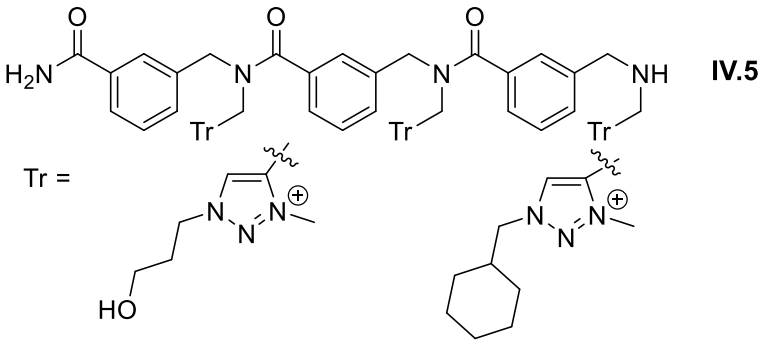

IV.5

Trimer **IV.5** was synthesised according to the standard procedure using 150 mg of Rink Amide resin (loading 0.62 mmol/g).

m_{crude}= 131 mg, 144% crude yield

m_{pure}= 80 mg (87% isolated yield, HPLC purity 97%),

LCMS pic at 2.13 min: HRMS (TOF MS ES+): *m/z* calcd for $C_{45}H_{59}N_{13}O_6$ $[M]^{2+}$: 438.73501 found: 438.7354 (0.91 ppm)

LCMS pic at 2.79 min: HRMS (TOF MS ES+): *m/z* calcd for $C_{49}H_{66}N_{13}O_5$ $[M]^{3+}$: 305.50978; found: 305.5101 (0.95 ppm).

LCMS pic at 3.56 min: HRMS (TOF MS ES+): *m/z* calcd for $C_{53}H_{72}N_{13}O_4$ $[M]^{3+}$: 318.19379; found: 318.1940 (0.65 ppm).

LCMS pic at 4.19 min: HRMS (TOF MS ES+): *m/z* calcd for $C_{57}H_{78}N_{13}O_3$ $[M]^{3+}$: 330.87780; found: 330.8780 (0.56 ppm)

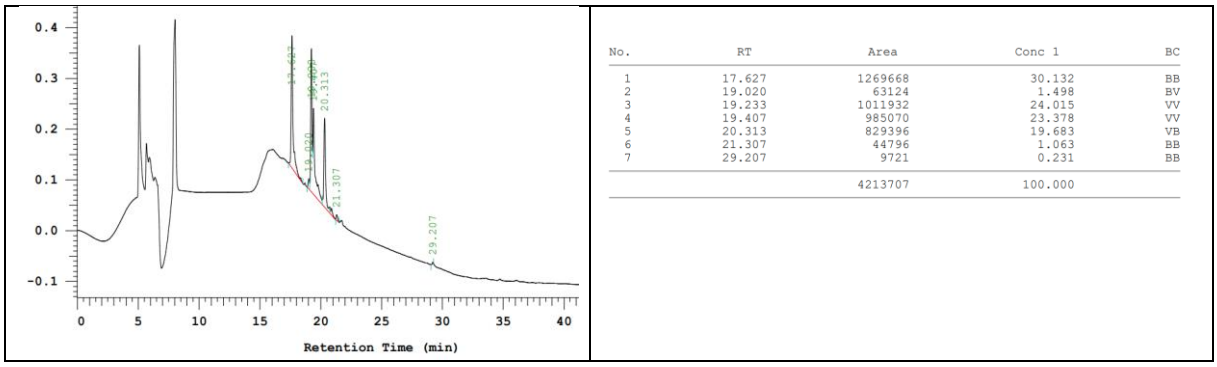

No.	RT	Area	Conc 1	BC
1	17.627	1269668	30.132	BB
2	19.020	63124	1.498	BV
3	19.233	1011932	24.015	VV
4	19.407	985070	23.378	VV
5	20.313	829396	19.683	VB
6	21.307	44796	1.063	BB
7	29.207	9721	0.231	BB
		4213707	100.000	

Figure S142. HPLC chromatogram (220nm) of the purified **IV.5**.

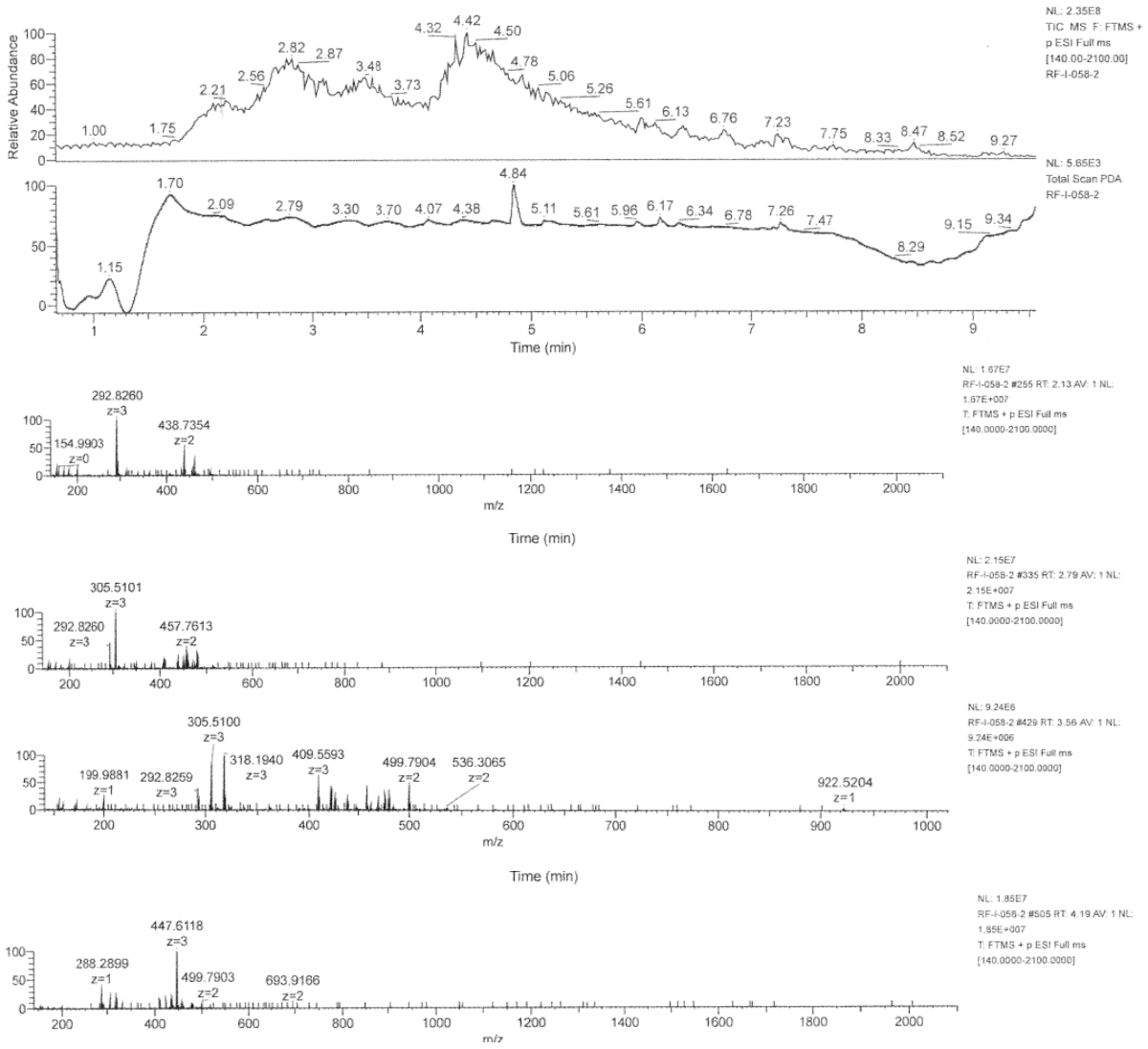

Figure S143. LCMS spectra of purified **IV.5**.

1.5. IV.6.

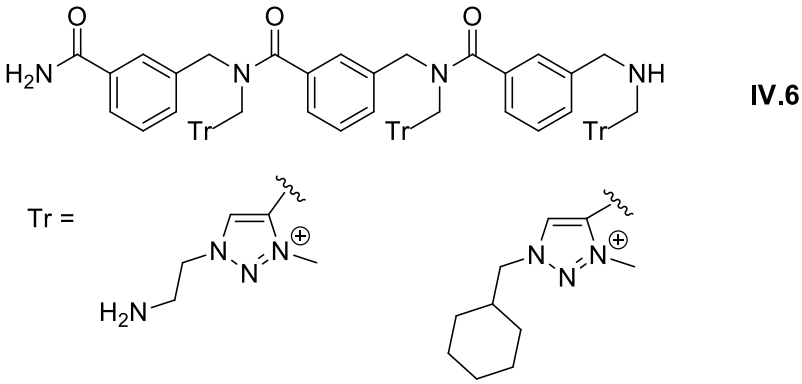

Trimer **IV.6** was synthesised according to the standard procedure (with 2 azides) using 150 mg of Rink Amide resin (loading 0.62 mmol/g).

m_{crude}= 136 mg, 168% crude yield

m_{pure}= 60 mg (67% isolated yield, purity 90%)

LCMS pic at 2.22 min: HRMS (TOF MS ES+): *m/z* calcd for $C_{42}H_{57}N_{16}O_3$ $[M]^{3+}$: 277.8261; found: 277.8264 (1.13 ppm)

LCMS pic at 2.44 min: HRMS (TOF MS ES+): *m/z* calcd for $C_{47}H_{64}N_{15}O_3$ $[M]^{3+}$: 295.5100; found: 295.5103 (0.85 ppm).

LCMS pic at 3.36 min: HRMS (TOF MS ES+): *m/z* calcd for $C_{52}H_{71}N_{14}O_3$ $[M]^{3+}$: 313.1939; found: 313.1941 (0.5 ppm).

LCMS pic at 3.96 min: HRMS (TOF MS ES+): *m/z* calcd for $C_{57}H_{78}N_{13}O_3$ $[M]^{3+}$: 330.87780; found: 330.8779 (0.19 ppm)

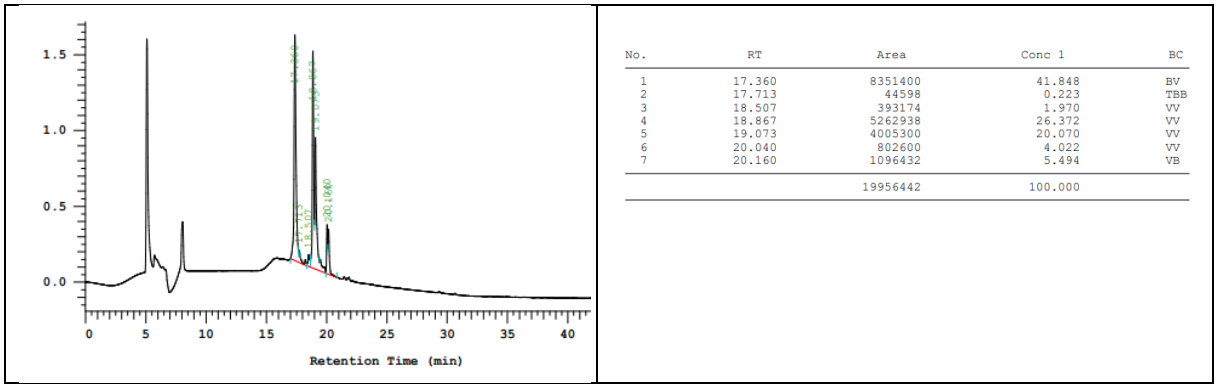

No.	RT	Area	Conc 1	BC
1	17.360	8351400	41.848	BV
2	17.713	44598	0.223	TBB
3	18.507	393174	1.970	VV
4	18.867	5262938	26.372	VV
5	19.073	4005300	20.070	VV
6	20.040	802600	4.022	VV
7	20.160	1096432	5.494	VB
		19956442	100.000	

Figure S144. HPLC chromatogram (220 nm) of the purified **IV.6**.

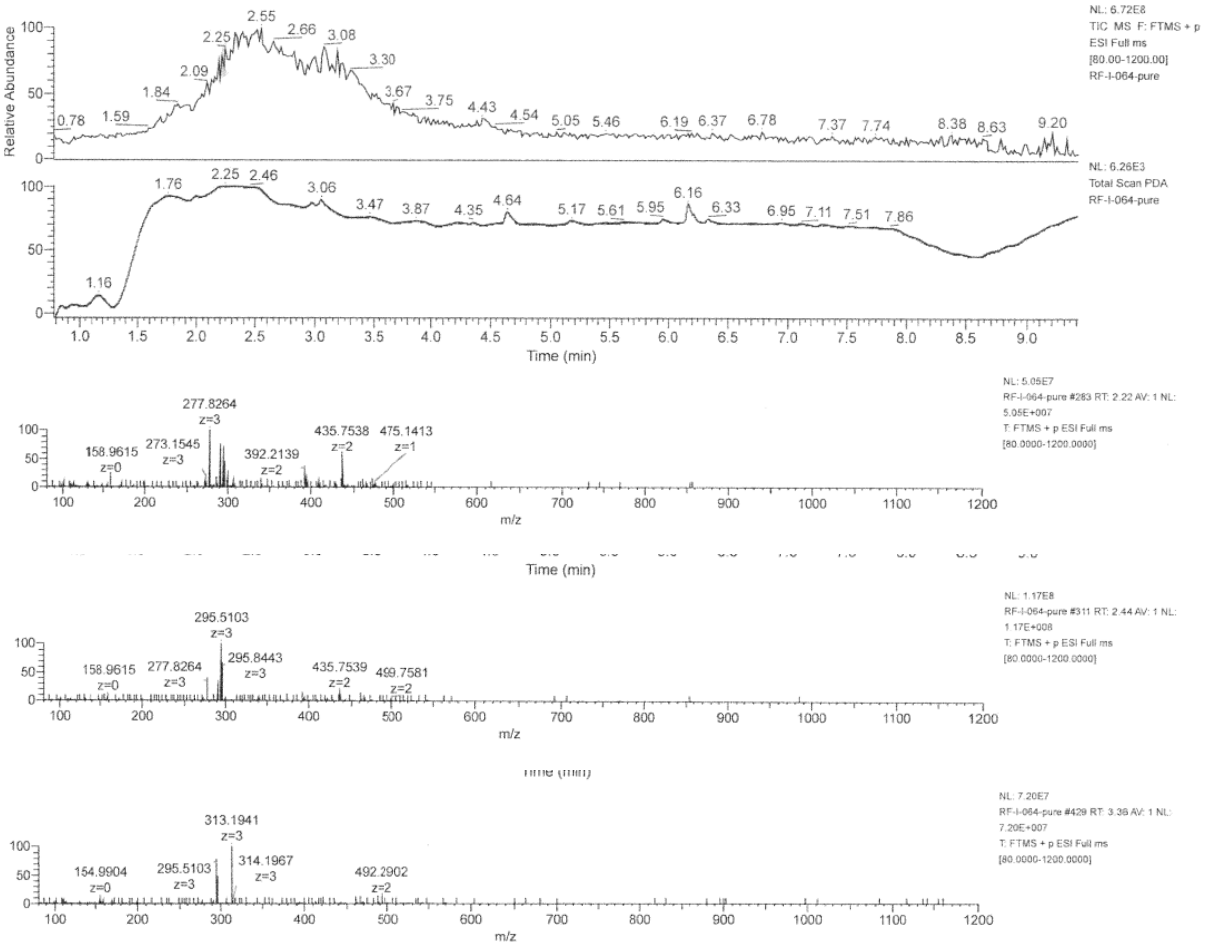

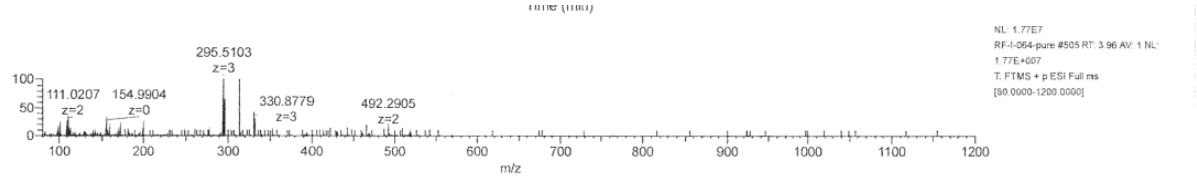

Figure S145. LCMS spectra of purified **IV.6**.

1.6. IV.7.

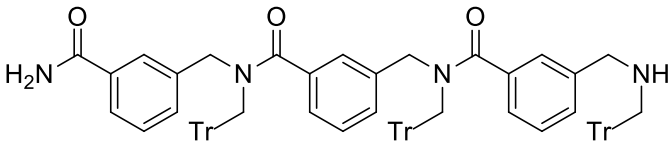

IV.7

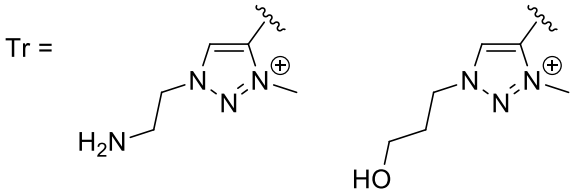

Trimer **IV.7** was synthesised according to the standard procedure using 150 mg of Rink Amide resin (loading 0.62 mmol/g).

m_{crude}= 126 mg, 157% crude yield

m_{pure}= 75 mg (92% isolated yield, HPLC purity 98%)

LCMS pic at 0.58 min: HRMS (TOF MS ES+): *m/z* calcd for $C_{44}H_{59}N_{14}O_5$ $[M]^{3+}$: 287.82588; found: 287.826 (0.27 ppm)

LCMS pic at 0.63 min: HRMS (TOF MS ES+): *m/z* calcd for $C_{43}H_{58}N_{15}O_4$ $[M]^{3+}$: 282.82599; found: 282.8264 (1.5 ppm).

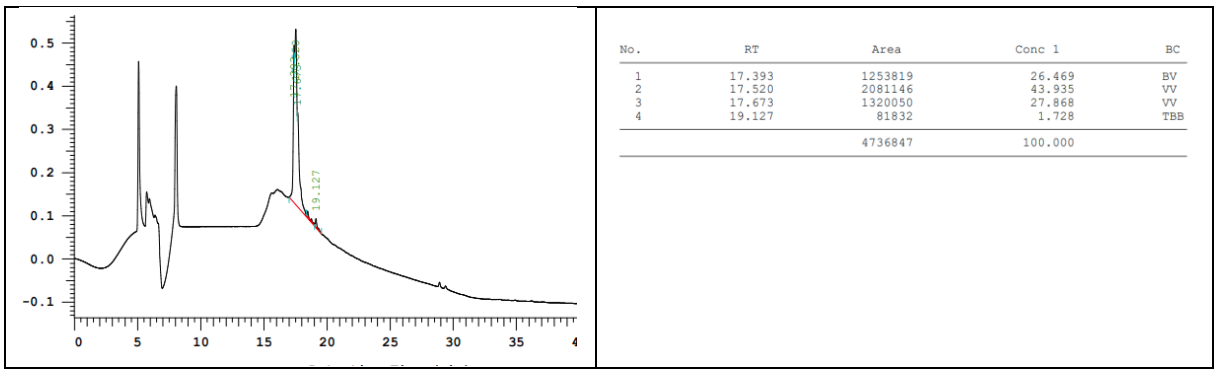

No.	RT	Area	Conc 1	BC
1	17.393	1253819	26.469	BV
2	17.520	2081146	43.935	VV
3	17.673	1320050	27.868	VV
4	19.127	81832	1.728	TBB
		4736847	100.000	

Figure S146. HPLC chromatogram (220 nm) of the purified **IV.7**.

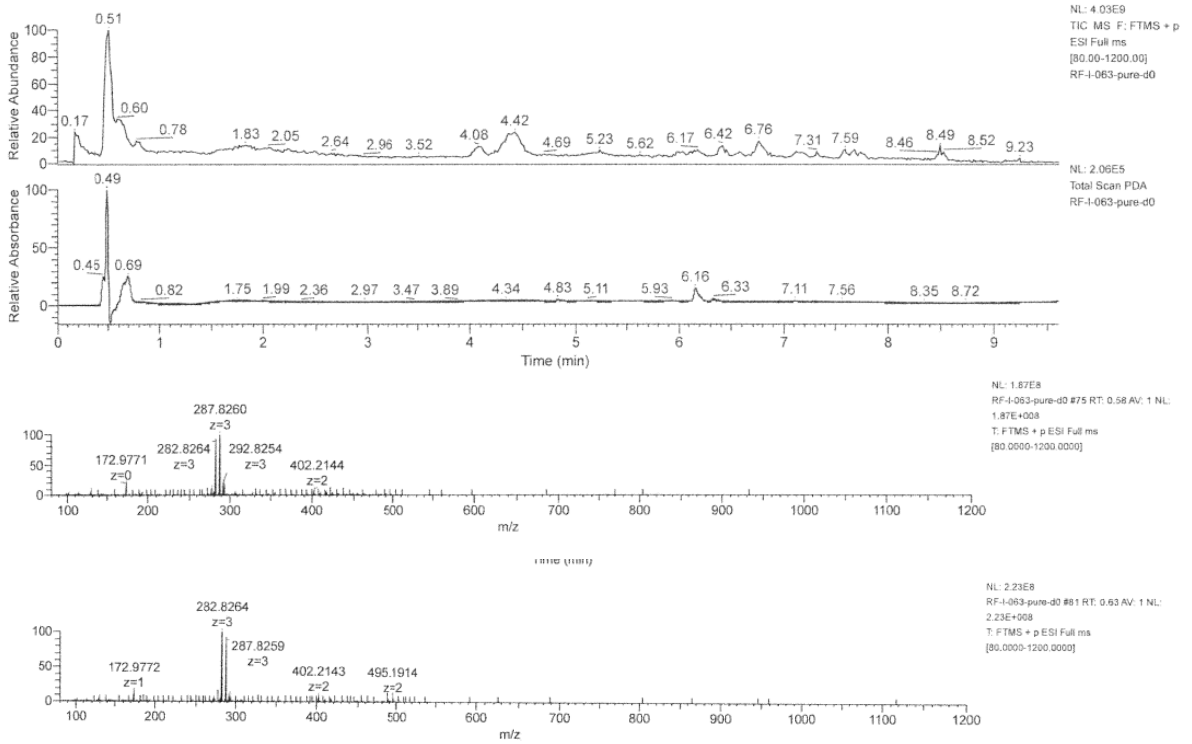

Figure S147. LCMS spectra of purified **IV.7**.

2.Series B

2.1. IV.8.

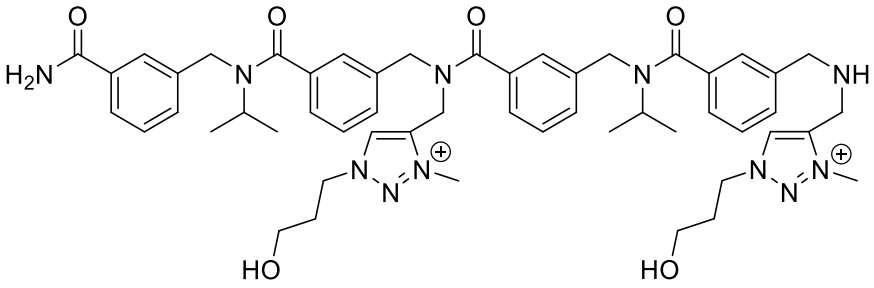

IV.8

Tetramer **IV.8** was synthesised according to the standard procedure using 150 mg of Rink Amide resin (loading 0.62 mmol/g).

m_{crude}= 98.7 mg, 114% crude yield

m_{pure}= 68 mg (78% isolated yield, HPLC purity 94%)

HRMS (TOF MS ES+): *m/z* calcd for $C_{52}H_{67}N_{11}O_6$ $[M]^{2+}$: 470.76324; found: 470.764 (1.63ppm).

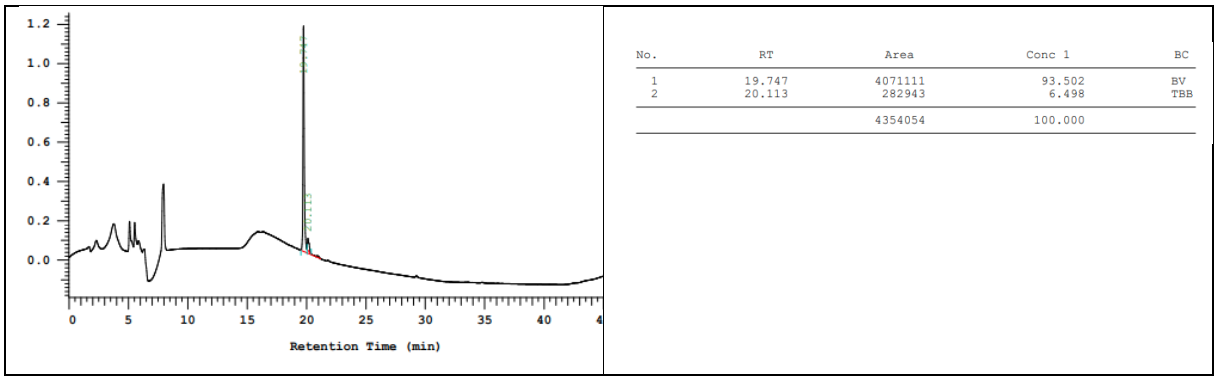

Figure S148. HPLC chromatogram (220 nm) of the purified **IV.8**.

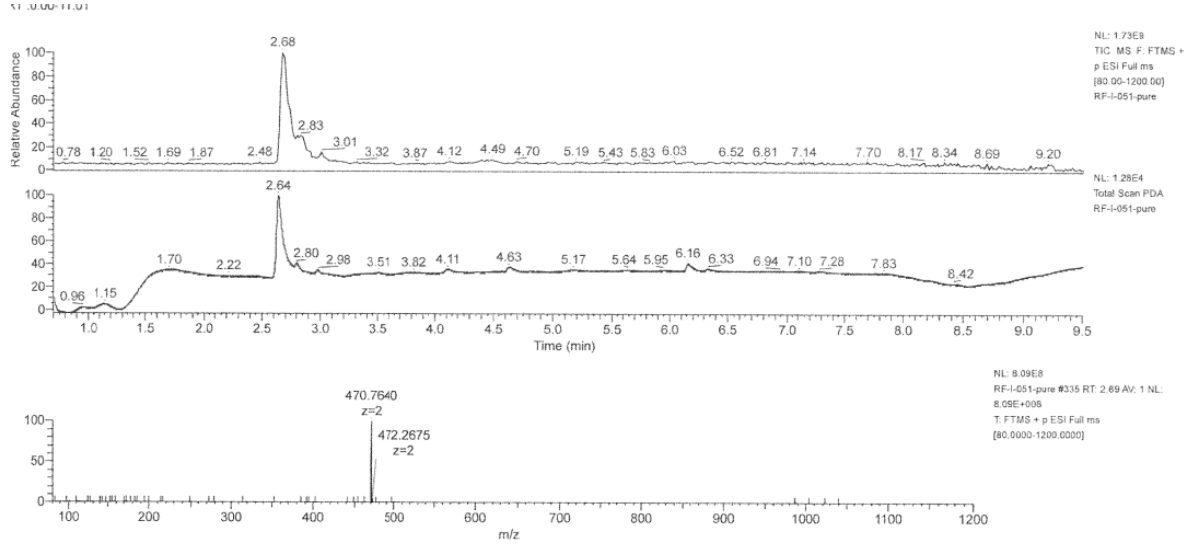

Figure S149. LCMS spectrum of purified **IV.8**.

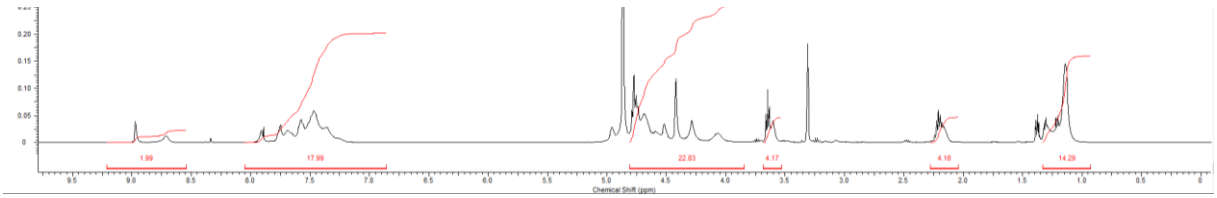

Figure S150. ^{1}H-NMR spectrum in MeOD of **IV.8**.

2.2. *IV.9.*

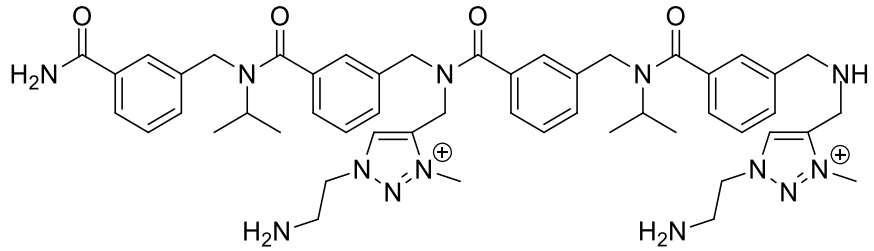

IV.9

Tetramer **IV.9** was synthesised according to the standard procedure using 150 mg of Rink Amide resin (loading 0.62 mmol/g).

m_{crude}= 116 mg, 136% crude yield

m_{pure}= 75 mg (88% isolated yield, HPLC purity 95%)

HRMS (TOF MS ES+): *m/z* calcd for $C_{50}H_{65}N_{13}O_4$ $[M+2H]^{2+}$: 455.76358; found: 455.7641 (1.15 ppm).

HRMS (TOF MS ES+): *m/z* calcd for $C_{50}H_{66}N_{13}O_4$ $[M+H]^{3+}$: 304.17814; found: 304.1784 (0.87 ppm).

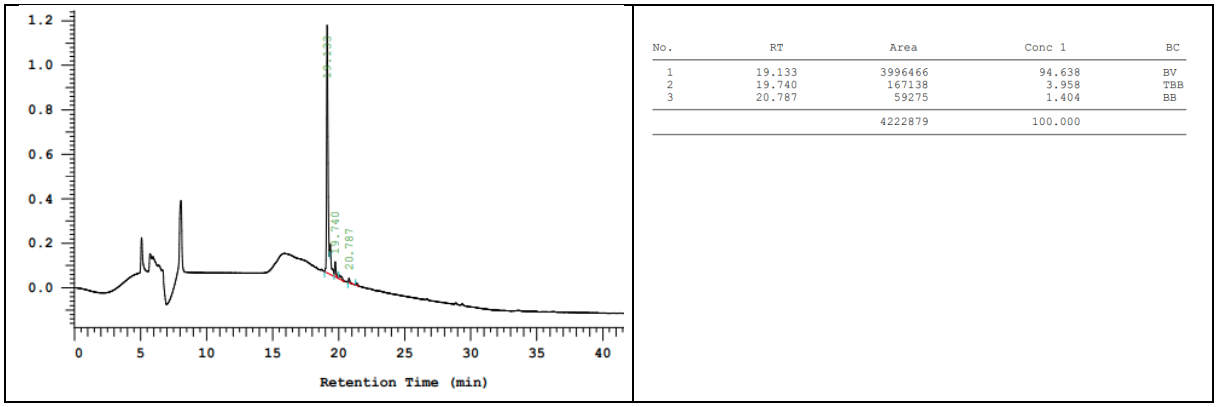

No.	RT	Area	Conc 1	BC
1	19.133	3996466	94.638	BV
2	19.740	167138	3.958	TBB
3	20.787	59275	1.404	BB
		4222879	100.000	

Figure S151. HPLC chromatogram (220 nm) of the purified **IV.9**.

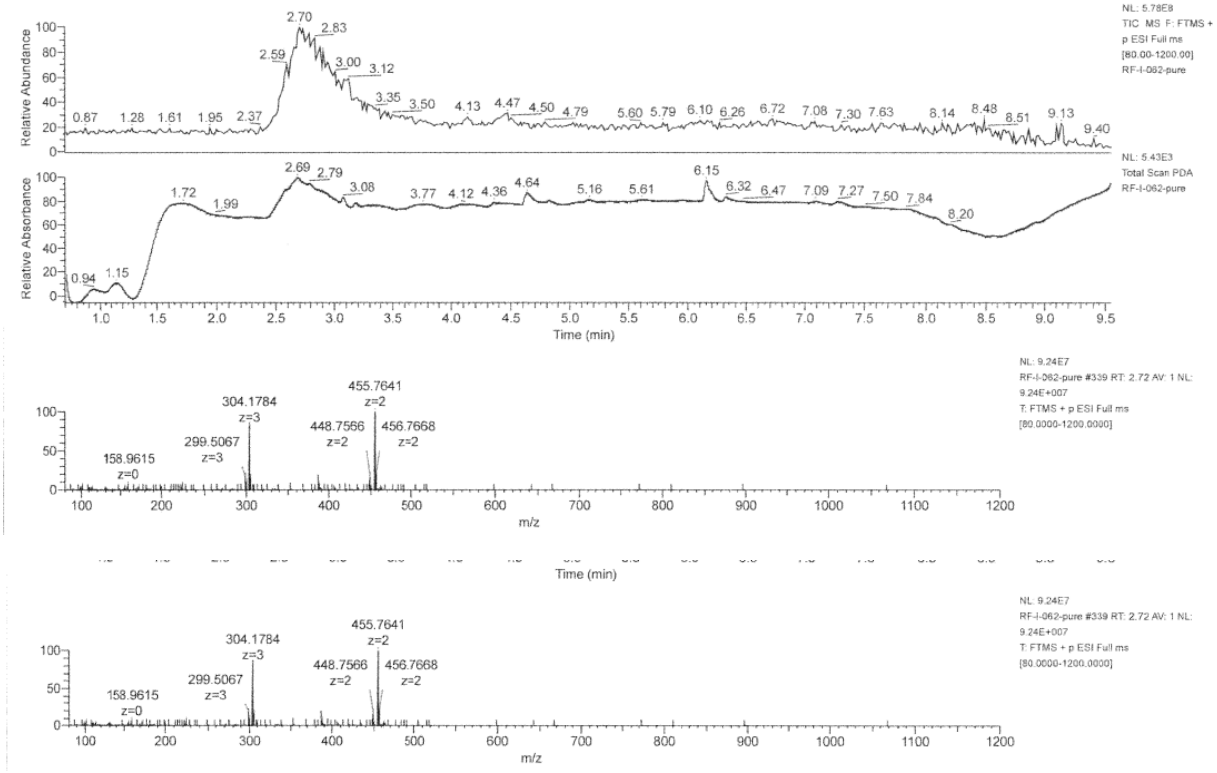

Figure S152 LCMS spectrum of the purified **IV.9**.

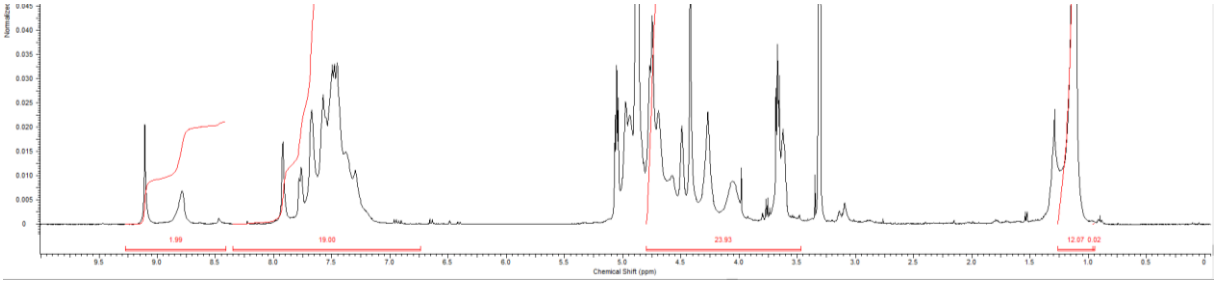

Figure S153. ^{1}H-NMR spectrum in MeOD of **IV.9**.

2.3. *IV.10.*

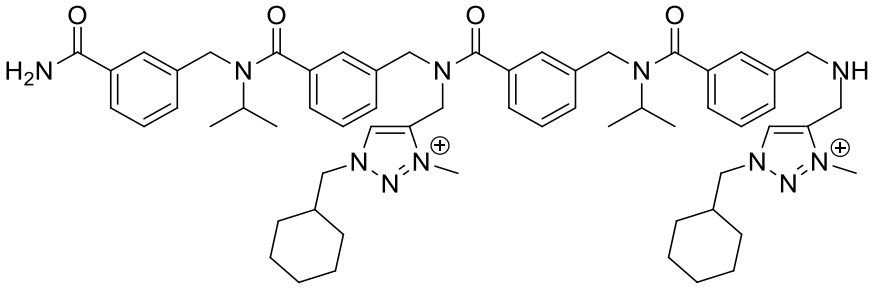

IV.10

Tetramer **IV.10** was synthesised according to the standard procedure using 100 mg of Rink Amide resin (loading 0.62 mmol/g).

m_{crude}= 94 mg, 150% crude yield

m_{pure}= 45 mg (71% isolated yield, HPLC purity 97%)

HRMS (TOF MS ES+): *m/z* calcd for $C_{60}H_{79}N_{11}O_4$ $[M+2H]^{2+}$: 508.81528; found: 508.8159 (1.14 ppm).

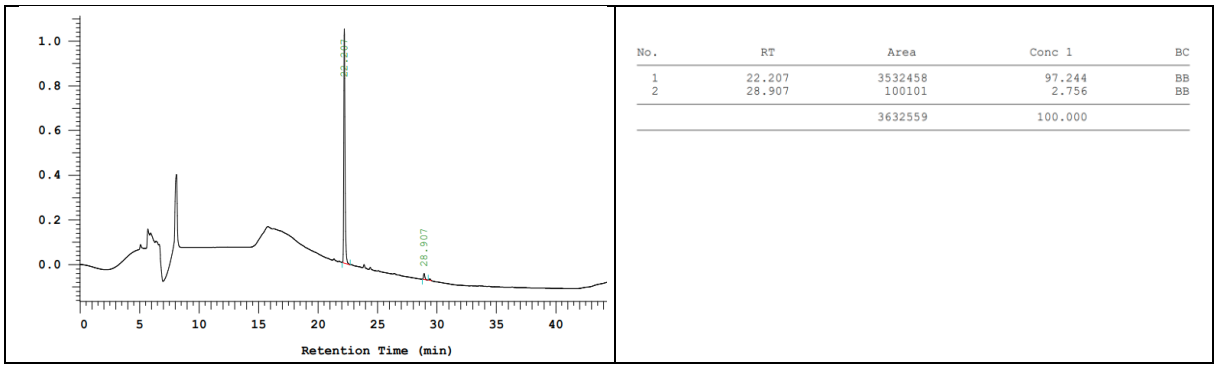

Figure S154. HPLC chromatogram (220 nm) of the purified **IV.10**.

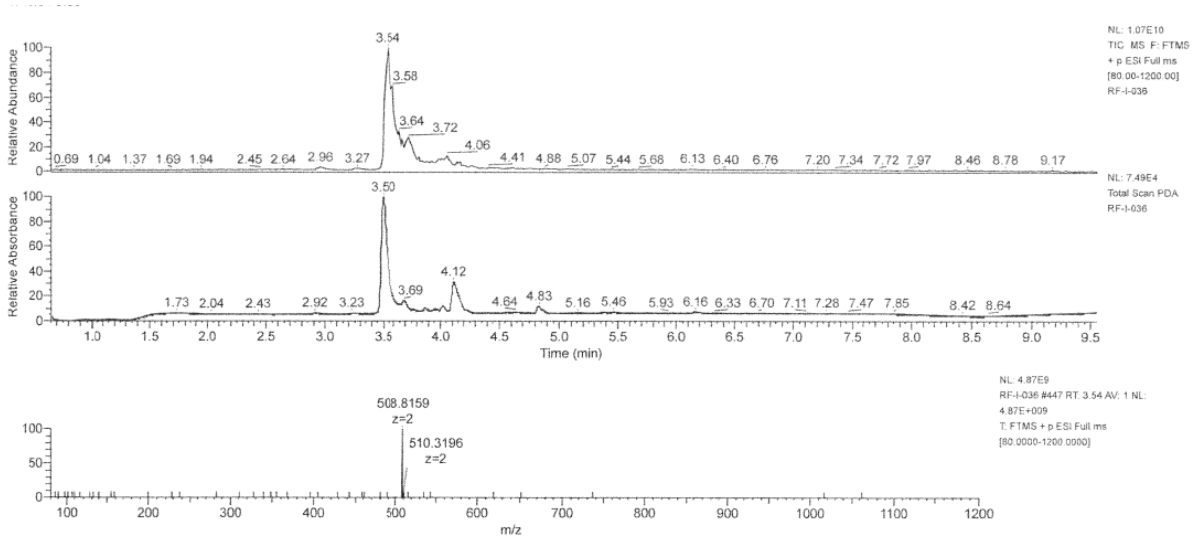

Figure S155. LCMS spectrum of purified **IV.10**.

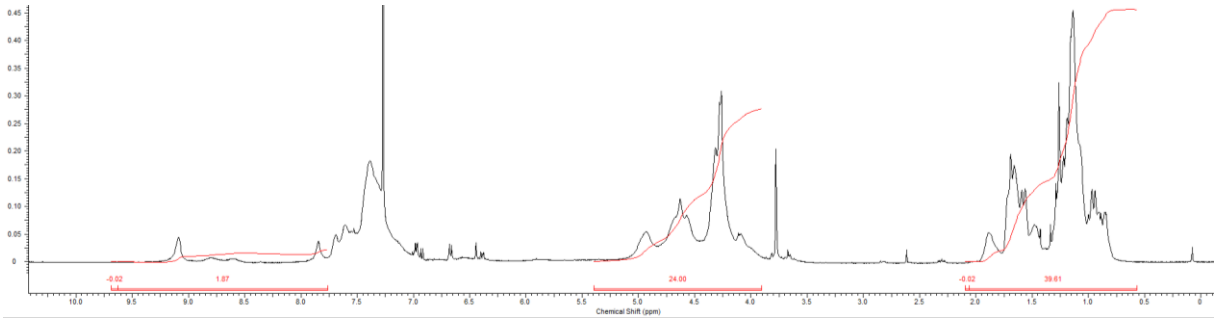

Figure S156. ^{1}H-NMR spectrum in $CDCl_3$ of **IV.10**.

2.4. *IV.11.*

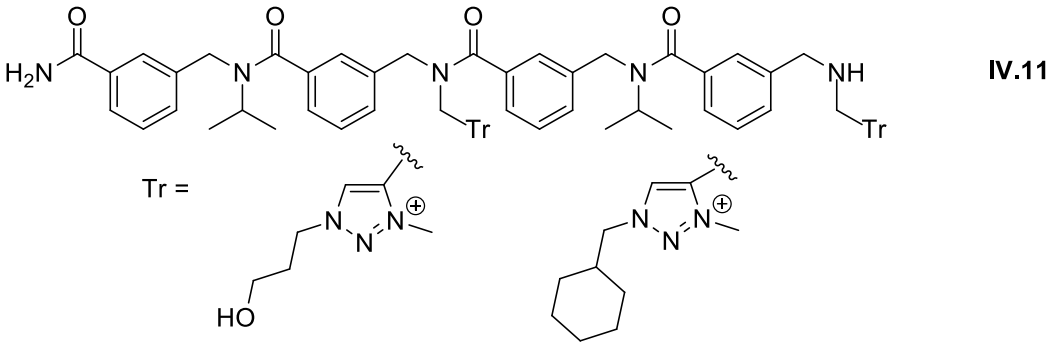

Tetramer **IV.11** was synthesised according to the standard procedure using 150 mg of Rink Amide resin (loading 0.62 mmol/g).

m_{crude}= 119 mg, 129% crude yield

m_{pure}= 95 mg (99% isolated yield, HPLC purity 86%).

LCMS pic at 2.66 min: HRMS (TOF MS ES+): *m/z* calcd for $C_{52}H_{67}N_{11}O_6$ $[M]^{2+}$: 470.76324 found: 470.7635 (0.59 ppm)

LCMS pic at 3.14 min: HRMS (TOF MS ES+): *m/z* calcd for $C_{56}H_{73}N_{11}O_5$ $[M]^{2+}$: 489.78926; found: 489.7898 (1.16 ppm).

LCMS pic at 3.74 min: HRMS (TOF MS ES+): *m/z* calcd for $C_{60}H_{79}N_{11}O_4$ $[M]^{2+}$: 508.81528; found: 508.8159 (1.26 ppm)

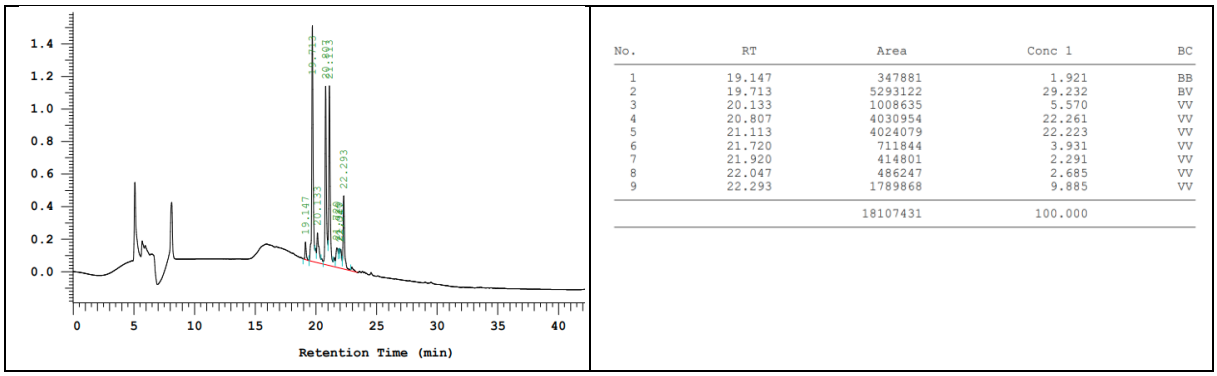

No.	RT	Area	Conc 1	BC
1	19.147	347881	1.921	BB
2	19.713	5293122	29.232	BV
3	20.133	1008635	5.570	VV
4	20.807	4030954	22.261	VV
5	21.113	4024079	22.223	VV
6	21.720	711844	3.931	VV
7	21.920	414801	2.291	VV
8	22.047	486247	2.685	VV
9	22.293	1789868	9.885	VV
		18107431	100.000	

Figure S157. HPLC chromatogram (220nm) of the purified **IV.11**.

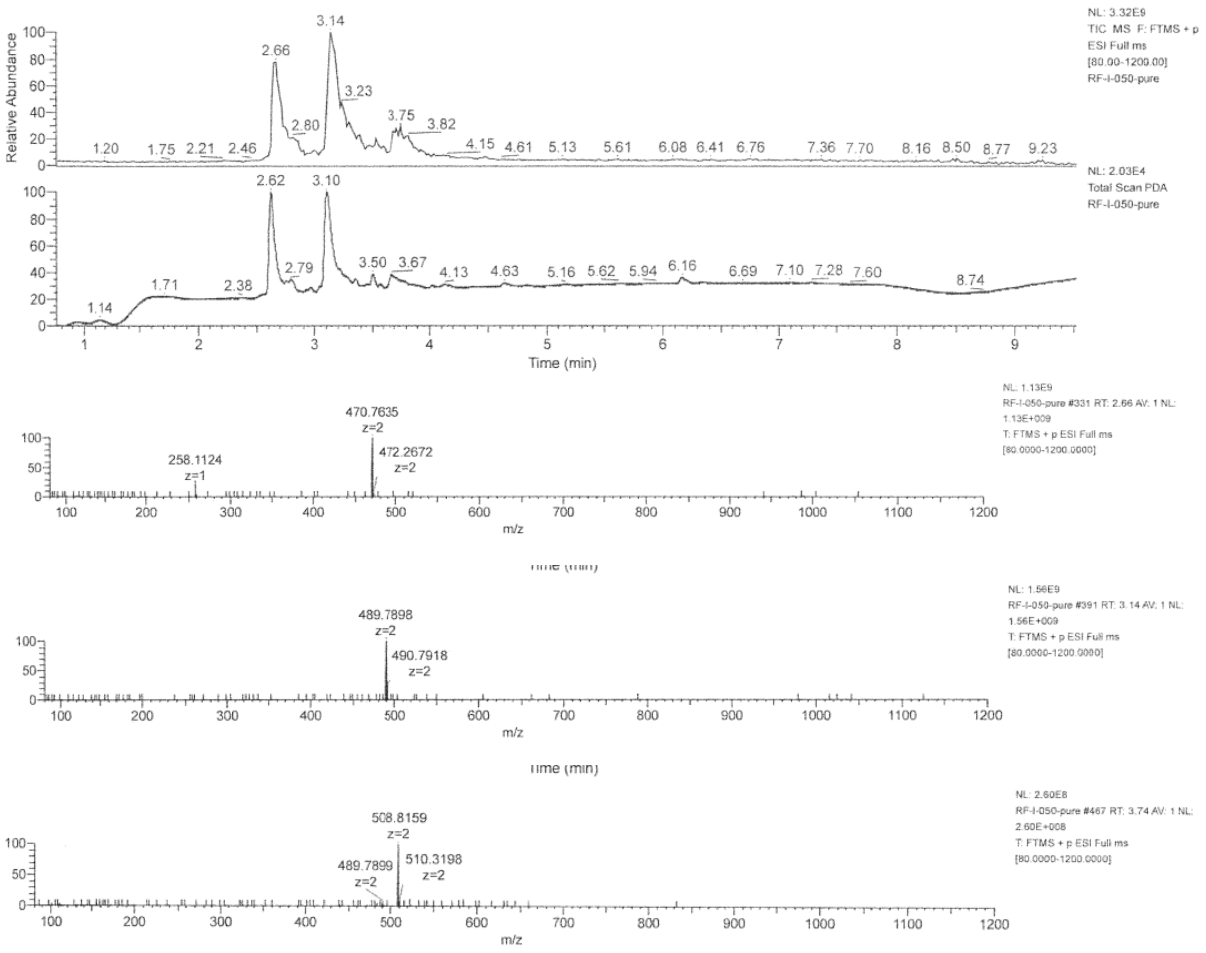

Figure S158. LCMS spectra of purified **IV.11**.

2.5. *IV.12.*

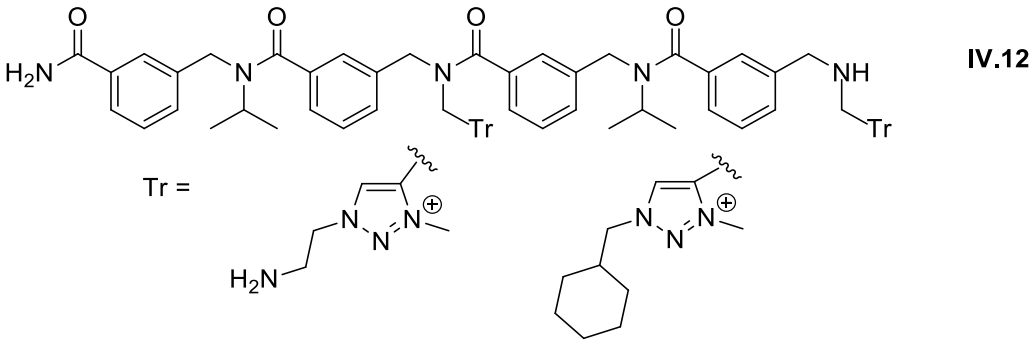

Tetramer **IV.12** was synthesised according to the standard procedure using 150 mg of Rink Amide resin (loading 0.62 mmol/g).

m_{crude}= 98.7 mg, 114% crude yield

m_{pure}= 65 mg (78% isolated yield, HPLC purity 94%).

LCMS pic at 2.85 min: HRMS (TOF MS ES+): *m/z* calcd for $C_{50}H_{65}N_{13}O_4$ $[M]^{2+}$: 455.76358 found: 455.7638 (0.48 ppm)

LCMS pic at 3.17 min: HRMS (TOF MS ES+): *m/z* calcd for $C_{55}H_{72}N_{12}O_4$ $[M]^{2+}$: 482.28943; found: 482.2897 (0.51 ppm).

LCMS pic at 3.17 min: HRMS (TOF MS ES+): *m/z* calcd for $C_{55}H_{73}N_{12}O_4$ $[M+H]^{3+}$: 321.86204; found: 321.8621 (0.15 ppm).

LCMS pic at 4.19 min: HRMS (TOF MS ES+): *m/z* calcd for $C_{60}H_{79}N_{11}O_4$ $[M]^{2+}$: 508.81528; found: 508.8159 (1.2 ppm)

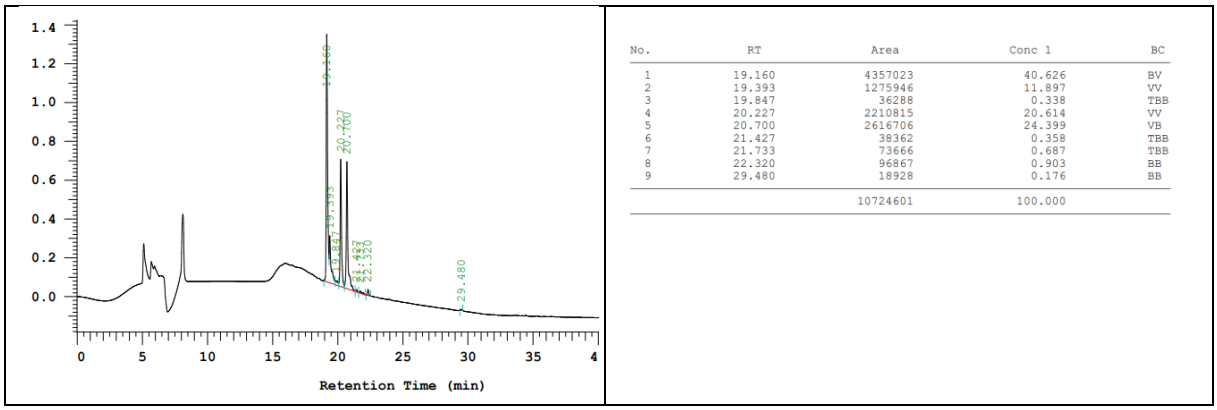

No.	RT	Area	Conc 1	BC
1	19.160	4357023	40.626	BV
2	19.393	1275946	11.897	VV
3	19.847	36288	0.338	TBB
4	20.227	2210815	20.614	VV
5	20.700	2616706	24.399	VB
6	21.427	38362	0.358	TBB
7	21.733	73666	0.687	TBB
8	22.320	96867	0.903	BB
9	29.480	18928	0.176	BB
		10724601	100.000	

Figure S159. HPLC chromatogram (220 nm) of the purified **IV.12**.

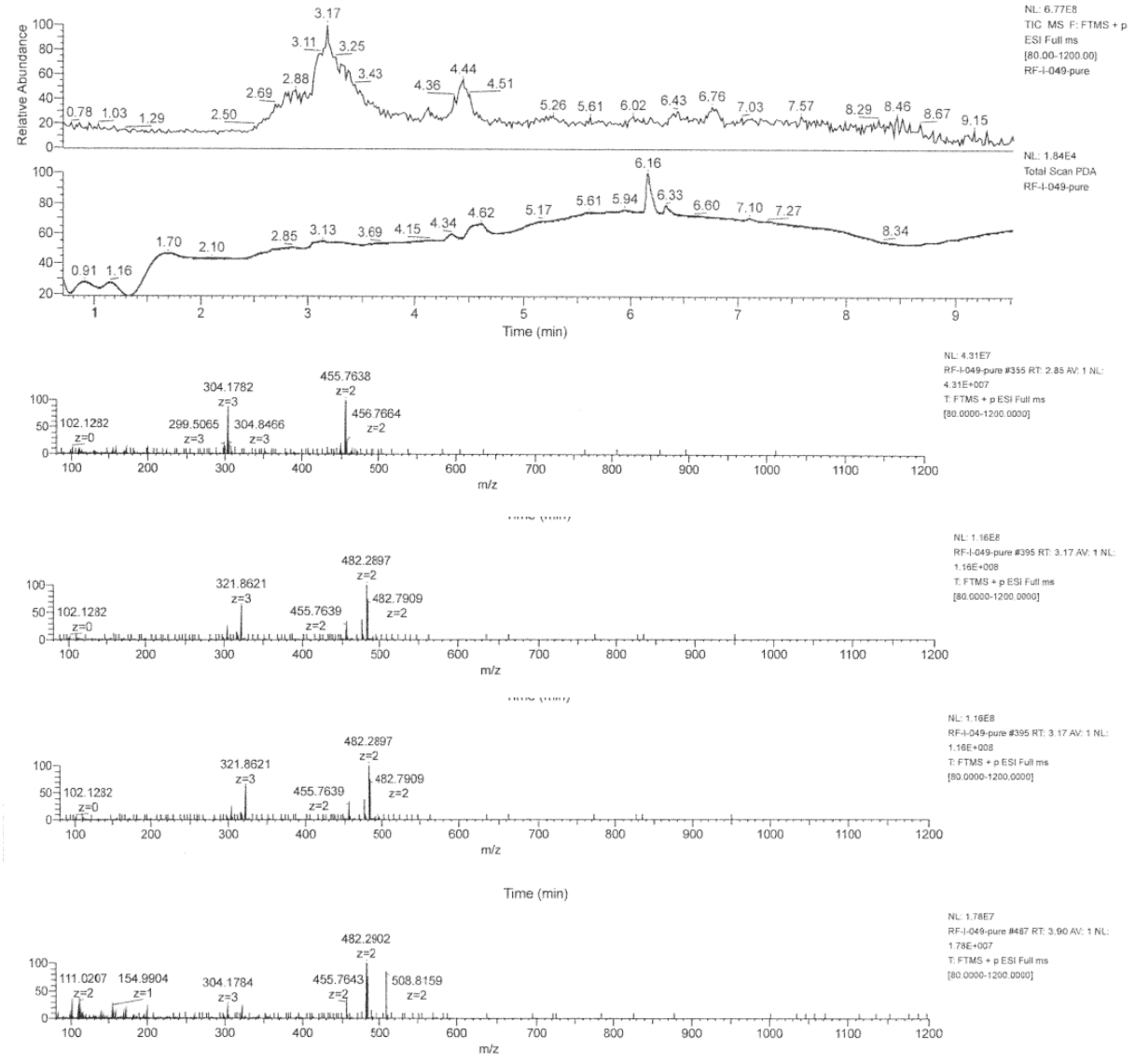

Figure S160. LCMS spectra of purified **IV.12**.

2.6. *IV.13.*

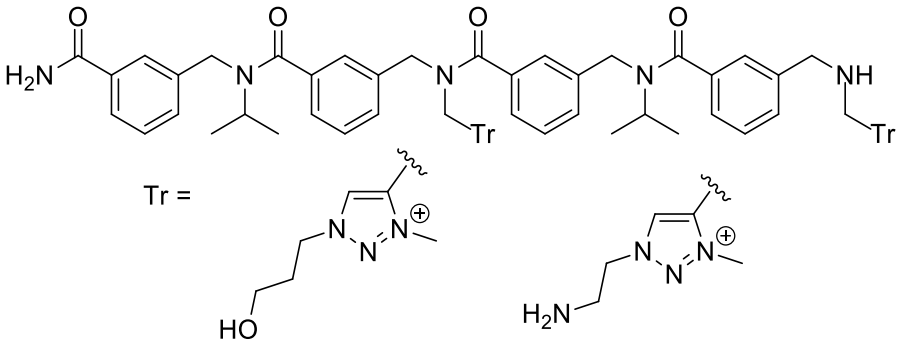

IV.13

Tetramer **IV.13** was synthesised according to the general procedure using 150 mg of Rink Amide resin (loading 0.62 mmol/g).

m_{crude}= 115 mg, 133% crude yield

m_{pure}= 46 mg (56% isolated yield, purity 97 %).

LCMS pic at 2.45 min: HRMS (TOF MS ES+): *m/z* calcd for $C_{50}H_{65}N_{13}O_4$ $[M]^{2+}$: 455.76358; found: 455.764 (0.88 ppm).

LCMS pic at 2.66 min: HRMS (TOF MS ES+): *m/z* calcd for $C_{51}H_{66}N_{12}O_5$ $[M]^{2+}$: 463.26341 found: 463.264 (1.29 ppm)

LCMS pic at 2.68 min: HRMS (TOF MS ES+): *m/z* calcd for $C_{52}H_{67}N_{11}O_6$ $[M]^{2+}$: 470.76234 found: 470.7639 (1.3 ppm)

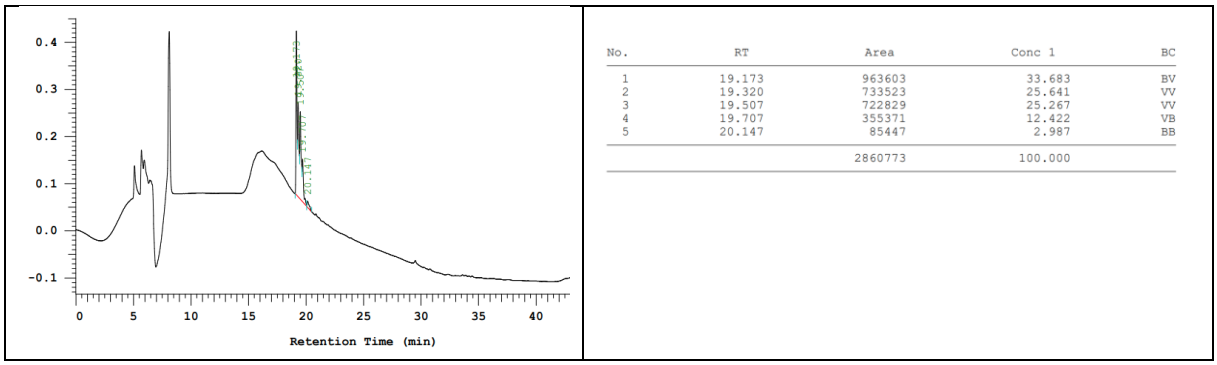

Figure S161. HPLC chromatogram (220 nm) of the purified **IV.13**.

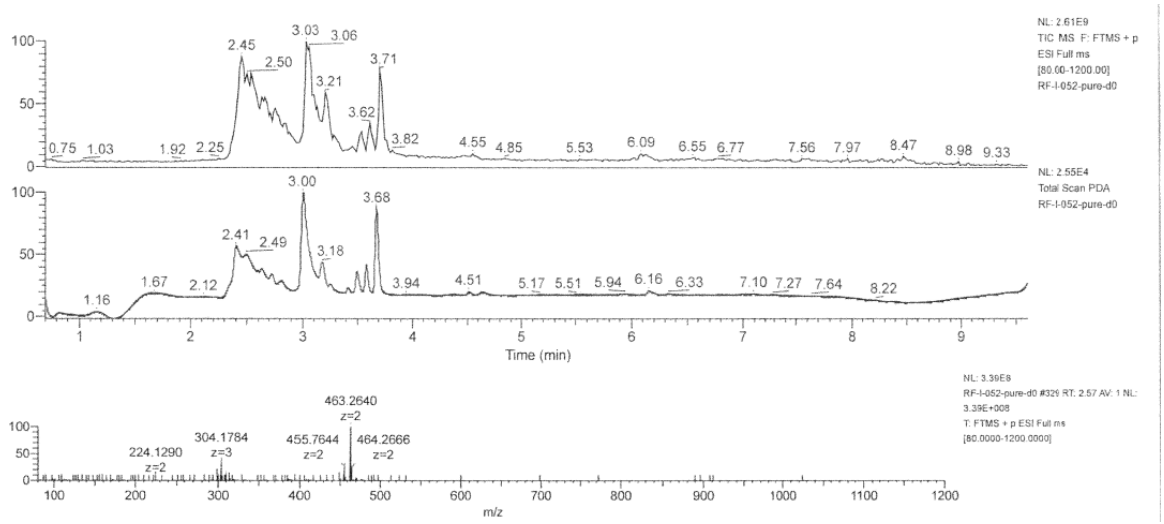

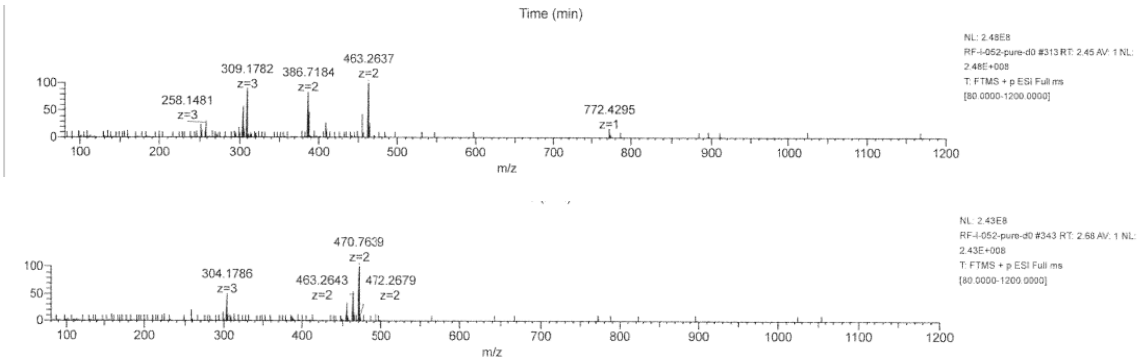

Figure S162. LCMS spectra of purified **IV.13**.

3.Series C

3.1. IV.15.

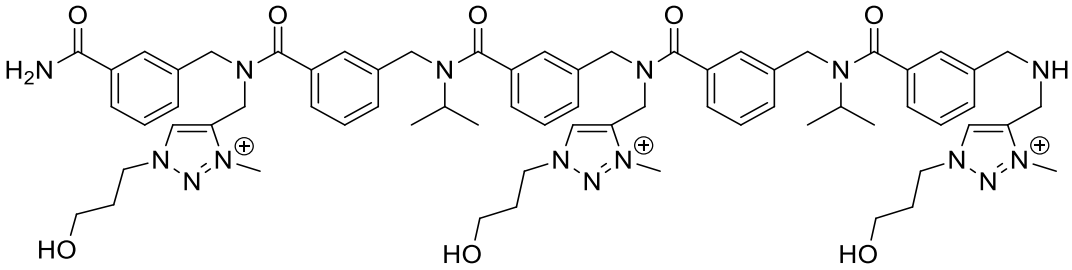

Pentamer **IV.15** was synthesised according to the standard procedure using 150 mg of Rink Amide resin (loading 0.62 mmol/g).

m_{crude}= 136 mg, 121% crude yield

m_{pure}= 62 mg (55% isolated yield, HPLC purity 90%),

HRMS (TOF MS ES+): *m/z* calcd for $C_{67}H_{86}N_{15}O_8$ $[M]^{3+}$: 409.55891; found: 409.5592 (0.71 ppm).

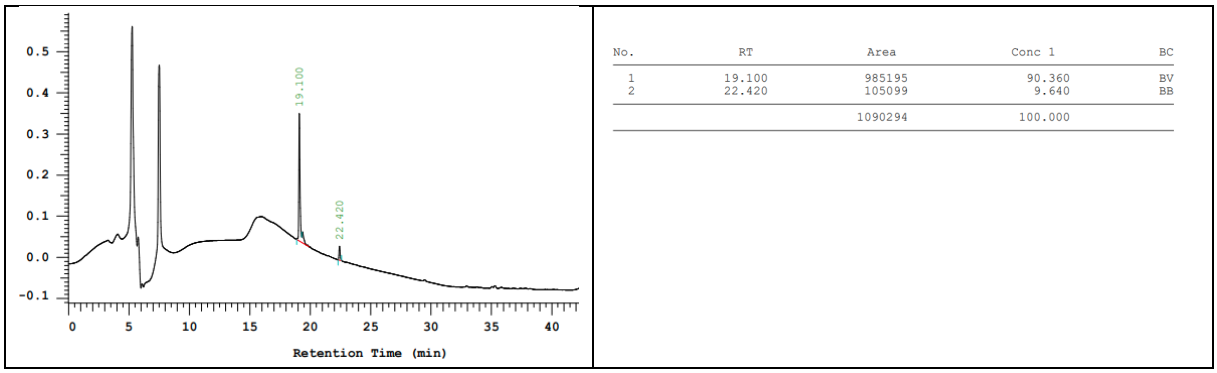

Figure S163. HPLC chromatogram (220 nm) of the purified **IV.15**.

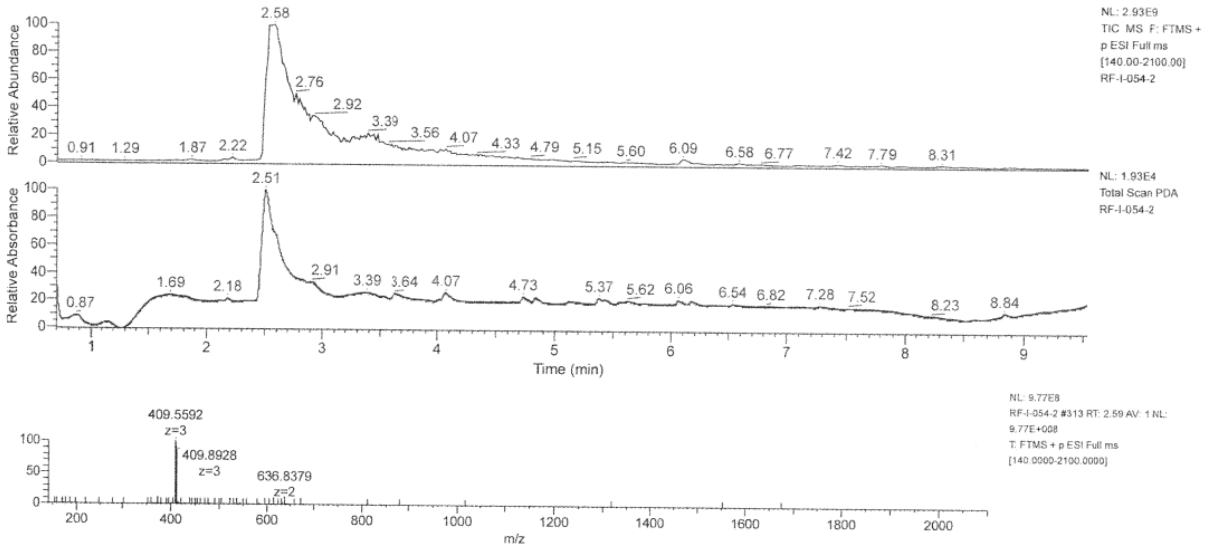

Figure 164. LCMS spectrum of the purified **IV.15**.

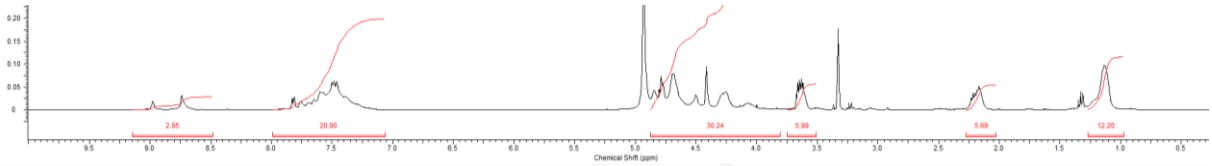

Figure S165. ^{1}H-NMR spectra in MeOD of **IV.15**.

3.2. *IV.16.*

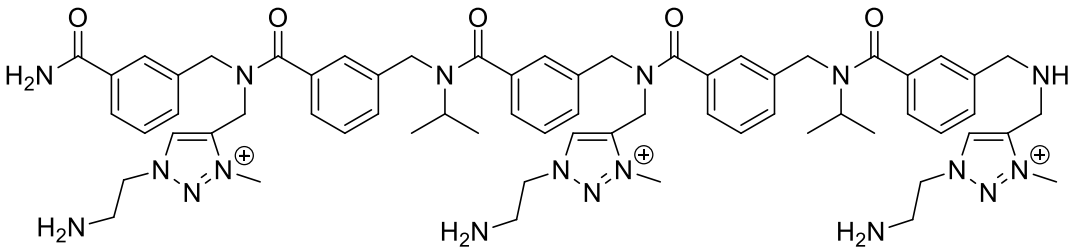

Pentamer **IV.16** was synthesised according to the standard procedure using 150 mg of Rink Amide resin (loading 0.62 mmol/g).

m_{crude}= 129 mg, 117% crude yield

m_{pure}= 101 mg (92% isolated yield, HPLC purity 99%).

HRMS (TOF MS ES+): *m/z* calcd for $C_{64}H_{83}N_{18}O_5$ $[M]^{3+}$: 394.55925; found: 394.5600 (1.83ppm).

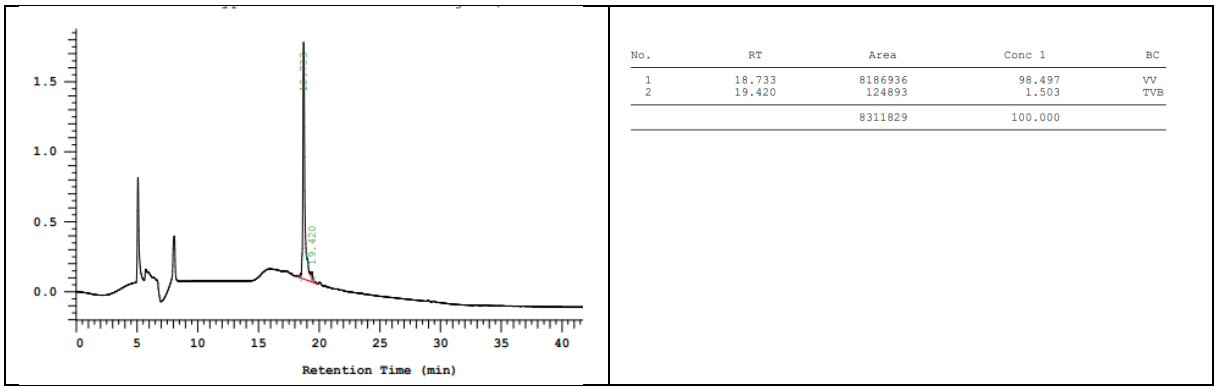

Figure S166. HPLC chromatogram (220 nm) of the purified **IV.16**.

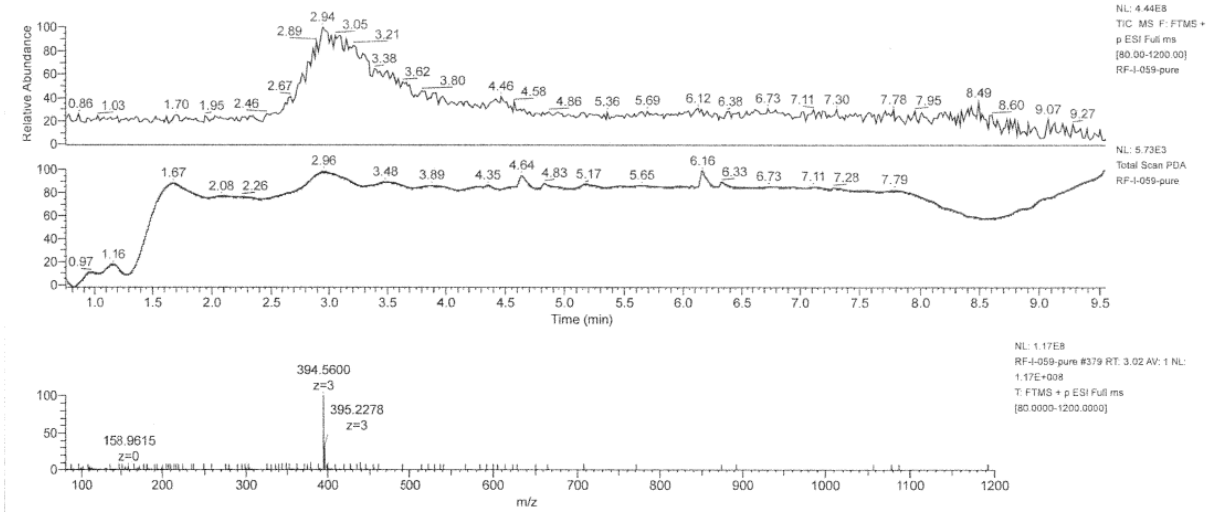

Figure S167. LCMS spectrum of purified **IV.16**.

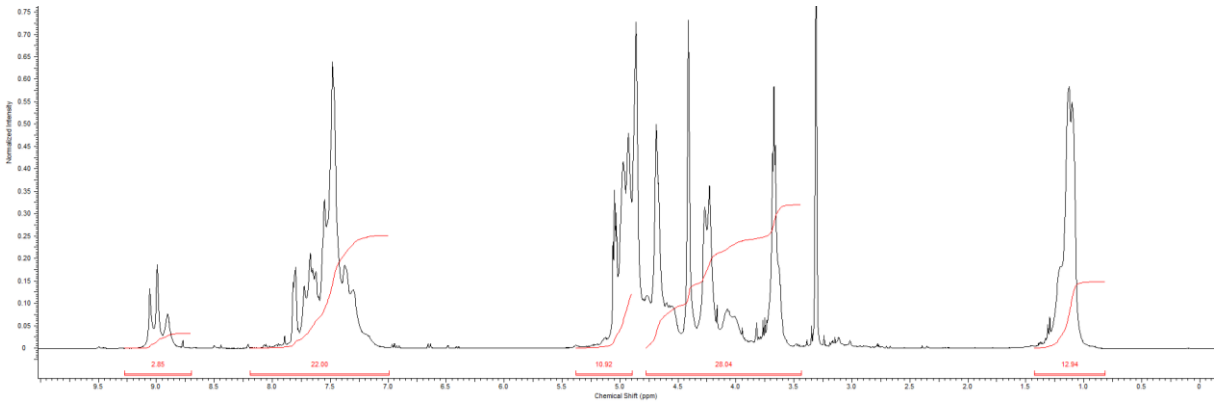

Figure S168 ^{1}H-NMR spectra in MeOD of **IV.16**.

3.3. IV.17.

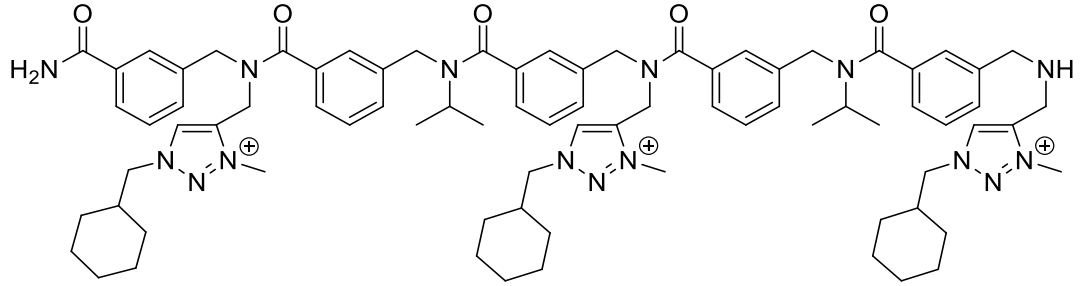

Pentamer **IV.17** was synthesised according to the standard procedure 150 mg of Rink Amide resin (loading 0.62 mmol/g).

m_{crude}= 167 mg, 133.8% crude yield

m_{pure}= 120 mg (96% isolated yield, HPLC purity 95%).

HRMS (TOF MS ES+): *m/z* calcd for $C_{79}H_{104}N_{51}O_5$ $[M]^{3+}$: 447.61095; found: 447.6116 (1.4ppm).

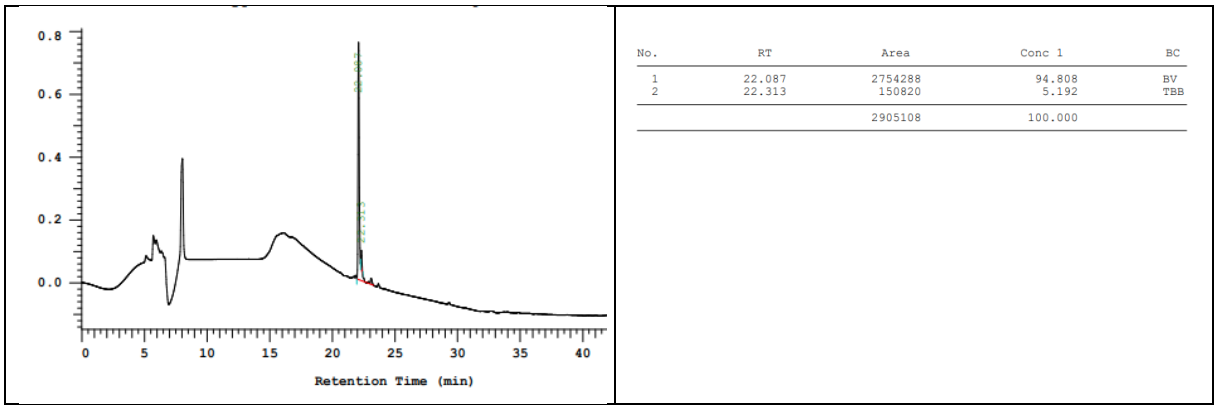

Figure S169. HPLC chromatogram (220 nm) of the purified **IV.17**.

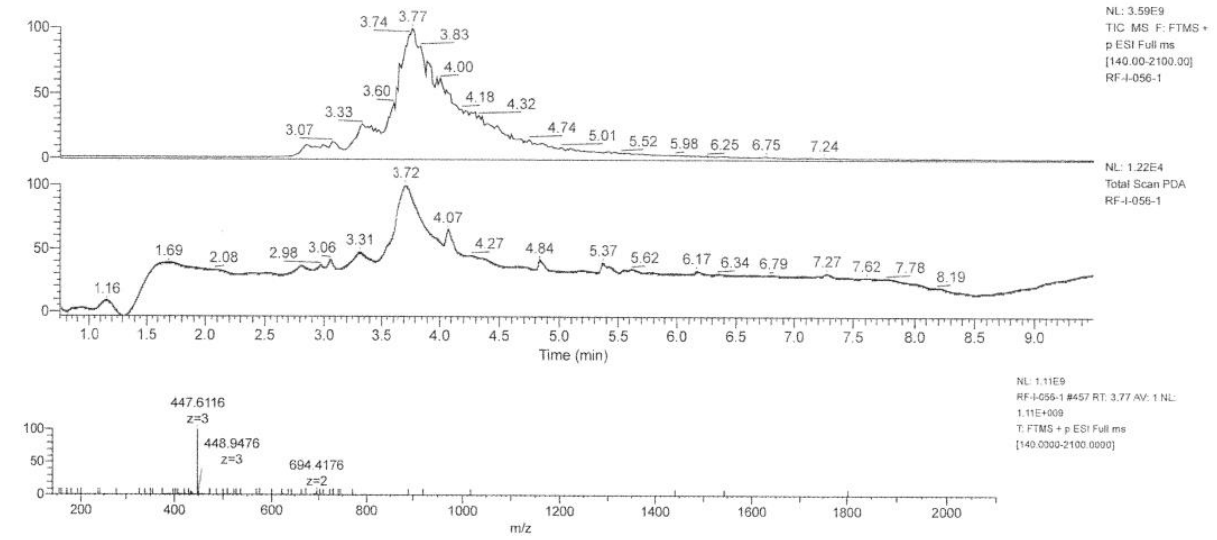

Figure S170. LCMS spectrum of purified **IV.17**.

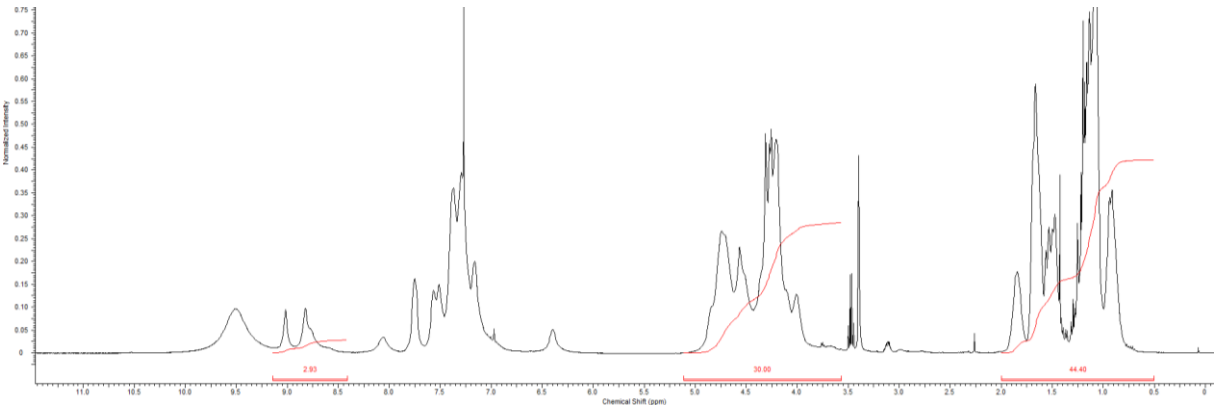

Figure S171. ^{1}H-NMR spectrum in $CDCl_3$ of **IV.17**.

3.4. *IV.18.*

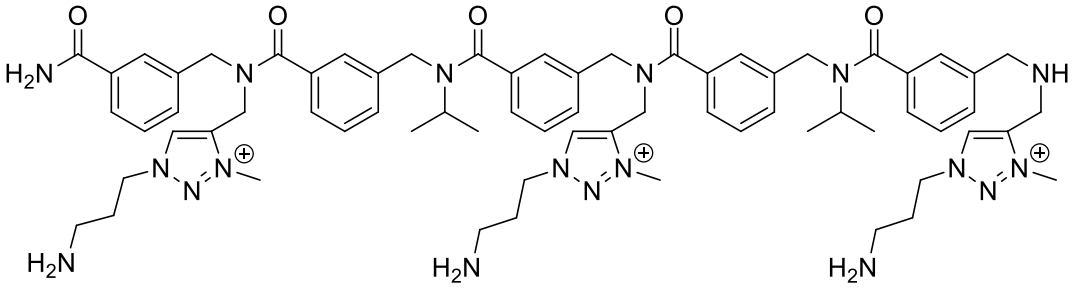

Pentamer **IV.18** was synthesised according to the standard procedue using 150 mg of Rink Amide resin (loading 0.62 mmol/g).

m_{crude}= 150 mg, 132% crude yield

m_{pure}= 105 mg (93% isolated yield, HPLC purity 99%) .

LCMS pic at 2.62 min: HRMS (TOF MS ES+): *m/z* calcd for $C_{67}H_{89}N_{18}O_5$ $[M]^{3+}$: 408.5749; found: 408.5753 (1.03 ppm).

LCMS pic at 2.7 min: HRMS (TOF MS ES+): *m/z* calcd for $C_{67}H_{90}N_{18}O_5$ $[M]^{3+}$: 306.68299; found: 306.683 (0.17 ppm).

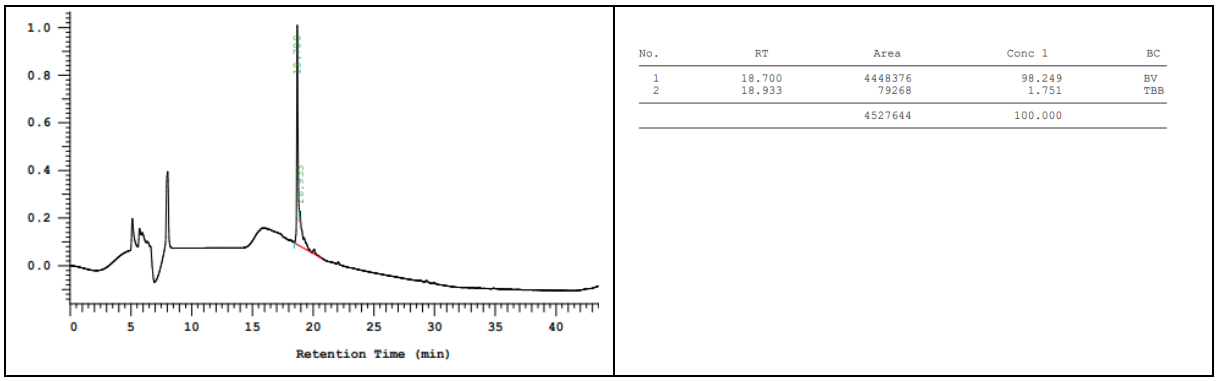

Figure S172. HPLC chromatogram (220 nm) of the purified **IV.18**.

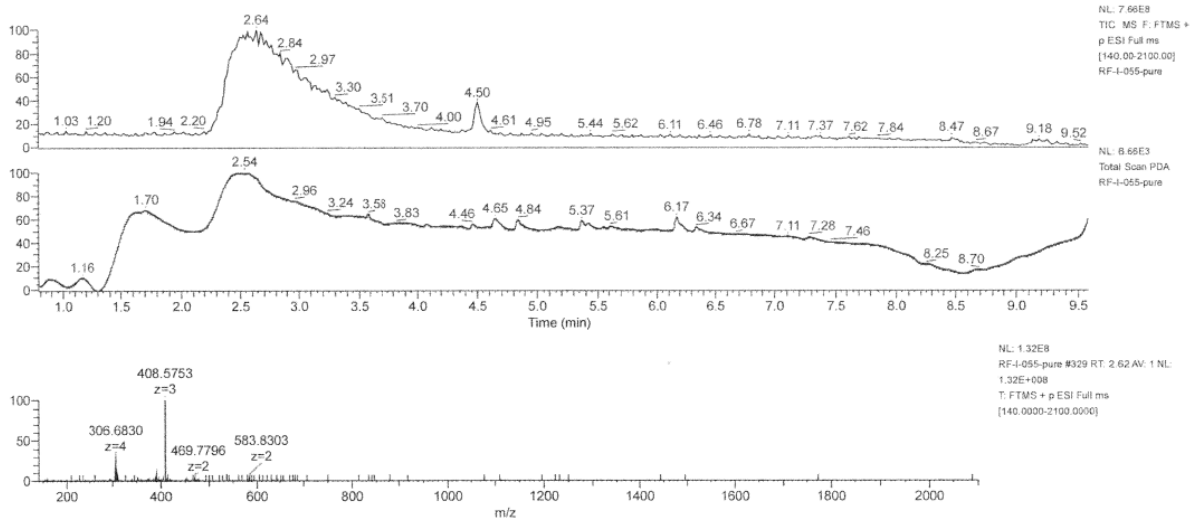

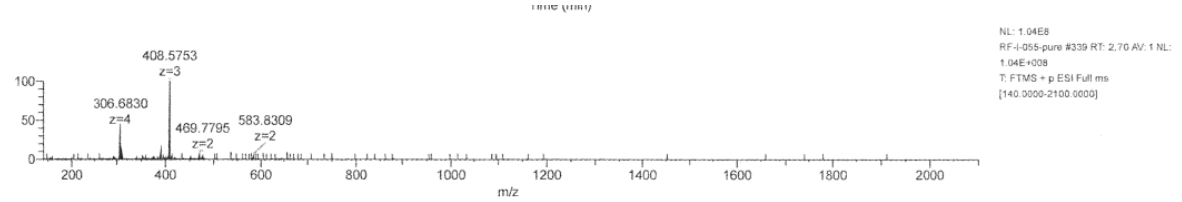

Figure S173. LCMS spectrum of purified **IV.18**.

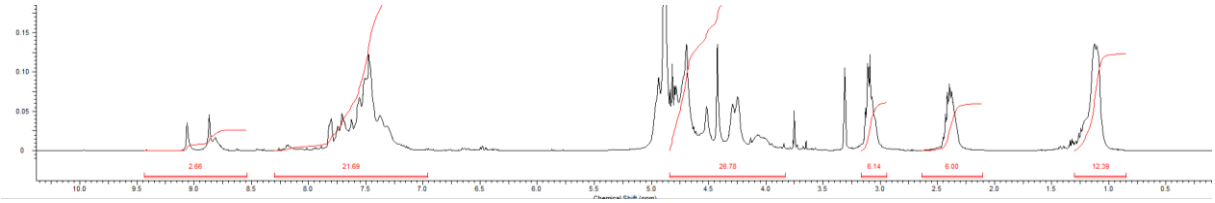

Figure S174. ^{1}H-NMR spectrum in MeOD of **IV.18**.

3.5. *IV.19*.

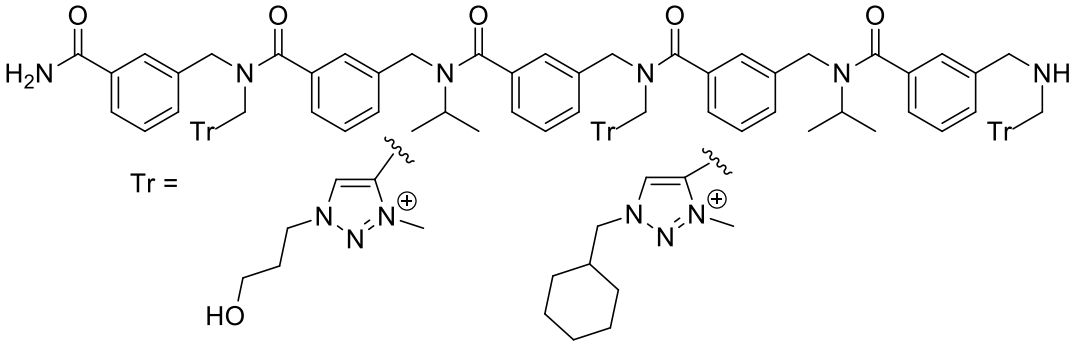

IV.19

Tr =

Pentamer **IV.19** was synthesised according to the standard procedure using 150 mg of Rink Amide resin (loading 0.62 mmol/g).

m_{crude}= 165 mg, 132% crude yield

m_{pure}= 101 mg (96% isolated yield, HPLC purity 95%) .

LCMS pic at 2.72 min: HRMS (TOF MS ES+): *m/z* calcd for $C_{67}H_{86}N_{15}O_8$ $[M]^{3+}$: 409.55891; found: 409.5592 (0.79 ppm).

LCMS pic at 3.16 min: HRMS (TOF MS ES+): *m/z* calcd for $C_{71}H_{92}N_{15}O_7$ $[M]^{3+}$: 422.24292; found: 422.2436 (1.51 ppm).

LCMS pic at 3.69 min: HRMS (TOF MS ES+): *m/z* calcd for $C_{75}H_{98}N_{15}O_5$ $[M]^{3+}$: 434.92694; found: 434.9272 (0.64 ppm).

LCMS pic at 4.5 min: HRMS (TOF MS ES+): *m/z* calcd for $C_{79}H_{104}N_{15}O_5$ $[M]^{3+}$: 447.61095; found: 447.6109 (-0.17 ppm).

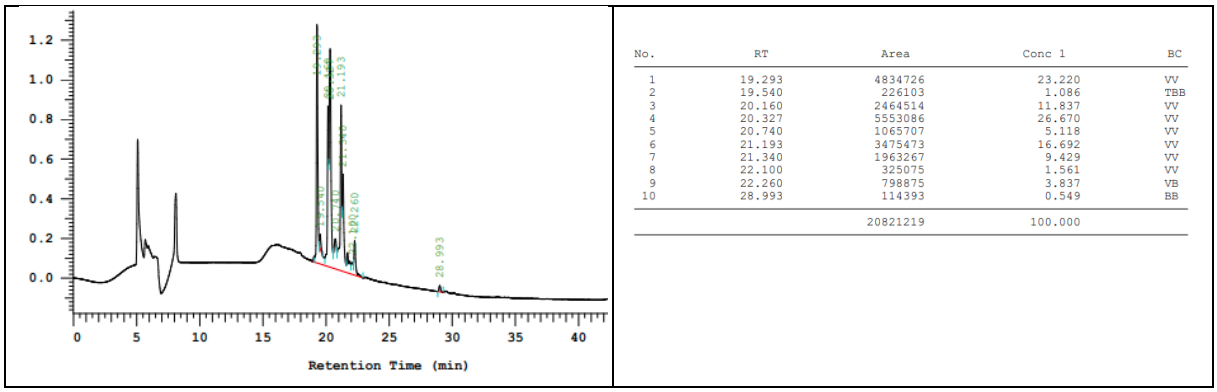

No.	RT	Area	Conc 1	BC
1	19.293	4834726	23.220	VV
2	19.540	226103	1.086	TBB
3	20.160	2464514	11.837	VV
4	20.327	5553086	26.670	VV
5	20.740	1065707	5.118	VV
6	21.193	3475473	16.692	VV
7	21.340	1963267	9.429	VV
8	22.100	325075	1.561	VV
9	22.260	798875	3.837	VB
10	28.993	114393	0.549	BB
		20821219	100.000	

Figure S175. HPLC chromatogram of the purified **IV.19**.

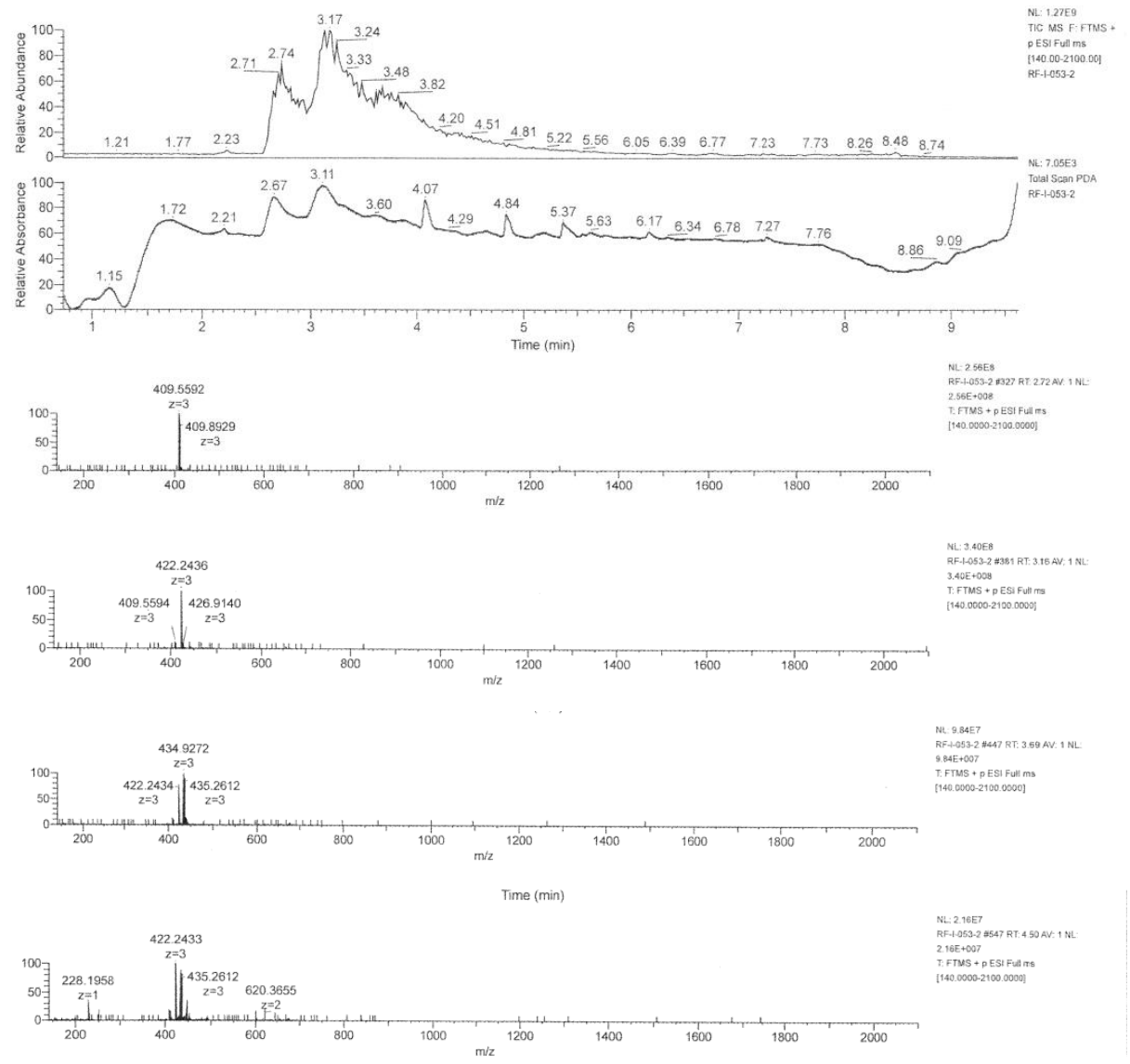

Figure S176. LCMS spectra of purified **IV.19**.

3.6. *IV.20.*

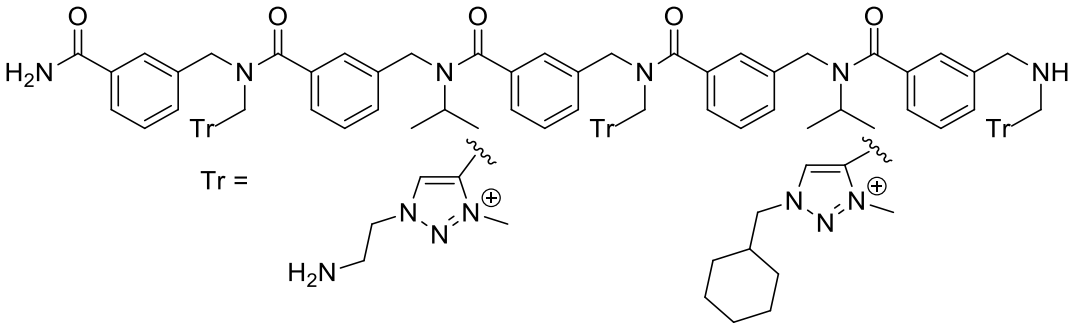

Pentamer **IV.20** was synthesised according to the standard procedure using 150 mg of Rink Amide resin (loading 0.62 mmol/g).

m_{crude}= 153 mg, 126% crude yield

m_{pure}= 101 mg (85% isolated yield, HPLC purity 99%)

LCMS pic at 3.0 min: HRMS (TOF MS ES+): *m/z* calcd for $C_{64}H_{83}N_{18}O_5$ $[M]^{3+}$: 394.55925; found: 394.5603 (2.76 ppm).

LCMS pic at 3.07 min: HRMS (TOF MS ES+): *m/z* calcd for $C_{69}H_{90}N_{17}O_5$ $[M]^{3+}$: 412.24315; found: 412.2443 (2.78 ppm).

LCMS pic at 3.57 min: HRMS (TOF MS ES+): *m/z* calcd for $C_{74}H_{97}N_{16}O_5$ $[M]^{3+}$: 429.92705; found: 429.9283 (2.81 ppm).

LCMS pic at 4.12 min: HRMS (TOF MS ES+): *m/z* calcd for $C_{79}H_{104}N_{15}O_5$ $[M]^{3+}$: 447.61095; found: 447.6120 (2.35 ppm).

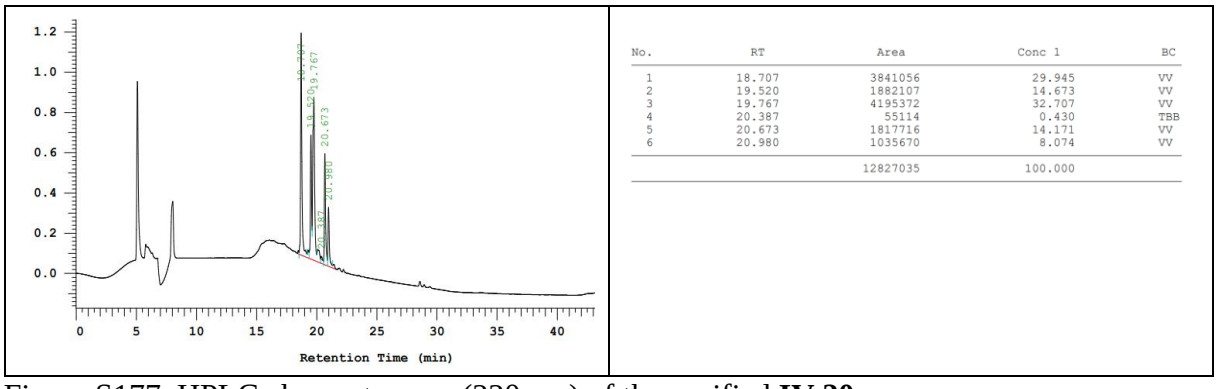

No.	RT	Area	Conc 1	BC
1	18.707	3841056	29.945	VV
2	19.520	1882107	14.673	VV
3	19.767	4195372	32.707	VV
4	20.387	55114	0.430	TBB
5	20.673	1817716	14.171	VV
6	20.980	1035670	8.074	VV
		12827035	100.000	

Figure S177. HPLC chromatogram (220 nm) of the purified **IV.20**.

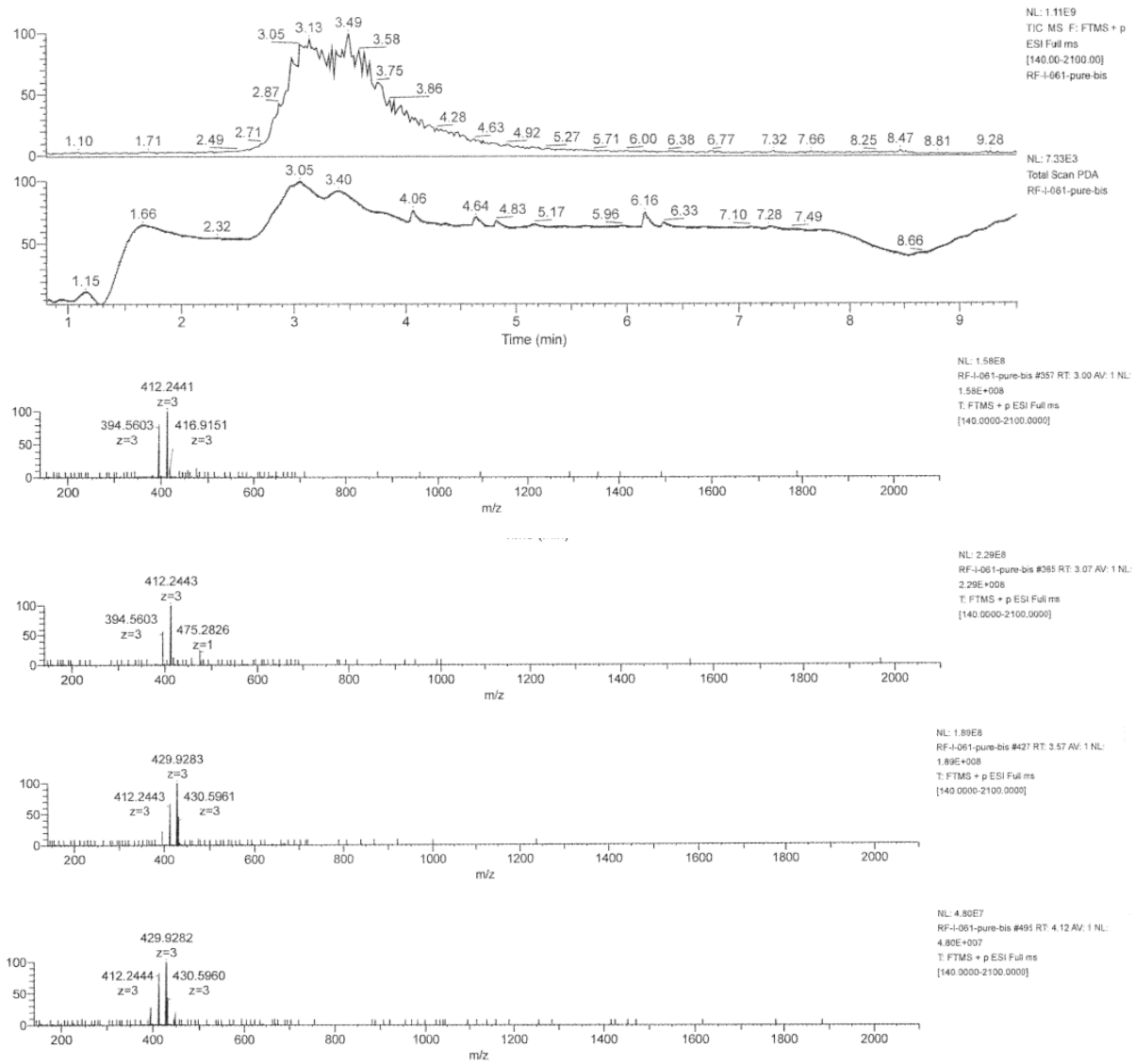

Figure S178. LCMS spectra of the purified **IV.20**.

3.7. IV.21.

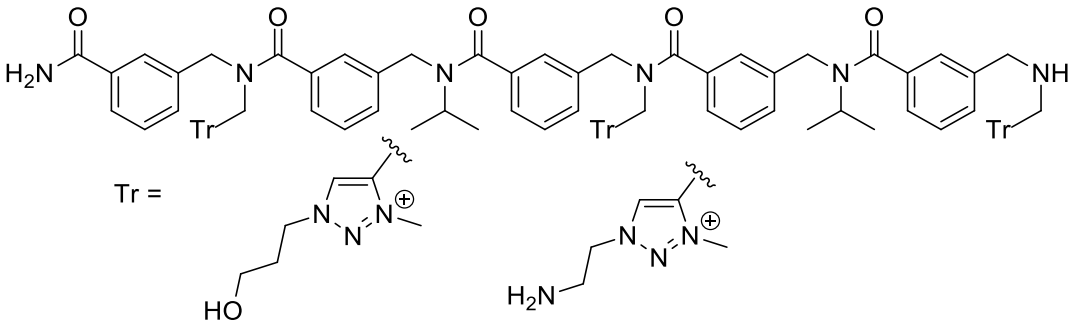

Pentamer **IV.21** was synthesised according to the standard procedure using 150 mg of Rink Amide resin (loading 0.62 mmol/g)

m_{crude}= 136 mg, 122% crude yield

m_{pure}= 69 mg (62% isolated yield, HPLC purity 99%)

LCMS pic at 2.6 min: HRMS (TOF MS ES+): *m/z* calcd for $C_{66}H_{85}N_{16}O_7$ $[M]^{3+}$: 404.55902; found: 404.56 (2.41 ppm).

LCMS pic at 2.9 min: HRMS (TOF MS ES+): *m/z* calcd for $C_{65}H_{84}N_{17}O_6$ $[M]^{3+}$: 399.55913; found: 399.5601 2.39 ppm).

LCMS pic at 3.37 min: HRMS (TOF MS ES+): *m/z* calcd for $C_{64}H_{83}N_{18}O_5$ $[M]^{3+}$: 394.55925; found: 394.5603 (2.6 ppm).

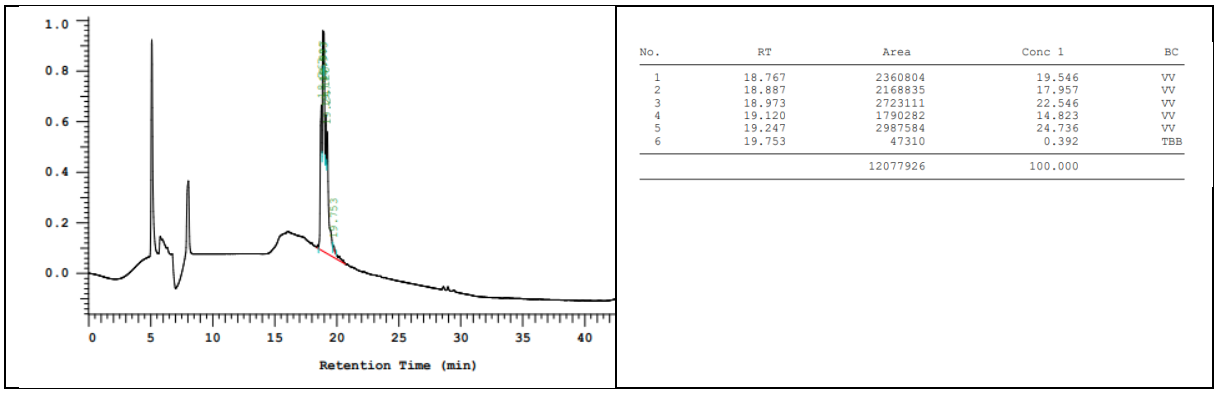

No.	RT	Area	Conc 1	BC
1	18.767	2360804	19.546	VV
2	18.887	2168835	17.957	VV
3	18.973	2723111	22.546	VV
4	19.120	1790282	14.823	VV
5	19.247	2987584	24.736	VV
6	19.753	47310	0.392	TBB
		12077926	100.000	

Figure S179. HPLC chromatogram (220 nm) of the purified **IV.21**.

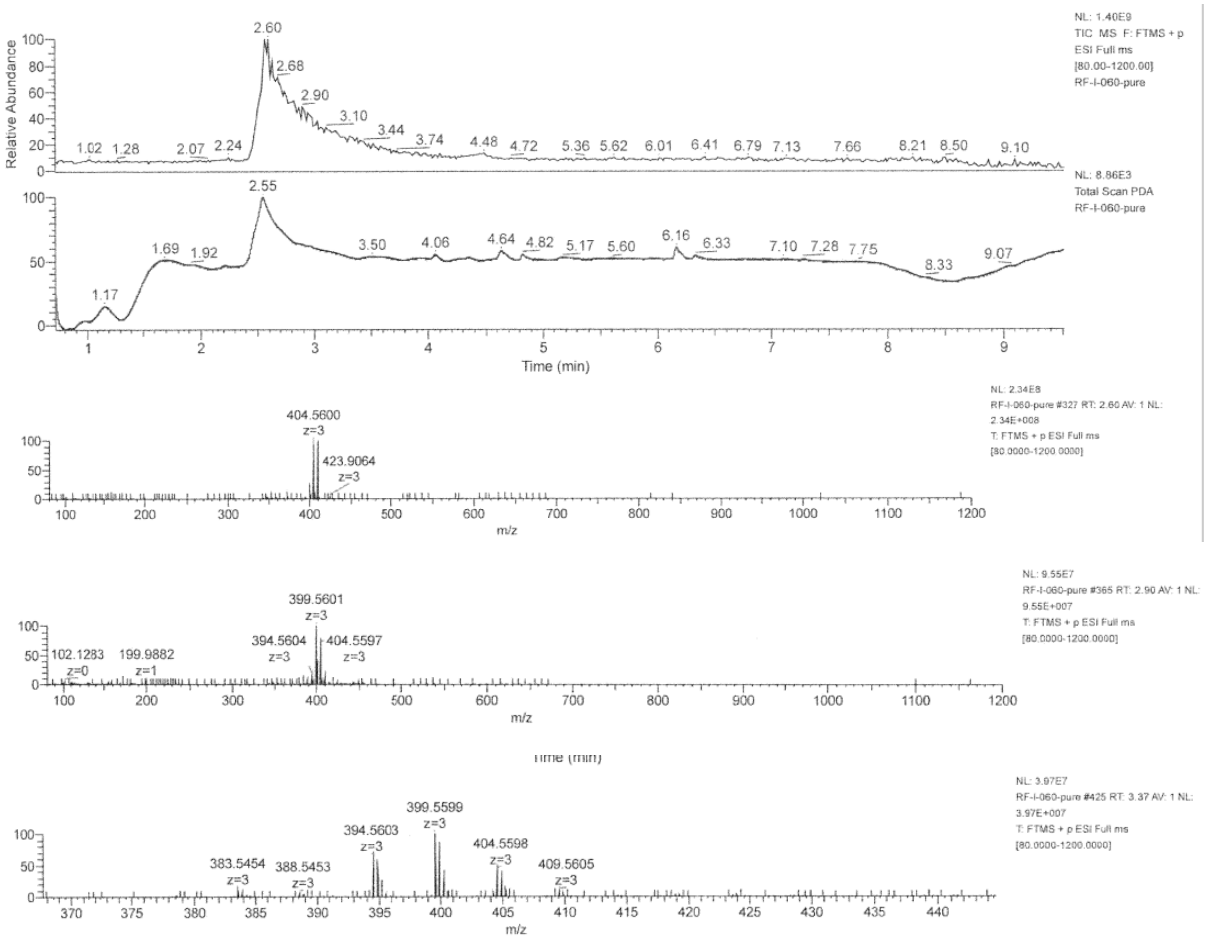

Figure S180. LCMS spectra of the purified **IV.21**.

4.Series D

4.1. IV.22.

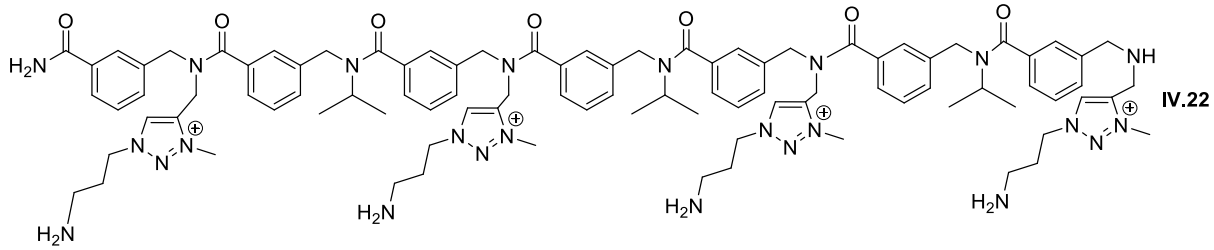

Heptamer **IV.22** was synthesised according to the standard procedure using 75 mg of Rink Amide resin (loading 0.62 mmol/g).

m_{pure}= 56.8 mg (78% isolated yield, HPLC purity 96%)

HRMS (TOF MS ES+): *m/z* calcd for $C_{93}H_{122}N_{20}O_7^{4+}$ $[M]^{4+}$: 421.74766; found: 421.7473 (-0.75 ppm).

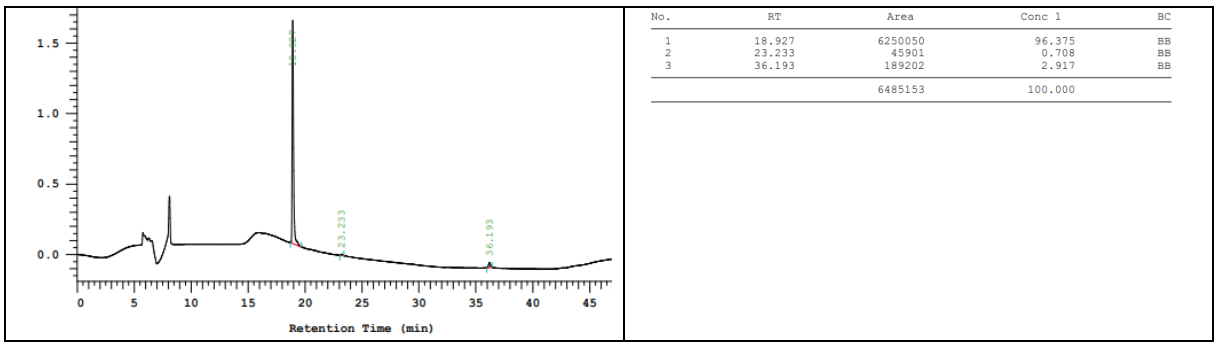

Figure S181. HPLC chromatogram (220 nm) of the purified **IV.22**.

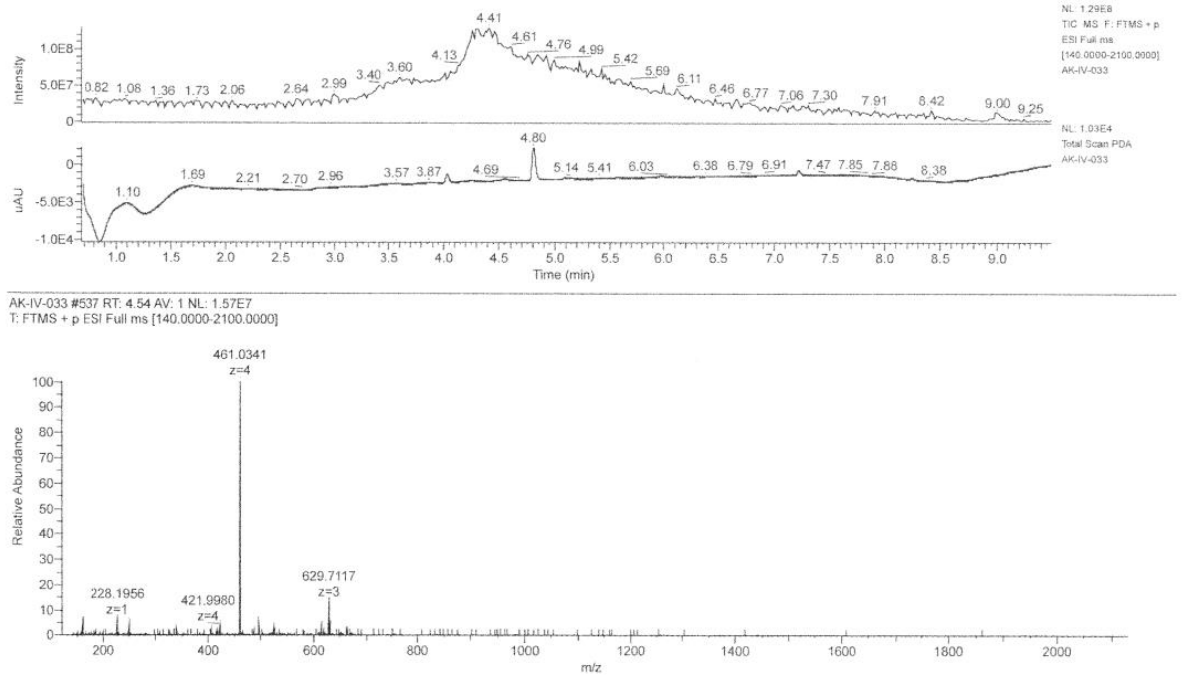

Figure S182. LCMS spectrum of the crude **IV.22**.

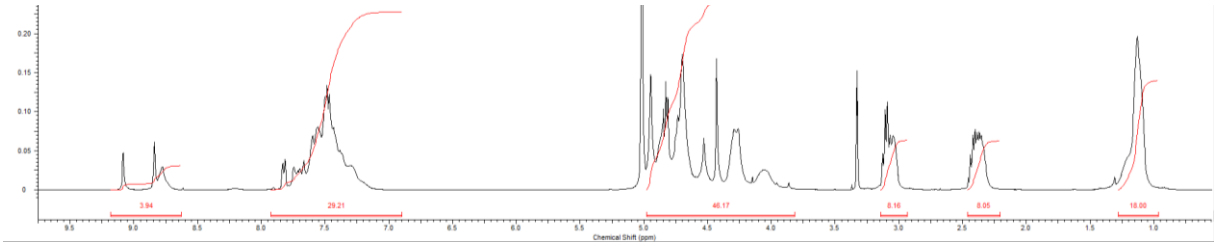

Figure S183. ^{1}H-NMR spectrum in MeOD of the pure **IV.22**.

4.2. IV.23.

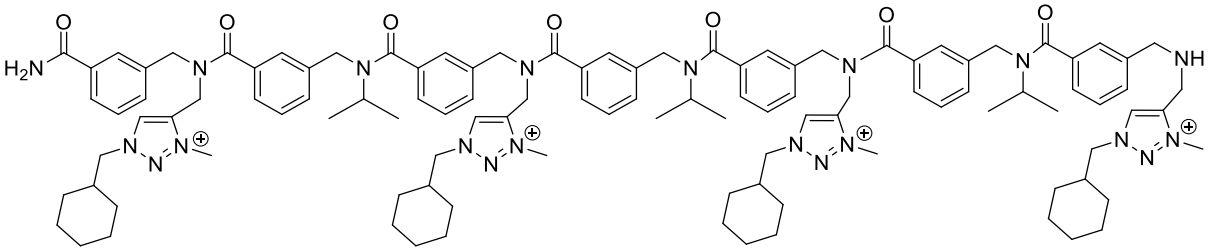

Heptamer **IV.23** was synthesised according to the standard procedure using 75 mg of Rink Amide resin (loading 0.62 mmol/g).

m_{pure}= 50 mg (87% isolated yield, HPLC purity 95%)

HRMS (TOF MS ES+): *m/z* calcd for $C_{109}H_{142}N_{20}O_7^{4+}$ $[M]^{4+}$: 460.78371; found: 460.7842 (1.08 ppm).

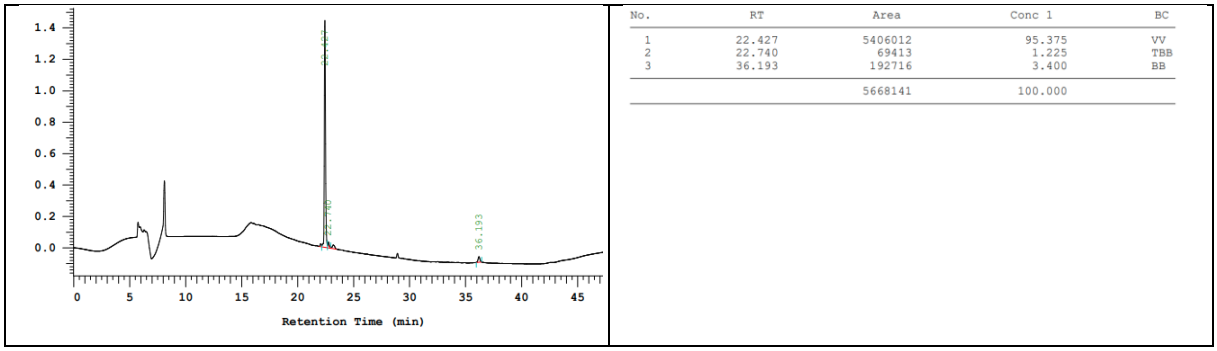

No.	RT	Area	Conc 1	BC
1	22.427	5406012	95.375	VV
2	22.740	69413	1.225	TBB
3	36.193	192716	3.400	BB
		5668141	100.000	

Figure S184. HPLC chromatogram (220 nm) of the purified **IV.23**.

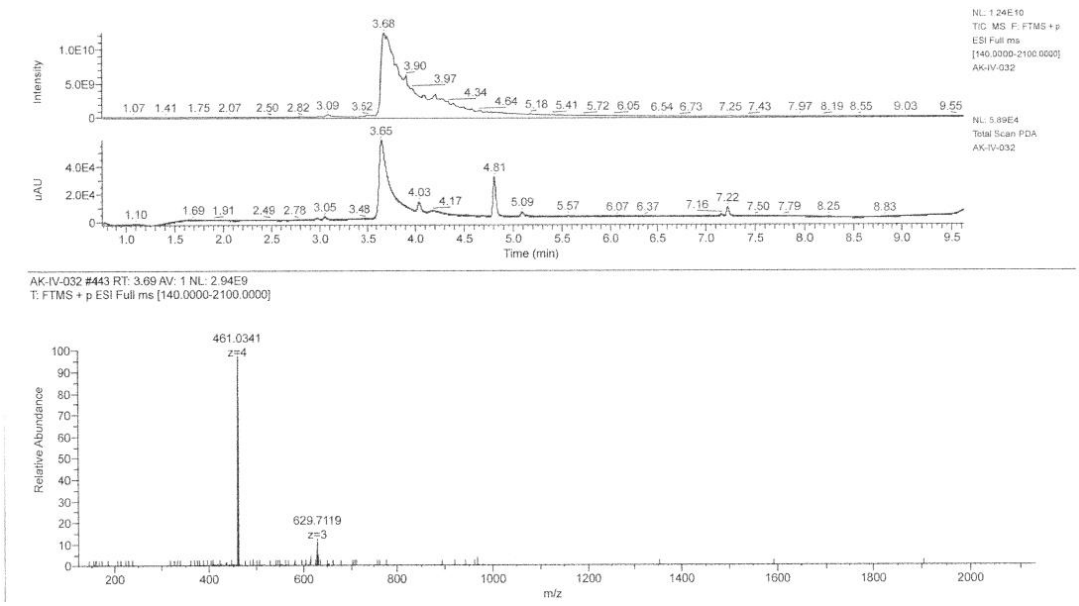

Figure S185. LCMS spectrum of the crude **IV.23**.

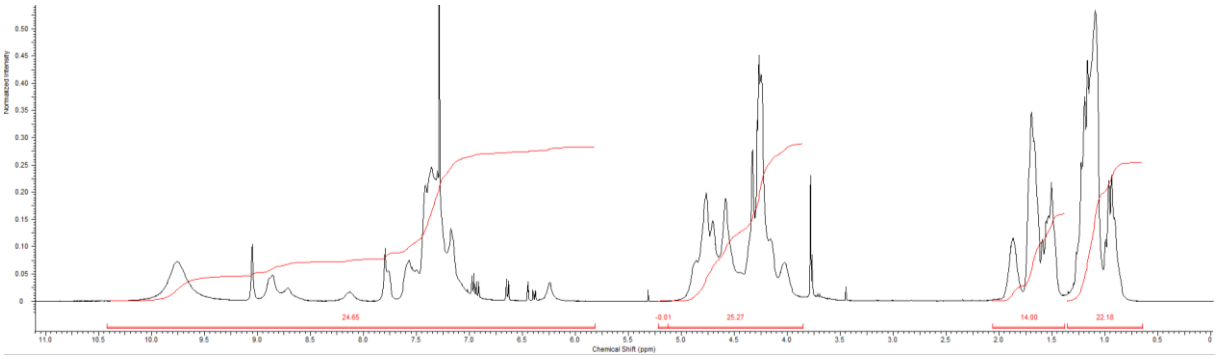

Figure S186. ^{1}H-NMR spectrum in $CDCl_3$ of the pure **IV.23**.

4.3. IV.24.

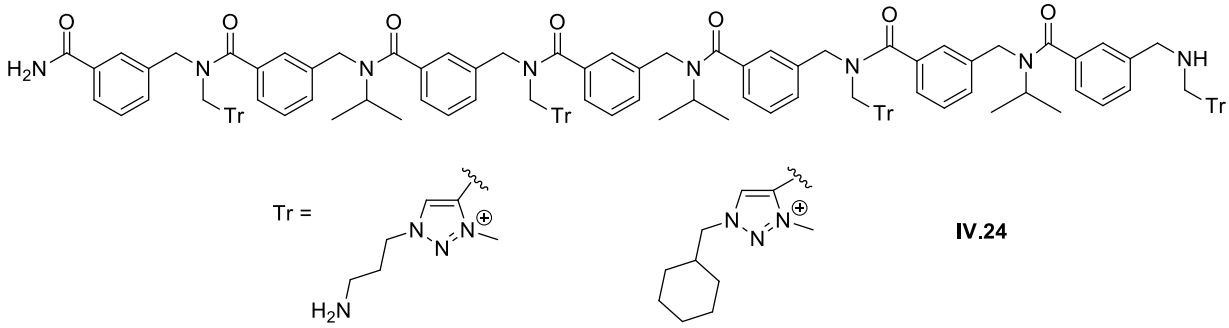

Heptamer **IV.24** was synthesised according to the standard procedure using 75 mg of Rink Amide resin (loading 0.62 mmol/g).

m_{pure}= 68 mg (91% isolated yield, HPLC purity 85%)

HRMS (TOF MS ES+): *m/z* calcd for $C_{93}H_{122}N_{24}O_7^{4+}$ $[M]^{4+}$: 421.74766; found: 421.7476 (-0.24 ppm).

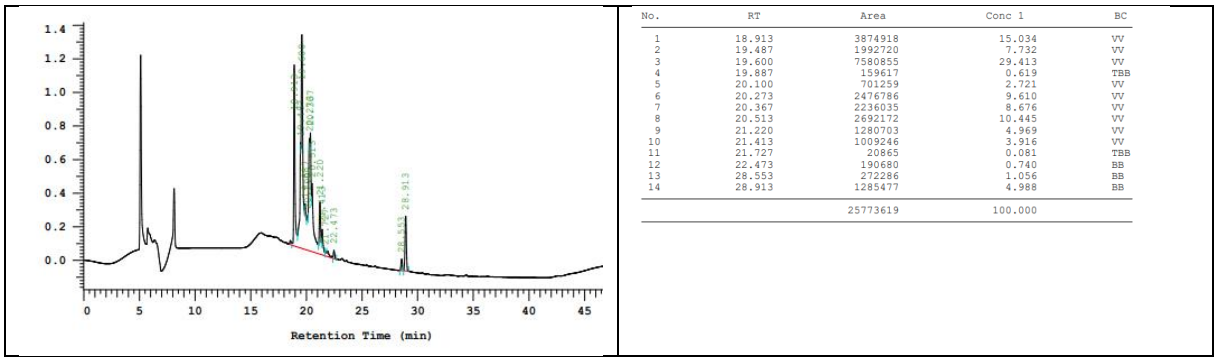

No.	RT	Area	Conc 1	BC
1	18.913	3874918	15.034	VV
2	19.487	1992720	7.732	VV
3	19.600	7580855	29.413	VV
4	19.887	159617	0.619	TBB
5	20.100	701259	2.721	VV
6	20.273	2476786	9.610	VV
7	20.367	2236035	8.676	VV
8	20.513	2692172	10.445	VV
9	21.220	1280703	4.969	VV
10	21.413	1009246	3.916	VV
11	21.727	20865	0.081	TBB
12	22.473	190680	0.740	BB
13	28.553	272286	1.056	BB
14	28.913	1285477	4.988	BB
		25773619	100.000	

Figure S187. HPLC chromatogram (220 nm) of the purified **IV.24**.

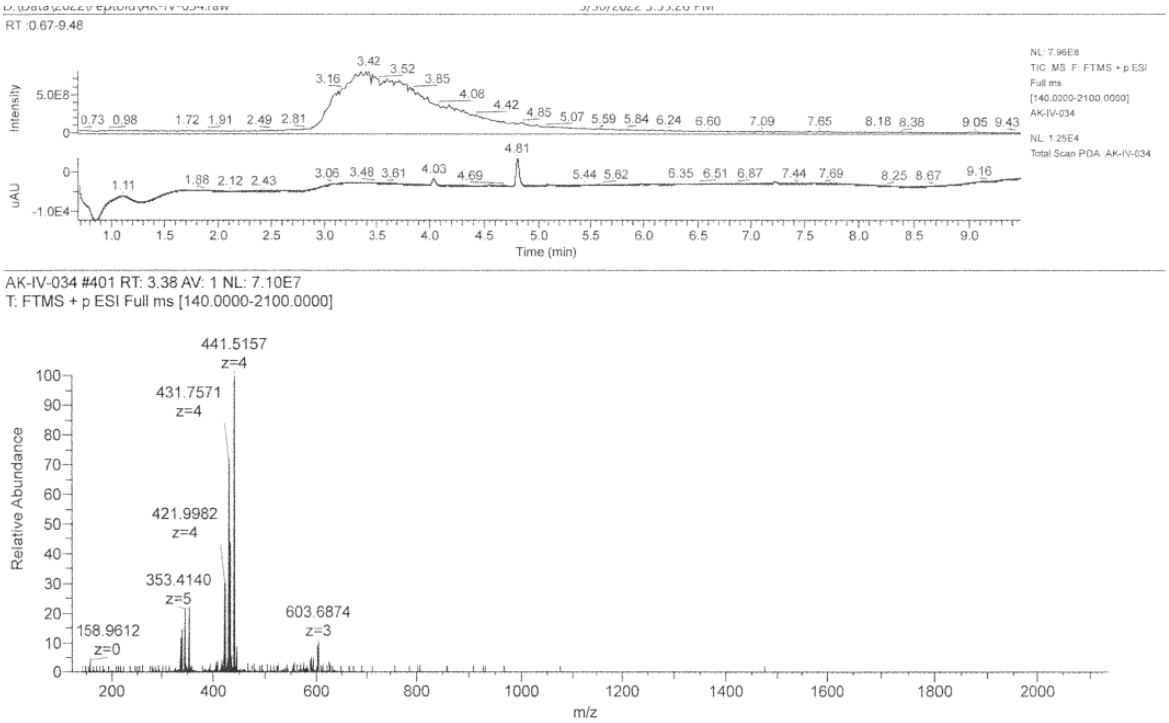

Figure S188. LCMS spectrum of the crude **IV.24**.

5.Series E

5.1. IV.26.

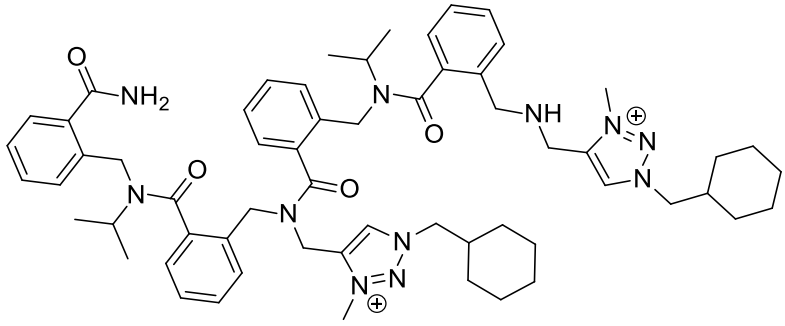

Tetramer **IV.26** was synthesised according to the standard procedure using 20 mg of Rink Amide resin (loading 0.62 mmol/g).

m_{pure}= 10 mg (80% isolated yield, HPLC purity 99%)

HRMS (TOF MS ES+): *m/z* calcd for $C_{60}H_{79}N_{11}O_4$ $[M]^{2+}$: 508.81528; found: 508.8157 (0.9 ppm).

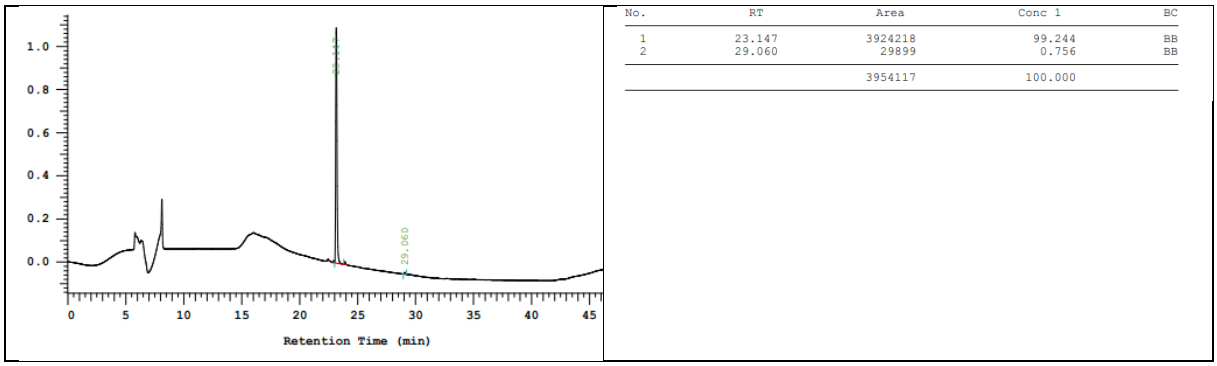

No.	RT	Area	Conc 1	BC
1	23.147	3924218	99.244	BB
2	29.060	29899	0.756	BB
		3954117	100.000	

Figure S189. HPLC chromatogram of the purified **IV.26**.

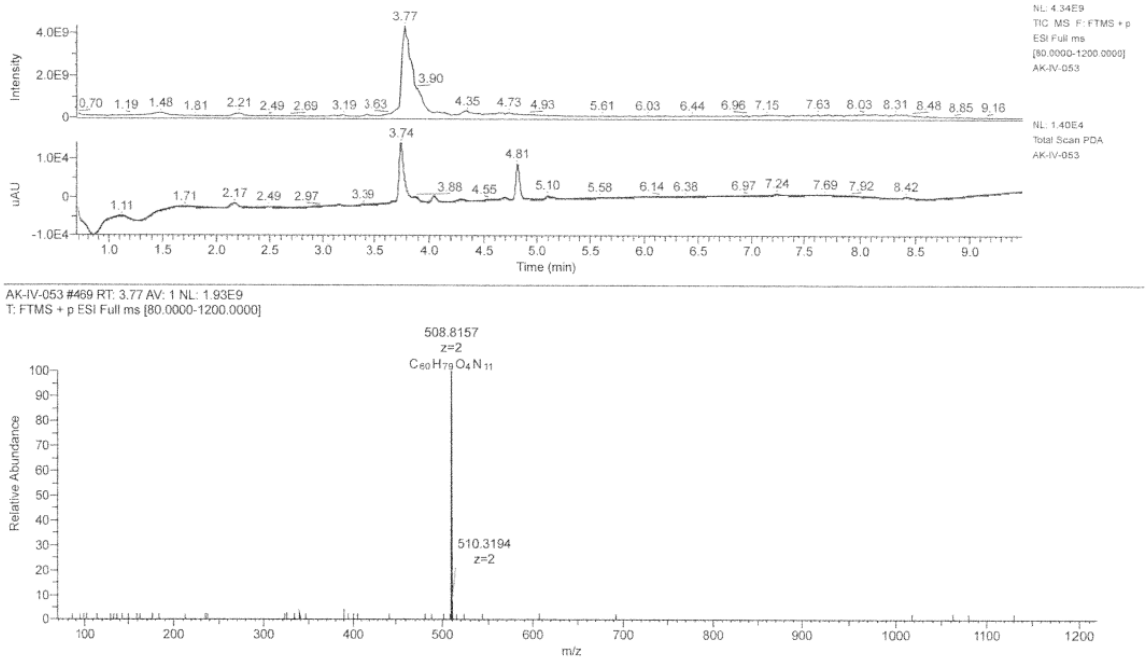

Figure S190. LCMS spectrum of the crude **IV.26**.

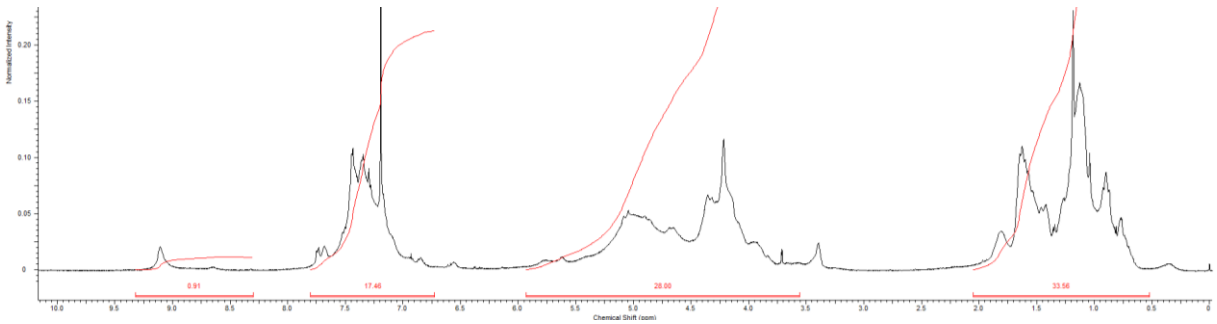

Figure S191. ^{1}H-NMR in $CDCl_3$of the pure **IV.26**.

5.2. *IV.25.*

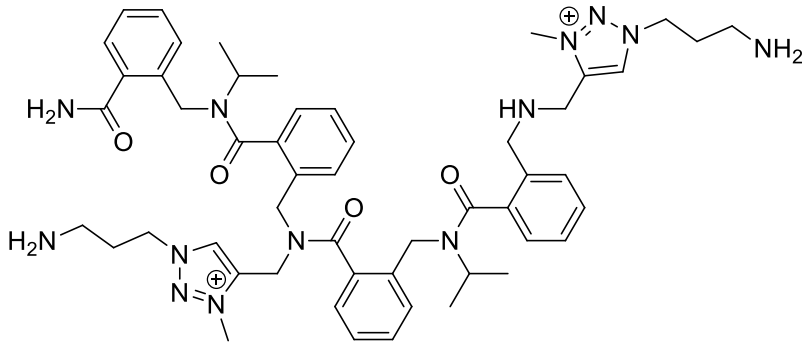

Tetramer **IV.25** was synthesised according to the standard procedure using 20 mg of Rink Amide resin (loading 0.62 mmol/g).

m_{pure}= 10 mg (86% isolated yield, HPLC purity 98%)

HRMS (TOF MS ES+): *m/z* calcd for $C_{52}H_{69}N_{13}O_4^{2+}[M]^{2+}$: 469.77923; found: 469.7791 (-0.17 ppm).

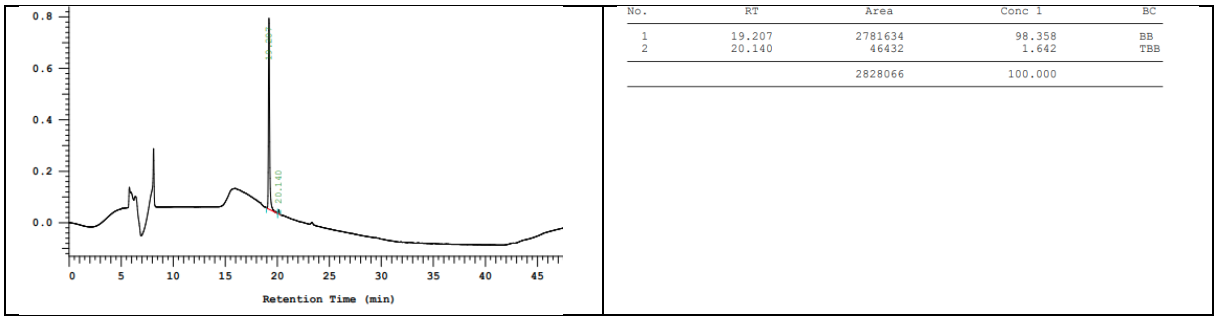

Figure S192. HPLC chromatogram (220 nm) of the purified **IV.25**.

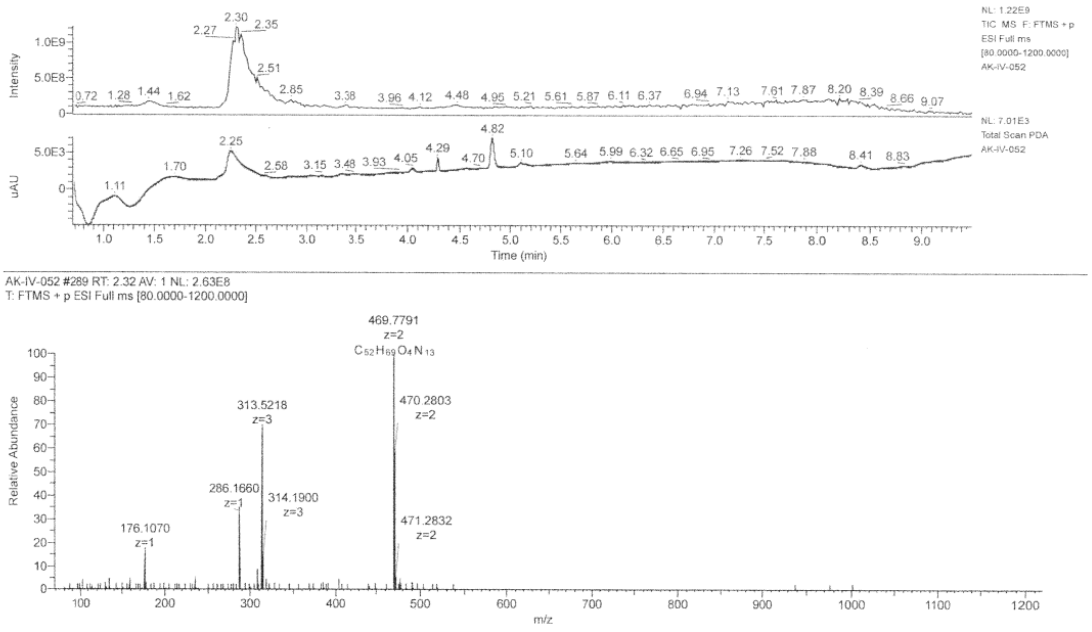

Figure S193. LCMS spectrum of the crude **IV.25**.

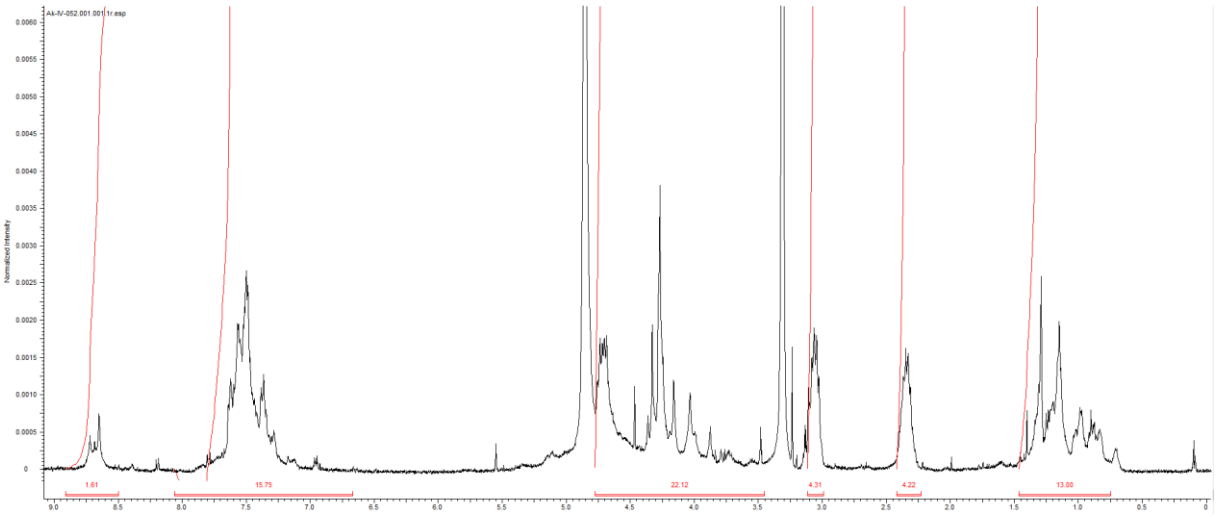

Figure S194. ^{1}H-NMR in MeOH of the pure **IV.25**.

6.Series F

6.1. IV.27.

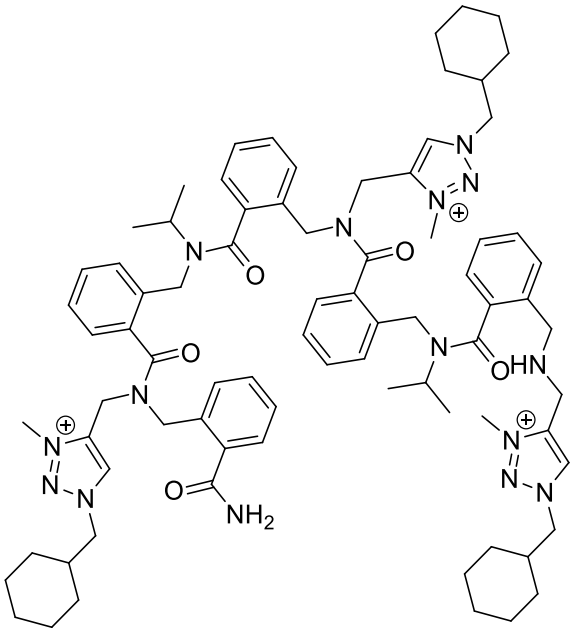

Pentamer **IV.27** was synthesised according to the standard procedure using 75 mg of Rink Amide resin (loading 0.62 mmol/g).

m_{pure}= 51 mg (82% isolated yield, HPLC purity 95%)

HRMS (TOF MS ES+): *m/z* calcd for $C_{79}H_{104}N_{15}O_5$ $[M]^{3+}$: 447.61095; found: 447.6108 (-0.38 ppm).

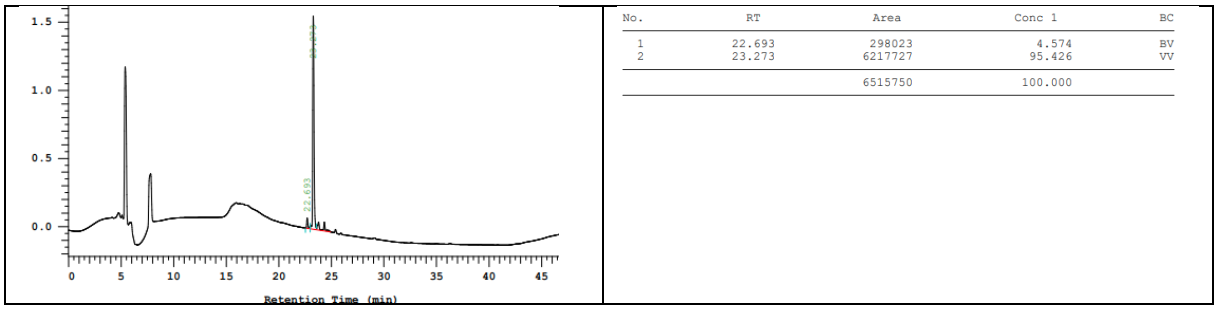

No.	RT	Area	Conc 1	BC
1	22.693	298023	4.574	BV
2	23.273	6217727	95.426	VV
		6515750	100.000	

Figure S195. HPLC chromatogram (220 nm) of the purified **IV.27**.

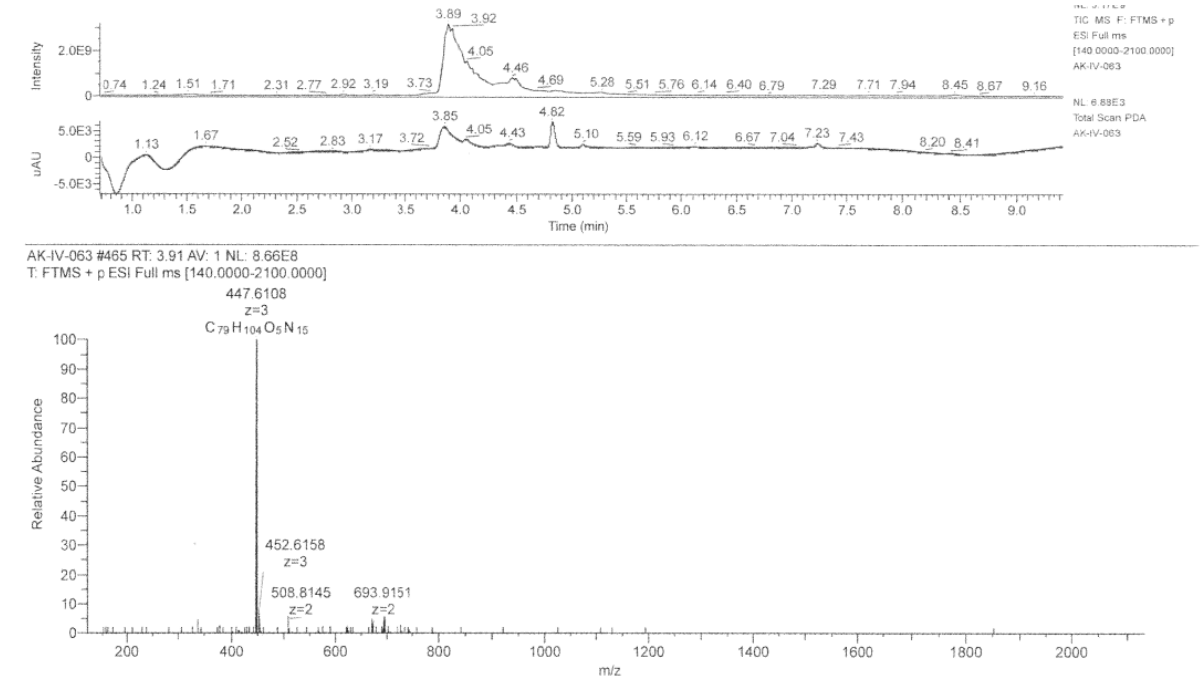

Figure S196. LCMS spectrum of the crude **IV.27**.

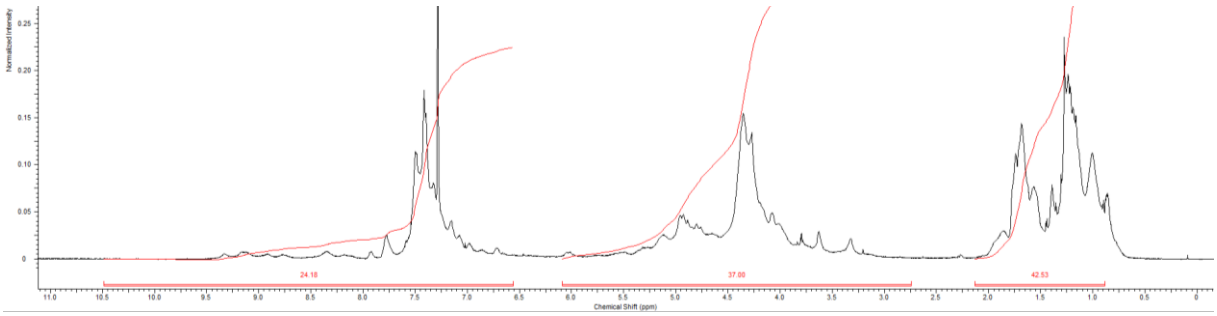

Figure S197. ^{1}H-NMR spectrum in $CDCl_3$ of **IV.27**.

6.2. *IV.28.*

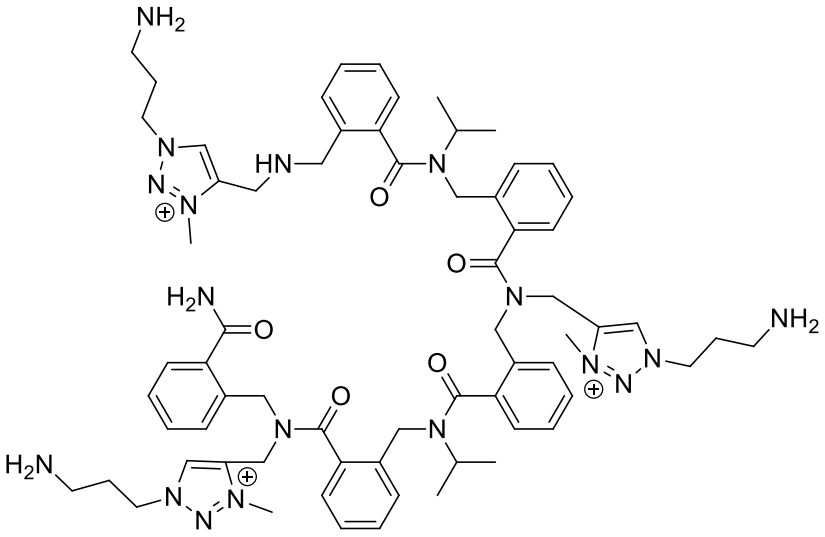

Pentamer **IV.28** was synthesised according to the standard procedure using 75 mg of Rink Amide resin (loading 0.62 mmol/g).

m_{pure}= 49 mg (86% isolated yield, HPLC purity 98%)

HRMS (TOF MS ES+): *m/z* calcd for $C_{67}H_{89}N_{18}O_5^{3+}$ $[M]^{3+}$: 408.5749; found: 408.5750 (0.14 ppm).

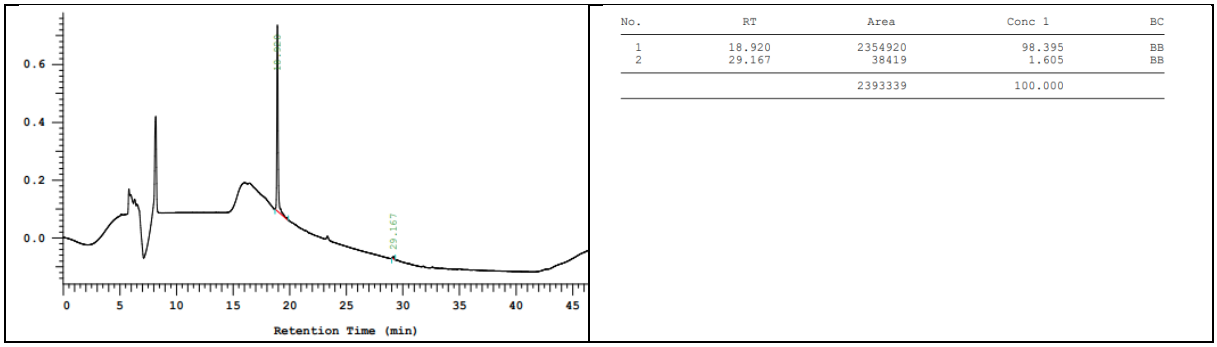

No.	RT	Area	Conc 1	BC
1	18.920	2354920	98.395	BB
2	29.167	38419	1.605	BB
		2393339	100.000	

Figure S198. HPLC chromatogram (220 nm) of the purified **IV.28**.

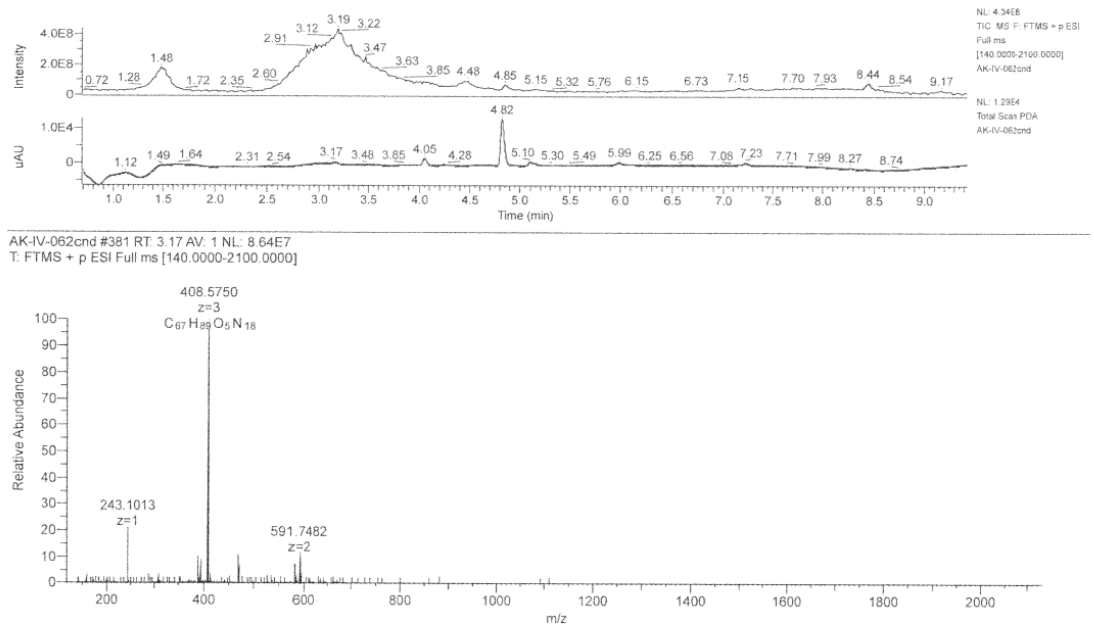

Figure S199. LCMS spectrum of crude **IV.28**.

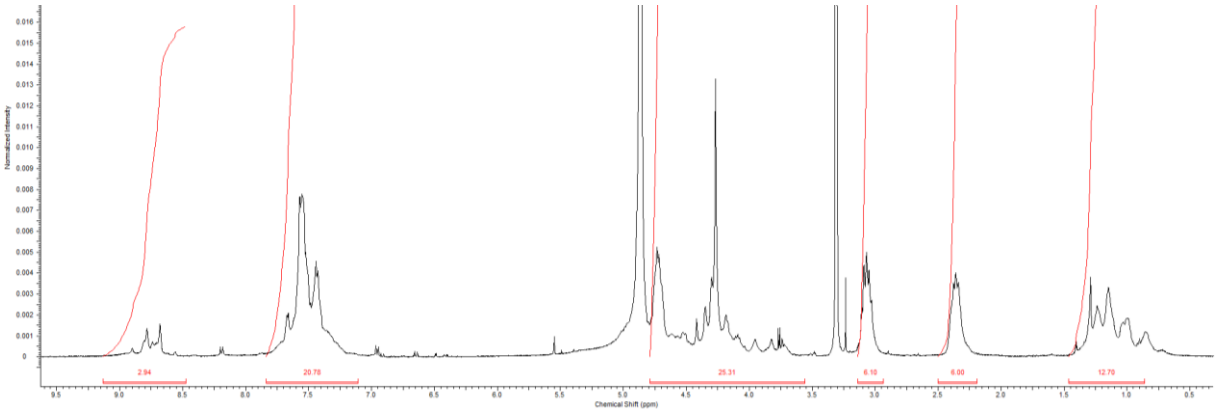

Figure S200. ^{1}H-NMR spectrum in MeOD of the pure **IV.28**.

6.3. IV.29.

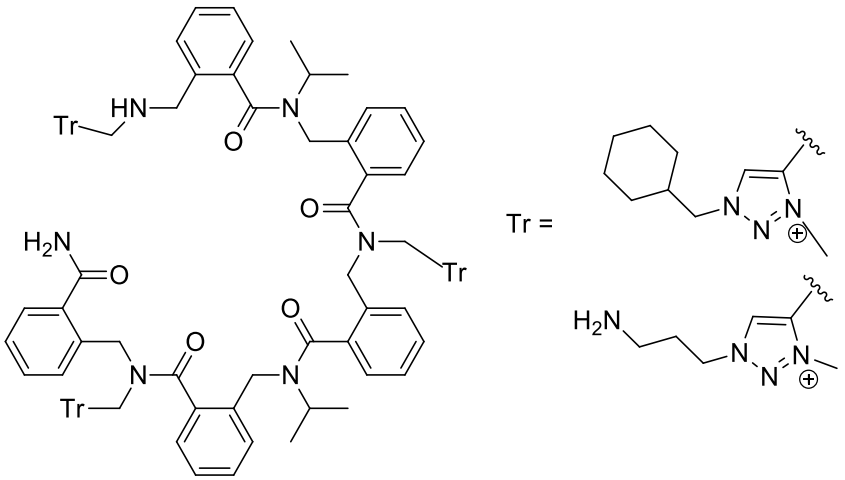

Pentamer **IV.29** was synthesised according to the standard procedure using 15 mg of Rink Amide resin (loading 0.62 mmol/g).

m_{pure}= 11 mg (95% isolated yield, HPLC purity 96%)

HRMS (TOF MS ES+) pic at 4.12: *m/z* calcd for $C_{79}H_{104}N_{15}O_5^{3+}$ $[M]^{3+}$: 447.61095; found: 447.6103 (-1.4 ppm).

HRMS (TOF MS ES+) pic at 3.67: *m/z* calcd for $C_{75}H_{99}N_{16}O_5^{3+}$ $[M]^{3+}$: 434.59893; found: 434.5981 (-1.88 ppm).

HRMS (TOF MS ES+) pic at 3.46: *m/z* calcd for $C_{67}H_{89}N_{18}O_5^{3+}$ $[M]^{3+}$: 408.57490; found: 408.5742 (-1.66 ppm).

HRMS (TOF MS ES+) pic at 3.41: *m/z* calcd for $C_{71}H_{94}N_{17}O_5^{3+}$ $[M]^{3+}$: 421.58691; found: 421.5861 (-1.88 ppm).

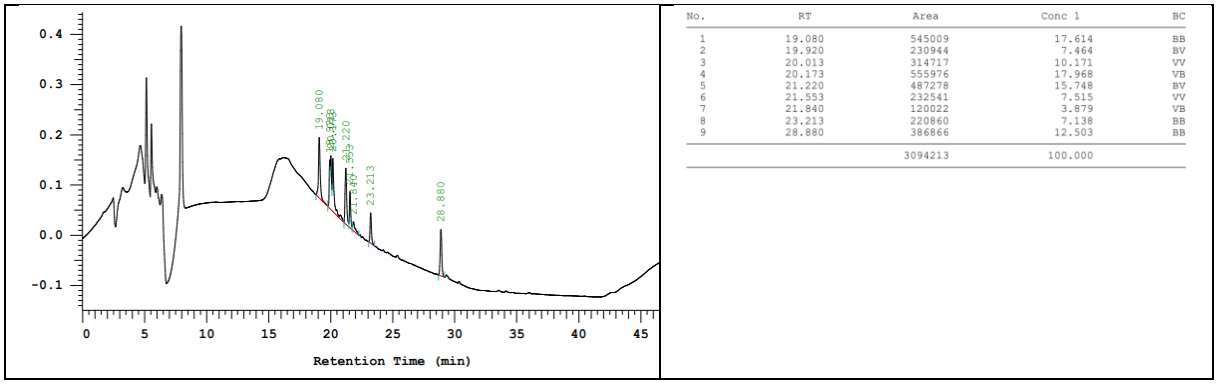

No.	RT	Area	Conc 1	BC
1	19.080	545009	17.614	BB
2	19.920	230944	7.464	BV
3	20.013	314717	10.171	VV
4	20.173	555976	17.968	VB
5	21.220	487278	15.748	BV
6	21.553	232541	7.515	VV
7	21.840	120022	3.879	VB
8	23.213	220860	7.138	BB
9	28.880	386866	12.503	BB
		3094213	100.000	

Figure S201. HPLC chromatogram (220 nm) of the **IV.29**.

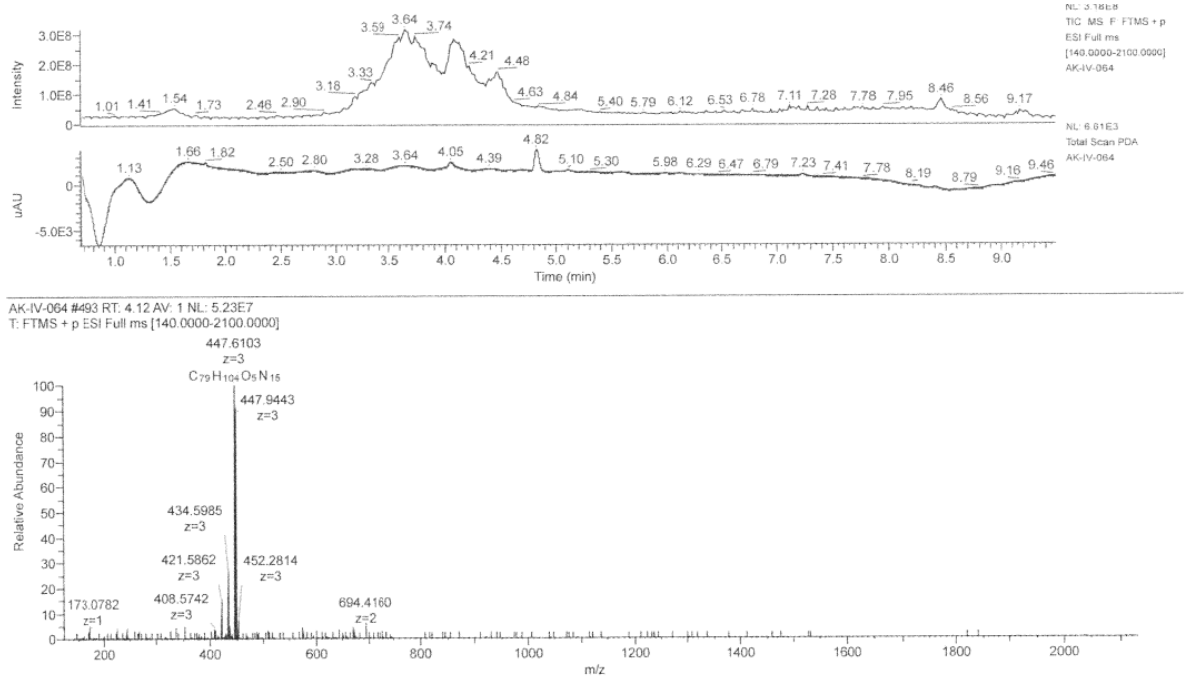

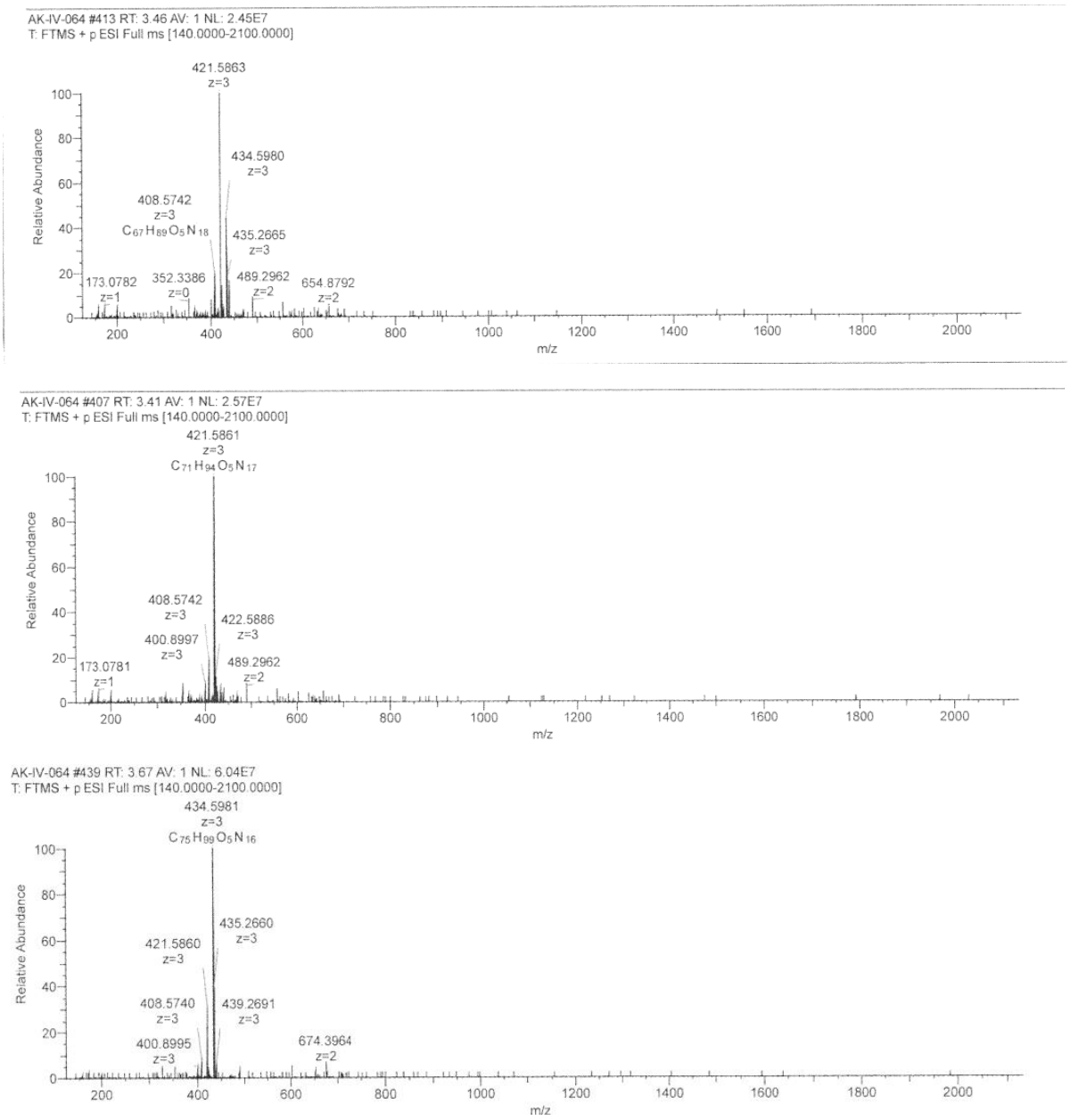

Figure S202. LCMS spectra of the crude **IV.29**.

7.Series G

7.1. IV.30.

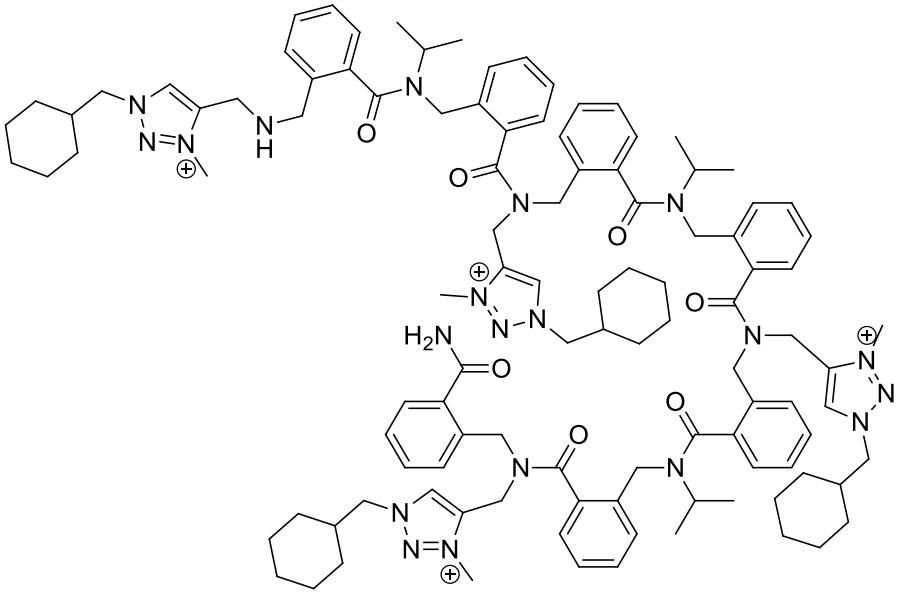

Heptamer **IV.30** was synthesised according to the standard procedure using 80 mg of Rink Amide resin (loading 0.62 mmol/g).

m_{pure}= 81.3 mg (89% isolated yield, HPLC purity 92%)

HRMS (TOF MS ES+): *m/z* calcd for $C_{109}H_{142}N_{20}O_7^{4+}$ $[M]^{4+}$: 460.78371; found: 460.7833 (-0.97 ppm).

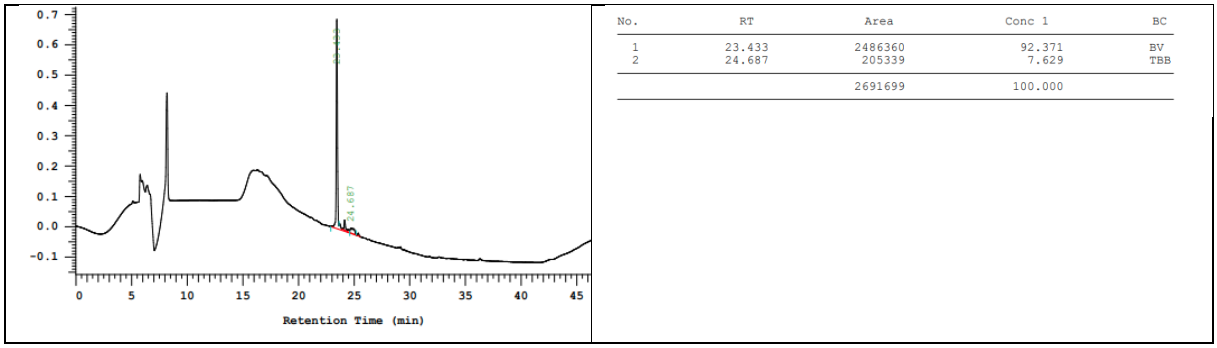

No.	RT	Area	Conc 1	BC
1	23.433	2486360	92.371	BV
2	24.687	205339	7.629	TBB
		2691699	100.000	

Figure S203. HPLC chromatogram (220 nm) of the pure **IV.30**.

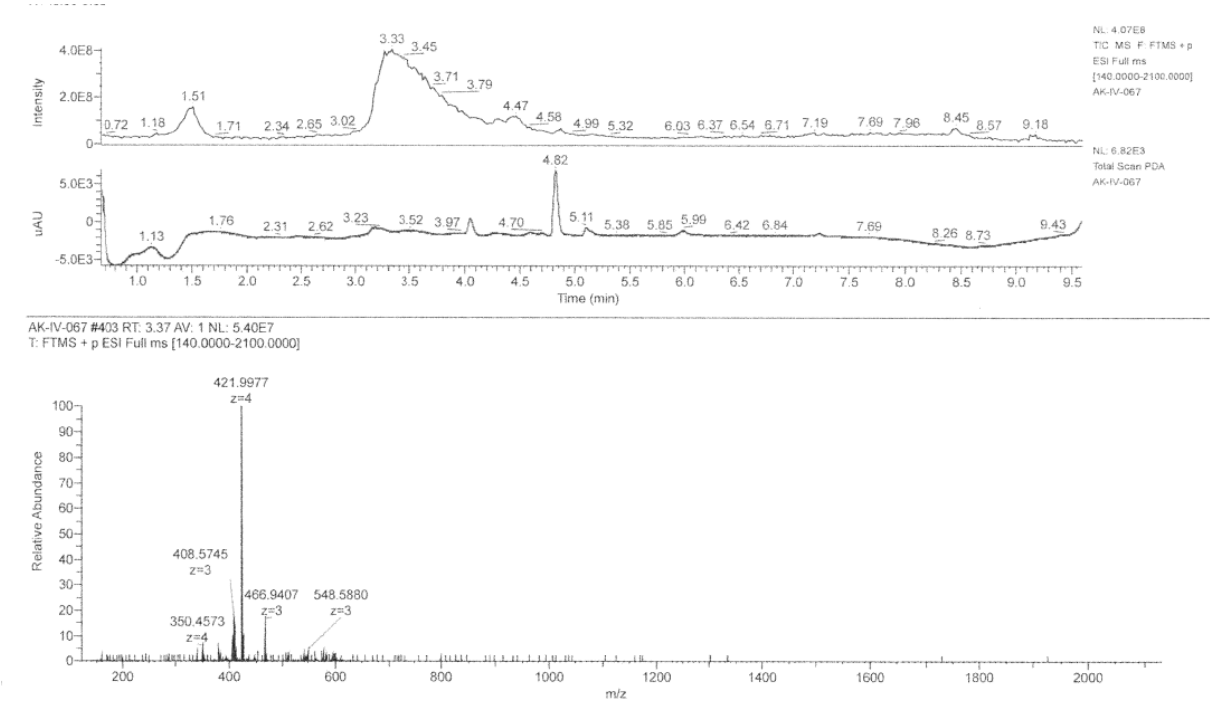

Figure S204. LCMS spectrum of the crude **IV.30**.

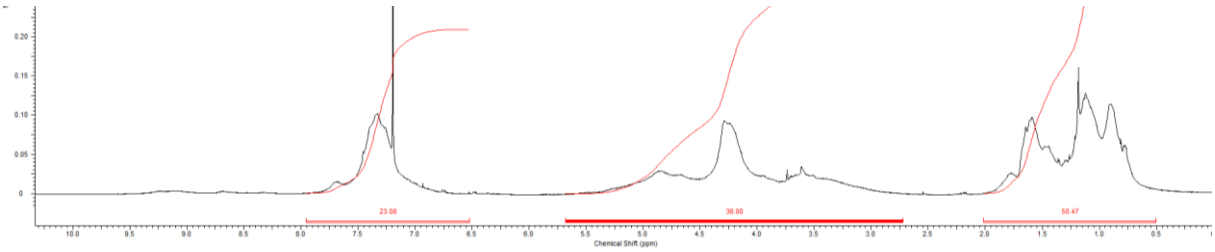

Figure S205. ^{1}H-NMR spectrum in $CDCl_3$ of the pure **IV.30**.

7.2. IV.31.

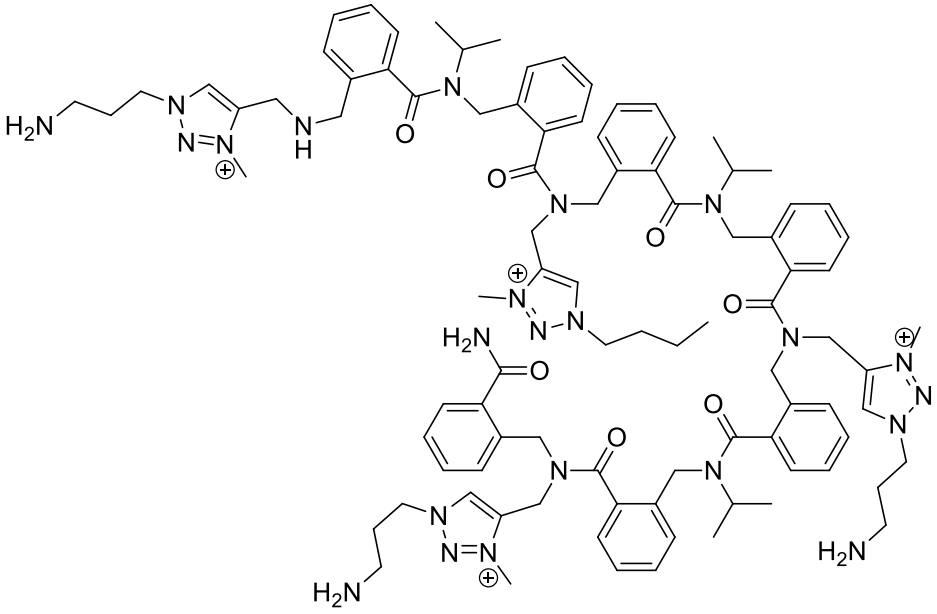

Heptamer **IV.31** was synthesised according to the standard procedure using 75 mg of Rink Amide resin (loading 0.62 mmol/g).

m_{pure}= 79 mg (95% isolated yield, HPLC purity 98%)

HRMS (TOF MS ES+): *m/z* calcd for $C_{93}H_{122}N_{24}O_7^{4+}$ $[M]^{4+}$: 421.74766; found: 421.7475 (-0.31 ppm).

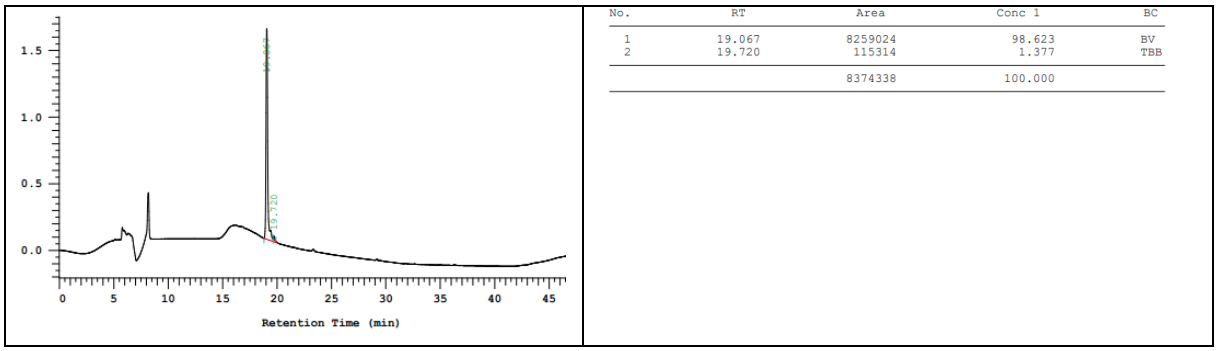

No.	RT	Area	Conc 1	BC
1	19.067	8259024	98.623	BV
2	19.720	115314	1.377	TBB
		8374338	100.000	

Figure S206. HPLC chromatogram (220 nm) of the pure **IV.31**.

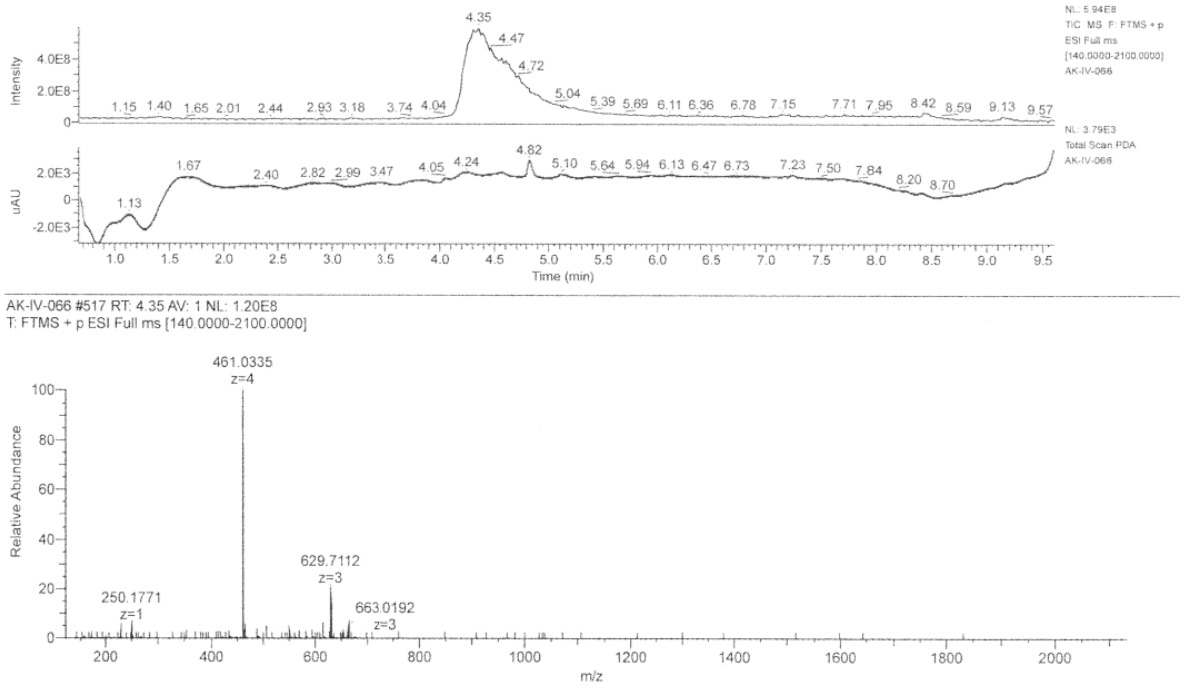

Figure S207. LCMS spectrum of the crude **IV.31**.

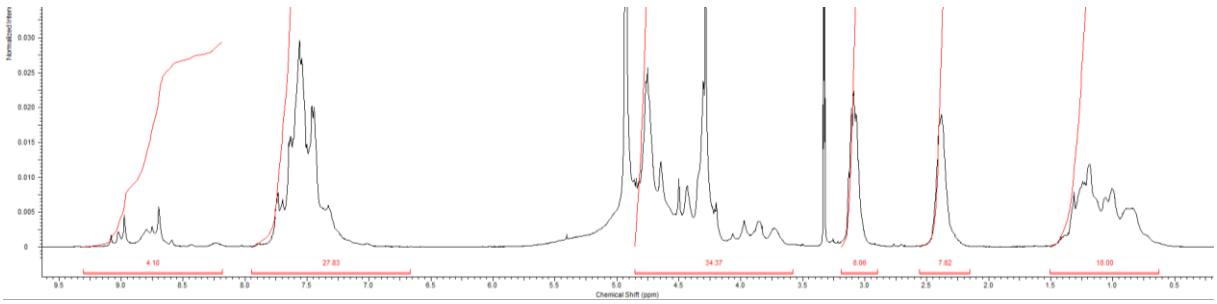

Figure S208. ^{1}H-NMR spectrum in MeOD of the pure **IV.31**.

Synthesis of compounds for conformational studies.

IV.32

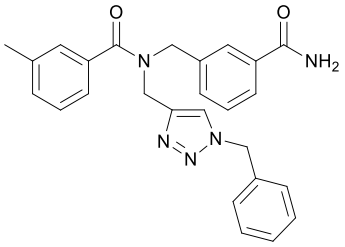

m_{pure}= 79 mg (purity 95%), 85% isolated yield.

HRMS (TOF MS ES+): *m/z* calcd for $C_{26}H_{26}N_5O_2[M+H]^+$: 440.20810; found: 440.2080 (-0.21 ppm).

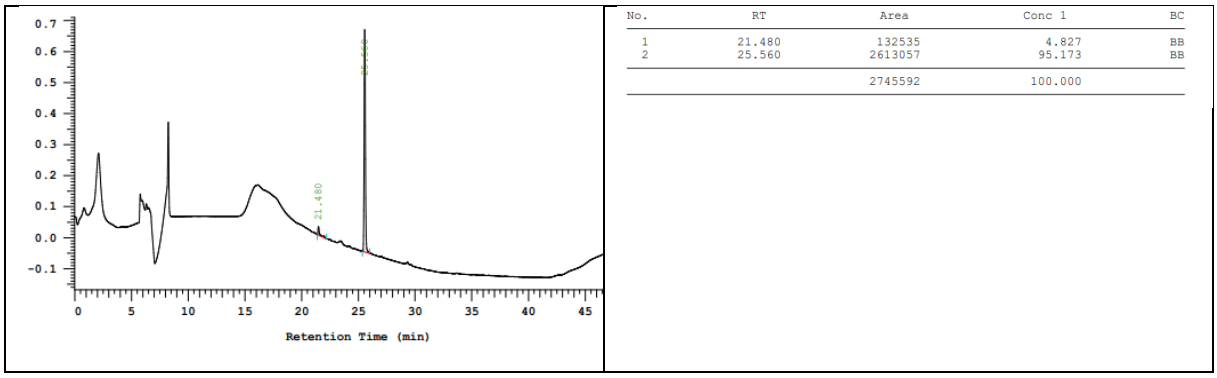

Figure S209. HPLC chromatogram (220 nm) of the pure **IV.32**.

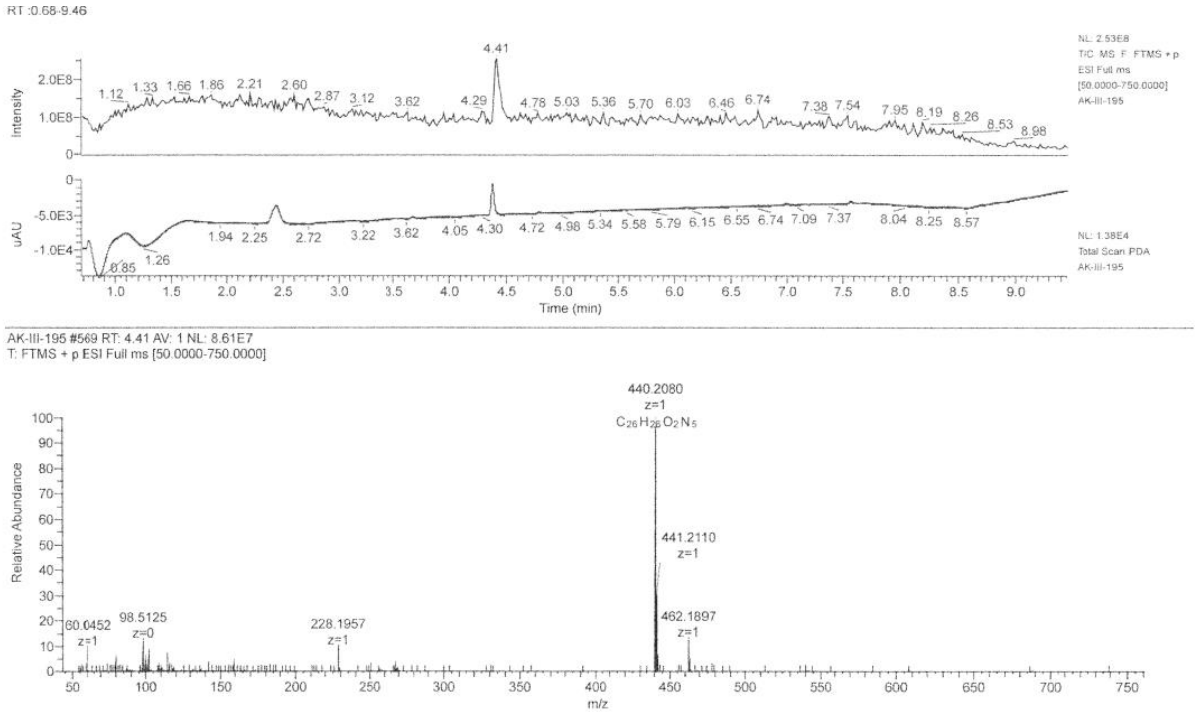

Figure S210. LCMS spectrum of the crude **IV.32**.

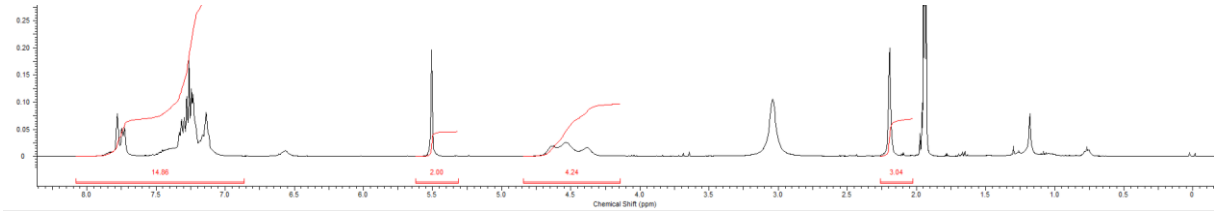

Figure S211. ^{1}H-NMR spectrum in acetonitrile of the pure **IV.32**.

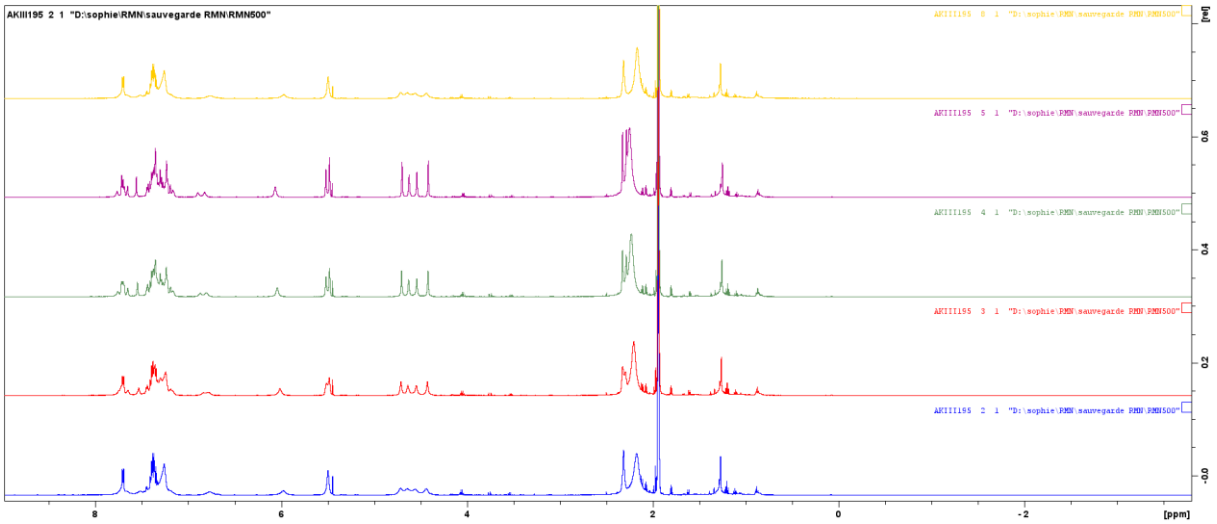

Figure S212. Variable temperature study of **IV.32** in CD_3CN: 298 K (blue curve), 288K (red curve), 278 K (green curve), 273 K (purple curve), 298 K at the end of the study (yellow curve).

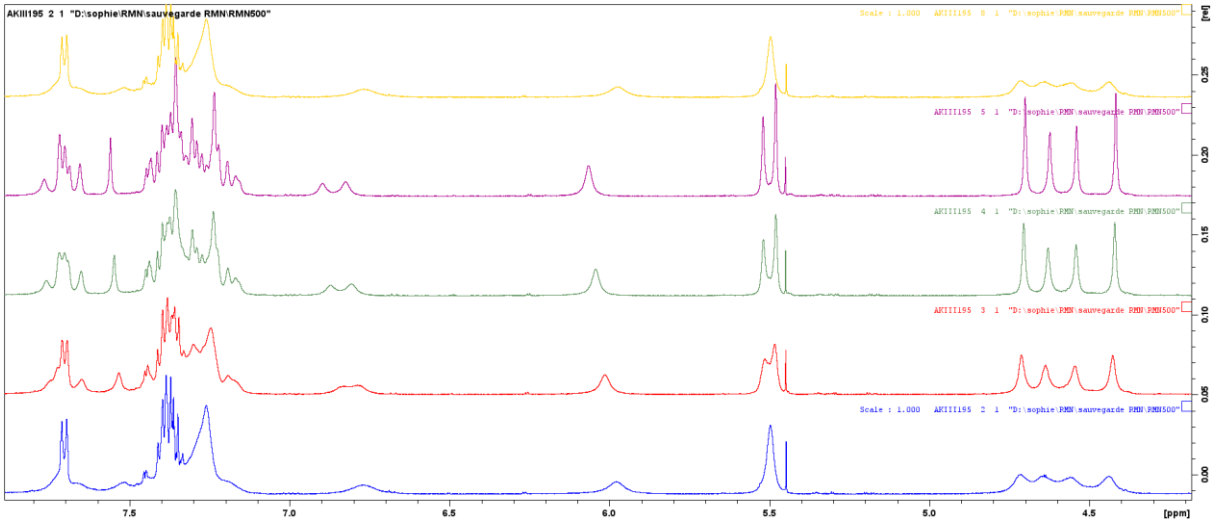

Figure S213. Variable temperature study of **IV.32** in CD_3CN (4-8 ppm region): 298 K (blue curve), 288K (red curve), 278 K (green curve), 273 K (purple curve), 298 K at the end of the study (yellow curve).

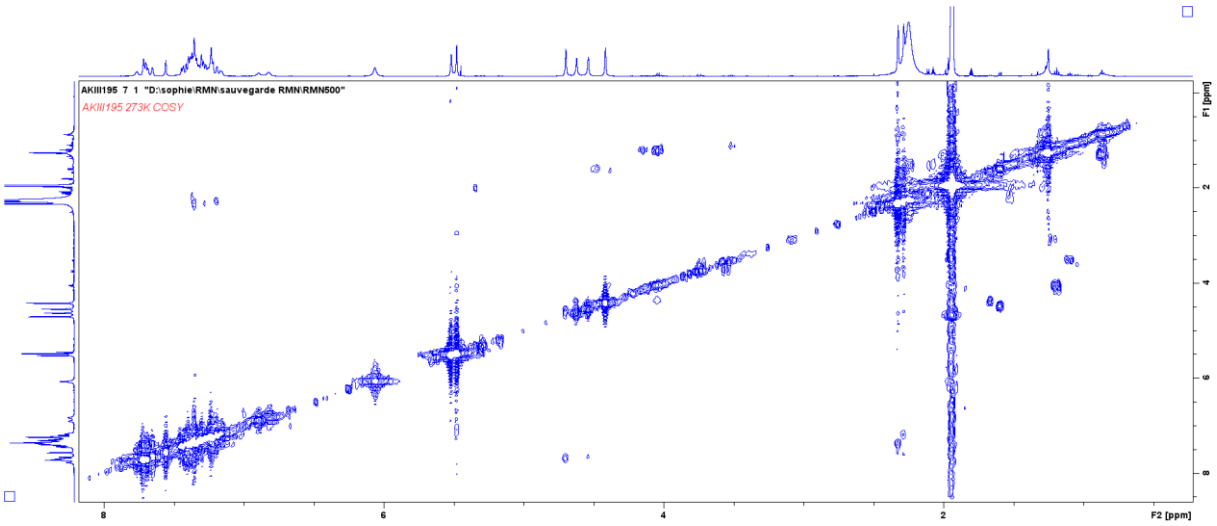

Figure S214. COSY spectrum of **IV.32** in CD_3CN at 273 K.

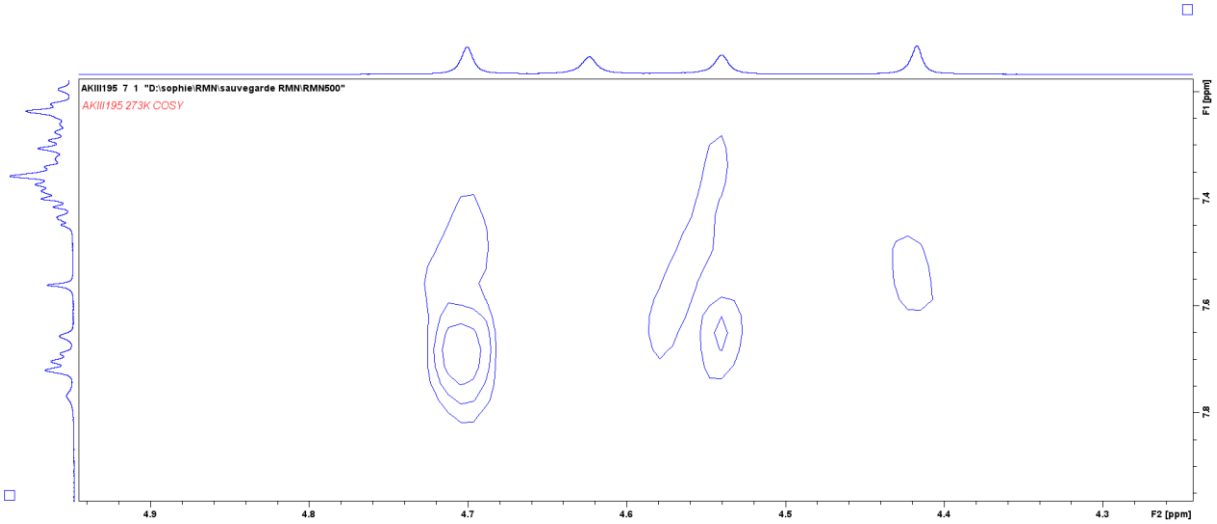

Figure S215. COSY spectrum of **IV.32** in CD_3CN at 273 K

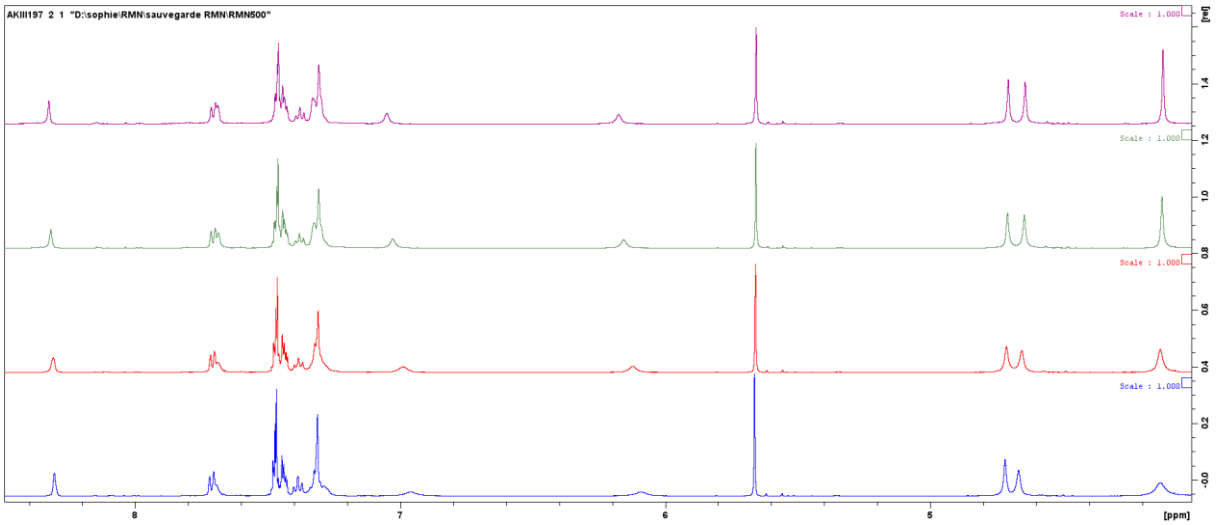

Figure S216. Variable temperature study of **IV.32** in CD_3CN (4-8 ppm region): 298 K (blue curve), 288K (red curve), 278 K (green curve), 273 K (purple curve).

IV.33

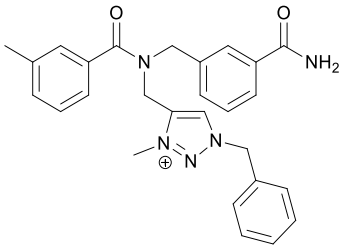

m_{pure}= 18.2 mg (purity 98%), 89% isolated yield.

HRMS (TOF MS ES+): *m/z* calcd for $C_{27}H_{28}N_5O_2^+[M]^+$: 454.22375; found: 454.2233 (-0.93 ppm).

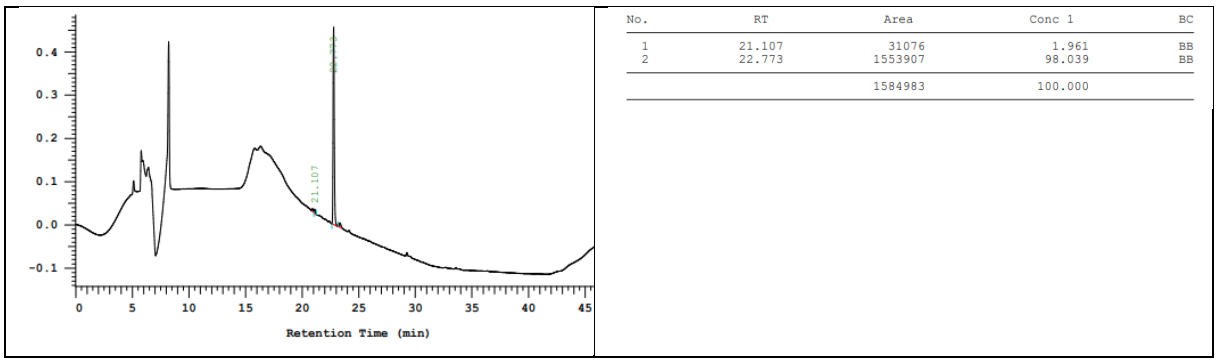

Figure S217 HPLC chromatogram (220 nm) of the pure **IV.33**.

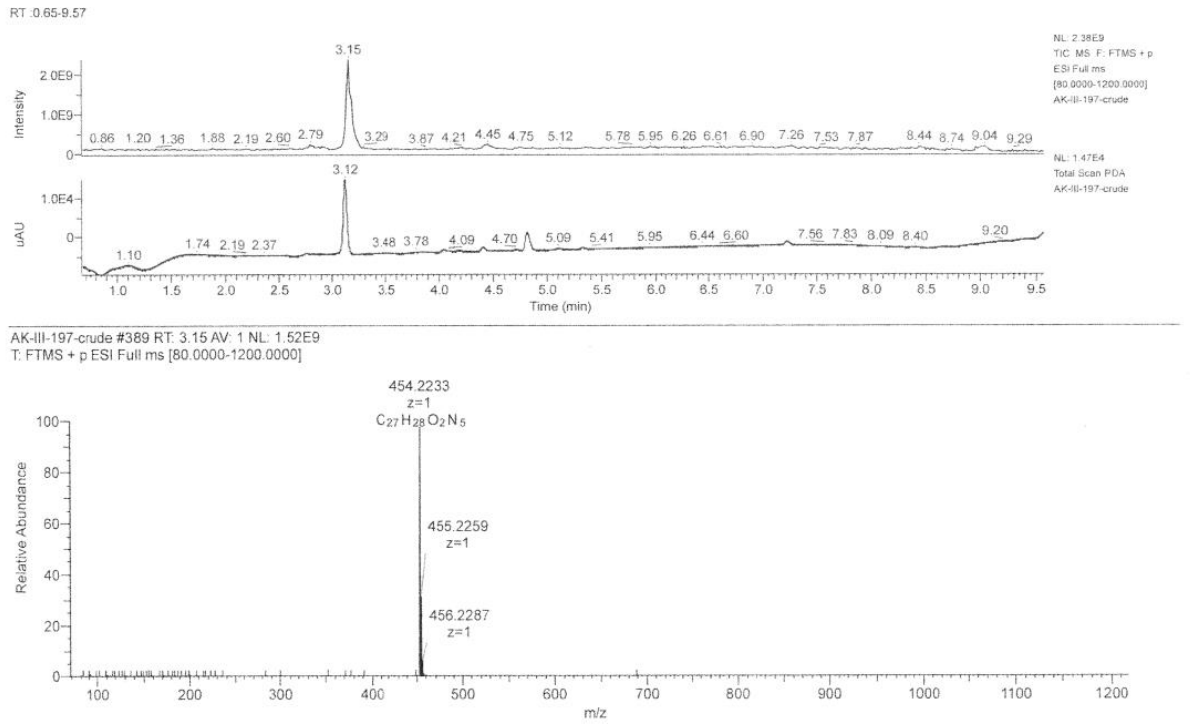

Figure S218 LCMS spectrum of the crude **IV.33**.

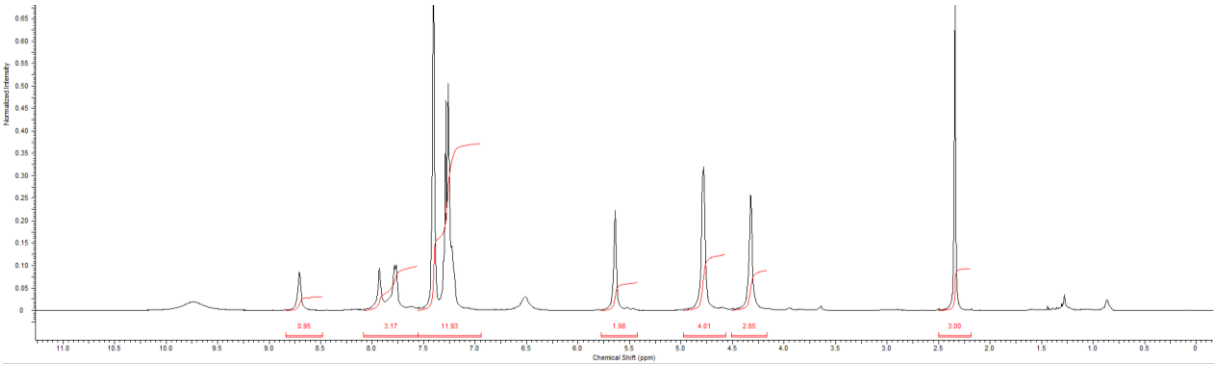

Figure S219. ^{1}H-NMR spectrum in $CDCl_3$ of the pure **IV.33**.

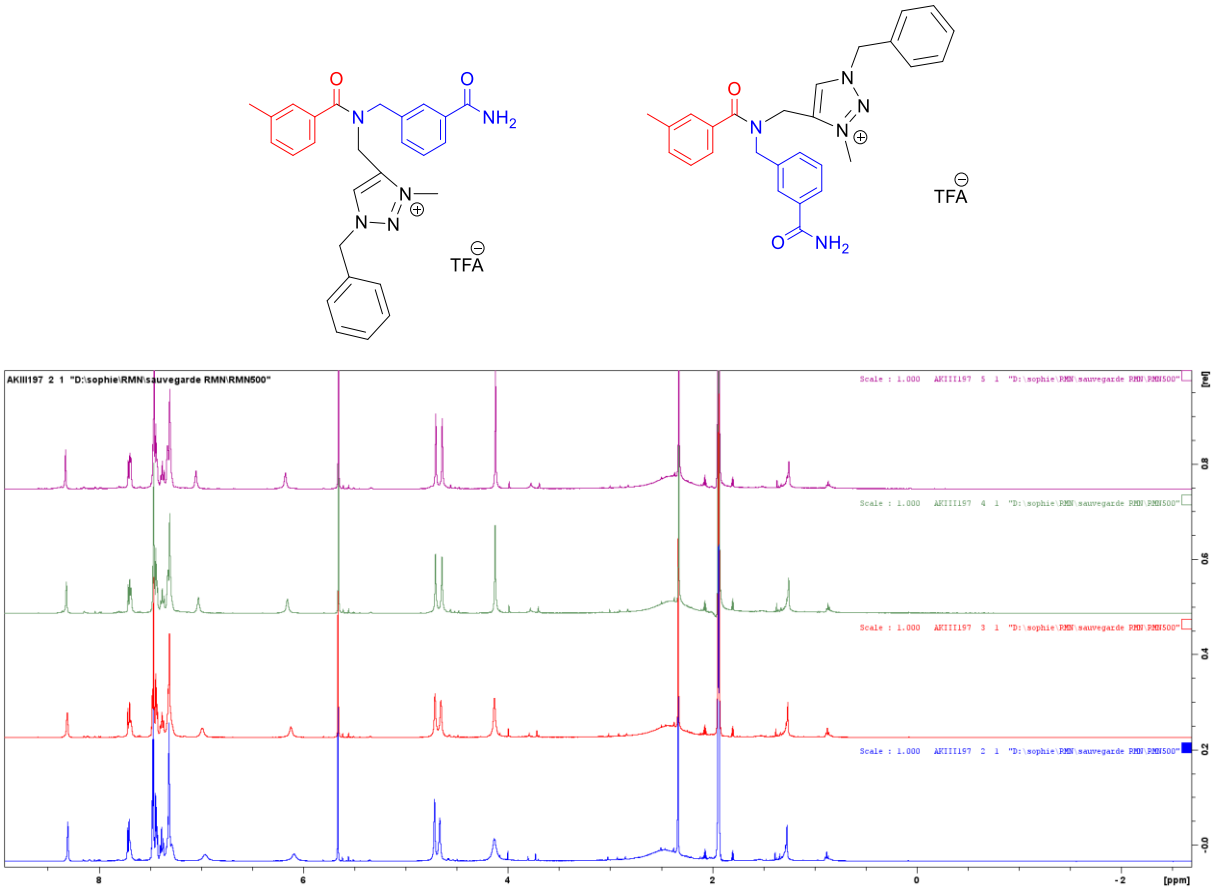

Figure S220. Variable temperature study of **IV.33** in CD_3CN: 298 K (blue curve), 288K (red curve), 278 K (green curve), 273 K (purple curve).

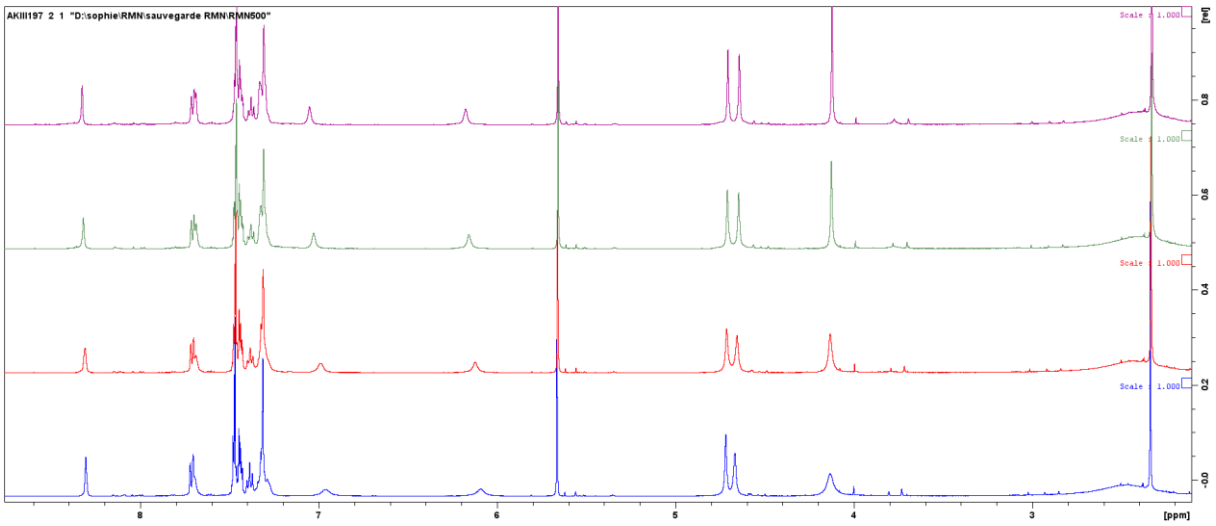

Figure S221. Variable temperature study of **IV.33** in CD_3CN: 298 K (blue curve), 288K (red curve), 278 K (green curve), 273 K (purple curve).

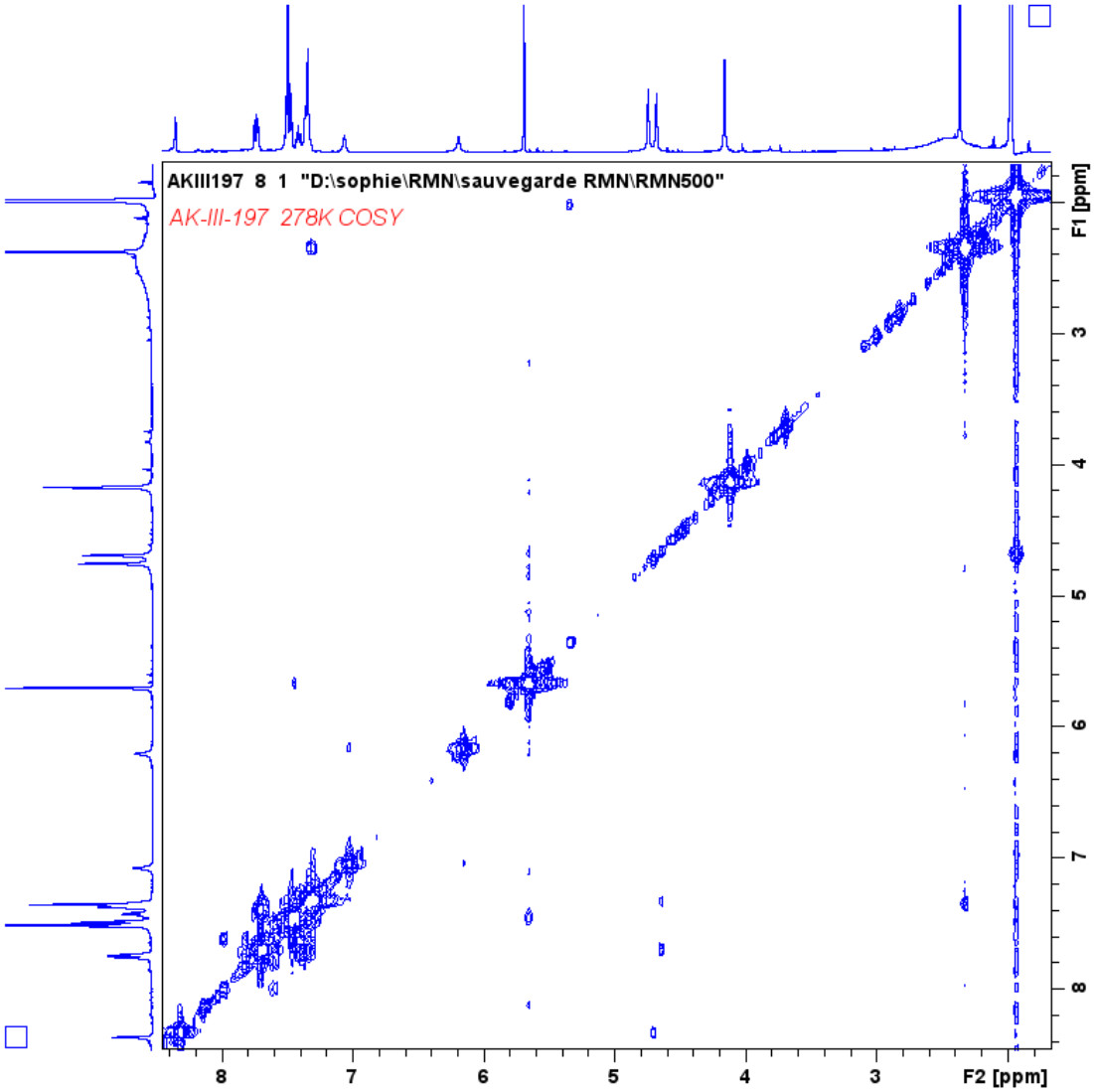

Figure S222. COSY spectrum of **IV.33** in CD_3CN at 278 K.

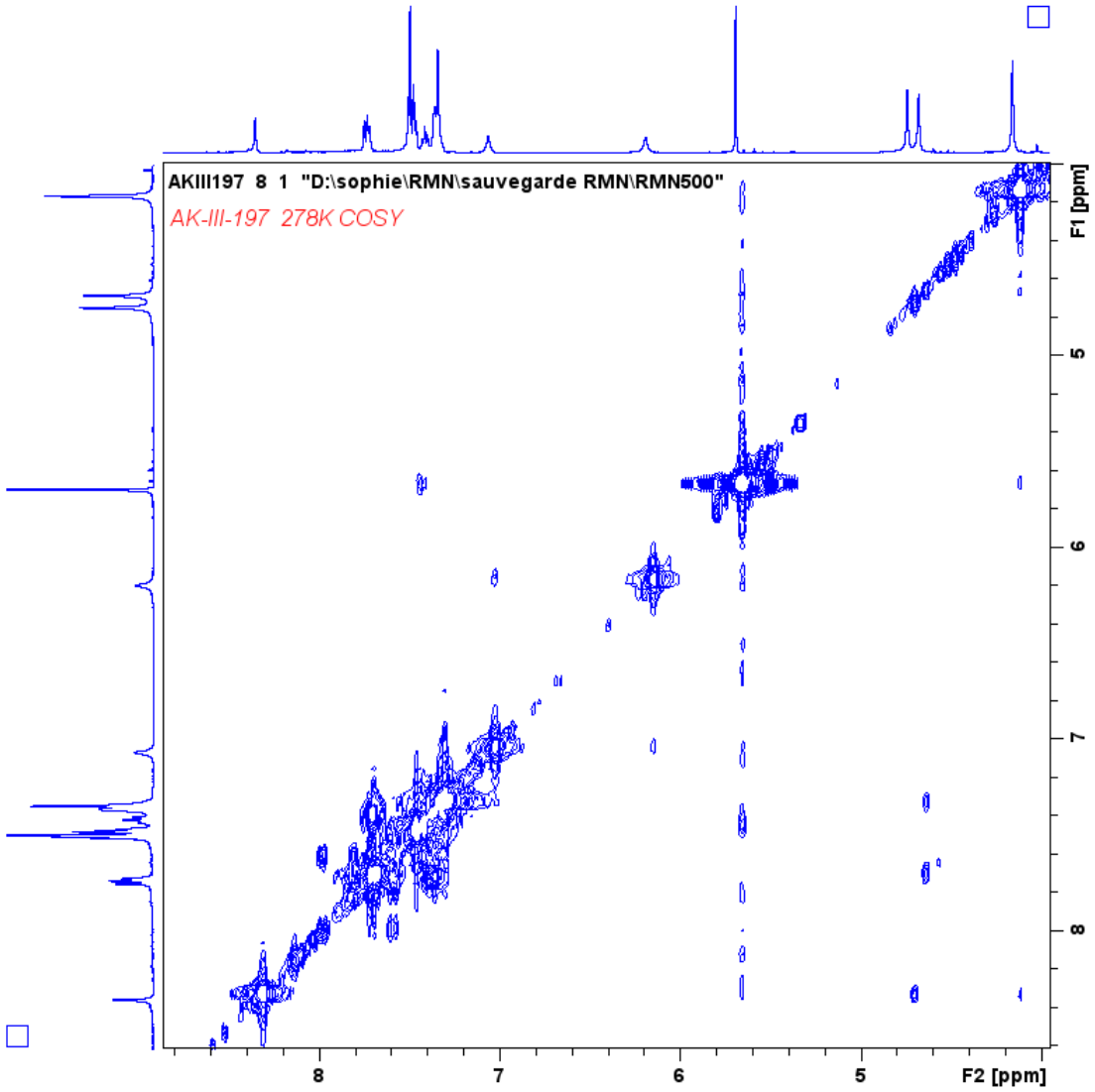

Figure S223. COSY spectra of **IV.33** in CD_3CN at 278 K.

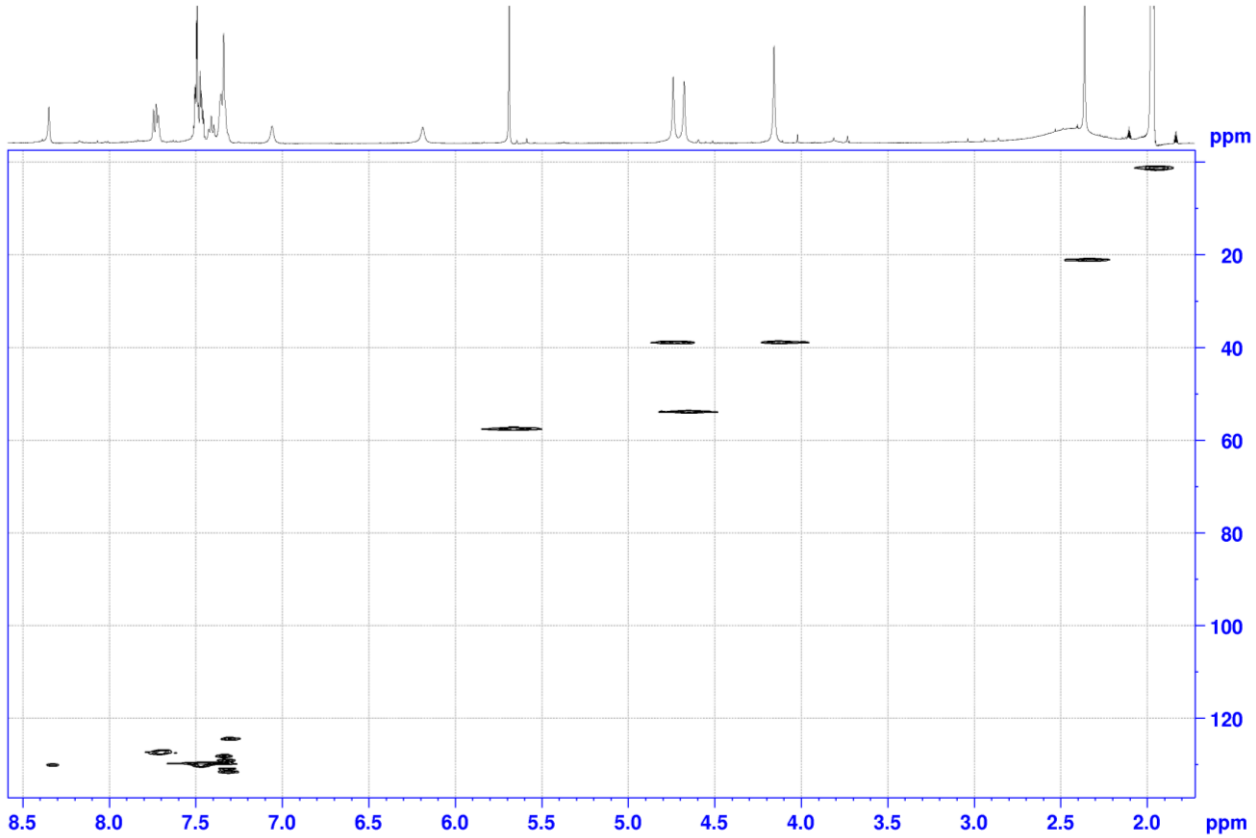

Figure S224. HSQC spectra of **IV.33** in CD3CN at 278 K.

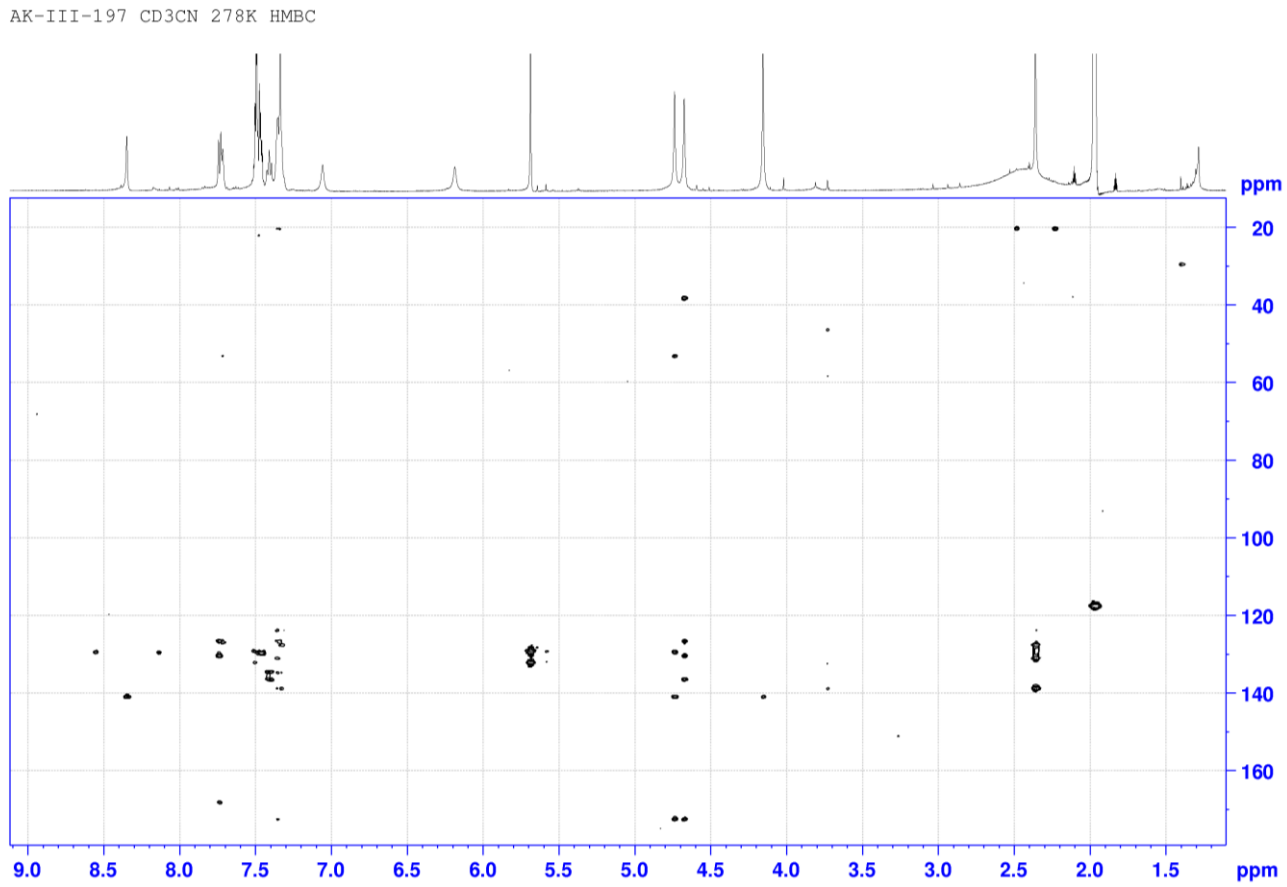

Figure S225. HMBC spectrum of **IV.33** in CD_3CN at 278 K.

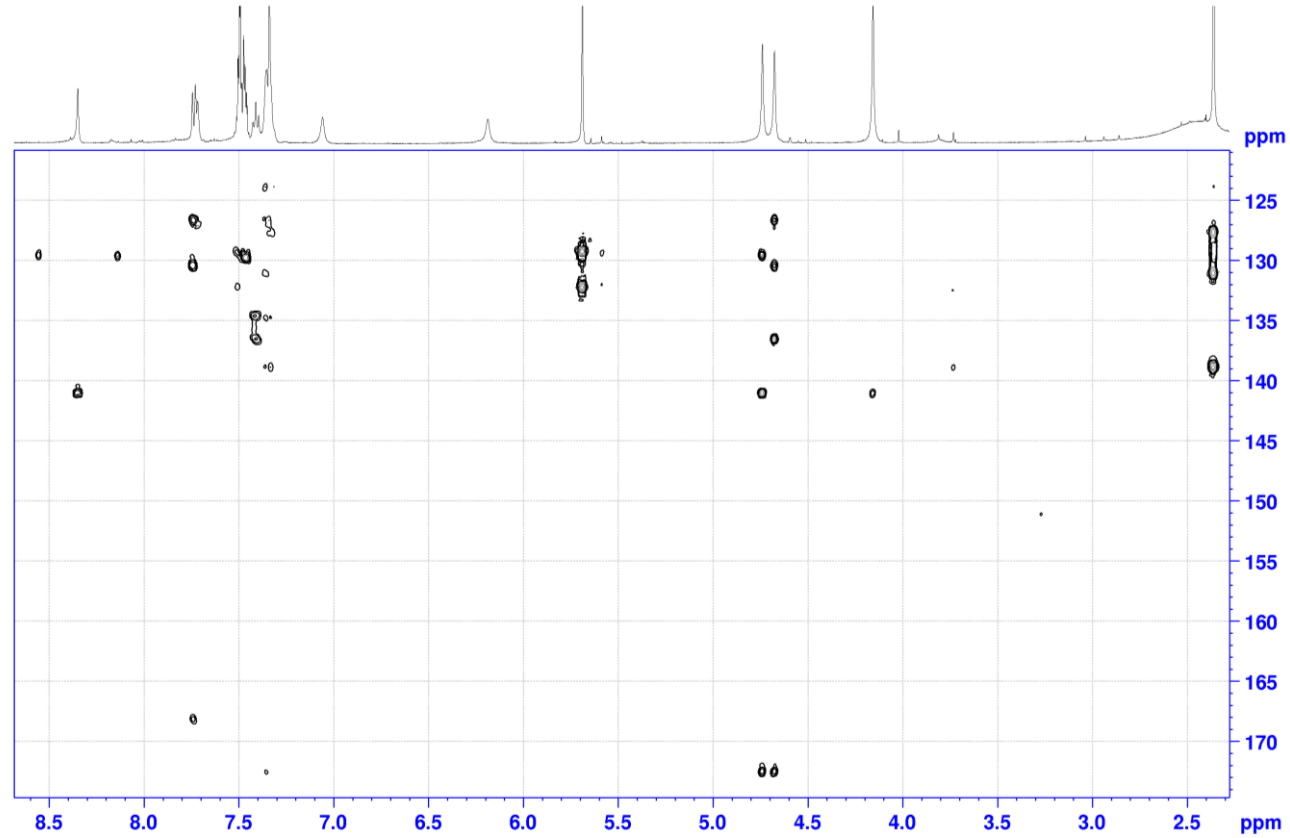

Figure 226 HMBC spectrum of **IV.33** in CD_3CN at 278 K.

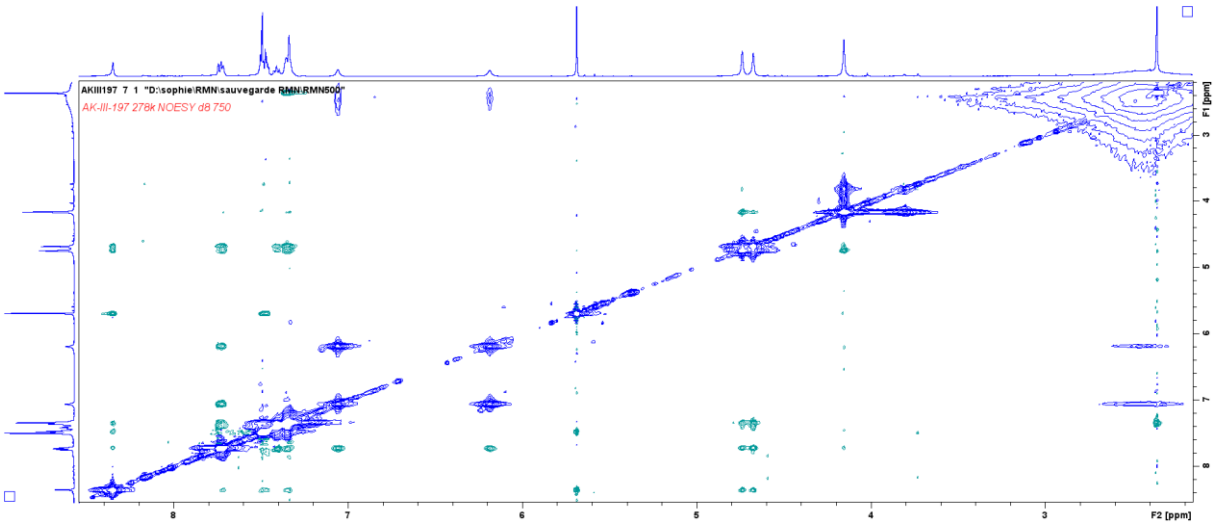

Figure S227. NOESY experiment of **IV.33** in CD_3CN at 278 K.

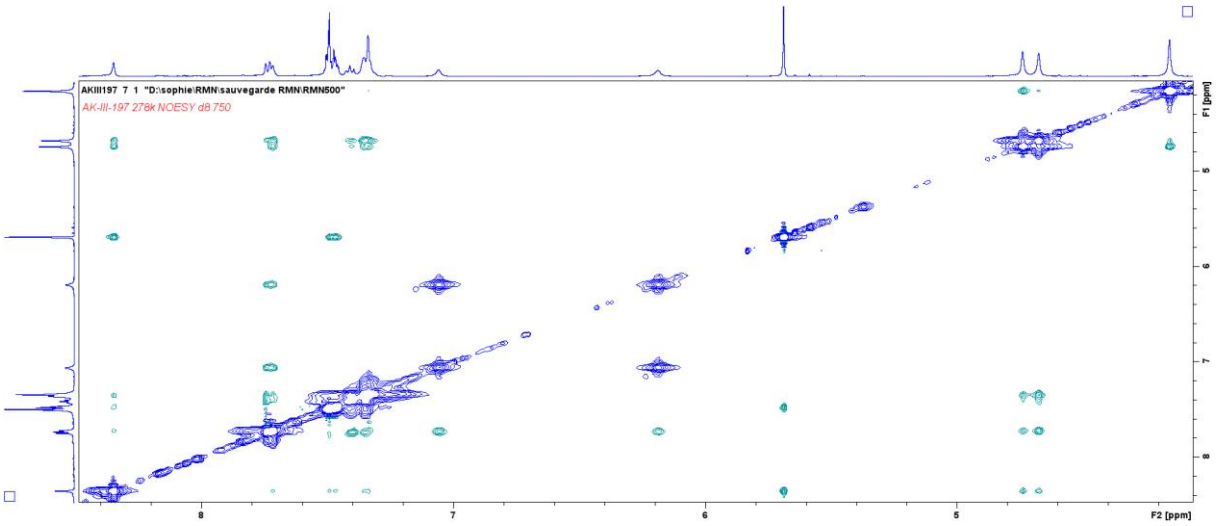

Figure S228. NOESY experiment of **IV.33** in CD_3CN at 278 K.

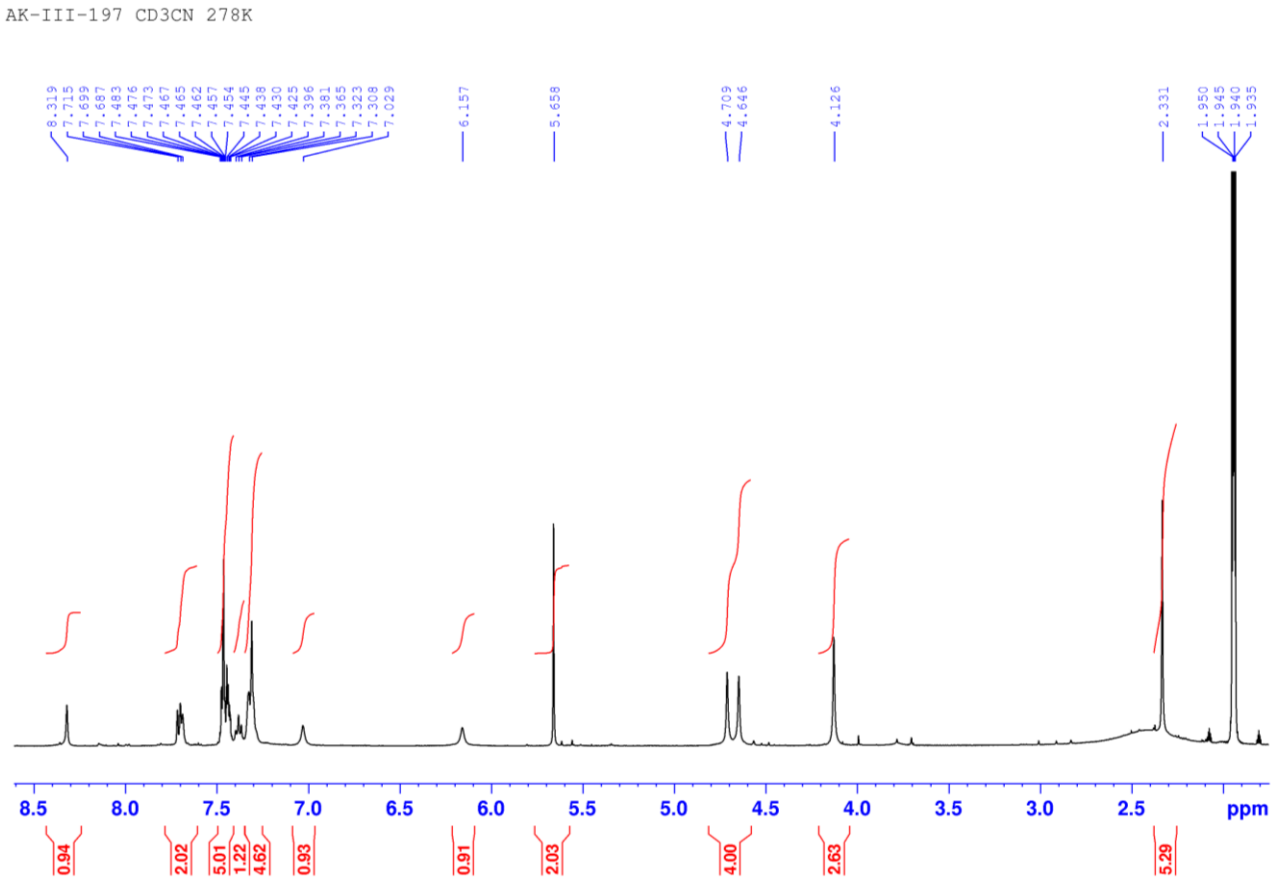

Figure S229. ^1H NMR spectra of **IV.33** in CD_3CN at 278 K.

Chapter V.

I-Chemicals

Chemicals: Rink amine resin (0.62mmol/g loading) was obtained from Novabiochem, piperidine and dichloromethane from Carlo Erba; 3-chloromethylbenzoylchloride, TFA, DIPEA, isopropyl, and propargyl amines from TCI; *N*-methylpyrrolidone from Alfa Aesar and DMSO from Acros. Benzyl azide (**1a**), (azidomethyl)cyclohexane (**1b**), *tert*-butyl azido acetate (**1c**), *tert*-butyl (2-azidoethyl)carbamate (**1d**) and 3-azido propane-1-ol (**1e**) were synthetized according to literature procedures. 10 mL jacketed reactors were purchased from Kamush and thermo-regulated using a Lauda thermostat. NMR was recorded on Bruker advance 400 spectrometer. Purification was performed on a Buchi Pure Chromatography system.

Analytical HPLC was recorded on a Hitachi liquid chromatograph (Oven 5310, 30°C; Pump 5160; DAD detector 5430) equipped with a C18 Acclaim column (4.6mm×250mm, 5µm, 120Å). Detection wavelength was 240nm or 280nm and flow rate 0.5mL/min. Gradient elution used (A) water/0.1% TFA; (B) methanol according to Method A: (Solvents A/B: 0 to 5 minutes isocratic at 95/5; 5 to 25 minutes gradient to 5/95; 25 to 35 minutes isocratic at 5/95; 35 to 45 minutes gradient to 95/5; 45 to 50 minutes 95/5) or Method B (Solvents A/B: 0 to 5 minutes isocratic at 95/5; 5 to 10 minutes gradient to 75/25; 10 to 50 minutes gradient to 40/60; 50 to 65 minutes gradient to 5/95; 65 to 70 minutes isocratic at 5/95; 70 to 80 minutes gradient to 95/5).

II.General Procedure

II.1. Synthesis of linear arylopeptoids

II.1.a. Linear ortho hexamer.

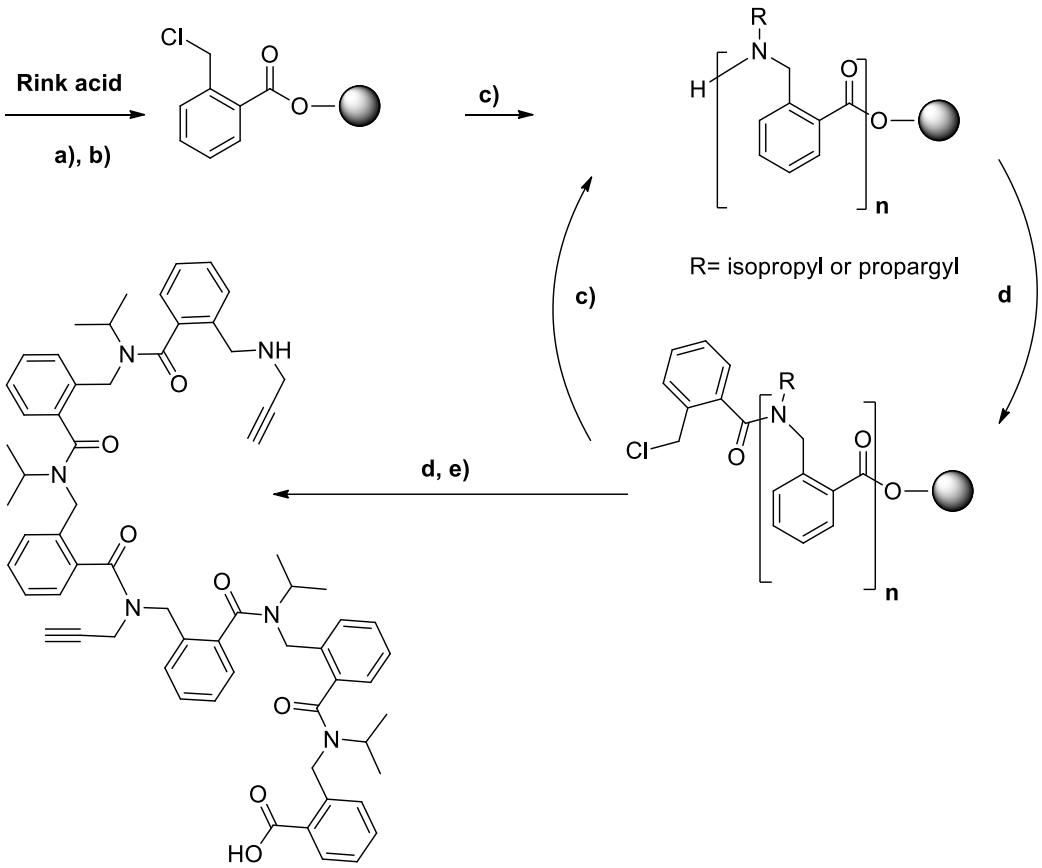

a) Swelling, CH_2Cl_2; b) 2-chloromethyl benzoylchloride, DIPEA, DMAP; CH_2Cl_2; c) Isopropyl amine or propargyl amine, dmso; d) 2-chloromethyl benzoylchloride, DIPEA, CH_2Cl_2 ;e) Cleavage: TFA/CH_2Cl_2 (20:80).

Scheme S4. Solid-phase submonomer synthesis on Rink acid resin

1-For 100mg of resin, swelling: 2 ml of CH_2Cl_2 at RT for 10 min

2- 2-chloromethylbenzoylchloride (3 equiv. per mmol loading), 4-DMAP (3 equiv. per mmol loading) DIPEA (3 equiv. per mmol loading) dissolved in 1 mL CH_2Cl_2 were added at RT, shaken 10 minutes. This step is repeated. The liquid was drawn down, then the solid phase was washed with CH_2Cl_2 (5x2ml), then with DMSO (5x2ml).

3- Isopropyl amine (20 equiv per mmol loading) dissolved in 0.5 mL of DMSO were added. The reaction was shaken for 1h at RT. The liquid was drawn down, then the solid phase was washed with DMSO (5x2ml), then with CH_2CL_2 (5x2ml).

4- 2-chloromethylbenzoylchloride (3 equiv. per mmol loading), DIPEA (6 equiv. per mmol loading) dissolved in 1 mL CH_2Cl_2 were added at RT, shaken 10 minutes. The liquid was drawn down, then the solid phase was washed with CH_2Cl_2 (5x2ml), then with DMSO (5x2ml).

5- Isopropyl amine or propargyl amine (20 equiv per mmol loading, 1M) dissolved in 0.5 mL of DMSO were added. The reaction was shaken for 1h at RT. The liquid was drawn down, then the solid phase was washed with DMSO (5x2ml), then with CH_2CL_2 (5x2ml).

Steps 4 and 5 were repeated to grow the targeted arylopeptoid oligomer until the expected sequence length.

6-The arylopeptoid was cleaved by the addition of 1ml of CH_2Cl_2/TFA (8:2) for 30 min at RT. The solution was collected and then the resin was washed with CH_2Cl_2 (5x2ml). The solution was evaporated under reduced pressure. The product was purified on Buchi LC auctomatic C18 column (Water + 0.1% TFA/MeOH) affording 90% of product (purity 96%).

HRMS (TOF MS ES+): *m/z* calcd for $C_{66}H_{73}N_6O_7$ $[M+H]^+$: 1061.55352; found: 1061.5520 (-1.43 ppm).

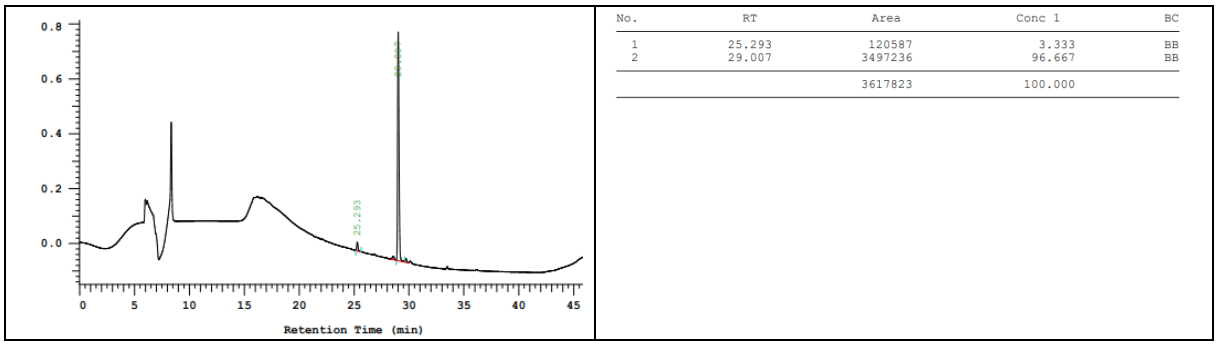

No.	RT	Area	Conc 1	BC
1	25.293	120587	3.333	BB
2	29.007	3497236	96.667	BB
		3617823	100.000	

Figure S230. HPLC chromatogram of the pure **Ia**.

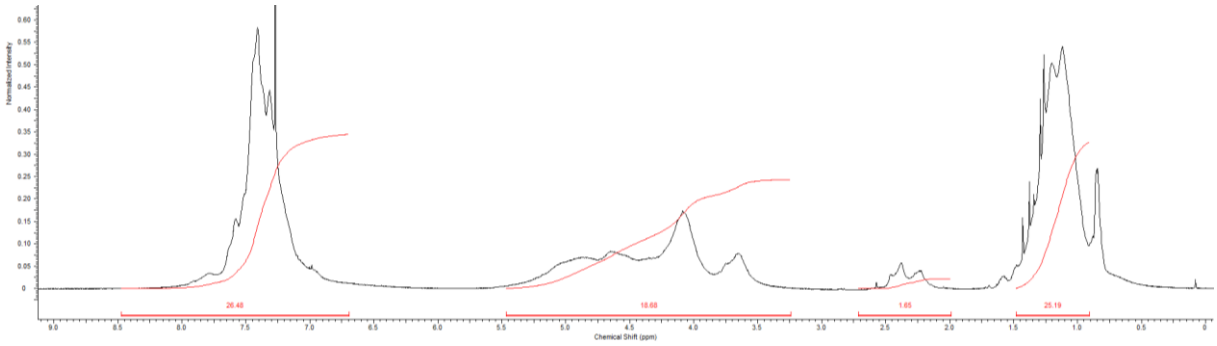

Figure S231. ^{1}H-NMR in $CDCl_3$ of the pure **Ia**.

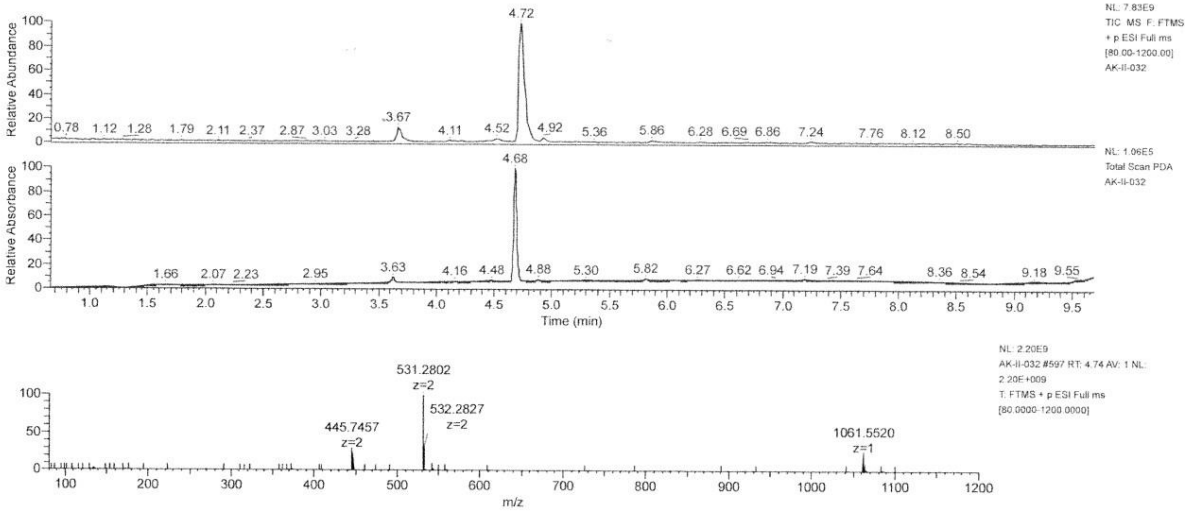

Figure S232. LCMS spectrum of the crude **Ia**.

Figure S233. Infra-red of **Ia**.

II.1.b. linear meta hexamer.

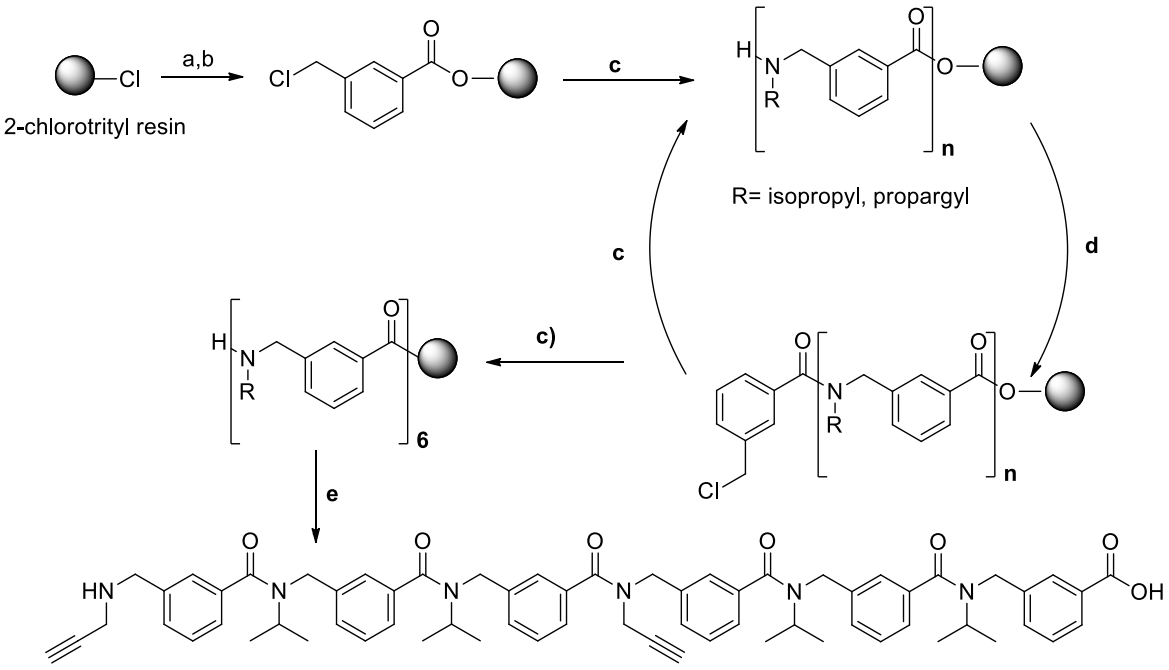

a) Swelling, CH_2Cl_2; b) 3-chloromethyl benzoic acid, DIPEA, CH_2Cl_2; c) Isopropyl amine or propargyl amine, dmso, 50°C; d) 3-chloromethyl benzoylchloride, DIPEA, CH_2Cl_2;e) Cleavage: TFA/CH_2Cl_2 (2:8).

Scheme S5. Synthesis of linear *meta*-arylopeptoid.

1-For 100mg of resin, swelling: 2 ml of CH_2Cl_2 at RT for 10 min

2- 3-chloromethylbenzoic acid (1.2 equiv. per mmol loading), DIPEA (5 equiv. per mmol loading) dissolved in 1 mL CH_2Cl_2 were added at RT and shaken 40 minutes. This step is repeated. The liquid was drawn down, then the solid phase was washed with CH_2Cl_2 (5x2ml), then with DMSO (5x2ml).

3- Isopropyl amine or propargyl amine (20 equiv per mmol loading, 1M) dissolved in 0.5 mL of DMSO were added. The reaction was shaken for 1h at 50°C. The liquid was drawn down, then the solid phase was washed with DMSO (5x2ml), then with CH_2CL_2 (5x2ml).

4- 3-chloromethylbenzoylchloride (3 equiv. per mmol loading), DIPEA (6 equiv. per mmol loading) dissolved in 1 mL CH_2Cl_2 were added at RT, shaken 10 minutes. The liquid was drawn down, then the solid phase was washed with CH_2Cl_2 (5x2ml), then with DMSO (5x2ml).

5- Isopropyl amine or propargyl amine (20 equiv per mmol loading) dissolved in 0.5 mL of DMSO were added. The reaction was shaken for 1h at 50°C. The liquid was drawn down, then the solid phase was washed with DMSO (5x2ml), then with CH_2CL_2 (5x2ml).

Steps 4 and 5 were repeated to grow the targeted arylopeptoid oligomer until the expected sequence length.

6-The arylopeptoid was cleaved by the addition of 1ml of CH_2Cl_2/TFA (8:2) for 30min at RT. The solution was collected and then the resin was washed with CH_2Cl_2 (5x2ml). The solution was evaporated under reduced pressure. The product was purified on LC Buchi C18 column (water +0.1%TFA/MeOH) affording 93% of product (purity 96%).

HRMS (TOF MS ES+): *m/z* calcd for $C_{66}H_{73}N_6O_7$ $[M+H]^+$: 1061.55352; found: 1061.5536 (0.06 ppm).

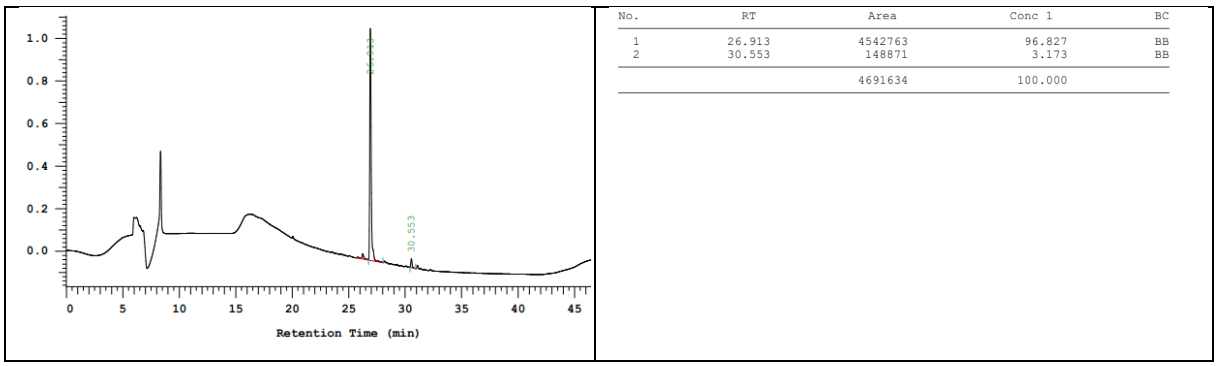

No.	RT	Area	Conc 1	BC
1	26.913	4542763	96.827	BB
2	30.553	148871	3.173	BB
		4691634	100.000	

Figure S234. HPLC chromatogram of pure **Ib**.

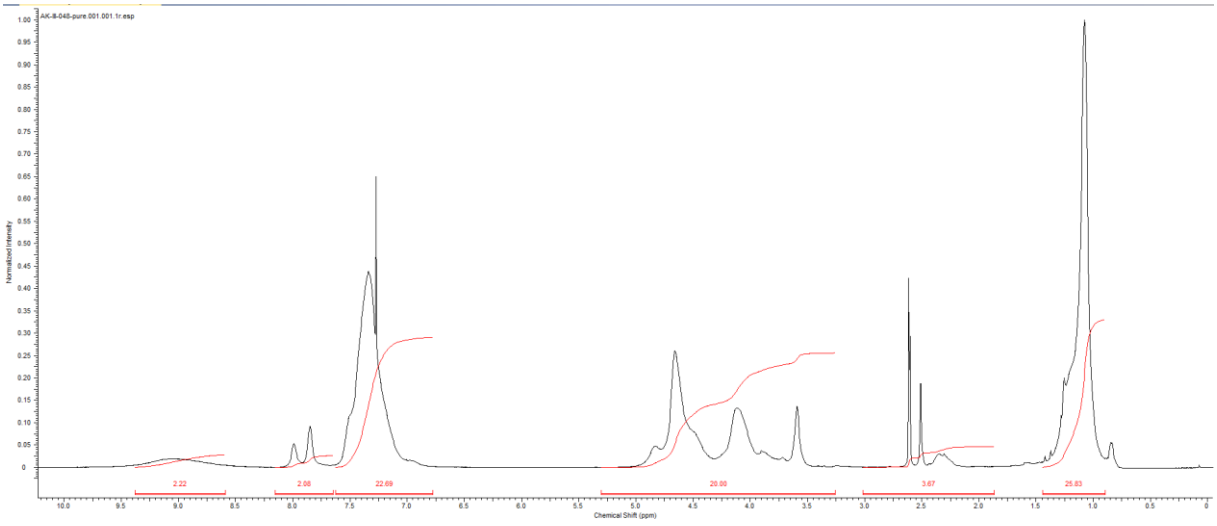

Figure S235. ^{1}H-NMR spectrum in $CDCl_3$ of pure **Ib**.

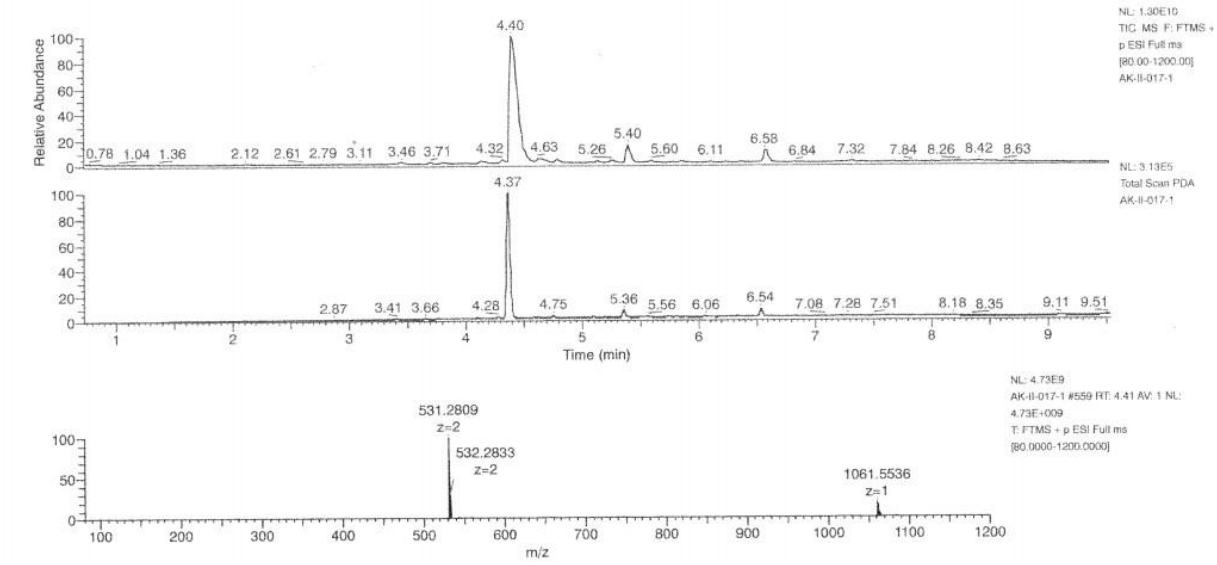

Figure S236. LCMS spectrum of the crude **Ib**.

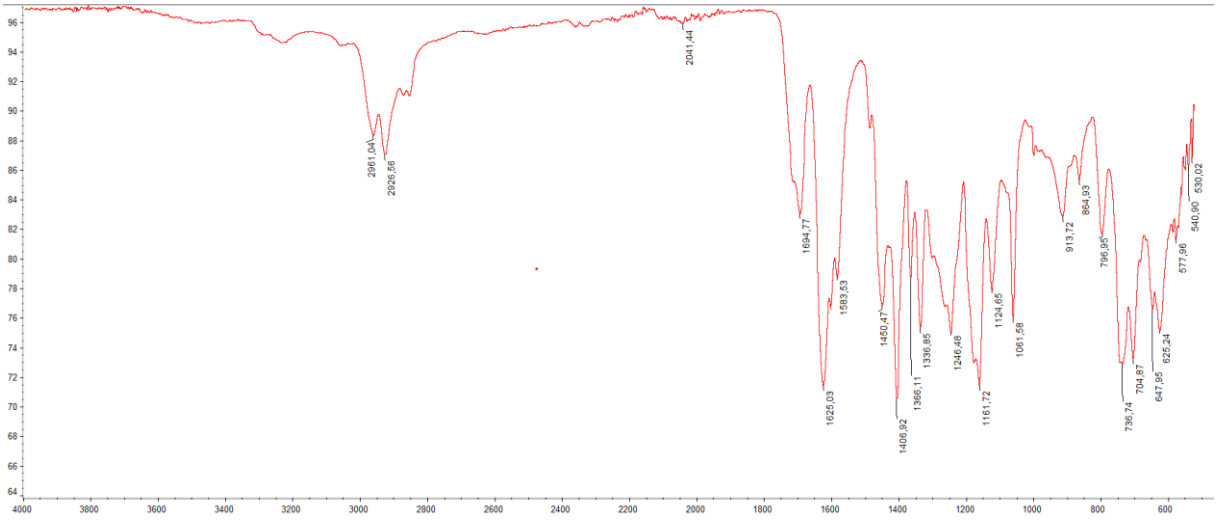

Figure S237. Infra-red of pure **Ib**.

II.2. Cyclisation

*II.2.a. Cyclic ortho hexamer **IIa**.*

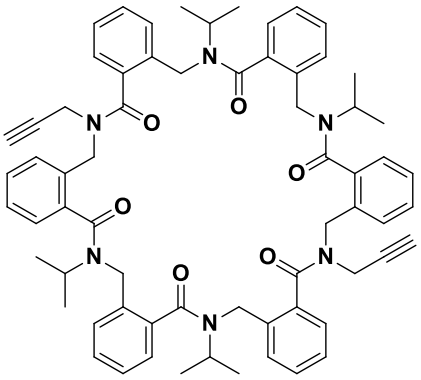

Molecular Weight: 1043,30

The *ortho*-hexamer was dissolved in CH_2Cl_2 (5 mmol/L), then 5 equiv. of DIPEA was added followed by 1.2 equiv. of HATU. The reaction was stirred overnight at RT. The solvent was evaporated under

reduced pressure and then the residue was evaporated with CH_2Cl_2 (2*20ml). The residue is then dissolved in EtOAc (20ml), extracted with $NaHCO_3$ (2*10ml) then brine (1*10ml). The organic layer was dried with $MgSO_4$, then evaporated under reduced pressure. The product was purified on C18 column (Water + 0.1% TFA/ MeOH) affording **IIa** in 70% yield (purity 95%).

On standing at RT for 1-2 days in the collecting tubes crystals forms from the solution. X-ray suitable crystals were collected after 2 weeks.

HRMS (TOF MS ES+): *m/z* calcd for $C_{66}H_{71}N_6O_6$ $[M+H]^+$: 1043.54296; found: 1043.5422 (-0.69 ppm).

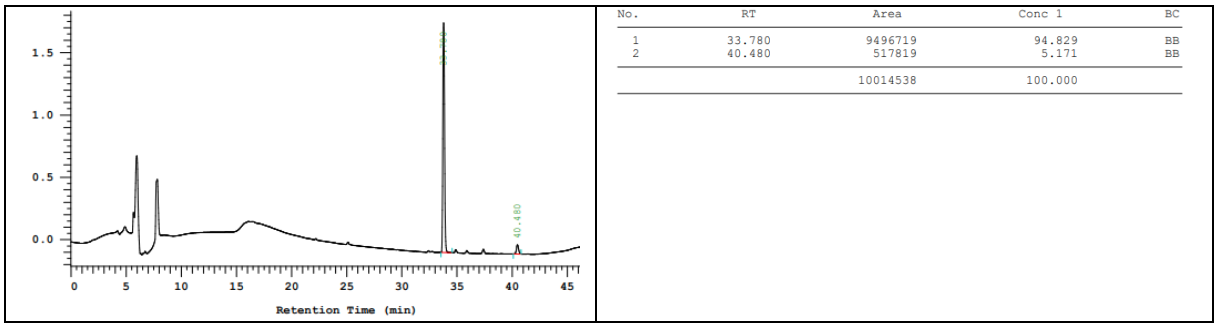

No.	RT	Area	Conc 1	BC
1	33.780	9496719	94.829	BB
2	40.480	517819	5.171	BB
		10014538	100.000	

Figure S238. HPLC chromatogram of the pure *ortho*-macrocycle (**IIa**).

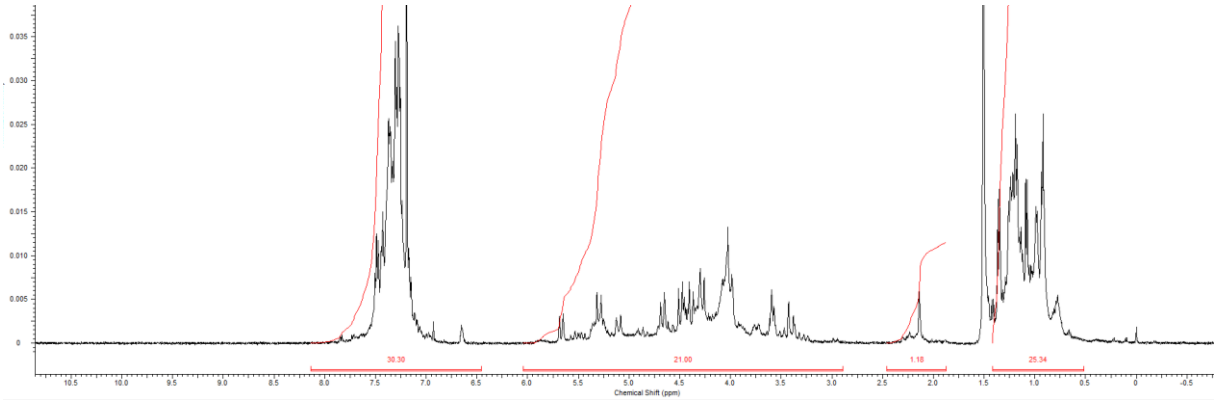

Figure S239 : ^{1}H-NMR spectrum in $CDCl_3$ of pure *ortho*-macrocycle (**IIa**)..

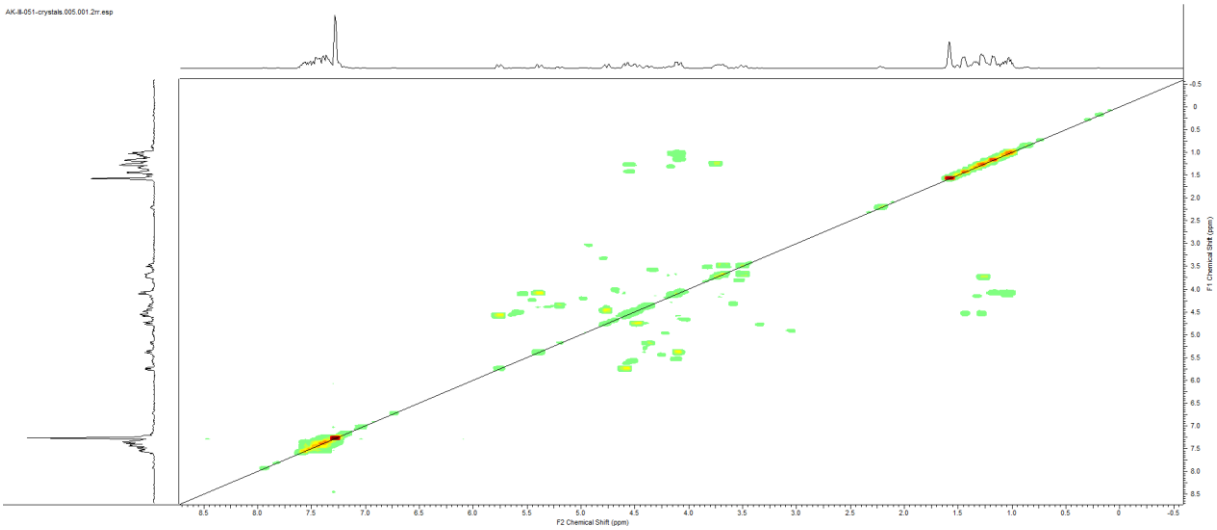

Figure S240. COSY spectrum in $CDCl_3$ of pure *ortho*-macrocycle (**IIa**).

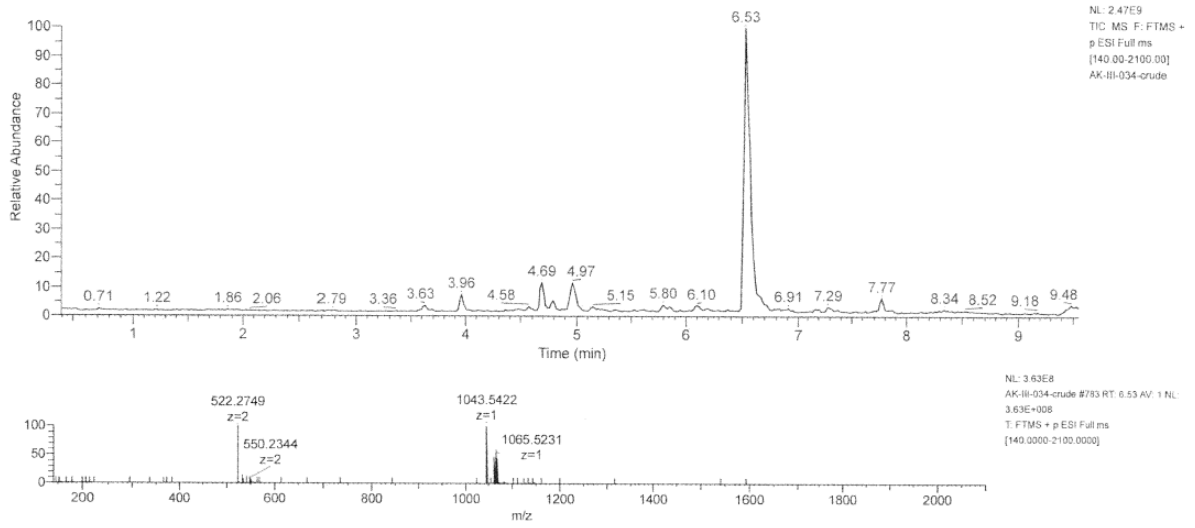

Figure S241. LCMS spectra of *ortho*-macrocycle (**IIa**).

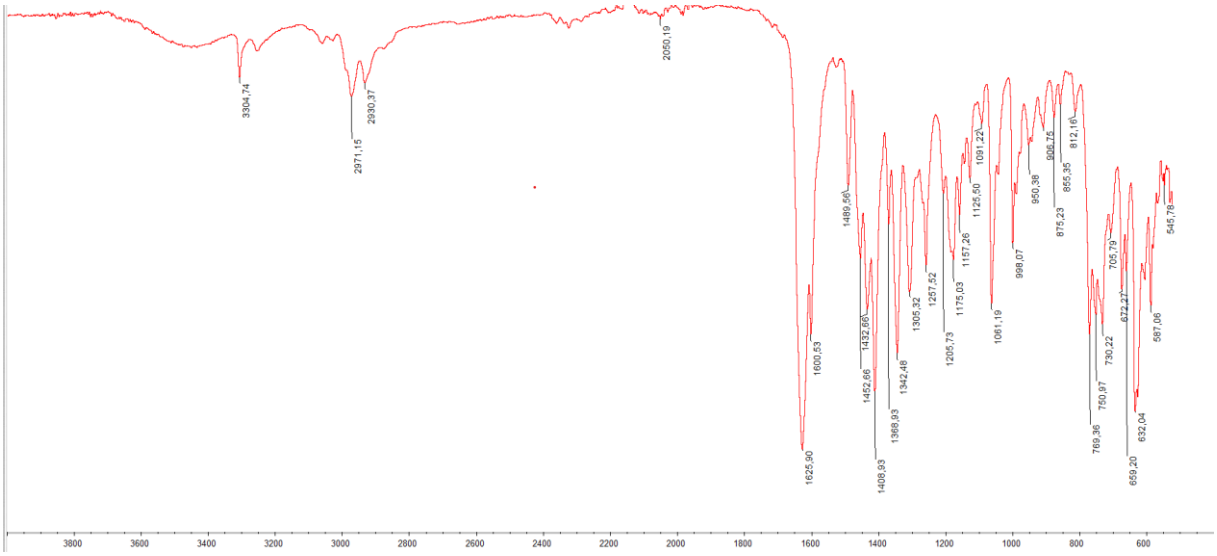

Figure S242. Infra-red of *ortho*-macrocycle (**IIa**).

II.2.b. Cyclic meta hexamer ***Ib.***

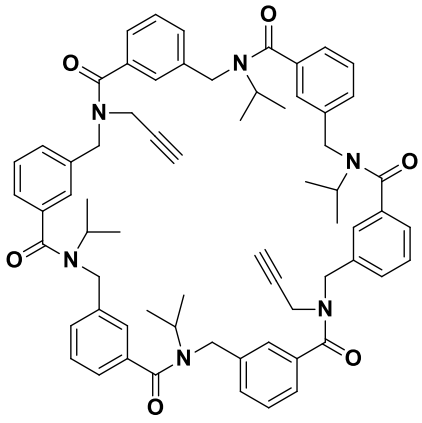

The *meta*-hexamer was dissolved in CH_2Cl_2 (5 mmol/L), then 5 equiv. of DIPEA was added followed by 1.2 equiv. of HATU. The reaction was stirred overnight at RT. The solvent was evaporated under reduced pressure and then the residue was evaporated with CH_2Cl_2 (2*20ml). The residue is then

dissolved in EtOAc (20ml), extracted with $NaHCO_3$ (2*10ml) then brine (1*10ml). The organic layer was dried with $MgSO_4$, then evaporated under reduced pressure. The product was purified on C18 column (Water + 0.1% TFA/ MeOH) affording **IIb** in 81% yield (purity 95%).

HRMS (TOF MS ES+): *m/z* calcd for $C_{66}H_{71}N_6O_6$ $[M+H]^+$: 1043.54296; found: 1043.5427 (-0.23 ppm).

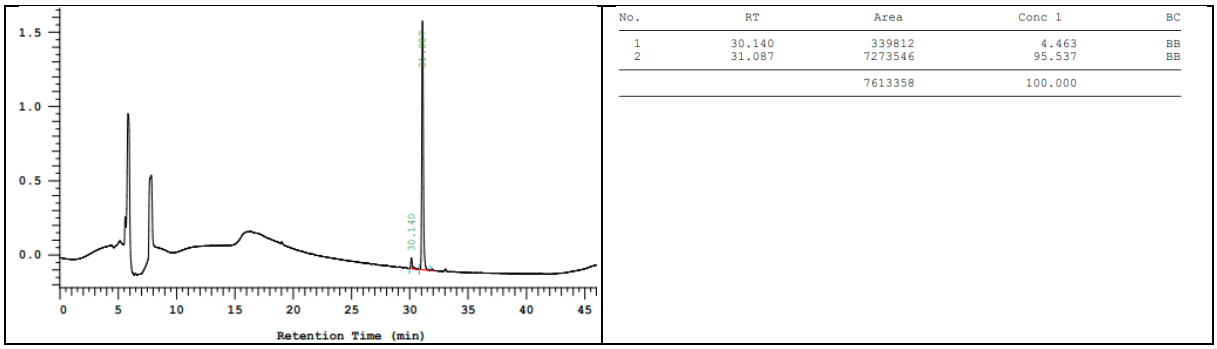

No.	RT	Area	Conc 1	BC
1	30.140	339812	4.463	BB
2	31.087	7273546	95.537	BB
		7613358	100.000	

Figure S243. HPLC of pure *meta*-macrocycle (**IIb**).

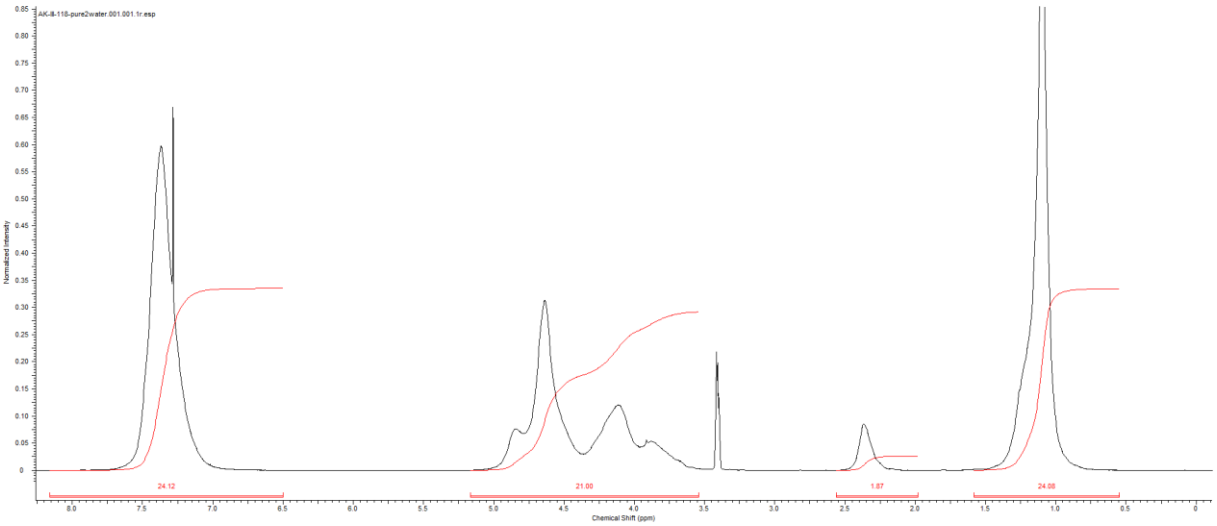

Figure S244. ^{1}H-NMR in $CDCl_3$ of pure *meta*-macrocycle (**IIb**).

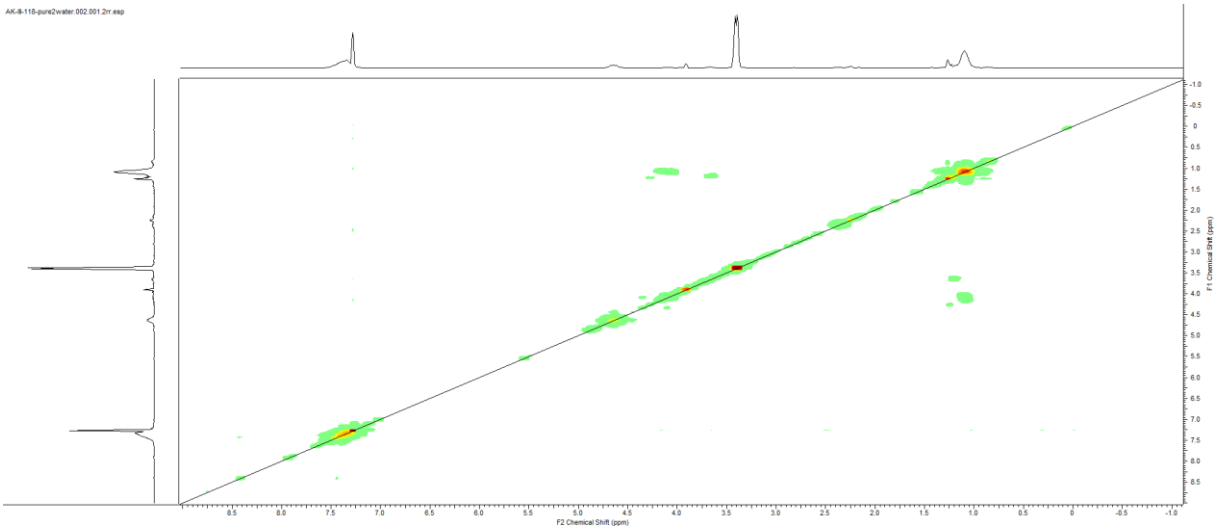

Figure S245. COSY in $CDCl_3$ of pure *meta*-macrocycle (**IIb**).

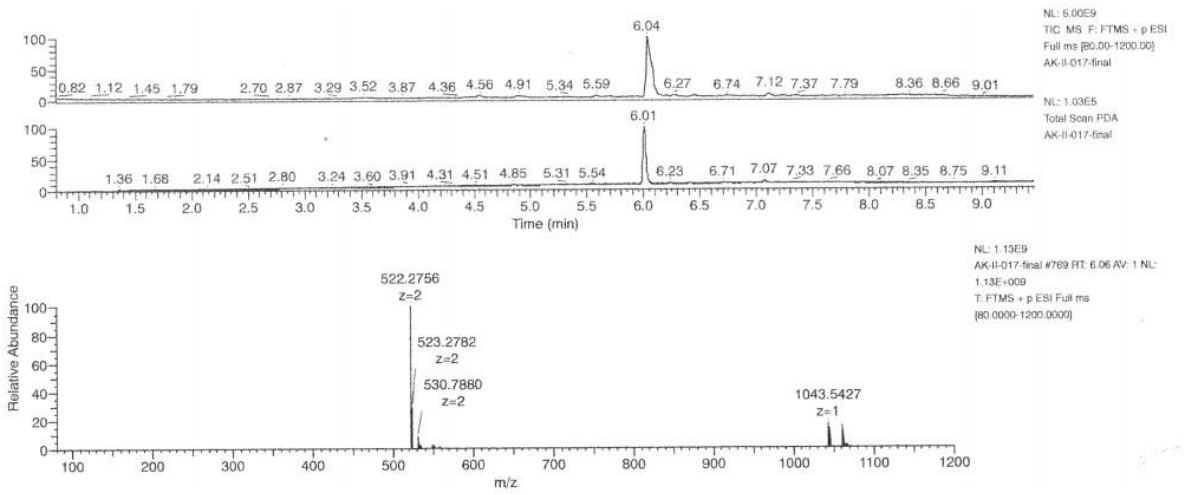

Figure S246. LCMS spectrum of the crude *meta*-macrocycle (**IIb**).

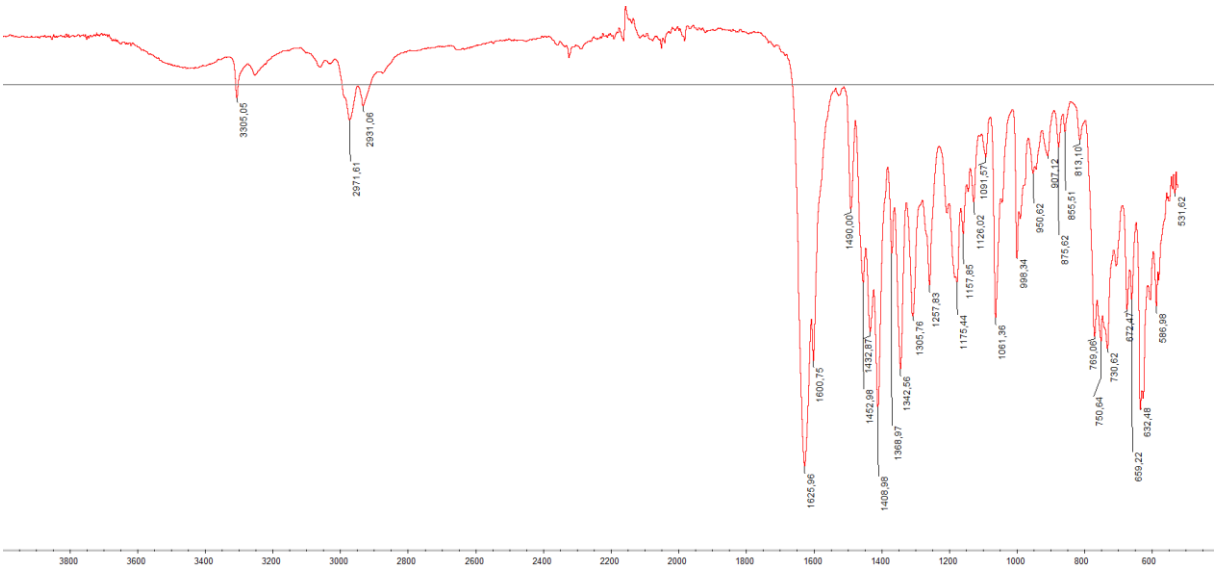

Figure S247. Infra-red of *meta*-macrocycle (**IIb**).

II.3. CuAAC reactions

General procedure :

High dilution procedure: the macrocycle **IIa** or **IIb** (1.0 equiv.) was dissolved in methanol (C = 1.0 mM). 1,4-bis(azidomethyl) benzene and catalyst **III** (10 mol-% per alkyne) were added. The reaction was stirred for 2 days at room temperature and the solvent was evaporated under reduced pressure.

High concentration procedure for ortho compounds: the macrocycle **IIa** was dissolved in methanol/CH_2Cl_2 (1/1) at concentration of 0.1 M. 1,4-bis(azidomethyl) benzene (1.1 equivalent) and catalyst **III** (10 mol-% per alkyne) were added. The reaction was stirred for 2 days at room temperature and the solvent was evaporated under reduced pressure.

High concentration procedure meta compounds **IIb**: the macrocycle **IIb** was dissolved in methanol (C = 0.1 M). 1,4-bis(azidomethyl) benzene (1.1 equivalent) and catalyst **III** (10 mol-% per alkyne) were added. The reaction was stirred for 2 days at room temperature and the solvent was evaporated under reduced pressure.

II.3.a. *Compounds* ***IVa***.

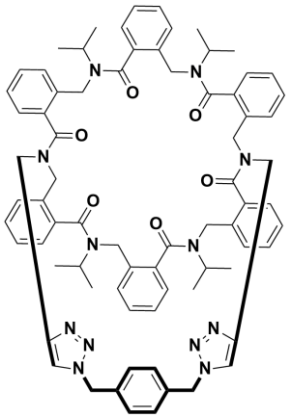

High dilution procedure: performed on 95 mg (0.09 mmol) of **IIa**. HRMS of the crude indicates the presence of crown like **IVa** as major compound and tube like **Va** as traces. The product **IVa** was purified by column chromatography (9/1: EtOAc/MeOH then 95/5 to 7/3: CH_2Cl_2/MeOH) followed by C18 purification (MeOH/H_2O + 0.1%TFA) furnishing 86 mg (98% purity), 78 % yield.

High concentration procedure: performed on 50 mg (0.045 mmol) of **Ia**. HRMS of the crude also indicates the presence of crown-like **IVa** as major compound and tube like **Va** as traces. The product **IVa** was purified by column chromatography (9/1: EtOAc/MeOH then 95/5 to 7/3: CH_2Cl_2/MeOH) followed by C18 purification (MeOH/H_2O + 0.1%TFA) furnishing 40 mg (98% purity), 76 % yield.

HRMS (TOF MS ES+): *m/z* calcd for $C_{74}H_{79}N_{12}O_6$ $[M+H]^+$: 1231.624; found: 1231.6248 (0.61 ppm)

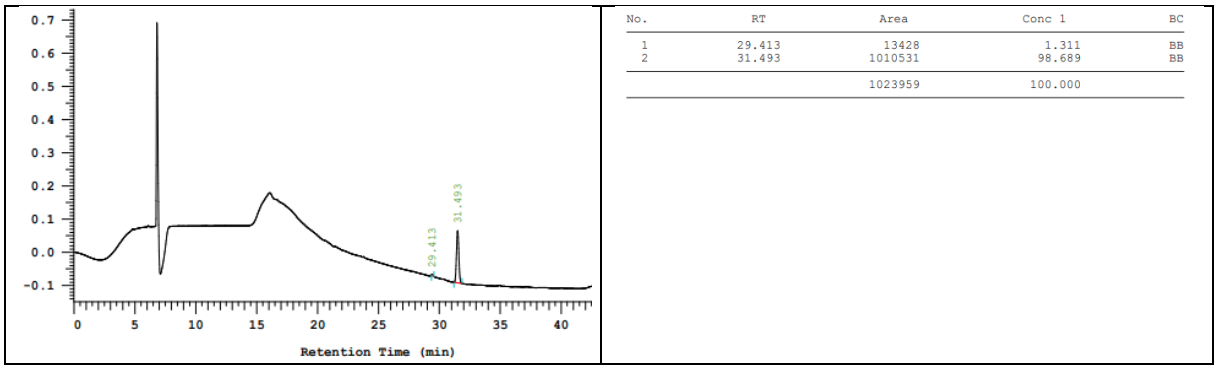

No.	RT	Area	Conc 1	BC
1	29.413	13428	1.311	BB
2	31.493	1010531	98.689	BB
		1023959	100.000	

Figure S248. HPLC of the pure *Ortho*-Crown-like **IVa**.

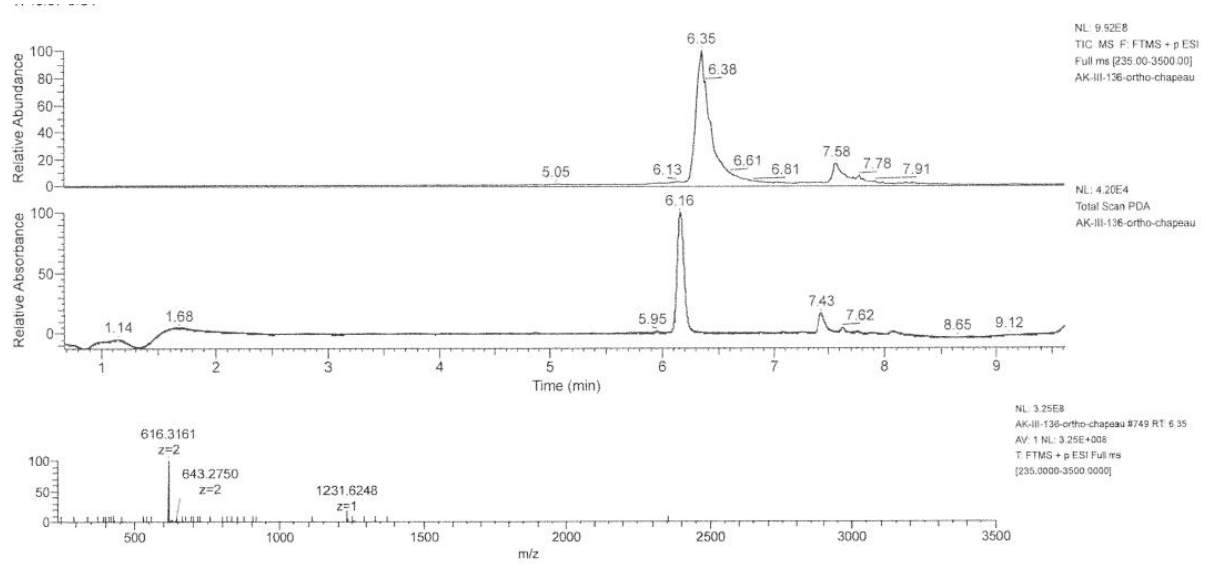

Figure S249 : spectra of the pure *Ortho*-Crown-like **IVa**.

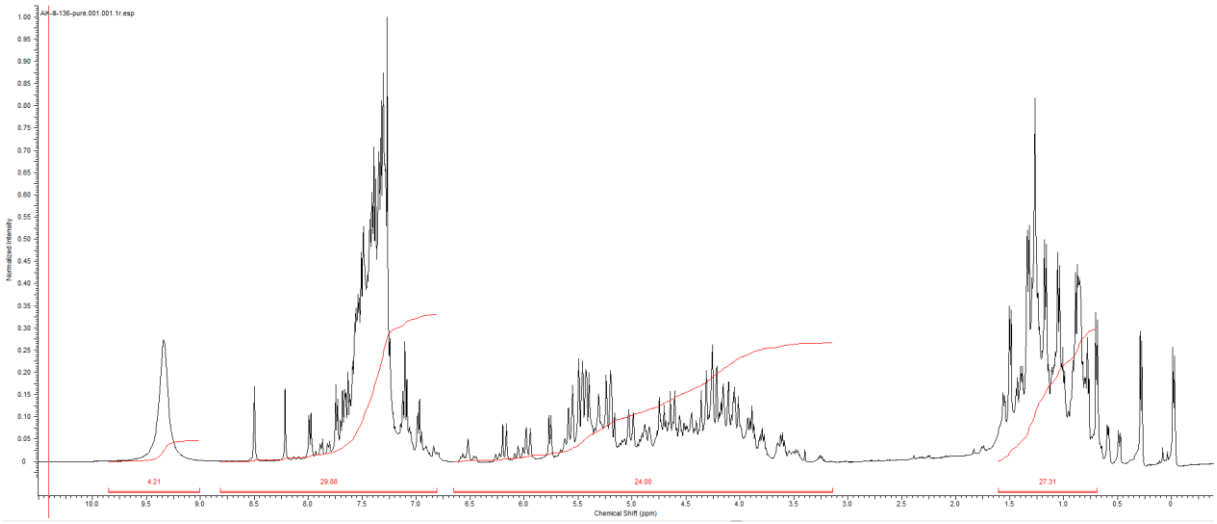

Figure S250 ^{1}H-NMR in $CDCl_3$ of the pure *Ortho*-Crown-like **IVa**.

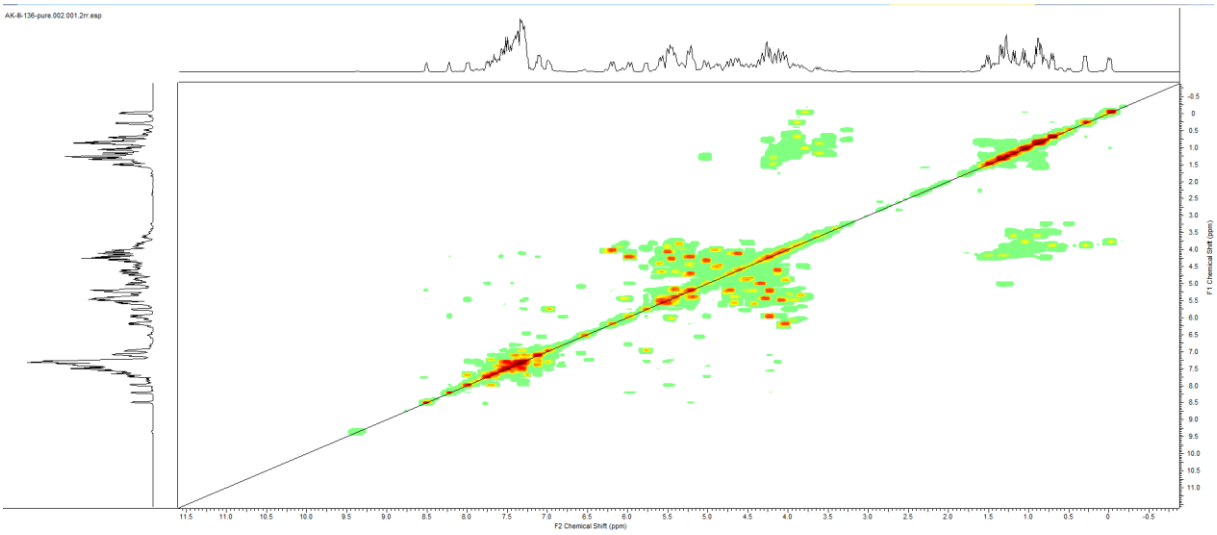

Figure S251 : COSY in $CDCl_3$ of the pure *Ortho*-Crown-like **Iva**.

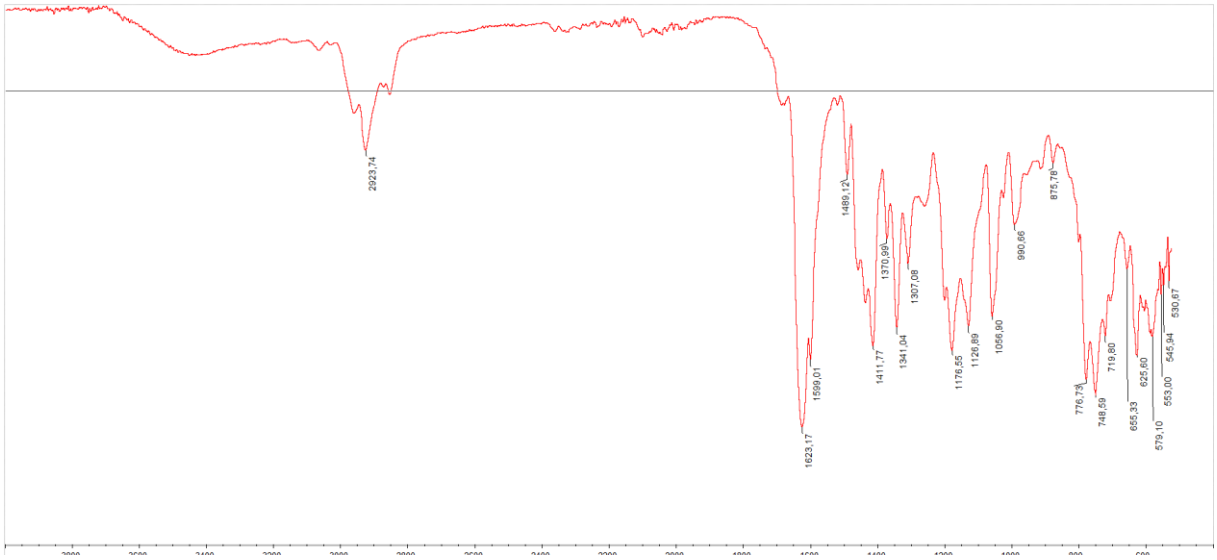

Figure S252. Infra-red of *Ortho*-Crown-like **IVa**.

*II.3.b. Compounds **IVb** and **Vb**.*

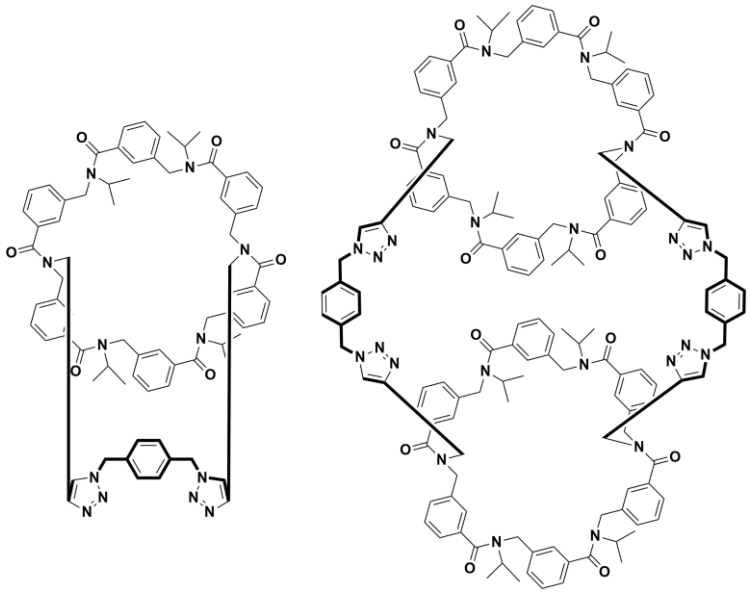

High dilution procedure: performed on 200 mg (0.19 mmol) of **Ib** furnishing 103 mg (98% purity), 44 % yield of crown-like and 88mg **IVb** (98.5% purity), 37% yield of tube like **Vb** structures.

High concentration procedure: performed on 100 mg (0.1 mmol) of **Ib** furnishing 48 mg (98% purity), 39 % yield of crown-like **IVb** and 50mg (98% purity), 41 % yield of tube like **Vb** structures.

Purification procedure: The products were purified by column chromatography (9/1: EtOAc/MeOH then 95/5 to 7/3: CH_2Cl_2/MeOH) affording mixture of crown-like **IVb** and tube like **Vb** Further C18 purification (MeOH/H_2O + 0.1%TFA)

IVb:

HRMS (TOF MS ES+): *m/z* calcd for $C_{74}H_{79}N_{12}O_6$ $[M+H]^+$: 1231.624; found: 1231.6257 (1.4 ppm).

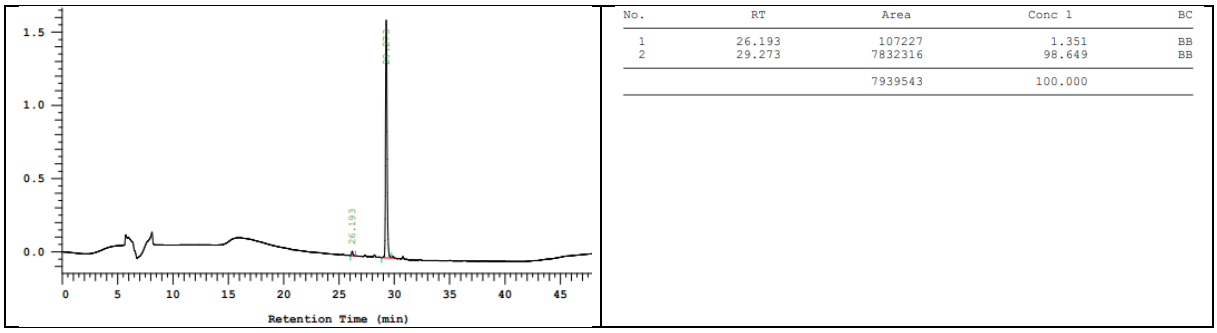

No.	RT	Area	Conc 1	BC
1	26.193	107227	1.351	BB
2	29.273	7832316	98.649	BB
		7939543	100.000	

Figure S253. HPLC chromatogram of the pure *Meta*-Crown-like **IVb**.

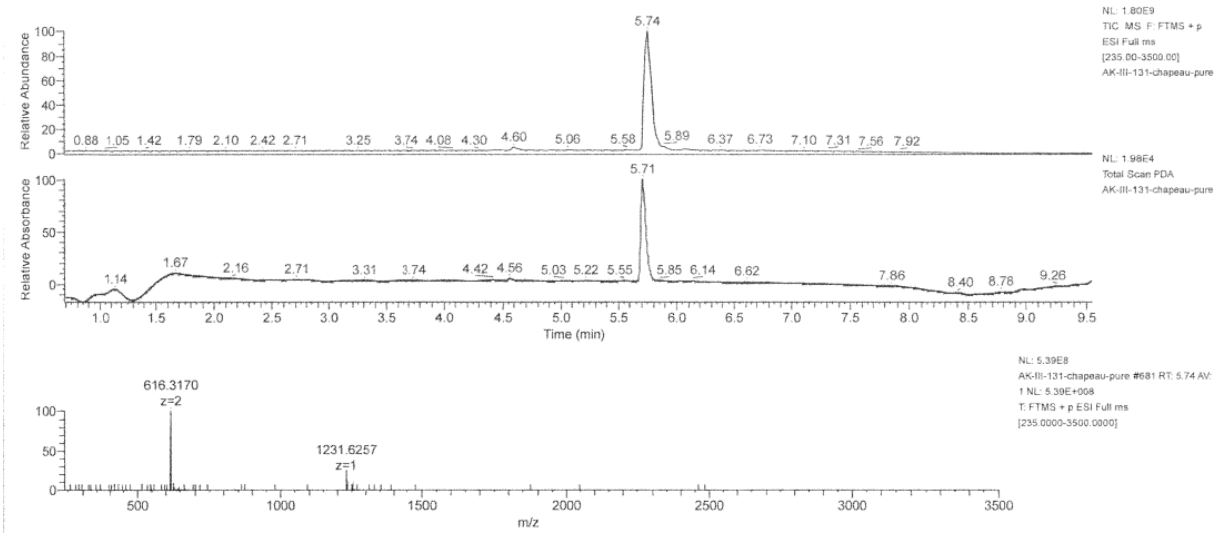

Figure S254. LCMS spectrum of crude *Meta*-Crown-like **IVb**.

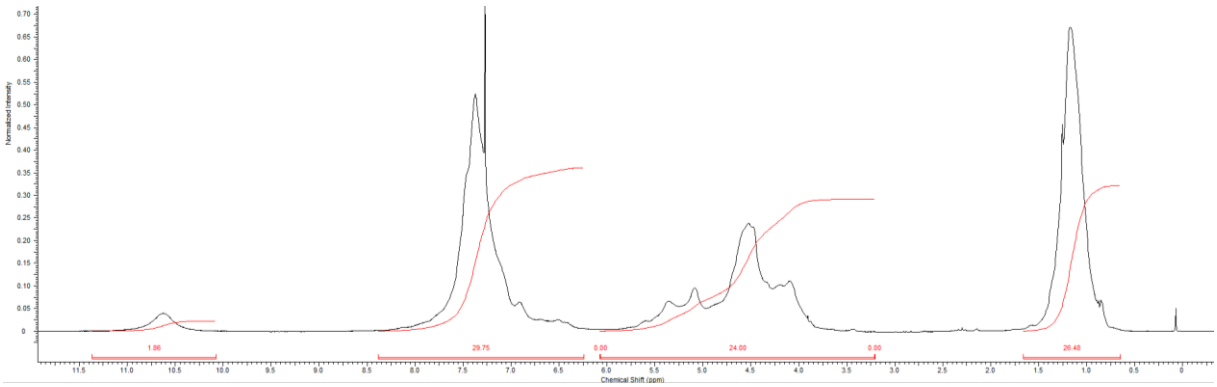

Figure S255. ^{1}H-NMR in $CDCl_3$ of the pure *Meta*-Crown-like **IVb**.

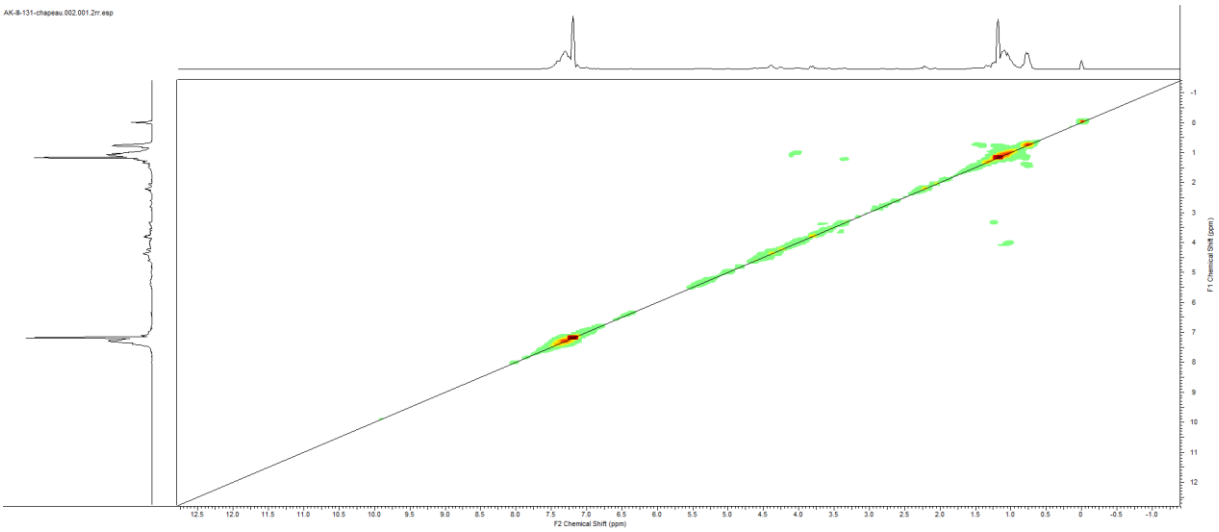

Figure S256. COSY in $CDCl_3$ of the pure *Meta*-Crown-like **IVb**.

Figure S257. Infra-red of *Meta*-Crown-like **IVb**.

Vb.

HRMS (TOF MS ES+): *m/z* calcd for $C_{148}H_{158}N_{24}O_{12}$ $[M+2H]^{2+}$: 1231.624; found: 1231.6252 (1.01 ppm).

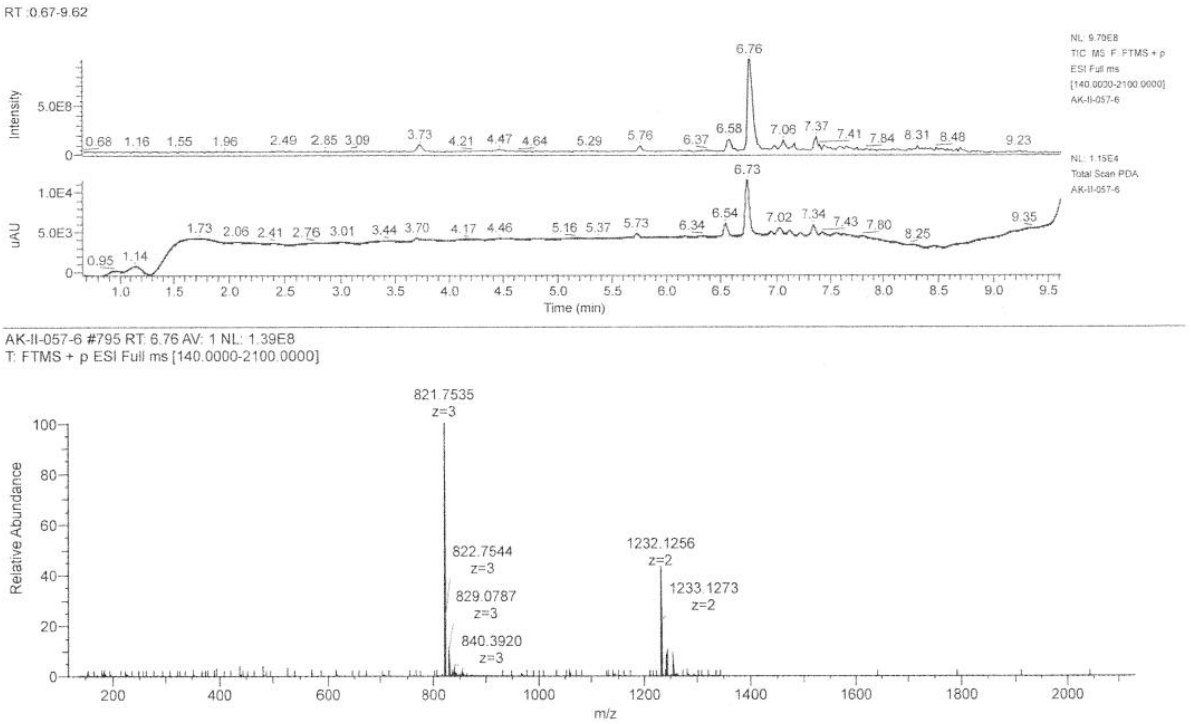

Figure S258. LCMS of the pure *Meta*-Tube-like **Vb.**

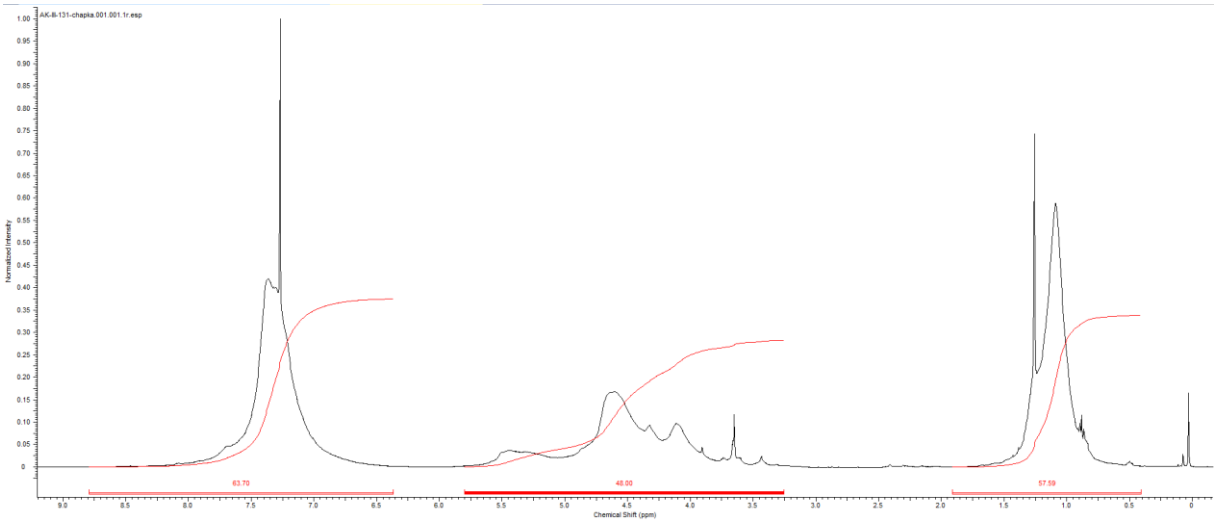

Figure S259. ^{1}H-NMR in $CDCl_3$ of the pure *Meta*-Tube-like **Vb**.

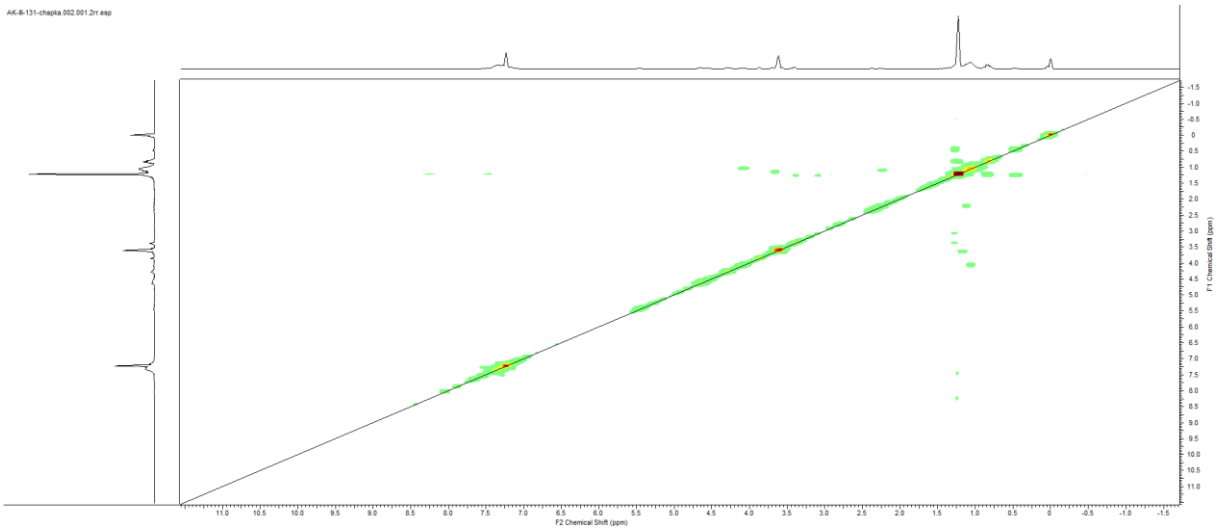

Figure S260. COSY in $CDCl_3$ of the pure *Meta*-Tube-like **Vb**.

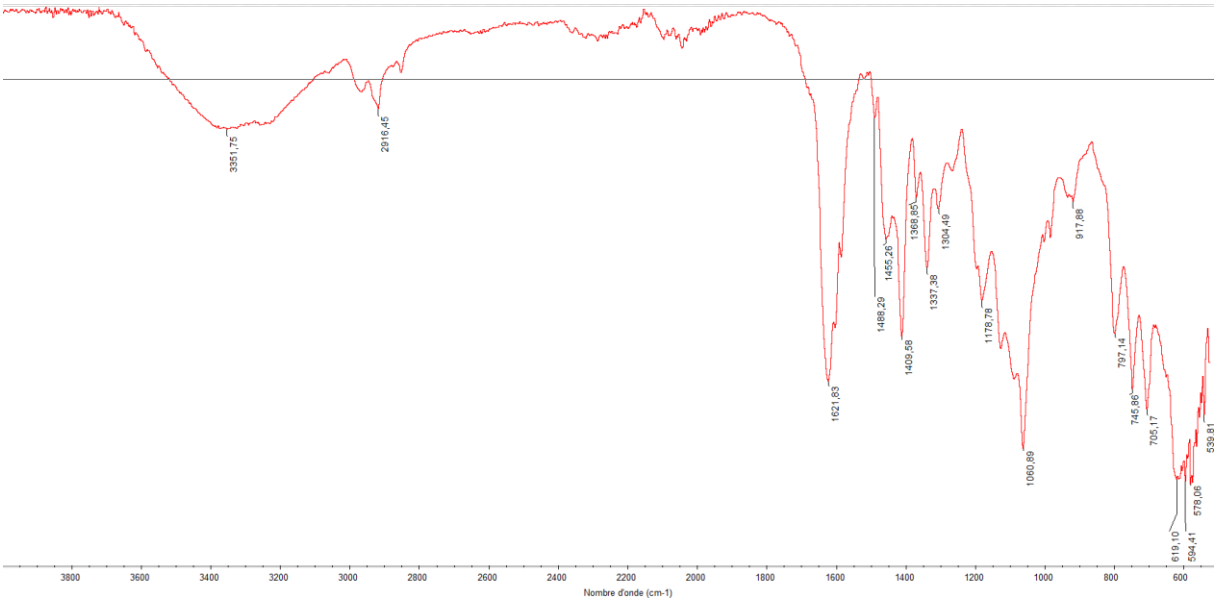

Figure S261. Infra-red of pure *Meta*-Tube-like **Vb**.

II.4. Methylation

The methylation of crown-like compounds I**Va** and I**Vb** was performed in ace pressure tube in pure MeI at 70°C, for 24 hours and produces the double methylated products **VIa** and **VIb** in quantitative yields.

*II.4.a. Ortho crown-like triazolium **VIa**.*

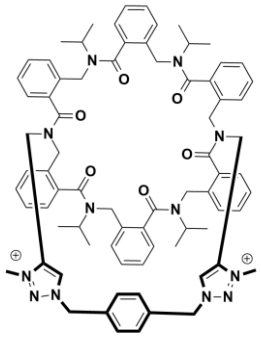

HRMS (TOF MS ES+): *m/z* calcd for $C_{76}H_{84}N_{12}O_6$ $[M]^{2+}$: 630.33129; found: 630.3325 (1.95 ppm).

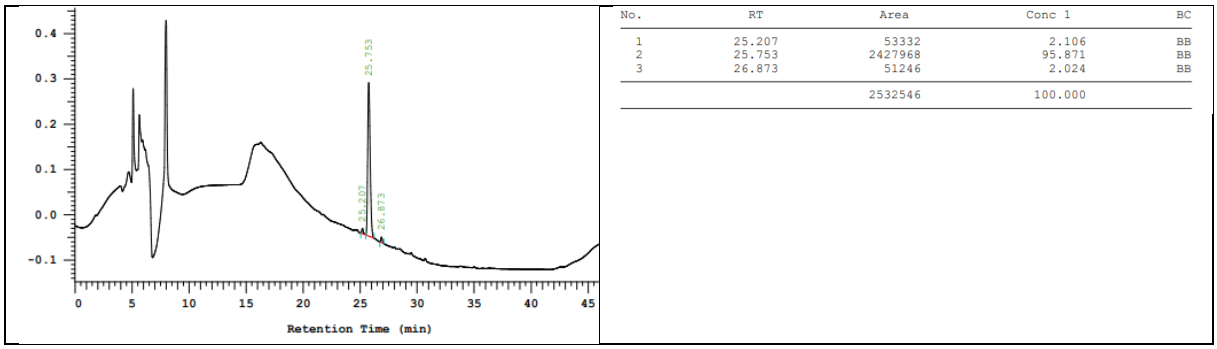

No.	RT	Area	Conc 1	BC
1	25.207	53332	2.106	BB
2	25.753	2427968	95.871	BB
3	26.873	51246	2.024	BB
		2532546	100.000	

Figure S262. HPLC of the crude *ortho* crown-like triazolium **VIa**.

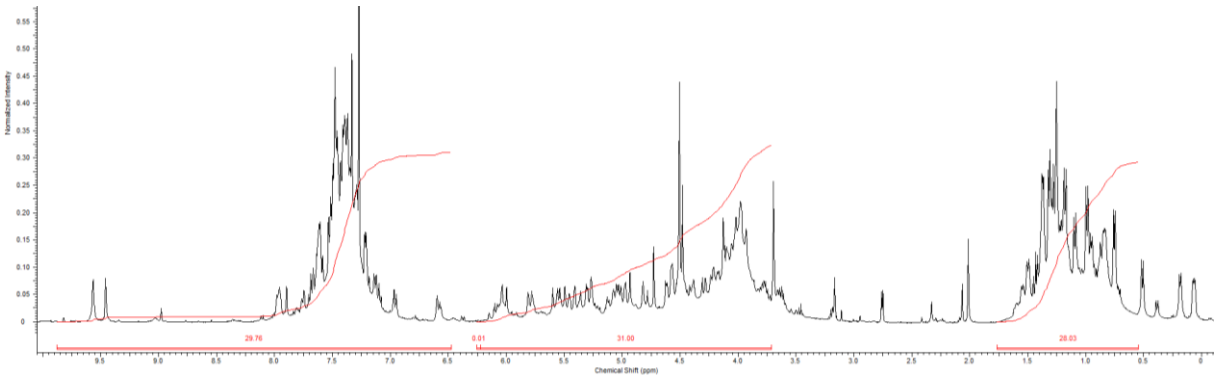

Figure S263. ^{1}H-NMR in $CDCl_3$ of the crude *ortho* crown-like triazolium **VIa**.

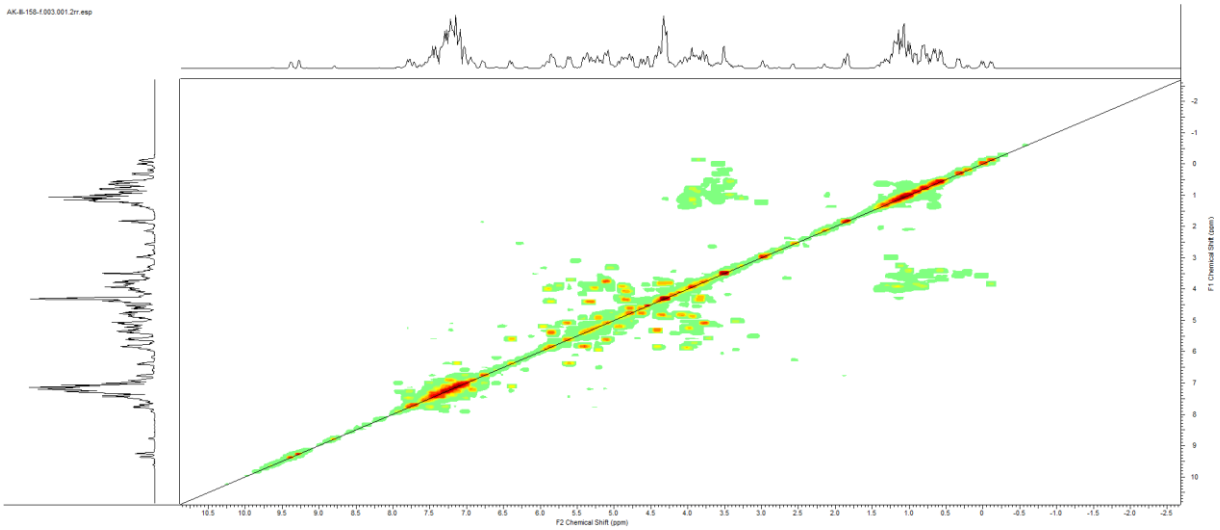

Figure S264 COSY in $CDCl_3$ of the crude *ortho* crown-like triazolium **VIa**.

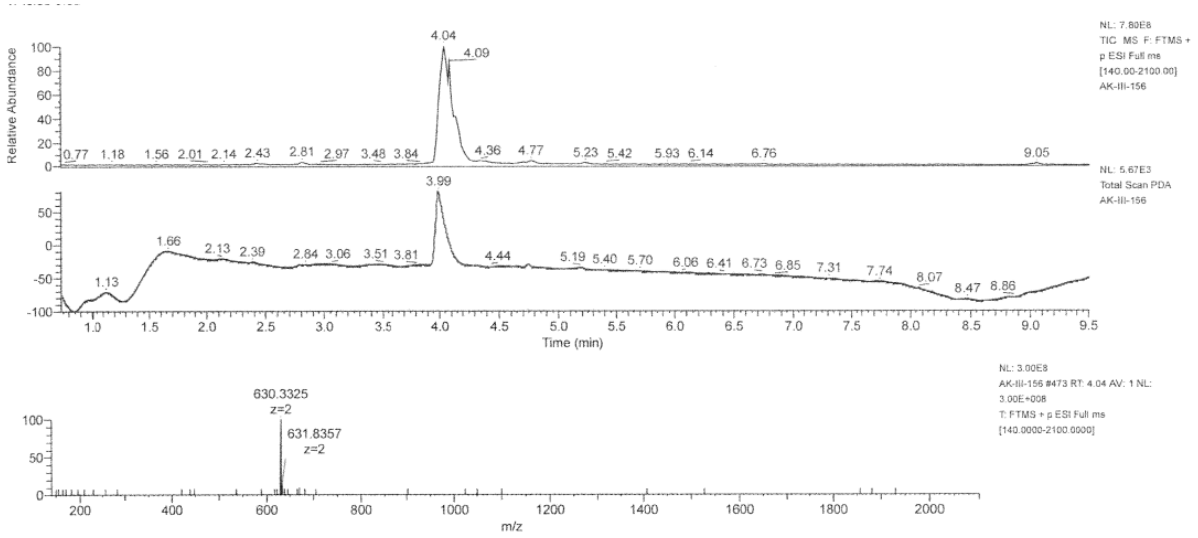

Figure S265 LCMS of the crude *ortho* crown-like triazolium **VIa**.

II.4.b.Meta-crown-like triazolium ***VIb****.*

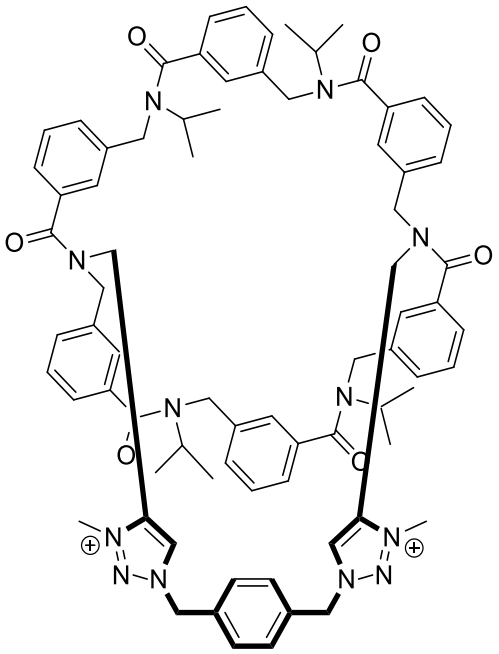

m_{crude} = 40 mg, (purity 96%), isolated yield 98%

HRMS (TOF MS ES+): *m/z* calcd for $C_{82}H_{90}N_{12}O_6$ $[M]^{2+}$: 669.35477; found: 669.3538 (-1.41 ppm).

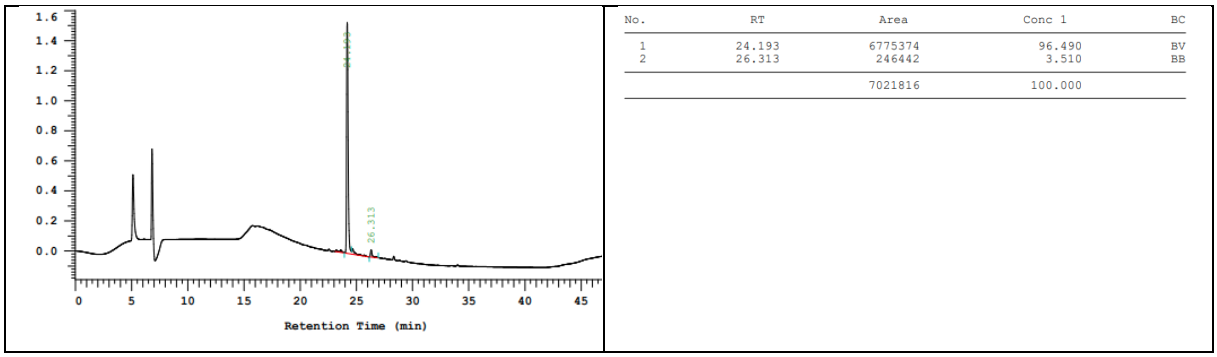

No.	RT	Area	Conc 1	BC
1	24.193	6775374	96.490	BV
2	26.313	246442	3.510	BB
		7021816	100.000	

Figure S266. HPLC chromatogram of *Meta*-crown-like triazolium **VIb**.

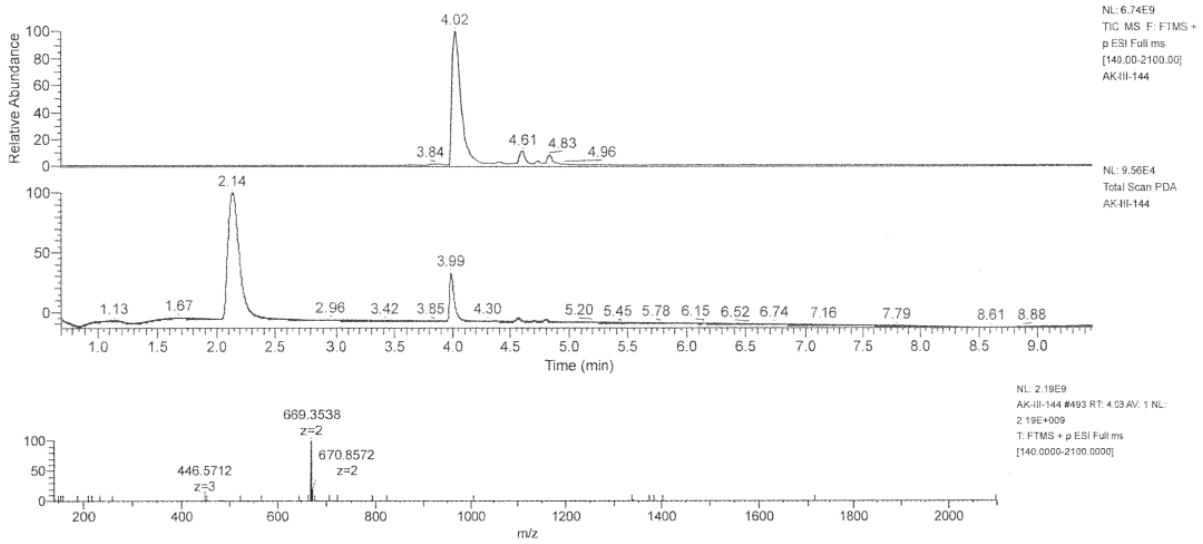

Figure S267. LCMS spectrum of *Meta*-crown-like triazolium **VIb**.

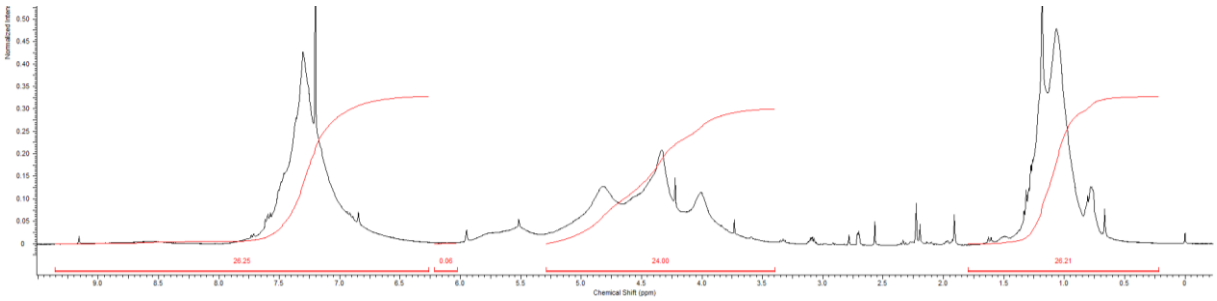

Figure S268. ^{1}H-NMR in $CDCl_3$ of the pure *Meta*-crown-like triazolium **VIb**.

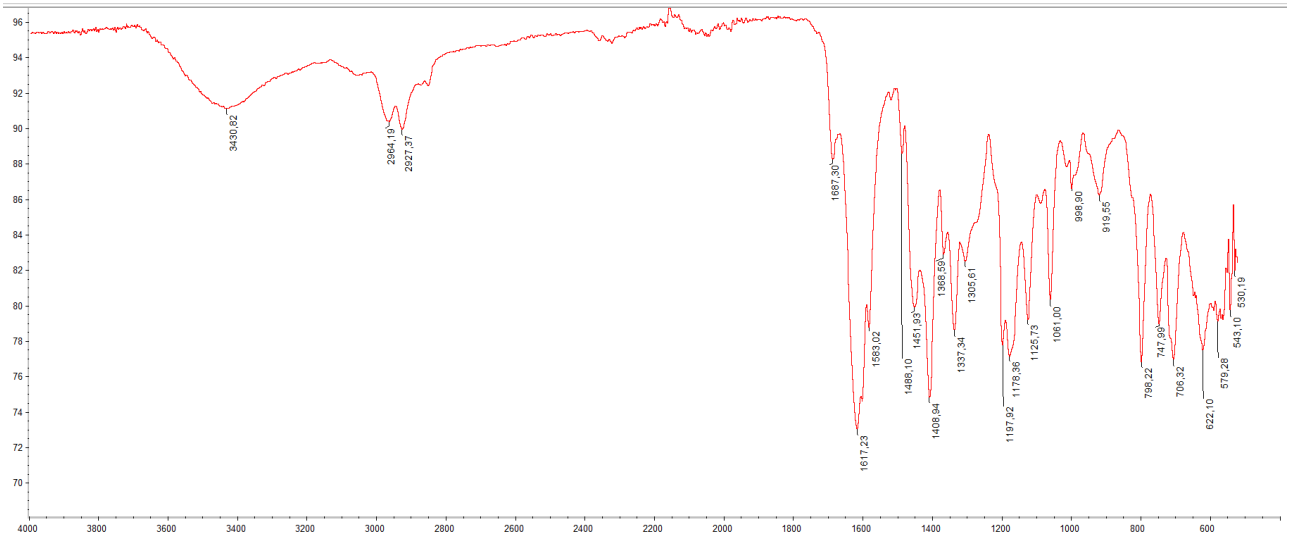

Figure S269. Infra-red of *Meta*-crown-like triazolium **VIb**.

IV.Extension of the publication.

IV.1. Click of BnN3

The macrocycle **Ib** was introduced into round bottom flask containing methanol (0.5 mM). Benzyl azide (2.2 equivalence) and 10 mol% of catalyst per alkyne were added. The reaction was stirred for 2 days at room temperature, then the solvent was evaporated to dryness under reduced pressure. The

product then was purified by column chromatography (95/5: EtOAc/MeOH) then (95/5: CH_2Cl_2/MeOH), followed by Buchi LC automatic C18 column and collected as pure macrocycle with 80% isolated yield.

The reaction results in 2 products: the expected bis-triazole in 70% ratio and a linked bis-triazole **V.2** in 30 % ratio (by HPLC and LCMS)

The macrocycle **Ib** was introduced into round bottom flask containing methanol (0.5 mM). Benzyl azide (2.2 equivalence) and 10 mol% of catalyst per alkyne were added. The reaction was stirred for 2 days at room temperature, then the solvent was evaporated to dryness under reduced pressure. The product then was purified by column chromatography (95/5: EtOAc/MeOH) then (95/5: CH_2Cl_2/MeOH), followed by Buchi LC automatic C18 column and collected as pure macrocycle with 80% isolated yield.

The reaction results in 2 products: the expected bis-triazole in 70% ratio and a linked bis-triazole **V.2** in 30 % ratio (by HPLC and LCMS)

IV.1.a. ***V.1.***

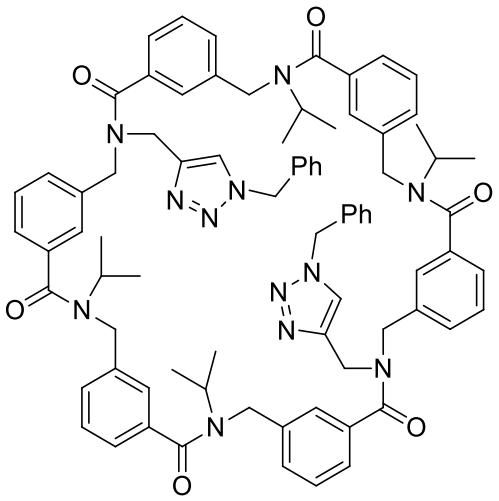

m_{pure}= 138 mg (purity 95%), isolated yield 56% (200 mg starting material)

HRMS (TOF MS ES+): *m/z* calcd for $C_{80}H_{84}N_{12}O_6$ $[M+2H]^{2+}$: 655.33912; found: 655.3386 (-0.84 ppm).

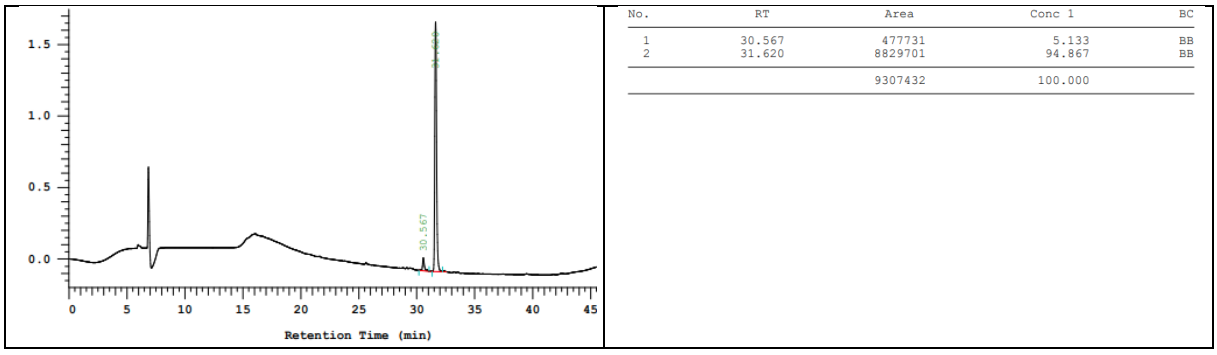

Figure S270. HPLC chromatogram of the pure bis-triazole **V.1**.

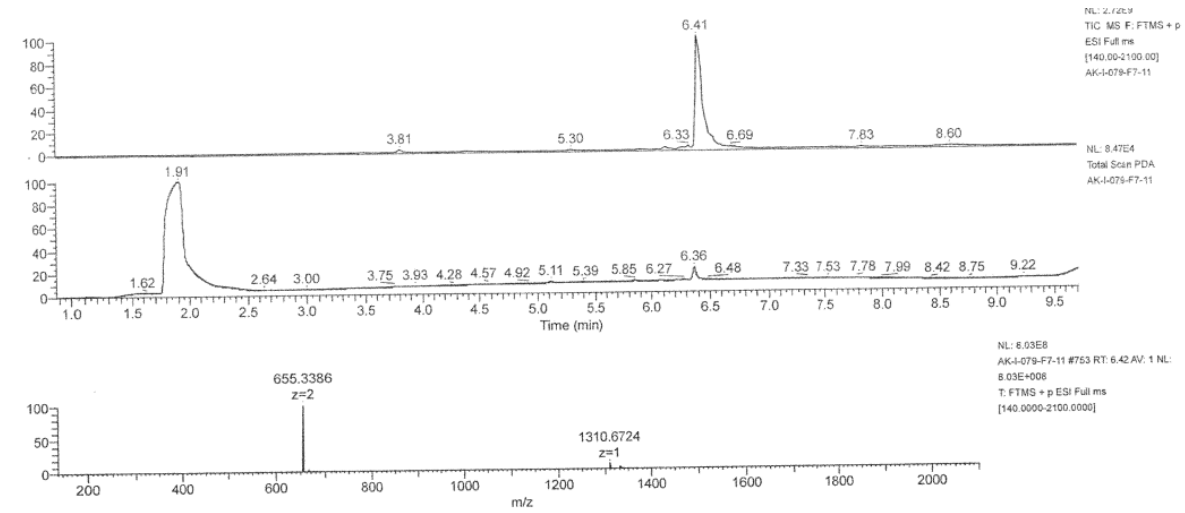

Figure S271. LCMS spectrum of pure bis-triazole **V.1**.

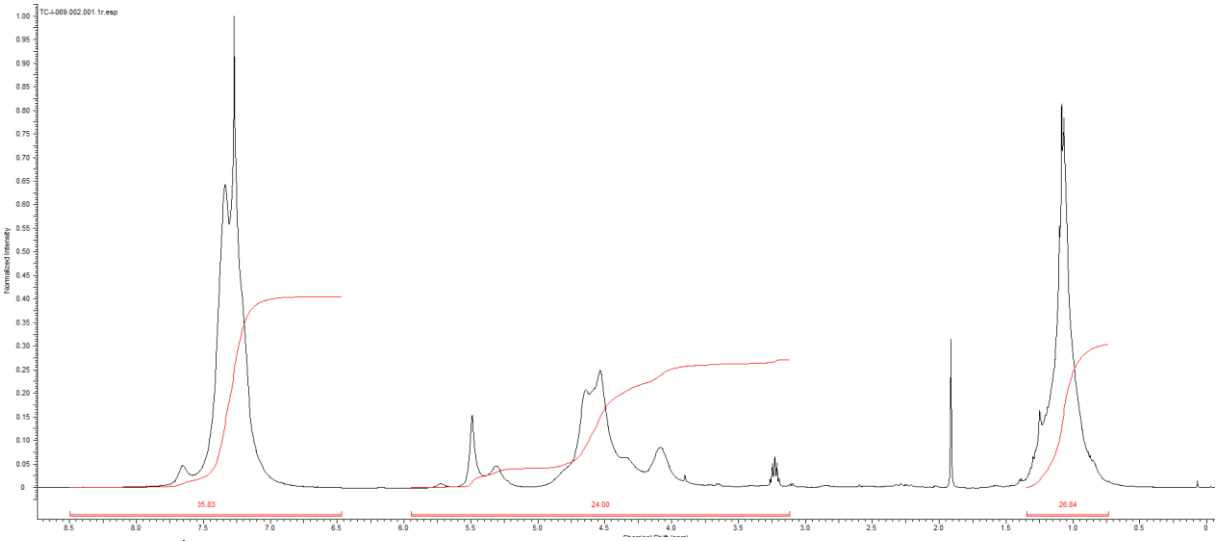

Figure S272. ^{1}H-NMR in $CDCl_3$ of pure bis-triazole **V.1**.

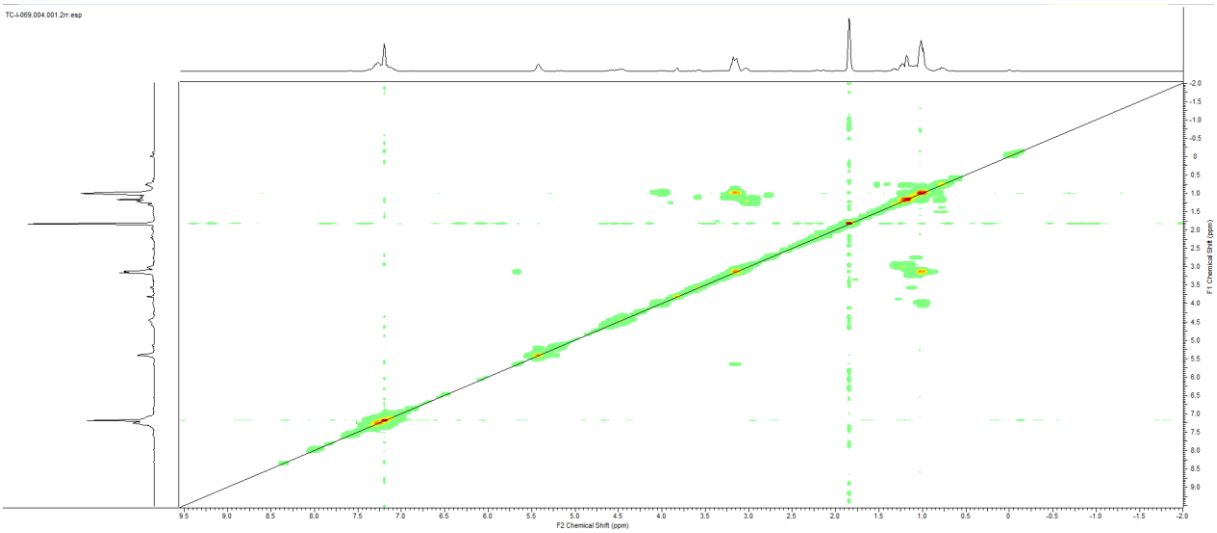

Figure S273. COSY in $CDCl_3$ of bis-triazole **V.1**.

IV.1.b. ***V.2.***

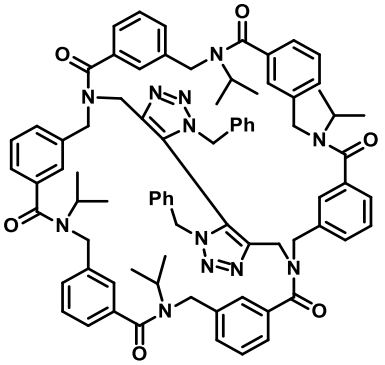

Chemical Formula: $C_{80}H_{82}N_{12}O_6$
Exact Mass: 1306,65
Molecular Weight: 1307,61

m_{pure}= 32.8 mg (purity 95%), isolated yield 13. 2 % (200 mg starting material)

HRMS (TOF MS ES-): *m/z* calcd for $C_{80}H_{82}N_{12}O_7$ $[M+OH]^-$: 1323.65022; found: 1323.6512 (0.77 ppm).

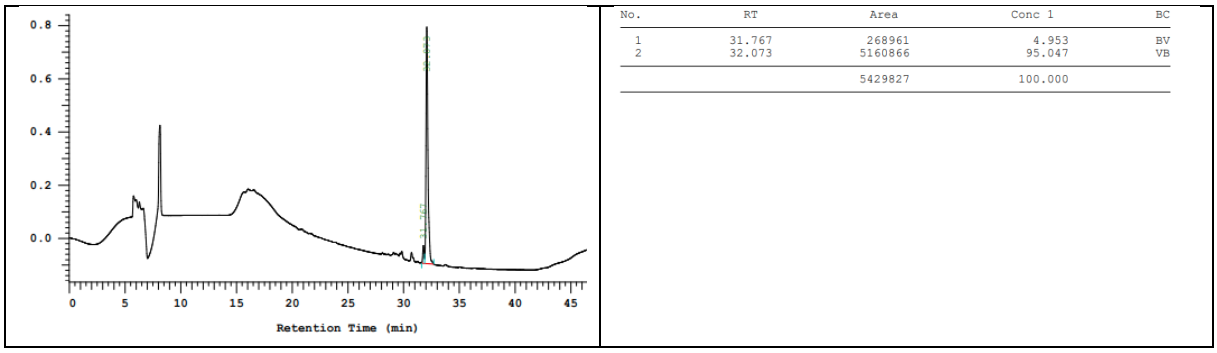

No.	RT	Area	Conc 1	BC
1	31.767	268961	4.953	BV
2	32.073	5160866	95.047	VB
		5429827	100.000	

Figure S274. HPLC of the pure linked-bistriazole **V.2**.

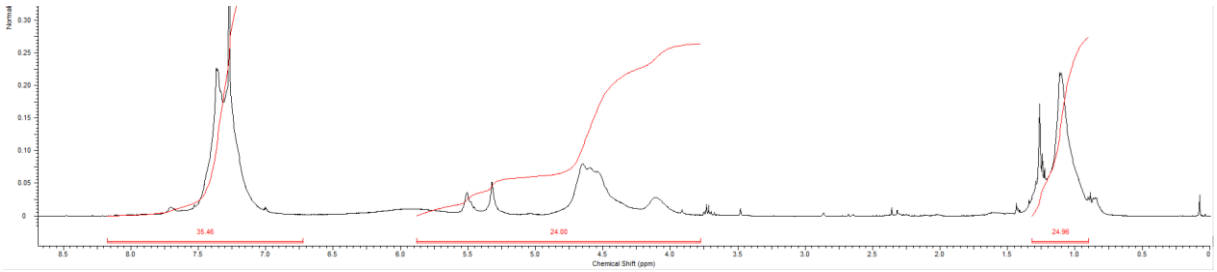

Figure S275. ^{1}H-NMR in $CDCl_3$ of the pure linked-bistriazole **V.2**.

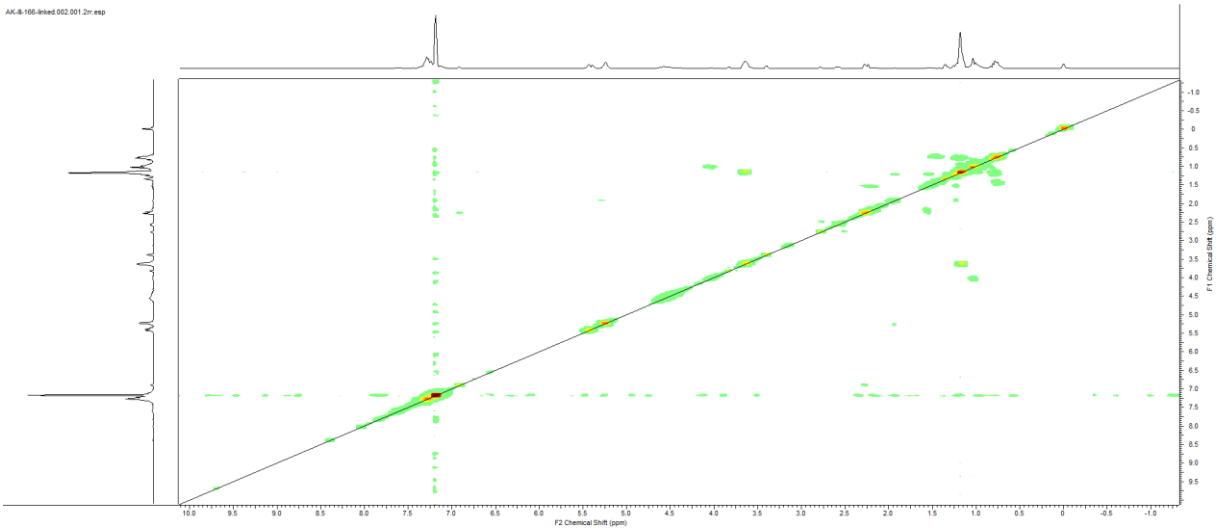

Figure S276. COSY in $CDCl_3$ of the linked-bistriazole **V.2**.

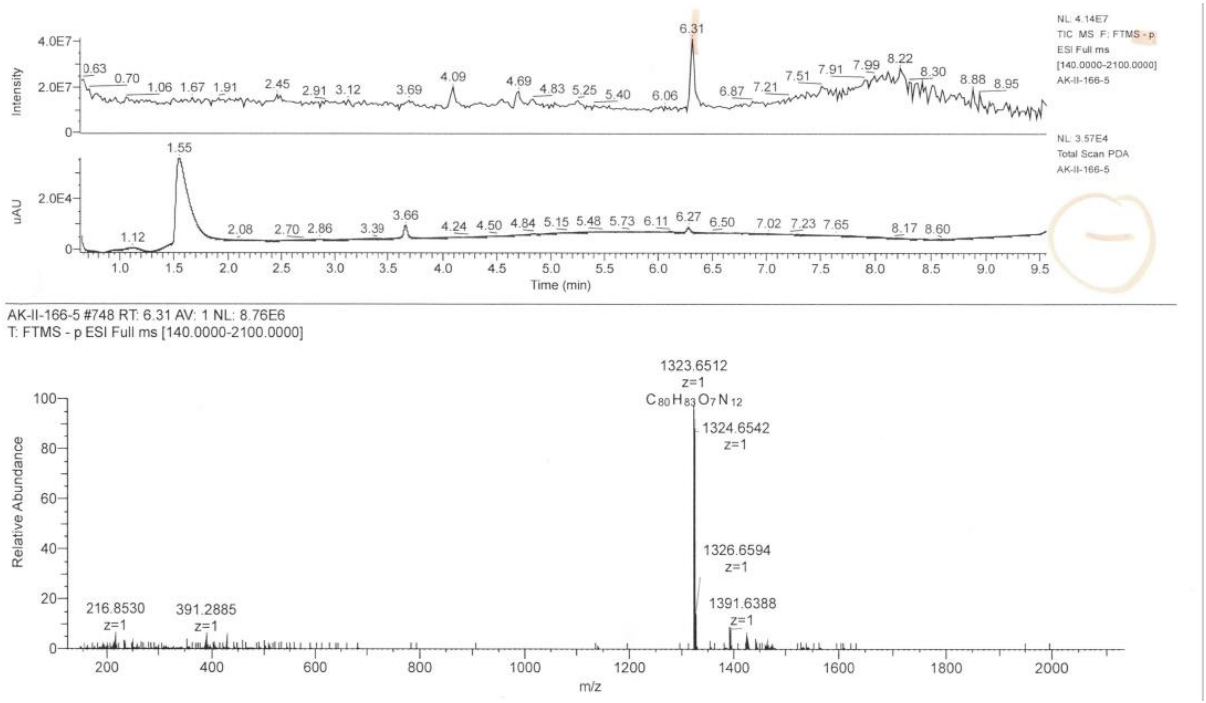

Figure S277. LCMS spectrum of the pure linked-bistriazole **V.2**.

IV.1.c. ***V.3.***

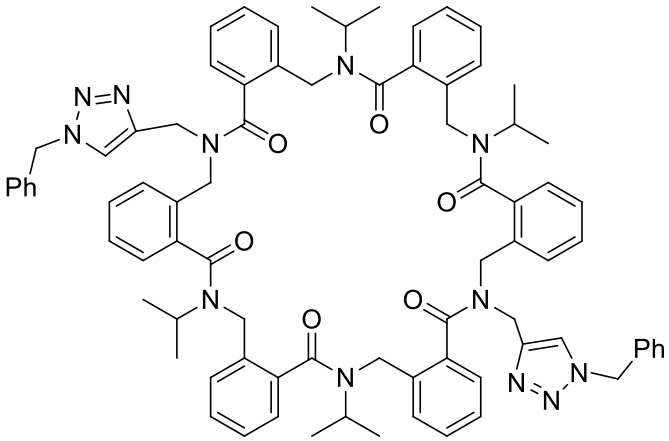

V.3 was synthesized using the same procedure.

m_{pure}= 170 mg (purity 93%), isolated yield 90% (starting from 150 mg macrocycle)

HRMS (TOF MS ES+): *m/z* calcd for $C_{80}H_{84}N_{12}O_6$ $[M+H]^+$: 1309.67095; found: 1309.6718 (0.61 ppm).

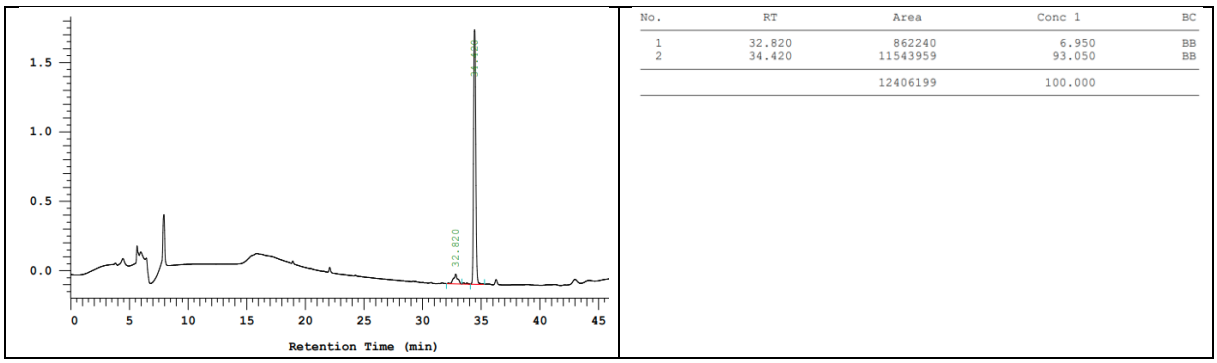

Figure S278. HPLC chromatogram of pure *ortho*-bistriazole **V.3**.

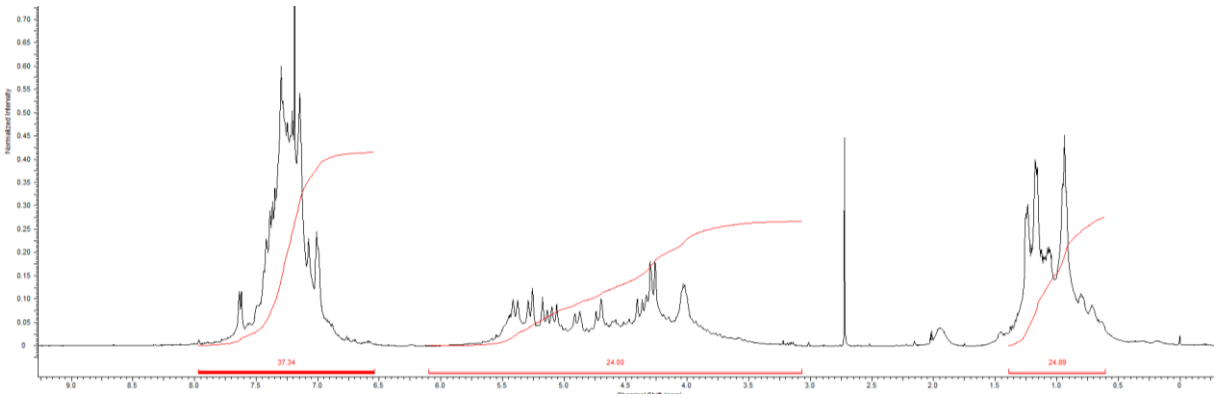

Figure S279. ^{1}H-NMR in $CDCl_3$ of the pure *ortho*-bistriazol **V.3**.

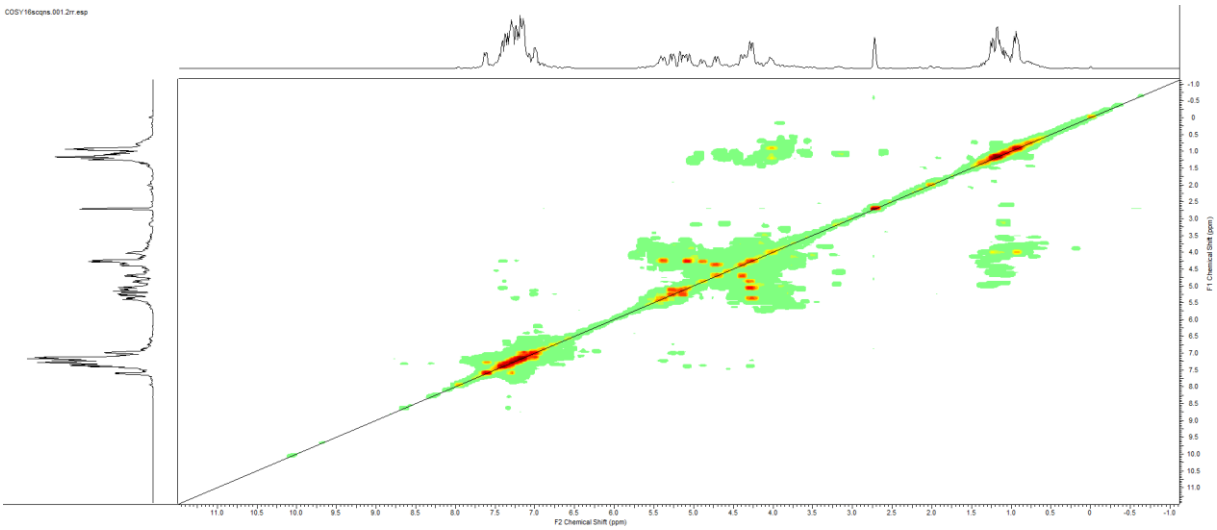

Figure S280. COSY in $CDCl_3$ of the pure *ortho*-bistriazol **V.3**.

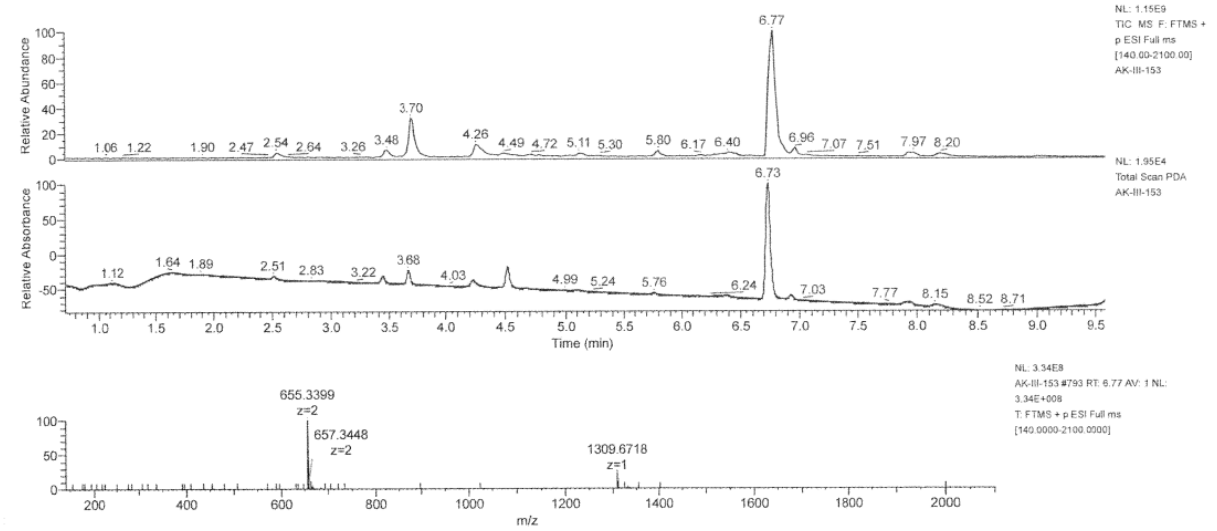

Figure S281. LCMS spectrum of the pure *ortho*-bistriazol **V.3**.

IV.2. Crown-like and Tube-like using 9,10-bis(azidomethyl)anthracene

Purification procedure: HRMS indicates the presence of crown like **V.4** as major compound and tube like **V.5** as traces. The product then was purified by column chromatography (9/1: EtOAc/MeOH then 95/5 to 7/3: CH_2Cl_2/MeOH) followed by C18 purification (MeOH/H_2O + 0.1%TFA)

High dilution conditions: performed on 160 mg (0.15 mmol) of **Ia** furnishing 115 mg (94% purity), 57 % yield.

High concentration procedure: performed on 28 mg (0.0268 mmol) of **Ia** furnishing 28 mg (94% purity), 80 % yield.

IV.2.a. ***V.4.***

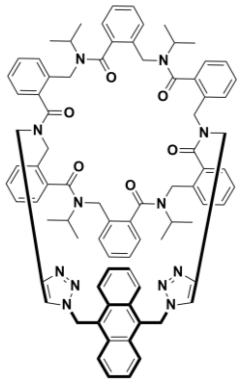

HRMS (TOF MS ES+): *m/z* calcd for $C_{82}H_{83}N_{12}O_6$ $[M+H]^+$: 1331.6553; found: 1331.657 (1.26 ppm)

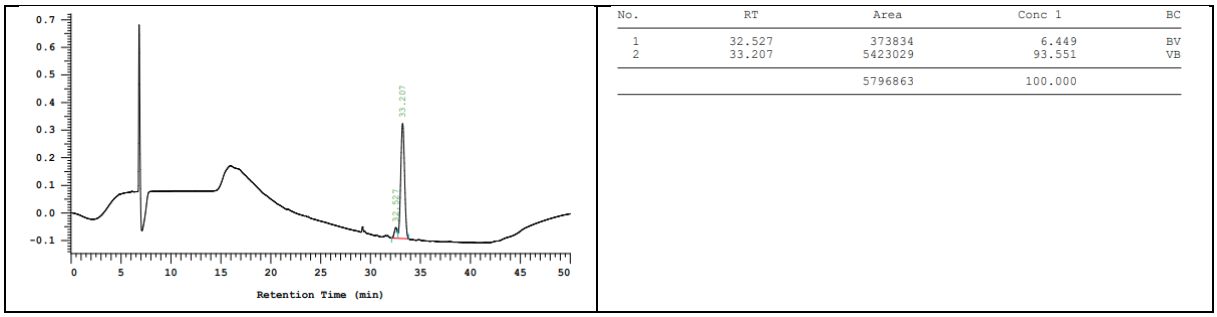

No.	RT	Area	Conc 1	BC
1	32.527	373834	6.449	BV
2	33.207	5423029	93.551	VB
		5796863	100.000	

Figure S282. HPLC chromatogram of the pure *Ortho*-Crown-like **V.4**.

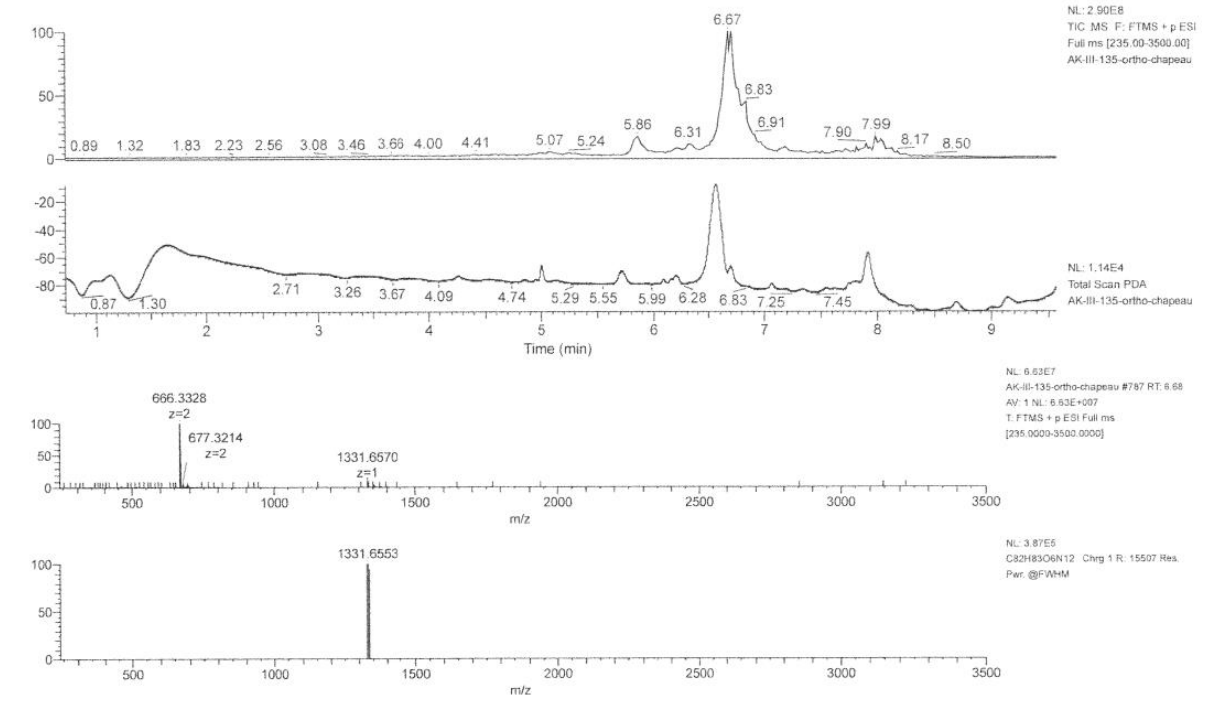

Figure S283. spectra of the pure *Ortho*-Crown-like **V.4**.

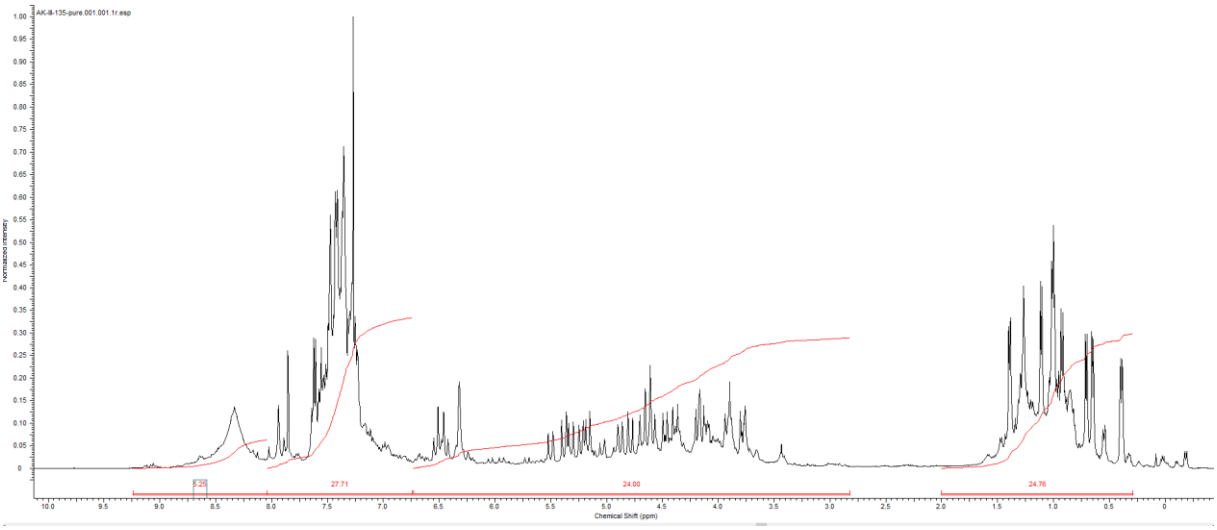

Figure S284. ^{1}H-NMR in $CDCl_3$ of the pure *Ortho*-Crown-like **V.4**.

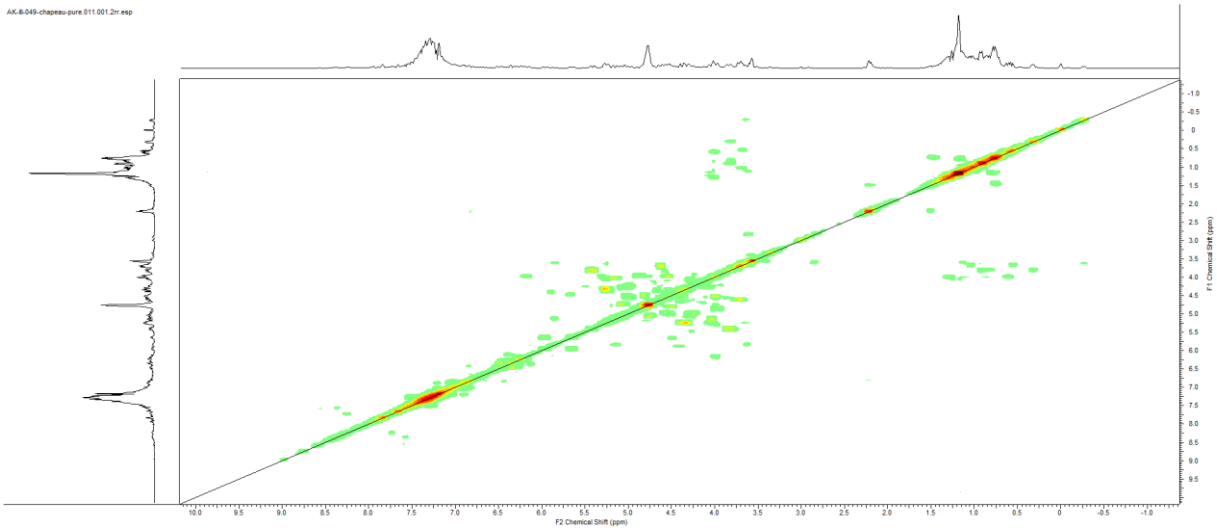

Figure S285. COSY in $CDCl_3$ of the pure *Ortho*-Crown-like **V.4**.

*IV.2.b. Compounds **V.6** and **V.7**.*

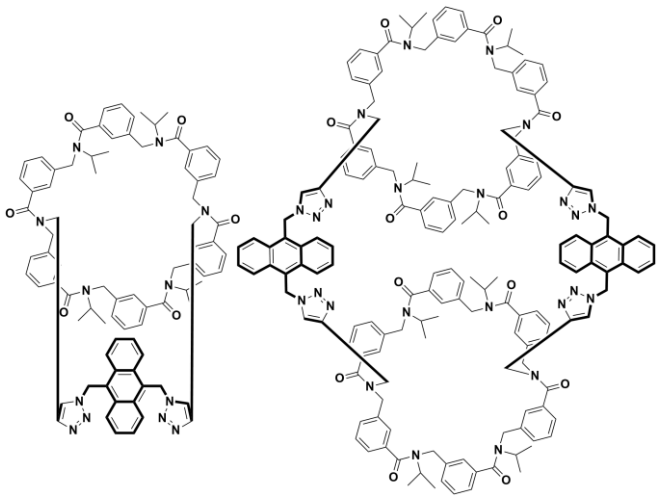

Purification procedure: the products were purified by column chromatography (9/1: EtOAc/MeOH then 95/5 to 7/3: CH_2Cl_2/MeOH) affording mixture of crown-like **V.6** and tube like **V.7**. Further automatic LC C18 purification (MeOH/H_2O + 0.1%TFA)

High dilution procedure: performed on 200 mg (0.19 mmol) of **Ib** furnishing 97 mg (96% purity), 38 % yield of crown-like and 92mg (96% purity), 36% yield of tube like structures.

High concentration procedure: performed on 100 mg (0.1 mmol) of **Ib** furnishing 49 mg (96% purity), 37 % yield of crown-like **V.6** and 52 mg, 39% yield of tube like **V.7** structures.

V.6:

HRMS (TOF MS ES+): *m/z* calcd for $C_{82}H_{83}N_{12}O_6$ $[M+H]^+$: 1331.6567; found: 1331.6553 (1.08 ppm).

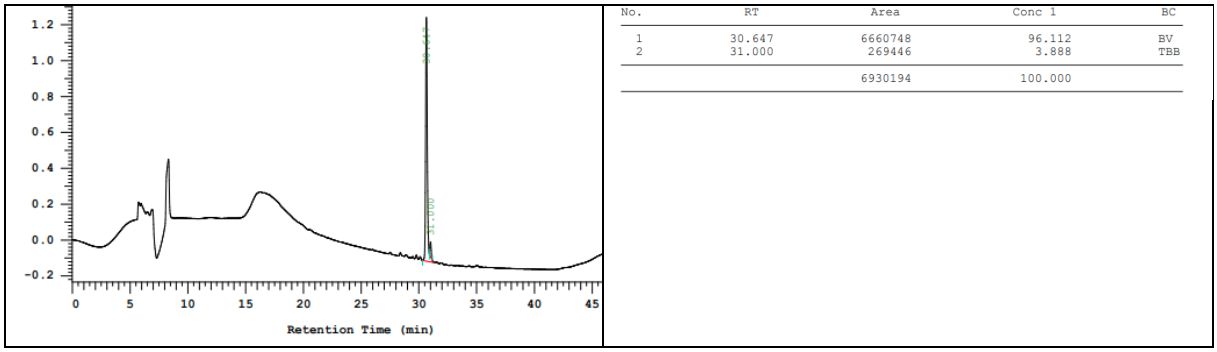

Figure S286. HPLC chromatogram of the pure Crown-like **V.6**.

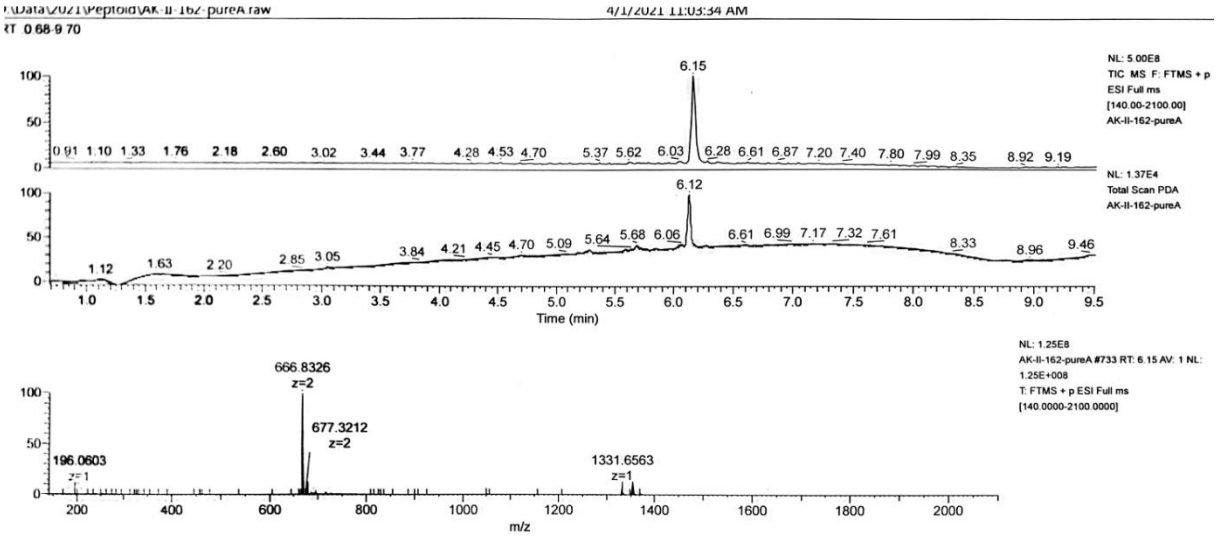

Figure S287. LCMS spectra of the pure Crown-like **V.6**.

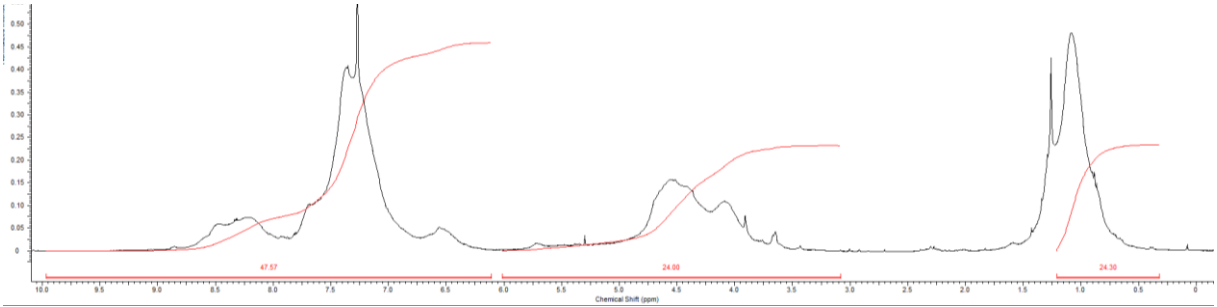

Figure S288. ^{1}H-NMR $CDCl_3$ spectrum of the pure Crown-like **V.6**.

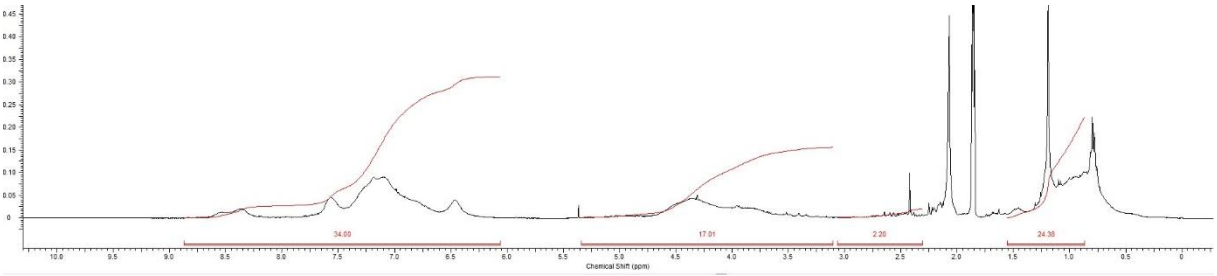

Figure S289. ^{1}H-NMR in acetonitrile of the pure Crown-like **V.6**.

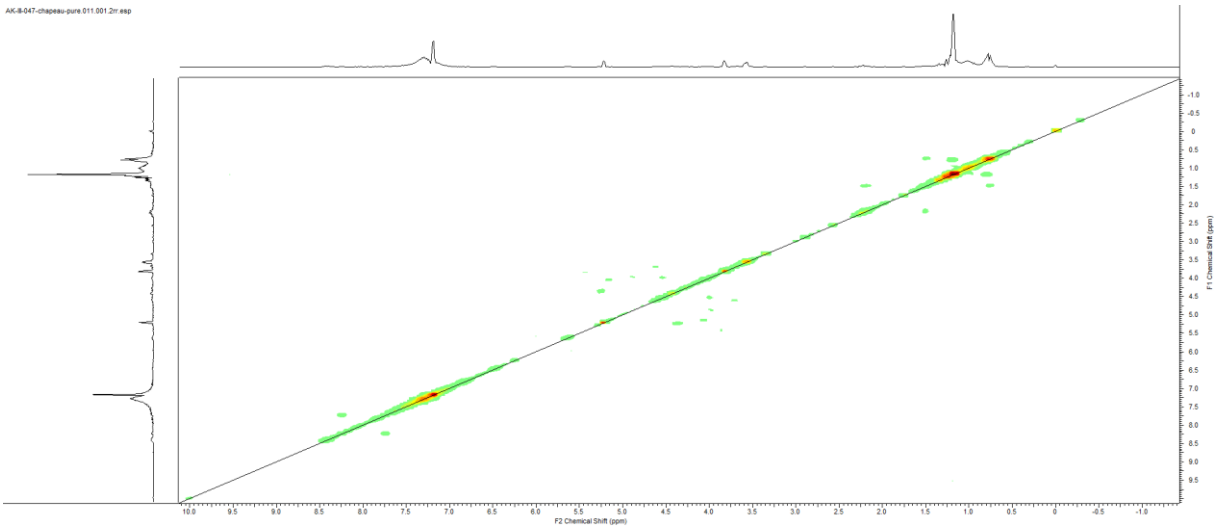

Figure S290. COSY in $CDCl_3$ of the pure Crown-like **V.6**.

V.7.

HRMS (TOF MS ES+): *m/z* calcd for $C_{164}H_{166}N_{24}O_{12}$ $[M+2H]^{2+}$: 1331.6553; found: 1331.6598 (1.08 ppm).

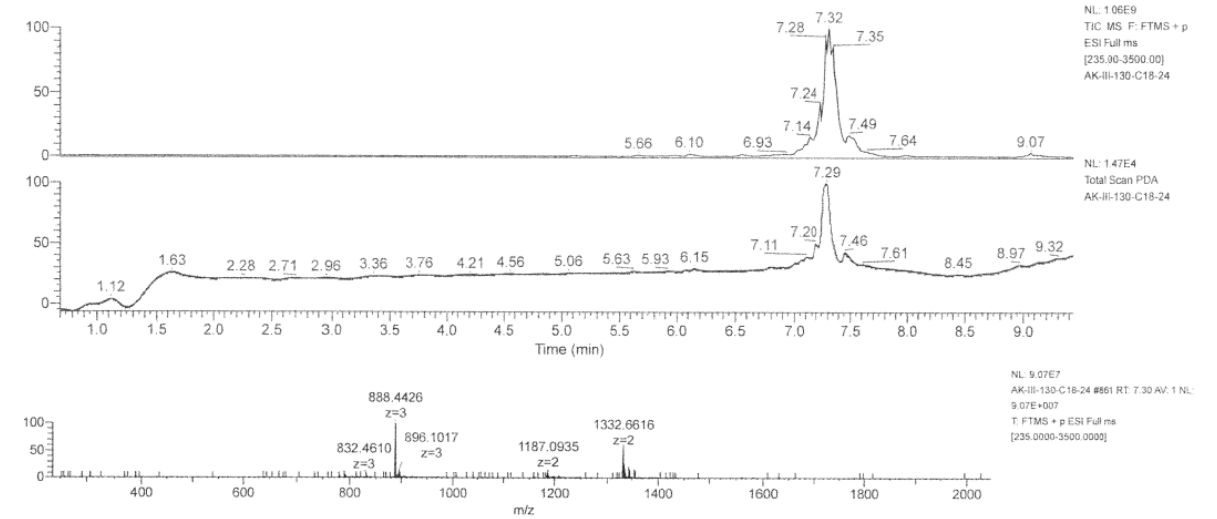

Figure S291. LCMS spectrum of the pure Tube-like **V.7**.

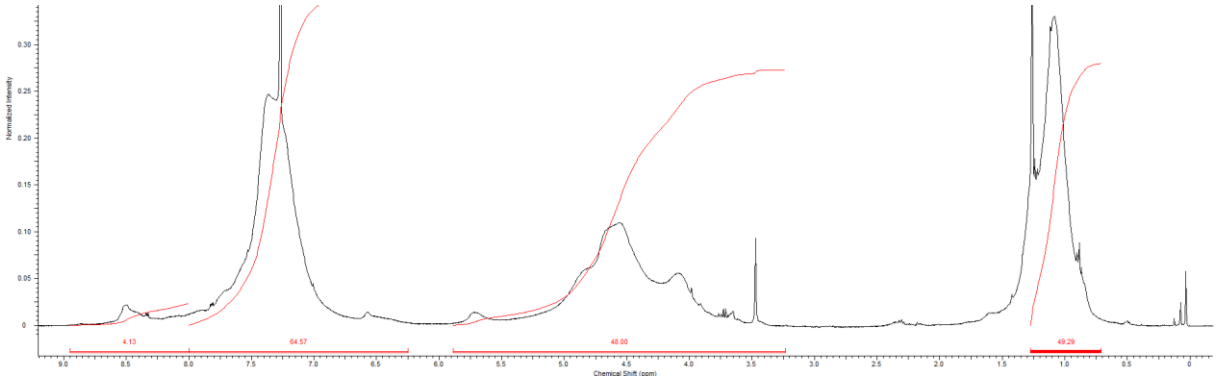

Figure S292. ^{1}H-NMR in $CDCl_3$ of pure Tube-like **V.7**.

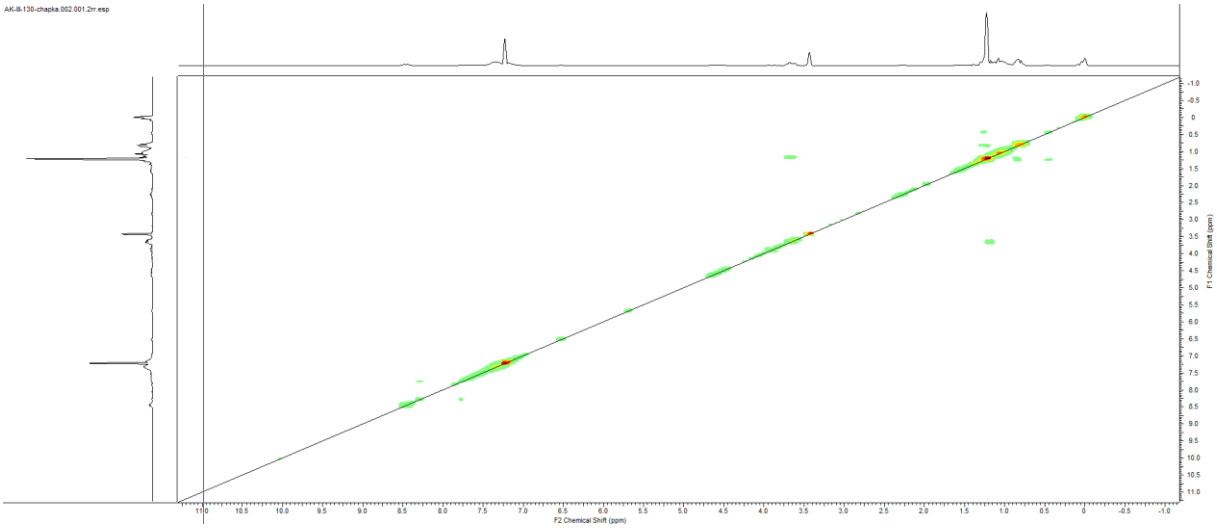

Figure S293. COSY in $CDCl_3$ of pure Tube-like **V.7**.

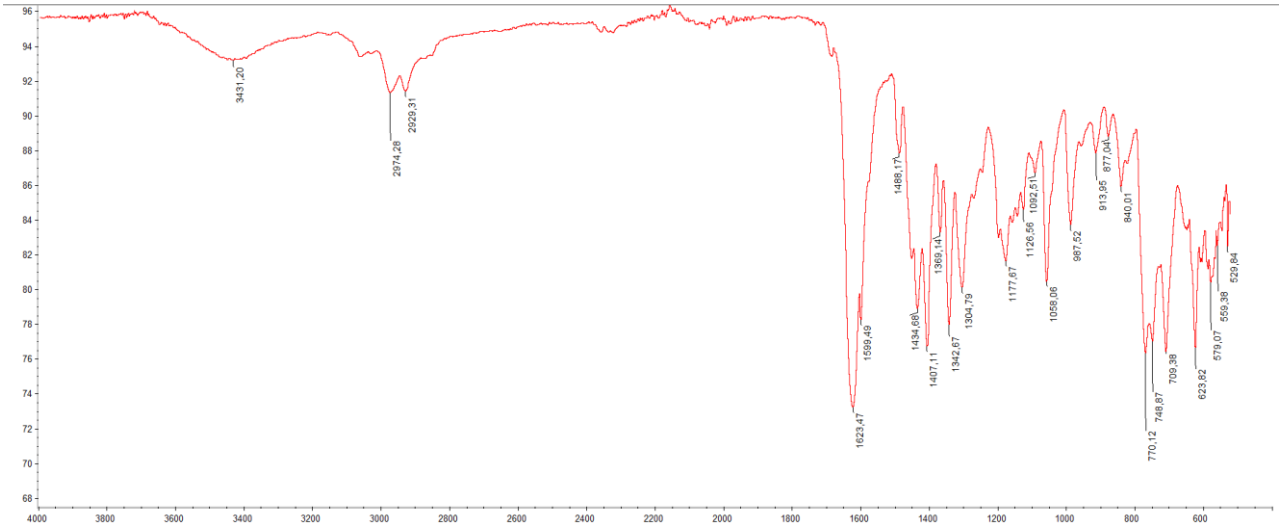

Figure S294. Infra-red of Tube-like **V.7**.

IV.3. Methylation

IV.3.a. ***V.8***.

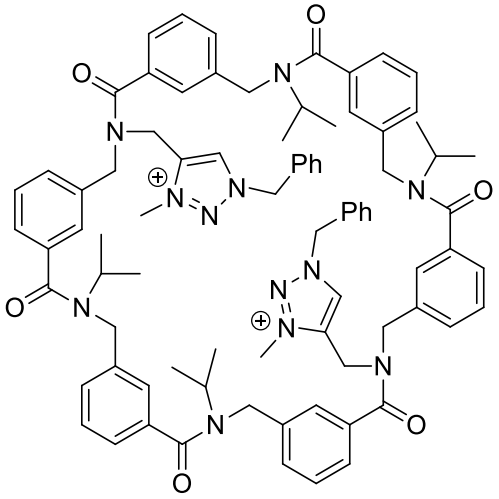

m_{crude} = 60 mg (purity 95%), isolated yield 98%.

HRMS (TOF MS ES+): *m/z* calcd for $C_{82}H_{90}N_{12}O_6$ $[M]^{2+}$: 669.35477; found: 669.3547 (-0.14 ppm).

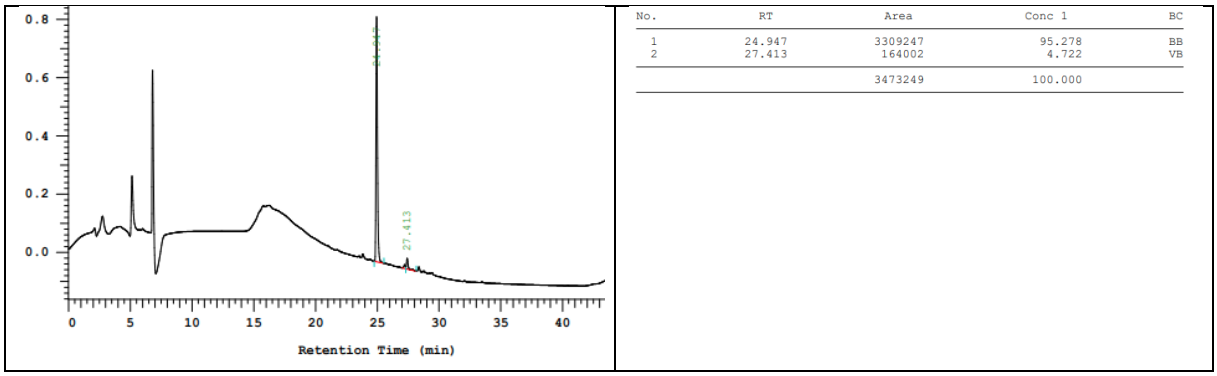

Figure S295. HPLC of the pure **V.8**.

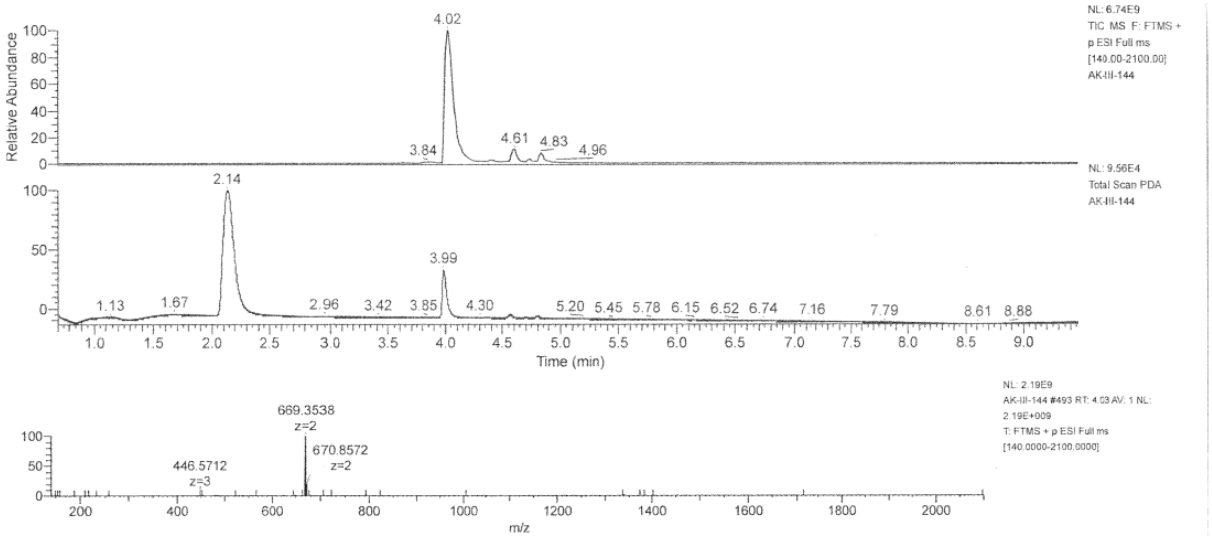

Figure S296. LCMS spectrum of crude **V.8**.

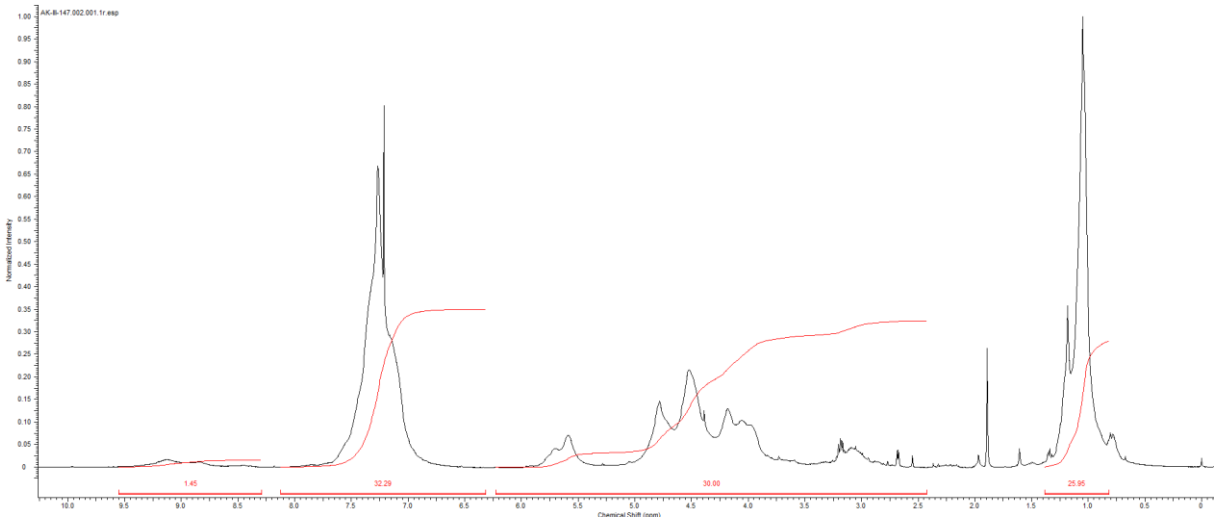

Figure S297. ^{1}H-NMR of the crude **V.8**.

IV.3.b. V.9.

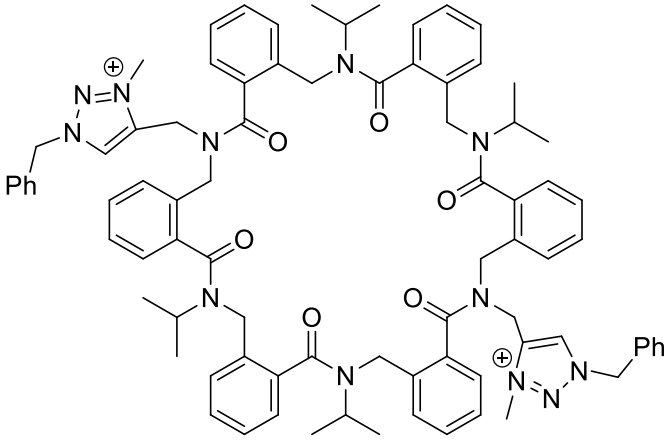

m_{crude} = 60 mg (purity 95%), isolated yield 98%

HRMS (TOF MS ES+): *m/z* calcd for $C_{82}H_{90}N_{12}O_6$ $[M]^{2+}$: 669.35477; found: 669.3547 (-0.14 ppm).

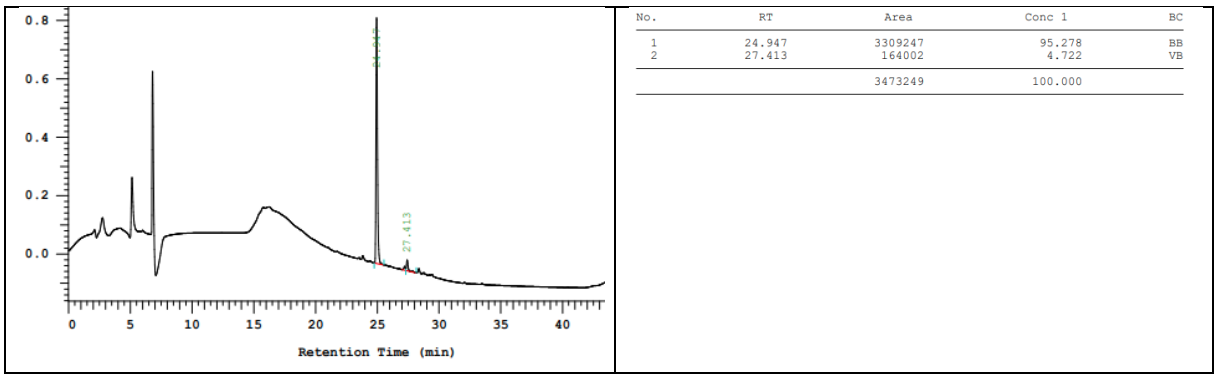

No.	RT	Area	Conc 1	BC
1	24.947	3309247	95.278	BB
2	27.413	164002	4.722	VB
		3473249	100.000	

Figure S298. HPLC of **V.9**.

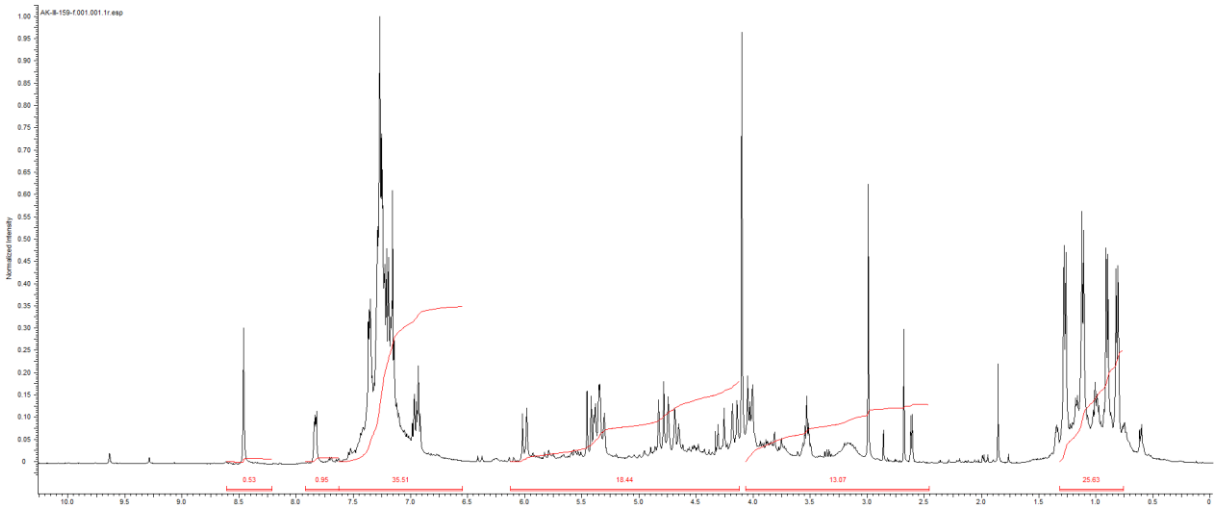

Figure S299. ^{1}H-NMR of the **V.9**.

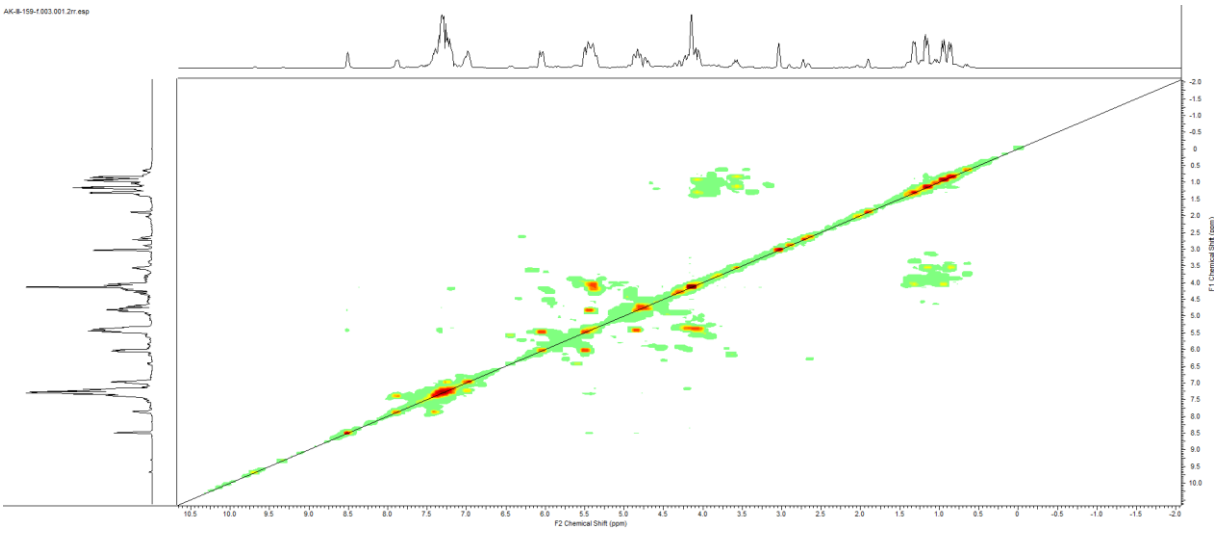

Figure S300. COSY in $CDCl_3$ of **V.9**.

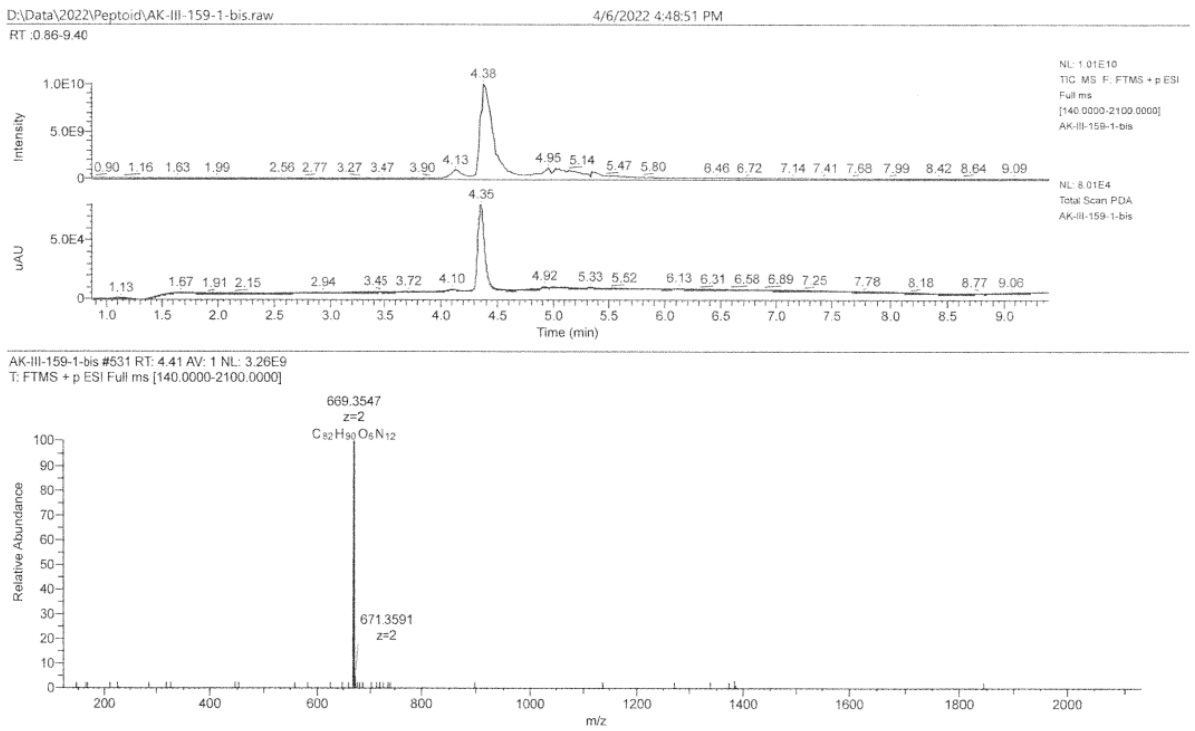

Figure S301. LCMS spectrum of the crude **V.9**.

V. New Macrocycles.

V.1. Linear hexamers.

The linear hexamers was synthesized in the same procedure described above (II.1)

*V.1.a. **V.10**.*

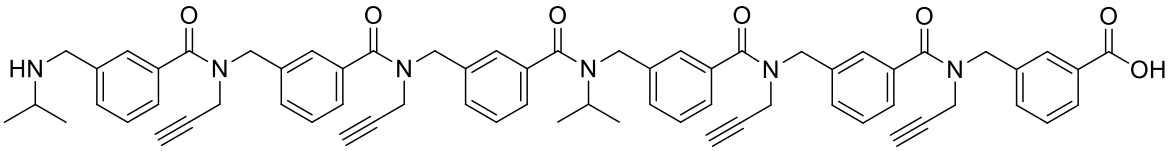

m_{pure} = 160 mg (purity 94%), isolated yield 72%

HRMS (TOF MS ES+): *m/z* calcd for $C_{66}H_{65}N_6O_7$ $[M+H]^+$: 1053.49092; found: 1053.4900 (-0.89 ppm).

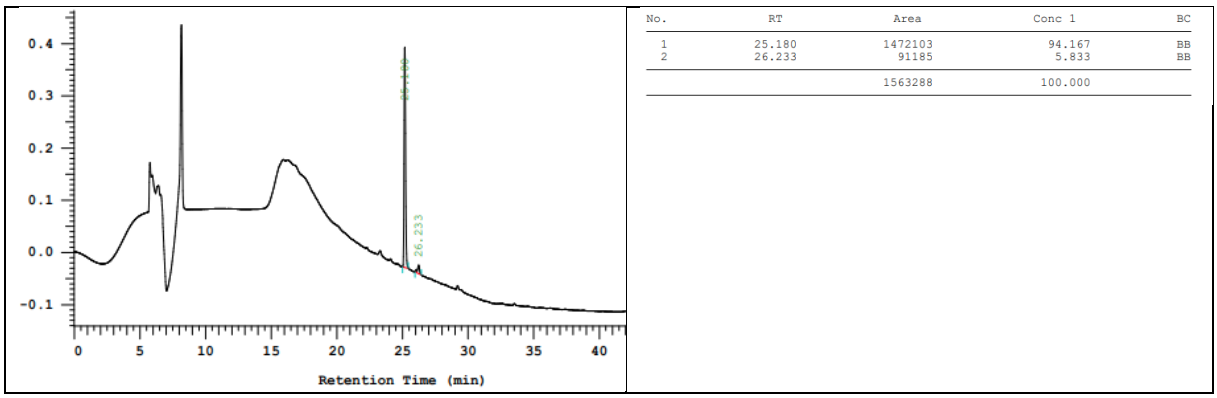

Figure S302. HPLC chromatogram of pure **V.10**.

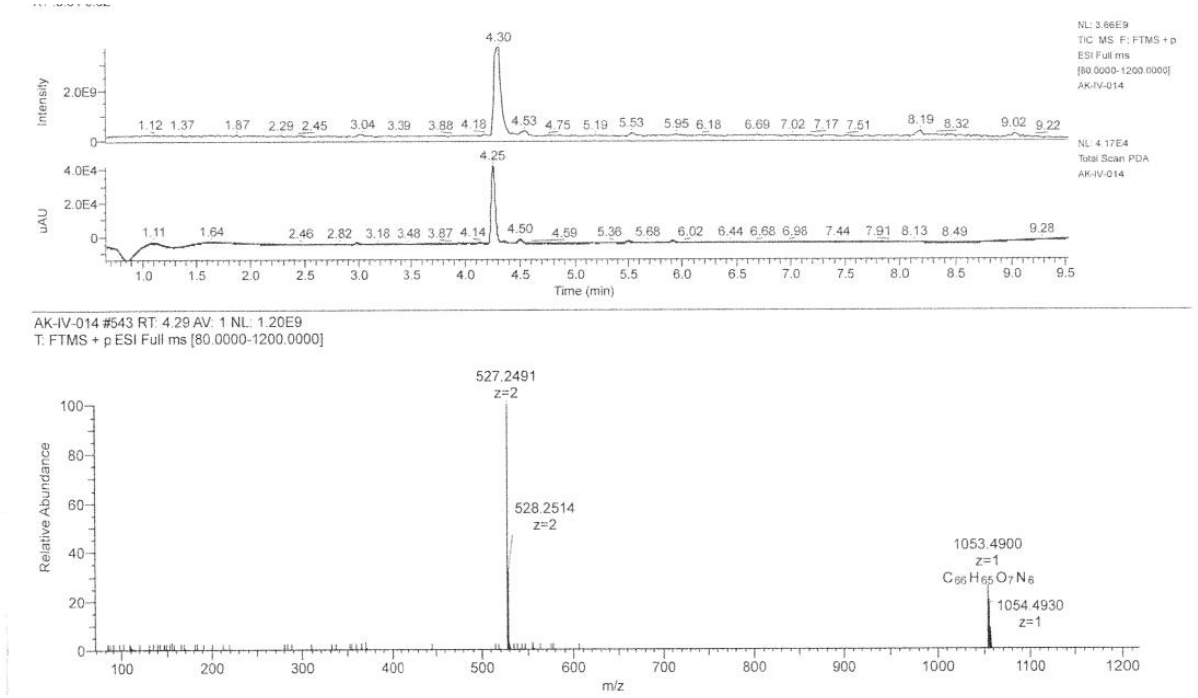

Figure S303. LCMS spectrum of crude **V.10**.

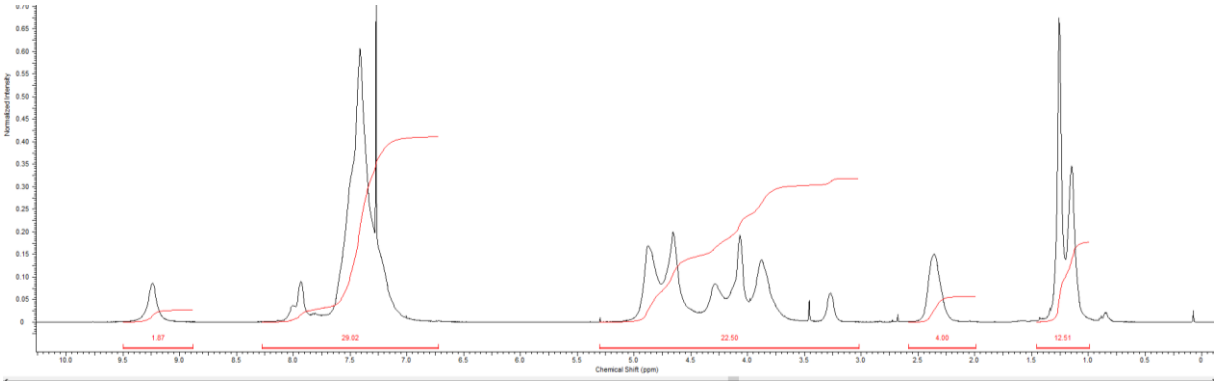

Figure S304. ^{1}H-NMR in $CDCl_3$ of pure **V.10**.

*V.1.a. **V.11**.*

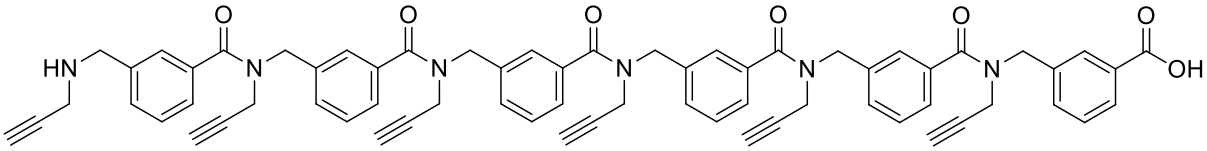

m_{pure} = 160 mg (purity 96%), isolated yield 73%

HRMS (TOF MS ES+): *m/z* calcd for $C_{66}H_{57}N_6O_7$ $[M+H]^+$: 1045.42832; found: 1045.4272 (-1.03 ppm).

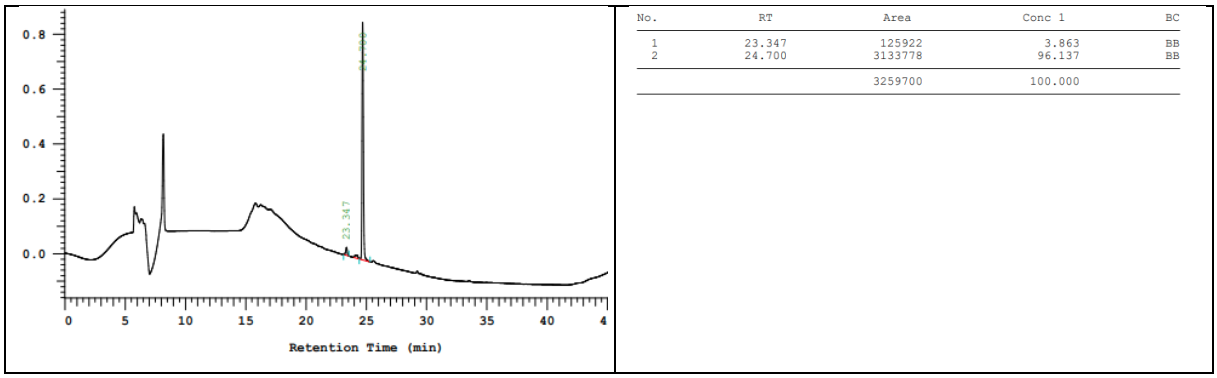

No.	RT	Area	Conc 1	BC
1	23.347	125922	3.863	BB
2	24.700	3133778	96.137	BB
		3259700	100.000	

Figure S305. HPLC chromatogram of pure **V.11**.

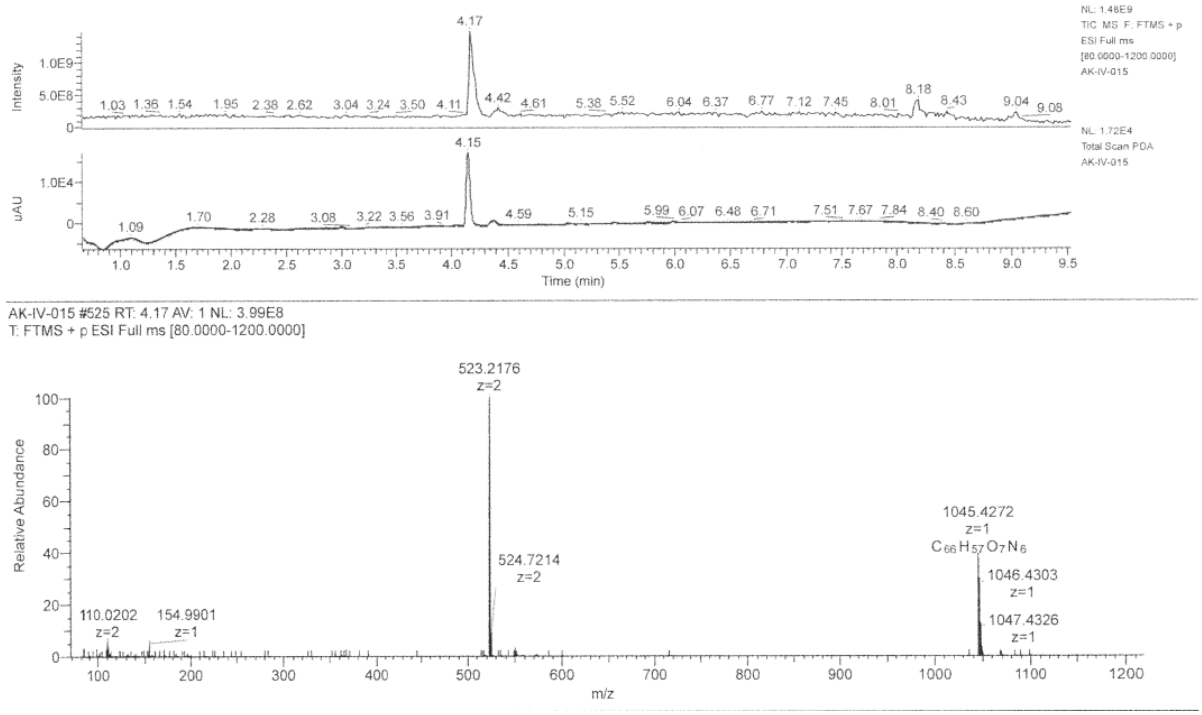

Figure S306. LCMS spectrum of crude **V.11**.

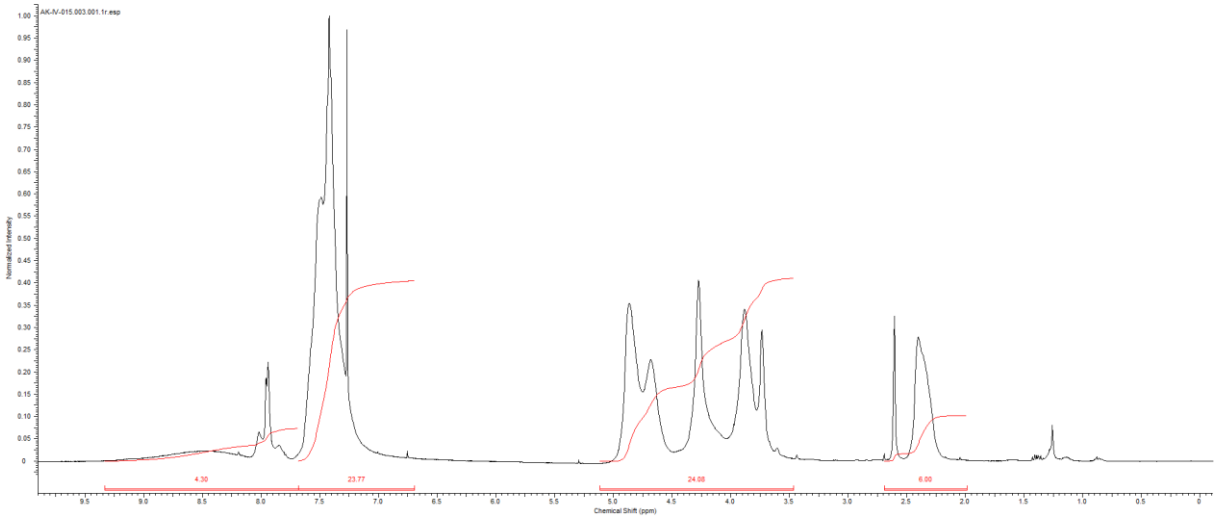

Figure S307. ^{1}H-NMR in $CDCl_3$ of pure **V.11**.

V.1.c. ***V.12.***

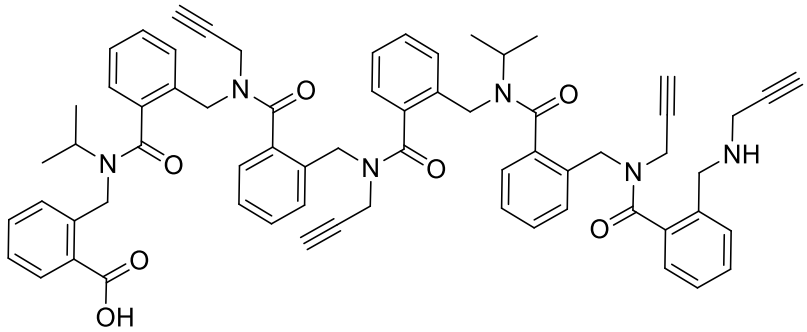

Molecular Weight: 1053,250

m_{pure} = 140 mg (purity 97%), isolated yield 84%

HRMS (TOF MS ES+): *m/z* calcd for $C_{66}H_{65}N_6O_7$ $[M+H]^+$: 1053.49092; found: 1053.4900 (-0.89 ppm).

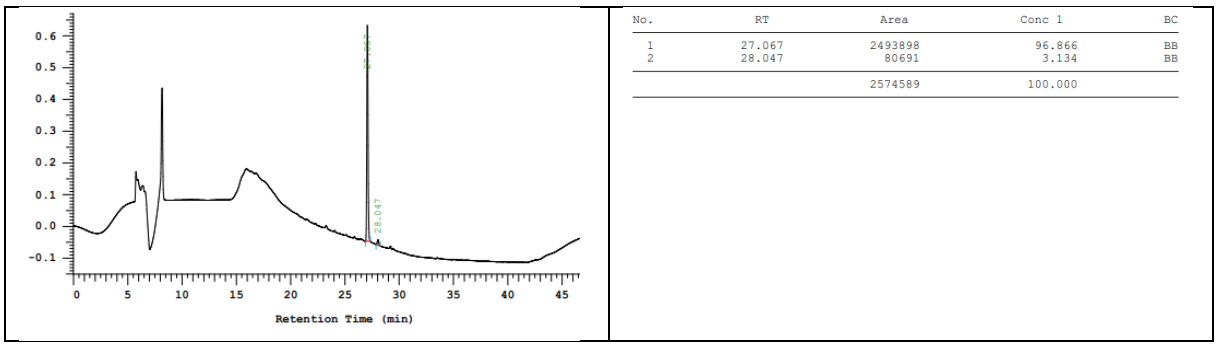

No.	RT	Area	Conc 1	BC
1	27.067	2493898	96.866	BB
2	28.047	80691	3.134	BB
		2574589	100.000	

Figure S308 HPLC chromatogram of **V.12**.

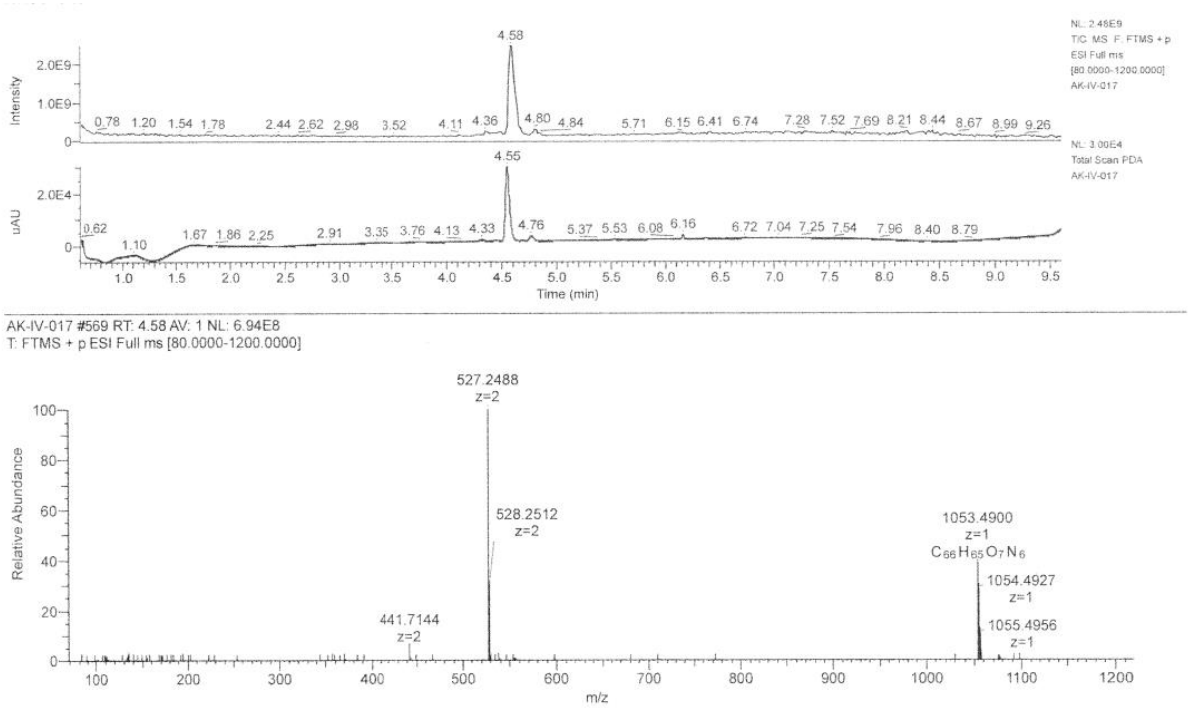

Figure S309. LCMS spectrum of the crude **V.12**.

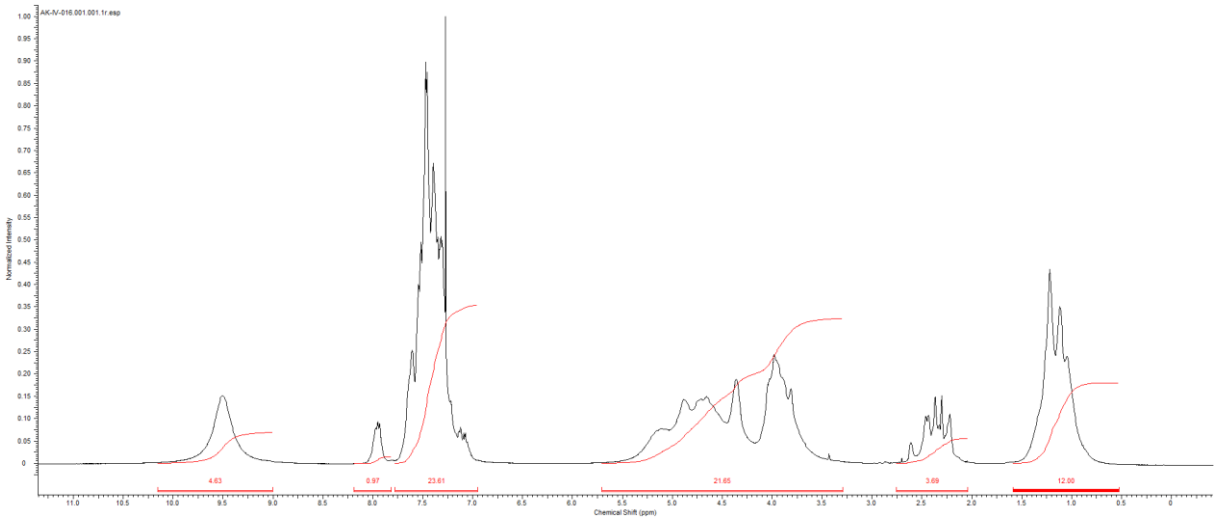

Figure S310. ^{1}H-NMR in $CDCl_3$spectrum of the pure **V.12**.

V.2. Macrocyclization.

The Macrocyclization procedure is the same than the one used in II.2

V.2.a. ***V.13.***

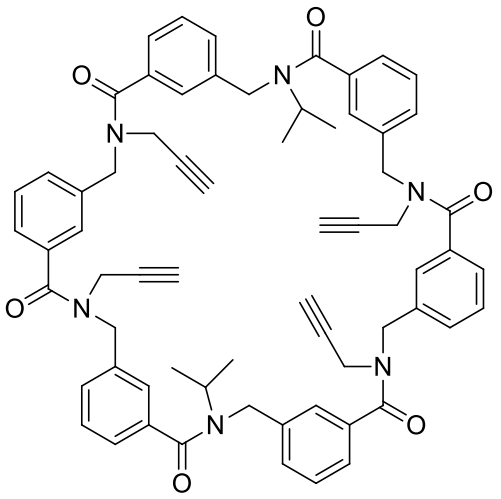

m_{pure} = 80 mg (purity 96%), isolated yield 68%

HRMS (TOF MS ES+): *m/z* calcd for $C_{66}H_{63}N_6O_6$ $[M+H]^+$: 1035.48036; found: 1035.4814 (1.05 ppm).

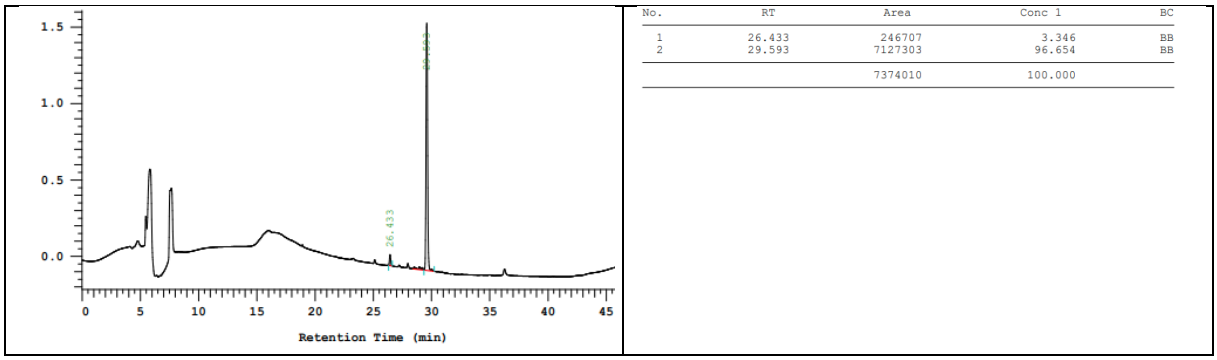

Figure S311. HPLC chromatogram of pure **V.13**.

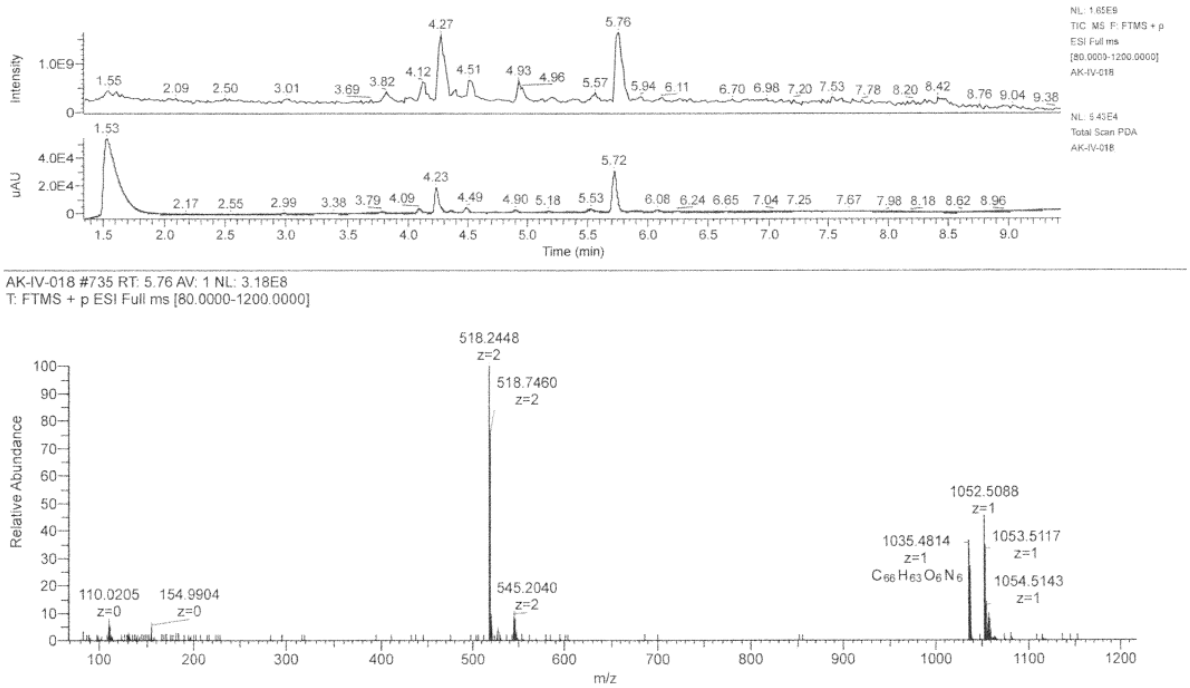

Figure S312 LCMS spectrum of the crude **V.13**.

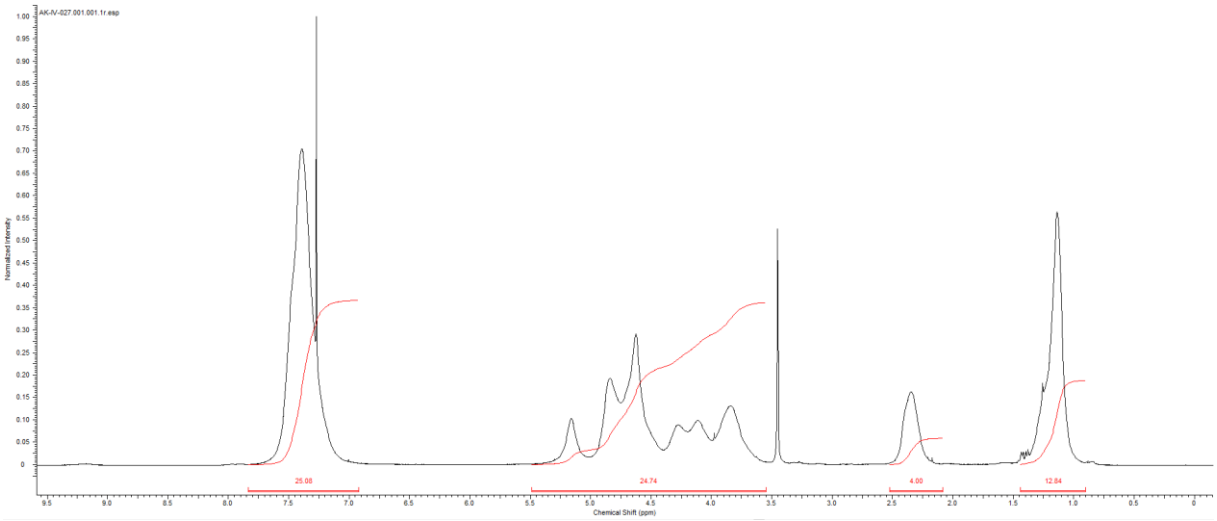

Figure S313. ^{1}H-NMR in $CDCl_3$ of pure **V.13**.

V.2.b. ***V.14.***

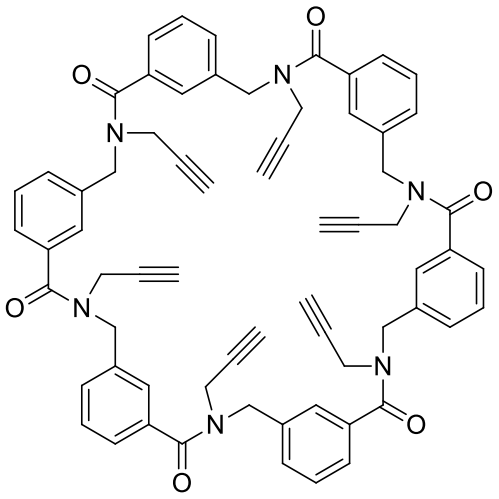

m_{pure} = 85 mg (purity 96%), isolated yield 74%

HRMS (TOF MS ES+): *m/z* calcd for $C_{66}H_{55}N_6O_6$ $[M+H]^+$: 1027.41776; found: 1027.4186 (0.8 ppm).

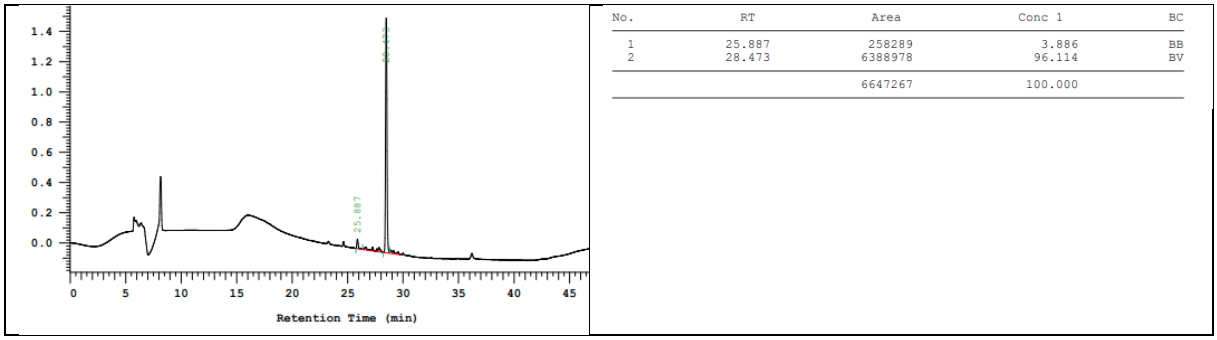

No.	RT	Area	Conc 1	BC
1	25.887	258289	3.886	BB
2	28.473	6388978	96.114	BV
		6647267	100.000	

Figure S314. HPLC chromatogram of pure **V.14**.

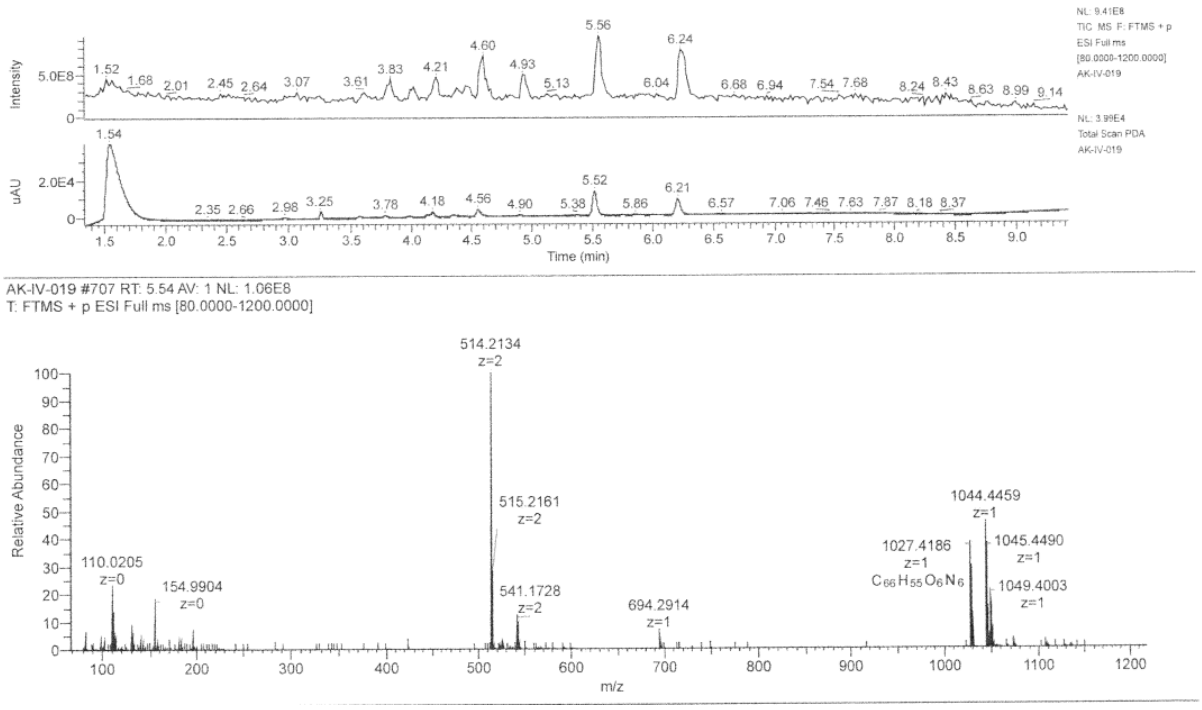

Figure S315. LCMS spectrum of crude **V.14**.

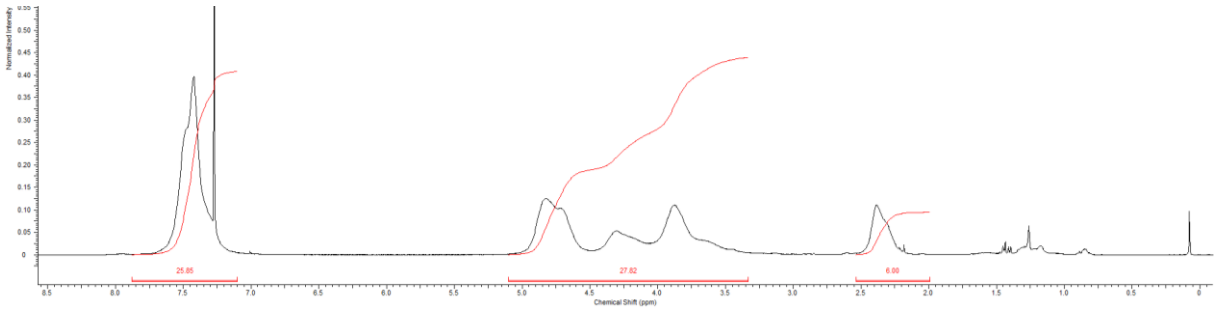

Figure S316. ^{1}H-NMR in $CDCl_3$ of pure **V.14**.

V.2.c. V.15.

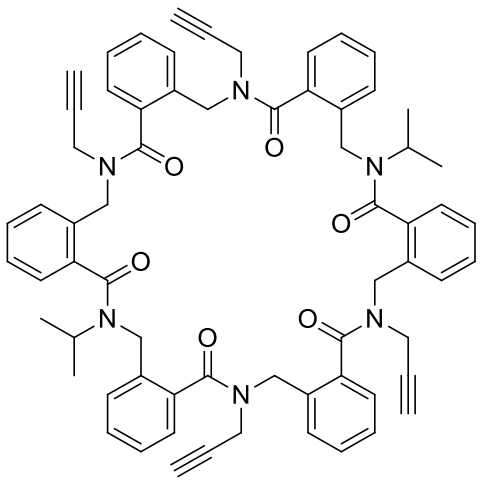

m_{pure} = 82 mg (purity 99%), isolated yield 70%

HRMS (TOF MS ES+): *m/z* calcd for $C_{66}H_{63}N_6O_6$ $[M+H]^+$: 1035.48036; found: 1035.4824 (1.99 ppm).

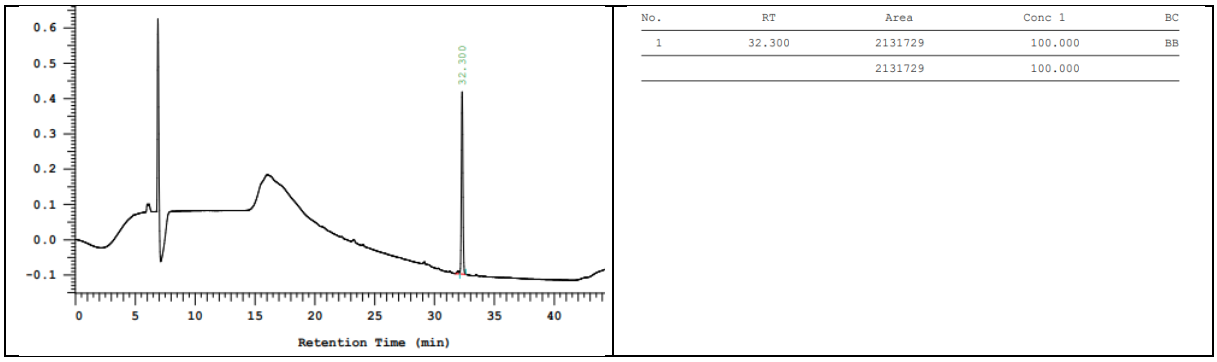

Figure S317. HPLC chromatogram of pure **V.15**.

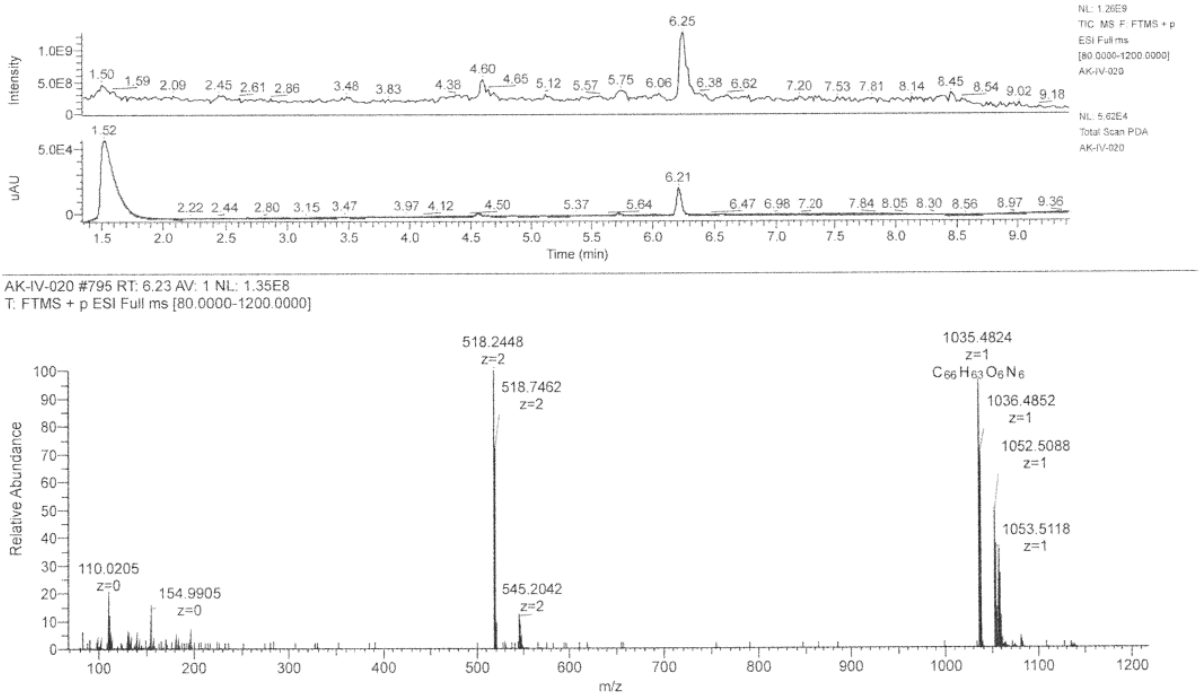

Figure S318. LCMS spectrum of the crude **V.15**.

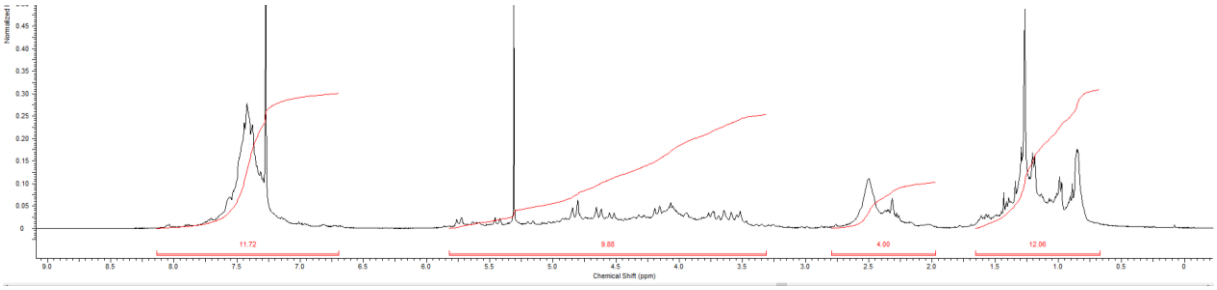

Figure S319. ^{1}H-NMR in $CDCl_3$ of pure **V.15**.

Chapter VI.

I-Chemicals

Chemicals: Rink amide resin (0.62 mmol/g loading) was obtained from Novabiochem, piperidine and dichloromethane from Carlo Erba; 3-chloromethylbenzoylchloride, TFA, DIPEA, isopropyl, and propargyl amines from TCI; *N*-methylpyrrolidone from Alfa Aesar and DMSO from Acros. Benzyl azide (**1a**), (azidomethyl)cyclohexane (**1b**), *tert*-butyl azido acetate (**1c**), *tert*-butyl (2-azidoethyl)carbamate (**1d**) and 3-azido propane-1-ol (**1e**) were synthetized according to literature procedures. 10 mL jacketed reactors were purchased from Kamush and thermo-regulated using a Lauda thermostat. NMR was recorded on Bruker advance 400 spectrometer. Purification was performed on a Buchi Pure Chromatography system.

High-resolution mass spectra (HRMS) are recorded using electrospray ionization in positive mode (ESI+) on or a Q Exactive Quadrupole-Orbitrap Mass Spectrometer. Liquid chromatography mass spectroscopy (LC-MS) were recorded on a Q Exactive Quadrupole-Orbitrap Mass Spectrometer coupled to a UPLC Ultimate 3000 (Kinetex EVO C18; 1,7µm; 100 mm x 2,1 mm column with a flow rate of 0.45 ml.min^{-1} with the following gradient: a linear gradient of solvent B from 5% to 95% over 7.5 min (solvent A = H_2O + 0.1% formic acid, solvent B = acetonitrile + 0.1% formic acid) equipped with a DAD UV/VIS 3000 RS detector)

Analytical HPLC was recorded on a Hitachi liquid chromatograph (Oven 5310, 30°C; Pump 5160; DAD detector 5430) equipped with a C18 Acclaim column (4.6mm×250mm, 5µm, 120Å). Detection wavelength was 240nm or 280nm and flow rate 0.5mL/min. Gradient elution used (A) water/0.1% TFA; (B) methanol according to Method A: (Solvents A/B: 0 to 5 minutes isocratic at 95/5; 5 to 25 minutes gradient to 5/95; 25 to 35 minutes isocratic at 5/95; 35 to 45 minutes gradient to 95/5; 45 to 50 minutes 95/5) or Method B (Solvents A/B: 0 to 5 minutes isocratic at 95/5; 5 to 10 minutes gradient to 75/25; 10 to 50 minutes gradient to 40/60; 50 to 65 minutes gradient to 5/95; 65 to 70 minutes isocratic at 5/95; 70 to 80 minutes gradient to 95/5).

II- Procedures

II-a. General procedure A.

Resin-bound arylopeptoid trimers obtained from 100 mg of resin were introduced in a reactor containing 1 mL of CH_2Cl_2/MeOH mixture (v/v = 8:2). Bis-azide (0.55 equiv. per alkyne) and 10 mol-% of catalyst per alkyne were added. The reactor is gently shaken for 4h at 50°C. The resin was washed with MeOH (5x2ml) at 50°C and then with CH_2Cl_2 (5 x 2 ml) at room temperature. Cleavage was performed by gently shaking in a 1 mL solution of TFA/TIS/H_2O (95:2.5:2.5) for 10 min at RT. The solution was drained out and evaporated to dryness under reduced pressure. The product was purified using Buchi LC automatic C18 column (Water + 0.1% TFA/MeOH).

II.b. General procedure B.

Resin-bound chloride intermediate **VI.5** obtained from 100 mg of resin, was introduced in a reactor containing 1 mL of CH_2Cl_2/MeOH mixture (v/v = 8:2). Bis-azide (0.55 equiv. per alkyne) and 10 mol-% of catalyst per alkyne were added. The reactor is gently shaken for 4h at 50°C. The resin was washed with MeOH (5x2ml) at 50°C and then with CH_2Cl_2 (5x2ml) at

room temperature. Then, the elongation of the arylopeptoid produced is performed using the standard solid-phase submonomer method described in chapter III, with isopropylamine or propargyl amine side chains. After the synthesis of the desired product, Cleavage was performed by gently shaking in a 1 mL solution of TFA/TIS/H_2O (95:2.5:2.5) for 10 min at RT. The solution was drained out and evaporated to dryness under reduced pressure. The product was purified using Buchi LC auctomatic C18 column (Water + 0.1% TFA/MeOH).

III.1. H-shaped arylopeptoids with General procedure A

*III.1.a. H-shaped arylopeptoid **VI.3**.*

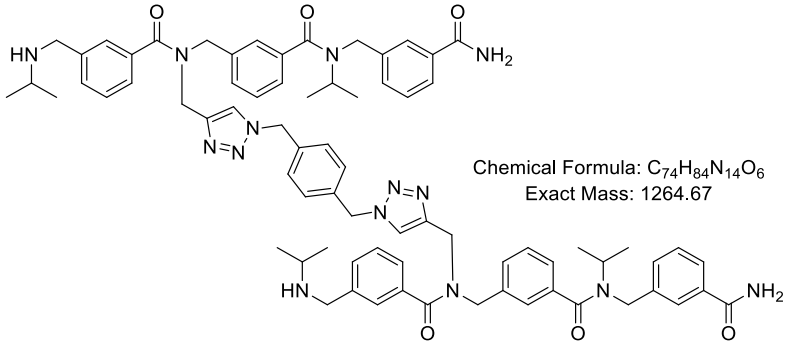

H-shaped **VI.3** was synthesised according to General procedure A using 100 mg of Rink Amide resin (loading 0.62mmol/g).

m_{pure}= 33 mg (purity 90%), isolated yield 84%

HRMS (TOF MS ES+): *m/z* calcd for $C_{74}H_{86}N_{14}O_6$ $[M+2H]^{2+}$: 633.34219; found: 633.3422 (0.05 ppm).

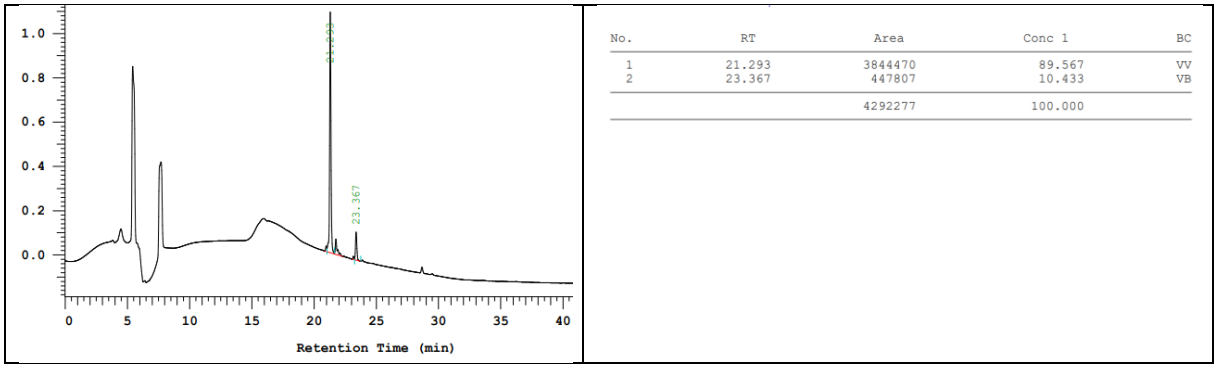

Figure S320. HPLC chromatogram of isolated **VI.3**.

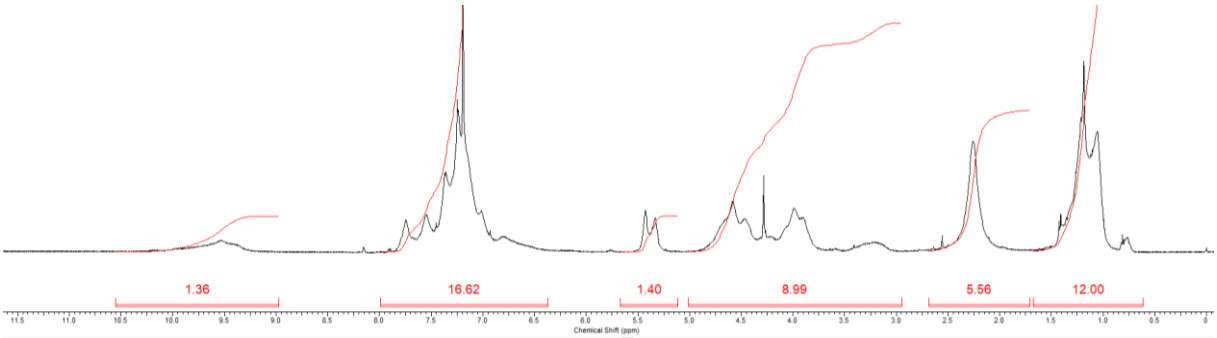

Figure S321. ^{1}H-NMR in $CDCl_3$ of isolated **VI.3**.

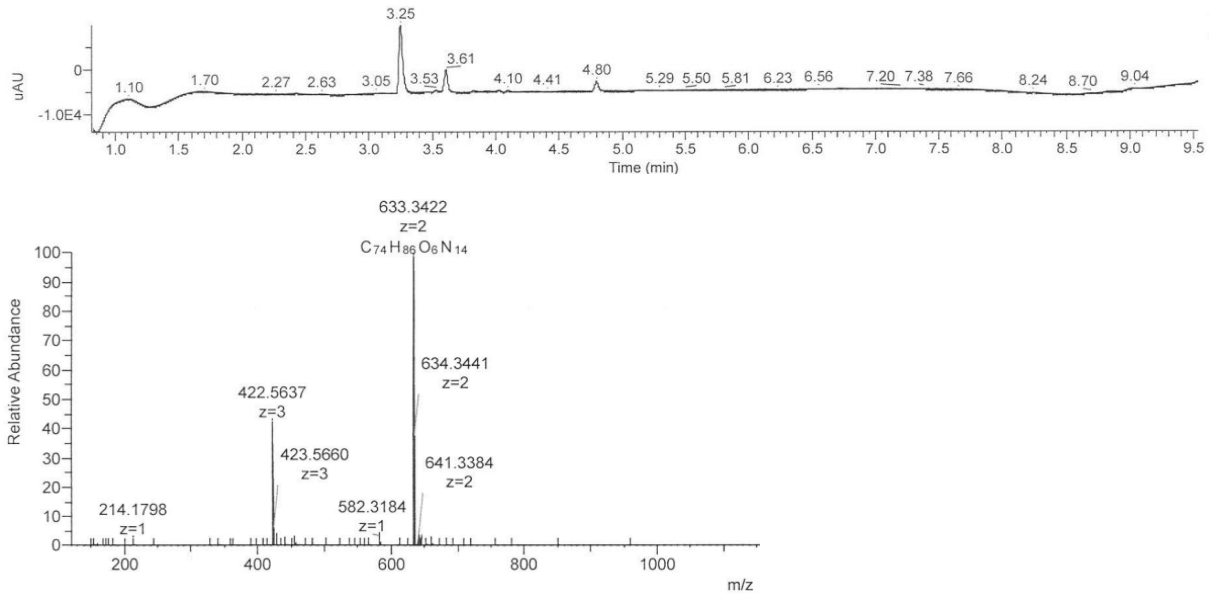

Figure S322. LCMS spectrum of **VI.3**.

*III.1.b. Mono-clicked triazole **VI.4**.*

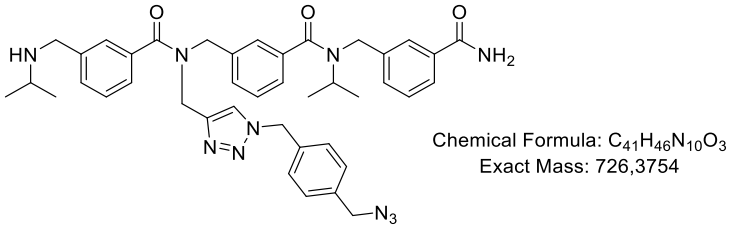

Monoclicked **VI.4** was synthesised according to General procedure A with increased amount of bis-azide to 10 equivalents, using 100 mg of Rink Amide resin (loading 0.62mmol/g).

m_{pure}= 35 mg (purity 97%), isolated yield 78%

HRMS (TOF MS ES+): *m/z* calcd for $C_{41}H_{47}N_{10}O_3$ $[M+H]^+$: 727.38271; found: 727.3835 (1.15 ppm).

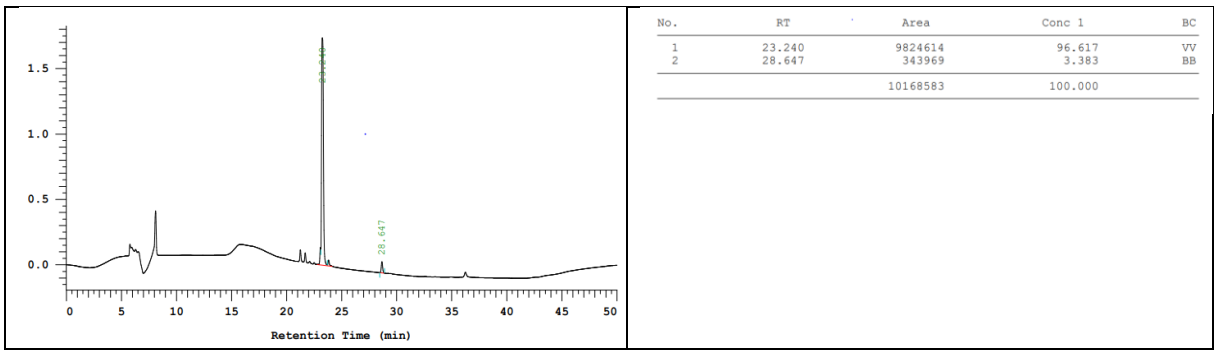

Figure S323. HPLC chromatogram of purified **VI.4**.

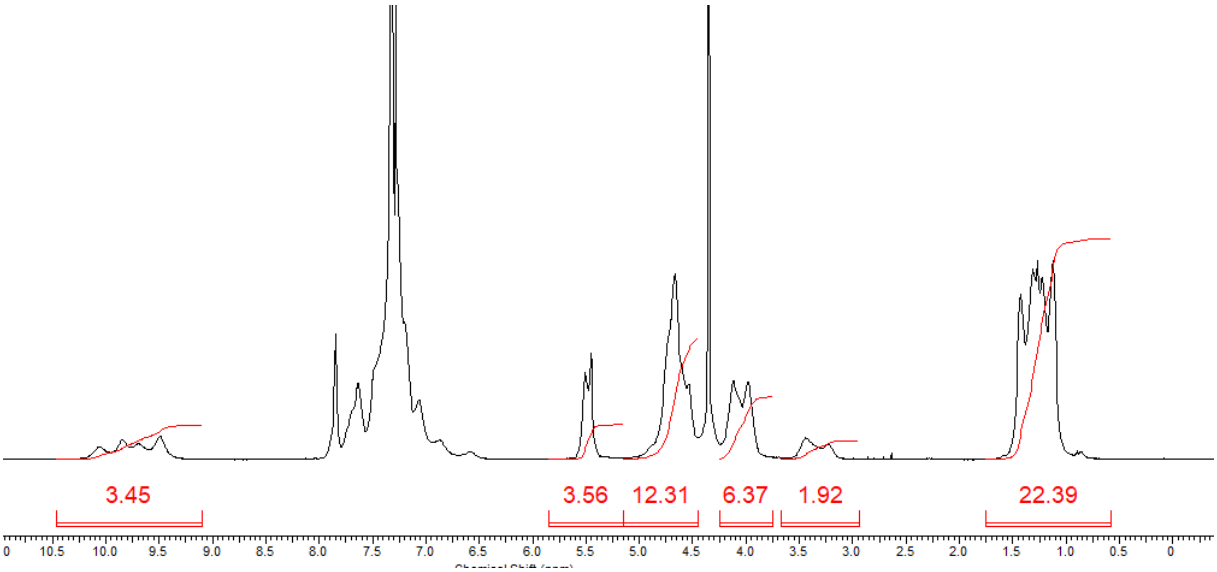

Figure S324. ^{1}H-NMR in $CDCl_3$ of purified **VI.4**.

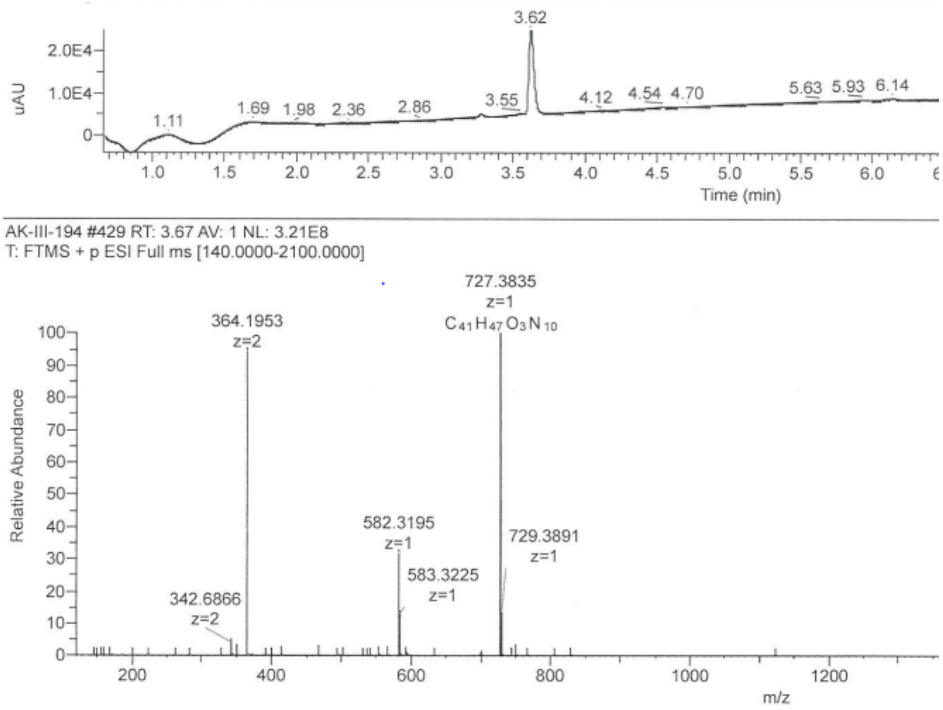

Figure S325. LCMS spectrum of **VI.4**.

III.2. H-shaped arylopeptoids with General procedure B.

III.2.a. ***VI.6***.

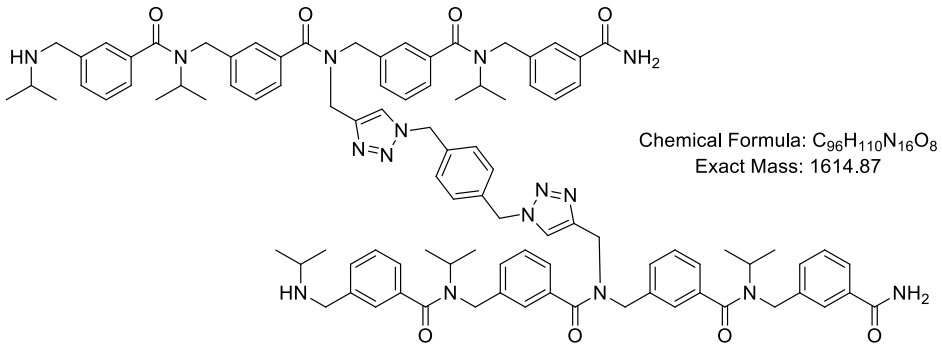

H-shaped **VI.6** was synthesised according to General procedure B, using 100 mg of Rink Amide resin (loading 0.62mmol/g).

m_{pure}= 39.5 mg (purity 94%), isolated yield 79%

HRMS (TOF MS ES+): *m/z* calcd for $C_{96}H_{112}N_{16}O_8$ $[M+2H]^{2+}$: 808.44190; found: 808.4412 (-0.92 ppm).

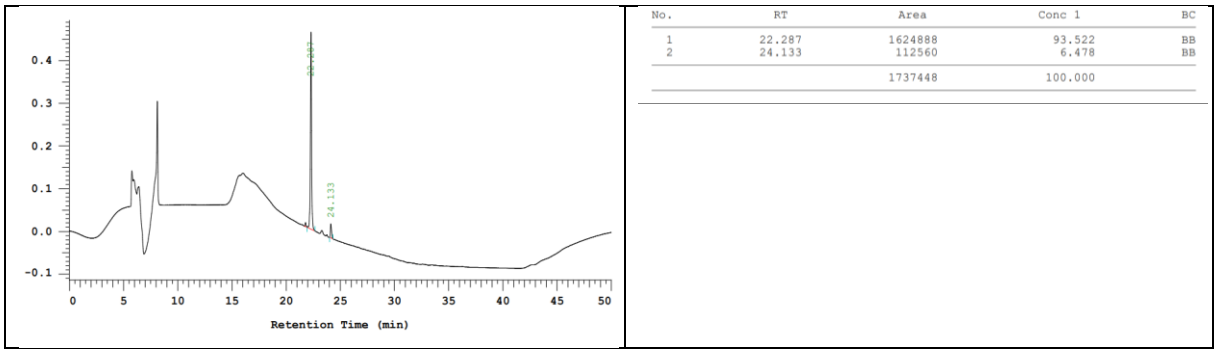

Figure S326. HPLC chromatogram of purified **VI.6**.

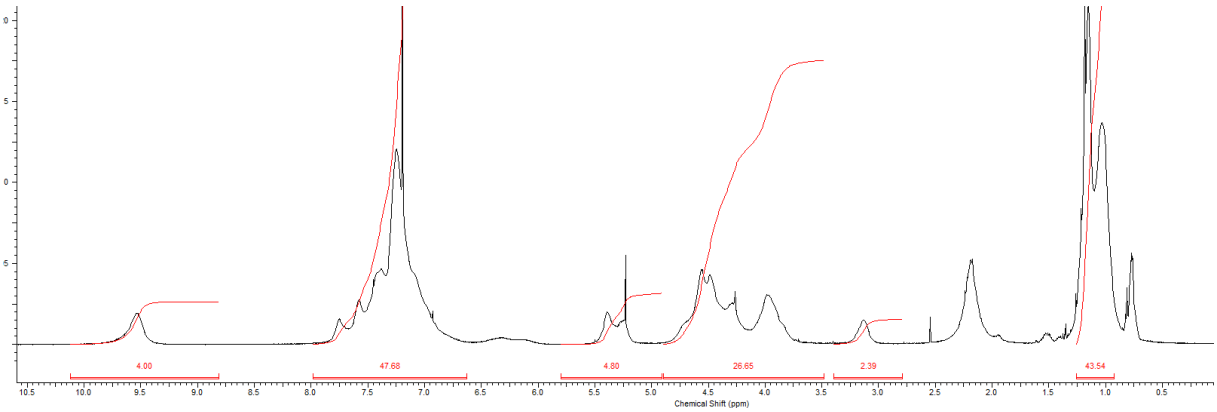

Figure S327. ^{1}H-NMR in $CDCl_3$ of purified **VI.6**.

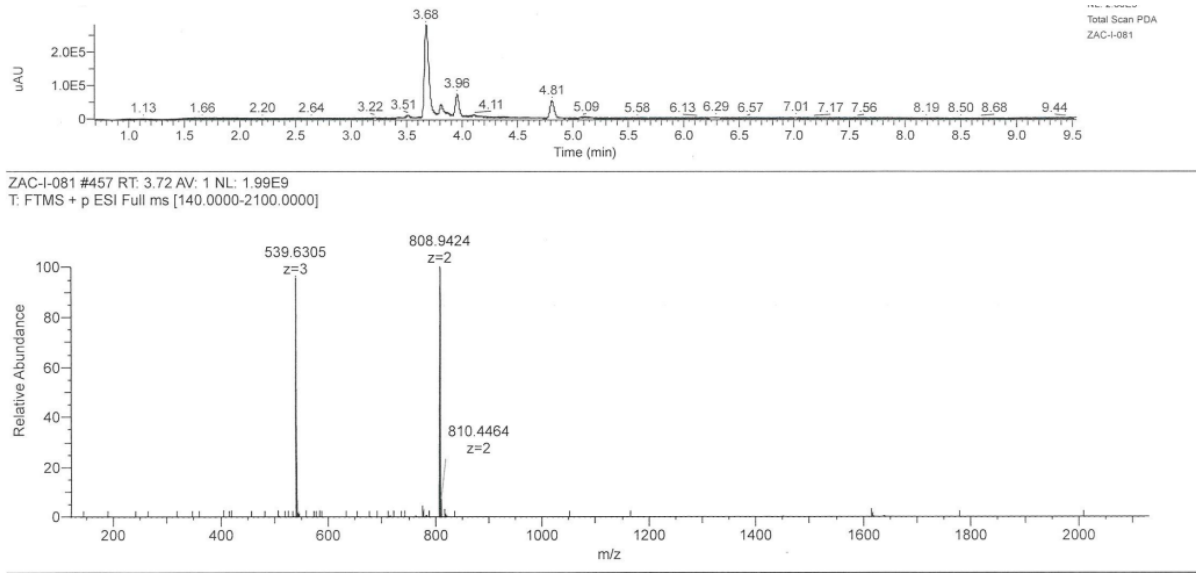

Figure S328. LCMS spectrum of crude **VI.6**.

III.2.b. VI.7.

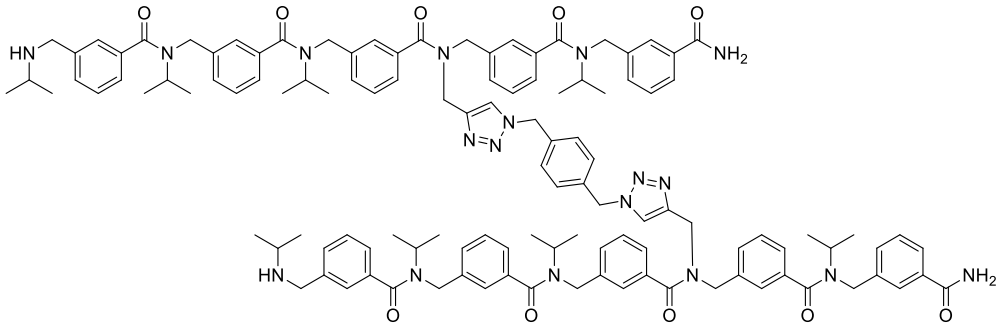

H-shaped **VI.7** was synthesised according to General procedure B, using 100 mg of Rink Amide resin (loading 0.62mmol/g).

m_{pure}= 49 mg (purity 91%), isolated yield 81%

HRMS (TOF MS ES+): *m/z* calcd for $C_{118}H_{138}N_{18}O_{10}$ $[M+2H]^{2+}$: 983.54126; found: 983.5405 (-1.11 ppm).

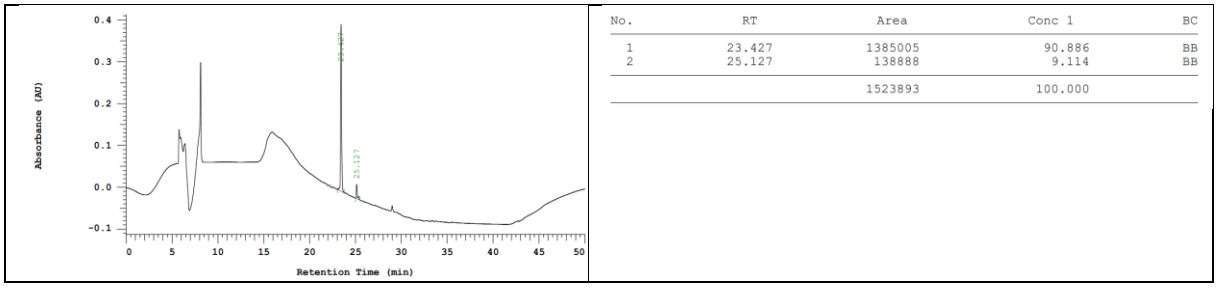

Figure S329. HPLC chromatogram of purified **VI.7**.

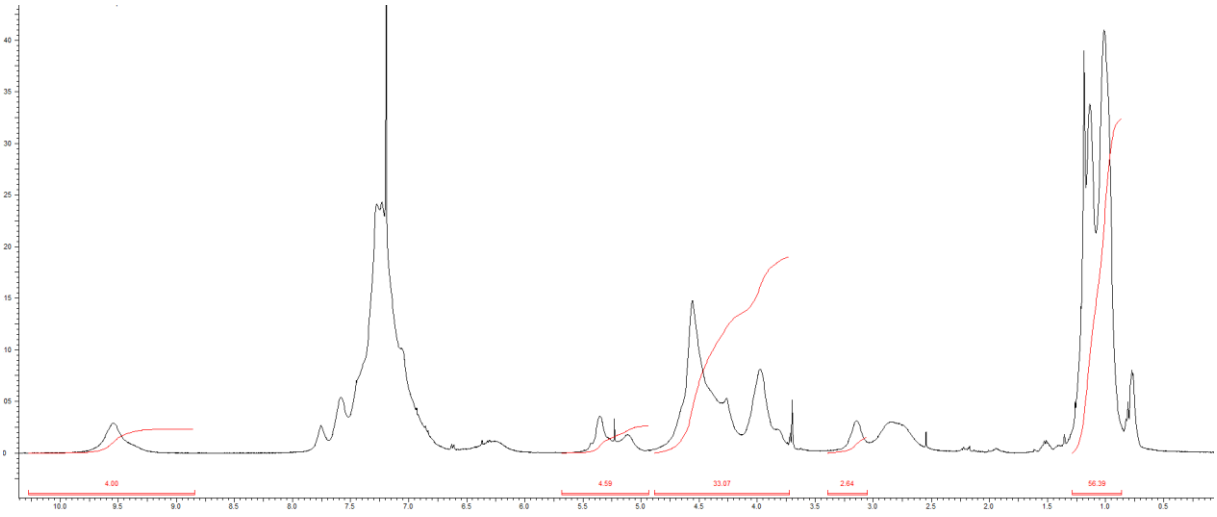

Figure S330. ^{1}H-NMR in $CDCl_3$ of purified **VI.7**.

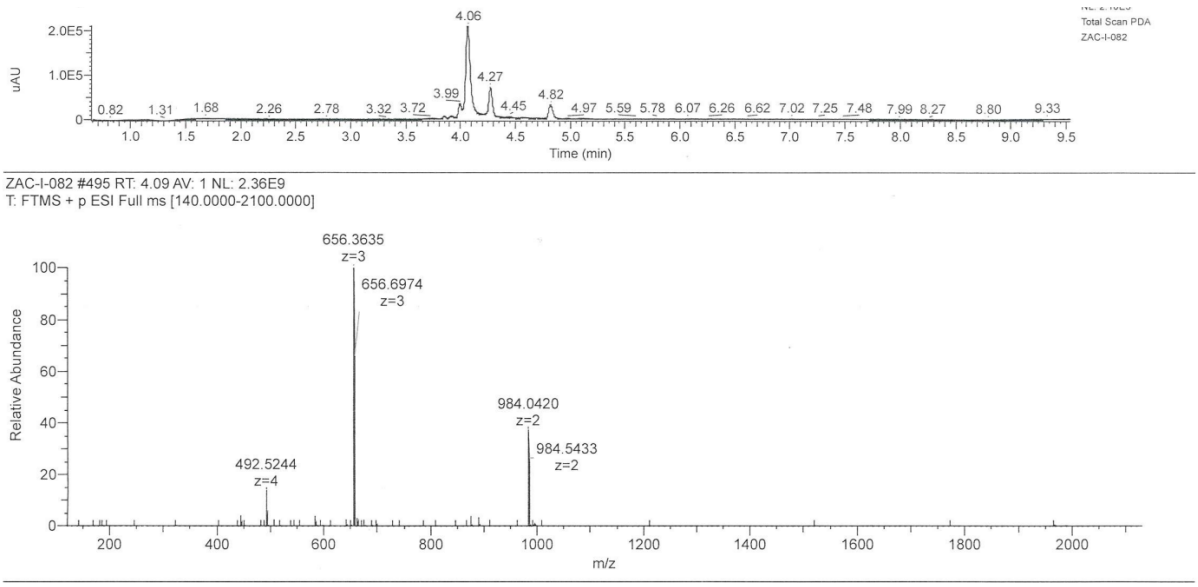

Figure S331. LCMS spectrum of crude **VI.7**.

III.2.c. ***VI.8.***

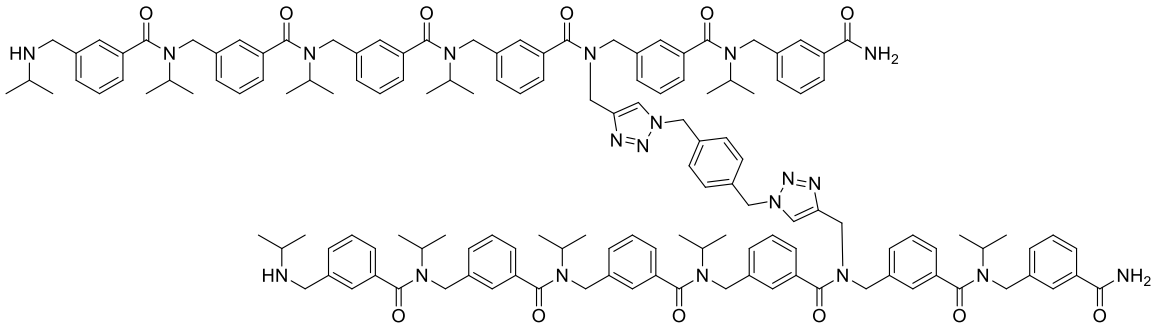

H-shaped **VI.8** was synthesised according to General procedure B, using 100 mg of Rink Amide resin (loading 0.62mmol/g).

m_{pure}= 59 mg (purity 99%), isolated yield 82%

HRMS (TOF MS ES+): *m/z* calcd for $C_{140}H_{165}N_{20}O_{12}$ $[M+3H]^{3+}$: 772.76331; found: 772.7634 (0.15 ppm).

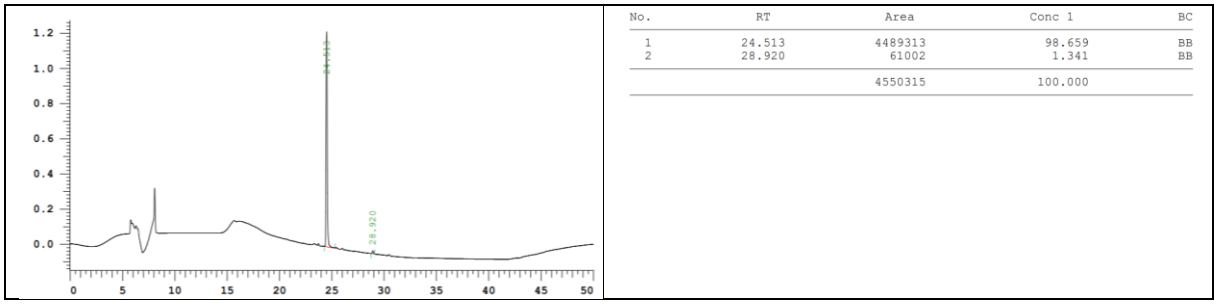

Figure S332. HPLC chromatogram of purified **VI.8**.

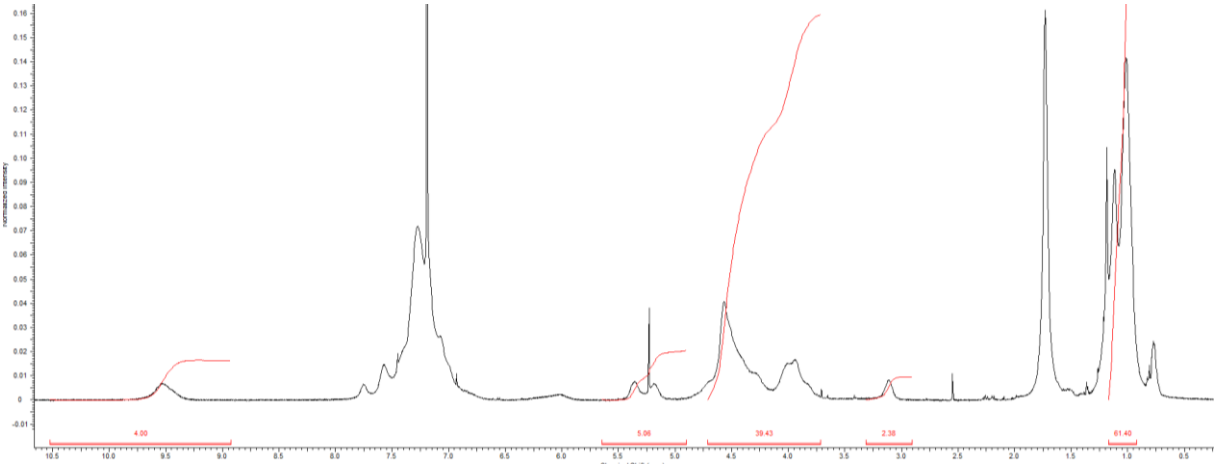

Figure S333. ^{1}H-NMR in $CDCl_3$ of purified **VI.8**.

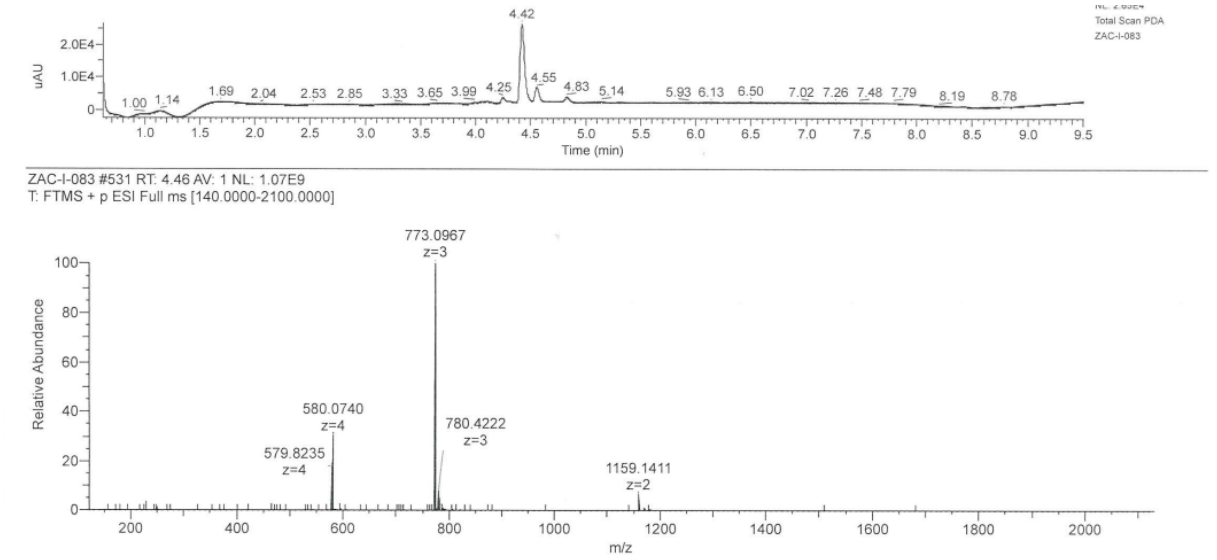

Figure S334. LCMS spectrum of crude **VI.8**.

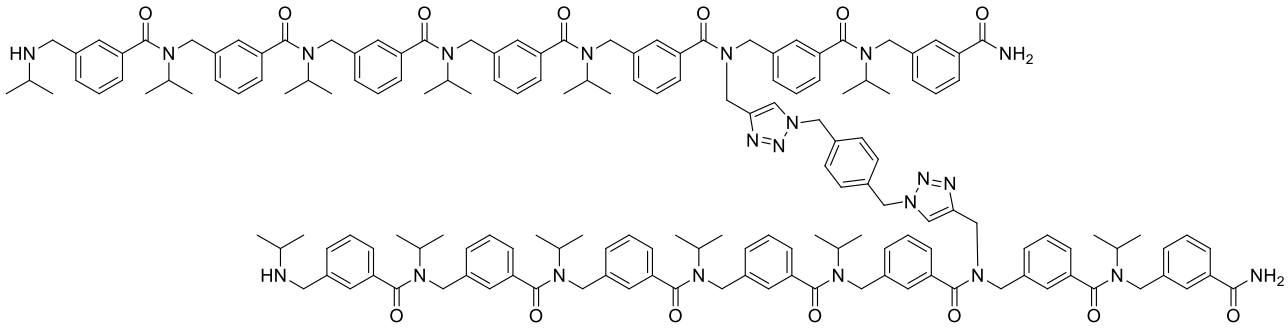

H-shaped **VI.9** was synthesised according to General procedure B, using 100 mg of Rink Amide resin (loading 0.62mmol/g).

m_{pure}= 73.5 mg (purity 98%), isolated yield 89%

HRMS (TOF MS ES+): *m/z* calcd for $C_{162}H_{191}N_{22}O_{14}$ $[M+3H]^{3+}$: 889.49646; found: 889.4958 (-0.68 ppm).

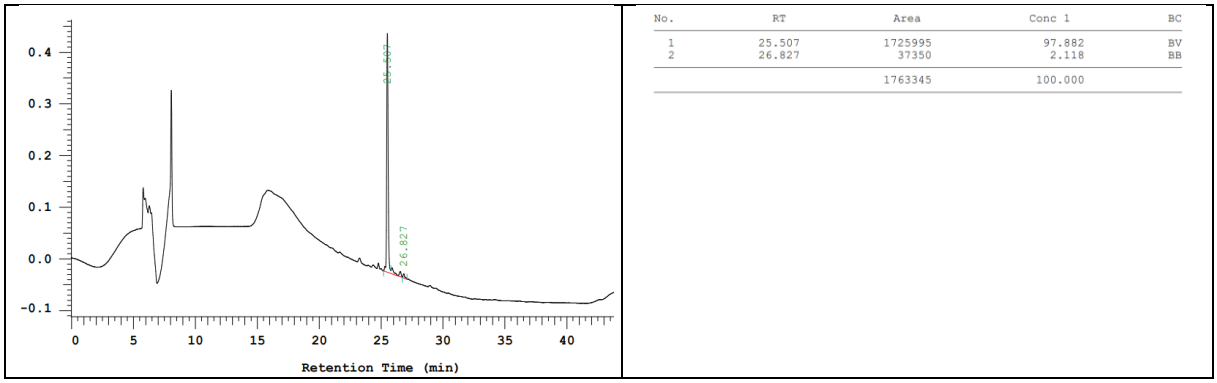

Figure S335. HPLC chromatogram of purified **VI.9**.

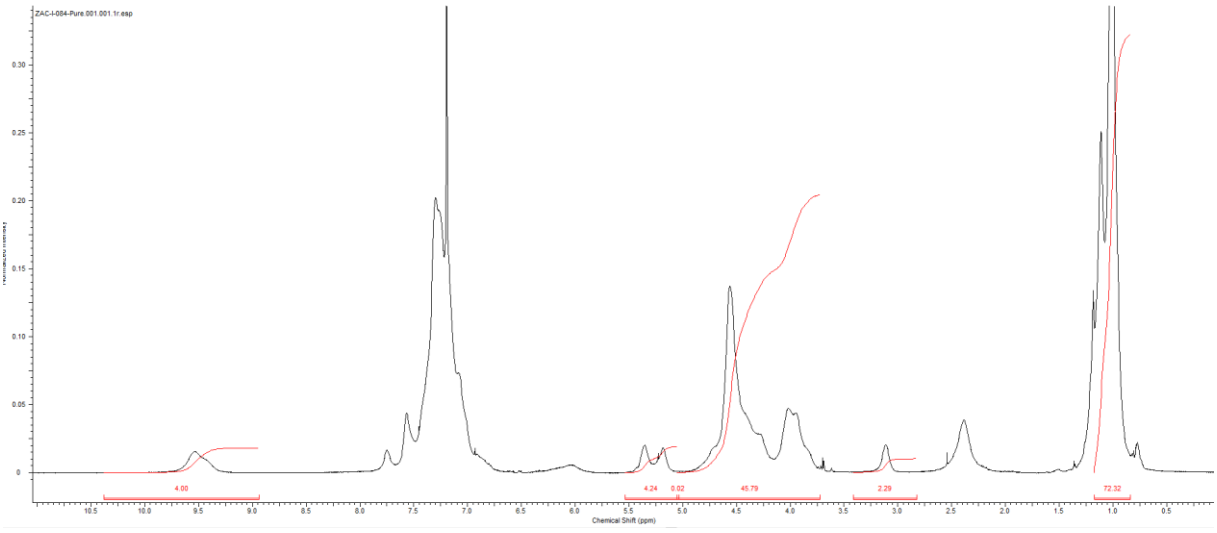

Figure S336. ^{1}H-NMR in $CDCl_3$ of purified **VI.9**.

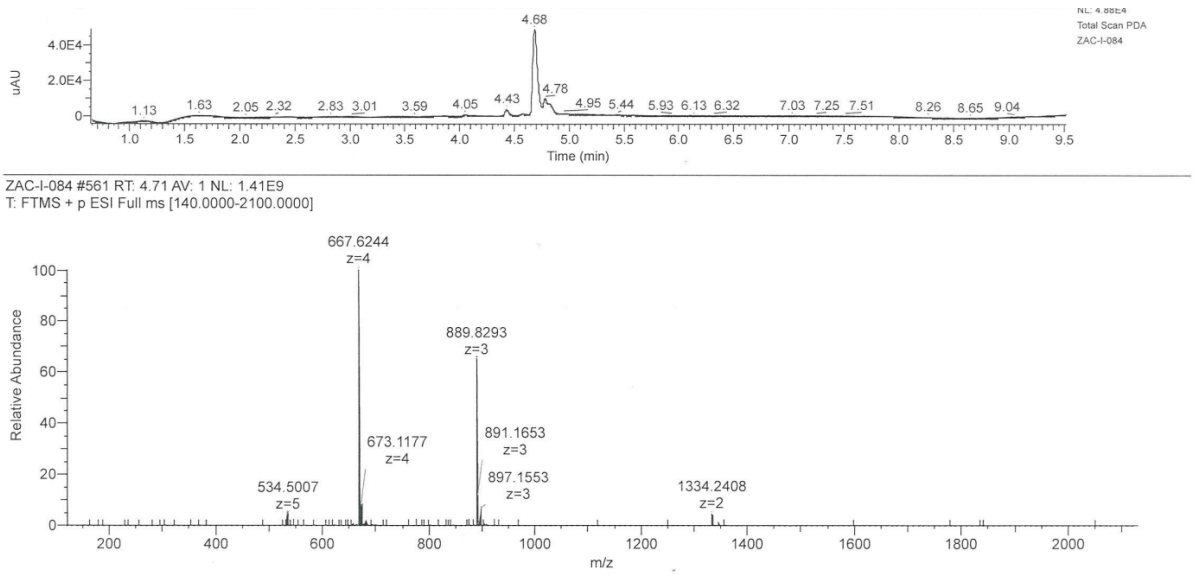

Figure S337. LCMS spectrum of crude **VI.9**.

III.2.e. VI.10.

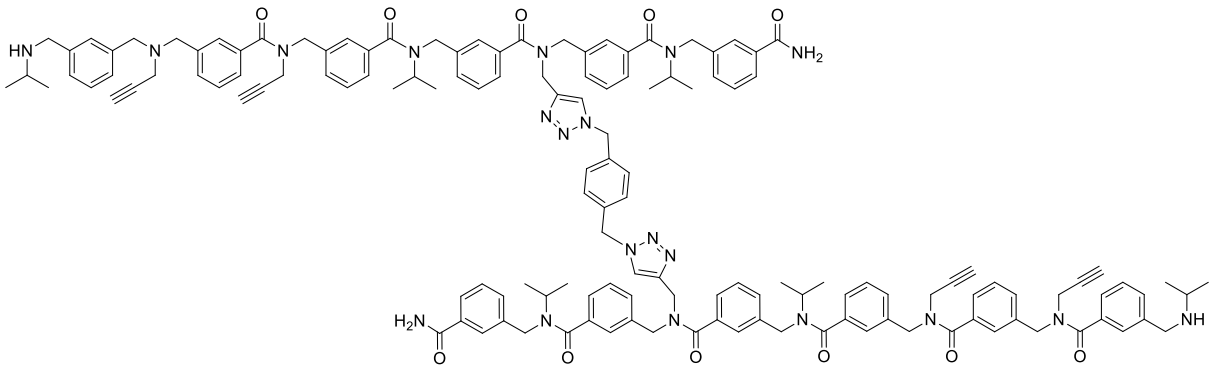

H-shaped **VI.10** was synthesised according to General procedure B, using 20 mg of Rink Amide resin (loading 0.62mmol/g).

m_{pure}= 11.5 mg, isolated yield 81%

HRMS (TOF MS ES+): *m/z* calcd for $C_{140}H_{149}N_{20}O_{12}$ $[M+3H]^{3+}$: 767.38825; found: 767.3898 (1.99 ppm).

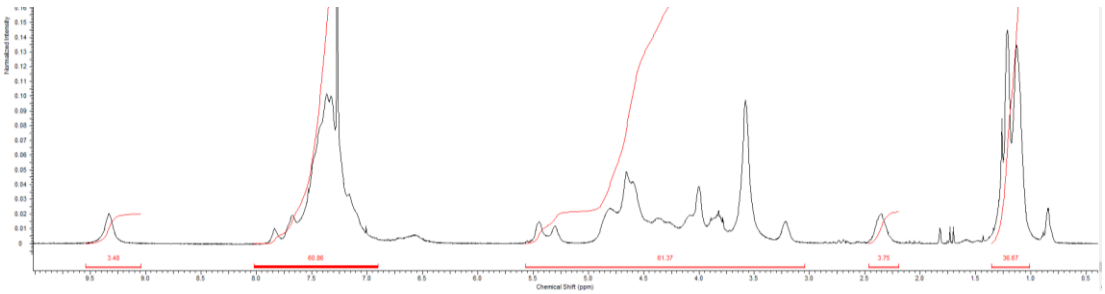

Figure S338. ^{1}H-NMR in $CDCl_3$ of pure **VI.10**.

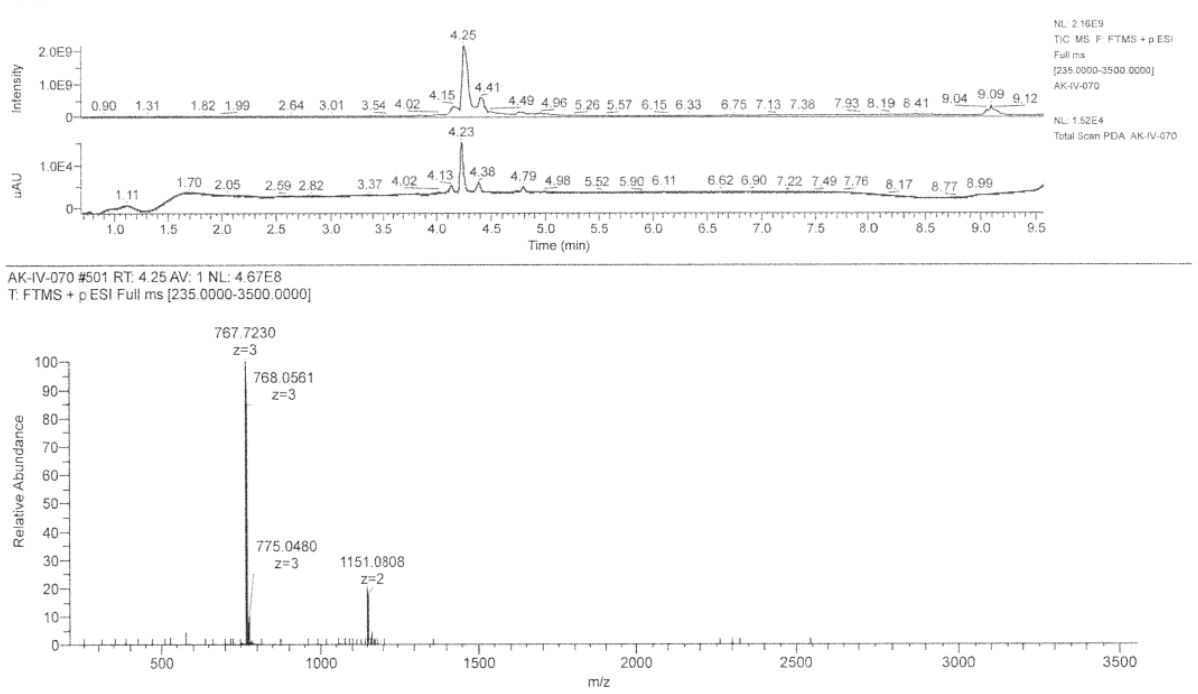

Figure S339. LCMS spectrum of crude **VI.10**.

III.3. H-shaped arylopeptoids with General procedure B followed with CuAAC.

*III.3.a. **VI.11**.*

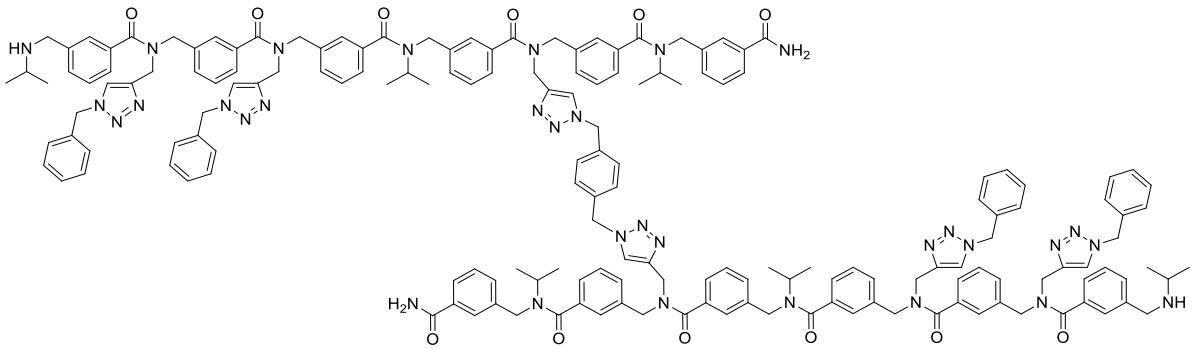

H-shaped **VI.11** was synthesised according to General procedure B followed with CuAAC using the optimized conditions from publication in chapter III, using 100 mg of Rink Amide resin (loading 0.62mmol/g).

m_{pure}= 61.8 mg, isolated yield 70%

HRMS (TOF MS ES+): *m/z* calcd for $C_{168}H_{178}N_{32}O_{12}$ $[M+4H]^{4+}$: 708.85700; found: 708.8564 (-0.78 ppm).

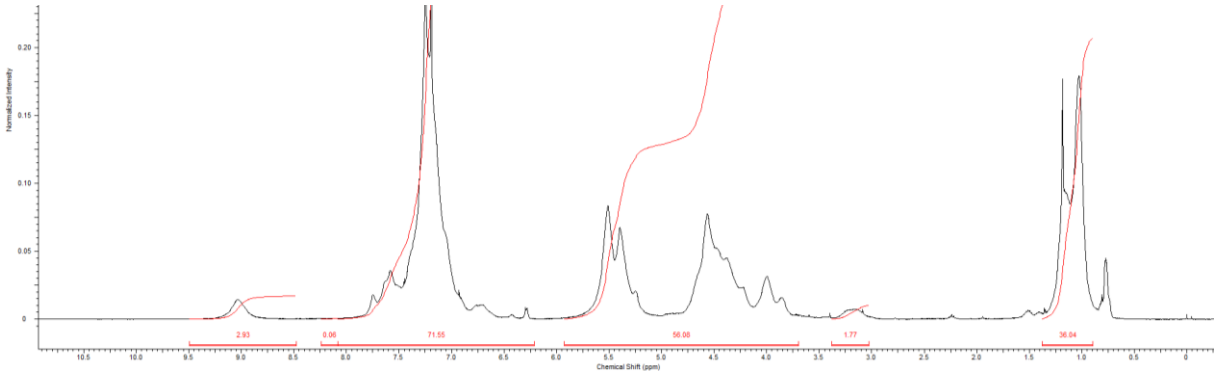

Figure S340. ^{1}H-NMR in $CDCl_3$ of purified **VI.11**.

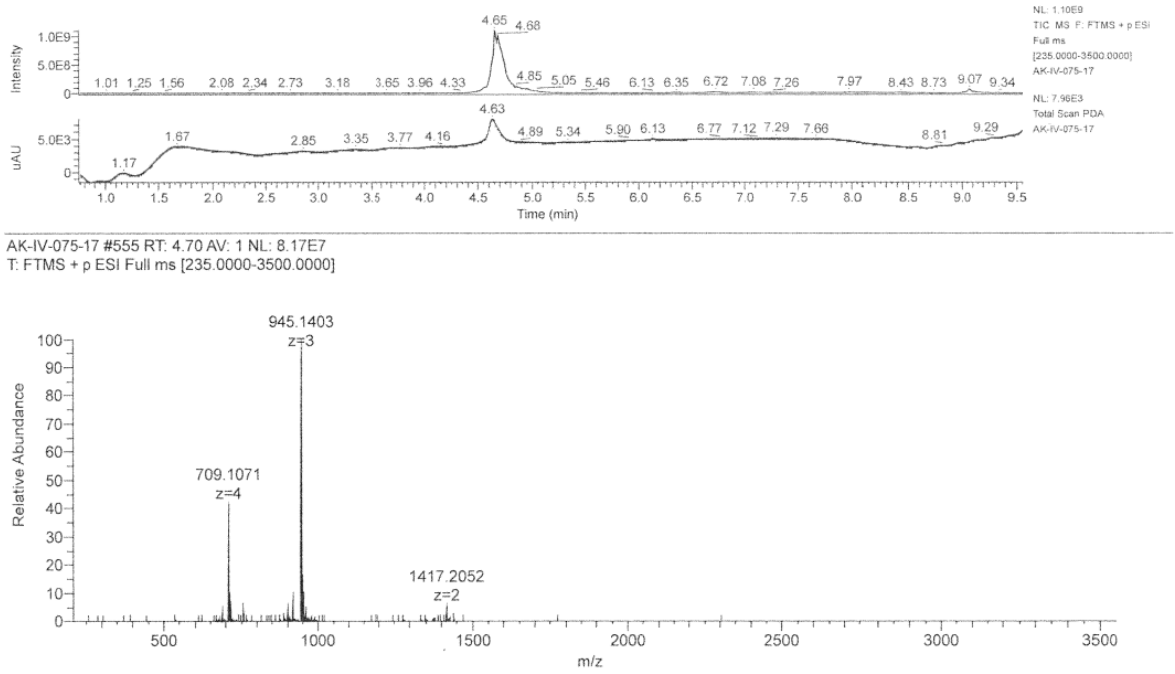

Figure S341. LCMS spectrum of crude **VI.11**.

III.3.b. VI.12.

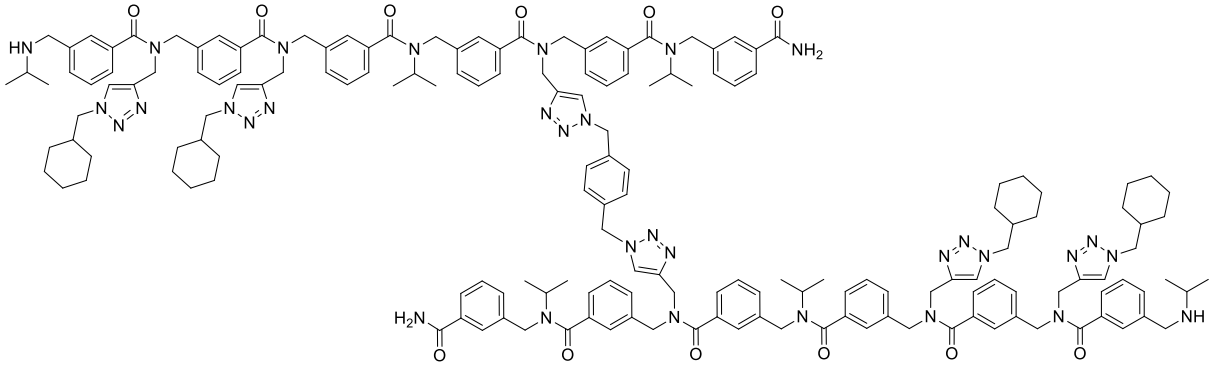

H-shaped **VI.12** was synthesised according to General procedure B followed with CuAAC using the optimized conditions from publication in chapter III, using 100 mg of Rink Amide resin (loading 0.62mmol/g).

m_{pure}= 63 mg, isolated yield 71%

HRMS (TOF MS ES+): *m/z* calcd for $C_{168}H_{202}N_{32}O_{12}$ $[M+4H]^{4+}$: 714.90395; found: 714.9028 (-1.65 ppm).

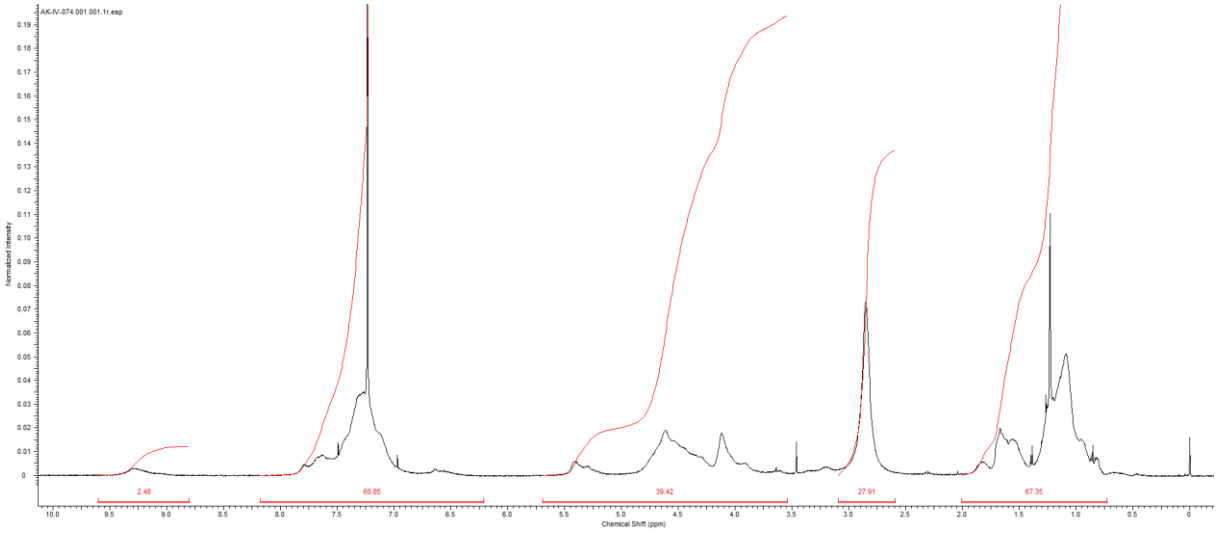

Figure S342. ^{1}H-NMR in $CDCl_3$ of purified **VI.12**.

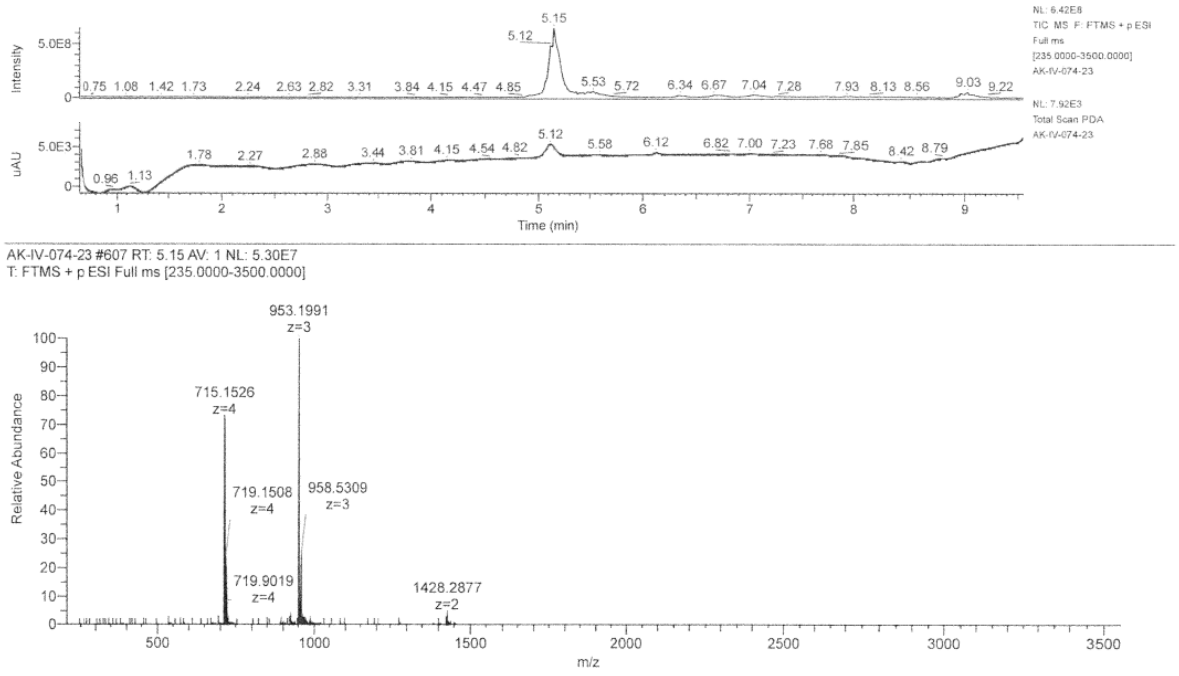

Figure S343. LCMS spectrum of crude **VI.12**.

Abstract

Arylopeptoids (*i.e.* oligomeric *N*-substituted aminomethyl benzamides) is a class of peptoid-inspired oligoamides with aromatic backbone. They retain advantageous features of peptoids such as straightforward synthesis by submonomer approach and conformational preferences governed by *cis-trans* isomerism of *N,N*-disubstituted amides. These *N*-alkylated aromatic oligoamides may be developed as proteomimetics or scaffolds for multivalent display. The aim of this thesis was to explore the chemical diversity accessible from linear and cyclic arylopeptoids through Click chemistry using Copper carbene as catalyst.

First, access and properties of Copper (I)-*N*-heterocyclic carbene catalyst was exposed. Also, an extension of the quantitative NMR was presented to study the purity of this catalyst and other organometallic compounds. The development of an efficient CuAAC protocol on-resin using Copper (I)-*N*-heterocyclic carbene catalyst for the functionalization of arylopeptoids has allowed the efficient preparation of a library of linear oligomers carrying several triazole-type side chains. Besides, combinatorial and sequential approaches have been implemented leading to huge accessible chemical diversity. Post-modification of the triazoles into triazoliums has led to several series of triazolium-based arylopeptoids exhibiting amphipathic character. Their antibacterial activity against a panel of bacterial strains has been evaluated. The access to 3-dimensional crown- and tube-like structures from constrained arylopeptoid macrocycles by CuAAC reaction using the Cu-NHC catalyst also proved to be efficient with a selectivity depending on the spatial preorganization of the cyclic core and proper choice of the NHC catalyst. Finally, the access to H-shaped arylopeptoids was studied using CuAAC reaction on resin. Overall, this work highlights the potential of the Copper (I)-*N*-heterocyclic carbene as catalyst for CuAAC to perform on-resin poly-functionalization of arylopeptoids and to build complex 3D-architectures.

Key words: *Click* chemistry; CuAAC reaction, Copper(I) N-heterocyclic carbene; *N*-alkylated aromatic oligoamides.

Les arylopeptoïdes (ou oligomères d'aminométhylbenzamides *N*-substitués) sont une classe d'oligoamides inspirés des peptoïdes et possédant un squelette aromatique. Ils conservent les caractéristiques intéressantes des peptoïdes telles que la synthèse par une approche submonomère et les préférences conformationnelles régies par l'isomérie cis-trans des amides *N,N*-disubstitués. Ces oligoamides aromatiques *N*-alkylés peuvent être développés en tant que protéomimétiques ou plateformes pour une présentation multivalente. L'objectif de cette thèse était d'explorer la diversité chimique accessible à partir des arylopeptoïdes linéaires et cycliques grâce à la chimie Click en utilisant un catalyseur de type carbène *N*-hétérocyclique de cuivre(I).

Tout d'abord, l'accès et les propriétés du catalyseur *N*-carbène hétérocyclique de cuivre (I) sont exposés. Aussi, une application de la RMN quantitative est présentée pour obtenir la pureté de ce catalyseur (ainsi que d'autres composés organométalliques). Le développement d'un protocole CuAAC efficace sur résine utilisant ce catalyseur carbène cuivre pour la fonctionnalisation des arylopeptoïdes a permis la préparation efficace d'une bibliothèque d'oligomères linéaires portant plusieurs chaînes latérales de type triazole. Parallèlement, des approches combinatoire et séquentielle ont été mises en œuvre conduisant à une plus grande diversité chimique. La post-modification des triazoles en triazoliums a conduit à plusieurs séries d'arylopeptoïdes à base de triazolium présentant un caractère amphipathique. Leur activité antibactérienne a été évaluée sur un panel de souches bactériennes. L'accès par la réaction CuAAC à des structures tridimensionnelles en forme de couronne et/ou de tube à partir de macrocycles arylopeptoïdes contraints s'est également avéré efficace avec une sélectivité dépendant de la pré-organisation spatiale du macrocycle et du choix approprié du catalyseur. Enfin, l'accès à des arylopeptoïdes branchés en forme de H a été étudié en utilisant la réaction CuAAC sur résine. Dans l'ensemble, ce travail met en évidence le potentiel du catalyseur de type carbène cuivre (I) pour effectuer la poly-fonctionnalisation d'arylopeptoïdes sur résine et pour construire des architectures 3D complexes.

Mots-clès : Chimie *Click* ; réaction CuAAC, carbène *N*-hétérocyclique de cuivre(I); oligoamides aromatiques *N*-alkylés.